VNIVERSITAT DE VALÈNCIA

FACULTY OF CHEMISTRY

PRINCIPE FELIPE
CENTRO DE INVESTIGACION

POLYMER THERAPEUTICS LABORATORY

Doctoral Program: **Chemistry**

DEVELOPMENT OF POLYPEPTIDE-BASED THERAPEUTICS FOR TOPICAL DELIVERY

Irene Dolz Pérez

Doctoral Thesis - University of Valencia

October 2019

Thesis Directors: **Dr. María J. Vicent Docón** and **Dr. Vicent J. Nebot Carda**

Dr. María J. Vicent Docón, Ph.D. in Chemistry and Head of the Polymer Therapeutics Laboratory at the Centro de Investigación Príncipe Felipe (Valencia Spain), and Dr. Vicent J. Nebot Carda, Ph.D. in Chemistry and Chief Technical Officer of the company Polypeptide Therapeutic Solutions S.L. CERTIFY, that the work

"DEVELOPMENT OF POLYPEPTIDE-BASED THERAPEUTICS FOR TOPICAL DELIVERY"

has been developed by Irene Dolz Pérez under their supervision in the Centro de Investigación Príncipe Felipe in Valencia, as a thesis project to obtain a Ph.D degree in Chemistry from the University of Valencia, Faculty of Chemistry.

A mi hermana

INDEX

ACKNOWLEDGMENTS.....17

ABBREVIATIONS.....21

ABSTRACT.....27

OBJECTIVES OF THE RESEARCH.....31

CHAPTER I: GENERAL INTRODUCTION AND BACKGROUND.....33

I.1. Biological Barriers to the Administration of Therapeutic Agents.....35

I.2. Skin as a Barrier.....37

I.2.1. Skin Structure and Function.....37

I.2.1.1. The Epidermis.....37

I.2.1.2. The Dermis.....39

I.2.2. Penetrating the Skin Barrier.....39

I.2.3. Penetrant Characteristics.....41

I.2.4. Methods to Improve Penetration through Skin.....41

I.2.4.1. Formulation Optimization.....41

I.2.4.2. Chemical Enhancers.....41

I.2.4.3. Physical Enhancers.....45

I.2.5. Techniques to Evaluate Skin Penetration.....46

I.2.5.1. Skin Models.....47

I.2.5.2. Monitoring Penetration in the Skin.....48

I.2.6. Skin Penetration as a Challenge.....49

I.3. Nanomedicine.....49

I.3.1. Nanomedicine Applications to the Skin.....50

I.4. Polymer Therapeutics: The First Polymeric Nanomedicines.....52

I.4.1. Definition and Classification.....52

I.4.2. Polymer Conjugates as Therapeutics.....55

I.4.2.1. Polymer-Protein Conjugates.....56

I.4.2.2. Polymer-Drug Conjugates.....60

I.4.2.2.1. Rational Design of Polymer-Drug Conjugates.....64

I.4.2.2.1.1. Polymeric Carrier 64
I.4.2.2.1.2. Bioresponsive Linkers 65
I.4.2.2.1.3. Physico-Chemical Properties of Polymer-Drug Conjugates 66
I.4.3. Polypeptide-Based Therapeutics 67
I.4.4. Characterization Techniques 69
I.4.5. Polymer Therapeutics for Skin Delivery 72
I.5. Psoriasis as a Target Pathology 74
I.5.1. Prevalence and Morbidity 75
I.5.2. Etiology 76
I.5.2.1. Triggering Factors 76
I.5.2.2. Genetic Factors 77
I.5.3. Immunopathological Features 78
I.5.4. Immunopathogenesis: Central Role of the Immune System 79
I.5.5. Current Therapeutic Approaches for Psoriasis 83
I.5.5.1. Topical Approaches 83
I.5.5.2. Systemic Approaches 84
I.5.5.2.1. Biologic Therapeutics 85
I.5.5.2.2. Non-Biologic Therapeutics 86
I.5.5.3. Phototherapy 87
I.5.6. Nanomedicine-Polymer Therapeutic Approaches to Psoriasis Treatment 87
I.6. References 91

<u>CHAPTER II</u>: *EX VIVO* AND *IN VIVO* MODELS OF PSORIASIS: DISEASE PROGRESSION AND HISTOPATHOLOGICAL FEATURES 111
II.1. Antecedents and Background 113
II.2. Results 117
II.2.1 *Ex Vivo* Human Skin Model 117
II.2.1.1. Characterization of *Ex Vivo* Human Skin Model 117
II.2.1.1.1. Tissue Viability Maintenance 117
II.2.1.1.2. Histological Features 117
II.2.1.2. Characterization of Inflammatory *Ex Vivo* Human Skin Model 118
II.2.1.2.1. Maintenance of Tissue Viability Following Inflammation 119
II.2.1.2.2. Inflammatory Features 120
II.2.1.2.3. Quantification of Cytokine Release following Inflammatory Insult. 122
II.2.2 *In Vivo* Model of Psoriasis 124

II.2.2.1. Monitoring Safety during Disease Induction via Animal Weight 124
II.2.2.2. Evaluation of Inflammation: Back Morphology and PASI Score 124
II.2.2.3. Increase in Ear Thickness 126
II.2.2.4. Histology of Ear and Back 127
II.2.2.5. Increase in Spleen Weight 129
II.2.2.6. Increased Pro-Inflammatory Cytokines Release in Serum and Tissue 130
II.2.2.7. Hematological Parameters 132
II.3. Discussion 133
II.3.1. Inflammatory *Ex Vivo* Human Skin Model Mimics the Features of Psoriasis 133
II.3.2. Suitability of Imiquimod Cream for Psoriasis Development 134
II.3.3. H&E Staining as a Tool to Evaluate Skin Inflammation 134
II.3.4. Interleukin Levels as a Critical Biomarker of Psoriatic Progression 135
II.4. Conclusions 136
II.5. Materials and Methods 137
II.5.1. *Ex Vivo* Models 137
II.5.1.1. Development of *Ex Vivo* Human Skin Model 137
II.5.1.1.1 Tissue Viability Assay 137
II.5.1.1.2. Histological Analysis and Imaging 138
II.5.1.2. Development of Inflammatory *Ex Vivo* Human Skin Model 138
II.5.1.2.1. Tissue Viability Assay 139
II.5.1.2.2. Histological Analysis and Imaging 139
II.5.1.2.3. Quantification of Pro-Inflammatory Cytokines Released to the Culture Medium 139
II.5.2. *In Vivo* Models 139
II.5.2.1. Mouse Strains 139
II.5.2.2. Ethical Considerations 139
II.5.2.3. Establishment of the Psoriatic Model 140
II.5.2.4. Scoring Severity of Skin Inflammation (PASI Score) 140
II.5.2.5. Ear Thickness 140
II.5.2.6. Spleen Weight 140
II.5.2.7. Histology 141
II.5.2.8. Pro-Inflammatory Cytokines Levels in Serum and Tissue 141
II.5.2.9. Hematological Analysis 141
II.6. References 142

CHAPTER III: DEVELOPMENT OF HYBRID POLYPEPTIDE-BASED CARRIERS TO ENHANCE DRUG DELIVERY THROUGH THE SKIN.....147

III.1. Antecedents and Background..... 151

III.2. Results and Discussion..... 154

III.2.1. Development of the Hyaluronic Acid-Poly-L-Glutamate Cross-Polymer (HA-CP) Vehicle: Synthesis and Physico-Chemical Characterization 154

III.2.1.1. Synthesis and Physico-Chemical Characterization of HA-CP 154

III.2.1.2. Development of Fluorescently-labeled HA-based Materials..... 157

III.2.2. Analysis of the HA-CP as a Biomaterial for Topical Skin Applications..... 159

III.2.2.1. Hyaluronidase Degradation Studies 159

III.2.2.2 Cell Viability *In Vitro*..... 160

III.2.2.3. Tissue Viability in an *Ex Vivo* Human Skin Model 161

III.2.2.4. *Ex Vivo* Human Skin Permeation by Franz Diffusion Cells 161

III.2.2.5. Hydration Assays in Human Volunteers 164

III.2.3. Hybrid Material: HA-CP Vehicle Combined with Polypeptidic Micelles for Transdermal Delivery of Hydrophobic APIs..... 165

III.2.3.1. Synthesis and Characterization of Block Copolymers 165

III.2.3.2. Characterization of Block Copolymer Micelle Formulation 167

III.2.3.3. Cell Viability Studies *In Vitro* of Selected Micelles 170

III.2.3.4. Characterization of the Hybrid Material..... 171

III.2.3.5. *Ex Vivo* Human Skin Permeation of Hybrid Material by Franz Diffusion Cells 172

III.2.3.6. Tissue Viability of Hybrid Material in an *Ex Vivo* Human Skin 175

III.3. Conclusions 176

III.4. Materials and Methods..... 177

III.4.1. Materials..... 177

III.4.2. Physico-Chemical Characterization Methods 178

III.4.2.1. Nuclear Magnetic Resonance (NMR) Spectroscopy..... 178

III.4.2.2. Gel Permeation Chromatography (GPC) in DMF..... 178

III.4.2.3. Gel Permeation Chromatography (GPC) in Aqueous Media 178

III.4.2.4. Circular Dichroism (CD) 179

III.4.2.5. Dynamic Light Scattering (DLS) 179

III.4.2.6. Fluorescence Spectroscopy..... 180

III.4.2.7. Ultraviolet-Visible (UV-Vis) Spectroscopy 180

III.4.2.8. Transmission Electron Microscopy (TEM) 181

III.4.2.9. Amine Quantification by TNBSA Assay 181

III.4.2.10. High-Performance Liquid Chromatography (HPLC) 181
III.4.2.11. Viscosity Measurements 181
III.4.3. Synthetic Protocols 182
III.4.3.1. Synthesis of Hyaluronic Acid-poly-L-Glutamate Cross-Polymer 182
III.4.3.2. Cyanine5.5 Labeling of HA-based Materials 182
III.4.3.3. Synthesis of Amphiphilic Block Copolymers 183
III.4.3.4. Preparation of the Micelles using the Block Copolymers 184
III.4.4. Biological Evaluation 184
III.4.4.1. *In Vitro* Evaluation 184
III.4.4.1.1. Cell Viability 184
III.4.4.2. *Ex Vivo* Evaluation 185
III.4.4.2.1. Permeation Studies by Franz Diffusion Cells 185
III.4.4.2.2. Evaluation of Tissue Viability in an *Ex Vivo* Human Skin Model .. 186
III.4.4.3. *In Vivo* Evaluation 186
III.4.4.3.1. Hydration Assays 186
III.5. References 187

CHAPTER IV: POLYMER THERAPEUTICS FOR THE TREATMENT OF SKIN DISEASES. PSORIASIS TREATMENT AS PROOF OF CONCEPT.....189
IV.1. Antecedents and Background 195
IV.2. Results 197
IV.2.1. Safety and Skin Penetration of Linear and Star PGAs 197
IV.2.2. Synthesis and Characterization of Poly-L-Glutamate Fluocinolone Acetonide Conjugates 198
IV.2.3. Self-assembling Behavior of PGA-FLUO 205
IV.2.4. FLUO Release Kinetics as a Crucial Feature Driving Sustained Release into the Skin 209
IV.2.5. Compatibility of PGA-FLUO with the HA-CP Vehicle 211
IV.2.6. *In Vitro* Skin Compatibility and Cell Trafficking Studies of PGA-FLUO Conjugates 212
IV.2.7. PGA-FLUO Reduces the Release of Pro-Inflammatory Cytokines *In Vitro* 214
IV.2.8. PGA-FLUO Biocompatibility and Anti-Inflammatory Effect in an Inflammatory Skin Equivalents Model and an Inflammatory *Ex Vivo* Human Skin Model 215
IV.2.9. FLUO Conjugation and the Use of HA-CP as Vehicle Enhances Skin Permeation 217

IV.2.10. Optimization of *In Vivo* Experiments 220
IV.2.10.1. Reduction of Skin Inflammation, Ear Thickness, and Splenomegaly.. 221
IV.2.10.2. Reduction of Epidermal Thickness 223
IV.2.10.3. Reduction of Pro-Inflammatory Cytokines Levels in Serum 224
IV.2.11. PGA-FLUO in HA-CP Reduces Imiquimod-Induced Skin Inflammation *In Vivo* 226
IV.2.12. Reduction of Skin Inflammation, Ear Thickness, and Splenomegaly 228
IV.2.13. PGA-FLUO Conjugates Reduce Pro-Inflammatory Cytokines Levels in Serum and Tissue 229
IV.3. Conclusions 231
IV.4. Materials and Methods 231
IV.4.1. Materials 231
IV.4.2. Physico-Chemical Characterization Methods 232
IV.4.2.1. Nuclear Magnetic Resonance (NMR) Spectroscopy 232
IV.4.2.2. Ultraviolet-Visible (UV-Vis) Spectroscopy 232
IV.4.2.3. Size Exclusion Chromatography (SEC) in Aqueous Media 233
IV.4.2.4. Fluorescence Spectroscopy 233
IV.4.2.5. Transmission Electron Microscopy (TEM) 234
IV.4.2.6. Dynamic Light Scattering (DLS) 234
IV.4.2.7. High-Performance Liquid Chromatography (HPLC) 234
IV.4.2.7.1. Recovery of FLUO in a Polymeric Matrix: Liquid-liquid Extraction 235
IV.4.2.7.2. Extraction and Quantification of FLUO in the Skin 236
IV.4.2.8. Circular Dichroism (CD) 236
IV.4.3. Synthetic Protocols 236
IV.4.3.1 Synthesis of Poly-L-glutamate Fluocinolone Acetonide Conjugates 236
IV.4.3.2 Oregon Green Labeling of PGA-FLUO Conjugates 237
IV.4.4. Biological Evaluation of Polymer-Drug Conjugates 238
IV.4.4.1. *In Vitro* Evaluation 238
IV.4.4.1.1. Cell Viability 238
IV.4.4.1.2. Cellular Uptake by Flow Cytometry 238
IV.4.4.1.3. Uptake Studies by Confocal Microscopy 239
IV.4.4.1.4. Anti-Inflammatory Activity 240
IV.4.4.1.5. Cathepsin B Activity 240
IV.4.4.2. *Ex Vivo* Evaluation 241
IV.4.4.2.1. Permeation Studies by Franz Diffusion Cells 241

IV.4.4.2.2. Tissue Viability and Evaluation of the Anti-Inflammatory Activity of PGA-FLUO Conjugates in an Inflammatory *Ex Vivo* Human Skin Model 242
IV.4.4.2.3. Development of a Skin Equivalents Construction Model and Cell Viability Assays 243
IV.4.4.2.4. Development of an Inflammatory Skin Equivalents Construction Model and Anti-Inflammatory Activity of PGA-FLUO conjugates 243
IV.4.4.3. *In Vivo* Evaluation 244
IV.4.4.3.1. Ethical Considerations 244
IV.4.4.3.2. Optimization of Optimal FLUO Concentration for Psoriatic Mice Model 244
IV.4.4.3.2.1. Establishment of Psoriatic Model 244
IV.4.4.3.2.1. Safety Evaluation of Treatments 244
IV.4.4.3.2.2. Scoring Severity of Skin Inflammation: PASI score 245
IV.4.4.3.2.3. Spleen Weight 245
IV.4.4.3.2.4. Ear Thickness 245
IV.4.4.3.2.5. Histology 245
IV.4.4.3.2.6. Pro-Inflammatory Interleukin Levels in Serum 246
IV.4.4.3.3. Evaluation of Anti-Inflammatory Activity of PGA-FLUO Conjugates in Psoriatic Mice Model 246
IV.4.4.3.3.1. Establishment of Psoriatic Model 246
IV.4.4.3.3.2. Safety Evaluation of Treatments 246
IV.4.4.3.3.3. Scoring Severity of Skin Inflammation: PASI score 247
IV.4.4.3.3.4. Spleen Weight 247
IV.4.4.3.3.5. Ear Thickness 247
IV.4.4.3.3.6. Histology 247
IV.4.4.3.3.7. Pro-Inflammatory Interleukin Levels in Serum and Tissue 247
IV.5. References 248

CHAPTER V: DEVELOPMENT OF POLYMER CONJUGATES FOR TISSUE HEALING 247
V.1. Antecedents and Background 255
V.1.1. Skin Wound Healing 255
V.1.2. Heart Tissue Damage by Induced Ischemia-Reperfusion Injury 259
IV.2. Results and Discussion 260
V.2.1. Synthesis and Characterization of Poly-L-Glutamate-Didocosahexaenoic Acid Conjugates 260

V.2.2. Enhanced Solubility and Stability upon diDHA Conjugation 264
V.2.3. Self-assembling Behavior of PGA-diDHA Conjugates 265
V.2.4. Drug Release Kinetics and Conformation of PGA-diDHA Conjugates 268
V.2.5. PGA-diDHA Treatment of Skin Wound Healing 270
V.2.5.1. Cell Viability Studies with PGA-diDHA Conjugates 270
V.2.5.2. Enhanced Cell Migration by PGA-diDHA Conjugates 271
V.2.5.3. PGA-diDHA Permeation into the Epidermis 272
V.2.6. PGA-diDHA Treatment of Ischemia-Reperfusion (I/R) Injury 274
V.2.6.1. Enhanced Cell Viability after diDHA Conjugation *In Vitro* 274
V.2.6.2. PGA-diDHA6.4 Treatment Decreases Myocardial Infarct Size in an I/R Model *In Vivo* 276
V.3. Conclusions 277
V.4. Materials and Methods 279
V.4.1. Materials 279
V.4.2. Physico-Chemical Characterization Methods 279
V.4.2.1. Nuclear Magnetic Resonance (NMR) Spectroscopy 279
V.4.2.2. Ultraviolet-Visible (UV-Vis) Spectroscopy 279
V.4.2.3. Fluorescence Spectroscopy 280
V.4.2.4. Transmission Electron Microscopy (TEM) 280
V.4.2.5. Dynamic Light Scattering (DLS) 280
V.4.2.6. Fast Protein Liquid Chromatography (FPLC) 281
V.4.2.7. Circular Dichroism (CD) 282
V.4.2.8. Stability Over Time by NMR Analysis 282
V.4.2.9. Stability Over Time by Malondialdehyde Colorimetric Assay 282
V.4.2.10. Quantitative Determination of the Triglyceride Content in the PGA-diDHA Conjugates 283
V.4.3. Synthetic Protocols 283
V.4.3.1 Synthesis of Poly-L-Glutamate Didocosahexaenoic Acid Conjugates 283
V.4.3.2 Oregon Green Labeling of PGA-diDHA Conjugates 284
V.4.4. Biological Evaluation of PGA-diDHA Conjugates 285
V.4.4.1. Skin Wound Healing 285
V.4.4.1.1. *In Vitro* Evaluation 285
V.4.4.1.1.1. Cell Viability 285
V.4.4.1.1.2. Scratch Assays 285
V.4.4.1.2. *Ex Vivo* Evaluation 286
V.4.4.1.2.1. Visualization of Dermal Penetration 286

V.4.4.1.2.2. Confocal Microscopy 286
V.4.4.2. Ischemia-Reperfusion Injury 287
V.4.4.2.1. *In Vitro* Evaluation 287
V.4.4.2.2. *In Vivo* Evaluation 287
V.5. References 288

GENERAL DISCUSSION 293
FINAL CONCLUSIONS 311
APPENDIX: THESIS PROJECT, OBJECTIVES, MAIN METHODOLOGY, RESULTS AND CONCLUSIONS IN SPANISH 317
1. Introducción, antecedentes y marco temático de la Tesis 319
2. Objetivos de la investigación 321
3. Metodología 322
4. Resultados 333
5. Conclusiones 339
6. Referencias 342

ACKNOWLEDGEMENTS

"Y una vez que la tormenta termine, no recordarás cómo lo lograste, cómo sobreviviste. Ni siquiera estarás seguro de si la tormenta ha terminado realmente. Pero una cosa sí es segura. Cuando salgas de esa tormenta, no serás la misma persona que entró en ella. De eso se trata esta tormenta" Haruki Murakami

Después de este largo camino, ha llegado el momento de dar las gracias a todas las personas que han hecho esto posible. En primer lugar, me gustaría dar las gracias a mis directores de tesis, María Jesús y Vicent. Recuerdo nuestra primera reunión en la que yo quería hacer prácticas en el laboratorio, pero solamente en algún proyecto relacionado con la piel…y aquí estamos…casi 5 años más tarde presentando mi tesis doctoral. María Jesús, gracias haberme guiado durante este camino, por apostar por mí y darme la oportunidad de comenzar una nueva línea de investigación en tu laboratorio casi desde cero. Gracias por brindarme un mundo de posibilidades y por dejarme formar parte de tu gran equipo. Vicent, gracias por tu esfuerzo enseñándome el mundo de los polímeros y de la química en general. Por confiar en mí en todo momento y entender mis tiempos. Sobre todo, siempre te agradeceré que te preocuparas por mí en épocas oscuras de la tesis, simplemente una palabra reconfortante es suficiente para continuar con más fuerza todavía.

Cuando llegué al laboratorio me encontré a una gran familia que no dudó en hacerme sentir una más y cuidarme desde el principio. He vivido la transición de ser la nueva del grupo hasta estos días, en los que soy una de las "veteranas". Muchos cambios, muchas despedidas y nuevas incorporaciones. Por ello, quiero dar las gracias en mayúsculas a las viejas glorias del I-36 por haberme enseñado y ayudado en todo lo posible. Sin vosotros estos años no hubieran sido igual. Gracias por dejarme crecer profesional y personalmente con vosotros. Gracias de corazón a toda la gente que forma parte del I-36, por ofrecerme vuestra ayuda cuando lo he necesitado, por todo. En especial, me gustaría agradecer a varias personas:

Esther, sin tí mi paso por el laboratorio no hubiera sido igual. Llegué al laboratorio perdida (el mundo de los pellejos todavía estaba por descubrir) pero no dudaste en ofrecerme tu ayuda desde el principio. Ojalá existieran más personas como tú. Gracias

por tu sinceridad, ánimo, humor y compañerismo. Los guarapitos vendrán conmigo siempre!

David, el bailongo del lab! Gracias por estar siempre dispuesto a ayudarnos y por hacernos la vida más fácil en el laboratorio. Me llevo muchas risas, bailes, comidas al sol, y por supuesto palabras en francés…cochon!!

Juanjo, has sido un gran apoyo durante todo este camino. Siempre dispuesto a ayudarme y a enseñarme tu sabiduría (el HPLC se va a sentir muy solo sin nosotros). Te agradezco infinitamente tus charlas motivacionales y tus consejos para esquivar problemas antes de caer en ellos. Gracias por la confianza, las risas y los abrazos.

Fer, mi compañera de batallas!! Sabes que has sido una pieza clave durante mi tesis. Con una mirada sabemos lo que piensa la otra, demasiadas horas juntas…Echaré mucho de menos nuestros ataques de risa (¿Cuánto es un crédito? Alf ha vuelto, en forma de chapa!), canciones de los 90, confidencias, etc. Me llevo a una gran amiga. Te deseo toda la suerte del mundo en tu etapa final, eres una curranta y vales muchísimo, nunca lo olvides.

Inma, tu vuelta fue un empujón para mí. Te has convertido en alguien imprescindible en mi día a día, siempre atenta y dispuesta a sacarme una sonrisa. Gracias por entenderme, enseñarme y ayudarme siempre. Eres luz. Tenemos mucha suerte de tener a una compañera como tú en el lab. Sigue siempre fiel a tus principios y no dejes que nadie cambie tu forma de hacer las cosas.

Me llevo grandes personas y amigos de mi paso por el I-36 y el CIPF en general. Ha sido un placer compartir estos años de mi vida con vosotros. Además, me gustaría agradecer a toda la gente que forma PTS por su paciencia y ayuda cuando lo he necesitado. Os he visto crecer desde el principio (cuando trabajaban Dani y Luz mano a mano), y me siento muy orgullosa de ver en lo que os habéis convertido con mucho trabajo y dedicación.

No me puedo olvidar de la gran experiencia vivida durante mi estancia en el laboratorio de Marcelo Calderon en Berlín. Gracias a TODO el grupo por la acogida desde el primer día que llegué, solo tengo palabras de agradecimiento!! Gracias por dejarme aprender de vosotros y por brindarme vuestra ayuda siempre que lo necesitaba. Nunca olvidaré las

cervezas después del lab, las barbacoas y las clases magistrales de alemán-español. Berlín, te has quedado con un trocito de mí.

Fuera de los laboratorios, tengo la suerte de contar con unos amigas/os inmejorables. Siempre han intentado sacarme una sonrisa en los peores momentos, haciéndome sentir querida, valorada y apoyada. Aunque no entendierais porque tenía que trabajar los fines de semana o porque no podía ir a las quedadas o a los festivales que tanto nos gustan, siempre me comprendíais y teníais una propuesta alternativa para poder vernos. Después de mil horas en el laboratorio, sentir que tus amigos van a estar para lo que necesites, ya sea en persona o por teléfono (no me olvido de las personas que se han preocupado por mí a km de distancia), es algo que os agradeceré eternamente. Mil veces gracias.

Y por último, me gustaría dar las gracias a mis grandes pilares durante este largo camino...

En primer lugar, gracias a mis padres, por estar siempre a mi lado y apoyarme en todas mis decisiones. Por aguantarme y reconfortarme en mis peores momentos. Nunca os podré agradecer tanta dedicación y cariño. Desde pequeña me habéis hecho sentir lo orgullosos que estabais de mí y que podía conseguir todo lo que me propusiera. Gracias por vuestro esfuerzo para abrirme las puertas de mi futuro.

En segundo lugar, gracias a Fran. Gracias por aparecer en mis peores momentos, quedarte y cambiar mi mundo. Has sido mi vía de escape durante este largo camino. Tus palabras de ánimo, cariño, paciencia, comprensión y tus abrazos interminables son algo que no olvidaré nunca…"si no confías en ti, confía en el mí que cree en ti". Te debo muchísimo. Gracias por ser mi calma en la tempestad.

Y por último, esta tesis se la quiero dedicar a mi hermana, a mi ejemplo a seguir. Gracias por agarrarme fuerte de la mano y no soltarme nunca. Desde pequeña siempre me has enseñado que con esfuerzo, dedicación y trabajo todo se puede conseguir, y por eso una parte de esta tesis es tuya. Eres ese ave fénix que resurge de sus cenizas con más fuerza todavía. Hasta en tus peores momentos te sigues preocupando por mí y sigues haciéndome sentir la persona más fuerte y con más suerte del mundo. Nunca dudes de todo lo que eres capaz. Arriba las Dolz!

GRACIAS

ABBREVIATIONS

Aa = Amino acid

ACN = Acetonitrile

AGM = Aminoglutethimide

AMI = Acute myocardial infarction

AMM = Activated monomer mechanism

APIs =Active pharmaceutical ingredients

Ar = Argon

Asp = Aspartate

ATRA = All-trans retinoic acid

Au-3MPS = Sodium 3-mercapto-1-propane sulfonate

BBB =Blood-brain barrier

BG = Benzyl-L-glutamate

BSA = Bovine serum albumin

CAC = Critical aggregation concentration

cAMP = Cyclic adenosine monophosphate

Cat. B = Cathepsin B

CD = Circular dichroism

Ck = Cytokeratin

CMC = Critical micelle concentration

COX-2 = Cyclooxygenase-II

CVD = Cardiovascular diseases

Cy5.5 = Cyanine 5.5

Đ = Polydispersity

Da = Dalton

DC = Diffusion coefficient

DCM = Dichloromethane

DCs = Dendritic cells

ddH_2O = MilliQ water

DHA = Docosahexaenoic acid

diDHA = Didocosahexaenoic acid

DIEA = N,N-Diisopropylethylamine

DiI = 1,1'-Dioctadecyl-3,3,3',3'-Tetramethylindocarbocyanine Perchlorate

DLS = Dynamic light scattering

DMAP = 4-Dimethylaminopyridine

DMEM = Dulbecco's Modified Eagle's Medium

DMF = N,N'-Dimethyl formamide

DMSO = Dimethyl sulphoxide

DMTMM = 4-(4,6-Dimethoxy-1,3,5-triazin-2-yl)-4- methylmorpholinium

dn/dc = Refractive index increment

DNA = Deoxyribonucleic acid

Dox = Doxorubicin

DP = Degree of polymerization

E.E = Encapsulation efficiency

ECM = Extracellular matrix

EDC = 1-Ethyl-3-(-3-dimethylaminopropyl) carbodiimide

EGF = Epidermal growth factor

EGFR = Epidermal growth factor receptor

EPA = Eicosapentaenoic acid

EPR = Enhanced permeability and retention

eq. = Equivalents

FBS = Fetal bovine serum

FD = Free drug

FDA = Food and drug administration

FLUO = Fluocinolone acetonide

F-NALP = Fusogenic nucleic acid lipid particle

FPLC = Fast protein liquid chromatography

GAU = Glutamic acid units

G-CSF = Granulocyte-colony stimulating factor

GFLG = Gly-Phe-Leu-Gly

GLFG = Gly-Leu-Phe-Gly

Gly = Glycine

GPC = Gel permeation chromatography

GPR120 = G-protein-coupled receptor 120

H&E = Hematoxilin-Eosin

HA = Hyaluronic acid

HAase = Hyaluronidase

HaCaT= Human immortalized non-tumorigenic keratinocyte cell line

HA-CP = Hyaluronic acid-poly-L-glutamate cross-polymer

hGH = Human growth hormone

HIH = National institute of health

HIV-1 = Human immunodeficiency virus type 1

HPLC = High pressure liquid chromatography

HPMA = Poly-*N*-hydroxypropyl methacrylamide

I/R = Ischemia-reperfusion

ICAM-1 = Intercellular adhesion molecule 1

Ig = Immunoglobulin

IKK = IkB kinase (IKK)

IL = Interleukin

IMQ = Imiquimod

INF-γ = Interferon gamma

IPA = Isopropanol

K = Keratins

kDa = Kilodalton

kHz = Kilohertz

LbL = Layer-by-layer

LCMS = Liquid chromatography–mass spectrometry

Leu = Leucine

LPS = Lipopolysaccharide

Lys = L-lysine

MDA = Malondialdehyde

mDCs = Dermal myeloid DCs

MeOH = Methanol

moDCs = Monocyte derived denditric cells

MTT = 3-(4,5-dimethyl-2-thiazolyl)-2,5-diphenyl-2H-tetrazolium

Mw = Molecular weight

MWCO = Molecular weight cut-off

N_2 = Nitrogen

NAM = Normal amine mechanism

NCA = N-carboxyanhydride

NCS = Neocarzinostatin

NF-kB = Nuclear factor kappa beta

nm = Nanometer

NMR = Nuclear Magnetic Resonance

OCT = Optimum cutting temperature

OG = Oregon green 488 cadaverine

PAMAM = Polyamidoamine

PASI = Psoriasis Area Severity Index

PB = Phosphate buffer

PBG = Poly-benzyl-L-glutamate

PBS = Phosphate-buffered saline

pDC = Plasmacytoid dendritic cells

PDEPT = Polymer-directed enzyme prodrug therapy

PDI = Polydispersity index

PDT = Photodynamic therapy

PEG = Polyethylene glycol

PELT = Polymer-enzyme liposome therapy

PFA = Paraformaldehyde

PGA = Poly(L-glutamic acid)

Phe = Phenylalanine

PLGA = Poly-lactic-co-glycolic acid

PPhe = Poly-L-phenylalanine

PPP = Palmoplantar pustulosis

PTS = Polypeptide Therapeutic Solutions S.L.

PTX = Paclitaxel

PUFAs = Polyunsaturated fatty acids

PUVA = Ultraviolet A plus psoralen

PVA = Polyvinyl alcohol

PVP = Polyvinyl pyrrolidone

r.t. = Room temperature

R_f = Retention factor

Rh = Hydrodynamic radius

RI = Refraction Index

RMN = Nuclear Magnetic Resonance

RNA = Ribonucleic acid

ROP = Ring opening polymerization

SANS = Small-angle neutron scattering

SAXS = Small-angle X-ray scattering

SC = Stratum corneum

SEC = Size exclusion chromatography

SEM = Standard error of the mean

siRNA = Small interfering RNA

SMA = Styrene-co-maleic acid

ST = Star polymer

STAT = Signal transducer and activator of transcription

TBA = Thiobarbituric acid

TBARS = Thiobarbituric acid reactive substance

TDL = Total drug loading

TEM = Transmission electron microscopy

TFA-d_1 = Deuterated trifluoroacetic acid

TG = Total tryglyceride

TLC = Thin-layer chromatography

TLR = Toll-like receptors

TNBSA = 2,4,6-Trinitrobenzene Sulfonic Acid

TNF = Tumor necrosis factor

TNFR1 = TNF receptor 1 (TNFR1)

TTC = 2,3,5 Triphenyltetrazolium chloride

UVA = Ultraviolet A

UVB = Ultraviolet B

UV-Vis = Ultraviolet-visible

VCAM-1 = Vascular cell adhesion molecule 1

w/w = Weight/weight

w/v = Weight/volume

WAXS = Wide angle X-ray scattering

wt% =Drug loading in weight percent

ABSTRACT

Topical administration represents the main route to attain local therapeutic activity of bioactive agents in several organs, such as the skin or the heart by means of devices that enhance drug transport through the endothelium acting as a reservoir.

The complex structure of the skin protects the human body against potentially harmful external agents; however, this protective mechanism inhibits the penetration of topically administering bioactive agents employed for the treatment of skin diseases. Unfortunately, many of the topical drugs currently used or under evaluation in clinical trials lack the appropriate physico-chemical characteristics required for delivery through the skin. However, various rational strategies have been employed in an attempt to improve the physico-chemical properties of bioactive agents according to the features of the desired site of action, thereby improving topical delivery and stability.

The research carried out in this thesis describes the application of polymer therapeutics, a nanomedicinal approach, to improve the physico-chemical properties and increase both the penetration of bioactive agents through the skin and retention time at the desired site of action. Well-defined polypeptide-based polymer therapeutic approaches offer particular advantages for dermal applications such as biodegradability, versatility, multivalence, and high drug loading capacity. The development of new polypeptide-drug conjugates employing stimuli-responsive linking moieties can enhance transdermal drug delivery into the skin, thereby improving the effectiveness of topical treatments for skin diseases such as psoriasis. Furthermore, we believe that our newly developed platforms may find wider use, and we also explore polypeptide-drug combinations as an approach to enhance wound healing and treat ischemia/reperfusion injury following myocardial infarction.

Psoriasis, a common and chronic inflammatory disease mediated by the immune system with predominantly cutaneous involvement, affects 2-3% of the adult population and 0.5-1% of children. Plaque psoriasis, the most prevalent type of psoriasis, is characterized by scaly skin, erythematous plaques, and inflammatory cell infiltration. Approximately 80% of patients are affected by mild to moderate disease, and topical treatment with corticosteroids remains a widely employed therapeutic approach. However, many topical corticosteroids that are currently employed or under assessment in clinical trials lack adequate physico-chemical properties and suffer from local

cutaneous and systemic side effects that correlate with the high doses required. Therefore, we propose the implementation of polymer conjugation approaches to overcome these limitations.

The knowledge base regarding the pathogenesis of human psoriasis has recently widened thanks to the development of accurate *ex vivo* and *in vivo* models. We now present the detailed characterization of an inflammatory *ex vivo* human skin model, including the assessment of tissue viability, immunohistopathology, and the quantification of pro-inflammatory cytokine release. Additionally, we developed an *in vivo* preclinically relevant imiquimod (IMQ)-induced model of psoriasis that reflects the critical features of the human disease. Our findings demonstrated the suitability of this murine model to mimic the main hallmarks of human psoriasis, including inflamed skin and the presence of increased levels of psoriasis-associated inflammatory cytokines in tissue and serum.

Furthermore, our newly described models permitted the evaluation of both the safety and therapeutic efficacy of our novel polypeptide-based therapeutics. To this end, we present the development of a biodegradable vehicle, comprising a cross-linked matrix of hyaluronic acid and poly-L-glutamic acid (hyaluronic acid-poly-L-glutamate cross-polymer or HA-CP), for the topical delivery of the advanced therapeutic agents. We exhaustively characterized and biologically evaluated our HA-CP vehicle *in vitro*, *ex vivo,* and *in vivo* revealing multiple advantageous properties regarding the topical administration of therapeutics. Our HA-CP vehicle functioned as a penetration enhancer, using a family of amphiphilic block copolymers of different nature (using PPhe and PBG with different degree of polymerization) and physico-chemical properties, significantly promoting the penetration into the viable epidermis while avoiding the systemic absorption and any associated adverse effects.

We also present a straightforward methodology for the synthesis of well-defined polypeptide-based drug conjugates based on poly-L-glutamic acid, or PGA, as the polymeric carrier. We synthesized and characterized a PGA-conjugated corticosteroid (fluocinolone acetonide) via a pH-responsive ester linker. PGA conjugation targeted the corticosteroid to the appropriate skin layer, and the implementation of bioresponsive polymer-drug linking moieties permitted the sustained release of the drug at the required site of action. Both these characteristics promote optimal drug release kinetics and the

attainment of a therapeutically relevant concentration of an active agent within the epidermis for the required period of time. We demonstrated that polymer conjugation significantly improved the pharmacological activity of the drug due to greater bioavailability in the required skin layer *in vitro*, *ex vivo*, and *in vivo*. Moreover, the combination of our polypeptide-conjugated corticosteroid within the HA-CP vehicle resulted in synergistic anti-psoriatic activity *in vivo*, providing a significant reduction in inflammation. Therefore, our novel combinatorial polymer-based approach represents a possible palliative treatment of inflammatory skin diseases.

Finally, we applied the knowledge acquired from the development of polymer-drug conjugates for the treatment of skin inflammation to the development of novel wound healing approaches via the PGA-conjugation of the omega-3 polyunsaturated fatty acid didocosahexaenoic acid (diDHA). PGA conjugation enhanced diDHA stability and decreased degradation, which promoted improved therapeutic activity for the conjugate when compared to free diDHA both in skin wound healing and in the treatment of ischemia-reperfusion injury in the mouse heart following myocardial infarction.

Overall, our findings highlight the suitability of polymer therapeutic approaches, and polypeptide conjugation in particular, to form drug delivery systems for dermal applications. Specifically, PGA-drug conjugates enhance the skin penetration of drugs, while bioresponsive linkers promote the specific release of the drug in the desired skin layer. Moreover, PGA conjugation of fatty acids has also demonstrated the improvement of both safety and effectiveness of the treatment in skin wound healing and in ischemia-reperfusion injury in the heart.

OBJECTIVES OF THE RESEARCH

The present thesis dissertation focuses on the development of polymeric platforms for drug delivery as novel treatment approaches for skin diseases or disorders, such as psoriasis and wound healing. The development of polymer-drug conjugates must follow well-established synthetic approaches and employ rational design; furthermore, polymer-drug conjugates require exhaustive physico-chemical characterization and biological evaluation in relevant models.

The general aims can be summarized as the following specific objectives:

1. **The development and exhaustive characterization of healthy and inflammatory *ex vivo* human skin models and a psoriatic mouse model as platforms to evaluate advanced treatment approaches** (Chapter II)

2. **The synthesis, full physico-chemical characterization, and biological evaluation of novel crosslinked hyaluronic acid and poly-L-glutamic acid-based materials that function as vehicles that enhance penetration through the skin** (Chapter III)

3. **The design, synthesis, and exhaustive physico-chemical characterization of poly-L-glutamic acid-drug conjugates incorporating bioresponsive linkers as a treatment for psoriasis and the *in vitro, ex vivo,* and *in vivo* biological evaluation of said conjugates to assess enhanced anti-inflammatory/anti-psoriatic activities** (Chapter IV)

4. **The design, synthesis, and exhaustive physico-chemical characterization of a family of poly-L-glutamic acid-drug conjugates for wound healing disorders and the biological evaluation of said conjugate to assess enhanced wound healing activity** (Chapter V)

CHAPTER I

GENERAL INTRODUCTION AND BACKGROUND

I.1. Biological Barriers to the Administration of Therapeutic Agents

The term "biological barriers" encompasses a group of protective mechanisms present throughout the body. These biological barriers, such as the blood-brain barrier (BBB), the skin, and the nasal and mouth mucosa, protect the body from unwanted exogenous material (including chemicals, viruses, bacteria), while selectively allowing molecules with specific characteristics to cross. However, the restrictive nature of these barriers also impedes the passage of a range of therapeutic agents, as in the case of the topical administration, thereby lowering overall effectiveness. This delivery "challenge" requires novel and rationally designed therapeutics, such as polymer therapeutics (discussed in detail in **Section I.4.**), that can conform to the different characteristics required to pass through specific biological barriers to reach disease sites, specific tissue and cell types, or even specific subcellular locations.

Biological barriers that inhibit the passage of therapeutic agents to their desired site of action can be categorized into five levels (**Figure I. 1**) and will be discussed below.

Level 1: Reaching the Bloodstream

Reaching the bloodstream is generally the first biological barrier faced by a given therapeutic. Intravenous injection represents the easiest and most direct administration route; however, alternative routes of administration, including topical [1, 2], inhalatory [3], and oral [4] administration involve different types of barriers [5, 6].

For the treatment of skin diseases/disorders, a given therapeutic agent may require targeting to specific skin layers, rather than the bloodstream, thereby requiring the rational design of delivery systems that can reach the desired site of action and avoid unwanted systemic side effects.

Level 2: Circulatory System Barriers

When a given therapeutic agent enters the bloodstream, various plasma proteins, including serum albumin, apolipoproteins, and immunoglobulins, adsorb to the surface of a therapeutic agent in a process known as opsonization [7]. This process promotes the recognition of foreign agents by phagocytes (immune cells) resulting in their removal from the bloodstream. Opsonization depends on specific physico-chemical and surface properties of the therapeutic agents, including size, surface charge and chemistry, and hydrophobicity [8].

Level 3: Tissue-specific Barriers

Several biological barriers separate the blood from the interstitial fluid that encloses tissues (including the blood-brain, blood-ocular, and blood-thymus barriers). The most selective and controlled of these barriers is the blood-brain barrier, or BBB, located in the central nervous system [9]. As an example, certain omega-3 fatty acids (including didocosahexaenoic acid [diDHA]) can attenuate neuroinflammation in the brain [10, 11], thereby demonstrating its capacity to cross the BBB. Of note, we will explain in detail how diDHA can enhance to cross biological barriers in **Chapter V** of this thesis.

Level 4: Cellular Barriers

The passive diffusion of molecules represents the main pathway used to cross cellular barriers. Therapeutic agents can be uptaken through endocytotic, macropinocytotic, or phagocytotic mechanisms [12, 13]. Cell internalization can be enhanced by modifying the physico-chemical characteristics of the therapeutic agent, including shape, charge, and/or the addition of different ligands.

Level 5: Subcellular Barriers

Some therapeutic agents have been designed to target the specific intracellular locations/organelles implicated in cellular dysfunction [14]; however, optimal delivery through membranes delineating each type of organelle represents a significant challenge. Of note, the mechanism employed for the internalization of a given therapeutic agent will influence subcellular targeting. Hence, a global understanding of these processes will provide relevant information for the rational design of therapeutic agents [15].

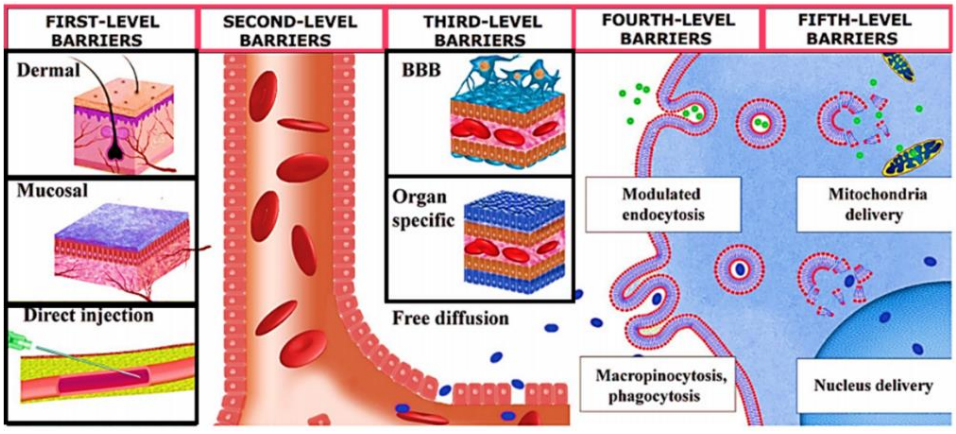

Figure I. 1: General representation of biological barriers present in the body. Adapted from [16].

I.2. Skin as a Barrier

I.2.1. Skin Structure and Function

The skin is the largest and most physiologically complex organ of the human body; it accounts for ~10% of total body mass and has a surface area of approximately 2-3 m^2, thereby representing the main biological barrier of the body [17]. The skin performs multiple functions, including the regulation of temperature, control of water ingress/egress, self-maintenance/self-repair, and protection against external threats [18, 19]. The skin also possesses a sizeable sensory surface containing three categories of skin sensory receptors: mechanoreceptors, thermoreceptors, and nociceptors. Therefore, the skin transmits sensory information, such as temperature, touch, pressure, and pain throughout the body. The skin displays a multilayer structure consisting of two main histological layers: the epidermis and the dermis.

I.2.1.1. The Epidermis

The epidermis is the outermost layer of the skin, whose thickness varies according to body area [19]. The ongoing production of lipids, glycosaminoglycans, and ceramides [20] in this layer contributes to the creation of the protective barrier. The epidermis lacks blood vessels and diffusion across the dermis supplies nutrients to cells in deeper layers. Although is composed mostly of keratinocytes, the epidermis also hosts other cell types, such as Langerhans cells (antigen-presenting cells), melanocytes (melanin-producing cells), and Merkel cells (mechanoreceptors). The epidermis comprises a stratified epithelium formed by several layers of keratinocytes that display increased levels of keratinization as the layers approach the skin surface (stratum corneum), creating five distinct layers or strata (**Figure I. 2**).

The stratum basale

Commonly known as the basal layer, the stratum basale is considered the deepest layer of the epidermis. In this layer, keratinocytes are interconnected and form further connections with the dermo-epidermal membrane via desmosomes and hemidesmosomes, respectively [21, 22]. The innermost metabolically active layer is formed by epidermal stem cells that continually provide keratinocytes from the inner

epidermis for the outer epidermis [23]. Interestingly, other cell types, such as melanocytes, Langerhans cells, and Merkel cells, are also found in this layer.

The stratum spinosum

This stratum spinosum (or spinous layer/prickle cell layer) is located above the stratum basale and comprises an average of two to six layers of keratinocytes that flatten as they approach the next layer towards the skin surface. These keratinocytes contain cytosol prolongations similar to prickles and are often called spiny cells [24]. The prickles of adjacent keratinocytes provide improved structural rigidity and increase the resistance of the skin to abrasion. Studies have also reported keratin production in this layer [25].

The stratum granulosum

The stratum granulosum is composed of one or more layers of flattened keratinocytes. The cytoplasm of these keratinocytes contains characteristic granules of keratohyalin, the precursor of keratin synthesis [26]. The apoptosis of keratinocytes begins in this layer, with cells beginning to lose their nucleus.

The stratum lucidum

The stratum lucidum is present only in thicker skin, such as that of the palms of the hands and the soles of the feet [27], and consists of a single layer of flattened homogeneous keratinocytes that lack a nucleus and display a consistent increase in keratinization compared to deeper stratum.

The stratum corneum

The stratum corneum is the last and outermost layer of the epidermis with protein (mainly keratin) and lipids (predominately triglycerides, cholesterol, and phospholipids) [28] representing major components. Both the stratum lucidum and the stratum corneum also contain dead keratinocytes that are replaced thanks to the upward migration of cells from the deepest epidermal layers - a renewal process known as desquamation [29]. The stratum corneum presents as a compacted, dehydrated, and keratinized multilayer whose keratinocytes transform into corneocytes (terminally differentiated, anucleated cells of the keratinocyte lineage).

In healthy skin, the rate of stratum corneum desquamation is generally similar to the ratio of epidermal cell synthesis, taking approximately 28 days; however, in skin

diseases such as psoriasis, the keratinocyte renewal cycle decreases from 28 to 7 days, leading to interrupted maturation and incorrect completion [30].

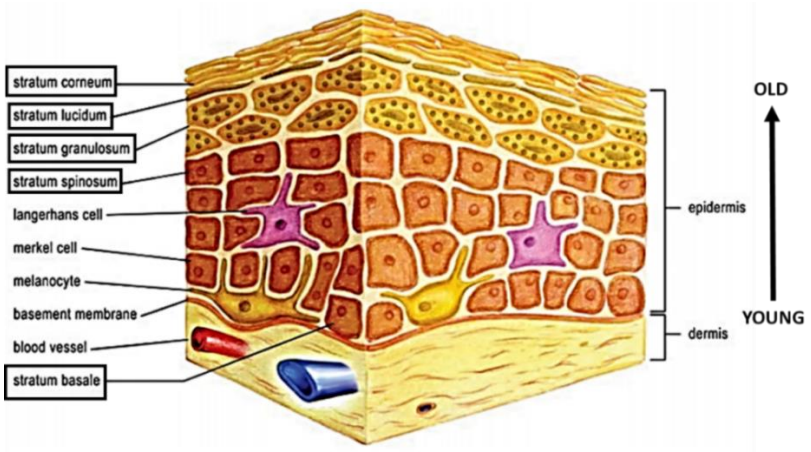

Figure I. 2: Structure of the epidermis separated into different strata. Adapted from [31].

I.2.1.2. The Dermis

The dermis, which constitutes the most significant proportion of the skin as a whole, lies directly below the epidermis and is considered as the support of the skin. The epidermal and dermal layers meet at the dermal-epidermal junction [32], a matrix of mechanically strong fibrous proteins (mainly collagen) immersed in a mixture of proteins, glucose, electrolytes, and water (generally known as the ground substance) [33]. Additionally, blood vessels, nerve tissues, and skin appendages such as sebaceous glands and hair follicles lie within this matrix. While the vasculature provides nutrients for the epidermis, it also transports substances absorbed across the skin barrier into the systemic circulation.

I.2.2. Penetrating the Skin Barrier

The skin represents an alternative route for the administration of therapeutic agents due to its sizeable available surface area, allowing for sustained and continuous delivery to the circulatory system. This approach enables wider spacing of doses than intravenous delivery, for example, while avoiding the unwanted side effects of other administration routes [34]. Transdermal delivery also promotes patient compliance due to the ease of administration and the option of safe self-administration. Importantly, the transdermal route represents an alternative for certain therapeutic agents where there exists a significant first-pass effect in the liver, which can lead to premature

metabolization, therefore avoiding systemic administration is advisable [35]. However, the barrier role of the multilayer stratum corneum makes transdermal delivery a challenging prospect. Transdermally administered therapeutic agents can reach the bloodstream if said therapeutic can perform three steps: i) penetration, entry into a specific skin layer, ii) permeation, penetration from one layer to another, and iii) resorption, entry into the vascular system [36].

There exist three proposed penetration pathways through the skin [37]: i) the intercellular penetration pathway, ii) the transcellular penetration pathway, and iii) the follicular penetration pathway [38, 39] (**Figure I. 3**). The intercellular route represents the most common pathway for permeation [40] - the therapeutic agent penetrates through the stratum corneum by passing between corneocytes. However, the transcellular pathway is more direct and rapid, with the therapeutic in question crossing the skin by directly passing through the lipid structures of the stratum corneum and the cytoplasm of keratinocytes. Significant resistance to permeation represents the major limitation to this route, given that therapeutic agents must cross both lipophilic and hydrophilic structures [41]. Studies had suggested a meager contribution of the follicular pathway (0.15%) in comparison to intercellular/transcellular penetration, given the relatively small area of skin covered by hair [34]. Nevertheless, recent studies have demonstrated that follicular penetration can create a reservoir of drugs that can be released slowly; therefore, this route may still have relevance to the delivery of therapeutic agents [42-46].

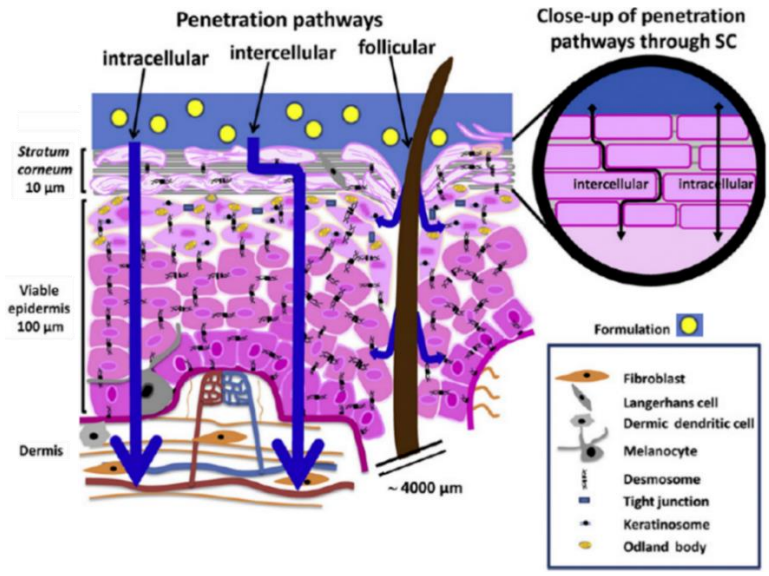

Figure I. 3: Representative image of the three penetration pathways: intracellular, intercellular, and follicular. Adapted from [34].

I.2.3. Penetrant Characteristics

The physico-chemical properties of the penetrant (the therapeutic agent in question) significantly influence the penetration route across the skin, with lipophilicity and molecular size representing critical parameters [47-49]. Other critical parameters that influence penetration include hydrogen bond acidity and basicity, excess molar refractivity, polarizability, molar refractivity, melting point, and molar volume [50, 51]. Penetrant properties influence skin permeation through two possible mechanisms: increasing absorption into or lowering the diffusion resistance through the stratum corneum lipid phase [52].

I.2.4. Methods to Improve Penetration through Skin

The structure of the skin provides resistance to permeation of therapeutic agents; however, different methodologies have been developed to increase transdermal penetration.

I.2.4.1. Formulation Optimization

Effective penetration through the skin not only depends on skin conditions and the characteristics of the therapeutic agent but also depends on the transport vehicle employed [53]. The vehicle plays a vital role in therapeutic potency and success since the characteristics of the vehicle can influence the rate and extent of therapeutic agent penetration and absorption, thereby modifying its bioavailability [54].

The application of hydrophilic and hydrophobic therapeutics to the skin requires the application of varying vehicles or formulations, including creams, gels, and patches. The vehicle must be selected and formulated with the characteristics of each therapeutic agent in mind to promote maximal release and penetration through the skin to ensure enhanced transdermal delivery. The vehicle should facilitate the rapid but controlled therapeutic release by permitting sustained release over time.

I.2.4.2. Chemical Enhancers

Chemicals can be incorporated into topical formulations to promote the penetration and enhance therapeutic agent release within skin layers. These chemicals must exhibit specific properties for their inclusion in different formulations [55].

Chemical enhancers must:

- Be pharmacologically inert
- Be non-toxic, non-irritating, and non-allergenic
- Allow immediate penetration of the therapeutic agent after application
- Allow the rapid and complete recovery of full barrier properties after use
- Be chemically and physically compatible with associated therapeutics and adjuvants
- Be suitable solvents for therapeutic agents
- Be well-tolerated by patients, organoleptically acceptable
- Be readily formulated into dermatological preparations, transdermal devices, and skin adhesives.

Chemical enhancers can increase the penetration of therapeutic agents through various mechanisms [56]:

- By increasing the diffusion coefficient of the therapeutic agent
- By increasing the effective concentration of the therapeutic agent in the vehicle
- By improving partitioning between formulation and stratum corneum
- By decreasing skin thickness

Several types of chemical enhancers have been studied and evaluated:

1. Water

The application of water represents one of the most used and safest means to improve skin permeation and permeability. The water content of human stratum corneum is typically around 15–20% [57]. Despite extensive research in the area, the mechanism of action involved remains unclear, although many hypothesize that water increases the hydration of the stratum corneum and also controls the transepidermal water loss.

2. Sulfoxides

Sulfoxides can aid both hydrophilic and hydrophobic permeants. One of the most widely used penetration enhancer is dimethyl sulfoxide or DMSO, also known as the “universal solvent” in pharmaceutical sciences. DMSO can denature proteins, changing the intercellular keratin configuration in human skin from helical to beta sheet [58].

Although DMSO has proven to be an excellent penetration accelerant, studies have encountered adverse effects at high concentrations of DMSO, such as erythema [56].

3. Azones

Azone (1-dodecylazacycloheptan-2-one or laurocapram), a colorless and odorless liquid with a melting point of -7°C, is considered as the first molecule exclusively designed as a skin penetration enhancer [57]. The mechanism of action comprises the fluidization of the intercellular lipid bilayers of the stratum corneum, thereby reducing the diffusional resistance of the skin barrier to permeation [59]. The application of azone has improved the skin penetration of a variety of drugs, including steroids, antibiotics, and antiviral agents [60, 61].

4. Pyrrolidones

Pyrrolidones have been employed as permeation enhancers for a wide range of molecules, including hydrophilic and lipophilic drugs. Treatment with pyrrolidones can generate drug reservoirs within skin layers, as pyrrolidones partition into the lipids of the stratum corneum and increase their fluidity, thereby permitting the release of an active agent from the stratum corneum over time [57, 58]. N-methyl-2-pyrrolidone is one of the most used enhancers of skin penetration, and has been applied with several drugs and active agents, such as caffeine [62].

5. Fatty Acids

Several long-chain fatty acids have been employed as enhancers of therapeutic agents penetration through the skin. Oleic acid, one of the principal long-chain fatty acids used for this purpose, increases the diffusivity of therapeutics through the skin by interacting and interfering with lipids within the stratum corneum [63]. Lauric acid, myristic acid, and capric acid can also enhance the delivery of various drugs [64].

6. Alcohols

Ethanol is the most used alcohol in transdermal formulations, often employed as a component of transdermal patches. Obtaining the desired effect depends on the concentration used, as high levels cause dehydration of biological membranes and therefore decrease permeation [56]. Fast evaporation of ethanol increases drug concentration, thereby altering solubility in the skin, and providing a supersaturated state with a greater driving force, promoting drug penetration.

7. Surfactants

Surfactants in formulations help to form micelles that solubilize the therapeutic agent in question and promote effective skin permeation. Surfactants are generally classified into three types: anionic (e.g., sodium lauryl sulfate), cationic (e.g., cetyltrimethylammonium bromide), and non-ionic (e.g., dodecyl betaine). Anionic and cationic surfactants can have adverse effects on human skin; for example, sodium lauryl sulfate is a powerful irritant and can increase transepidermal water loss *in vivo* [65]. In contrast, non-ionic surfactants tend to be considered safe for application to human skin.

8. Urea

Urea is regarded as a hydrating agent (a hydrotrope) and has been widely applied in the treatment of diseases such as psoriasis [57]. Urea induces transdermal permeation by facilitating significant stratum corneum hydration and the formation of hydrophilic diffusion channels [66]. Moreover, salicylic acid provides keratolytic properties to urea, allowing application in skin diseases characterized by an increment of epidermis thickening (e.g., keratosis, sometimes associated with the development of psoriasis) [67]. Several analogs containing more potent enhancing moieties have been developed to improve the penetration-enhancing activity of urea, including cyclic, alkyl, and aryl urea analogs [68].

9. Essential oils, Terpenes, and Terpenoids

Terpenes are found in essential oils and have been employed as medicines, flavorings, and fragrance agents. The size of terpenes influences their activity; smaller terpenes tend to be more active permeation enhancers than larger terpenes (such as sesquiterpenes) [57]. Terpenes can transform the solvent nature of the stratum corneum, thereby modifying and enhancing diffusivity through the skin [56]. Essential oils of eucalyptus, chenopodium, and ylang-ylang have been shown to improve the penetration of 5-fluorouracil in human skin [69].

10. Phospholipids

Several pharmaceutical formulations have employed phospholipids to carry therapeutic agents into and through human skin due to their capacity to create vesicles (liposomes) that surround and protect said therapeutic agent. The application of the phospholipids as vesicles promotes fusion with stratum corneum lipids, while

phospholipids also alter the solvent nature of the human skin and improve the permeation of different drugs, demonstrating the most significant positive effect on hydrophilic drugs [70, 71].

I.2.4.3. Physical Enhancers

Physical enhancers can improve the penetration of therapeutic agents by physical disruption of the structure of the skin, using for this purpose different techniques.

1. Iontophoresis

Permeation is enhanced by the application of a low-level electric current directly over the skin [72-74], a strategy which can be adapted to each case [75]. Modifiable parameters include electrode type, system pH, current intensity, competitive ion effect, and permeant type [76]. Several mechanisms can increase permeability: i) the anode-cathode charge directs the therapeutic agent towards specific layers of skin [77]; ii) the electric current itself deconstructs skin layers and inhibits barrier function [78]; and iii) the accumulation of water increases by electroosmosis, which improves the hydration of the skin and favors penetration [79].

2. Sonophoresis or Phonophoresis

This technique involves the usage of high- or low-frequency ultrasound waves. Sonophoresis enlarges existing skin pores and also creates more pores in the skin leading to the disruption of the stratum corneum [80]. Parameters that can affect the effectiveness of this technique include the duration, intensity, and frequency of the treatment [75]. Several studies have demonstrated the improvement of insulin delivery using ultrasound [81, 82].

3. Magnetophoresis

Magnetophoresis, the application of a magnetic field, represents a novel approach to improve therapeutic agent permeation across the skin. The presence of a magnetic field induces structural alterations, thereby modifying the protective properties of the skin and increasing permeability. This technique has been used to improve the penetration of a multitude of drugs/active agents, demonstrating its versatility [83, 84].

4. Electroporation

Electroporation is the transitory structural modification of the lipid bilayer membranes due to the application of short and high voltage pulses to the skin [85], which leads to transient pore formation allowing the transit of compounds into cells [58]. The electrical parameters and physico-chemical properties of the drugs determine the effectiveness of transport.

5. Thermophoresis

Thermophoresis employs higher than physiological temperature to favor percutaneous absorption [86] thanks to induced vasodilation of the subcutaneous blood vessels [87] and increased drug diffusivity through the vehicle and skin because of improved lipid fluidity [88]. *In vitro* [89] and *in vivo* [90] studies have demonstrated the contribution of this technique to the improvement of drug permeation.

6. Radiofrequency

Radiofrequency is a versatile technology employed for generating therapeutic intensities of heat, thereby producing structural and biological responses. This technique focuses on the exposure of skin to high-frequency alternating current (preferably from 100 to 500 kHz), which induces the formation of membrane microchannels in response to the heat caused by electrical current application, facilitating the penetration of hydrophilic drugs [91].

7. Microneedles

Microneedle devices facilitate the penetration by piercing the stratum corneum to deliver therapeutic agents into the epidermis. Microneedles have been fabricated with different size, shape, geometry, and materials [92] for applications with a wide range of molecules and nanoparticles [93, 94].

I.2.5. Techniques to Evaluate Skin Penetration

The assessment of skin penetration represents a critical challenge in the evaluation of the suitability and effectiveness of a given therapeutic agent as a treatment for skin diseases. The development of real skin models that can better mimic the characteristic features of disease has generated an ever-expanding knowledge base regarding penetration. Furthermore, the development of new specific techniques that can track the

drug through the skin will allow a better understanding of the processes that mediate the localization of a given therapeutic agent.

I.2.5.1. Skin Models

Widely accepted models for skin-permeation studies include *ex vivo* human or animal skin either frozen or in culture; however, several alternative *in vitro* models to *in vivo* animal models have been developed applying the 3R principle (replace, reduce and refine [95]) (**Table I. 1**).

The latest advances comprise the creation of skin models through artificial membranes or reconstructed skin models.

Table I. 1: Different skin models. Adapted from [96].

Model	Advantages	Disadvantages
Human skin		
In vivo	Gold standard	Often precluded for ethical and practical reasons
Ex vivo skin	Best surrogate for in vivo humans	Not readily available, variability
Animal skin		
In vivo	Reasonably easy to obtain animals, can be scaled up to humans, hairless species available	Pigs: similar barrier to humans, but difficult to handle Rodents: different barrier properties from humans
In vivo chimeric model	Human skin xenografts on mice allows testing on living human skin	Technically difficult
Ex vivo skin	Easy to obtain	Different barrier properties, variability
Artificial membranes		
Simple polymeric models	Useful for studying basic diffusion mechanisms, consistent and homogenous	Not representative of human skin
Lipid-based models	Useful for screening	Not representative of human skin
Reconstructed skin models		
Reconstructed human epidermis	Built-in barrier properties	Usually more permeable than human skin
Living skin equivalents	Can be engineered to include a range of normal or disease features	Usually more permeable than human skin

Artificial and reconstructed skin models represent suitable tools for the evaluation of transdermal absorption. Artificial skin models are particularly convenient for the study of the underlying mechanisms of passive transport through a membrane [97-99]. The development of these models is reproducible and straightforward due to the elimination of the complexity of human or animal skin [96]. Although simplicity represents one of the main advantages of these models, oversimplification also represents a limitation, as these skin models do not provide an adequate representation of complexities of *in vivo* skin [100].

Reconstructed skin models are created from layers of different human cells cultured on a polymeric matrix, thereby obtaining the desired organization and a degree of complexity. Reconstructed human epidermis models can be generated to mimic the epidermis or the entire human skin (living skin equivalents) [101, 102]. Interestingly, these models also mimic the physiopathology of various diseases states, such as psoriasis or atopic dermatitis [96]. Therefore, reconstructed skin models can be used not only to understand the molecular pathways responsible for specific diseases but also to examine the penetration, delivery, and effects of topical therapies.

I.2.5.2. Monitoring Penetration in the Skin

Several advanced physicochemical techniques have been used to investigate skin penetration pathways, which allow the study of the internal structure of skin layers and their physiological behavior, as well as the penetration of different drugs through the skin, and the interactions between therapeutic agents and skin components [103-105]. Techniques employed to detect penetration include infrared and Raman spectroscopy, confocal microscopy, and mass spectrometry.

Fourier transform infrared spectroscopy permits the investigation of stratum corneum lipids under controlled conditions [106] and the evaluation of changes in stratum corneum barrier function *in vivo* after the application of compounds, such as sucrose oleate and sucrose laurate [107]. Also, Fourier-transform infrared spectroscopy represents a useful screening tool for the evaluation of guidelines in the design of chemical enhancers to increase skin permeability [108].

Raman spectroscopy provides specific vibrational signatures of chemical bonds, allowing the precise skin layer-location of the studied therapeutic agent [109, 110], while confocal microscopy permits the visualization and localization of fluorescent compounds in the skin [111]. Recent studies have employed a novel technique based on confocal-Raman microspectroscopy [112], demonstrating its suitability in assessing the effect of skin penetration enhancers [113, 114], the penetration of different compounds [115, 116], and the status of skin features and conditions, such as hydration [117, 118].

Recently, mass spectrometry methods have been used to image the spatial distribution of compounds in various skin layers, providing high chemical specificity

[119]; as an example, mass spectrometry has allowed the observation of differences in penetration profiles for four different drugs [120].

I.2.6. Skin Penetration as a Challenge

The complex structure of the skin provides the necessary protection to the human body against external agents; however, this protection also has a negative consequence when topically administering drugs or active agents, as the skin prevents penetration.

Many of the topical drugs currently used or under clinical trials lack appropriate physico-chemical characteristics for adequate delivery through the skin. Various rational strategies have been evolved to improve the physico-chemical properties of drug/therapeutic agents according to the features of the desired site of action, improving topical delivery and stability. Some methods include the development of the prodrug approach [121] or the development of nanomedicines via the conjugation of therapeutic agents to carriers with different characteristics [122]. Said nanomedicines protect the therapeutic agent against premature degradation and interact with various components of the skin, increasing the penetration of the therapeutic agents through the different layers of the skin, and increase retention time in the desired site of action [123, 124].

We will detail the main characteristics and advantages of nanomedicine in the field of topical applications in the next section.

I.3. Nanomedicine

Nanotechnology involves controlling the properties and structures with particle sizes in the nanometer range, typically ranging from less than 100 to 1000 nm [125, 126]. Nanomedicines are nano-sized agents employed for the diagnosis, prevention, and treatment of diseases/disorders, and have allowed a deeper understanding of the complex pathophysiology of disease [127]. Nanomedicinal advances, mainly in cancer, have demonstrated huge potential and utility as systemic treatment approaches [128].

The first classes of nanomedicinal platforms present distinct physico-chemical properties (**Figure I. 4**) and can be classified into separate groups depending on size ranges in the nanoscale: liposomes (80 - 200 nm), nanoparticles (20 - 1000 nm), polymer

therapeutics (5 - 25 nm), block copolymer micelles (50 - 200 nm), gold nanoparticles (5 - 50 nm), and nanosized drug crystals (100 - 1000 nm).

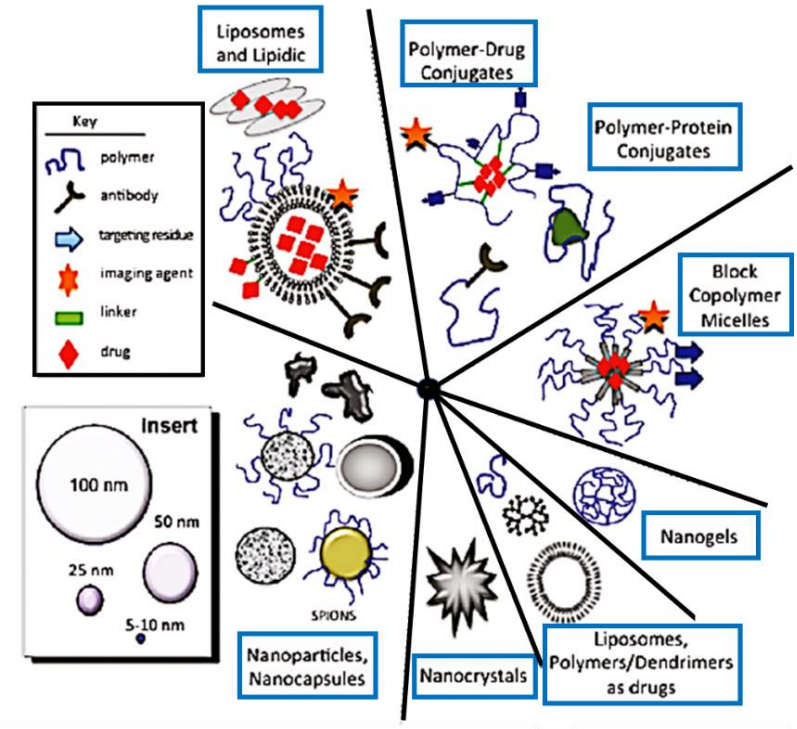

Figure I. 4. Schematic illustration of established first generation nanomedicines platforms. Adapted from [127].

Different nanoparticle-based formulations are used in clinics as a potential strategy to deliver a range of therapeutic agents [129], including polymeric nanoparticles [130], micelles [131], liposomes [132], antibody-drug conjugates [133], virosomes as nanoparticles [134], nanocrystals [135], gene therapy and immunotherapy-based treatment [129].

I.3.1. Nanomedicine Applications to the Skin

The improvement of transdermal delivery remains the main target of current research. The nanomedicinal approaches in topical applications hope to overcome many of the limitations of current transdermal delivery formulations. Nanosized carriers, or nanocarriers, are especially useful for the passive delivery of therapeutic agents, inducing transit through the skin without the need for energy input or specific receptors.

Nanocarriers offer several advantages over conventional carriers, including higher solubility, controlled size, delivery to specific targets, controlled and sustained release of

therapeutic agents, delivery of hydrophilic and lipophilic molecules, weakened skin irritancy, protection from degradation, increased loading, and enhanced permeation through the skin [136-138]. Due to these advantages, nanocarriers can enhance the pharmacokinetic profile and effectiveness of therapeutic agents when compared to "free" forms [139]. Moreover, nanocarriers interact with the skin and can modify barrier properties, contributing to penetration [140].

Some of the most used nanocarriers include nanoparticles (e.g., nanocapsules and nanospheres), liposomes, microparticles (e.g., microcapsules and microspheres), nanocrystals, polymersomes, niosomes, cubosomes, dendrimers, and fullerenes, amongst notable others [141, 142]. Of these, nanoparticles represent the most promising systems due to their high physico-chemical stability and ability to incorporate different therapeutic agents.

The application of nanocarriers as treatment approaches for skin diseases has given rise to the field of "nanodermatology". First introduced by the Nanodermatology Society [143], nanodermatology consists of the application of nanotechnology to the skin for diagnostic, therapeutic, or cosmetic purposes (**Table I. 2**).

Table I. 2: Promising areas in nanodermatology research. Adapted from [144].

Area of Development	Potential Areas of Application
Consumer Products	Sunscreen, antimicrobials, dressings, slow liberation volatile compounds (such as perfumes and insect repellents).
Diagnostic Equipment	Real time visualisation of tumours and sentinel lymphnodules, real time diagnosis of infections and malignant diseases, minimally invasive biopsies.
Therapeutic Agents	Antimicrobials, skin fillers, cutaneous paralyzing agents, corticosteroids located in the epidermis, gene silencers, cutaneous vaccines, induced skin treatments (for example, optical, magnetic, thermal, and radiofrequency).

This new area of research allows the development of delivery systems to transport therapeutic agents through the epidermis and direct them towards their required site of action [145, 146]. Therefore, the features of the delivery systems in the skin not only depend on the therapeutic agents but also the transporting nanocarrier.

This thesis describes a particular nanomedicinal approach, polymer therapeutics, to increase the penetrability of bioactive agents through the skin and improve the physico-chemical properties.

I.4. Polymer Therapeutics: The First Polymeric Nanomedicines

Polymer therapeutics represent exciting first-generation nanomedicines and are generally considered as the first polymeric nanomedicines [147, 148]. The term "Polymer Therapeutics", coined by Prof. Ruth Duncan, includes an extensive family of nano-sized medicines (5 - 100 nm in diameter). More than twenty polymer therapeutics have found in routine clinical use [149] with two polymer therapeutics becoming top-selling drugs in the USA in the last decade: the polymeric drug glatiramer acetate for the treatment of multiple sclerosis (Copaxone®, Teva Pharm) and a polyethylene glycol (PEG)-filgrastim polymer conjugate for the treatment of neutropenia (Neulasta®, Amgen) [148].

Polymer therapeutics-based treatments have demonstrated suitability in a range of disease/disorders, including cancer [150-152], neurodegenerative disorders [153, 154], hepatitis [155], and autoimmune diseases [156], thereby reflecting the huge potential of this nanomedicinal approach.

I.4.1. Definition and Classification

Polymer therapeutics fall into five distinct families: polymeric drugs (polymers with inherent activity) [157], polymer-protein conjugates [158], polymer-drug conjugates [159], polyplexes (multi-component systems used as non-viral vectors for gene/small interfering RNA delivery) [160], and polymeric micelles (where drug attachment occurs via covalent bonding) [161] (**Figure I. 5**).

This thesis focuses most of its attention on the development of polymer-drug conjugates, which will be described in detail (**Section I.4.2.2.**).

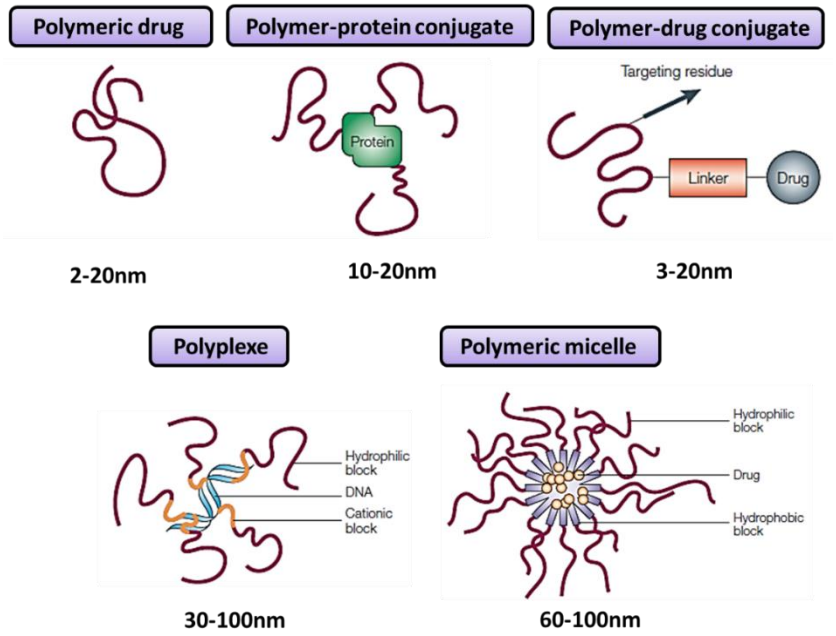

Figure I. 5: Schematic representation of the polymer therapeutics family. Redrawn from [159].

Polymer therapeutics employ specific water-soluble polymers, a crucial factor for systemic administrations of these systems, acting as an inert structural component or as an active agent (polymeric drug) [159]. While most polymer therapeutics in the clinics employ intravenous administration, other options include oral, intramuscular, subcutaneous, and local administration routes [162]. Of particular interest to this thesis, polymer therapeutics have been clinically developed as a topical administration; as an example, VivaGel® (Starpharma), a lysine-based dendrimer (a type of branched polymer) that acts as microbiocide is currently in Phase III clinical trials [163, 164] as an HIV-1 preventative agent.

When used as a delivery system for an active agent, be it a small molecule drug, protein, targeting moiety, etc., polymer therapeutic-based approaches allow for targeted release at the desired site of action and controlled and sustained release within a suitable therapeutic window [165]. The conjugation of a therapeutic agent to a polymer backbone offers several advantages over other nanomedicines, including (1) increased water solubility; (2) controlled size and size-dependent properties; (3) protection of the therapeutic agent against degradation by proteolytic enzymes or unspecific cellular uptakes; (4) enhanced plasma half-life due to the increase in hydrodynamic volume and the decrease in kidney clearance; (5) prevention or reduction of aggregation, immunogenicity, and antigenicity; (6) modified pharmacokinetics both at cellular and even subcellular level.

The design of nanosized medicines like polymer therapeutics has been inspired by the "enhanced permeability and retention (EPR) effect" first described by Matsumura and Maeda [166]. After intravenous administration, nanomedicines of specific sizes can passively extravasate from the bloodstream and accumulate in the tumor interstitium due to the enhanced permeability of the angiogenic tumor vasculature and defective lymphatic drainage (**Figure I. 6**).

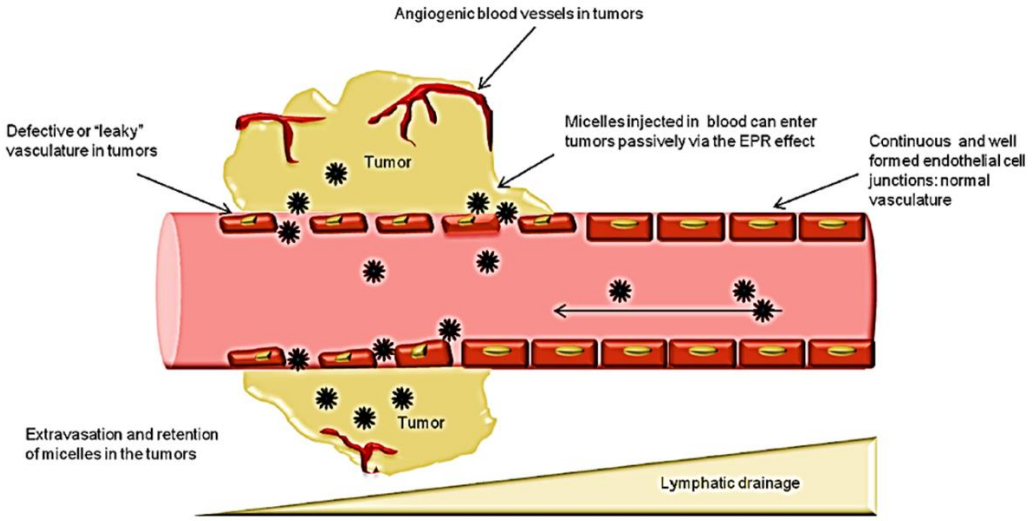

Figure I. 6: Enhanced permeability and retention (EPR) effect and passive targeting. Adapted from [167].

The EPR effect also plays a vital role in inflammatory tissues, as in the case of psoriatic skin, supporting and justifying the design and use of this class of nanocarriers in infectious and inflammatory conditions [168]. However, studies have shown that the EPR effect is a complex phenomenon with a heterogeneous presentation, which in the case of cancer is also affected by tumor type, tumor region, and tumor vascularization. As tumor vascularization represents an important factor regarding the uptake of nanomedicines, poorly-vascularized damaged tissues are less susceptible passively-targeted nanosized therapeutics [169], thereby highlighting the need for the integration of targeting strategies into polymer therapeutics-based approaches.

Following accumulation around the tumor or target tissue, endocytic mechanisms promote the cellular uptake of polymer-based nanomedicines through invaginations of the cell membrane, creating vesicles called endosomes that undergo a complex succession of fusion events until the formation of the lysosome. Lysosomes contain a high concentration of proteolytic enzymes and display an acidic pH (5.5) [170] that can aid the

degradation of the polymer-based nanomedicines with degradable linkers or the polymer backbone, and release the therapeutic agent from the polymer (**Figure I. 7**).

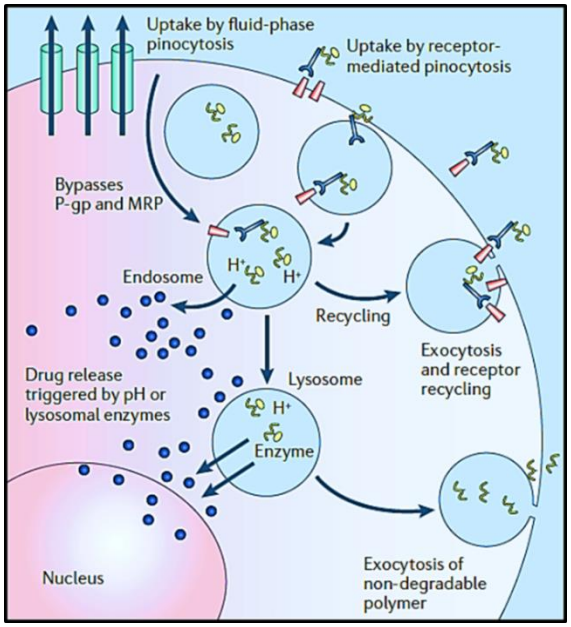

Figure I. 7: Lysosomotropic intracellular drug delivery process followed by polymer-drug conjugates. Adapted from [171].

I.4.2. Polymer Conjugates as Therapeutics

Polymer conjugates fall into two groups: polymer-protein and polymer-drug conjugates. The choice of an adequate polymeric carrier and a suitable linker(s) or spacer(s) depends on the physico-chemical properties of the bioactive agents(s) to deliver to the molecular target and also the biological activity or aim pursued in each case.

The exponential increase in the number of polymer conjugates on the market for different medical applications reflects the enormous future potential for polymer therapeutics (**Table I. 3**).

Table I. 3: Marketed polymer conjugates. PEG: polyethylene glycol; G-CSF: granulocyte-colony stimulating factor.

Name	Polymer carrier	Drug	Company	Indication(s)	Year approved
Adagen	PEG	Adenosine deaminase	Enzon Pharmaceuticals	ADA-SCID	1990
SMANCS	Poly(styrene-co-maleic acid)	Neocarzinostatin	Astellas Pharma	Liver and renal cancer	1993 (Japan)
Oncaspar	PEG	L-asparaginase	Enzon Pharmaceuticals	Acute lymphoblastic leukemia	1994
PegIntron	PEG	Interferon α-2b	Merck	Hepatitis C	2000
Pegasys	PEG	Interferon α-2a	Genentech	Hepatitis B Hepatitis C	2002
Neulasta	PEG	G-CSF	Amgen	Chemotherapy induced neutropenia	2002
Somavert	PEG	HGH receptor antagonist	Pfizer	Acromegaly	2003
Macugen	PEG	Anti-VEGF aptamer	Bausch & Lomb	Neovascular agerelated macular degeneration	2004
Mircera	PEG	Epoetin beta	Roche	Anemia associated with chronic kidney disease	2007
Cimzia	PEG	Anti-TNFα Fab' fragment	UCB Pharma	Crohn's disease, rheumatoid arthritis, psoriatic arthritis, ankylosing spondylitis	2008
Krystexxa	PEG	Uricase	Horizon Pharma	Chronic gout	2010
Plegridy	PEG	Interferon β-1a	Biogen	Relapsing multiple sclerosis	2014
Movantik	PEG	Naloxone	AstraZeneca	Opioid-induced constipation	2014
Adynovate	PEG	Factor VIII	Baxalta	Hemophilia	2015
Palynziq	PEG	Phenylalanine ammonia lyase	BioMarin	Phenylketonuria	2018

I.4.2.1. Polymer-Protein Conjugates

Most therapeutics that contain peptides, proteins, or antibodies present limitations such as short circulation times, low stability, limited therapeutic effects, and possible immunogenic responses. Protein conjugation addresses these limitations by increasing stability in serum and decreasing immunogenicity. Although the development of polymer-protein conjugates began in the 1990s with the appearance of SMANCS, a poly-(styrene-co-maleic acid) (SMA) conjugate of neocarzinostatin (NCS) for hepatocellular

carcinoma treatment [172], polymer-protein conjugates only became relevant following the description of the US Food and Drug Administration (FDA)-approved PEGylation technique [173, 174]. The mechanism comprises the covalent attachment of polyethylene glycol (PEG) to proteins, and examples abound in the market [147].

PEG, an artificial non-biodegradable polymer that displays flexibility, extreme water-solubility, and a lack of charge, has found common use in the pharmaceutical industry as an excipient and a starting product. PEG conjugation to proteins improves immunogenicity and solubility, and prolongs blood plasma half-life [175]. The hydrophilic character of PEG contributes to steric stability and protects the system against degradation, thereby allowing a reduction in the required dosing frequency, which enhances the safety profile of the therapeutic in question.

Encouragingly, PEGylation has had substantial clinical impact in the treatment of various pathologies, including hepatitis C and rheumatoid arthritis. As a consequence, this impact has encouraged the clinical approval of PEG-protein conjugates by the FDA (**Table I. 3**), and several products are in clinical development since 2018 (**Table I. 4**).

However, reported toxic effects limit the application of PEG [176] as the non-biodegradable nature of PEG provokes progressive accumulation following continuous administration, leading to adverse side effects [177]. Also, the functional molecular weight (Mw) used has limits; studies have demonstrated that oligomers with < 400 Da are toxic due to oxidation into diacid and hydroxyl acid metabolites by alcohol and aldehyde dehydrogenase enzymes [178].

Table I. 4: Polymer-protein conjugates in clinical development. Adapted from [179].

Name	Polymer carrier	Drug	Company	Indication(s)	Stage (ClinicalTrials.gov identifier)
Damoctocog alfa pegol	PEG	Factor VIII	Bayer	Hemophilia A	Pre-registration (NCT01580293)
Turoctocog alfa pegol	PEG	Factor VIII	Novo Nordisk	Hemophilia A	Pre-registration (NCT01480180)
Calaspargase pegol	PEG	Asparaginase	Shire	Acute lymphoblastic leukemia and lymphoblastic lymphoma	Pre-registration (NCT01574274)
Pegvorhyaluronidase alfa	PEG	Hyaluronidase	Halozyme Therapeutics	Pancreatic cancer	Phase 3 (NCT02715804)
TransCon Growth Hormone	PEG	Human growth hormone	Ascendis Pharma	Growth hormone deficiency	Phase 3 (NCT03344458)
Pegilodecakin	PEG	IL-10	BioSciences	Pancreatic cancer	Phase 3 (NCT02923921)
Elapegademase	PEG	Adenosine deaminase	Leadiant Biosciences	ADA-SCID	Phase 3 (NCT01420627)
Pegargiminase	PEG	Arginine deiminase	Polaris Pharmaceuticals	Mesothelioma	Phase 2/3 (NCT02709512)
BCT-100	PEG	Arginase 1	Bio-Cancer Treatment International	Acute myeloid leukemia	Phase 2 (NCT02899286)
Pegsiticase	PEG	Uricase Selecta	Biosciences	Chronic gout	Phase 2 (NCT02959918)
Sanguinate	PEG	Carboxyhemog lobin	Prolong Pharmaceuticals	Sickle cell disease	Phase 2 (NCT02411708)
Pegzilarginase	PEG	Arginase I Aeglea	BioTherapeutics	Arginase I deficiency	Phase 2 (NCT03378531)
BMS-986036	PEG	FGF21	Bristol-Myers Squibb	Nonalcoholic steatohepatitis	Phase 2 (NCT03486899)

Table I. 4: Polymer-protein conjugates in clinical development (continuation). Adapted from [179].

Name	Polymer carrier	Drug	Company	Indication(s)	Stage (ClinicalTrials.gov identifier)
Dapirolizumab pegol	PEG	Anti-CD40L Fab' fragment	UCB Pharma Systemic	Systemic lupus erythematosus	Phase 2 (NCT02804763)
Zimura	PEG	Aptamer complement C5 inhibitor	Ophthotech Corporation	Neovascular age-related macular degeneration	Phase 2 (NCT03362190)
NKTR-214	PEG	IL-2	Nektar Therapeutics	Solid tumors	Phase 1/2 (NCT02869295)
Olaptesed pegol	PEG	Anti-CXCL12 aptamer	NOXXON Pharma	Colorectal cancer and pancreatic cancer	Phase 1/2 (NCT03168139)
Fovista	PEG	Anti-PDGF-B aptamer	Ophthotech Corporation	Ocular von Hippel-Lindau syndrome	Phase 1/2 (NCT02859441)
BMS-986171	PEG	FGF21	Bristol-Myers Squibb	Nonalcoholic steatohepatitis	Phase 1 (NCT02538874)
NKTR-358	PEG	IL-2	Nektar Therapeutics	Autoimmune diseases	Phase 1 (NA)

I.4.2.2. Polymer-Drug Conjugates

Polymer-drug conjugates, a term coined by Ringsdorf in 1975 [180], are composed of three main components: a water-soluble polymer, a bioresponsive linker, and a bioactive agent (**Figure I. 8**). Polymer-drug conjugates are formulated to influence drug pharmacokinetics at the whole body and cellular level, and to aid passage through various biological barriers. Moreover, conjugation improves cellular specificity, controls drug release rate in specific targets, and therefore, decreases non-specific toxicities.

Importantly, inherent polymer multivalency permits the conjugation of more than one compound to the polymeric backbone, allowing the introduction of targeting residues (promoting receptor-mediated endocytosis) [181], diagnostic moieties [182], or more than one drug (polymer-based combination therapy) [183].

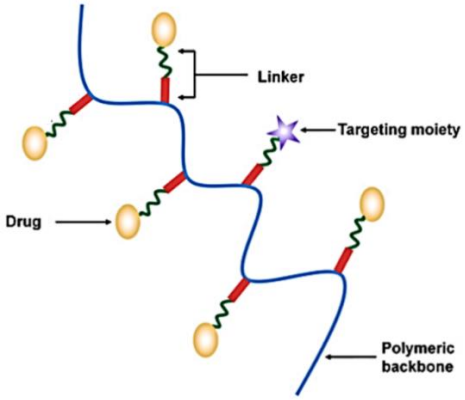

Figure I. 8: Schematic illustration of polymer-drug conjugates. Adapted from [184].

In general, the development and application of polymer-drug conjugates have generally focused on cancer treatment. In 1994, Kopecek and Duncan developed the first polymer-anti-cancer drug conjugate clinically evaluated, the poly-*N*-hydroxypropyl methacrylamide (HPMA) copolymer-doxorubicin (DOX) conjugate (HPMA-DOX or PK1, FCE 28068), which employed a lysosomally-cleavable peptidyl linker [159]. Although PK1 displayed a 15-fold improvement in plasma half-life, an enhanced safety profile, and higher anti-tumor efficacy in comparison with free DOX in preclinical animal models [185], clinical trials demonstrated low efficacy, thereby halting PK1 development.

Overall, only a small fraction of the first generation of polymer-drug conjugates have had success in clinical trials:

- Poly (*N*-hydroxypropyl methacrylamide) (polyHPMA)-DOX [186-189].
- Poly (glutamic acid) (PGA) conjugates of paclitaxel (Xyotax™ or Opaxio™) or camptothecin (CT-2106) [190-192].
- PEG-cyclodextrin-camptothecin nanoparticulate conjugates (CRLX101 or IT-101) [193, 194].
- PEG-polypeptide block copolymer conjugated with SN-38 (NK-012), Doxorubicin (NK-911) or Cisplatin (NC-6004) [195-197].

And currently, only one polymer-drug conjugate is already in the market, Movantik™ (PEGylated derivative of naloxol, a metabolite of naloxone) used to treat opioid-induced constipation [198]**,** and more than 20 products are in clinical development (**Table I. 5**).

Opaxio™ [199] (previously called Xyotax™), a PGA-conjugate form of paclitaxel (PTX) using an ester linker (PGA-PTX), represents one of the most advanced polymer-drug conjugate and is currently in Phase III clinical trials for the treatment of ovarian, prostate and esophageal cancer, which can be applied in combination with cisplatin or radiotherapy. Opaxio™ has an average Mw of 38.5 kDa and a drug loading between 36 - 37% w/w (1 drug molecule in each 11 glutamic acid (GA) units). In comparison with other nanosystems with PTX, Opaxio™ has higher drug loading (37 wt% *vs.* 5 wt% for the discontinued HPMA-PTX conjugate [200] and therefore presents with enhanced stability in blood.

Interestingly, the Opaxio™ clinical trial results demonstrated a relationship between polymer-drug conjugate therapeutic effect and patient hormone status: pre-menopausal women with higher estrogen levels responded, while post-menopausal women and men did not. The current hypothesis states that higher estrogen levels increase cathepsin B activity, with cathepsin B responsible for the PTX release from the PGA backbone. Hence, cathepsin B activity represents one of the few examples of biomarker assessment in nanomedicine clinical trial patient selection [150]. In 2012, the FDA awarded Opaxio™ orphan drug designation for the treatment of glioblastoma multiforme in combination with temozolomide and radiotherapy. Opaxio™ development has been a reference for the expansion of PGA and polypeptide-based conjugates alone or in combination therapy, revealing the huge potential of these systems as therapeutics [16,

201]. One of the major strategies to move forward with polymer conjugates is the use of biodegradable nanocarriers, such as polypeptides, to avoid undesired side effect as those observed with PEG related with vacuolization and lysosomal storage diseases [13, 183].

Table I. 5: Polymer-drug conjugates in clinical development. Adapted from [179].

Name	Polymer carrier	Drug	Company	Indication(s)	Stage (ClinicalTrials.gov identifier)
Onzeald	PEG	Irinotecan	Nektar Therapeutics	Breast cancer	Pre-registration (NCT02915744)
PEX168	PEG	Loxenatide	Jiangsu Hansoh Pharmaceutical	Type 2 diabetes	Pre-registration (NCT02477969)
NKTR-181	PEG	μ-opioid receptor agonist	Nektar Therapeutics	Chronic low back pain and chronic noncancer pain	Phase 3 (NCT02367820)
NC-6004	PEG-bpoly(glutamic acid) micelle	Cisplatin	NanoCarrier	Pancreatic cancer	Phase 3 (NCT02043288)
Opaxio	Polyglutamic acid	Paclitaxel	CTI BioPharma	Ovarian cancer, peritoneal cancer, and fallopian tube cancer	Phase 3 (NCT00108745)
APL-2	PEG	Cyclic peptide complement C3 inhibitor	Apellis Pharmaceuticals	Paroxysmal nocturnal hemoglobinuria	Phase 3 (NCT03500549)
CRLX101	CyclodextrinPEG that selfassembles into nanoparticles	Camptothecin	BlueLink Pharmaceuticals	Ovarian cancer, peritoneal cancer, and fallopian tube cancer	Phase 2 (NCT01652079)
NK012	PEG-bpoly(glutamic acid) micelle	SN-38	Nippon Kayaku	Breast cancer	Phase 2 (NCT00951054)
OsteoDex	Dextran	Alendronate	DexTech Medical	Prostate cancer	Phase 2 (NCT02825628)
Somadex	Dextran	Somatostatin	DexTech	Medical Neuroendocrine tumors and acromegalia	Phase 2 (NA)
BP-C1	Benzo-polycarbonic acid polymer	Platinum(II)	Meabco A/S	Breast cancer	Phase 2 (NCT02783794)

Table I. 5: Polymer-drug conjugates in clinical development (continuation). Adapted from [179].

Name	Polymer carrier	Drug	Company	Indication(s)	Stage (ClinicalTrials.gov identifier)
Pegcantratini b	PEG	TrkA inhibitor	Sienna Biopharmaceuticals	Pruritus	Phase 2 (NCT03322137)
NC-6300	PEG-bpoly(aspartic acid) micelle	Epirubicin	NanoCarrier	Solid tumors and soft tissue sarcoma	Phase 1/2 (NCT03168061)
CRLX301	CyclodextrinPEG that selfassembles into nanoparticles	Docetaxel	BlueLink Pharmaceuticals	Solid tumors	Phase 1/2 (NCT02380677)
DEP cabazitaxel	PEGpolylysine dendrimer	Cabazitaxel	Starpharma	Solid tumors	Phase 1/2 (NA)
DEP docetaxel	PEGpolylysine dendrimer	Docetaxel	Starpharma	Solid tumors	Phase 1 (NA)
CriPec docetaxel	Core crosslinked PEGpolymer micelle	Docetaxel	Cristal Therapeutics	Solid tumors	Phase 1 (NCT02442531)
NC-4016	PEG-bpoly(glutamic acid) micelle	Oxaliplatin	NanoCarrier	Solid tumors and lymphoma	Phase 1 (NCT03168035)
RadProtect	PEG-bpoly(glutamic acid) chelating complex micelle	Amifostine	Original BioMedicals	Acute radiation syndrome	Phase 1 (NCT02587442)
SER-214	Poly(2-ethyl2-oxazoline)	Rotigotine	Serina Therapeutics	Parkinson's disease	Phase 1 (NCT02579473)
DFP-13318	PEG	SN-38	ProLynx	Solid tumors	Phase 1 (NCT02646852)

I.4.2.2.1. Rational Design of Polymer-Drug Conjugates

The design of polymer-drug conjugates for the treatment of a given disease or disorder must follow a rational stepwise design in consideration of the different processes that the conjugate faces following patient administration [202]. The physico-chemical characteristics of the polymer-drug conjugates will determine its capacity to cross the required biological barriers, such as the skin, and, therefore, the biological activity. The successful activity of the conjugate depends mainly on its response to the specific physiological environments found in the whole body. The essential components studied for the effective development of polymer-drug conjugates are the biodegradable polymer carrier itself and the bioresponsive linker between the polymer and the therapeutic agent involved.

I.4.2.2.1.1. Polymeric Carrier

In general, the polymeric carrier of choice should present the following properties:

(1) Biodegradability or a suitably small molecular weight, thereby facilitating excretion *in vivo*.
(2) Low polydispersity, providing homogeneity of the final conjugate.
(3) Prolonged half-life in the blood, enhancing adequate biodistribution and accumulation in body compartments, thus promoting optimal activity.
(4) Multivalency, allowing adequate drug loading, combinatorial drug loading, or the application of targeting/diagnostic moieties.

Biodegradability represents one of the most important characteristics of potential carriers, as this avoids accumulations in the body and possible related adverse side effects. The non-biodegradability and molecular weight restrictions of the first-generation conjugates of PEG and HPMA revealed limitations to pharmacokinetics and systemic toxicity. Thus, current research focuses on developing new and advanced biodegradable and biocompatible water-soluble polymers [203]. Polymer carriers include natural polymers as dextran (α-1,6 polyglucose), dextrin (α-1,4 polyglucose), cyclodextrin, and hyaluronic acid, and synthetic polymers such as PEG, HPMA copolymers (a polymer derived from more than one types of monomer), polyacetals, and polypeptides.

Moreover, polymer structural versatility has allowed the synthesis of a massive number of different systems, from linear or branched homopolymers to block

copolymers. Branched polymers involve several types, such as star, hyperbranched and dendritic-like polymers, dendrimers, graft, brush, and comb-like polymers, and polymer networks [204]. The high multifunctionality of branched polymers provides several advantages compared to their linear analogs, such as enhanced stimuli-responsiveness and the conjugation of a vast amount of different bioactive agents [205]. Moreover, branched polymers have demonstrated superior biodistribution, pharmacokinetic profiles [206], and *in vivo* biodistribution in healthy mice. Overall, the required functionality will drive the final use of linear or branched polymers.

I.4.2.2.1.2. Bioresponsive Linkers

The choice of the bioresponsive linker represents another critical parameter in the rational design of polymer-drug conjugates [207]. The application of stimuli-responsive materials, both endogenous (e.g., pH, redox environments or reactive oxygen species) and exogenous (e.g., magnetic field, temperature, light), has exponentially grown in recent times. Linker chemistry can optimize drug release profiles in specific microenvironments or the presence of particular enzymes, thereby ensuring the release of the active agent(s) within the target area and improving biological activity.

Different types of linkers have been described according to their susceptibility [16]:

(i) pH-responsive linkers: including acetal or ester bonds, N-cis-aconityl acid, or hydrazone linkers [208, 209].

(ii) Lysosomal enzyme-responsive linkers: normally oligopeptides cleaved by lysosomal enzymes such as cathepsin B or D, or metalloproteinases. Examples of such linkers include GFLG (Gly-Phe-Leu-Gly) and GLFG (Gly-Leu-Phe-Gly) [210].

(iii) Self-immolative linkers: These linkers can disassemble into constituent fragments, provoking the rapid disassembly of the polymer [211, 212].

(iv) Reductive-sensitive linkers: Drug release is produced in reducing environments, mainly due to the presence of glutathione [213].

(v) Drug release by anchimeric-assisted hydrolysis: firstly, drug-linkers release from the polymer following hydrolysis (first prodrug), activating the linker (second prodrug) which releases the free and active form of the drug [214].

I.4.2.2.1.3. Physico-Chemical Properties of Polymer-Drug Conjugates

The selection of the polymeric carrier and the linker significantly influences the physico-chemical parameters of the polymer-drug conjugate, such as the size (hydrodynamic radius), surface charge, and conformation.

The size of the conjugate determines its ability to cross biological barriers, such as the skin, and also the mechanism of cellular uptake. Therapeutic agents with sizes larger than 200 nm do not penetrate through the different layers of the epidermis well, although conjugates of this size may be captured by other mechanisms, such as through hair follicles [215, 216].

Within the circulatory system, nanosystems with sizes smaller than 5 nm penetrate capillary fenestrae and become rapidly eliminated by renal glomerular capillaries; however, larger particles exhibit prolonged circulation in the bloodstream, thereby increasing the time in which the nanosystem can play an active therapeutic role. Hence, nanosized therapeutics suitable for systemic applications should be in the range from 5 to 200 nm.

The self-assembly behavior of nanosystems also affects the final size and is determined by the characteristics of the assembling polymers and the conjugated drug(s), among other driving forces specific for each nanosystem implicated in its regulation [206]. Remarkably, several hydrophilic polymers fail to aggregate in the presence of water, but conjugation with a hydrophobic drug can induce self-assembly. As an example, both PEG-P(L-Asp) and PEG-P(L-Glu) create nanosized systems only after conjugation with DOX, resulting in the well-known polymeric micelles, some of them in advanced clinical development [217, 218].

The type of polymeric carrier employed also influences the surface charge (positive, neutral or negative), while after conjugation to different moieties or drugs, the zeta (ξ) potential value (the relative magnitude of the charges) of the system can also change. The surface charge impacts the *in vivo* effect of conjugates, conditioning the type of interactions with cell membranes and therefore cellular uptake, recognition and elimination from the bloodstream, and toxicity [219, 220].

In terms of cellular uptake, surface charge regulates the interactions between the nanosystem and the lipid cell membrane; due to the presence of sulfated proteoglycans in

the lipid bilayer, the cellular surface charge is ordinarily negative [221]. Hence, nanosystems with positive surface charges, such as poly-lysine, can bind strongly to the membrane, enhancing cellular uptake. However, positively charged nanosystems are not recommended for direct application *in vivo*, as these systems interact with negatively charged serum proteins (albumin) and red blood cells in the bloodstream and produce a precipitate over the cell surface [222], thereby destabilizing the plasma membrane and inducing instantaneous toxicity [223]. Thus, nanosystems should be modified with small or neutral charges by conjugation or complexation with anionic molecules (e.g., siRNA), to decrease the positive charge. Interestingly, surface charge also affects the physical stability and aggregation of the nanosystem in the circulatory system.

Conjugate conformation also represents an important parameter in the design of polymer-drug conjugates. Polymer chain conformation can modulate the stability of the nanosystem and the interaction with cellular membranes, and therefore, the final biological activity. The conformation of polymer-drug conjugates also affects the exposure of the therapeutic agent(s) involved to the factors that trigger its release, such as pH or specific enzymes, which can significantly influence release rate, activity, and effectiveness of the treatment at the desired target. The conformation of the nanosystem can also vary according to the type and pH of the solvent. This effect is especially significant in the case of polypeptides, where pH changes promote an ionization or neutralization of functional groups in the amino acid residues, which then encourages conformational transitions [224]. Furthermore, conjugated moieties or drugs can introduce extra charged elements that can modify the electrostatic equilibrium of the nanosystem, acting as a stabilizing or destabilizing force [225].

The polymer-drug conjugates synthesized, characterized, and evaluated in this thesis are based on the poly-L-glutamic acid (PGA) as polypeptidic carrier (discussed below). Ester bond linkers have been used in the majority of the systems due to their susceptibility to pH changes, leading to the drug release in the lysosomal compartment or in specific tissue areas showing an inflammation or a pathological situation.

I.4.3. Polypeptide-Based Therapeutics

Giving the described problems with previously developed non-biodegradable or bioaccumulative polymers, the use of natural biodegradable polymers in polymer therapeutics has greatly expanded, especially as a component of drug delivery systems

[226]. In particular, poly-amino acids or polypeptide-based materials (such as PGA) have had the most significant impact in the field of biomedicine as they provide the previously described advantages of polymers (**see section I.4.2.2.1.1.**) while avoiding some of the unwanted side effects.

The intrinsic characteristics of polypeptide-based materials have justified the trend to move away from non-natural polymers. Polypeptides mimic natural proteins, demonstrating remarkable biocompatibility and biodegradability due to controlled sequences and composition of the constitutive monomers. Therefore, the application of polypeptide-based materials suits diseases that require prolonged and continuous treatment, such as chronic or infectious diseases, neurological disorders, or tissue regeneration. Moreover, polypeptides present low immunogenicity [227, 228], thereby contributing to their suitability for constant parenteral administration and allowing the use of high doses of polymer [127]. The emergence of polymerization techniques, mainly ring-opening polymerization of α-amino-N-carboxyanhydrides [229-231], has led to the controlled synthesis of polypeptides with narrow polydispersity, high reproducibility, and specific functionalization of the polymeric backbone [204, 230].

Several important properties must be considered in the design of advanced biodegradable polypeptide-based materials [232]. Characteristics include (i) the avoidance of a sustained inflammatory response, (ii) a degradation time according to their function, (iii) suitable mechanical characteristics for their final use, (iv) the production of easily resorbable or excretable non-toxic degradation products, and (v) the possession of adequate permeability and processability for the designed purpose.

Polypeptide-based conjugates have found use in multiple areas of medicine, with an ever-increasing number of polypeptide-based compounds reaching preclinical and clinical trials [233]. These products include anti-cancer [234, 235], anti-tuberculosis [236], anti-diabetic [237], anti-microbial [238, 239], anti-virus [240], and anti-apoptotic conjugates [241], alongside magnetic resonance imaging agents [6], and theranostic agents (diagnostic and therapeutic applications in the same agent) [242]. These examples demonstrate the structural versatility of the polypeptide conjugates, facilitating the conjugation of therapeutic agents with different origin and physico-chemical properties (e.g., size, hydrophilicity) and diverse loading rates.

In this thesis, the synthesized polymer-drug conjugates employed PGA as a biodegradable polymer to take advantage of the intrinsic properties explained above.

I.4.4. Characterization Techniques

The rational design of drug delivery systems will significantly influence the final activity of the drug, and the exhaustive physico-chemical characterization of developed systems can provide information regarding structure-activity relationships, safety, and efficacy. Characterization contributes to the broader understanding of the conformation, dynamics, dimensions, and also the interactions with the biological environment. Purity, identity, molecular weight, polydispersity, drug content, free drug content, and quantification of targeting units represent just some of the critical characteristics of a nanosized drug-delivery system.

A growing interest in new biodegradable polymeric systems has led to the development of complex systems, creating the need for establishing adequate physico-chemical techniques for their characterization. The application of multiple and complementary techniques has provided knowledge on shape, size, and conformation. **Table I. 6** describes some of the most important techniques used in the physicochemical characterization of the nanosystems. Novel physico-chemical techniques such as SAXS (small-angle X-ray scattering), SANS (small-angle neutron scattering) [243, 244], wide angle X-ray scattering (WAXS), and Cryo-TEM (Transmission Electron Microscopy) [245, 246] have provided for significant advances in the characterization field.

Table I. 6: Summary of the most relevant techniques used to elucidate physico-chemical descriptors in physiological media. Adapted from [247].

Technique	Strenghts	Drawbacks	Descriptor Measured
UV-Vis	Quantitative, non-destructive, fast measurements, time-course studies, physiological conditions (aqueous, pH, ionic strength)	Necessity of chromophores, signal overlapping	Composition, conformation, non-covalent interactions
Differential Refractometry	Quantitative, non-destructive, fast measurements, time-course studies, physiological conditions (aqueous, pH ionic strenght), universal	Reference cell, not specific	Concentration
FS	Quantitative, selective, time-course studies, non-destructive, physiological conditions (aqueous, pH, ionic strength)	Necessity of fluorophores, fluorescence quenching	Concentration, composition, CMC stability
FRET	Quantitative, selective, low sample concentration, physiological conditions (aqueous, pH, ionic strength)	Insufficient spectral separation (false negatives), donor reabsorbs emission, high background noise	Structure, binding affinities, stability conformational change
FCS	Sensitive to single-entities, very small sample volumes, fast measurement, in vivo measurement possible	Dimerization not observable, high preparation time, requires fluorophore	Size (R_h), Size distribution
IR	Fast measurement, small sample volumes, time-course studies	Water masks part of the spectra, signal overlapping	Composition, conformation, non-covalent interactions
ATR-FTIR	Fast measurement, small sample volumes, null sample preparation, aqueous samples, time-course studies	Needs ATR correction software, signal overlapping	Composition, conformation, interactions
RS	Quantitative, minimal sample preparation, relative fast measurements, physiological conditions (pH, ionic strength, biological fluids), mapping of biological tissues	Auto-fluorescence, signal overlapping	Composition, conformation, Interaction with biological environment
CD	Quantitative, non-destructive, fast measurement, minimal sample preparation, time-course studies, physiological conditions (aqueous, pH ionic strength)	Signal overlapping	Conformation, non-covalent interactions, binding affinities
1D-NMR ^{1}H NMR	Non-destructive, minimal sample preparation, semi-quantitative, time-course studies, physiological conditions (aqueous, pH, ionic strength), highly selective, water signals can be eliminated	Relatively long measurments, expertise required, relativelly large concentration required, signal overlapping	Composition, binding affinities, interactions
^{19}F NMR	Biological samples, tissues	Long measurement time, biological sample preparation	Quantification in tissues
NOESY NMR	Non-destructive, minimal sample preparation, semi-quantitative, physiological conditions (aqueous, pH, ionic strength), highly selective, water signals can be eliminated	Very long measurement times, expertise required, relatively large concentration required, signal overlapping	Conformation at the molecular level, non-covalent interactions, epitope mapping, dynamics
PGSE NMR	Non-destructive, minimal sample preparation, semi-quantitative, complex mixtures, physiological conditions (aqueous, pH, ionic strength), highly selective, water signals can be eliminated, biological fluids	Relatively long measurement times, expertise required, relatively large concentration required, signal overlapping	Size (R_h), conformation, non-covalent interactions, co-assembling systems, fast screening of interacting components within complex mixtures dynamics

Table I. 6: Summary of the most relevant techniques used to elucidate physico-chemical descriptors in physiological media (continuation). Adapted from [247].

Technique	Strenghts	Drawbacks	Descriptor Measured
STD NMR	Non-destructive, minimal sample preparation, semi-quantitative, physiological conditions (aqueous, pH, ionic strength), highly selective, water signals can be eliminated	Long measurement times, expertise required, relatively large concentration required, signal overlapping	Binding affinities, epitope maping, screening of interacting components within complex mixtures, dynamics
NMR Relaxometry	Non-destructive, minimal sample preparation, semi-quantitative, physiological conditions (aqueous, pH, ionic strength), highly selective, water signals can be eliminated	Long measurement times, expertise required, relatively large concentration required, signal overlapping	Conformation, mobility, flexibility (or rigidity, structure topology, dynamics
SANS	Non-destructive, minimal sample preparation, physiological conditions (aqueous, pH, ionic strength), possibility of contrast variation scattering studies	Long measurments, expertise required, relatively large concentration required	Size , conformation, flexibility (or rigidity), 3D shape
SAXS	Non-destructive, minimal sample preparation, physiological conditions (aqueous, pH, ionic strength)	Relatively long measurement time, expertise required, relatively large concentration required, heavier elements mask the scattering from lighter elements	Size, conformation, flexibility (or rigidity), 3D shape
SLS	Non-destructive, small sample volumes, physiological conditions (aqueous, pH, ionic strength)	Requires sample preparation, interferences (dust, aggregation)	Size (R_h, Rg), size distribution, form factor (ρ), molecular weight
DLS	Non-destructive, small sample volumes, physiological conditions (aqueous, pH, ionic strength), biological fluids	Requires sample preparation, interferences (dust, aggregation), can´t differentiate similar sized populations	Size (R_h), size Distribution
ITC	Quantitative, aqueous samples	High preparation time, high precision in sample preparation is required	Non-covalent interactions, binding affinities and associated thermodynamic data
ESEM	Non-destructive, 3D mapping, physiological conditions	Expertise required	Size, size distribution, surface morphology, shape
Cryo-TEM	Physiological conditions, 3D mapping	Expertise required	Size, size distribution, surface morphology, shape
AFM	Non-destructive, 3D mapping, minimal sample preparation	Overestimation of measurements	Size, size distribution, surface morphology, shape
PT	Non-destructive, aqueous sample	Salts and pH might interfere the measurements	Salt ratio, ionization state, pKa
Z-potential	Non-destructive, physiological conditions (aqueous, pH, ionic strength)	Salts and pH might interfere the measurements	Surface charge, stability Binding affinities
NTA	Small sample volumes, minimal sample preparation, physiological conditions (aqueous, pH, ionic strength), selective measuremen through fluorescent labelling	Interferences (Dust, aggregation), limited particle concentration range	Size (R_h) distribution, particle size concentration, selective filtering through fluorescence
SPR	Quantitative, small sample volumes, physiological conditions	Artefacts	Interactions, binding rates

I.4.5. Polymer Therapeutics for Skin Delivery

Transdermal drug delivery systems based on polymer therapeutics represent a non-invasive administration strategy for both local and systemic therapies. The topical route presents several advantages compared to other types of administration, mainly due to the reduction of the frequency of dose and bypassing hepatic first-pass elimination [248, 249].

One of the most widely used polymeric carriers for transdermal delivery of bioactive molecules is the biodegradable and biocompatible natural polymer, hyaluronic acid (HA) [250], a glycosaminoglycan found in the extracellular matrix that binds and retains water molecules [251]. As an example of the potential of HA, Yang *et al*. assessed the penetration capacity of an HA-conjugated form of the human growth hormone (hGH) [252]. hGH has been commonly employed for the treatment of short stature by injection over months to years. As hGH receptors are distributed throughout the skin, especially in fibroblasts, and influence cell proliferation and differentiation [253, 254], topical administration of hGH represents an exciting alternative to intravenous injection. The topical application of the HA-hGH conjugate led to increased penetration and reached the dermis, thereby drastically enhancing the bioavailability of hGH in the bloodstream when compared to free hGH.

The bioresorbable polymer chitosan represents another natural polymer carrier that can enhance skin penetration by modifying the secondary structure of keratin in the skin, thereby increasing the hydration of the stratum corneum and cell membrane fluidity [255]. Chitosan is a type of mucopolysaccharide found in the shell of crustaceans, and many other organisms, including insects and fungi [256]. Pawar *et al*. prepared a chitosan hydrogel containing the covalently conjugated antibiotic cefuroxime by an ester linker for the treatment of wound infections in the skin. The results revealed a potent antibacterial activity using the agar well diffusion method (Kirby-Bauer assay [257]), thereby extending the therapeutic time span of the antibiotic [258].

The conjugation of various drugs (e.g., retinal [Vitamin A], pyridoxal [Vitamin B_6], and pyridoxal phosphate [metabolically active coenzyme of vitamin B_6]) to a polyamidoamine based dendrimer (PAMAM), a type of branched polymer, has also been used as a means to effectively penetrate the skin [259]. Due to the intrinsic characteristics of these branched polymers, such as monodispersity and a compact spherical structure

(1 - 10 nm), the reduced size of the PAMAM dendrimers improved the penetration of the conjugates in the skin [260, 261].

A study by Castleberry *et al*. reported the conjugation of all-trans retinoic acid (ATRA) to a hydrophilic polymer, polyvinyl alcohol (PVA), through a hydrolytically degradable ester linkage (PATRA), as a potential means to improve transdermal penetration. Franz diffusion cell studies using an explant pig skin model demonstrated that topical application of the PATRA conjugate for 12 hours led to the improved dermal accumulation of ATRA. *In vivo* irritation studies demonstrated that PATRA generated a more significant reduction in inflammation at the site of application site when compared to free ATRA [262].

In another study, Bonina *et al.* developed polyoxyethylene ester prodrug conjugates of different anti-inflammatory drugs (e.g., ketoprofen, naproxen, and diclofenac). Ester synthesis employed the conjugation of drugs with polyoxyethylene glycols using a succinic acid spacer. *In vitro* transdermal absorption studies established that esters with elevated levels of ethylene oxide groups displayed an increased flux through the skin when compared to the application of the free drugs. The evaluation of the anti-inflammatory activity of the conjugates in a methyl nicotinate-induced skin erythema model in healthy human volunteers demonstrated the appreciable and sustained activity of ketoprofen and diclofenac esters with higher PEG molecular mass compared with the free drugs [263].

Polymer therapeutic approaches have also been employed to develop a topical chemotherapy strategy for the treatment of melanoma. Capanema *et al*. developed a carbohydrate-based prodrug composed of a carboxymethylcellulose polymer conjugated with the anticancer drug DOX via covalent amide bonds. Additionally, cross-linking of the polymer with citric acid produced advanced hydrogels. The results established the influence of the carboxymethylcellulose structure (different degree of substitution) on DOX release kinetics *in vitro* and its cytotoxicity towards melanoma cancer cells *in vitro* [264].

Overall, polymer therapeutics offer particular advantages that can enhance transdermal drug delivery. Although the skin presents certain challenges to the delivery of therapeutic agents, such as the stratum corneum barrier and constant cell shedding, polymer therapeutics can overcome barrier properties and promote drug penetration to

deeper skin layers. The use of polymer therapeutic-based formulations for various skin diseases could revolutionize current therapeutic strategies employed in dermatology by overcoming old challenges and offering new perspectives for the treatment and prevention of dermatological diseases.

To this end, we will discuss the skin disorder psoriasis in the following section as one of the main focuses of this thesis.

I.5. Psoriasis as a Target Pathology

Damage to the skin barrier function leads to the development of several skin diseases or disorders [265]. Skin barrier integrity is essential for the protection of the whole body, and its dysfunction can enhance the risk of developing infective and inflammatory disorders [266]. In some disorders, such as psoriasis, the inflammatory process impedes the correct synthesis and maintenance of skin barrier elements and prevents or diminishes the effectiveness of topical treatments. Our challenge is to develop a suitable and effective topical treatment for our target pathology, psoriasis, through the application of a polymer therapeutic-based approach.

Psoriasis is a common and chronic inflammatory disease mediated by the immune system with predominantly cutaneous involvement. Psoriasis is characterized by the unpredictable nature of pathological evolution, presenting with periods free of disease followed by periods of outbreaks with highly variable appearance and duration. There are several clinical phenotypes of psoriasis, which can be classified based on the characteristics of the disease, including patient age at disease onset, degree of skin involvement, morphologic pattern, and anatomic location [267]. While the most common manifestation of psoriasis is plaque psoriasis or psoriasis vulgaris (90% of psoriatic patients [268]), other forms of this disease include psoriasis-like pustular psoriasis, erythrodermic psoriasis, and guttate psoriasis (**Figure I. 9**) [269, 270]. Psoriasis can have a considerable impact on patient quality of life, due, in most cases, to the perceived embarrassment regarding the appearance of the skin, therefore affecting both the physical and emotional health of the patients [271].

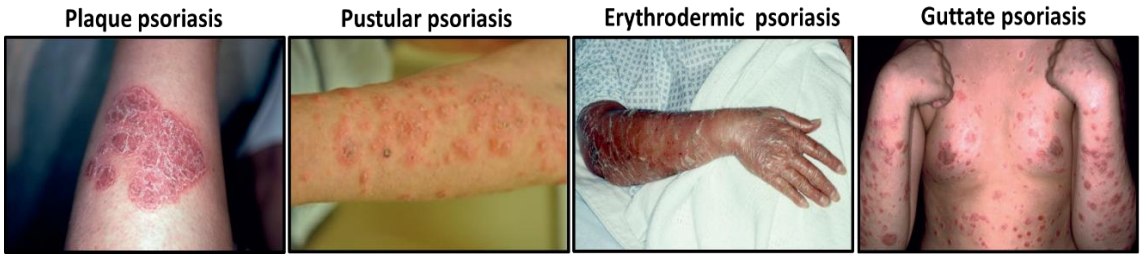

Figure I. 9: Clinical presentation of psoriasis. Adapted from [272, 273].

I.5.1. Prevalence and Morbidity

Psoriasis is a relatively common disease, affecting 2 - 3% of the adult population and 0.5 - 1% of children [274]. Studies have indicated that the incidence of psoriasis doubled between the years 1970 and 2000 [275] and can appear at any age, although normally between the ages of 15 - 30 and 50 - 60 [276]. According to the National Institute of Health (NIH), as many as 7.5 million Americans suffer from some form of psoriasis, with more than 150,000 new diagnoses of psoriasis reported every year; however, most new cases are in persons under 30 years of age [277]. These numbers translate to annual health care costs of around $135 billion in the USA alone [278].

Recently, the importance of gender in psoriasis prevalence has been demonstrated [279] in a study that demonstrated a significantly higher presence of the disease in male than in female in the Japanese and Thai populations (**Figure I. 10**) [280, 281].

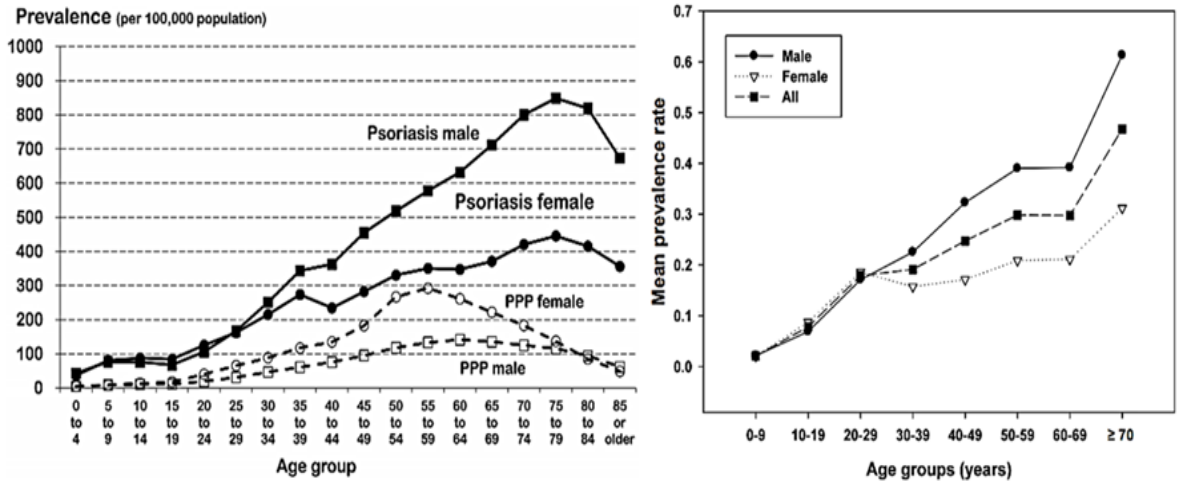

Figure I. 10: Prevalence of psoriasis and the palmoplantar pustulosis (PPP) (localized forms of pustular psoriasis) in the Japanese (left) and Thai (right) population. Adapted from [280, 281].

The onset of psoriasis usually leads to the development of new associated disorders, as the chronic systemic inflammation associated with psoriasis leads to an

increased risk of suffering from cardiovascular diseases [271] such as hypertension, diabetes mellitus, and obesity [282]. Furthermore, psoriasis can trigger the appearance of other autoimmune diseases, such as psoriatic arthritis and Crohn's disease [283].

I.5.2. Etiology

Psoriasis is a complex disease that involves a range of factors or causes. The development of the disease has a genetic predisposition, along with several factors that can trigger its appearance.

I.5.2.1. Triggering Factors

1. Trauma and Infection

In 1872, Koebner discovered that psoriatic skin lesions appeared in unaffected areas following trauma in patients [284]. The "Koebner phenomenon" describes the characteristic distribution of psoriatic lesions on extensor surfaces, such as the elbows, knees, and sacral region. Additionally, infections can induce and/or exacerbate the onset of psoriasis by triggering a cascade of internal alterations. Infections by *Streptococcus*, *Staphylococcus aureus*, *Malassezia* fungi, *Candida*, and some viruses can all induce psoriasis [285].

2. Obesity

Psoriasis can represent both the cause and consequence of the appearance of obesity, along with other cardiovascular diseases. Recent studies have shown that patients with obesity have a high risk of developing psoriasis. For instance, the Nurses' Health Study followed around 100,000 women over 12 years, assessing if obesity was a potential triggering factor. The authors demonstrated the presence of a significant association between increasing body mass index and the risk of suffering psoriasis [286].

3. Medication

Certain medications can cause the appearance of psoriasis in patients with a genetic predisposition and can also intensify or exacerbate existing disease. Some of the drugs evaluated as potential triggers of the disease include beta-blockers, lithium, hydroxychloroquine, some antibiotics (penicillin, amoxicillin, ampicillin, and doxycycline), and non-steroidal anti-inflammatory drugs [285, 287, 288].

4. Stress, Alcohol, and Smoking

Periods of stress can lead to the appearance of psoriasis, and while the exact mechanisms involved have yet to be clarified, one study established that stress produces alterations in the hypothalamic-pituitary-adrenal axis that provokes changes in the expression of some hormones [289, 290]. Furthermore, unhealthy habits such as smoking or the excessive consumption of alcohol can trigger the disease, with studies directly linking tobacco/alcohol consumption to the appearance of psoriasis [291, 292].

5. Endocrine factors

Some hormones related to the hypothalamic-pituitary-adrenal axis, such as androgens, prolactin, and thyroid hormone, influence psoriasis directly [293]. Abrupt changes in hormonal levels, such as those that occur during pregnancy, can produce the appearance of psoriasis or worsen preexisting disease [294].

I.5.2.2. Genetic Factors

Psoriasis is also related to a strong hereditary character, involved a complex genetic basis [295]. Multiple genes are involved in the molecular genetic basis of psoriasis, confirming the complexity of the disease [296]. Although there exists heterogeneity between different populations, previous studies identified ten loci as common potential psoriasis susceptibility regions [297] (**Table I. 9**).

Table I. 7: The ten psoriasis susceptibility regions identified using linkage studies. Adapted from [293].

Loci name	Location
PSORS1	6p21.3
PSORS2	17q25
PSORS3	4q
PSORS4	1q21
PSORS5	3q21
PSORS6	19p13
PSORS7	1p
PSORS8	16q
PSORS9	4q31-34
PSORS10	18p11.23

The primary susceptibility locus for psoriasis is at 6p21, referred to as PSORS1, which is over-expressed in all populations tested [298-301]. Additional studies found a

relationship between psoriasis and other genes implicated in inflammatory pathways, including nuclear factor kappa beta (NF-kB), tumor necrosis factor (TNF), and interleukin (IL)-23/17 pathways [297] demonstrating a central role of both the innate and the adaptive immune system.

I.5.3. Immunopathological Features

While initial analyses suggested that the aberrant activity of keratinocytes and the associated uncontrolled proliferation of the epidermal cell layers causes psoriasis, recent studies have demonstrated that the evolution of psoriatic skin inflammation seems to be influenced by the presence of immune cells, especially dendritic cells and T cells [274]. Therefore, psoriasis is no longer considered merely as a disease caused by an ineffective skin barrier, but rather a more complex and systemic disease. Moreover, studies have established a dependence on the interaction between systemic pro-inflammatory factors and keratinocyte overproliferation [302-304]. Alterations to the immune system are now considered the primary inducing factor for psoriasis [293].

Psoriasis vulgaris is characterized by aberrant keratinocyte hyperproliferation in the basal layer when compared with healthy skin, causing the increment in epidermal thickening (acanthosis) that produces the plaques that characterize this subtype [305, 306]. Additionally, the premature maturation of keratinocytes produces the incomplete conversion of keratinocytes into corneocytes, with the retention of nuclei in the stratum corneum (parakeratosis) [307]. Inflammatory infiltration, consisting mainly of dendritic cells, macrophages, and T cells (**Figure I. 11**), is also observed in psoriatic lesions. Psoriasis also affects the regulation of the synthesis of essential keratins (K) for the correct functioning of keratinocytes; one study found that hyperproliferation-associated keratins (K6, K16, and K17) replaced keratins typical of suprabasal cells (K1 and K10) [308, 309].

Figure I. 11: **(A)** Characteristics plaques together with erythema, in different sizes and shapes. **(B)** Histopathological features characterized by increased epidermis thickness, parakeratosis, elongated rete ridges, and a mixed cellular infiltrate CD3+ T cells **(C)** and CD8+ T cells **(D)**. Adapted from [307].

I.5.4. Immunopathogenesis: Central Role of the Immune System

The contributions of dysfunctional skin cells and the immune system establish a pro-inflammatory environment within the skin that prevents the normal functioning of the skin barrier. During the development of psoriasis, there exists a close relationship between the innate and adaptive immune system; the innate immune system provides an early response mechanism, and after its activation, the adaptive immunity becomes involved.

As described Nestle *et al*. [307] (**Figure I. 12**), the onset of psoriasis begins with the activation of the innate immune system, in particular, the activation of dendritic cells (DCs), which are antigen-presenting cells that connect innate and adaptive immunity. Different types of DCs can be found in the skin, expressing different surface markers and immune mediators. Following inflammation, studies have revealed an increase in the numbers of specific DC populations, including plasmacytoid DCs (pDCs) and dermal myeloid DCs (mDCs) [274]. During disease initiation, pDCs become activated in huge

numbers. Following a disease trigger, keratinocytes respond by producing LL-37, an antimicrobial peptide, that complexes with self-DNA and RNA. LL-37/DNA and LL-37/RNA complexes can be uptaken by dendritic cells and activate them, stimulating two Toll-like receptors (TLR) types, TLR-9, and TLR-7, respectively.

Adaptive immunity-related mechanisms begin to function following the activation of the innate immune system. Activated dendritic cells produce the synthesis of pro-inflammatory cytokines such as IL-12 and IL-23 [310] to promote T-cell induction of Th1 and Th17 class expansion, respectively. This interaction begins a cascade of inflammation and the synthesis of proinflammatory cytokines such as IL-17A, IL-17F, IL-22, IL-26, IL-6, IL-21, TNF-α, and interferon gamma (INF-γ) [274, 310]. The cytokine IL-17 plays an essential role in the amplification of the inflammatory signal, and several studies have indicated that the development of psoriasis occurs primarily through the IL-23/IL-17 axis, which, therefore, represents a primary therapeutic target. Binding of IL-17 to receptors on keratinocytes [311] produces several responses, including heightened proliferation.

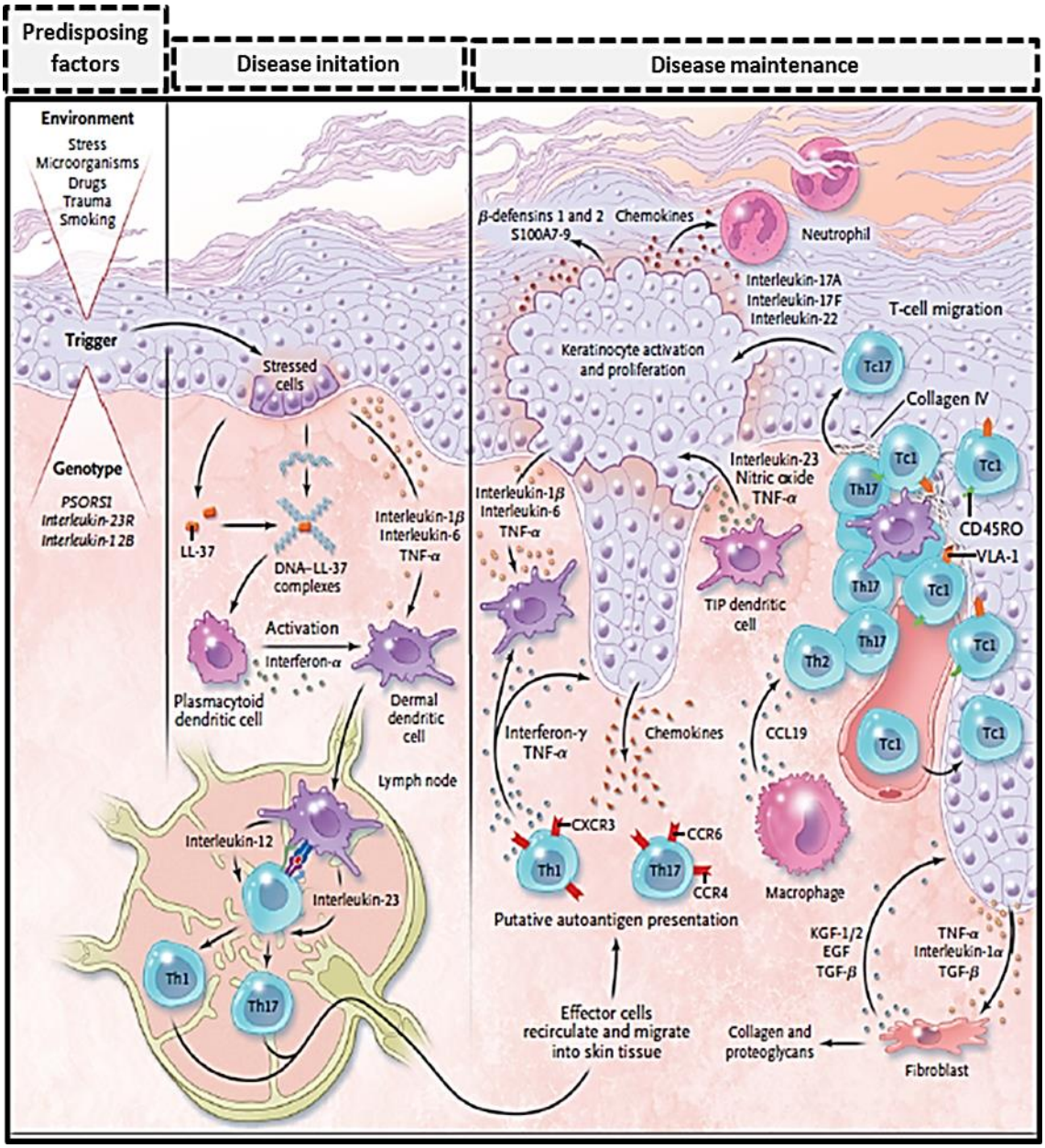

Figure I. 12: Evolution of a psoriatic lesion from initiation to maintenance of disease. Adapted from [307].

Other than the activation of Th17 cells, IL-23 has been implicated in several other effects related to the development of psoriasis [312]. IL-23 receptor complex is formed by IL-12Rb1 and IL-23R subunits, which are associated with the Jak family members. IL-23 stimulation activates receptor-associated Jaks [310], which, in turn, phosphorylate tyrosine residues that serve as docking sites for the signal transducer and activator of transcription (STAT) molecules, with STAT3 the most relevant member in the IL-23 signaling pathway. After activation, STAT3 homodimers translocate into the nucleus and bind DNA promoter regions of target genes, thereby promoting the synthesis of cytokines

related with psoriasis (IL-17A, IL-17F, and INF-γ) (**Figure I. 13**). Moreover, IL-23 alters the expression of TNF-α by stimulating macrophages [293] and has a direct impact in keratinocytes by promoting keratin 16 (K16) gene expression, which is associated with epidermal hyperplasia [308, 313].

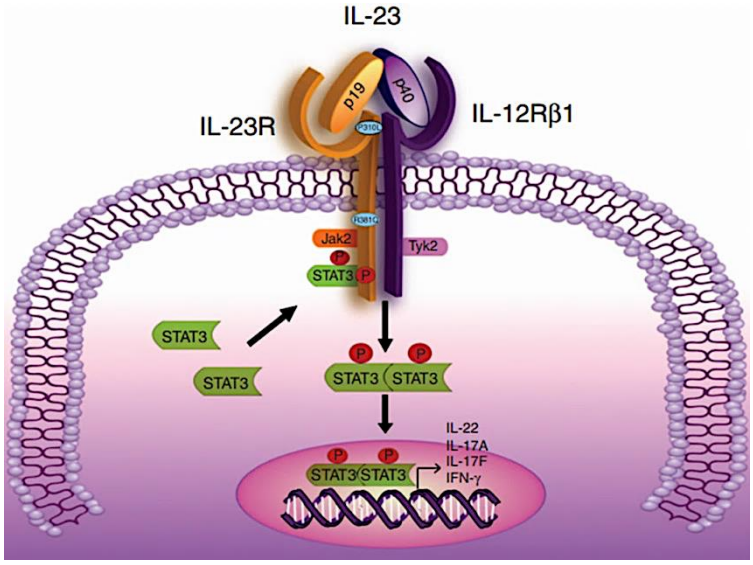

Figure I. 13: IL-23 signaling pathway. Adapted from [310].

Other cytokines with essential roles in the development of psoriasis include TNF-α and INF-γ. A multitude of cells involved in the pathophysiology of psoriasis produce TNF-α, including keratinocytes, DCs, and Th1, Th17 and Th22 cells [314], which participates in both acute and chronic phase disease. The pro-inflammatory functions of TNF-α include the initiation of several secondary mediators and the induction of adhesion molecules [315].

INF-γ also represents a crucial mediator that prolongs the inflammatory process. Type I IFNs play various roles in the antiviral host defense, due to their ability to prevent viral replication and promote immune system activation [316]. Activated pDCs secrete large amounts of INF-γ in response to the release of nucleic acids, which induces epidermal regeneration. This type of interferon is mainly involved in the acute phase of psoriasis (appearance of skin lesions), where pDCs infiltrate into early developing lesions [317]. INF-γ also affects the expression levels of IL-17, contributes to cytokine release [318], and induces the expression of the IL-22 receptor by acting indirectly on keratinocytes [314]. Moreover, continuous type I IFNs activity prevents wounds healing, thereby enhancing the development of psoriatic lesions [319, 320].

In summary, psoriasis is a complex disease based on interconnected immunological mechanisms. Although there are several pathways implied in the onset of the disease, the IL-23/IL-17 axis plays an essential role in the beginning, development, and maintenance of the disease.

I.5.5. Current Therapeutic Approaches for Psoriasis

The complexity of psoriasis has prompted the development of a multitude of treatments against the various mechanisms involved in psoriasis. Treatment approaches are generally patient-specific, factoring in the severity of the disease (critical factor to select the most adequate therapeutic), comorbidities, patient compliance, and safety. Furthermore, the body surface area affected must be taken into account, and while topical treatment suit mild to moderate psoriasis, moderate to severe psoriasis may require systemic medications and/or phototherapy.

Currently developed therapeutics for psoriasis are classified into three types: topical, systemic, and phototherapy-based approaches.

I.5.5.1. Topical Approaches

Topical therapies are the most widely employed treatment for psoriasis and can be combined with systemic therapies in patients with more severe forms of the disease. Topical anti-psoriatic drugs typically aim to diminish local epidermal inflammation and thereby reduce both the epidermal layer thickness and desquamation in the stratum corneum. This approach can avoid or slow down the formation of characteristic skin plaques. Furthermore, decreasing inflammation through topical therapies eliminates the red coloration characteristic of erythema, and can, therefore, improve patient quality of life from an emotional health point of view.

Recommended topicals treatments include corticosteroids, vitamin D analogs, calcineurin inhibitors, retinoids, and their combination [293]. Topical corticosteroids represent the most common and effective topical treatments, with the variety of vehicles/formulations (such as ointment, cream, lotion, gel, foams, etc.) allowing patient-specific approaches based on location and severity of lesions [321].

Of note, the correct selection of the vehicle for drug delivery is a critical parameter controlling the effectiveness and acceptability of topical formulations. As previously

mentioned, drug permeability through the different layers of the skin is modulated and related by the properties of the vehicle used [322]. The main parameters that ensure successful topical treatment, such as drug release, drug penetration through the stratum corneum and drug permeation through the skin layers, are determined by the interaction between the vehicle, the skin, and the drug [323]. The formulation of therapeutic agents includes ointments, creams, lotions, gels, foams, and a range of other similar examples.

The physico-chemical properties of the vehicle condition the effect of the therapeutic agents on the skin. Paraffin, fats, and oils are occlusive and lipophilic vehicles, which enhance the moisture content in the skin, and hence increase drug penetration. The term occlusion refers to skin coverage by impermeable films or substances that are widely utilized to enhance the penetration of applied drugs [324]. In contrast, hydrogels consisting mainly of water do not display an occlusive effect but can improve the hydration level of the skin, thereby promoting drug penetration and preventing additional symptoms related to dry skin.

The combination of aqueous and oily solutions results in emulsions; water-in-oil emulsions have a less occlusive nature than the lipid solutions but are more occlusive than the oil-in-water emulsions [322]. Recently, the development of Pickering emulsions, emulsions stabilized by solid particles in place of surfactants, has improved such vehicles. Adsorbed solid particles avoid coalescence to a greater degree than surfactants, a process in which two or more droplets merge to form a single larger droplet, stabilizing the emulsions. The elimination of surfactants in these vehicles allows for long term skin applications, where surfactants often cause irritancy [325]. Importantly, formulations that increase patient compliance will improve outcomes thanks to the stricter adherence to treatment regimens.

I.5.5.2. Systemic Approaches

Systemic therapies are generally the most effective treatments for psoriasis. An increase in our understanding of the mechanisms and mediators involved in psoriasis has prompted the development of new systemic therapies specifically targeting various critical pathways, thereby increasing the effectiveness of the treatment. These therapies have two distinct approaches: biologic or non-biologic therapeutics.

I.5.5.2.1. Biologic Therapeutics

The discovery of biologic drugs has supposed a revolution in the therapeutic management of patients suffering psoriasis. A multitude of research articles have revealed the efficacy and safety profile in the long term of the biologic treatments. Therefore, this treatment represents an excellent therapeutic tool for chronic diseases like psoriasis [326, 327]. Living organisms can be employed to generate biological therapeutics [328], which include monoclonal antibodies, cytokines, kinase inhibitors, etc [329]. The involved mechanisms of action focus on attacking specific targets of the immune system, and so have colossal relevance and potential for the treatment of autoimmune diseases.

Biological therapeutics are classified according to the therapeutic target on which they act, although each one will have a different mechanism of action. Based on the immunopathogenesis of psoriasis, therapeutic targets with the best clinical results are the primary mediators of the inflammatory process of the disease, such as TNF-α, IL-17, and IL-23. Schadler *et al.* [293] described some of the most effective biologic treatments approved by the FDA, according to the target on which they act:

1. **<u>TNF-α inhibitors</u>**

Etanercept (Enbrel®, Amgen): a TNF-receptor fusion protein that acts by competitively inhibiting the binding of TNF-α to TNF receptors 1 and 2. Etanercept was approved for the treatment of psoriatic arthritis in 2002 and the treatment of plaque psoriasis in adults in 2005.

Adalimumab (Humira®, AbbVie): a monoclonal antibody against TNF-α that acts by binding host TNF ligands, thereby inhibiting interaction with TNF receptors. Adalimumab was approved for the treatment of moderate to severe plaque psoriasis in adults in 2008.

Infliximab (Remicade®, Janssen Pharmaceutica): a monoclonal anti-TNF-α antibody that acts through the same mechanism of action as Adalimumab, and was approved for the treatment of psoriatic arthritis in 2005 and chronic plaque psoriasis in 2006.

Certolizumab Pegol (Cimzia®, UCB): a Polymer Therapeutic, specifically a PEG-TNF-α antibody fragment conjugate first approved for use in Crohn's disease, rheumatoid arthritis, psoriatic arthritis, and ankylosing spondylitis. The PEG moiety induces

improvements to the activity of the drug, due to the increment lifetime of the molecule in circulation. Certolizumab Pegol received approval for the treatment of moderate to severe plaque psoriasis in adults in 2018.

2. IL-17 inhibitors

Secukinumab (Cosentyz®, Novartis): a humanized IgG monoclonal antibody that specifically targets IL-17A. Secukinumab was the first anti-IL-17 antibody on the market for the treatment of psoriasis in adults and was approved in 2015.

Ixekizumab (Taltz®, Eli Lilly and Company): a humanized monoclonal antibody which targets IL-17A to inhibit interaction with its receptor that was approved in 2016 for the treatment of adults with plaque psoriasis.

Brodalumab (Siliq®; Valeant Pharmaceuticals): a monoclonal antibody targeted against IL-17 receptor A. The IL-17 receptor is a dimer complex of which receptor A is a shared subunit and binding of this subunit by Brodalumab prevents IL-17 from complexing with the receptor. Brodalumab was approved in 2017 for use in adults with chronic plaque psoriasis.

3. IL-23 Inhibitors

Guselkumab (Tremfya®; Janssen Pharmaceutica): a monoclonal antibody that specifically targets the p19 subunit of IL-23. Guselkumab was approved in 2017 for use in adults and became the first selective IL-23 inhibitor on the market.

Tildrakizumab (Ilumya®, Sun Pharmaceutical Industries Ltd.): An IgG humanized antibody that also targets the p19 subunit of IL-23. In 2018, Tildrakizumab received approval for treatment of adults with moderate to severe plaque psoriasis.

New drugs in phase III clinical trials for the treatment of moderate to severe plaque psoriasis and psoriatic arthritis, including bimekizumab (IL-17 inhibitors) and risankizumab (IL-23 inhibitor) [293, 330].

I.5.5.2.2. Non-Biologic Therapeutics

Non-biologic therapeutics for moderate to severe psoriasis represent less specific systemic treatments with generally lower efficacy than biologic therapeutics. Commonly employed non-biologic therapeutics include methotrexate, a dihydrofolate reductase inhibitor that reduces the synthesis of purines and pyrimidines required for DNA

synthesis. However, methotrexate also displays anti-inflammatory, anti-proliferative, and immunosuppressive activities in psoriatic patients [331].

Apremilast, a phosphodiesterase 4 inhibitor, inhibits the breakdown of cyclic adenosine monophosphate and the decreased production of inflammatory cytokines and clinical trials have established Apremilast as an effective treatment for plaque, nail, scalp, and palmoplantar psoriasis [332, 333].

Cyclosporine, an immunosuppressive drug that inhibits calcineurin and decreases the synthesis of IL-2, is a conventional oral treatment for psoriasis treatment alongside methotrexate [334].

Finally, Acitretin, a vitamin-A-derived retinoid that interferes with epidermal cell growth and differentiation [335], is used in combination with topical or systemic treatments as alone it presents only weak effects on outcomes in psoriasis patients [336].

I.5.5.3. Phototherapy

Phototherapy consists of repeated exposure of the skin to ultraviolet (UV) radiation as a treatment and is often employed following the failure of topical medications. While recent improvements have improved utility and accessibility, the mechanism of action has yet to be fully delineated [337]. However, studies have discovered that phototherapy intensifies cutaneous immunosuppression, mainly by altered cytokine expression and lymphocyte apoptosis [338].

Different types of radiation have been used; ultraviolet B (UVB), ultraviolet A plus psoralen (PUVA), and photodynamic therapy (PDT) [339]. Ultraviolet B radiation at 311 nm represents the most common and effective phototherapeutic modality in psoriasis patients; however, the strategy of employing ultraviolet A plus psoralen (PUVA) is no longer used to the heightened associated risk of skin cancer [293]. To improve patient compliance, home UV units were developed to allow patients to avoid medical facilities, and this has improved access to treatment and increased patient satisfaction [340].

I.5.6. Nanomedicine-Polymer Therapeutic Approaches to Psoriasis Treatment

Several polymer-based nanocarriers have been employed as drug delivery systems for the treatment of skin diseases such as psoriasis, as they permit the sustained diffusion

of the drug into the skin following the formation of a high drug concentration gradient at the skin surface [341]. These advantages allow the sustained and controlled drug release at the target site for prolonged periods when compared to the free drug [342, 343]. Furthermore, polymer-based nanocarriers can also reduce the number of doses and spacing times, producing higher levels of patient acceptability and treatment compliance [344]. In the following section, we will discuss the few studies that have directly addressed psoriasis.

In 2016, Bessar *et al*. employed gold nanoparticles functionalized by sodium 3-mercapto-1-propane sulfonate (Au-3MPS) to encapsulate methotrexate and studied the absorption behavior in a C57BL/6 mouse normal skin model. They discovered that this formulation reached the epidermis, with a lower amount also reaching the dermis [345]. Ultraviolet-visible spectroscopy after 24 hours of skin application revealed the presence of the conjugate in the mouse skin, with higher delivery of methotrexate to the epidermis and dermis using the gold nanoparticles when compared to treatment with the free drug. The authors confirmed their findings *in vitro* by scanning transmission electron microscopy images, observing gold nanoparticles distribution inside the keratinocytes from primary cell cultures.

Another study developed by Crisan *et al*. employed silver and gold nanoparticles to carry polyphenols-rich extracts from the *Cornus mas.* shrub recently revealed to have promising anti-inflammatory activity *in vivo* [346]. The application of nanoparticle-based ointments in psoriatic patients for six weeks prompted a considerable improvement of psoriasis plaques, with reduced peeling, erythema, and plaque thickness. Immunofluorescence of skin biopsies demonstrated that nanoparticles significantly reduced CD68-positive macrophages and TNF-α production in the psoriasis plaques.

Nemati *et al*. developed novel nanoparticles conjugating the epidermal growth factor receptor (EGFR) siRNAs to gold nanoparticles. Treatment (three times per week for three weeks) with EGFR-siRNA gold nanoparticles mixed with Aquaphor®, a marketed ointment for skin application of active agents, in an acute imiquimod-induced psoriasis murine model revealed reduced epidermal thickness when compared free EGFR-siRNA [347].

Thapa *et al*. studied the effect of tacrolimus (immunosuppressive drug)-loaded liquid crystalline nanoparticles in a psoriatic mice model, finding the retention of 65% of

the total drug when applied as a nanoparticle formulation at 24 hours when compared to only 25% when used as a solution [348].

However, the use of non-biodegradable gold, silver or liquid crystalline nanoparticles can provoke local and/or systemic accumulation, producing adverse effects in the body. Currently, lipidic and polymeric nanoparticles represent the most applied type of nanoparticle for the treatment of skin diseases. As an example, the encapsulation of capsaicin [349] or a combination of methotrexate and etanercept [350] in lipidic nanoparticles increases the amount of drug that reaches the viable epidermis when compared to the application of the drug alone. The controlled synthesis of polymeric nanoparticles also allows more controllable development of chemical and physical characteristics and can help the nanoparticle (and hence the associated drug(s)) to penetrate through the skin and improve therapeutic outcomes.

The application of polymersomes [351, 352] has led to further improvements in drug treatment for psoriasis. As an example, Marepally *et al*. developed a polymersome based on a fusogenic nucleic acid lipid particle (F-NALP) system, encapsulating two therapeutic nucleic acids, anti-STAT3 and anti-TNF-α siRNA. Results revealed that F-NALPs efficiently carried both therapeutics into the dermis and synergistically functioned to improve psoriatic-like plaques in an imiquimod-induced psoriatic-like plaque mouse model.

Several studies revealed the potential of drug encapsulation in polymeric nanoparticles as a delivery system. For instance, the use of curcumin-loaded poly-lactic-co-glycolic acid) (PLGA) nanoparticles in a psoriasis-like mouse model prompted a reduction of psoriasis symptoms, mainly due to the higher penetration through the skin of the PLGA nanoparticles in comparison with free curcumin in gel [353]. In studies carried out by Mao *et al*. aiming to increase the encapsulation efficiency of curcumin, researchers synthesized new self-assembled nanoparticles formed by a new amphiphilic polymer, RRR-α-tocopheryl succinate-grafted-ε-polylysine. The application of these curcumin-loaded nanoparticles in gel in an imiquimod-induced psoriatic mouse revealed that the nanoparticles displayed better activity than the free curcumin in gel, with a higher therapeutic effect and significant inhibition of the expression of inflammatory cytokines (TNF-α, NF-kB, and IL-6) [354].

Gurny and co-workers developed a new formulation for tacrolimus encapsulation, using a methoxy-poly (ethylene glycol)-hexyl substituted poly (lactic acid)-based nanocarrier and subsequently loaded it into a carbopol hydrogel. The authors compared the activity of the developed formulation with the commercial formulation Protopic™, an ointment containing free tacrolimus used as a benchmark. The results revealed that the skin delivery of tacrolimus composite hydrogel in an imiquimod-induced psoriasis mouse model was twice as high as for the Protopic™. Furthermore, the tacrolimus composite hydrogel showed significant enhancements on both the histopathological score in the mice model as well as the *in vivo* clinical score (erythema and skin thickness) [355].

In 2017, Wan *et al*. synthesized a novel hybrid system based on self-assembling nanoparticles of HA-conjugated cholesterol for the encapsulation of nicotinamide and tacrolimus. Antipsoriatic activity assessed in an imiquimod-induced psoriasis mouse model found that the newly developed nanoparticles functioned as well as a positive control for psoriasis treatment (clobetasol propionate) and better than a commercial ointment Protopic® [356].

To the best of our knowledge, there exist only a few reports of the development of polymer-conjugated psoriatic drugs. Jin *et al*. conjugated zinc phthalocyanine (core) to a biocompatible amphiphilic polymer called Brij 58 (a type of polyoxyethylene acyl ether) (shell), to create a novel compound for photodynamic therapy of psoriasis. Anti-psoriatic activity assessments in guinea pig psoriasis model suggested that treatment with the conjugate prompted an almost complete disappearance of the signs of psoriasis according to the histopathological investigation, compared to groups treated with saline, light alone, zinc phthalocyanine polymer conjugate alone, and the combination of light and zinc phthalocyanine polymer conjugate [357].

Summarising, although not many examples of nanomedicine and in particular Polymer Therapeutics have been so far reported for the topical treatment of psoriasis it is clear that a rational design and a control drug release at the adeaquate skin layer and correct cell type significantly improves psoriasis plaque and inflammation.

I.6. References

[1] J.B. Rothbard, S. Garlington, Q. Lin, T. Kirschberg, E. Kreider, P.L. McGrane, P.A. Wender, P.A. Khavari, Conjugation of arginine oligomers to cyclosporin A facilitates topical delivery and inhibition of inflammation, Nat Med 6(11) (2000) 1253-7.
[2] K. Sahu, M. Sharma, H. Bansal, A. Dube, P.K. Gupta, Topical photodynamic treatment with poly-L-lysine-chlorin p6 conjugate improves wound healing by reducing hyperinflammatory response in Pseudomonas aeruginosa-infected wounds of mice, Lasers Med Sci 28(2) (2012) 465-71.
[3] S. Mignani, S. El Kazzouli, M. Bousmina, J.P. Majoral, Expand classical drug administration ways by emerging routes using dendrimer drug delivery systems: a concise overview, Adv Drug Deliv Rev 65(10) (2013) 1316-30.
[4] Y. Ikumi, T. Kida, S. Sakuma, S. Yamashita, M. Akashi, Polymer-phloridzin conjugates as an anti-diabetic drug that inhibits glucose absorption through the Na+/glucose cotransporter (SGLT1) in the small intestine, J Control Release 125(1) (2007) 42-9.
[5] M.J. Alonso, Nanomedicines for overcoming biological barriers, Biomed Pharmacother 58(3) (2004) 168-72.
[6] M.A. Islam, P. Bajracharya, S.K. Kang, C.H. Yun, E.M. Kim, H.J. Jeong, Y.J. Choi, E.B. Kim, C.S. Cho, Mucoadhesive alginate/poly (L-lysine)/thiolated alginate microcapsules for oral delivery of Lactobacillus salivarius 29, J Nanosci Nanotechnol 11(8) (2011) 7091-5.
[7] E. Blanco, H. Shen, M. Ferrari, Principles of nanoparticle design for overcoming biological barriers to drug delivery, Nat Biotechnol 33(9) (2015) 941-51.
[8] A.E. Nel, L. Mädler, D. Velegol, T. Xia, E.M. Hoek, P. Somasundaran, F. Klaessig, V. Castranova, M. Thompson, Understanding biophysicochemical interactions at the nano-bio interface, Nat Mater 8(7) (2009) 543-57.
[9] J. Keaney, M. Campbell, The dynamic blood-brain barrier, FEBS J 282(21) (2015) 4067-79.
[10] M. Picq, P. Chen, M. Perez, M. Michaud, E. Véricel, M. Guichardant, M. Lagarde, DHA metabolism: targeting the brain and lipoxygenation, Mol Neurobiol 42(1) (2010) 48-51.
[11] A. Lo Van, N. Sakayori, M. Hachem, M. Belkouch, M. Picq, M. Lagarde, N. Osumi, N. Bernoud-Hubac, Mechanisms of DHA transport to the brain and potential therapy to neurodegenerative diseases, Biochimie 130 (2016) 163-167.
[12] I. Canton, G. Battaglia, Endocytosis at the nanoscale, Chem Soc Rev 41 (2012) 2718-39.
[13] R. Duncan, S.C. Richardson, Endocytosis and intracellular trafficking as gateways for nanomedicine delivery: opportunities and challenges, Mol Pharm 9 (2012) 2380-402.
[14] J.G. Huang, T. Leshuk, F.X. Gu, Emerging nanomaterials for targeting subcellular organelles, Nano Today 6(5) (2011) 478-492.
[15] I.A. Khalil, K. Kogure, H. Akita, H. Harashima, Uptake pathways and subsequent intracellular trafficking in nonviral gene delivery, Pharmacol Rev 58(1) (2006) 32-45.
[16] O. Zagorodko, J.J. Arroyo-Crespo, V.J. Nebot, M.J. Vicent, Polypeptide-Based Conjugates as Therapeutics: Opportunities and Challenges, Macromol Biosci 17 (2017) 1600316.
[17] P.A.J. Kolarsick, M.A. Kolarsick, C. Goodwin, Anatomy and Physiology of the Skin, J Dermatol Nurses Assoc 3(4) (2011) 203-213.

[18] L.T. Agache P., Mac-Mary S., Fanian F., Humbert P. (2017) The Human Skin: An Overview. In: Humbert P., Fanian F., Maibach H., Agache P. (eds) Agache's Measuring the Skin. Springer, Cham.
[19] E. Proksch, J.M. Brandner, J.M. Jensen, The skin: an indispensable barrier, Exp Dermatol 17(12) (2008) 1063-72.
[20] E.N. Tessema, T. Gebre-Mariam, R.H.H. Neubert, J. Wohlrab, Potential Applications of Phyto-Derived Ceramides in Improving Epidermal Barrier Function, Skin Pharmacol Physiol 30(3) (2017) 115-138.
[21] A.P. Kowalczyk, K.J. Green, Structure, function, and regulation of desmosomes, Prog Mol Biol Transl Sci 116 (2013) 95-118.
[22] A. Morrow, T. Lechler, Studying cell biology in the skin, Mol Biol Cell 26(23) (2015) 4183-6.
[23] O. Akinduro, K. Sully, A. Patel, D.J. Robinson, A. Chikh, G. McPhail, K.M. Braun, M.P. Philpott, C.A. Harwood, C. Byrne, R.F.L. O'Shaughnessy, D. Bergamaschi, Constitutive Autophagy and Nucleophagy during Epidermal Differentiation, J Invest Dermatol 136(7) (2016) 1460-1470.
[24] D.J. Tobin, Biochemistry of human skin--our brain on the outside, Chem Soc Rev 35(1) (2006) 52-67.
[25] B. Wang, W. Yang, J. McKittrick, M.A. Meyers, Keratin: Structure, mechanical properties, occurrence in biological organisms, and efforts at bioinspiration, Prog Mater Sci 76 (2016) 229-318.
[26] J.M. Wierzbicka, M.A. Zmijewski, J. Antoniewicz, M. Sobjanek, A.T. Slominski, Differentiation of Keratinocytes Modulates Skin HPA Analog, J Cell Physiol 232(1) (2017) 154-66.
[27] G. Raju, N. Katiyar, S. Vadukumpully, S.A. Shankarappa, Penetration of gold nanoparticles across the stratum corneum layer of thick-Skin, J Dermatol Sci 89(2) (2017) 146-154.
[28] J. van Smeden, J.A. Bouwstra, Stratum Corneum Lipids: Their Role for the Skin Barrier Function in Healthy Subjects and Atopic Dermatitis Patients, Curr Probl Dermatol 49 (2016) 8-26.
[29] T. Egelrud, Desquamation in the stratum corneum, Acta Derm Venereol Suppl (Stockh) 208 (2000) 44-5.
[30] B.D. G.J.Tortora, Principles of Anatomy and Physiology.11th ed. John Willey and Sons, Inc USA. 2007. p. 575-93.
[31] M.A. Farage, K.W. Miller, P. Elsner, H.I. Maibach, Structural characteristics of the aging skin: a review, Cutan Ocul Toxicol 26(4) (2007) 343-57.
[32] R.E. Burgeson, A.M. Christiano, The dermal-epidermal junction, Curr Opin Cell Biol 9(5) (1997) 651-8.
[33] S.H. Hussain, B. Limthongkul, T.R. Humphreys, The biomechanical properties of the skin, Dermatol Surg 39(2) (2013) 193-203.
[34] M.-A. Bolzinger, S. Briançon, J. Pelletier, Y. Chevalier, Penetration of drugs through skin, a complex rate-controlling membrane, Curr Opin Colloid Interface Sci 17(3) (2012) 156-165.
[35] M.R. Prausnitz, R. Langer, Transdermal drug delivery, Nat Biotechnol 26(11) (2008) 1261-8.
[36] B. Kammerau, U. Klebe, A. Zesch, H. Schaefer, Penetration, permeation, and resorption of 8-methoxypsoralen. Comperative in vitro and in vivo studies after topical application of four standard preparations, Arch Dermatol Res 255(1) (1976) 31-42.

[37] U. Blume-Peytavi, L. Massoudy, A. Patzelt, J. Lademann, E. Dietz, U. Rasulev, N. Garcia Bartels, Follicular and percutaneous penetration pathways of topically applied minoxidil foam, Eur J Pharm Biopharm 76(3) (2010) 450-453.
[38] J. Lademann, F. Knorr, H. Richter, U. Blume-Peytavi, A. Vogt, C. Antoniou, W. Sterry, A. Patzelt, Hair follicles--an efficient storage and penetration pathway for topically applied substances. Summary of recent results obtained at the Center of Experimental and Applied Cutaneous Physiology, Charité -Universitätsmedizin Berlin, Germany, Skin Pharmacol Physiol 21(3) (2008) 150-5.
[39] N. Otberg, A. Teichmann, U. Rasuljev, R. Sinkgraven, W. Sterry, J. Lademann, Follicular penetration of topically applied caffeine via a shampoo formulation, Skin Pharmacol Physiol 20(4) (2007) 195-8.
[40] J. Hadgraft, Skin deep, Eur J Pharm Biopharm 58(2) (2004) 291-9.
[41] H. Trommer, R.H. Neubert, Overcoming the stratum corneum: the modulation of skin penetration. A review, Skin Pharmacol Physiol 19(2) (2006) 106-21.
[42] H. Schaefer, J. Lademann, The role of follicular penetration. A differential view, Skin Pharmacol Appl Skin Physiol 14 Suppl 1 (2001) 23-7.
[43] E.A. Genina, A.N. Bashkatov, Y.P. Sinichkin, V.I. Kochubey, N.A. Lakodina, G.B. Altshuler, V.V. Tuchin, In vitro and in vivo study of dye diffusion into the human skin and hair follicles, J Biomed Opt 7(3) (2002) 471-7.
[44] F. Knorr, J. Lademann, A. Patzelt, W. Sterry, U. Blume-Peytavi, A. Vogt, Follicular transport route--research progress and future perspectives, Eur J Pharm Biopharm 71(2) (2008) 173-80.
[45] T. Ogiso, T. Shiraki, K. Okajima, T. Tanino, M. Iwaki, T. Wada, Transfollicular drug delivery: penetration of drugs through human scalp skin and comparison of penetration between scalp and abdominal skins in vitro, J Drug Target 10(5) (2002) 369-78.
[46] A. Vogt, U. Blume-Peytavi, Biology of the human hair follicle. New knowledge and the clinical significance, Hautarzt 54(8) (2003) 692-8.
[47] A.L. Bunge, R.L. Cleek, A new method for estimating dermal absorption from chemical exposure: 2. Effect of molecular weight and octanol-water partitioning, Pharm Res 12(1) (1995) 88-95.
[48] G.B. Kasting, Kinetics of finite dose absorption through skin 1. Vanillylnonanamide, J Pharm Sci 90(2) (2001) 202-12.
[49] R.O. Potts, R.H. Guy, Predicting skin permeability, Pharm Res 9(5) (1992) 663-9.
[50] M.H. Abraham, F. Martins, Human skin permeation and partition: general linear free-energy relationship analyses, J Pharm Sci 93(6) (2004) 1508-23.
[51] M.D. Barratt, Quantitative structure-activity relationships for skin permeability, Toxicol In Vitro 9(1) (1995) 27-37.
[52] J.T. Chittenden, J.E. Riviere, Assessment of penetrant and vehicle mixture properties on transdermal permeability using a mixed effect pharmacokinetic model of ex vivo porcine skin, Biopharm Drug Dispos 37(7) (2016) 387-396.
[53] J. Wohlrab, Topical preparations and their use in dermatology, J Dtsch Dermatol Ges 14(11) (2016) 1061-1070.
[54] M.R Prausnitz, P.M. Elias, T.J. Franz, M. Schmuth, et al. Skin barrier and transdermal drug delivery. In: Bolognia JL, Jorizzo JL, Schaffer JV, editors. Dermatology, 3rd edn. Philadelphia, PA: Elsevier Saunders; 2012. pp. 2065–74.
[55] S.D.M. S.S. Jagannath, S.R. Bhanudas, Chemical penetration enhancers-a review, World J Pharmacy Pharma Sciences, 3(2) (2014) 1068-1080.
[56] B.M.a.S. Gulam Ahmed, S., Chemical permeation enhancement through skin, Int J Adv Res 3(8) (2015) 644-651.

[57] A.C. Williams, B.W. Barry, Penetration enhancers, Adv Drug Deliv Rev 56(5) (2012) 128-137.
[58] S.B.C. S. Saini, S.S. Agrawal, Recent development in penetration enhancers and techniques in transdermal drug delivery system, J. Adv. Pharm, (4) (2014) 31–40.
[59] J.C. Beastall, J. Hadgraft, C. Washington, Mechanism of action of Azone as a percutaneous penetration enhancer: Lipid bilayer fluidity and transition temperature effects, Int J Pharm 43(3) (1988) 207-213.
[60] J.W. Wiechers, R.A. de Zeeuw, Transdermal drug delivery: efficacy and potential applications of the penetration enhancer Azone, Drug Des Deliv 6(2) (1990) 87-100.
[61] M.I. Afouna, T.K. Fincher, A.A. Zaghloul, I.K. Reddy, Effect of Azone upon the in vivo antiviral efficacy of cidofovir or acyclovir topical formulations in treatment/prevention of cutaneous HSV-1 infections and its correlation with skin target site free drug concentration in hairless mice, Int J Pharm 253(1-2) (2003) 159-68.
[62] e.a. G.N. Sharma, Penetration Enhancement of Medicinal Agents, Int Res J Pharm, 3(5) (2012) 83-88.
[63] M.E. Lane, Skin penetration enhancers, Int J Pharm 447(1-2) (2013) 12-21.
[64] A.P. Funke, R. Schiller, H.W. Motzkus, C. Günther, R.H. Müller, R. Lipp, Transdermal delivery of highly lipophilic drugs: in vitro fluxes of antiestrogens, permeation enhancers, and solvents from liquid formulations, Pharm Res 19(5) (2002) 661-8.
[65] R.A. Tupker, J. Pinnagoda, J.P. Nater, The transient and cumulative effect of sodium lauryl sulphate on the epidermal barrier assessed by transepidermal water loss: inter-individual variation, Acta Derm Venereol 70(1) (1990) 1-5.
[66] L. Celleno, Topical urea in skincare: A review, Dermatol Ther 31(6) (2018) e12690.
[67] P. Gholam, C. Fink, I. Bosselmann, A.H. Enk, Retrospective analysis evaluating the effect of a keratolytic and physical pretreatment with salicylic acid, urea and curettage on the efficacy and safety of photodynamic therapy of actinic keratoses with methylaminolaevulinate, J Eur Acad Dermatol Venereol 30(4) (2016) 619-23.
[68] O. Wong, N. Tsuzuki, B. Nghiem, J. Kuehnhoff, T. Itoh, K. Masaki, J. Huntington, R. Konishi, J.H. Rytting, T. Higuchi, Unsaturated cyclic ureas as new non-toxic biodegradable transdermal penetration enhancers. II. Evaluation study, Int J Pharm 52(3) (1989) 191-202.
[69] A.C. Williams, B.W. Barry, Essential oils as novel human skin penetration enhancers, Int J Pharm 57(2) (1989) R7-R9.
[70] J. Li, X. Wang, T. Zhang, C. Wang, Z. Huang, X. Luo, Y. Deng, A review on phospholipids and their main applications in drug delivery systems, Asian J Pharm Sci 10(2) (2015) 81-98.
[71] K.B. Ita, J. Du Preez, M.E. Lane, J. Hadgraft, J. du Plessis, Dermal delivery of selected hydrophilic drugs from elastic liposomes: effect of phospholipid formulation and surfactants, J Pharm Pharmacol 59(9) (2007) 1215-22.
[72] Y. Wang, L.V. Allen, L.C. Li, Y.H. Tu, Iontophoresis of hydrocortisone across hairless mouse skin: investigation of skin alteration, J Pharm Sci 82(11) (1993) 1140-4.
[73] N.G. Turner, Y.N. Kalia, R.H. Guy, The effect of current on skin barrier function in vivo: recovery kinetics post-iontophoresis, Pharm Res 14(9) (1997) 1252-7.
[74] R.H. Guy, Y.N. Kalia, M.B. Delgado-Charro, V. Merino, A. López, D. Marro, Iontophoresis: electrorepulsion and electroosmosis, J Control Release 64(1-3) (2000) 129-32.
[75] Y.S. V. Mathur, and M.S. Rajput, Physical and chemical penetration enhancers in transdermal drug delivery system, Asian J. Pharmacol, (4) (2014) 173.

[76] A.K. Banga, S. Bose, T.K. Ghosh, Iontophoresis and electroporation: comparisons and contrasts, Int J Pharm 179(1) (1999) 1-19.
[77] V. Dhote, P. Bhatnagar, P.K. Mishra, S.C. Mahajan, D.K. Mishra, Iontophoresis: a potential emergence of a transdermal drug delivery system, Sci Pharm 80(1) (2012) 1-28.
[78] B.W. Barry, Novel mechanisms and devices to enable successful transdermal drug delivery, Eur J Pharm Sci 14(2) (2001) 101-14.
[79] M.J. Pikal, The role of electroosmotic flow in transdermal iontophoresis, Adv Drug Deliv Rev 46(1-3) (2001) 281-305.
[80] S. Mitragotri, D. Blankschtein, R. Langer, Transdermal drug delivery using low-frequency sonophoresis, Pharm Res 13(3) (1996) 411-20.
[81] R. Rao, S. Nanda, Sonophoresis: recent advancements and future trends, J Pharm Pharmacol 61(6) (2009) 689-705.
[82] J.J. Escobar-Chavez, D. Bonilla-Martinez, M.A. Villegas-Gonzalez, I.M. Rodriguez-Cruz, C.L. Dominguez-Delgado, The use of sonophoresis in the administration of drugs throughout the skin, J Pharm Pharm Sci 12(1) (2009) 88-115.
[83] S.N. Murthy, S.M. Sammeta, C. Bowers, Magnetophoresis for enhancing transdermal drug delivery: Mechanistic studies and patch design, J Control Release 148(2) (2010) 197-203.
[84] S.M. Sammeta, M.A. Repka, S. Narasimha Murthy, Magnetophoresis in combination with chemical enhancers for transdermal drug delivery, Drug Dev Ind Pharm 37(9) (2011) 1076-1082.
[85] A.R. Denet, R. Vanbever, V. Préat, Skin electroporation for transdermal and topical delivery, Adv Drug Deliv Rev 56(5) (2004) 659-74.
[86] I.H. Blank, R.J. Scheuplein, D.J. MacFarlane, Mechanism of percutaneous absorption. 3. The effect of temperature on the transport of non-electrolytes across the skin, J Invest Dermatol 49(6) (1967) 582-9.
[87] T.O. Klemsdal, K. Gjesdal, J.E. Bredesen, Heating and cooling of the nitroglycerin patch application area modify the plasma level of nitroglycerin, Eur J Clin Pharmacol 43(6) (1992) 625-8.
[88] T. Ogiso, T. Hirota, M. Iwaki, T. Hino, T. Tanino, Effect of temperature on percutaneous absorption of terodiline, and relationship between penetration and fluidity of the stratum corneum lipids, Int J Pharm 176(1) (1998) 63-72.
[89] P. Clarys, K. Alewaeters, A. Jadoul, A. Barel, R.O. Manadas, V. Preat, In vitro percutaneous penetration through hairless rat skin: influence of temperature, vehicle and penetration enhancers, Eur J Pharm Biopharm 46(3) (1998) 279-83.
[90] T.S. Shomaker, J. Zhang, M.A. Ashburn, A pilot study assessing the impact of heat on the transdermal delivery of testosterone, J Clin Pharmacol 41(6) (2001) 677-82.
[91] A.C. Sintov, I. Krymberk, D. Daniel, T. Hannan, Z. Sohn, G. Levin, Radiofrequency-driven skin microchanneling as a new way for electrically assisted transdermal delivery of hydrophilic drugs, J Control Release 89(2) (2003) 311-20.
[92] Y.-C. Kim, J.-H. Park, M.R. Prausnitz, Microneedles for drug and vaccine delivery, Adv Drug Deliv Rev 64(14) (2012) 1547-1568.
[93] M.R. Prausnitz, Microneedles for transdermal drug delivery, Adv Drug Deliv Rev 56(5) (2004) 581-7.
[94] S. Henry, D.V. McAllister, M.G. Allen, M.R. Prausnitz, Microfabricated microneedles: a novel approach to transdermal drug delivery, J Pharm Sci 87(8) (1998) 922-5.
[95] National centre for the replacement, refinement and reduction of animals in research. https://www.nc3rs.org.uk/the-3rs.

[96] E. Abd, S.A. Yousef, M.N. Pastore, K. Telaprolu, Y.H. Mohammed, S. Namjoshi, J.E. Grice, M.S. Roberts, Skin models for the testing of transdermal drugs, Clin Pharmacol 8 (2016) 163-176.
[97] J. Zhang, M. Sun, A. Fan, Z. Wang, Y. Zhao, The effect of solute–membrane interaction on solute permeation under supersaturated conditions, Int J Pharm 441(1) (2013) 389-394.
[98] G. Oliveira, J. Hadgraft, M.E. Lane, The role of vehicle interactions on permeation of an active through model membranes and human skin, Int J Cosmet Sci 34(6) (2012) 536-45.
[99] S.F. Ng, J.J. Rouse, F.D. Sanderson, G.M. Eccleston, The relevance of polymeric synthetic membranes in topical formulation assessment and drug diffusion study, Arch Pharm Res 35(4) (2012) 579-93.
[100] A.K. Dąbrowska, G.M. Rotaru, S. Derler, F. Spano, M. Camenzind, S. Annaheim, R. Stämpfli, M. Schmid, R.M. Rossi, Materials used to simulate physical properties of human skin, Skin Res Technol 22(1) (2015) 3-14.
[101] S. Küchler, K. Strüver, W. Friess, Reconstructed skin models as emerging tools for drug absorption studies, Expert Opin Drug Metab Toxicol 9(10) (2013) 1255-63.
[102] G.E. Flaten, Z. Palac, A. Engesland, J. Filipovic-Grcic, Z. Vanic, N. Skalko-Basnet, In vitro skin models as a tool in optimization of drug formulation, Eur J Pharm Sci 75 (2015) 10-24.
[103] S. Wartewig, R.H. Neubert, Pharmaceutical applications of Mid-IR and Raman spectroscopy, Adv Drug Deliv Rev 57(8) (2005) 1144-70.
[104] A. Tfayli, E. Guillard, M. Manfait, A. Baillet-Guffroy, Raman spectroscopy: feasibility of in vivo survey of stratum corneum lipids, effect of natural aging, Eur J Dermatol 22(1) (2012) 36-41.
[105] M. Forster, M.A. Bolzinger, G. Montagnac, S. Briancon, Confocal Raman microspectroscopy of the skin, Eur J Dermatol 21(6) (2011) 851-63.
[106] D.J. Moore, M.E. Rerek, Insights into the molecular organization of lipids in the skin barrier from infrared spectroscopy studies of stratum corneum lipid models, Acta Derm Venereol Suppl (Stockh) 208 (2000) 16-22.
[107] H.A. Ayala-Bravo, D. Quintanar-Guerrero, A. Naik, Y.N. Kalia, J.M. Cornejo-Bravo, A. Ganem-Quintanar, Effects of sucrose oleate and sucrose laureate on in vivo human stratum corneum permeability, Pharm Res 20(8) (2003) 1267-73.
[108] P. Karande, A. Jain, K. Ergun, V. Kispersky, S. Mitragotri, Design principles of chemical penetration enhancers for transdermal drug delivery, Proc Natl Acad Sci U S A 102(13) (2005) 4688-93.
[109] G. Mao, C.R. Flach, R. Mendelsohn, R.M. Walters, Imaging the distribution of sodium dodecyl sulfate in skin by confocal Raman and infrared microspectroscopy, Pharm Res 29(8) (2012) 2189-201.
[110] C.W. Freudiger, W. Min, B.G. Saar, S. Lu, G.R. Holtom, C. He, J.C. Tsai, J.X. Kang, X.S. Xie, Label-free biomedical imaging with high sensitivity by stimulated Raman scattering microscopy, Science 322(5909) (2008) 1857-61.
[111] R. Alvarez-Román, A. Naik, Y.N. Kalia, H. Fessi, R.H. Guy, Visualization of skin penetration using confocal laser scanning microscopy, Eur J Pharm Biopharm 58(2) (2004) 301-16.
[112] M. Mélot, P.D. Pudney, A.M. Williamson, P.J. Caspers, A. Van Der Pol, G.J. Puppels, Studying the effectiveness of penetration enhancers to deliver retinol through the stratum cornum by in vivo confocal Raman spectroscopy, J Control Release 138(1) (2009) 32-9.

[113] A.N.C. Anigbogu, A.C. Williams, B.W. Barry, H.G.M. Edwards, Fourier transform raman spectroscopy of interactions between the penetration enhancer dimethyl sulfoxide and human stratum corneum, Int J Pharm 125(2) (1995) 265-282.
[114] G. Zhang, C.R. Flach, R. Mendelsohn, Tracking the dephosphorylation of resveratrol triphosphate in skin by confocal Raman microscopy, J Control Release 123(2) (2007) 141-147.
[115] G. Zhang, D.J. Moore, K.B. Sloan, C.R. Flach, R. Mendelsohn, Imaging the Prodrug-to-Drug Transformation of a 5-Fluorouracil Derivative in Skin by Confocal Raman Microscopy, J Invest Dermatol 127(5) (2007) 1205-1209.
[116] A. Tfayli, O. Piot, F. Pitre, M. Manfait, Follow-up of drug permeation through excised human skin with confocal Raman microspectroscopy, Eur Biophys J 36(8) (2007) 1049-58.
[117] P.J. Caspers, H.A. Bruining, G.J. Puppels, G.W. Lucassen, E.A. Carter, In Vivo Confocal Raman Microspectroscopy of the Skin: Noninvasive Determination of Molecular Concentration Profiles, J Invest Dermatol 116(3) (2001) 434-442.
[118] L. Chrit, C. Hadjur, S. Morel, G. Sockalingum, G. Lebourdon, F. Leroy, M. Manfait, In vivo chemical investigation of human skin using a confocal Raman fiber optic microprobe, J Biomed Opt 10(4) (2005) 44007.
[119] P. Sjövall, L. Skedung, S. Gregoire, O. Biganska, F. Clément, G.S. Luengo, Imaging the distribution of skin lipids and topically applied compounds in human skin using mass spectrometry, Sci Rep 8(1) (2018) 16683.
[120] D. Bonnel, R. Legouffe, A.H. Eriksson, R.W. Mortensen, F. Pamelard, J. Stauber, K.T. Nielsen, MALDI imaging facilitates new topical drug development process by determining quantitative skin distribution profiles, Anal Bioanal Chem 410(11) (2018) 2815-2828.
[121] J.Y. Fang, Y.L. Leu, Prodrug strategy for enhancing drug delivery via skin, Curr Drug Discov Technol 3(3) (2006) 211-24.
[122] R. Saraceno, A. Chiricozzi, M. Gabellini, S. Chimenti, Emerging applications of nanomedicine in dermatology, Skin Res Technol 19(1) (2013) e13-9.
[123] F. Alexis, E. Pridgen, L.K. Molnar, O.C. Farokhzad, Factors affecting the clearance and biodistribution of polymeric nanoparticles, Mol Pharm 5(4) (2008) 505-15.
[124] A. Kumari, S.K. Yadav, S.C. Yadav, Biodegradable polymeric nanoparticles based drug delivery systems, Colloids Surf B Biointerfaces 75(1) (2009) 1-18.
[125] B. Baroli, Skin absorption and potential toxicity of nanoparticulate nanomaterials, J Biomed Nanotechnol 6(5) (2010) 485-96.
[126] L.A. DeLouise, Applications of Nanotechnology in Dermatology, J Invest Dermatol 132(3, Part 2) (2012) 964-975.
[127] R. Duncan, Polymer therapeutics as nanomedicines: new perspectives, Curr Opin Biotech 22(4) (2011) 492-501.
[128] A. Wicki, D. Witzigmann, V. Balasubramanian, J. Huwyler, Nanomedicine in cancer therapy: Challenges, opportunities, and clinical applications, J Control Release 200 (2015) 138-157.
[129] F. Dilnawaz, S. Acharya, S.K. Sahoo, Recent trends of nanomedicinal approaches in clinics, Int J Pharm 538(1) (2018) 263-278.
[130] N. Desai, V. Trieu, Z. Yao, L. Louie, S. Ci, A. Yang, C. Tao, T. De, B. Beals, D. Dykes, P. Noker, R. Yao, E. Labao, M. Hawkins, P. Soon-Shiong, Increased antitumor activity, intratumor paclitaxel concentrations, and endothelial cell transport of cremophor-free, albumin-bound paclitaxel, ABI-007, compared with cremophor-based paclitaxel, Clin Cancer Res 12(4) (2006) 1317-24.

[131] A.D. Bhatt, A.A. Ranade, A retrospective observational study of efficacy and safety of Genexol-PM, a novel Cremophor-free, polymeric micelle formulation of paclitaxel, in patients with solid tumours, Ann Oncol 27(suppl_9) (2016).
[132] T.E. Kubal, C. Salamanca, R.S. Komrokji, D.A. Sallman, K.L. Sweet, E. Padron, A.F. List, J.E. Lancet, Safety and feasibility of outpatient induction chemotherapy with CPX-351 in selected older adult patients with newly diagnosed AML, Clin Oncol 36(15_suppl) (2018) e19013-e19013.
[133] A. Thomas, B.A. Teicher, R. Hassan, Antibody–drug conjugates for cancer therapy, Lancet 17(6) (2016) e254-e262.
[134] E.M. Gordon, G.H. Cornelio, C.C. Lorenzo, J.P. Levy, R.A. Reed, L. Liu, F.L. Hall, First clinical experience using a 'pathotropic' injectable retroviral vector (Rexin-G) as intervention for stage IV pancreatic cancer, Int J Oncol 24(1) (2004) 177-85.
[135] R.W.G. Johnson, Sirolimus (Rapamune) in renal transplantation, Curr Opin Nephrol Hypertens 11(6) (2002) 603-607.
[136] M.P. Vinardell, M. Mitjans, Nanocarriers for Delivery of Antioxidants on the Skin, Cosmetics 2(4) (2015).
[137] M.J. Abla, A.K. Banga, Formulation of tocopherol nanocarriers and in vitro delivery into human skin, Int J Cosmet Sci 36(3) (2014) 239-46.
[138] W. Abramovits, P. Granowski, P. Arrazola, Applications of nanomedicine in dermatology: use of nanoparticles in various therapies and imaging, J Cosmet Dermatol 9(2) (2010) 154-9.
[139] W. Gao, Y. Chen, Y. Zhang, Q. Zhang, L. Zhang, Nanoparticle-based local antimicrobial drug delivery, Adv Drug Deliv Rev 127 (2018) 46-57.
[140] M. Rahman, S. Akhter, J. Ahmad, M.Z. Ahmad, S. Beg, F.J. Ahmad, Nanomedicine-based drug targeting for psoriasis: potentials and emerging trends in nanoscale pharmacotherapy, Expert Opin Drug Deliv 12(4) (2014) 635-52.
[141] B.C. Palmer, L.A. DeLouise, Nanoparticle-Enabled Transdermal Drug Delivery Systems for Enhanced Dose Control and Tissue Targeting, Molecules 21(12) (2016).
[142] B.D. Kurmi, P. Tekchandani, R. Paliwal, S.R. Paliwal, Transdermal Drug Delivery: Opportunities and Challenges for Controlled Delivery of Therapeutic Agents Using Nanocarriers, Curr Drug Metab 18(5) (2017) 481-495.
[143] A. Nasir, A. Friedman, Nanotechnology and the Nanodermatology Society, J Drugs Dermatol 9(7) (2010) 879-82.
[144] J.R. Antonio, C.R. Antônio, I.L. Cardeal, J.M. Ballavenuto, J.R. Oliveira, Nanotechnology in dermatology, An Bras Dermatol 89(1) (2014) 126-36.
[145] M.M. Abdel-Mottaleb, C. Try, Y. Pellequer, A. Lamprecht, Nanomedicine strategies for targeting skin inflammation, Nanomedicine 9(11) (2014) 1727-43.
[146] K. Embil, S. Nacht, The Microsponge® Delivery System (MDS): a topical delivery system with reduced irritancy incorporating multiple triggering mechanisms for the release of actives, J Microencapsul 13(5) (1996) 575-588.
[147] R. Duncan, R. Gaspar, Nanomedicine(s) under the microscope, Mol Pharm 8(6) (2011) 2101-41.
[148] R. Duncan, Polymer therapeutics: Top 10 selling pharmaceuticals — What next?, J Control Release 190 (2014) 371-380.
[149] R. Duncan, Polymer therapeutics at a crossroads? Finding the path for improved translation in the twenty-first century, J Drug Target 25(9-10) (2017) 759-780.
[150] S.P. Atkinson, Z. Andreu, M.J. Vicent, Polymer Therapeutics: Biomarkers and New Approaches for Personalized Cancer Treatment, J Pers Med 8(1) (2018).
[151] J.J. Arroyo-Crespo, A. Armiñán, D. Charbonnier, L. Balzano-Nogueira, F. Huertas-López, C. Martí, S. Tarazona, J. Forteza, A. Conesa, M.J. Vicent, Tumor

microenvironment-targeted poly-L-glutamic acid-based combination conjugate for enhanced triple negative breast cancer treatment, Biomaterials 186 (2018) 8-21.
[152] A. Armiñán, M. Palomino-Schätzlein, C. Deladriere, J.J. Arroyo-Crespo, S. Vicente-Ruiz, M.J. Vicent, A. Pineda-Lucena, Metabolomics facilitates the discrimination of the specific anti-cancer effects of free- and polymer-conjugated doxorubicin in breast cancer models, Biomaterials 162 (2018) 144-153.
[153] B. Newland, H. Newland, C. Werner, A. Rosser, W. Wang, Prospects for polymer therapeutics in Parkinson's disease and other neurodegenerative disorders, Prog Polym Sci 44 (2015) 79-112.
[154] F. Rodriguez-Otormin, A. Duro-Castano, I. Conejos-Sánchez, M.J. Vicent, Envisioning the future of polymer therapeutics for brain disorders, Wiley Interdiscip Rev Nanomed Nanobiotechnol 11(1) (2018) e1532.
[155] K. Rajender Reddy, M.W. Modi, S. Pedder, Use of peginterferon alfa-2a (40 KD) (Pegasys®) for the treatment of hepatitis C, Adv Drug Deliv Rev 54(4) (2002) 571-586.
[156] L. Lang, FDA Approves Cimzia to Treat Crohn's Disease, Gastroenterology 134(7) (2008) 1819.
[157] L.G. Donaruma, Synthetic biologically active polymers, Prog Polym Sci 4 (1975) 1-25.
[158] M.J. Vicent, H. Ringsdorf, R. Duncan, Polymer therapeutics: clinical applications and challenges for development, Adv Drug Deliv Rev 61(13) (2009) 1117-20.
[159] R. Duncan, The dawning era of polymer therapeutics, Nat Rev Drug Discov 2 (2003) 347-60.
[160] D.W. Pack, A.S. Hoffman, S. Pun, P.S. Stayton, Design and development of polymers for gene delivery, Nat Rev Drug Discov 4(7) (2005) 581-593.
[161] Y. Matsumura, K. Kataoka, Preclinical and clinical studies of anticancer agent-incorporating polymer micelles, Cancer Sci 100(4) (2009) 572-9.
[162] J.I. Hare, T. Lammers, M.B. Ashford, S. Puri, G. Storm, S.T. Barry, Challenges and strategies in anti-cancer nanomedicine development: An industry perspective, Adv Drug Deliv Rev 108 (2017) 25-38.
[163] R. Gaspar, R. Duncan, Polymeric carriers: Preclinical safety and the regulatory implications for design and development of polymer therapeutics, Adv Drug Deliv Rev 61(13) (2009) 1220-1231.
[164] M.Y. Chen, I.Y. Millwood, H. Wand, M. Poynten, M. Law, J.M. Kaldor, S. Wesselingh, C.F. Price, L.J. Clark, J.R. Paull, C.K. Fairley, A randomized controlled trial of the safety of candidate microbicide SPL7013 gel when applied to the penis, J Acquir Immune Defic Syndr 50(4) (2009) 375-80.
[165] W.B. Liechty, D.R. Kryscio, B.V. Slaughter, N.A. Peppas, Polymers for drug delivery systems, Annu Rev Chem Biomol Eng 1 (2010) 149-73.
[166] H. Maeda, J. Fang, T. Inutsuka, Y. Kitamoto, Vascular permeability enhancement in solid tumor: various factors, mechanisms involved and its implications, Int Immunopharmacol 3(3) (2003) 319-328.
[167] A.M. Jhaveri, V.P. Torchilin, Multifunctional polymeric micelles for delivery of drugs and siRNA, Front Pharmacol 5 (2014) 77.
[168] K. Greish, J. Fang, T. Inutsuka, A. Nagamitsu, H. Maeda, Macromolecular therapeutics: advantages and prospects with special emphasis on solid tumour targeting, Clin Pharmacokinet 42(13) (2003) 1089-105.
[169] M.K. Danquah, X.A. Zhang, R.I. Mahato, Extravasation of polymeric nanomedicines across tumor vasculature, Adv Drug Deliv Rev 63(8) (2011) 623-639.

[170] M.E.H. El-Sayed, A.S. Hoffman, P.S. Stayton, Smart polymeric carriers for enhanced intracellular delivery of therapeutic macromolecules, Expert Opin Biol Ther 5(1) (2005) 23-32.
[171] R. Duncan, Polymer conjugates as anticancer nanomedicines, Nat Rev Cancer 6 (2006) 688-701.
[172] a.T.K. H. Maeda, (1997) Metamorphosis of Neocarzinostatin to SMANCS: Chemistry, Biology, Pharmacology, and Clinical Effect of the First Prototype Anticancer Polymer Therapeutic. In: Maeda H., Edo K., Ishida N. (eds) Neocarzinostatin. Springer, Tokyo.
[173] F. Fuertges, A. Abuchowski, The clinical efficacy of poly(ethylene glycol)-modified proteins, J Control Release 11(1) (1990) 139-148.
[174] F.F. Davis, The origin of pegnology, Adv Drug Deliv Rev 54(4) (2002) 457-8.
[175] A. Abuchowski, J.R. McCoy, N.C. Palczuk, T. van Es, F.F. Davis, Effect of covalent attachment of polyethylene glycol on immunogenicity and circulating life of bovine liver catalase, J Biol Chem 252(11) (1977) 3582-6.
[176] e.a. R. Webster, (2009) PEG and PEG conjugates toxicity: towards an understanding of the toxicity of PEG and its relevance to PEGylated biologicals. In: Veronese F.M. (eds) PEGylated Protein Drugs: Basic Science and Clinical Applications. Milestones in Drug Therapy. Birkhäuser Basel.
[177] K. Knop, R. Hoogenboom, D. Fischer, U.S. Schubert, Poly(ethylene glycol) in drug delivery: pros and cons as well as potential alternatives, Angew Chem Int Ed Engl 49(36) (2010) 6288-308.
[178] G.L. Liua, Y.; Yangd, L.; Weia, Y.; Wangb, X.; Wangc, Z.; Tao, L., Cytotoxicity study of polyethylene glycol derivatives, RSC Adv 7 (2017) 18252-18259.
[179] I. Ekladious, Y.L. Colson, M.W. Grinstaff, Polymer–drug conjugate therapeutics: advances, insights and prospects, Nat Rev Drug Discov 18(4) (2019) 273-294.
[180] H. Ringsdorf, Structure and properties of pharmacologically active polymers, J Polymer Sci. Polymer Symp, (51) (1975) 135–153.
[181] J. Shi, P.W. Kantoff, R. Wooster, O.C. Farokhzad, Cancer nanomedicine: progress, challenges and opportunities, Nat Rev Cancer 17 (2016) 20.
[182] S.E. Stiriba, H. Frey, R. Haag, Dendritic polymers in biomedical applications: from potential to clinical use in diagnostics and therapy, Angew Chem Int Ed Engl 41(8) (2002) 1329-34.
[183] R. Duncan, M.J. Vicent, Polymer therapeutics-prospects for 21st century: the end of the beginning, Adv Drug Deliv Rev 65 (2013) 60-70.
[184] X. Pang, Y. Jiang, Q. Xiao, A.W. Leung, H. Hua, C. Xu, pH-responsive polymer-drug conjugates: Design and progress, J Control Release 222 (2015) 116-29.
[185] D.L. Stirland, J.W. Nichols, S. Miura, Y.H. Bae, Mind the gap: a survey of how cancer drug carriers are susceptible to the gap between research and practice, J Control Release 172(3) (2013) 1045-64.
[186] L.W. Seymour, D.R. Ferry, D. Anderson, S. Hesslewood, P.J. Julyan, R. Poyner, J. Doran, A.M. Young, S. Burtles, D.J. Kerr, C.R.C.P.I.I.I.C.T. committee, Hepatic drug targeting: phase I evaluation of polymer-bound doxorubicin, J Clin Oncol 20(6) (2002) 1668-76.
[187] L.W. Seymour, D.R. Ferry, D.J. Kerr, D. Rea, M. Whitlock, R. Poyner, C. Boivin, S. Hesslewood, C. Twelves, R. Blackie, A. Schatzlein, D. Jodrell, D. Bissett, H. Calvert, M. Lind, A. Robbins, S. Burtles, R. Duncan, J. Cassidy, Phase II studies of polymer-doxorubicin (PK1, FCE28068) in the treatment of breast, lung and colorectal cancer, Int J Oncol 34(6) (2009) 1629-36.

[188] J. Kopecek, P. Kopecková, T. Minko, Z. Lu, HPMA copolymer-anticancer drug conjugates: design, activity, and mechanism of action, Eur J Pharm Biopharm 50(1) (2000) 61-81.
[189] R. Duncan, Biological effects of soluble synthetic polymers as drug carriers, Crit Rev Ther Drug Carrier Syst 1(4) (1985) 281-310.
[190] C. Li, D.F. Yu, R.A. Newman, F. Cabral, L.C. Stephens, N. Hunter, L. Milas, S. Wallace, Complete regression of well-established tumors using a novel water-soluble poly(L-glutamic acid)-paclitaxel conjugate, Cancer Res 58(11) (1998) 2404-9.
[191] J.W. Singer, Paclitaxel poliglumex (XYOTAX™, CT-2103): A macromolecular taxane, J Control Release 109(1) (2005) 120-126.
[192] J. Homsi, G.R. Simon, C.R. Garrett, G. Springett, R. De Conti, A.A. Chiappori, P.N. Munster, M.K. Burton, S. Stromatt, C. Allievi, P. Angiuli, A. Eisenfeld, D.M. Sullivan, A.I. Daud, Phase I trial of poly-L-glutamate camptothecin (CT-2106) administered weekly in patients with advanced solid malignancies, Clin Cancer Res 13(19) (2007) 5855-61.
[193] M.E. Davis, Design and development of IT-101, a cyclodextrin-containing polymer conjugate of camptothecin, Adv Drug Deliv Rev 61(13) (2009) 1189-92.
[194] E. Pham, M.J. Birrer, S. Eliasof, E.G. Garmey, D. Lazarus, C.R. Lee, S. Man, U.A. Matulonis, C.G. Peters, P. Xu, C. Krasner, R.S. Kerbel, Translational impact of nanoparticle-drug conjugate CRLX101 with or without bevacizumab in advanced ovarian cancer, Clin Cancer Res 21(4) (2014) 808-18.
[195] H. Cabral, K. Kataoka, Progress of drug-loaded polymeric micelles into clinical studies, J Control Release 190 (2014) 465-76.
[196] F. Koizumi, M. Kitagawa, T. Negishi, T. Onda, S. Matsumoto, T. Hamaguchi, Y. Matsumura, Novel SN-38-incorporating polymeric micelles, NK012, eradicate vascular endothelial growth factor-secreting bulky tumors, Cancer Res 66(20) (2006) 10048-56.
[197] H. Uchino, Y. Matsumura, T. Negishi, F. Koizumi, T. Hayashi, T. Honda, N. Nishiyama, K. Kataoka, S. Naito, T. Kakizoe, Cisplatin-incorporating polymeric micelles (NC-6004) can reduce nephrotoxicity and neurotoxicity of cisplatin in rats, Br J Cancer 93(6) (2005) 678-87.
[198] J. Wotring, S. Countryman, F.N. Wallace, E.C. Strickland, O.T. Cummings, G.L. McIntire, Movantik™ and the Frequency of Positive Naloxone in Urine, J Anal Toxicol 42(3) (2017) e38-e40.
[199] S.D. Chipman, F.B. Oldham, G. Pezzoni, J.W. Singer, Biological and clinical characterization of paclitaxel poliglumex (PPX, CT-2103), a macromolecular polymer-drug conjugate, Int J Nanomedicine 1(4) (2006) 375-83.
[200] R. Duncan, Development of HPMA copolymer–anticancer conjugates: Clinical experience and lessons learnt, Adv Drug Deliv Rev 61(13) (2009) 1131-1148.
[201] N.J. Leong, D. Mehta, V.M. McLeod, B.D. Kelly, R. Pathak, D.J. Owen, C.J.H. Porter, L.M. Kaminskas, Doxorubicin Conjugation and Drug Linker Chemistry Alter the Intravenous and Pulmonary Pharmacokinetics of a PEGylated Generation 4 Polylysine Dendrimer in Rats, J Pharm Sci 107(9) (2018) 2509-2513.
[202] C.J. Cheng, G.T. Tietjen, J.K. Saucier-Sawyer, W.M. Saltzman, A holistic approach to targeting disease with polymeric nanoparticles, Nat Rev Drug Discov 14(4) (2015) 239-47.
[203] F.T. Tsai, Y. Wang, D.J. Darensbourg, Environmentally Benign CO2-Based Copolymers: Degradable Polycarbonates Derived from Dihydroxybutyric Acid and Their Platinum-Polymer Conjugates, J Am Chem Soc 138(13) (2016) 4626-33.
[204] A. Duro-Castano, J. Movellan, M.J. Vicent, Smart branched polymer drug conjugates as nano-sized drug delivery systems, Biomater Sci 3(10) (2015) 1321-34.

[205] C. Fasting, C.A. Schalley, M. Weber, O. Seitz, S. Hecht, B. Koksch, J. Dernedde, C. Graf, E.W. Knapp, R. Haag, Multivalency as a chemical organization and action principle, Angew Chem Int Ed Engl 51(42) (2012) 10472-98.
[206] A. Duro-Castano, V.J. Nebot, A. Niño-Pariente, A. Armiñán, J.J. Arroyo-Crespo, A. Paul, N. Feiner-Gracia, L. Albertazzi, M.J. Vicent, Capturing "Extraordinary" Soft-Assembled Charge-Like Polypeptides as a Strategy for Nanocarrier Design, Adv Mater 29(39) (2017).
[207] J.J. Arroyo-Crespo, et al., Anticancer activity driven by drug linker modification in a polyglutamic acid-based combination-drug conjugate. Adv Funct Mater, 28 (2018) 13.
[208] E. Gianasi, R.G. Buckley, J. Latigo, M. Wasil, R. Duncan, HPMA copolymers platinates containing dicarboxylato ligands. Preparation, characterisation and in vitro and in vivo evaluation, J Drug Target 10(7) (2002) 549-56.
[209] F. Kratz, U. Beyer, M.T. Schütte, Drug-polymer conjugates containing acid-cleavable bonds, Crit Rev Ther Drug Carrier Syst 16(3) (1999) 245-88.
[210] B. Apostolovic, S.P. Deacon, R. Duncan, H.A. Klok, Hybrid polymer therapeutics incorporating bioresponsive, coiled coil peptide linkers, Biomacromolecules 11(5) (2010) 1187-95.
[211] S. Iamsaard, F. Seidi, N. Dararatana, D. Crespy, Redox-Responsive Polymer with Self-Immolative Linkers for the Release of Payloads, Macromol Rapid Commun 39(12) (2018) e1800071.
[212] Y. Xie, T. Murray-Stewart, Y. Wang, F. Yu, J. Li, L.J. Marton, R.A. Casero, D. Oupický, Self-immolative nanoparticles for simultaneous delivery of microRNA and targeting of polyamine metabolism in combination cancer therapy, J Control Release 246 (2016) 110-119.
[213] G. Saito, J.A. Swanson, K.D. Lee, Drug delivery strategy utilizing conjugation via reversible disulfide linkages: role and site of cellular reducing activities, Adv Drug Deliv Rev 55(2) (2003) 199-215.
[214] A. Guiotto, M. Canevari, M. Pozzobon, S. Moro, P. Orsolini, F.M. Veronese, Anchimeric assistance effect on regioselective hydrolysis of branched PEGs: a mechanistic investigation, Bioorg Med Chem 12(19) (2004) 5031-5037.
[215] A. Patzelt, H. Richter, L. Dähne, P. Walden, K.H. Wiesmüller, U. Wank, W. Sterry, J. Lademann, Influence of the vehicle on the penetration of particles into hair follicles, Pharmaceutics 3(2) (2011) 307-14.
[216] R. Su, W. Fan, Q. Yu, X. Dong, J. Qi, Q. Zhu, W. Zhao, W. Wu, Z. Chen, Y. Li, Y. Lu, Size-dependent penetration of nanoemulsions into epidermis and hair follicles: implications for transdermal delivery and immunization, Oncotarget 8(24) (2017) 38214-38226.
[217] J. Vega, S. Ke, Z. Fan, S. Wallace, C. Charsangavej, C. Li, Targeting doxorubicin to epidermal growth factor receptors by site-specific conjugation of C225 to poly(L-glutamic acid) through a polyethylene glycol spacer, Pharm Res 20(5) (2003) 826-32.
[218] Y. Mochida, H. Cabral, K. Kataoka, Polymeric micelles for targeted tumor therapy of platinum anticancer drugs, Expert Opin Drug Deliv 14(12) (2017) 1423-1438.
[219] E. Fröhlich, The role of surface charge in cellular uptake and cytotoxicity of medical nanoparticles, Int J Nanomedicine 7 (2012) 5577-91.
[220] S. Behzadi, V. Serpooshan, W. Tao, M.A. Hamaly, M.Y. Alkawareek, E.C. Dreaden, D. Brown, A.M. Alkilany, O.C. Farokhzad, M. Mahmoudi, Cellular uptake of nanoparticles: journey inside the cell, Chem Soc Rev 46(14) (2017) 4218-4244.
[221] S. Nadel, N. Klein, R. Heyderman, M. Levin, Endotoxin antibody for sepsis in infants, Lancet 339(8794) (1992) 678.

[222] D. Fischer, T. Bieber, Y. Li, H.P. Elsässer, T. Kissel, A novel non-viral vector for DNA delivery based on low molecular weight, branched polyethylenimine: effect of molecular weight on transfection efficiency and cytotoxicity, Pharm Res 16(8) (1999) 1273-9.
[223] H. Lv, S. Zhang, B. Wang, S. Cui, J. Yan, Toxicity of cationic lipids and cationic polymers in gene delivery, J Control Release 114(1) (2006) 100-9.
[224] S.C. Shukla, A. Singh, A.K. Pandey, A. Mishra, Review on production and medical applications of ε-polylysine, Biochem Eng J 65 (2012) 70-81.
[225] M.V. Pimm, A.C. Perkins, S.J. Gribben, G. Mezö, D. Gaál, F. Hudecz, Gamma scintigraphy of 111In-labelled branched chain polypeptides (BCP) with a poly(L-lysine) backbone in mice with mammary carcinoma: effect of charge on biodistribution and tumour imaging potential, Ann Nucl Med 9(4) (1995) 247-51.
[226] S. Mitragotri, J. Lahann, Physical approaches to biomaterial design, Nat Mater 8(1) (2009) 15-23.
[227] S. Svenson, Clinical translation of nanomedicines, Curr Opin Solid St M 16(6) (2012) 287-294.
[228] S.A. Shaffer, C. Baker-Lee, J. Kennedy, M.S. Lai, P. de Vries, K. Buhler, J.W. Singer, In vitro and in vivo metabolism of paclitaxel poliglumex: identification of metabolites and active proteases, Cancer Chemother Pharmacol 59(4) (2006) 537-48.
[229] H.R. Kricheldorf, Polypeptides and 100 years of chemistry of alpha-amino acid N-carboxyanhydrides, Angew Chem Int Ed Engl 45(35) (2006) 5752-84.
[230] N. Hadjichristidis, H. Iatrou, M. Pitsikalis, G. Sakellariou, Synthesis of well-defined polypeptide-based materials via the ring-opening polymerization of alpha-amino acid N-carboxyanhydrides, Chem Rev 109(11) (2009) 5528-78.
[231] e.a. I. Conejos-Sánchez, A controlled and versatile NCA polymerization method for the synthesis of polypeptides. Polym Chem 4 (2013) 3182.
[232] B.D. Ulery, L.S. Nair, C.T. Laurencin, Biomedical Applications of Biodegradable Polymers, J Polym Sci B Polym Phys 49(12) (2011) 832-864.
[233] A. Duro-Castano, I. Conejos-Sánchez, J.M. Vicent, Peptide-Based Polymer Therapeutics, Polymers (Basel) 6 (2014) 515-551.
[234] M.E. Fox, S. Guillaudeu, J.M. Fréchet, K. Jerger, N. Macaraeg, F.C. Szoka, Synthesis and in vivo antitumor efficacy of PEGylated poly(l-lysine) dendrimer-camptothecin conjugates, Mol Pharm 6(5) (2009) 1562-72.
[235] L.V. Kiew, S.K. Cheong, K. Sidik, L.Y. Chung, Improved plasma stability and sustained release profile of gemcitabine via polypeptide conjugation, Int J Pharm 391(1-2) (2010) 212-20.
[236] M. Silva, N.L. Ricelli, O. El Seoud, C.S. Valentim, A.G. Ferreira, D.N. Sato, C.Q. Leite, E.I. Ferreira, Potential tuberculostatic agent: micelle-forming pyrazinamide prodrug, Arch Pharm (Weinheim) 339(6) (2006) 283-90.
[237] S. Karmaker, T.K. Saha, Y. Yoshikawa, H. Yasui, H. Sakurai, A novel drug delivery system for type 1 diabetes: Insulin-mimetic vanadyl-poly(γ-glutamic acid) complex, J Inorg Biochem 100(9) (2006) 1535-1546.
[238] A.C. Engler, A. Shukla, S. Puranam, H.G. Buss, N. Jreige, P.T. Hammond, Effects of side group functionality and molecular weight on the activity of synthetic antimicrobial polypeptides, Biomacromolecules 12(5) (2011) 1666-74.
[239] C.R. Cohen, J. Brown, A.B. Moscicki, E.A. Bukusi, J.R. Paull, C.F. Price, S. Shiboski, A phase I randomized placebo controlled trial of the safety of 3% SPL7013 Gel (VivaGel®) in healthy young women administered twice daily for 14 days, PLoS One 6(1) (2011) e16258.

[240] C.F. Price, D. Tyssen, S. Sonza, A. Davie, S. Evans, G.R. Lewis, S. Xia, T. Spelman, P. Hodsman, T.R. Moench, A. Humberstone, J.R. Paull, G. Tachedjian, SPL7013 Gel (VivaGel®) retains potent HIV-1 and HSV-2 inhibitory activity following vaginal administration in humans, PLoS One 6(9) (2011) e24095.
[241] M.J. Vicent, E. Pérez-Payá, Poly-L-glutamic acid (PGA) aided inhibitors of apoptotic protease activating factor 1 (Apaf-1): an antiapoptotic polymeric nanomedicine, J Med Chem 49(13) (2006) 3763-5.
[242] Xing T, Yang X, Wang F, Lai B, Y. L., Synthesis of polypeptide conjugated with near infrared fluorescence probe and doxorubicin for pH-responsive and image-guided drug delivery., J Mater Chem 22 (2012) 22290.
[243] V. Giménez, C. James, A. Armiñán, R. Schweins, A. Paul, M.J. Vicent, Demonstrating the importance of polymer-conjugate conformation in solution on its therapeutic output: Diethylstilbestrol (DES)-polyacetals as prostate cancer treatment, J Control Release 159(2) (2012) 290-301.
[244] A. Paul, C. James, R.K. Heenan, R. Schweins, Drug mimic induced conformational changes in model polymer-drug conjugates characterized by small-angle neutron scattering, Biomacromolecules 11(8) (2010) 1978-82.
[245] A.A. Khorasani, J.L. Weaver, C. Salvador-Morales, Closing the gap: accelerating the translational process in nanomedicine by proposing standardized characterization techniques, Int J Nanomedicine 9 (2014) 5729-51.
[246] P.-C. Lin, S. Lin, P.C. Wang, R. Sridhar, Techniques for physicochemical characterization of nanomaterials, Biotechnol Adv 32(4) (2014) 711-726.
[247] A. Nino-Pariente, V.J. Nebot, M.J. Vicent, Relevant Physicochemical Descriptors of "Soft Nanomedicines" to Bypass Biological Barriers, Curr Pharm Des 22(9) (2016) 1274-91.
[248] X. Pang, X. Yang, G. Zhai, Polymer-drug conjugates: recent progress on administration routes, Expert Opin Drug Deliv 11(7) (2014) 1075-86.
[249] A.C. Anselmo, Y. Gokarn, S. Mitragotri, Non-invasive delivery strategies for biologics, Nat Rev Drug Discov (2018).
[250] E.J. Oh, K. Park, K.S. Kim, J. Kim, J.-A. Yang, J.-H. Kong, M.Y. Lee, A.S. Hoffman, S.K. Hahn, Target specific and long-acting delivery of protein, peptide, and nucleotide therapeutics using hyaluronic acid derivatives, J Control Release 141(1) (2010) 2-12.
[251] E. Papakonstantinou, M. Roth, G. Karakiulakis, Hyaluronic acid: A key molecule in skin aging, Dermatoendocrinol 4(3) (2012) 253-8.
[252] J.A. Yang, E.S. Kim, J.H. Kwon, H. Kim, J.H. Shin, S.H. Yun, K.Y. Choi, S.K. Hahn, Transdermal delivery of hyaluronic acid -- human growth hormone conjugate, Biomaterials 33(25) (2012) 5947-54.
[253] S.R. Oakes, K.M. Haynes, M.J. Waters, A.C. Herington, G.A. Werther, Demonstration and localization of growth hormone receptor in human skin and skin fibroblasts, J Clin Endocrinol Metab 75(5) (1992) 1368-73.
[254] A. Tavakkol, J.T. Elder, C.E.M. Griffiths, K.D. Cooper, H. Talwar, G.J. Fisher, K.M. Keane, S.K. Foltin, J.J. Voorhees, Expression of Growth Hormone Receptor, Insulin-Like Growth Factor 1 (IGF-1) and IGF-1 Receptor mRNA and Proteins in Human Skin, J Invest Dermatol 99(3) (1992) 343-349.
[255] K.R. Pawar, R.J. Babu, Polymeric and lipid-based materials for topical nanoparticle delivery systems, Crit Rev Ther Drug Carrier Syst 27(5) (2010) 419-59.
[256] M.N.V. Ravi Kumar, A review of chitin and chitosan applications, React Funct Polym 46(1) (2000) 1-27.

[257] J.J. Biemer, Antimicrobial susceptibility testing by the Kirby-Bauer disc diffusion method, Ann Clin Lab Sci 3(2) (1973) 135-40.
[258] V. Pawar, M. Dhanka, R. Srivastava, Cefuroxime conjugated chitosan hydrogel for treatment of wound infections, Colloids Surf B Biointerfaces 173 (2018) 776-787.
[259] A. Filipowicz, S. Wołowiec, Bioconjugates of PAMAM dendrimers with trans-retinal, pyridoxal, and pyridoxal phosphate, Int J Nanomedicine 7 (2012) 4819-28.
[260] V.V.K. Venuganti, O.P. Perumal, Poly(amidoamine) dendrimers as skin penetration enhancers: Influence of charge, generation, and concentration, J Pharm Sci 98(7) (2009) 2345-2356.
[261] Y. Yang, S. Sunoqrot, C. Stowell, J. Ji, C.W. Lee, J.W. Kim, S.A. Khan, S. Hong, Effect of size, surface charge, and hydrophobicity of poly(amidoamine) dendrimers on their skin penetration, Biomacromolecules 13(7) (2012) 2154-62.
[262] S.A. Castleberry, M.A. Quadir, M.A. Sharkh, K.E. Shopsowitz, P.T. Hammond, Polymer conjugated retinoids for controlled transdermal delivery, J Control Release 262 (2017) 1-9.
[263] F.P. Bonina, C. Puglia, T. Barbuzzi, P. de Caprariis, F. Palagiano, M.G. Rimoli, A. Saija, In vitro and in vivo evaluation of polyoxyethylene esters as dermal prodrugs of ketoprofen, naproxen and diclofenac, Eur J Pharm Sci 14(2) (2001) 123-34.
[264] N.S.V. Capanema, A.A.P. Mansur, S.M. Carvalho, I.C. Carvalho, P. Chagas, L.C.A. de Oliveira, H.S. Mansur, Bioengineered carboxymethyl cellulose-doxorubicin prodrug hydrogels for topical chemotherapy of melanoma skin cancer, Carbohydr Polym 195 (2018) 401-412.
[265] M. Schmuth, S. Blunder, S. Dubrac, R. Gruber, V. Moosbrugger-Martinz, Epidermal barrier in hereditary ichthyoses, atopic dermatitis, and psoriasis, J Dtsch Dermatol Ges 13(11) (2015) 1119-23.
[266] C. Mattozzi, G. Paolino, A.G. Richetta, S. Calvieri, Psoriasis, vitamin D and the importance of the cutaneous barrier's integrity: An update, J Dermatol 43 (2016) 507-14.
[267] S.K. Raychaudhuri, E. Maverakis, S.P. Raychaudhuri, Diagnosis and classification of psoriasis, Autoimmun Rev 13 (2014) 490-5.
[268] D. Levine, A. Gottlieb, Evaluation and management of psoriasis: an internist's guide, Med Clin North Am 93(6) (2009) 1291-303.
[269] D.M. Pariser, J. Bagel, J.M. Gelfand, N.J. Korman, C.T. Ritchlin, B.E. Strober, A.S. Van Voorhees, M. Young, S. Rittenberg, M.G. Lebwohl, E.J. Horn, National Psoriasis Foundation clinical consensus on disease severity, Arch Dermatol 143(2) (2007) 239-42.
[270] S.P. Raychaudhuri, J. Gross, A comparative study of pediatric onset psoriasis with adult onset psoriasis, Pediatr Dermatol 17(3) (2000) 174-8.
[271] J. Takeshita, S. Grewal, S.M. Langan, N.N. Mehta, A. Ogdie, A.S. Van Voorhees, J.M. Gelfand, Psoriasis and comorbid diseases: Epidemiology, J Am Acad Dermatol 76(3) (2017) 377-390.
[272] R.I.a.K. Hartman, A.B. (2016) Clinical presentation of psoriasis and psoriatic arthritis. In: Warren R., Menter A. (eds) Handbook of Psoriasis and Psoriatic Arthritis. Adis, Cham.
[273] V.-P.M. Johnston A. (2018) Pustular Psoriasis. In: Wallach D., Valerio Marzano A. (eds) Neutrophilic Dermatoses. Springer, Cham.
[274] F.C. Eberle, J. Brück, J. Holstein, K. Hirahara, K. Ghoreschi, Recent advances in understanding psoriasis, F1000Res 5 (2016).
[275] M. Icen, C.S. Crowson, M.T. McEvoy, F.J. Dann, S.E. Gabriel, H. Maradit Kremers, Trends in incidence of adult-onset psoriasis over three decades: A population-based study, J Am Acad Dermatol 60(3) (2009) 394-401.

[276] G.K. Perera, P. Di Meglio, F.O. Nestle, Psoriasis, Annu Rev Pathol 7 (2012) 385-422.
[277] J.T. Elder, A.T. Bruce, J.E. Gudjonsson, A. Johnston, P.E. Stuart, T. Tejasvi, J.J. Voorhees, G.R. Abecasis, R.P. Nair, Molecular dissection of psoriasis: integrating genetics and biology, J Invest Dermatol 130(5) (2009) 1213-26.
[278] E.A. Brezinski, J.S. Dhillon, A.W. Armstrong, Economic Burden of Psoriasis in the United States: A Systematic Review, JAMA Dermatol 151(6) (2015) 651-8.
[279] D. Hägg, M. Eriksson, A. Sundström, M. Schmitt-Egenolf, The higher proportion of men with psoriasis treated with biologics may be explained by more severe disease in men, PLoS One 8(5) (2013) e63619.
[280] K. Kubota, Y. Kamijima, T. Sato, N. Ooba, D. Koide, H. Iizuka, H. Nakagawa, Epidemiology of psoriasis and palmoplantar pustulosis: a nationwide study using the Japanese national claims database, BMJ Open 5(1) (2015) e006450.
[281] Y.T. Chang, T.J. Chen, P.C. Liu, Y.C. Chen, Y.J. Chen, Y.L. Huang, J.S. Jih, C.C. Chen, D.D. Lee, W.J. Wang, M.W. Lin, H.N. Liu, Epidemiological study of psoriasis in the national health insurance database in Taiwan, Acta Derm Venereol 89(3) (2009) 262-6.
[282] C. Ryan, B. Kirby, Psoriasis is a systemic disease with multiple cardiovascular and metabolic comorbidities, Dermatol Clin 33(1) (2015) 41-55.
[283] E. Christophers, Comorbidities in psoriasis, Clin Dermatol 25(6) (2007) 529-534.
[284] H. Kobner, Zur Atiologie der Psoriasis, Vjschr Dermatol 3 (1876) 559.
[285] L. Fry, B.S. Baker, Triggering psoriasis: the role of infections and medications, Clin Dermatol 25(6) (2007) 606-615.
[286] S. Kumar, J. Han, T. Li, A.A. Qureshi, Obesity, waist circumference, weight change and the risk of psoriasis in US women, J Eur Acad Dermatol Venereol 27(10) (2012) 1293-8.
[287] H. Tagami, Triggering factors, Clin Dermatol 15(5) (1997) 677-685.
[288] A.R. Setty, G. Curhan, H.K. Choi, Obesity, waist circumference, weight change, and the risk of psoriasis in women: Nurses' Health Study II, Arch Intern Med 167(15) (2007) 1670-5.
[289] C. Zhou, X. Yu, D. Cai, C. Liu, C. Li, Role of corticotropin-releasing hormone and receptor in the pathogenesis of psoriasis, Med Hypotheses 73(4) (2009) 513-515.
[290] A.W. Evers, E.W. Verhoeven, F.W. Kraaimaat, E.M. de Jong, S.J. de Brouwer, J. Schalkwijk, F.C. Sweep, P.C. van de Kerkhof, How stress gets under the skin: cortisol and stress reactivity in psoriasis, Br J Dermatol 163(5) (2010) 986-91.
[291] L. Naldi, L. Peli, F. Parazzini, Association of early-stage psoriasis with smoking and male alcohol consumption: evidence from an Italian case-control study, Arch Dermatol 135(12) (1999) 1479-84.
[292] E. Adisen, S. Uzun, F. Erduran, M.A. Gurer, Prevalence of smoking, alcohol consumption and metabolic syndrome in patients with psoriasis, An Bras Dermatol 93(2) (2018) 205-211.
[293] E.D. Schadler, B. Ortel, S.L. Mehlis, Biologics for the primary care physician: Review and treatment of psoriasis, Dis Mon 65(3) (2018) 51-90.
[294] I.I. Roman, A.M. Constantin, M.E. Marina, R.I. Orasan, The role of hormones in the pathogenesis of psoriasis vulgaris, Clujul Med 89(1) (2016) 11-8.
[295] J.L. Melero, S. Andrades, L. Arola, A. Romeu, Deciphering psoriasis. A bioinformatic approach, J Dermatol Sci 89(2) (2018) 120-126.
[296] R.G. Langley, G.G. Krueger, C.E. Griffiths, Psoriasis: epidemiology, clinical features, and quality of life, Ann Rheum Dis 64 Suppl 2 (2005) ii18-23; discussion ii24-5.

[297] R. Gupta, M.G. Debbaneh, W. Liao, Genetic Epidemiology of Psoriasis, Curr Dermatol Rep 3(1) (2014) 61-78.
[298] R.C. Trembath, R.L. Clough, J.L. Rosbotham, A.B. Jones, R.D. Camp, A. Frodsham, J. Browne, R. Barber, J. Terwilliger, G.M. Lathrop, J.N. Barker, Identification of a major susceptibility locus on chromosome 6p and evidence for further disease loci revealed by a two stage genome-wide search in psoriasis, Hum Mol Genet 6(5) (1997) 813-20.
[299] R.P. Nair, P. Stuart, T. Henseler, S. Jenisch, N.V. Chia, E. Westphal, N.J. Schork, J. Kim, H.W. Lim, E. Christophers, J.J. Voorhees, J.T. Elder, Localization of psoriasis-susceptibility locus PSORS1 to a 60-kb interval telomeric to HLA-C, Am J Hum Genet 66(6) (2000) 1833-44.
[300] F. Capon, S. Semprini, B. Dallapiccola, G. Novelli, Evidence for interaction between psoriasis-susceptibility loci on chromosomes 6p21 and 1q21, Am J Hum Genet 65(6) (1999) 1798-800.
[301] C.D. Veal, R.L. Clough, R.C. Barber, S. Mason, D. Tillman, B. Ferry, A.B. Jones, M. Ameen, N. Balendran, S.H. Powis, A.D. Burden, J.N. Barker, R.C. Trembath, Identification of a novel psoriasis susceptibility locus at 1p and evidence of epistasis between PSORS1 and candidate loci, J Med Genet 38(1) (2001) 7-13.
[302] Y. Sun, J. Zhang, Z. Zhou, P. Wu, R. Huo, B. Wang, Z. Shen, H. Li, T. Zhai, B. Shen, X. Chen, N. Li, CCN1, a Pro-Inflammatory Factor, Aggravates Psoriasis Skin Lesions by Promoting Keratinocyte Activation, J Invest Dermatol 135(11) (2015) 2666-2675.
[303] N. Garzorz-Stark, K. Eyerich, Psoriasis Pathogenesis: Keratinocytes Are Back in the Spotlight, J Invest Dermatol 139(5) (2019) 995-996.
[304] A. Rendon, K. Schakel, Psoriasis Pathogenesis and Treatment, Int J Mol Sci 20(6) (2019).
[305] A.J. Cox, W. Watson, Histological variations in lesions of psoriasis, Arch Dermatol 106(4) (1972) 503-6.
[306] M. Gordon, W.C. Johnson, C.F. Burgoon, Histopathology and histochemistry of psoriasis. II. Dynamics of lesions during treatment, Arch Pathol 84(5) (1967) 443-50.
[307] F.O. Nestle, D.H. Kaplan, J. Barker, Psoriasis, N Engl J Med 361 (2009) 496-509.
[308] I.M. Leigh, H. Navsaria, P.E. Purkis, I.A. McKay, P.E. Bowden, P.N. Riddle, Keratins (K16 and K17) as markers of keratinocyte hyperproliferation in psoriasis in vivo and in vitro, Br J Dermatol 133(4) (1995) 501-11.
[309] M. Murphy, P. Kerr, J.M. Grant-Kels, The histopathologic spectrum of psoriasis, Clin Dermatol 25(6) (2007) 524-8.
[310] A. Di Cesare, P. Di Meglio, F.O. Nestle, The IL-23/Th17 Axis in the Immunopathogenesis of Psoriasis, J Invest Dermatol 129(6) (2009) 1339-1350.
[311] J. Kim, J.G. Krueger, The immunopathogenesis of psoriasis, Dermatol Clin 33(1) (2015) 13-23.
[312] A.T. Pietrzak, A. Zalewska, G. Chodorowska, D. Krasowska, A. Michalak-Stoma, P. Nockowski, P. Osemlak, T. Paszkowski, J.M. Roliński, Cytokines and anticytokines in psoriasis, Clin Chim Acta 394(1-2) (2008) 7-21.
[313] J.R. Chan, W. Blumenschein, E. Murphy, C. Diveu, M. Wiekowski, S. Abbondanzo, L. Lucian, R. Geissler, S. Brodie, A.B. Kimball, D.M. Gorman, K. Smith, R. de Waal Malefyt, R.A. Kastelein, T.K. McClanahan, E.P. Bowman, IL-23 stimulates epidermal hyperplasia via TNF and IL-20R2-dependent mechanisms with implications for psoriasis pathogenesis, J Exp Med 203(12) (2006) 2577-87.
[314] L. Grine, L. Dejager, C. Libert, R.E. Vandenbroucke, An inflammatory triangle in psoriasis: TNF, type I IFNs and IL-17, Cytokine Growth Factor Rev 26(1) (2014) 25-33.

[315] W.H. Boehncke, Etiology and Pathogenesis of Psoriasis, Rheum Dis Clin North Am 41(4) (2015) 665-75.
[316] J. Baliwag, D.H. Barnes, A. Johnston, Cytokines in psoriasis, Cytokine 73(2) (2015) 342-350.
[317] C. Albanesi, C. Scarponi, S. Pallotta, R. Daniele, D. Bosisio, S. Madonna, P. Fortugno, S. Gonzalvo-Feo, J.D. Franssen, M. Parmentier, O. De Pità, G. Girolomoni, S. Sozzani, Chemerin expression marks early psoriatic skin lesions and correlates with plasmacytoid dendritic cell recruitment, J Exp Med 206(1) (2008) 249-58.
[318] B.J. Nickoloff, F.O. Nestle, Recent insights into the immunopathogenesis of psoriasis provide new therapeutic opportunities, J Clin Invest 113 (2004) 1664-75.
[319] J. Gregorio, S. Meller, C. Conrad, A. Di Nardo, B. Homey, A. Lauerma, N. Arai, R.L. Gallo, J. Digiovanni, M. Gilliet, Plasmacytoid dendritic cells sense skin injury and promote wound healing through type I interferons, J Exp Med 207(13) (2010) 2921-30.
[320] M. Tohyama, L. Yang, Y. Hanakawa, X. Dai, Y. Shirakata, K. Sayama, IFN-alpha enhances IL-22 receptor expression in keratinocytes: a possible role in the development of psoriasis, J Invest Dermatol 132(7) (2012) 1933-5.
[321] L. Iversen, E. Dauden, S. Segaert, K. Freeman, S. Magina, D. Rigopoulos, D. Thaci, Reformulations of well-known active ingredients in the topical treatment of psoriasis vulgaris can improve clinical outcomes for patients, J Eur Acad Dermatol Venereol 31 (2017) 1271-1284.
[322] G.E. Flaten, Z. Palac, A. Engesland, J. Filipović-Grčić, Ž. Vanić, N. Škalko-Basnet, In vitro skin models as a tool in optimization of drug formulation, Eur J Pharm Sci 75 (2015) 10-24.
[323] R. Daniels, U. Knie, Galenics of dermal products--vehicles, properties and drug release, J Dtsch Dermatol Ges 5(5) (2007) 367-83.
[324] H. Zhai, H.I. Maibach, Occlusion vs. skin barrier function, Skin Res Technol 8(1) (2002) 1-6.
[325] E. Lémery, S. Briançon, Y. Chevalier, C. Bordes, T. Oddos, A. Gohier, M.-A. Bolzinger, Skin toxicity of surfactants: Structure/toxicity relationships, COLLOID SURF A PHYSICOCHEM ENG ASP 469 (2015) 166-179.
[326] M.H. Rustin, Long-term safety of biologics in the treatment of moderate-to-severe plaque psoriasis: review of current data, Br J Dermatol 167 Suppl 3 (2012) 3-11.
[327] A. Campanati, M. Orciani, S. Gorbi, F. Regoli, R. Di Primio, A. Offidani, Effect of biologic therapies targeting tumour necrosis factor-alpha on cutaneous mesenchymal stem cells in psoriasis, Br J Dermatol 167(1) (2012) 68-76.
[328] P.K. Patel, C.R. King, S.R. Feldman, Biologics and biosimilars, J Dermatol Treat 26(4) (2015) 299-302.
[329] J.G. Turbeville, N.U. Patel, L.A. Cardwell, E. Oussedik, S.R. Feldman, Recent Advances in Small Molecule and Biological Therapeutic Approaches in the Treatment of Psoriasis, Clin Pharmacol Ther 102(1) (2017) 70-85.
[330] J.E. Hawkes, T.C. Chan, J.G. Krueger, Psoriasis pathogenesis and the development of novel targeted immune therapies, J Allergy Clin Immunol 140 (2017) 645-653.
[331] M. Czarnecka-Operacz, A. Sadowska-Przytocka, The possibilities and principles of methotrexate treatment of psoriasis - the updated knowledge, Postepy Dermatol Alergol 31(6) (2014) 392-400.
[332] P. Schafer, Apremilast mechanism of action and application to psoriasis and psoriatic arthritis, Biochem Pharmacol 83(12) (2012) 1583-90.
[333] P. Rich, M. Gooderham, H. Bachelez, J. Goncalves, R.M. Day, R. Chen, J. Crowley, Apremilast, an oral phosphodiesterase 4 inhibitor, in patients with difficult-to-treat nail

and scalp psoriasis: Results of 2 phase III randomized, controlled trials (ESTEEM 1 and ESTEEM 2), J Am Acad Dermatol 74(1) (2016) 134-42.
[334] T. Soleymani, J.M. Vassantachart, J.J. Wu, Comparison of Guidelines for the Use of Cyclosporine for Psoriasis: A Critical Appraisal and Comprehensive Review, J Drugs Dermatol 15(3) (2016) 293-301.
[335] T. Pilkington, R.N. Brogden, Acitretin : A Review of its Pharmacology and Therapeutic Use, Drugs 43(4) (1992) 597-627.
[336] S. Dogra, S. Yadav, Acitretin in psoriasis: an evolving scenario, Int J Dermatol 53(5) (2014) 525-38.
[337] M. Nakamura, B. Farahnik, T. Bhutani, Recent advances in phototherapy for psoriasis, F1000Res 5 (2016).
[338] T. Wong, L. Hsu, W. Liao, Phototherapy in psoriasis: a review of mechanisms of action, J Cutan Med Surg 17(1) (2013) 6-12.
[339] F. Almutawa, L. Thalib, D. Hekman, Q. Sun, I. Hamzavi, H.W. Lim, Efficacy of localized phototherapy and photodynamic therapy for psoriasis: a systematic review and meta-analysis, Photodermatol Photoimmunol Photomed 31(1) (2015) 5-14.
[340] M.B. Koek, E. Buskens, H. van Weelden, P.H. Steegmans, C.A. Bruijnzeel-Koomen, V. Sigurdsson, Home versus outpatient ultraviolet B phototherapy for mild to severe psoriasis: pragmatic multicentre randomised controlled non-inferiority trial (PLUTO study), BMJ 338 (2009) b1542.
[341] T. Garg, G. Rath, A.K. Goyal, Nanotechnological approaches for the effective management of psoriasis, Artif Cells Nanomed Biotechnol 44(6) (2016) 1374-82.
[342] D. Joshi, T. Garg, A.K. Goyal, G. Rath, Development and Characterization of Novel Medicated Nanofibers Against Periodontitis, Curr Drug Deliv 12(5) (2015) 564-77.
[343] M.I. Siddique, H. Katas, M.C. Amin, S.F. Ng, M.H. Zulfakar, A. Jamil, In-vivo dermal pharmacokinetics, efficacy, and safety of skin targeting nanoparticles for corticosteroid treatment of atopic dermatitis, Int J Pharm 507(1-2) (2016) 72-82.
[344] e.a. E.C. Murphy, Nanotechnology for Psoriasis Therapy. Curr Derm Rep, (8) (2019) 14.
[345] H. Bessar, I. Venditti, L. Benassi, C. Vaschieri, P. Azzoni, G. Pellacani, C. Magnoni, E. Botti, V. Casagrande, M. Federici, A. Costanzo, L. Fontana, G. Testa, F.F. Mostafa, S.A. Ibrahim, M.V. Russo, I. Fratoddi, Functionalized gold nanoparticles for topical delivery of methotrexate for the possible treatment of psoriasis, Colloids Surf B Biointerfaces 141 (2016) 141-147.
[346] D. Crisan, K. Scharffetter-Kochanek, M. Crisan, S. Schatz, A. Hainzl, L. Olenic, A. Filip, L.A. Schneider, A. Sindrilaru, Topical silver and gold nanoparticles complexed with Cornus mas suppress inflammation in human psoriasis plaques by inhibiting NF-kappaB activity, Exp Dermatol 27(10) (2018) 1166-1169.
[347] H. Nemati, M.H. Ghahramani, R. Faridi-Majidi, B. Izadi, G. Bahrami, S.H. Madani, G. Tavoosidana, Using siRNA-based spherical nucleic acid nanoparticle conjugates for gene regulation in psoriasis, J Control Release 268 (2017) 259-268.
[348] R.K. Thapa, B.K. Yoo, Evaluation of the effect of tacrolimus-loaded liquid crystalline nanoparticles on psoriasis-like skin inflammation, J Dermatolog Treat 25(1) (2014) 22-5.
[349] U. Agrawal, M. Gupta, S.P. Vyas, Capsaicin delivery into the skin with lipidic nanoparticles for the treatment of psoriasis, Artif Cells Nanomed Biotechnol 43(1) (2015) 33-9.
[350] M. Ferreira, L. Barreiros, M.A. Segundo, T. Torres, M. Selores, S.A. Costa Lima, S. Reis, Topical co-delivery of methotrexate and etanercept using lipid nanoparticles: A

targeted approach for psoriasis management, Colloids Surf B Biointerfaces 159 (2017) 23-29.
[351] D.E. Discher, V. Ortiz, G. Srinivas, M.L. Klein, Y. Kim, D. Christian, S. Cai, P. Photos, F. Ahmed, Emerging applications of polymersomes in delivery: From molecular dynamics to shrinkage of tumors, Prog Polym Sci 32(8) (2007) 838-857.
[352] D.A. Christian, S. Cai, D.M. Bowen, Y. Kim, J.D. Pajerowski, D.E. Discher, Polymersome carriers: From self-assembly to siRNA and protein therapeutics, Eur J Pharm Biopharm 71(3) (2009) 463-474.
[353] L. Sun, Z. Liu, L. Wang, D. Cun, H.H.Y. Tong, R. Yan, X. Chen, R. Wang, Y. Zheng, Enhanced topical penetration, system exposure and anti-psoriasis activity of two particle-sized, curcumin-loaded PLGA nanoparticles in hydrogel, J Control Release 254 (2017) 44-54.
[354] K.L. Mao, Z.L. Fan, J.D. Yuan, P.P. Chen, J.J. Yang, J. Xu, D.L. ZhuGe, B.H. Jin, Q.Y. Zhu, B.X. Shen, Y. Sohawon, Y.Z. Zhao, H.L. Xu, Skin-penetrating polymeric nanoparticles incorporated in silk fibroin hydrogel for topical delivery of curcumin to improve its therapeutic effect on psoriasis mouse model, Colloids Surf B Biointerfaces 160 (2017) 704-714.
[355] D. Gabriel, T. Mugnier, H. Courthion, K. Kranidioti, N. Karagianni, M.C. Denis, M. Lapteva, Y. Kalia, M. Moller, R. Gurny, Improved topical delivery of tacrolimus: A novel composite hydrogel formulation for the treatment of psoriasis, J Control Release 242 (2016) 16-24.
[356] T. Wan, W. Pan, Y. Long, K. Yu, S. Liu, W. Ruan, J. Pan, M. Qin, C. Wu, Y. Xu, Effects of nanoparticles with hydrotropic nicotinamide on tacrolimus: permeability through psoriatic skin and antipsoriatic and antiproliferative activities, Int J Nanomedicine 12 (2017) 1485-1497.
[357] Y. Jin, X. Zhang, B. Zhang, H. Kang, L. Du, M. Li, Nanostructures of an amphiphilic zinc phthalocyanine polymer conjugate for photodynamic therapy of psoriasis, Colloids Surf B Biointerfaces 128 (2015) 405-409.

CHAPTER II

EX VIVO AND *IN VIVO* MODELS OF PSORIASIS: DISEASE PROGRESSION AND HISTOPATHOLOGICAL FEATURES

II.1. Antecedents and Background

Psoriasis, a human-specific and genetically heterogeneous autoimmune chronic inflammatory skin disease, currently lacks effective treatment options. At the histological level, psoriatic lesions present with acanthosis (thickened epidermis due to rapid keratinocyte proliferation), elongated epidermal rate ridges (epithelial extensions that project into the underlying connective tissue in both skin and mucous membranes), aberrant differentiation of keratinocytes, dilation of blood vessels in papillary dermis causing visible erythema (redness of the skin or mucous membranes), and elevated levels of inflammatory cell infiltration [1, 2]. During the last decade, our knowledge base regarding psoriasis pathogenesis has widened, leading to the development of accurate *ex vivo* and *in vivo* models.

Ex vivo models represent valuable research tools for investigations into psoriasis and are considered more relevant than *in vitro* research involving cell lines. Reconstructed epidermal models and *ex vivo* human skin models are the most relevant, and although both can test the topical application of different active agents at similar concentrations to real dosage conditions [3], the use of human skin from different types of surgeries (e.g., abdominal) is considered the most representative model to mimic the complexity and interactions in human physiology [4]. Reconstructed epidermal models do not include all human skin cell types as they develop from specific cell lines (keratinocytes and fibroblasts) and present with a more permeable stratum corneum [5, 6].

During the development of this thesis, we employed both models to evaluate the safety of the synthesized conjugates and their anti-inflammatory activity. We developed healthy reconstructed epidermal models following well-established methodologies that employed primary human keratinocytes and fibroblasts from juvenile foreskin [7, 8] through a collaboration with Prof. Sarah Hedtrich (University of British Columbia, Vancouver, Canada). To develop an inflammatory phenotype in the reconstructed epidermal models emulating characteristics of psoriatic skin, such as hyperproliferation [9], we added recombinant TNF-α to the culture medium to induce the release of pro-inflammatory cytokines to the culture medium. The assessment of the conjugates in these reconstructed epidermal models will be detailed in **Chapter IV**. We anticipate that the application of these models will provide complementary information to the *ex vivo* human skin models.

Concurrently, in our laboratory, we have developed *ex vivo* human skin models from skin explants from patients. The methodology involved in the development of *ex vivo* human skin model comprises the culture of skin samples in wells containing metal grid supports held over liquid culture medium, allowing epidermal exposure to air and contact of the dermis with the culture medium for several days. This approach enables the study of several parameters, including tissue viability, drug penetration, intradermal vaccination, photosafety evaluation, skin barrier repair, and genotoxicity [3, 6, 10-13].

Of note, *ex vivo* human skin models allow the development of inflammatory models through the application of bacterial lipopolysaccharide (LPS) and pro-inflammatory cytokines or mediators.

Inflammatory *ex vivo* skin models allow us to monitor the processes involved following activation of the immune system in healthy human skin [14], such as the release of pro-inflammatory cytokines or the increment in the thickness of the epidermis due to inflammatory processes. These models mimic the physiological characteristics of inflammatory skin diseases, such as psoriasis [15, 16], and therefore, allow the screening of anti-psoriatic drugs in topical treatments. *Ex vivo* human skin models also enable the testing of pharmaceutical products without the need for animals [17-19], thereby abiding by the *3R* principle [20]*: replacement* (replace the use of animals), *reduction* (reduce the number of animals), and *refinement* (minimize animal suffering). However, limited accessibility to skin biopsies, donor variability [4], and the lack a real immune system to mimic the features of an autoimmune disease such as psoriasis represent significant problems with *ex vivo* human skin models. Therefore, the application of *in vivo* models will complement the information obtained from the *ex vivo* models.

The development of *in vivo* preclinical mouse models may help us to understand the genetic and immune mechanisms contributing to disease development. Thus, any animal model developed must reflect the critical features of the human disease and respond similarly to previously developed psoriasis treatments [21].

Recent decades have seen the development and characterization of a wide range of mouse models of psoriasis, as described in **Figure II. 1**. The most representative models for the study of psoriasis are classified into three types: i) acute (inducible) [22-24], ii) genetically engineered (transgenic) [25-28], and iii) xenograft (humanized)

models [29, 30]. The advantages and limitations associated with each type of model highlight the complexity of mimicking multifactorial human diseases in animals [31].

We have developed and studied the features of an imiquimod (IMQ)-induced model of acute skin inflammation in immunocompetent (BALB/c) mice for the preclinical study of psoriasis. IMQ (or 1-(2-methylpropyl)-1H-imidazo[4,5-c] quinolin-4-amine) is an imidazoquinoline derivative with a small size and high hydrophobicity [32]. IMQ has displayed antiviral and antitumor activity in animal models, enhancing both the innate and the adaptive immune system [33].

Drugs like IMQ represent a new therapeutic approach to modify and enhance the immune response [34]. The first formulation of IMQ (Aldara^{TM} cream) was developed by 3M Pharmaceuticals, with IMQ 5% cream clinically applied to treat genital and perianal warts commonly caused by different viruses. Overall, patients tolerated this treatment well, with some measure of effectiveness observed [35, 36].

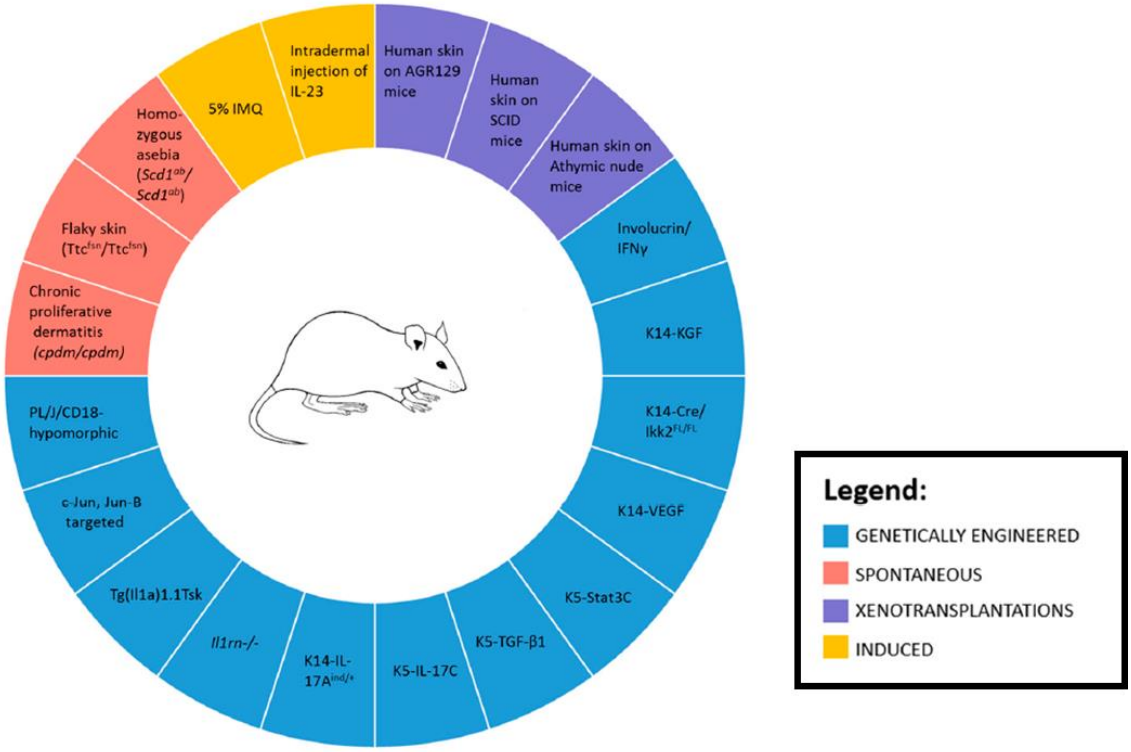

Figure II. 1: Summary of the major types of preclinical mouse models currently employed to study psoriasis. Adapted from [10].

Van der Fits *et al*. described the first use of IMQ to generate a psoriasis mouse model, establishing that the repeated application of IMQ produced phenotypic changes in the skin similar to psoriasis and modulated the IL-23/17 axis [37]. The primary mode of action of IMQ occurs through the activation of the Toll-like receptors (TLRs), with TLR7 specifically involved in psoriatic disease [38-40]. The TLR family is composed of ten human pathogen-recognition receptors (TLR-1-10) and represents a central component of the innate immune response, allowing cytokine synthesis in response to different stimuli [41]. Nevertheless, several studies have demonstrated that IMQ can activate other mechanisms independently of TLR7 signaling. For example, IMQ can antagonize A_{2A} adenosine receptors to diminish the activation of adenylyl cyclase and the accumulation of cyclic adenosine monophosphate (cAMP), thereby decreasing immunosuppression and promoting inflammation [42].

The IMQ mouse model of acute skin inflammation presents several advantages when compared to other model systems, including the straightforward application of IMQ (directly to the back of the mouse), the low costs compared to xenograft or knockout models, and the rapid induction of inflammation that reduces the treatment duration required to produce acute skin inflammation. However, there do exist limitations to this model, as the topical application of IMQ can produce a systemic inflammatory response and dehydration [39]. Moreover, the establishment of certain aspects of human psoriasis is limited due to the acute and non-chronic induction of the disease. Even given these limitations, the IMQ-induced psoriasis mouse model has rapidly become one of the most widely employed for the study of human psoriasis [43-45].

In this chapter, we focus on fully characterizing disease progression using an inflammatory *ex vivo* human skin model and an *in vivo* mice model of psoriasis. In the *ex vivo* model, we focus on the histopathological characteristics of the inflamed skin and the release of pro-inflammatory cytokines into the culture medium. The *in vivo* model provides information regarding disease progression during the seven days of IMQ application in immunocompetent mice, concentrating on the identification of functional features in the skin and the expression of pro-inflammatory cytokines considered crucial for disease development. Due to the fact that the application of IMQ cream produces acute rather than chronic inflammation, we also study the maintenance and progression of the disease for a further ten days after the IMQ application ceases to determine the optimum

time for subsequent studies into the application of different anti-psoriatic treatments (without the disappearance of the main features of the disease).

II.2. Results

II.2.1 *Ex Vivo* Human Skin Model

II.2.1.1. Characterization of *Ex Vivo* Human Skin Model

II.2.1.1.1. Tissue Viability Maintenance

We developed and characterized an *ex vivo* human skin model [46] and then assessed skin viability over 11 days using the MTT cell metabolic activity assay. The results revealed constant tissue viability from day 0 to day 4 in culture medium (**Figure II. 2**) [18]; however, we observed a marked decrease in tissue viability from day 4 to 7, after which point, tissue viability remained constant until day 11. These results indicate that keratinocytes within the *ex vivo* human skin model maintain their metabolic activity for the first 4 days, therefore mirroring the properties of healthy human body skin.

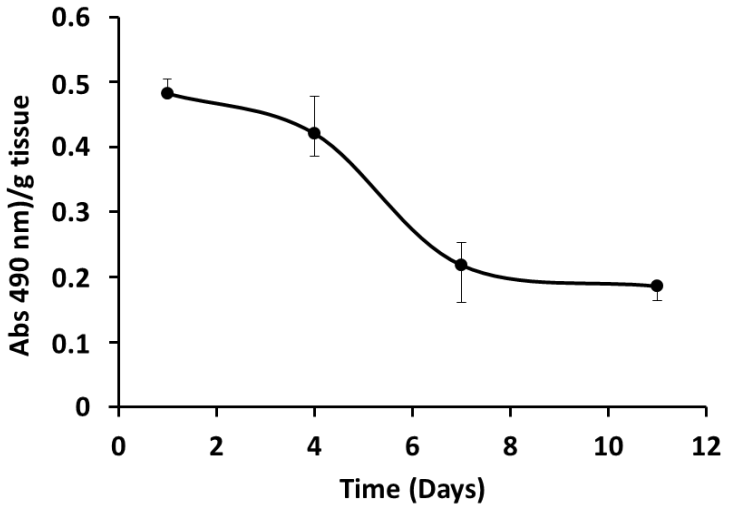

Figure II. 2: Tissue viability of skin samples in culture medium for 11 days by MTT assay (n=3).

II.2.1.1.2. Histological Features

Analysis of the histological features of the *ex vivo* human skin model also confirmed tissue viability during the experimental time in culture (**Figure II. 3**). Hematoxylin-Eosin (H&E) staining of skin samples (**Figure II. 3 – Top Row**) revealed the maintenance of skin structure and physiology for the 11 days in culture medium;

overall, the different skin layers appeared similar to day 0 at all other experimental time points. Furthermore, we observed a clear differentiation between the epidermis and the dermis layer at all times studied, without unwanted alterations such as tears or epidermal thickening.

Additionally, we established the presence of the Ki67 marker in keratinocytes at all studied times (**Figure II. 3 – Middle Row**), indicating the proliferative nature of these cells. Finally, we studied the expression of the cytokeratin (Ck) 5/6 basal cell marker in the epidermis (**Figure II. 3 – Bottom Row)** (Ck5 stabilizes the epidermis and Ck6 is considered as a hyperproliferative cytokeratin [47]), finding positive staining at all times under investigation. Again, this reinforces the adequate maintenance of morphology, proliferation, and the capacity for cytokeratin synthesis.

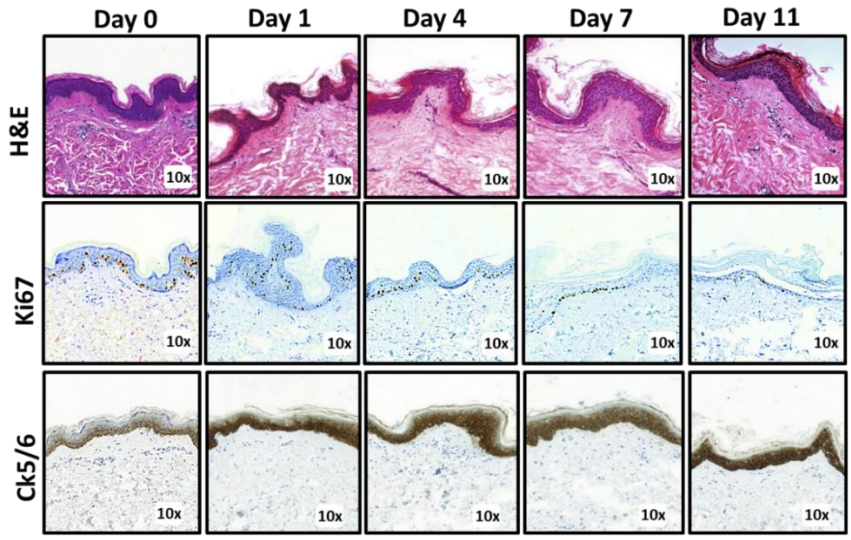

Figure II. 3: Histological features of the *ex vivo* human skin model by H&E staining (first row), Ki67 marker (second row) and Ck5/6 marker (third row). Original magnification displayed in each image was 10x. One representative picture is shown for each time point.

II.2.1.2. Characterization of Inflammatory *Ex Vivo* Human Skin Model

A combination of epidermal growth factor (EGF) and bacterial LPS in the culture medium in contact with the skin *ex vivo* can mimic the histological and biochemical features of psoriatic lesions [48]. Although this system lacks an immune system, the epidermal keratinocytes in such inflammatory model can produce and release pro-inflammatory cytokines to the culture medium in response to triggers, such as LPS. Moreover, the activity of EGF and the local inflammation produced by LPS produces an

increment of epidermal thickness, thereby imitating the typical ridges and hyperkeratosis that occur in psoriasis. Also, this inflammatory model offers complementary information to *in vitro* experiments and can provide results similar to those obtained from *in vivo* experiments.

Importantly, this model allows for the extensive evaluation of anti-psoriatic therapeutics after application on the skin. For example, penetrative capacity can be studied qualitatively and quantitatively with techniques including confocal microscopy, high-performance liquid chromatography (HPLC), or liquid chromatography-mass spectrometry (LCMS). Also, the model permits both the histological evaluation of epidermal thickness modulation and the assessment of anti-inflammatory capacity via quantification of the pro-inflammatory cytokines released to the culture medium.

In the following sections, we report the results of our exhaustive characterization of the developed inflammatory model to ensure the presence of psoriasis-like characteristics.

II.2.1.2.1. Maintenance of Tissue Viability Following Inflammation

We evaluated tissue viability after the addition of a combination of LPS and EGF in the culture medium to induce inflammation at 24 and 48 h by MTT assay. We maintained a constant concentration of EGF (2.5 ng/mL) but varied the level of LPS from 10 to 30 µg/mL at 24 h and from 10 to 15 µg/mL at 48 h (**Figure II. 4**).

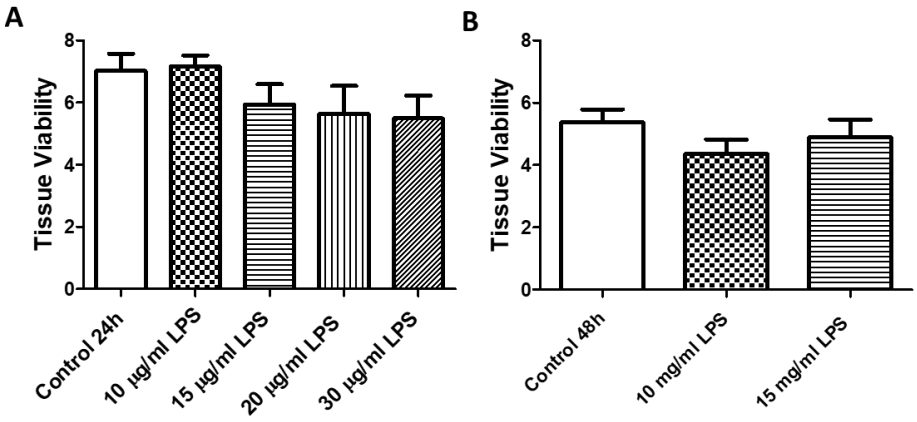

Figure II. 4: Tissue viability after the treatments with different concentrations of LPS (10 - 30 µg/mL) and a constant concentration of EGF (2.5 ng/mL) at 24 **(A)** and 48 h **(B)** in culture medium by MTT assay (n=3).

The results obtained suggest that tissue remains viable, with no significant differences observed between any combination of inflammatory insults and control. However, we do note the overall trend for a reduction in cell viability with the increasing levels of LPS at 24 h.

II.2.1.2.2. Inflammatory Features

We next assessed tissue viability after inflammatory insult by monitoring the histological modification of tissue over time. H&E staining for histomorphologic analysis revealed that the skin maintained its structure in response to the various inflammatory insults (**Figure II. 5A**). However, we observed a general increase in epidermal thickness in response to the combined action of the LPS and EGF, therefore suggesting that this inflammatory model mimics the features of skin suffering from inflammatory diseases as psoriasis.

We immunohistochemically studied keratinocyte viability (Ck5/6 marker) and proliferation (Ki67 marker) and assessed inflammation through the detection of typical pro-inflammatory cytokines and mediators, such as the IL-1b, INF-γ, and NF-kB. Analyses of Ck5/6 and Ki67 confirmed the viability and proliferation of the keratinocytes at all the concentrations of LPS and EGF tested. However, we failed to find significantly different levels of inflammation between the control and the treatments, perhaps due to the induction of inflammation in the control samples following the surgical procedures employed to isolate the samples (**Figure II. 5A**).

While keratinocytes are present in considerable numbers in the skin, there also exist other cell types such as fibroblasts (synthesis of fibers and maintenance of the extracellular tissue matrix), Langerhans cells (initiation and regulation of the immune response) and melanocytes (melanin synthesis). After treatment with the lowest concentrations (10 and 15 µg/mL of LPS) for 24 and 48 h, immunostaining with Hsp47 (fibroblasts) [49], langerin (Langerhans cells) and melanin A (melanocytes) markers revealed the presence of all three cell types described above in the skin. This finding suggests that treatment with LPS and EGF failed to influence other cells of the skin significantly, and therefore, the cellular viability of these cell types is not affected (**Figure II. 5B**).

Histologically, these findings indicate that the inflammatory insults employed do not affect the proliferative capacity, morphology, or cellular composition of the skin.

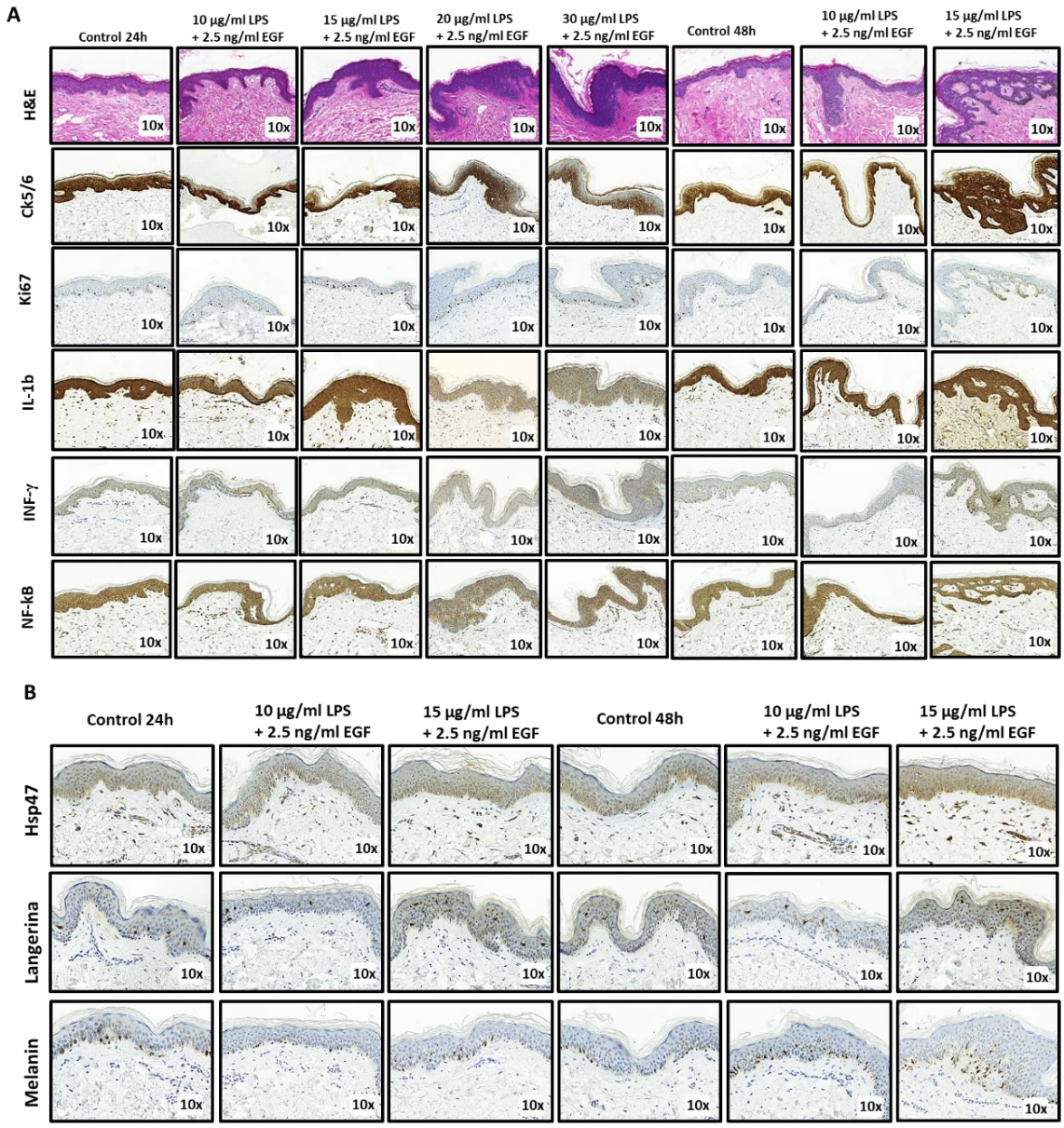

Figure II. 5: **(A)** H&E stained images (first row) of representative skin sections showing intact skin structure. Immunohistochemical staining of skin for Ck5/6 (second row) and Ki67 (third row) demonstrates the viability and proliferative capacity of keratinocytes. Positive cells for IL-1b (fourth row), INF-γ (fifth row), and NF-kB (sixth row) demonstrated the induction of inflammation (10x magnification). **(B)** Immunohistochemical staining of fibroblasts (first row), Langerhans cells (second row) and melanocytes (third row) provides evidence that the inflammatory insults employed failed to affect the cellular composition of the skin (10x magnification).

II.2.1.2.3. Quantification of Cytokine Release following Inflammatory Insult

To confirm the results obtained by histology, we assessed cytokine release after inflammatory insult to corroborate the establishment of the inflammatory model. We quantified the release of cytokines to the culture medium using a LUMINEX kit after inflammatory insult at 24 and 48 h. As shown in **Figure II. 6A**, the application of LPS at 10 and 15 µg/mL for 24 h led to a significant increase in the levels of the pro-inflammatory cytokines IL-1b and TNF-α, and the granulocyte macrophage colony stimulating factor (GM-CSF). In contrast, higher concentrations of LPS (20 and 30 µg/mL) failed to produce further increases in the release of pro-inflammatory cytokines and so studies at 48 h only employed 10 and 15 µg/mL of LPS (**Figure II. 6B**). Interestingly, we observed a trend for the increased expression of the INF-γ pro-inflammatory cytokine at 24 h, but we failed to observe a similar induction using 10 and 15 µg/mL of LPS at 48 h. At 48 h, as for 24 h, we observed a marked increase in the levels of IL-1b, TNF-α, and GM-CSF.

Moreover, we also assessed the release of IL-6, a key cytokine involved in the inflammatory processes, after induction with specific concentrations of LPS: 10, 15 and 20 µg/mL at 24 h and 15 µg/mL at 48 h (**Figure II. 6C**). Each inflammatory insult led to an increase in IL-6 when compared to the control – 4 times larger than control at 24 h and 15 - 20 times at 48 h.

Of note, we evaluated the levels of IL-10 anti-inflammatory cytokine [50] in the culture medium (**Figure II. 7**); the increased expression of the IL-10 after the inflammatory insult at 24 and 48 h indicates the development of inflammation in the skin, as the release of this cytokine counteracts the inflammatory response.

Summarizing, these results revealed that low concentrations of LPS lead to acute inflammation in the proposed *ex vivo* model without affecting tissue viability and morphology. Therefore, we performed further studies in this model using a final concentration of 15 µg/mL of LPS and 2.5 ng/mL of EGF.

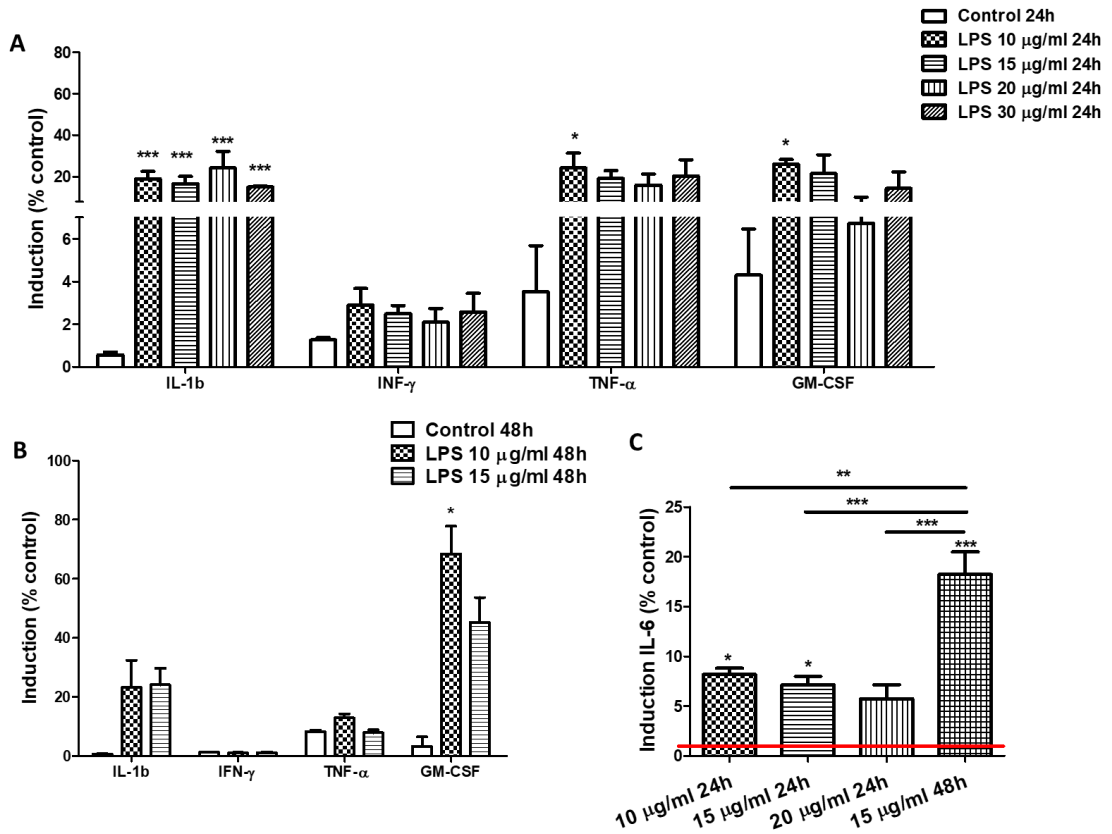

Figure II. 6: Quantification of pro-inflammatory cytokines released to the culture medium after 24 **(A)** and 48 h **(B)** of treatment with different concentrations of LPS (10 - 30 µg/mL) and a constant concentration of EGF (2.5 ng/mL). **(C)** Quantification of IL-6 released to the culture medium after 24 and 48 h of treatment with varying levels of LPS (10 - 20 µg/mL) and EGF (2.5 ng/mL). Asterisks indicate statistically significant differences after ANOVA analyses followed Bonferroni's post hoc tests, mean ± SEM. In all cases, we considered differences to be significant when p***<0.001; p**<0.01; p*<0.05.

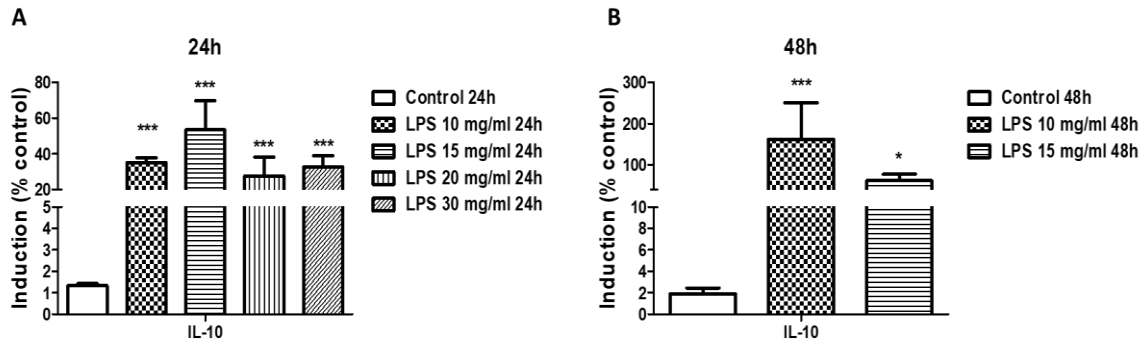

Figure II. 7: Quantification of IL-10 released to the culture medium after 24 **(A)** and 48 h **(B)** of treatment with different concentrations of LPS (10 - 30 µg/mL) and a constant concentration of EGF (2.5 ng/mL). Asterisks indicate statistically significant differences after ANOVA analyses followed Bonferroni's post hoc tests, mean ± SEM. In all cases, we considered differences to be significant when p***<0.001; p**<0.01; p*<0.05.

II.2.2 *In Vivo* Model of Psoriasis

II.2.2.1. Monitoring Safety during Disease Induction via Animal Weight

We applied IMQ cream for seven consecutive days to the mouse dorsal region and on the right ear, and then sacrificed animals at day 7, 10, 12, 14, and 17 following the first day of treatment with IMQ (**Figure II. 8A**). We evaluated IMQ cream safety by monitoring body weight and comparing observed values to those derived from healthy animals. We discovered that the application of IMQ cream for seven days produced a slight decrease in animal weight, whereas we observed a recovery in weight after the administration of the drug had terminated, eventually reaching the values observed at day 0 (**Figure II. 8B**).

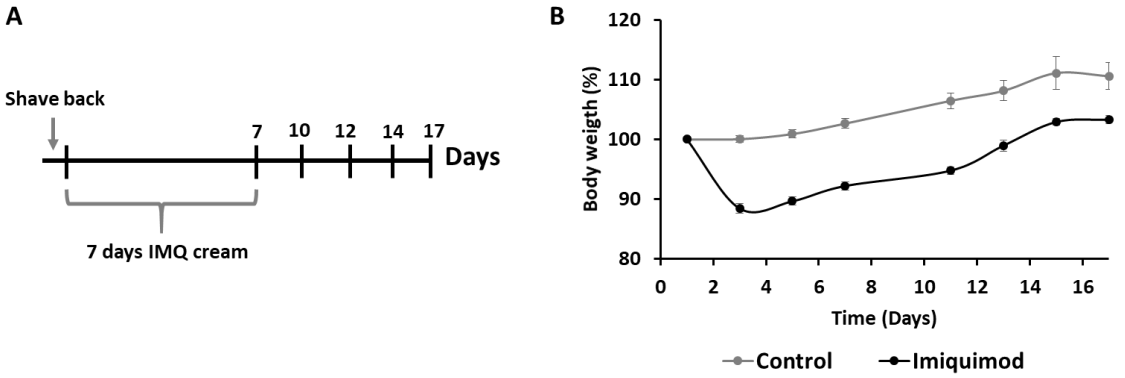

Figure II. 8: **(A)** General scheme of the establishment of the psoriatic model. **(B)** Mouse body weight measurement over time with no significant alterations in body weight. Animals recovered weight following the last day of application of the IMQ cream (day 7) with a 100% survival rate.

II.2.2.2. Evaluation of Inflammation: Back Morphology and PASI Score

Several studies have demonstrated that IMQ produces a robust immune response, inducing psoriasis-like inflammation by activating the production of immune cells via TLR activation and thereby mimicking the development of psoriatic features observed in mice [51, 52]. In our model, we stopped IMQ cream application after seven consecutive days of application and then monitored main psoriatic features.

At the gross morphological level, we observed the maximum level of erythema, scaling, and skin thickness on the back at day 7, which remained for up to 5 days later (day 12). After day 12, we observed a decrease in these characteristic disease parameters (**Figure II. 9**).

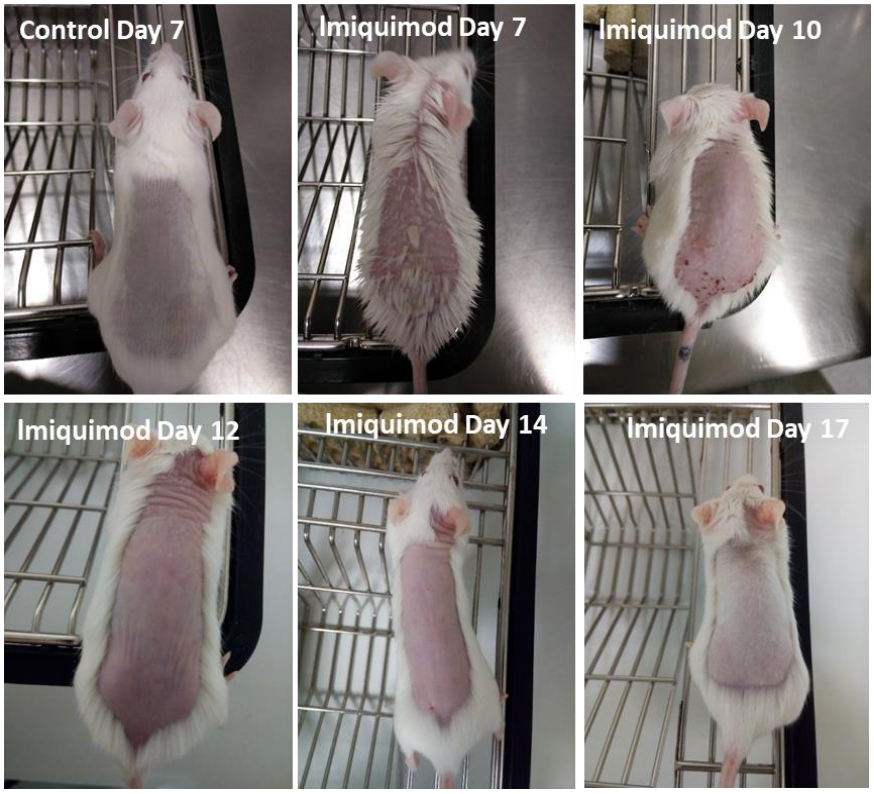

Figure II. 9: Morphological changes observed on the dorsal skin of the animals from 7 days of treatment with IMQ (day 7), in comparison with day 10, 12, 14 and 17 after the first dose of IMQ.

We assessed other key psoriatic features, including erythema, scaling, itching, and skin epidermal thickening, with the Psoriasis Area Severity Index (PASI) score. Doctors use this score to record psoriasis severity in the patients and is the most widely employed tool for measuring the psoriasis stage and evaluating the progress of people receiving psoriasis treatment. During the optimization stage of the psoriatic mice model, this score allowed us to appraise the appearance of the characteristics of the disease while applying IMQ cream (7 days) and their subsequent disappearance over time following the cessation of IMQ cream application.

PASI scoring from day 0 to day 17 revealed the expected progressive increase in score until 7 days of IMQ application (**Figure II. 10**). Examination of the back of the mouse every two days following the termination of IMQ treatment revealed a reduction in the signs of psoriasis, especially from day 12.

Overall, both the morphological and PASI parameters provided similar results in our IMQ-induced mouse model of psoriasis.

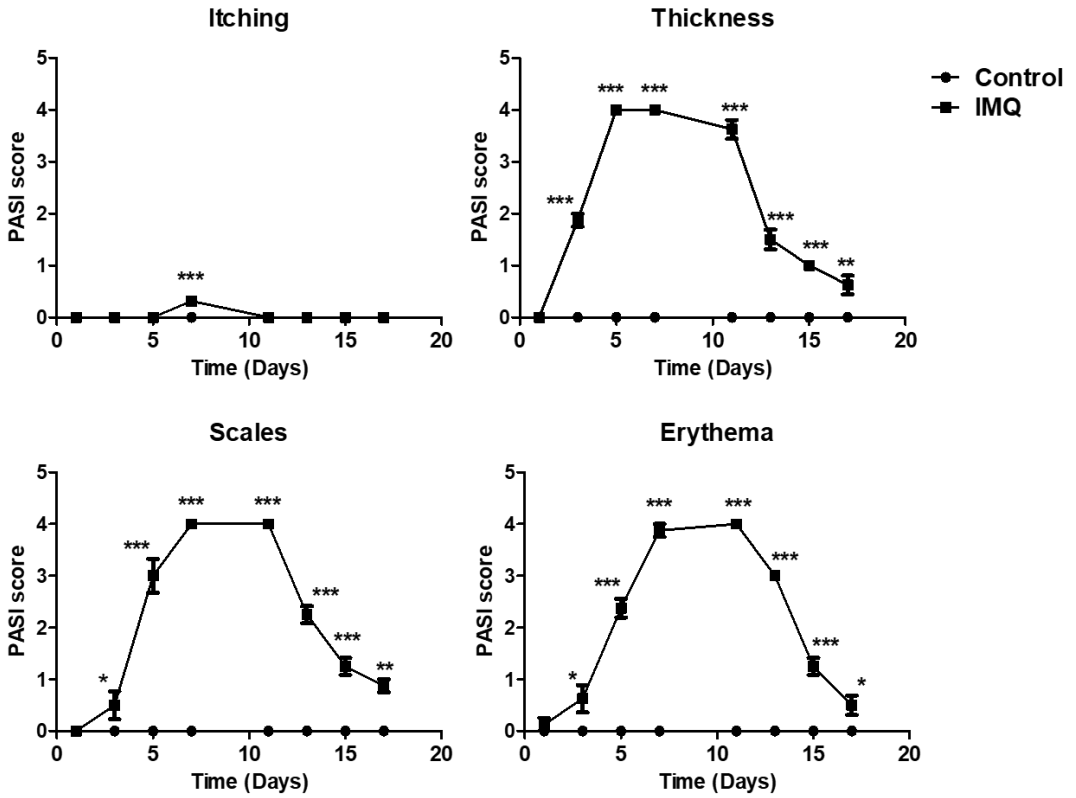

Figure II. 10: Severity of dorsal skin inflammation of the mouse indicted by PASI scoring (itching, thickness, scaling, and erythema) using a scale from 0 to 4. Asterisks indicate statistically significant differences after ANOVA analyses followed Bonferroni's post hoc tests (mean ± SEM displayed). In all cases, we considered differences to be significant when p***<0.001; p**<0.01; p*<0.05.

II.2.2.3. Increase in Ear Thickness

We measured ear thickness with a caliper every two days, discovering an increase in the thickness during the application of IMQ up to day seven (**Figure II. 11**). We found a significantly increased ear thickness at day five and day seven of IMQ treatment, and this remained until five days after the last application of IMQ (day 12) when compared to the contralateral untreated control ear. From day 12, we observed a decrease in the thickness of the IMQ-treated ear due to the disappearance of the inflammation produced by IMQ application.

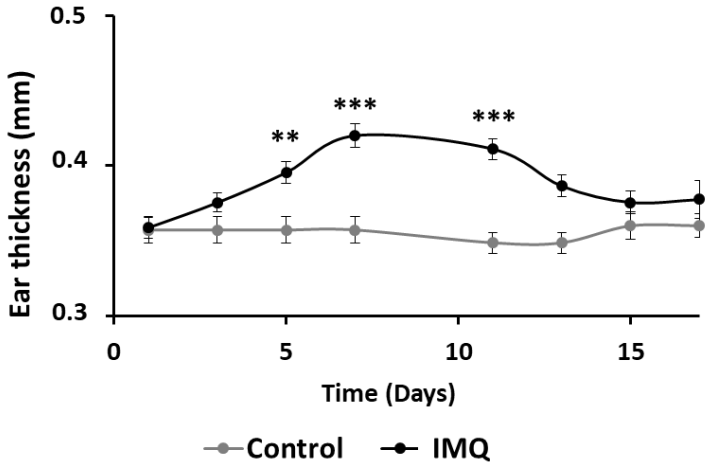

Figure II. 11: Ear thickness measurements every two days demonstrate IMQ-induced epidermal thickening. Asterisks indicate statistically significant differences after ANOVA analyses followed Bonferroni's post hoc tests (mean ± SEM displayed). In all cases, we considered differences to be significant when p***<0.001; p**<0.01; p*<0.05.

II.2.2.4. Histology of Ear and Back

Histological examination of the ears and back sections via H&E staining revealed a marked difference in epidermal thickening between the healthy control and the IMQ-treated mice (**Figure II. 12**). Right ear samples treated with IMQ cream displayed an increase in epidermal thickness that was maintained up to 12 days after the first application of IMQ (five days after the termination of IMQ treatment). However, analysis of samples from day 14 and day 17 revealed a slight decrease in epidermal thickness, although the differences remained pronounced when compared to the contralateral healthy ear.

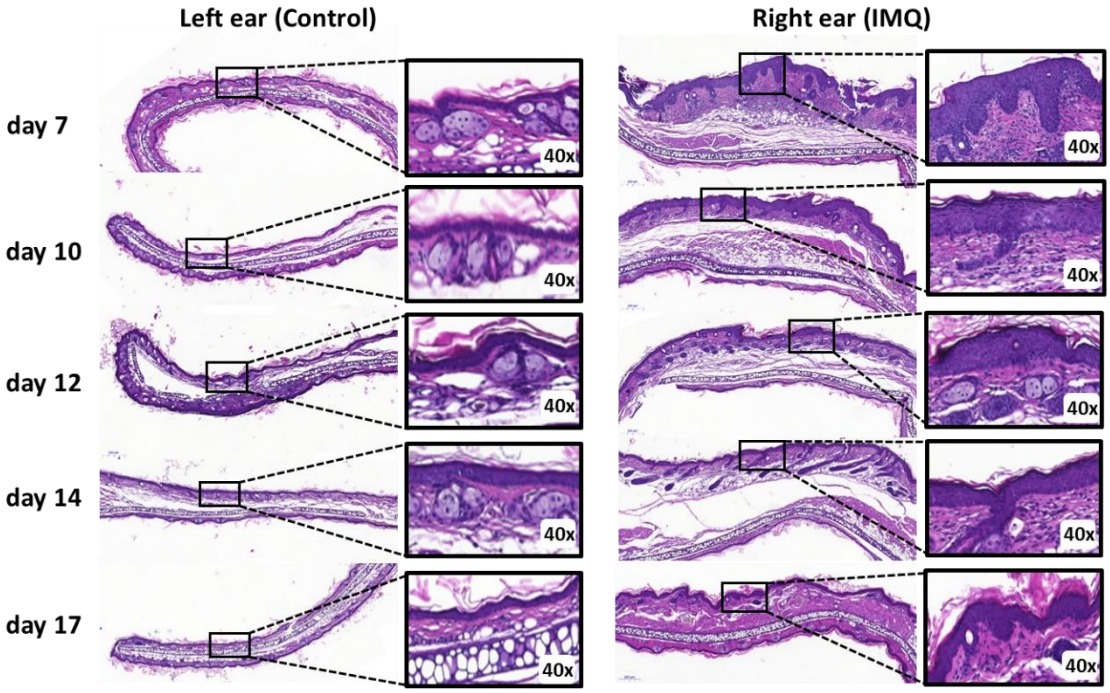

Figure II. 12: H&E staining of the ears in IMQ-treated mice. Original magnification displayed in each image was 10x. One representative picture is shown for each time point.

The histological examination of the dorsal skin of the IMQ-treated mouse revealed a similar pattern to the treated right ear. Analysis of back skin samples treated with IMQ until day seven revealed a considerable increase in epidermal thickness in comparison with healthy control. The thickening was maintained up to five days after the termination of treatment (day 12), although we observed decreases in epidermal thickness on days 14 and day 17 as the mouse recovered (**Figure II. 13**).

Both the ear and the back of the mice displayed marked epidermal hyperplasia and hyperkeratosis, evidencing increased epidermal growth in these lesions and thereby confirming the mimicry of histopathologic changes observed in human psoriasis [53].

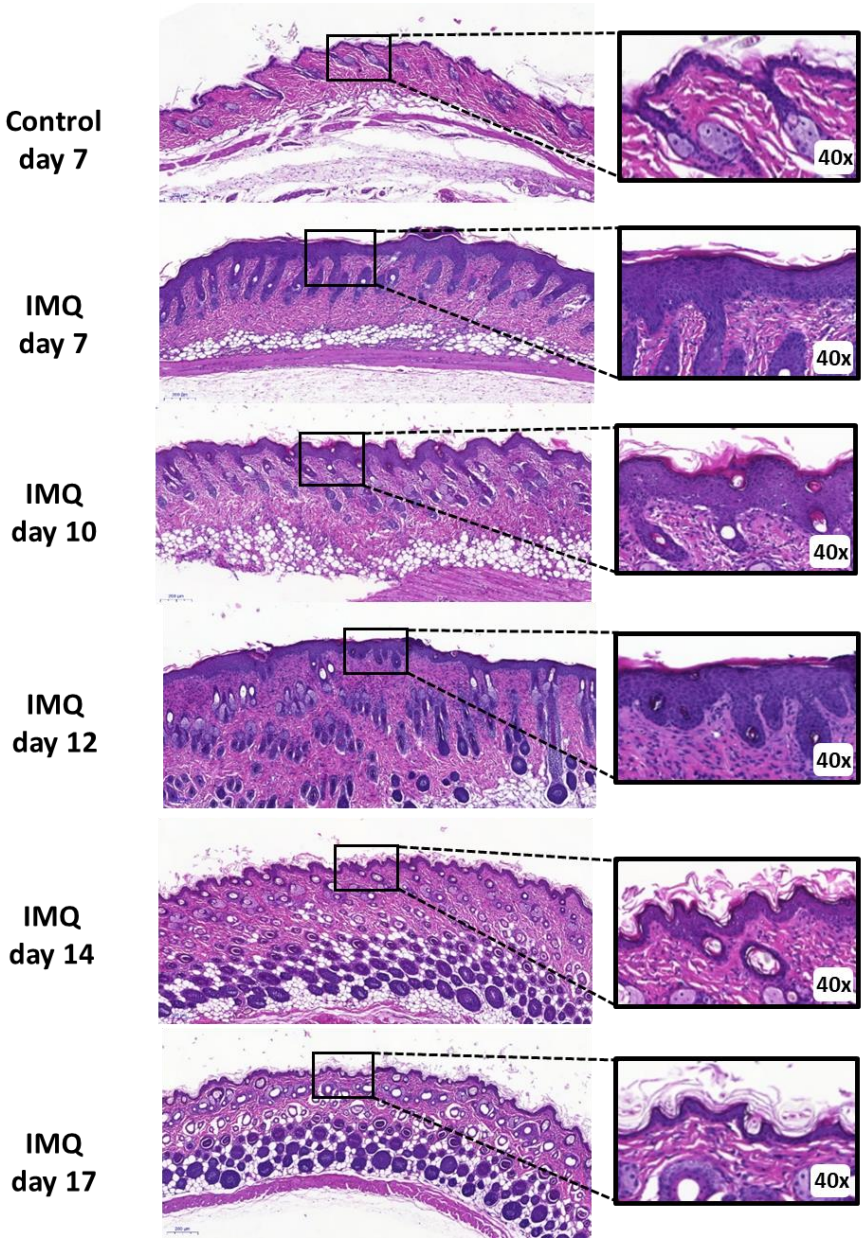

Figure II. 13: H&E staining of the dorsal skin in IMQ-treated mice. Original magnification displayed in each image is 10x. One representative picture is shown for each time point.

II.2.2.5. Increase in Spleen Weight

Several studies have reported that IMQ produces significant spleen enlargement and a general increase in weight due to the release of pro-inflammatory cytokines [37, 54, 55]. Our analyses revealed a considerable increase in spleen weight when compared to healthy control at days 7, 10, and 12 (0, 3, and 5 days after IMQ treatment termination) (**Figure II. 14**). The results demonstrated that the application of the IMQ cream in our

model produced a significant increase in spleen weight even at our experimental endpoint 17 days after the first application and 10 days after removal of IMQ treatment. This increase in spleen weight correlates to the known increase in the synthesis of pro-inflammatory cytokines in psoriasis.

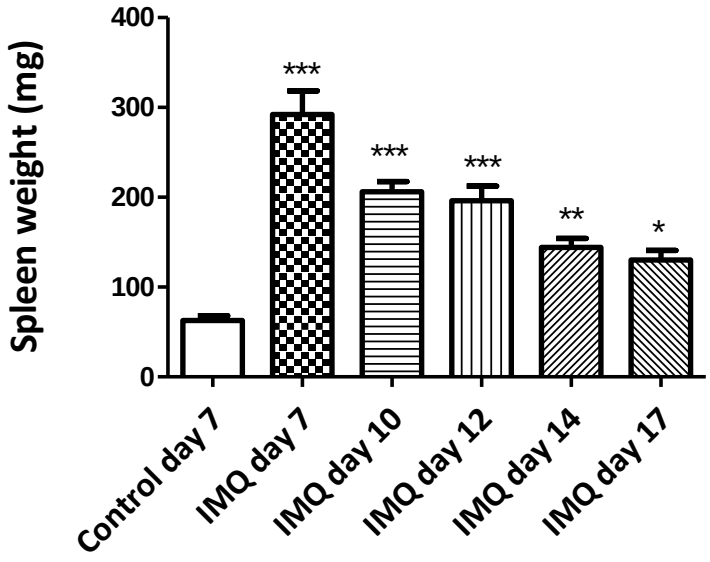

Figure II. 14: Spleen weight determined after treatment with IMQ cream. Analysis demonstrated significant increase when compared to the untreated control group. Asterisks indicate statistically significant differences after ANOVA analyses followed Bonferroni's post hoc tests, (results displayed as mean ± SEM). In all cases, we considered differences to be significant when p***<0.001; p**<0.01; p*<0.05.

II.2.2.6. Increased Pro-Inflammatory Cytokines Release in Serum and Tissue

IL-1b, IL-23, IL-17, INF-γ, and TNF-α act as major inflammatory mediators of psoriasis and are induced upon IMQ treatment [37, 56, 57]. We employed proteins extracted from frozen dorsal tissue and blood serum from IMQ treated and control animals to study IL-23 and INF-γ protein expression using a LUMINEX Kit according to the manufacturer's instructions.

Figure II. 15 depicts the levels of cytokines in dorsal tissue over the 17 days of the experiment. We observed a trend for maximal induction of cytokines levels on day seven (seven days of IMQ treatment) in comparison with healthy control mice. Following the cessation of IMQ cream application, we observed a general decrease in all cytokine

levels except for IL-23, whose expression increased significantly over time. Of note, IL-23 is a crucial cytokine for disease progression and maintenance in humans.

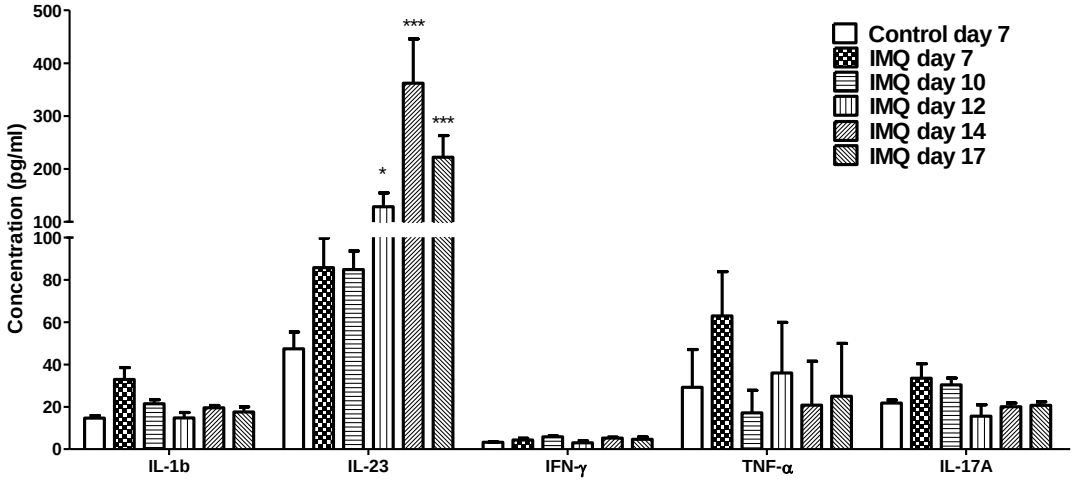

Figure II. 15: Induction of the synthesis of pro-inflammatory cytokines related to psoriasis in mouse dorsal skin tissue as measured by LUMINEX kit. Asterisks indicate statistically significant differences after ANOVA analyses followed Bonferroni's post hoc tests, results displayed as mean ± SEM. In all cases, we considered differences to be significant when p***<0.001; p**<0.01; p*<0.05.

We also assessed the levels of pro-inflammatory cytokines in serum only in the last day of the experiment (day 17). While we failed to observe the induction of IL-1b or IL-17a synthesis when compared to healthy controls, we observed significantly higher values of IL-23, INF-γ, and TNF-α in IMQ-treated animals when compared to healthy controls (**Figure II. 16**).

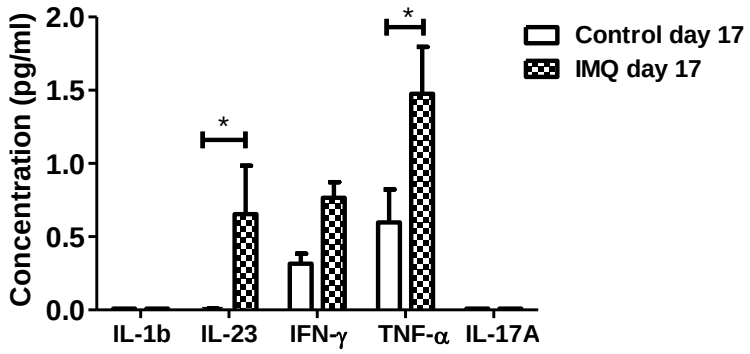

Figure II. 16: Induction of the synthesis of pro-inflammatory cytokines in serum related to psoriasis measured by LUMINEX kit. Asterisks indicate statistically significant differences after ANOVA analyses followed Bonferroni's post hoc tests, results displayed as mean ± SEM. In all cases, we considered differences to be significant when p***<0.001; p**<0.01; p*<0.05.

These results corroborate a robust immune response not only at the local level in the skin but also at the systemic level.

II.2.2.7. Hematological Parameters

The assessment of various hematological parameters can contribute to the detection of the systemic pathology development in psoriasis. We evaluated the levels of leukocytes, platelets, lymphocytes, and monocytes throughout the experimental time course. We observed specific alterations related to immune system status with significantly higher levels of leukocytes and monocytes after seven days of IMQ treatment (**Figure II. 17**).

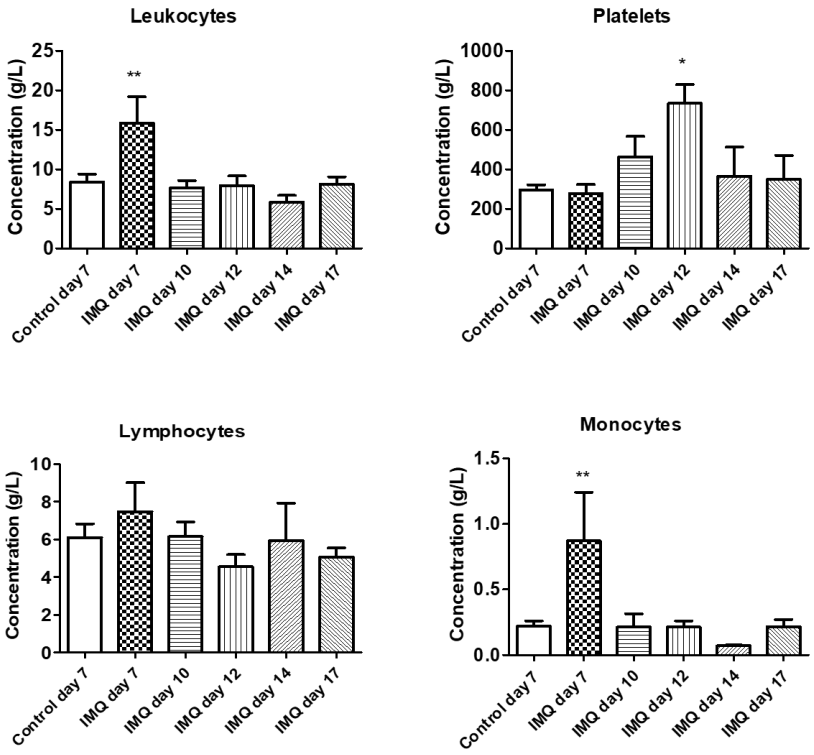

Figure II. 17: Complete hemogram of IMQ-induced psoriasis model. Asterisks indicate statistically significant differences after ANOVA analyses followed Bonferroni's post hoc tests, results displayed as mean ± SEM. In all cases, we considered differences to be significant when p***<0.001; p**<0.01; p*<0.05.

Both cell types are actively involved in the immune system [58] and, interestingly, monocyte-derived cells play a role in psoriasis development through the production of pro-inflammatory cytokines that increase the activation of skin-resident T cells [59].

However, we failed to observe significantly higher lymphocyte levels as expected from an autoimmune disease such as psoriasis.

Following the withdrawal of IMQ treatment, levels of leukocytes and monocytes reduced over time; however, we observed a peak in platelet production at day 12 (five days after IMQ withdrawal), perhaps due to the increase in the number of wounds that occur due to scaling and dryness of psoriatic skin.

II.3. Discussion

II.3.1. Inflammatory *Ex Vivo* Human Skin Model Mimics the Features of Psoriasis

The development of new models that lie between *in vitro* and *in vivo* methods allow the investigation of the structure and functions of healthy and diseased skin under conditions close to the *in vivo* situation. We have developed healthy and inflammatory *ex vivo* human skin models that ensure the maintenance of skin architecture and properties. The implementation of this inflammatory model plays a vital role throughout this thesis, as we can simulate the characteristics of the human psoriasis disease and, therefore, evaluate different therapeutic agents developed before moving to *in vivo* models.

Culturing skin with stimuli such as bacterial LPS and EGF represents a suitable means to induce skin inflammation. Histologically, we observed a marked increment in epidermal thickening, similar to that which occurs in psoriasis, without altering cell viability (including keratinocytes, fibroblasts, melanocytes, and Langerhans cells) and proliferation. Also, we failed to observe disruption to the stratum corneum, suggesting that the barrier function of the skin remains intact, thereby simulating the properties of human skin. Of note, LPS/EGF stimulation induced the secretion of pro-inflammatory cytokines to the culture medium, and depending on the concentration of LPS used, we can modulate the release of different cytokines involved in the pathology of psoriasis (e.g., IL-1b, IL-6, and GM-CSF) [14].

This *ex vivo* model provides a straightforward method for using human skin in tissue viability and drug penetration studies. Furthermore, this approach will also allow the rapid screening of drugs employed for the treatment of a range of skin diseases, including psoriasis, by evaluating the decrease in epidermal thickness and pro-inflammatory cytokines released to the culture medium.

II.3.2. Suitability of Imiquimod Cream for Psoriasis Development

While psoriasis is a uniquely human disease, a wide range of mouse models have been developed to mimic the main characteristics of the human condition, and these have allowed for the ever-widening understanding of disease pathology [21, 60]. However, the absence of animal models that reflect the intrinsic characteristics of the disease in humans remains a significant challenge to the development of new anti-psoriatic therapies [61]. Taking into consideration all currently available models, the *in vivo* IMQ-induced model [37, 43] has become the most straightforward model with the greatest potential for assessing the development of inflammatory skin diseases in humans [44, 51, 62, 63].

Although this model does not represent a chronic disease model, but rather an acute model of inflammation, IMQ-induced psoriasis in mice provides a powerful model with relevance to human psoriatic disease due to its simplicity, rapidity, and general applicability to different mouse strains [32, 64]. This simple model presents several features of human psoriatic skin lesions, such as the activation of plasmacytoid dendritic cells (pDCs) and the production of pro-inflammatory cytokines (IL-23, INF-γ, and TNF-α) [65].

However, we do note certain limitations of IMQ application; results following IMQ in different mouse strains have reached contradictory conclusions regarding the inflammatory and cellular mediators as well as the disease mechanism leading to the development of the psoriasis form phenotype [66].

II.3.3. H&E Staining as a Tool to Evaluate Skin Inflammation

The daily topical application of IMQ cream in mice for seven days led to inflamed skin lesions similar to psoriatic plaques and inflammatory cell activation, mimicking human psoriasis, in agreement with other studies [67]. IMQ functions through the ligation of TLR7 in mice [38] or TLR7 and TLR8 in humans [68], which then activates the STAT1 and STAT3 pathways required for optimal cytokine production by dendritic cells (DCs) [69]. The importance of STAT3 pathway activation in the pathogenesis of psoriasis was initially assessed through the use of transgenic mice [70]. The overexpression of STAT3 in keratinocytes through activation with IMQ triggered a psoriatic phenotype reproducing characteristic features of the disease, including parakeratosis, hyperkeratosis, and inflammatory cell infiltration. Moreover, the epidermal thickening caused by increased

keratinocyte proliferation reflects the increased mitotic activity within the basal layer [71, 72].

Histologically, the characteristics of our model include many hallmarks of human psoriasis, including acanthosis, hyperkeratosis, erythema, and desquamation, a phenomenon related to the hyperkeratosis that occurs in the stratum corneum after the application of IMQ cream. This phenotype has shown to be critically dependent on the IL-23/IL-17 axis in human psoriasis [37, 73] as in our mouse model.

II.3.4. Interleukin Levels as a Critical Biomarker of Psoriatic Progression

IMQ application affects both innate and acquired immunity [34], and our IMQ model displayed alterations to key immunological pathways and inflammatory cellular mediators present in the human disease [32]. As discussed above, IMQ is a ligand for TLR of macrophages, monocytes, and pDCs in mice [10], and therefore, TLR7 overexpression in macrophages and DCs can influence the development of an IMQ-induced mouse model of psoriasis.

Consequently, IMQ contributes to the strong activation of the immune system. Monocyte-derived cells (moDCs) and macrophages located in the dermis [74, 75] play a decisive role in the production of pro-inflammatory cytokines that increase the activation of skin T cells and epidermal thickening [59, 62, 76]. Hence, IMQ-treated mice exhibited increased tissue levels of several inflammatory cytokines characteristic of psoriasis (IL-1b, IL-23, INF-γ, TNF-α, and IL-17) by activating moDCs, in good agreement with several studies [59, 77].

Studies have demonstrated that IL-23 present in serum and tissue acts preferentially on memory T cells to trigger psoriasis followed by the production and proliferation of IFN-γ [78-81]. While there exist contradictory studies regarding the presence of IFN-γ [82-85], we have demonstrated the elevated presence of IFN-γ, together with TNF-α and IL-23, both in serum and tissue in our disease model in comparison with healthy animals. Several studies observed the overexpression of TNF-α in lesioned psoriatic skin [86, 87] and plasma [88, 89] from human patients, in agreement with our discoveries within our mouse model.

Importantly, we emphasize the enlarged spleen (splenomegaly) detected in our model after the topical application of IMQ cream, with an increase in weight of two-fold

encountered. Studies have demonstrated that IMQ induces systemic effects on the cellular composition of the spleen, with a shift from lymphoid to myeloid cells, with an increased number of Th17 cells [37]. This finding supports a role for IMQ in the induction of the synthesis of pro-inflammatory cytokines. As previously mentioned, psoriasis induction occurs in an acute and non-chronic manner, so once the action of the IMQ cream ceases, we observed a recovery of normal weight levels.

Based on the observations described above, analysis of IMQ treatment of mouse skin confirms its suitability in the development of a mouse model of psoriasis by mimicking many of the described features of the human disease [32, 37, 59] with regards to immunological pathways and inflammatory cellular mediators.

II.4. Conclusions

Within this chapter, we have developed and fully characterized *ex vivo* human skin models that can maintain tissue viability after four days in the culture medium, as evidenced by tissue viability assays and histological characteristics. The inflammatory skin model allows us to understand the peculiarities of inflammatory skin diseases, such as psoriasis. Also, *ex vivo* models permit drug screening as well as the evaluation of both drug penetration and anti-inflammatory activity of the desired drug before starting *in vivo* studies.

Moreover, we have described psoriasis progression in a preclinical mouse model widely employed for the appraisal of anti-psoriatic or anti-inflammatory therapies. We evaluated disease progression for 10 days after 7 days of disease induction by IMQ cream treatment (day 17 as endpoint). We focused our study on the pathological features that characterize the disease and compromise patient health. The exhaustive and detailed characterization of the psoriatic model over time has allowed us to assess the moment where the animals recover to a basal healthy-like state close to the endpoint studied.

We also discovered that five days after the termination of IMQ treatment (day 12), animals maintained the immune system activation and thickening of the epidermis, together with the ongoing presence of hyperkeratosis and acanthosis. Finally, after the optimization of our IMQ-induced psoriasis model, we confirmed the maintenance of the

main characteristics of the disease for five days after the last application of IMQ, thereby allowing us to evaluate the activity of anti-psoriatic therapeutic agents in further steps.

II.5. Materials and Methods

II.5.1. *Ex Vivo* Models

II.5.1.1. Development of *Ex Vivo* Human Skin Model

Breast skin samples were obtained with informed consent from healthy women undergoing plastic surgery (kindly donated from Hospital la Fe, Valencia, Spain). The skin was cut to approximately 1 cm^2 and placed in 6-well plates so that the dermal side was in contact with Dulbecco's modified Eagle medium (DMEM) supplemented with 50 mL fetal bovine serum (FBS), 5.5 mL penicillin/streptomycin, and 50 µL amphotericin B (all from Gibco, Spain). The epidermis was exposed to the air. After each time point (1, 4, 7, 11 days) in culture medium, skin samples were washed twice with 0.1 % PBS-BSA (PBS supplemented with bovine serum albumin (BSA)) and kept in 4% paraformaldehyde (PFA) for 24 h at room temperature (r.t.). Then, the samples were washed with 30% sucrose in PBS solution and stored in this solution for 24 h at 4ºC. Finally, skin samples were washed twice with PBS and preserved in a cryopreservation solution (40% 0.1M PB, 30% ethylene glycol, and 30% glycerol) at 4ºC until use.

II.5.1.1.1 Tissue Viability Assay

The skin pieces were incubated at 37ºC under 5% CO_2 for 11 days, and the media was changed every day. Tissue viability after 1, 4, 7, 11 days was evaluated by MTT assay. Skin samples were washed twice with PBS and were introduced in 4 mL of MTT solution (2 mg/mL) at 37ºC. MTT assay is a colorimetric assay for assessing cell metabolic activity; the activity of NAD(P)H-dependent cellular oxidoreductase enzymes reflect the number of viable cells present. These enzymes are capable of reducing the tetrazolium dye MTT 3-(4,5-dimethylthiazol-2-yl)-2,5-diphenyltetrazolium bromide to insoluble formazan (Sigma, Spain). After 4 h of incubation, skin samples were washed twice with PBS and placed in 4 mL of dimethyl sulfoxide (DMSO) to extract the formazan from the skin. After 15 h of extraction, the absorbance was read at 490 nm using Victor^{2}Wallac™ plate reader (Perkin Elmer, Spain).

II.5.1.1.2. Histological Analysis and Imaging

Tissue samples were processed for histological analysis. Skin fragments preserved in a cryopreservation solution were washed with PBS under shaking conditions three separate times. A common dehydration and paraffin-inclusion procedure was carried out, leading to blocks that were sliced into 5 μm sections.

H&E staining and immunostaining (Ki67 and Ck5/6) were performed as required (Dako Autostainer 48, US) and the slides were observed under the microscope, and those of interest were scanned with a Panoramic 250 Flash II slide scanner and processed with CaseViewer software (both from 3DHISTECH Ltd, Hungary).

II.5.1.2. Development of Inflammatory *Ex Vivo* Human Skin Model

Breast skin samples were obtained with written informed consent from healthy women undergoing plastic surgery (donated from Hospital la Fe, Valencia, Spain). The skin samples were cut to approximately 1 cm^2 and placed in 6-well plates so that the dermal side was in contact with DMEM medium supplemented with 50 mL FBS, 5.5 mL penicillin/streptomycin, and 50 μL amphotericin B (all from Gibco, Spain). The epidermis remained exposed to the air. The skin was incubated at 37ºC under 5% CO_2.

The inflammatory model was induced by the addition of a constant concentration of EGF (2.5 ng/mL) (Sigma, Spain) and different concentrations of LPS from *E. coli* (InvivoGen, US) (10 μg/mL, 15 μg/mL, 20 μg/mL, or 30 μg/mL) to the culture medium and further incubation for 24 and 48 h at 37ºC under 5% CO_2. After each time point, skin samples were washed twice with 0.1 % PBS-BSA and kept in 4% PFA for 24 h at r.t. Then, the samples were washed with 30% sucrose in PBS solution and stored in this solution for 24 h at 4ºC. Finally, skin samples were washed twice with PBS and preserved in a cryopreservation solution (40% 0.1M PB, 30% ethylene glycol, and 30% glycerol) at 4ºC until use.

The model was evaluated by MTT assay, histology and immunohistochemistry (H&E, Ki67, Ck5/6, INF-γ, IL-1b, NF-kB), and also the quantification of the pro-inflammatory cytokines released to the culture medium.

II.5.1.2.1. Tissue Viability Assay

Tissue viability after 24 and 48 h was evaluated by MTT assay. Skin pieces were washed twice with PBS and introduced into 4 mL of MTT solution (2 mg/mL) at 37ºC. After 4 h of incubation, skin samples were washed twice with PBS and introduced into 4 mL of DMSO, to extract the formazan from the skin. After 15 h of extraction, the absorbance was read at 490 nm using Victor^{2}Wallac™ plate reader (Perkin Elmer, Spain).

II.5.1.2.2. Histological Analysis and Imaging

Tissue samples were processed for histological analysis. Skin fragments preserved in a cryopreservation solution were washed with PBS under shaking conditions three separate times. A common dehydration and paraffin-inclusion procedure was carried out, leading to blocks that were sliced into 5 μm sections. Then, tissue samples were processed for histopathological analysis as described above.

II.5.1.2.3. Quantification of Pro-Inflammatory Cytokines Released to the Culture Medium

Culture medium was collected under standardized conditions from skin cultures after 24 and 48 h of incubation with the inflammatory treatment and kept at -80ºC until use. Cytokines concentrations were measured by LUMINEX kit (Affymetrix, eBioscience, Spain) and cytokine levels were determined according to standard solutions.

II.5.2. *In Vivo* Models

II.5.2.1. Mouse Strains

The 6-week-old male inbred immunocompetent BALB/c (BALB/cOlaHsd) mice used for all the experimental procedures were purchased from Envigo Laboratories Inc. (Spain).

II.5.2.2. Ethical Considerations

Animal experiments were performed in accordance with the European Communities Council Directive (86/609/ECC) guidelines and by the Spanish Royal Decree 1201/2005. All experimental procedures were approved by the Institutional Animal Care and Use Committee and accomplished by certified and trained staff, meeting the animal care rules. Mice were maintained in a specific-pathogen-free facility, under

constant temperature and humidity, using a 12 h light-dark cycle. Food pellets and water were provided ad-libitum during all experiments, and general aspect, body weight, grooming conduct, and behavior were evaluated daily from the beginning of the experiment to ensure animal welfare.

II.5.2.3. Establishment of the Psoriatic Model

The back of the mice was shaved one day before the start of the study. Mice at 6 weeks of age received a daily topical dose of 62.5 mg of commercially available IMQ cream (5%) (Imunocare®; Industrial Farmacéutica Cantabria, S.A., Spain) on the shaved back and the right ear (left ear acting as control for each animal) for 7 consecutive days, translating to a daily dose of 3.125 mg of the active compound. This dose was empirically determined to cause optimal and reproducible skin inflammation in mice [37]. Animals were sacrificed after different days (day 7, day 10, day 12, day 14, and day 17) after the the onset of treatment with IMQ to determine the time to apply the different treatments without the disappearance of the disease.

II.5.2.4. Scoring Severity of Skin Inflammation (PASI Score)

An objective scoring system was used to score the severity of the disease and the inflammation of the dorsal skin based on the clinical Psoriasis Area and Severity Index. Erythema, scaling, itching, and thickening were scored independently on a scale from 0 to 4: 0, none; 1, slight; 2, moderate; 3, marked; 4, very marked.

II.5.2.5. Ear Thickness

Ear thickness was evaluated by measuring using a caliper every two days and comparing with the healthy ear (control).

II.5.2.6. Spleen Weight

At the end of the 7 days of IMQ treatment, mice were sacrificed via CO_2 inhalation at different days (7, 10, 12, 14, and 17 days), and spleen weight was then measured compared to healthy animals.

II.5.2.7. Histology

H&E staining was carried out in both ears and the back. All the samples were removed from euthanized mice at relevant time points, and then tissues were washed in fresh PBS, carefully dried, weighed, and fixed in 4% PFA for 24 h. PFA was eliminated by successive washing with PBS, dehydration and paraffin-inclusion procedures were carried, and blocks were then sliced into 5 μm sections. The slides were observed under the microscope, scanned with a Panoramic 250 Flash III slide scanner, and processed with CaseViewer software (both from 3DHISTECH Ltd, Hungary).

II.5.2.8. Pro-Inflammatory Cytokines Levels in Serum and Tissue

The pro-inflammatory cytokine levels were measured in serum and dorsal skin tissue. Fresh serum was isolated from the blood through centrifugation (4000 rpm, 10 min, 4ºC), and both were stored at -80ºC. To performed protein extraction from frozen dorsal tissue, the skin was mixed with PBS (pH 7.4) containing a protease and phosphatase inhibitor cocktail and then treated in an ice bath by Ultra Turrax Scatter at 10000 ref/min for 20 min. Immediately after incubation, the tube was centrifuged at 4000 rpm for 20 min at 4°C and supernatants were collected and stored at -80ºC until use. For the LUMINEX assays, IL-1b, IL-23, INF-γ, TNF-α, and IL-17A protein expression in skin lysates and serum were quantified with according to the manufacturer's instruction (Invitrogen, Spain).

II.5.2.9. Hematological Analysis

Blood was extracted immediately after sacrifice by cardiac puncture with a 1 mL heparinized syringe and transferred to a 2 mL Eppendorf tube. Blood was gently homogenized and then kept at 4ºC until analysis (within the first 30 min after extraction). Serum was isolated by centrifugation (4000 rpm, 10 min, 4ºC) and analyzed using an automated hematologic analyzer (Sysmex XT-2000i).

II.6. References

[1] K. Nakajima, S. Sano, Mouse models of psoriasis and their relevance, J Dermatol 45(3) (2017) 252-263.
[2] E.F. Wagner, H.B. Schonthaler, J. Guinea-Viniegra, E. Tschachler, Psoriasis: what we have learned from mouse models, Nat Rev Rheumatol 6(12) (2010) 704-14.
[3] A.A. Reus, M. Usta, C.A. Krul, The use of ex vivo human skin tissue for genotoxicity testing, Toxicol Appl Pharmacol 261(2) (2012) 154-63.
[4] E. Desmet, A. Ramadhas, J. Lambert, M. Van Gele, In vitro psoriasis models with focus on reconstructed skin models as promising tools in psoriasis research, Exp Biol Med (Maywood) 242(11) (2017) 1158-1169.
[5] F. Netzlaff, C.M. Lehr, P.W. Wertz, U.F. Schaefer, The human epidermis models EpiSkin, SkinEthic and EpiDerm: an evaluation of morphology and their suitability for testing phototoxicity, irritancy, corrosivity, and substance transport, Eur J Pharm Biopharm 60(2) (2005) 167-78.
[6] A.A. Reus, R.N. van Meeuwen, N. de Vogel, W.J. Maas, C.A. Krul, Development and characterisation of an in vitro photomicronucleus test using ex vivo human skin tissue, Mutagenesis 26(2) (2010) 261-8.
[7] S. Hönzke, L. Wallmeyer, A. Ostrowski, M. Radbruch, L. Mundhenk, M. Schäfer-Korting, S. Hedtrich, Influence of Th2 Cytokines on the Cornified Envelope, Tight Junction Proteins, and β-Defensins in Filaggrin-Deficient Skin Equivalents, Journal of Investigative Dermatology 136(3) (2016) 631-639.
[8] S. Kuchler, D. Henkes, K.M. Eckl, K. Ackermann, J. Plendl, H.C. Korting, H.C. Hennies, M. Schafer-Korting, Hallmarks of atopic skin mimicked in vitro by means of a skin disease model based on FLG knock-down, Altern Lab Anim 39(5) (2011) 471-80.
[9] M. Giulbudagian, G. Yealland, S. Honzke, A. Edlich, B. Geisendorfer, B. Kleuser, S. Hedtrich, M. Calderon, Breaking the Barrier - Potent Anti-Inflammatory Activity following Efficient Topical Delivery of Etanercept using Thermoresponsive Nanogels, Theranostics 8 (2018) 450-463.
[10] K. Bocheńska, E. Smolińska, M. Moskot, J. Jakóbkiewicz-Banecka, M. Gabig-Cimińska, Models in the Research Process of Psoriasis, Int J Mol Sci 18(12) (2017).
[11] K.W. Ng, M. Pearton, S. Coulman, A. Anstey, C. Gateley, A. Morrissey, C. Allender, J. Birchall, Development of an ex vivo human skin model for intradermal vaccination: tissue viability and Langerhans cell behaviour, Vaccine 27(43) (2009) 5948-55.
[12] M.O. Danso, T. Berkers, A. Mieremet, F. Hausil, J.A. Bouwstra, An ex vivo human skin model for studying skin barrier repair, Exp Dermatol 24(1) (2014) 48-54.
[13] E. Vega, M.A. Egea, M.L. Garduño-Ramírez, M.L. García, E. Sánchez, M. Espina, A.C. Calpena, Flurbiprofen PLGA-PEG nanospheres: role of hydroxy-β-cyclodextrin on ex vivo human skin permeation and in vivo topical anti-inflammatory efficacy, Colloids Surf B Biointerfaces 110 (2013) 339-46.
[14] A.R. Companjen, L.I. van der Wel, L. Wei, J.D. Laman, E.P. Prens, A modified ex vivo skin organ culture system for functional studies, Arch Dermatol Res 293(4) (2001) 184-90.
[15] J. Varani, S. Kang, S. Stoll, J.T. Elder, Human psoriatic skin in organ culture: comparison with normal skin exposed to exogenous growth factors and effects of an antibody to the EGF receptor, Pathobiology 66(6) (1998) 253-9.
[16] Y. Yoshinaga, M. Higaki, S. Terajima, E. Ohkubo, T. Nogita, N. Miyasaka, M. Kawashima, Detection of inflammatory cytokines in psoriatic skin, Arch Dermatol Res 287(2) (1995) 158-64.

[17] M.A. Frade, T.A. Andrade, A.F. Aguiar, F.A. Guedes, M.N. Leite, W.R. Passos, E.B. Coelho, P.K. Das, Prolonged viability of human organotypic skin explant in culture method (hOSEC), An Bras Dermatol 90(3) (2015) 347-50.
[18] C. Gélis, S. Girard, A. Mavon, M. Delverdier, N. Paillous, P. Vicendo, Assessment of the skin photoprotective capacities of an organo-mineral broad-spectrum sunblock on two ex vivo skin models, Photodermatol Photoimmunol Photomed 19(5) (2003) 242-53.
[19] G.P. Sidgwick, D. McGeorge, A. Bayat, Functional testing of topical skin formulations using an optimised ex vivo skin organ culture model, Arch Dermatol Res 308(5) (2016) 297-308.
[20] National Centre for the Replacement Refinement & Reduction of Animals in Research. . https://www.nc3rs.org.uk/the-3rs.
[21] J.E. Gudjonsson, A. Johnston, M. Dyson, H. Valdimarsson, J.T. Elder, Mouse models of psoriasis, J Invest Dermatol 127(6) (2007) 1292-308.
[22] T. Kopp, P. Lenz, C. Bello-Fernandez, R.A. Kastelein, T.S. Kupper, G. Stingl, IL-23 production by cosecretion of endogenous p19 and transgenic p40 in keratin 14/p40 transgenic mice: evidence for enhanced cutaneous immunity, J Immunol 170(11) (2003) 5438-44.
[23] L. Rose, C. Schneider, C. Stock, T.M. Zollner, W.D. Docke, Extended DNFB-induced contact hypersensitivity models display characteristics of chronic inflammatory dermatoses, Exp Dermatol 21(1) (2012) 25-31.
[24] S. Sano, K.S. Chan, S. Carbajal, J. Clifford, M. Peavey, K. Kiguchi, S. Itami, B.J. Nickoloff, J. DiGiovanni, Stat3 links activated keratinocytes and immunocytes required for development of psoriasis in a novel transgenic mouse model, Nat Med 11(1) (2005) 43-9.
[25] A. Stratis, M. Pasparakis, R.A. Rupec, D. Markur, K. Hartmann, K. Scharffetter-Kochanek, T. Peters, N. van Rooijen, T. Krieg, I. Haase, Pathogenic role for skin macrophages in a mouse model of keratinocyte-induced psoriasis-like skin inflammation, J Clin Invest 116(8) (2006) 2094-104.
[26] A. Johnston, Y. Fritz, S.M. Dawes, D. Diaconu, P.M. Al-Attar, A.M. Guzman, C.S. Chen, W. Fu, J.E. Gudjonsson, T.S. McCormick, N.L. Ward, Keratinocyte overexpression of IL-17C promotes psoriasiform skin inflammation, J Immunol 190(5) (2013) 2252-62.
[27] J.A. Wolfram, D. Diaconu, D.A. Hatala, J. Rastegar, D.A. Knutsen, A. Lowther, D. Askew, A.C. Gilliam, T.S. McCormick, N.L. Ward, Keratinocyte but not endothelial cell-specific overexpression of Tie2 leads to the development of psoriasis, Am J Pathol 174(4) (2009) 1443-58.
[28] R. Zenz, R. Eferl, L. Kenner, L. Florin, L. Hummerich, D. Mehic, H. Scheuch, P. Angel, E. Tschachler, E.F. Wagner, Psoriasis-like skin disease and arthritis caused by inducible epidermal deletion of Jun proteins, Nature 437(7057) (2005) 369-75.
[29] O. Boyman, H.P. Hefti, C. Conrad, B.J. Nickoloff, M. Suter, F.O. Nestle, Spontaneous development of psoriasis in a new animal model shows an essential role for resident T cells and tumor necrosis factor-alpha, J Exp Med 199(5) (2004) 731-6.
[30] H.L. Ma, S. Liang, J. Li, L. Napierata, T. Brown, S. Benoit, M. Senices, D. Gill, K. Dunussi-Joannopoulos, M. Collins, C. Nickerson-Nutter, L.A. Fouser, D.A. Young, IL-22 is required for Th17 cell-mediated pathology in a mouse model of psoriasis-like skin inflammation, J Clin Invest 118(2) (2008) 597-607.
[31] J.E. Hawkes, J.A. Adalsteinsson, J.E. Gudjonsson, N.L. Ward, Research Techniques Made Simple: Murine Models of Human Psoriasis, J Invest Dermatol 138(1) (2018) e1-e8.

[32] B. Flutter, F.O. Nestle, TLRs to cytokines: mechanistic insights from the imiquimod mouse model of psoriasis, Eur J Immunol 43(12) (2013) 3138-46.
[33] A.K. Gupta, M. Browne, R. Bluhm, Imiquimod: a review, J Cutan Med Surg 6(6) (2002) 554-60.
[34] D.N. Sauder, Immunomodulatory and pharmacologic properties of imiquimod, J Am Acad Dermatol 43(1 Pt 2) (2000) S6-11.
[35] L. Edwards, A. Ferenczy, L. Eron, D. Baker, M.L. Owens, T.L. Fox, A.J. Hougham, K.A. Schmitt, Self-administered topical 5% imiquimod cream for external anogenital warts. HPV Study Group. Human PapillomaVirus, Arch Dermatol 134(1) (1998) 25-30.
[36] K.R. Beutner, S.L. Spruance, A.J. Hougham, T.L. Fox, M.L. Owens, J.M. Douglas, Jr., Treatment of genital warts with an immune-response modifier (imiquimod), J Am Acad Dermatol 38(2 Pt 1) (1998) 230-9.
[37] L. van der Fits, S. Mourits, J.S. Voerman, M. Kant, L. Boon, J.D. Laman, F. Cornelissen, A.M. Mus, E. Florencia, E.P. Prens, E. Lubberts, Imiquimod-induced psoriasis-like skin inflammation in mice is mediated via the IL-23/IL-17 axis, J Immunol 182 (2009) 5836-45.
[38] H. Hemmi, T. Kaisho, O. Takeuchi, S. Sato, H. Sanjo, K. Hoshino, T. Horiuchi, H. Tomizawa, K. Takeda, S. Akira, Small anti-viral compounds activate immune cells via the TLR7 MyD88-dependent signaling pathway, Nat Immunol 3(2) (2002) 196-200.
[39] J.E. Hawkes, J.E. Gudjonsson, N.L. Ward, The Snowballing Literature on Imiquimod-Induced Skin Inflammation in Mice: A Critical Appraisal, J Invest Dermatol 137(3) (2016) 546-549.
[40] M. Gilliet, C. Conrad, M. Geiges, A. Cozzio, W. Thürlimann, G. Burg, F.O. Nestle, R. Dummer, Psoriasis triggered by toll-like receptor 7 agonist imiquimod in the presence of dermal plasmacytoid dendritic cell precursors, Arch Dermatol 140(12) (2004) 1490-5.
[41] D. Bilu, D.N. Sauder, Imiquimod: modes of action, Br J Dermatol 149 Suppl 66 (2003) 5-8.
[42] M.P. Schön, M. Schön, K.N. Klotz, The small antitumoral immune response modifier imiquimod interacts with adenosine receptor signaling in a TLR7- and TLR8-independent fashion, J Invest Dermatol 126(6) (2006) 1338-47.
[43] K. Sakai, K.M. Sanders, M.R. Youssef, K.M. Yanushefski, L. Jensen, G. Yosipovitch, T. Akiyama, Mouse model of imiquimod-induced psoriatic itch, Pain 157(11) (2016) 2536-2543.
[44] S. Pantelyushin, S. Haak, B. Ingold, P. Kulig, F.L. Heppner, A.A. Navarini, B. Becher, Rorγt+ innate lymphocytes and γδ T cells initiate psoriasiform plaque formation in mice, J Clin Invest 122(6) (2012) 2252-6.
[45] S. Bezdek, A. Hdnah, T. Sezin, S. Mousavi, D. Zillikens, S. Ibrahim, R.J. Ludwig, C.D. Sadik, The genetic difference between C57Bl/6J and C57Bl/6N mice significantly impacts Aldara™-induced psoriasiform dermatitis, Exp Dermatol 26(4) (2016) 349-351.
[46] T.A. Andrade, A.F. Aguiar, F.A. Guedes, M.N. Leite, G.F. Caetano, E.B. Coelho, P.K. Das, M.A. Frade, Ex vivo Model of Human Skin (hOSEC) as Alternative to Animal use for Cosmetic Tests, Procedia Engineering 110 (2015) 67-73.
[47] C. Jacques, A.M. de Aquino, M. Ramos-e-Silva, Cytokeratins and dermatology, Skinmed 4(6) (2005) 354-60; quiz 360-1.
[48] M. Frušić-Zlotkin, Y. Soroka, R. Tivony, L. Larush, L. Verkhovsky, F.M. Brégégère, R. Neuman, S. Magdassi, Y. Milner, Penetration and biological effects of topically applied cyclosporin A nanoparticles in a human skin organ culture inflammatory model, Exp Dermatol 21 (2012) 938-43.
[49] K. Kuroda, S. Tajima, HSP47 is a useful marker for skin fibroblasts in formalin-fixed, paraffin-embedded tissue specimens, J Cutan Pathol 31 (2004) 241-6.

[50] W. Ouyang, S. Rutz, N.K. Crellin, P.A. Valdez, S.G. Hymowitz, Regulation and functions of the IL-10 family of cytokines in inflammation and disease, Annu Rev Immunol 29 (2011) 71-109.
[51] A. Walter, M. Schäfer, V. Cecconi, C. Matter, M. Urosevic-Maiwald, B. Belloni, N. Schönewolf, R. Dummer, W. Bloch, S. Werner, H.D. Beer, A. Knuth, M. van den Broek, Aldara activates TLR7-independent immune defence, Nat Commun 4 (2013) 1560.
[52] A.B. Van Belle, M. de Heusch, M.M. Lemaire, E. Hendrickx, G. Warnier, K. Dunussi-Joannopoulos, L.A. Fouser, J.C. Renauld, L. Dumoutier, IL-22 is required for imiquimod-induced psoriasiform skin inflammation in mice, J Immunol 188 (2011) 462-9.
[53] M. Murphy, P. Kerr, J.M. Grant-Kels, The histopathologic spectrum of psoriasis, Clin Dermatol 25(6) (2007) 524-8.
[54] M.J. Reiter, T.L. Testerman, R.L. Miller, C.E. Weeks, M.A. Tomai, Cytokine induction in mice by the immunomodulator imiquimod, J Leukoc Biol 55(2) (1994) 234-40.
[55] A. Ueyama, M. Yamamoto, K. Tsujii, Y. Furue, C. Imura, M. Shichijo, K. Yasui, Mechanism of pathogenesis of imiquimod-induced skin inflammation in the mouse: a role for interferon-alpha in dendritic cell activation by imiquimod, J Dermatol 41(2) (2014) 135-43.
[56] H.L. Ma, S. Liang, J. Li, L. Napierata, T. Brown, S. Benoit, M. Senices, D. Gill, K. Dunussi-Joannopoulos, M. Collins, C. Nickerson-Nutter, L.A. Fouser, D.A. Young, IL-22 is required for Th17 cell-mediated pathology in a mouse model of psoriasis-like skin inflammation, J Clin Invest 118 (2008) 597-607.
[57] S. Shibata, Y. Tada, Y. Asano, K. Yanaba, M. Sugaya, T. Kadono, N. Kanda, S. Watanabe, S. Sato, IL-27 activates Th1-mediated responses in imiquimod-induced psoriasis-like skin lesions, J Invest Dermatol 133 (2012) 479-88.
[58] J. Hawiger, Innate immunity and inflammation: a transcriptional paradigm, Immunol Res 23(2-3) (2001) 99-109.
[59] T.P. Singh, H.H. Zhang, I. Borek, P. Wolf, M.N. Hedrick, S.P. Singh, B.L. Kelsall, B.E. Clausen, J.M. Farber, Monocyte-derived inflammatory Langerhans cells and dermal dendritic cells mediate psoriasis-like inflammation, Nat Commun 7 (2016) 13581.
[60] M.P. Schön, Animal models of psoriasis: a critical appraisal, Exp Dermatol 17(8) (2008) 703-12.
[61] F.O. Nestle, P. Di Meglio, J.Z. Qin, B.J. Nickoloff, Skin immune sentinels in health and disease, Nat Rev Immunol 9(10) (2009) 679-91.
[62] L. Tortola, E. Rosenwald, B. Abel, H. Blumberg, M. Schäfer, A.J. Coyle, J.C. Renauld, S. Werner, J. Kisielow, M. Kopf, Psoriasiform dermatitis is driven by IL-36-mediated DC-keratinocyte crosstalk, J Clin Invest 122(11) (2012) 3965-76.
[63] Y. Cai, X. Shen, C. Ding, C. Qi, K. Li, X. Li, V.R. Jala, H.G. Zhang, T. Wang, J. Zheng, J. Yan, Pivotal role of dermal IL-17-producing γδ T cells in skin inflammation, Immunity 35(4) (2011) 596-610.
[64] W.R. Swindell, K.A. Michaels, A.J. Sutter, D. Diaconu, Y. Fritz, X. Xing, M.K. Sarkar, Y. Liang, A. Tsoi, J.E. Gudjonsson, N.L. Ward, Imiquimod has strain-dependent effects in mice and does not uniquely model human psoriasis, Genome Med 9(1) (2017) 24.
[65] S. Rodríguez-Martínez, J.C. Cancino-Diaz, I. Martínez- Torrez, S. M. Pérez-Tapia, M. E. Cancino-Diaz, Psoriatic Animal Models Developed for the Study of the Disease, in: A. Chiriac (Ed.), An Interdisciplinary Approach to Psoriasis, IntechOpen, Croatia, 2017.

[66] G.A. Churchill, Misleading results: don't blame the mice, Science 343(6169) (2014) 370.
[67] K. Yanaba, M. Kamata, N. Ishiura, S. Shibata, Y. Asano, Y. Tada, M. Sugaya, T. Kadono, T.F. Tedder, S. Sato, Regulatory B cells suppress imiquimod-induced, psoriasis-like skin inflammation, J Leukoc Biol 94(4) (2013) 563-73.
[68] M. Jurk, F. Heil, J. Vollmer, C. Schetter, A.M. Krieg, H. Wagner, G. Lipford, S. Bauer, Human TLR7 or TLR8 independently confer responsiveness to the antiviral compound R-848, Nat Immunol 3(6) (2002) 499.
[69] A. Larangé, D. Antonios, M. Pallardy, S. Kerdine-Römer, TLR7 and TLR8 agonists trigger different signaling pathways for human dendritic cell maturation, J Leukoc Biol 85(4) (2009) 673-83.
[70] S. Sano, K.S. Chan, S. Carbajal, J. Clifford, M. Peavey, K. Kiguchi, S. Itami, B.J. Nickoloff, J. DiGiovanni, Stat3 links activated keratinocytes and immunocytes required for development of psoriasis in a novel transgenic mouse model, Nat Med 11(1) (2004) 43-9.
[71] G.D. Weinstein, E.J. Van Scott, Autoradiographic analysis of turnover times of normal and psoriatic epidermis, J Invest Dermatol 45(4) (1965) 257-62.
[72] G.D. Weinstein, J.L. McCullough, P.A. Ross, Cell kinetic basis for pathophysiology of psoriasis, J Invest Dermatol 85(6) (1985) 579-83.
[73] K. El Malki, S.H. Karbach, J. Huppert, M. Zayoud, S. Reissig, R. Schüler, A. Nikolaev, K. Karram, T. Münzel, C.R. Kuhlmann, H.J. Luhmann, E. von Stebut, S. Wörtge, F.C. Kurschus, A. Waisman, An alternative pathway of imiquimod-induced psoriasis-like skin inflammation in the absence of interleukin-17 receptor a signaling, J Invest Dermatol 133(2) (2012) 441-51.
[74] S. Tamoutounour, M. Guilliams, F. Montanana Sanchis, H. Liu, D. Terhorst, C. Malosse, E. Pollet, L. Ardouin, H. Luche, C. Sanchez, M. Dalod, B. Malissen, S. Henri, Origins and functional specialization of macrophages and of conventional and monocyte-derived dendritic cells in mouse skin, Immunity 39(5) (2013) 925-38.
[75] S. Henri, L.F. Poulin, S. Tamoutounour, L. Ardouin, M. Guilliams, B. de Bovis, E. Devilard, C. Viret, H. Azukizawa, A. Kissenpfennig, B. Malissen, CD207+ CD103+ dermal dendritic cells cross-present keratinocyte-derived antigens irrespective of the presence of Langerhans cells, J Exp Med 207(1) (2009) 189-206.
[76] F.O. Nestle, L.A. Turka, B.J. Nickoloff, Characterization of dermal dendritic cells in psoriasis. Autostimulation of T lymphocytes and induction of Th1 type cytokines, J Clin Invest 94(1) (1994) 202-9.
[77] Y. Tsurekawa, M. Morita, M.A. Suico, M. Moriuchi, Y. Nakano, M. Piruzyan, M. Takada, S. Fukami, T. Shuto, H. Kai, Mild electrical stimulation with heat shock reduces inflammatory symptoms in the imiquimod-induced psoriasis mouse model, Exp Dermatol 27(10) (2018) 1092-1097.
[78] L. Grine, L. Dejager, C. Libert, R.E. Vandenbroucke, An inflammatory triangle in psoriasis: TNF, type I IFNs and IL-17, Cytokine Growth Factor Rev 26(1) (2014) 25-33.
[79] B. Oppmann, R. Lesley, B. Blom, J.C. Timans, Y. Xu, B. Hunte, F. Vega, N. Yu, J. Wang, K. Singh, F. Zonin, E. Vaisberg, T. Churakova, M. Liu, D. Gorman, J. Wagner, S. Zurawski, Y. Liu, J.S. Abrams, K.W. Moore, D. Rennick, R. de Waal-Malefyt, C. Hannum, J.F. Bazan, R.A. Kastelein, Novel p19 protein engages IL-12p40 to form a cytokine, IL-23, with biological activities similar as well as distinct from IL-12, Immunity 13(5) (2000) 715-25.
[80] K.L. Elkins, A. Cooper, S.M. Colombini, S.C. Cowley, T.L. Kieffer, In vivo clearance of an intracellular bacterium, Francisella tularensis LVS, is dependent on the

p40 subunit of interleukin-12 (IL-12) but not on IL-12 p70, Infect Immun 70(4) (2002) 1936-48.
[81] A.T. Pietrzak, A. Zalewska, G. Chodorowska, D. Krasowska, A. Michalak-Stoma, P. Nockowski, P. Osemlak, T. Paszkowski, J.M. Roliński, Cytokines and anticytokines in psoriasis, Clin Chim Acta 394(1-2) (2008) 7-21.
[82] J.F. Schlaak, M. Buslau, W. Jochum, E. Hermann, M. Girndt, H. Gallati, K.H. Meyer zum Büschenfelde, B. Fleischer, T cells involved in psoriasis vulgaris belong to the Th1 subset, J Invest Dermatol 102(2) (1994) 145-9.
[83] K. Uyemura, M. Yamamura, D.F. Fivenson, R.L. Modlin, B.J. Nickoloff, The cytokine network in lesional and lesion-free psoriatic skin is characterized by a T-helper type 1 cell-mediated response, J Invest Dermatol 101(5) (1993) 701-5.
[84] N.Y. el Barnawi, A.S. Giasuddin, M.M. Ziu, M. Singh, Serum cytokine levels in psoriasis vulgaris, Br J Biomed Sci 58(1) (2001) 40-4.
[85] O. Arican, M. Aral, S. Sasmaz, P. Ciragil, Serum levels of TNF-alpha, IFN-gamma, IL-6, IL-8, IL-12, IL-17, and IL-18 in patients with active psoriasis and correlation with disease severity, Mediators Inflamm 2005(5) (2005) 273-9.
[86] C. Bonifati, M. Carducci, P. Cordiali Fei, E. Trento, G. Sacerdoti, M. Fazio, F. Ameglio, Correlated increases of tumour necrosis factor-alpha, interleukin-6 and granulocyte monocyte-colony stimulating factor levels in suction blister fluids and sera of psoriatic patients--relationships with disease severity, Clin Exp Dermatol 19(5) (1994) 383-7.
[87] P. Ettehadi, M.W. Greaves, D. Wallach, D. Aderka, R.D. Camp, Elevated tumour necrosis factor-alpha (TNF-alpha) biological activity in psoriatic skin lesions, Clin Exp Immunol 96(1) (1994) 146-51.
[88] A. Mussi, C. Bonifati, M. Carducci, G. D'Agosto, F. Pimpinelli, D. D'Urso, L. D'Auria, M. Fazio, F. Ameglio, Serum TNF-alpha levels correlate with disease severity and are reduced by effective therapy in plaque-type psoriasis, J Biol Regul Homeost Agents 11(3) (1997) 115-8.
[89] G. Chodorowska, Plasma concentrations of IFN-gamma and TNF-alpha in psoriatic patients before and after local treatment with dithranol ointment, J Eur Acad Dermatol Venereol 10(2) (1998) 147-51.

CHAPTER III

DEVELOPMENT OF HYBRID POLYPEPTIDE-BASED CARRIERS TO ENHANCE DRUG DELIVERY THROUGH THE SKIN

III.1. Antecedents and Background

Transdermal drug delivery systems promote the non-invasive delivery of a drug or active pharmaceutical ingredients (APIs) through the skin for the localized or systemic treatment of various diseases or disorders [1]. This administration route avoids any adverse effect associated with hypodermic injection or oral administration [2, 3]. Biocompatibility, biodegradability, and high permeation efficiency through the skin barrier represent some of the desired characteristics for such delivery systems.

Hydrogels are commonly employed in nanomedicine for dermal applications and cosmetic skincare [4] as many hydrogel-based biomaterials mimic specific properties of the skin extracellular matrix [5]. Cross-linking of polymers represents a common synthetic approach to obtain hydrogels, providing materials with useful properties when compared to linear polymers, including higher viscosity in aqueous solutions, higher molecular weights (Mw), and greater resistance to degradation [6]. These advantageous properties have promoted the application of cross-polymers in tissue engineering, injectable hydrogel formulations, skin delivery, and dermal fillers, among notable others [7-9].

Polysaccharides, and hyaluronic acid (HA) in particular, represent the most widely used biopolymers for dermal applications [8]. HA, a natural heteropolysaccharide with a linear structure composed of altered residues of D-glucuronic and N-acetyl-D-glucosamide, was discovered by Meyer and Palmer in 1934 [10]. HA represents one of the primary components of the skin extracellular matrix and disappearance of epidermal HA content can occur during natural aging and oxidative processes generated by exposure to ultraviolet rays from sunlight [11, 12]. HA has been widely employed in the composition of different vehicles for dermal applications [6], wound healing [13, 14], and for the penetration of drugs into the skin as part of dermal drug delivery systems [15, 16].

The characteristics of biodegradable polypeptides have also prompted their exploration as part of dermal drug delivery systems [17-19]. Poly-glutamic acid (PGA) (specifically poly-γ-glutamic acid – a polymeric chain where the peptide bonds are formed between NH_2 and gamma COOH at glutamic acid side chain) moisturizes the skin and acts as a hydrophilic humectant (a substance that moisturizes and softens the skin) due to the creation of a smooth and elastic film after application to the skin [20]. PGA

administration also enhances the synthesis of natural moisturizing factors in the skin, such as lactic acid, pyrrolidone carboxylic acid, and urocanic acid, and also improves skin elasticity when compared with HA or collagen [21, 22]. Of note, studies have reported that PGA inhibits the activity of hyaluronidases, a family of enzymes that degrades dermal HA, therefore maintaining skin elasticity [23]. Moreover, the free glutamate units produced during PGA degradation act as nutrients for the skin [24].

Although polyglutamates are mainly used as drug delivery agents itself in nanomedicine approaches employed to treat several systemic diseases, such as cancer or Alzheimer's disease [25-27], it has also been found to be used as skin penetration enhancers for pharmaceuticals such as insulin (through the use of polymer microneedles composed by γ-PGA and polyvinyl alcohol/polyvinyl pyrrolidone ([PVA/PVP] supporting structures) [24]. PGA can also increase water absorption rates and swelling ratios, so it has been widely applied in biomaterials for biological adhesive (natural polymeric compounds that can act as adhesives in the skin) and tissue engineering [28, 29]. Therefore, PGA not only increases the skin penetration of bioactive agents but also maintains a moist microenvironment that promotes effective wound healing [30, 31].

Motivated by the desire to develop an advanced biodegradable platform for the topical delivery of drugs and also considering the advantageous properties of PGA as well as HA in dermal applications, we decided to rationally design our platform using both materials. We based our design on well-established strategies using cross-linked HA and γ-PGA for skin applications [32-34], but using the synthetic poly-L-α-glutamic acid instead.

In close collaboration with the company Polypeptide Therapeutic Solutions S.L. (PTS, Valencia, Spain) we developed a cross-polymer vehicle composed by HA and PGA cross-linked through L-lysine (Lys) residues (hyaluronic-poly-L-glutamate cross-polymer or HA-CP). This vehicle is a biodegradable and biocompatible material which is completely assimilable by the organism and allows the modulation of its rheological properties; this viscous gel-like vehicle does not behave as a hydrogel at our working concentration (1% w/v) in terms of rheological or mechanical behavior, but can form viscoelastic hydrogels at higher concentrations or higher cross-linking degrees. We exhaustively characterized HA-CP using a battery of techniques and then evaluated HA-CP *in vitro, ex vivo, in vivo* (see **Chapter IV**) and even in human volunteers. To

demonstrate the property of this material as skin penetration enhancer we studied the capacity of HA-CP to act as a vehicle of hydrophobic APIs (using fluorescence probes as model system) encapsulated in amphiphilic micelles based on polyethylene glycol (PEG)-polyamino acids (amphiphilic block copolymers). The encapsulation of hydrophobic drugs or APIs in aqueous solution by amphiphilic PEG-polyamino acid micelles has been widely described in the literature [35], with examples for transdermal skin delivery [2] and the treatment of skin diseases such as psoriasis [36, 37].

The combination of HA-CP with the adequate polymeric nanomicelles could be considered an efficient hybrid transdermal delivery system for a variety of therapeutic applications where the required drug is not capable to bypass this challenging biological barrier, the skin (**Figure III. 1**).

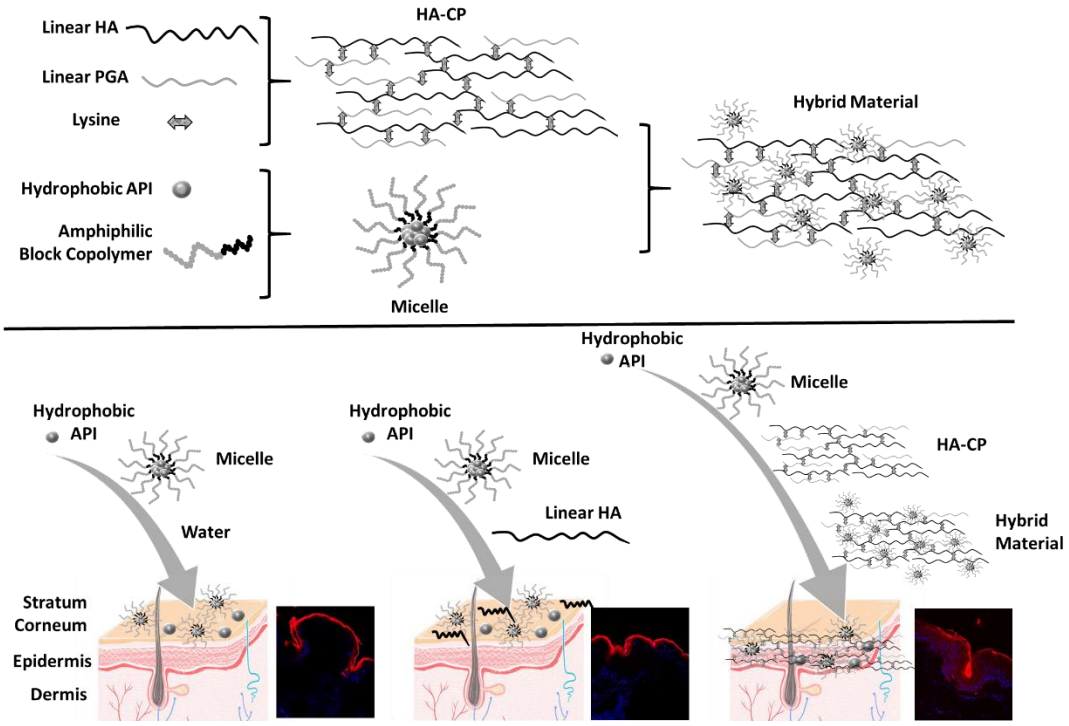

Figure III. 1: **Upper Section:** Scheme of the hyaluronic acid-poly-L-glutamate cross-polymer (HA-CP) vehicle, the micelle composed by amphiphilic block copolymer encapsulating a hydrophobic API, and the hybrid material (composed by micelles embedded into the HA-CP matrix). **Lower Section:** Schematic representation of the developed skin delivery platforms: (i) hydrophobic API in micelle applied in water, (ii) hydrophobic API in micelle applied with linear hyaluronic acid and (iii) hydrophobic API in micelle applied in HA-CP vehicle. Representative confocal microscopy images obtained from the penetration studies with each platform are shown next to the skin schema as demonstrative examples.

III.2. Results and Discussion

III.2.1. Development of the Hyaluronic Acid-Poly-L-Glutamate Cross-Polymer (HA-CP) Vehicle: Synthesis and Physico-Chemical Characterization

Cross-linked reactions for HA can use several established methodologies, including Schiff-base reaction, thiol-Michael addition, Diels-Alder click cross-linking, ionic-crosslinking, amide or ester bond formation, supramolecular-cross-linking, and photo-crosslinking [6, 38]. HA possesses various reactive groups, including carboxylic acid and hydroxylic groups, which can be easily chemically modified. We selected carboxylic acid moieties for cross-linking due to the presence of these groups in PGA. Many activating reagents condense carboxyl and amino groups to create amide bonds, including carbodiimides, carbonyl diimidazole, 1-ethyl-3-(3-dimethyl aminopropyl)-1-carbodiimide hydrochloride (EDC), N-hydroxysuccinimide (NHS), and 4-(4,6-Dimethoxy-1,3,5-triazin-2-yl)-4-methylmorpholinium chloride (DMTMM·Cl) [5]. A common mechanism of action is the initial activation of the carboxyl group via adduct formation, followed by the nucleophilic attack of the amine moiety to create the amide bond. This mechanism precludes the activating agent from being incorporated into the final product [6].

Focusing on the development of a biodegradable skin delivery platform, our synthetic cross-linking approach employed amide bond formation between carboxylic groups of HA and PGA, using the amines of the lysine residue as the cross-linker moiety and DMTMM·Cl as the activating coupling agent. The use of DMTMM·Cl for peptidic coupling of HA [5, 39] and PGA [40-42] through amine moiety in aqueous solutions is reported widely in the literature.

III.2.1.1. Synthesis and Physico-Chemical Characterization of HA-CP

We obtained HA-CP through the activation of the carboxylic groups of linear HA (50 kDa) and PGA with DMTMM·Cl, employing lysine as coupling moiety. **Figure III. 2** shows the ^{1}H-NMR spectra of HA-CP, demonstrating the presence of HA and PGA moieties within the cross-polymer. The low stoichiometric amounts of lysine employed for the cross-linking reaction and the fact that epsilon (ε) methylene near to the amino

group might experience a significant downfield shift precludes the identification of lysine within the HA-CP via NMR after extensive purification by dialysis.

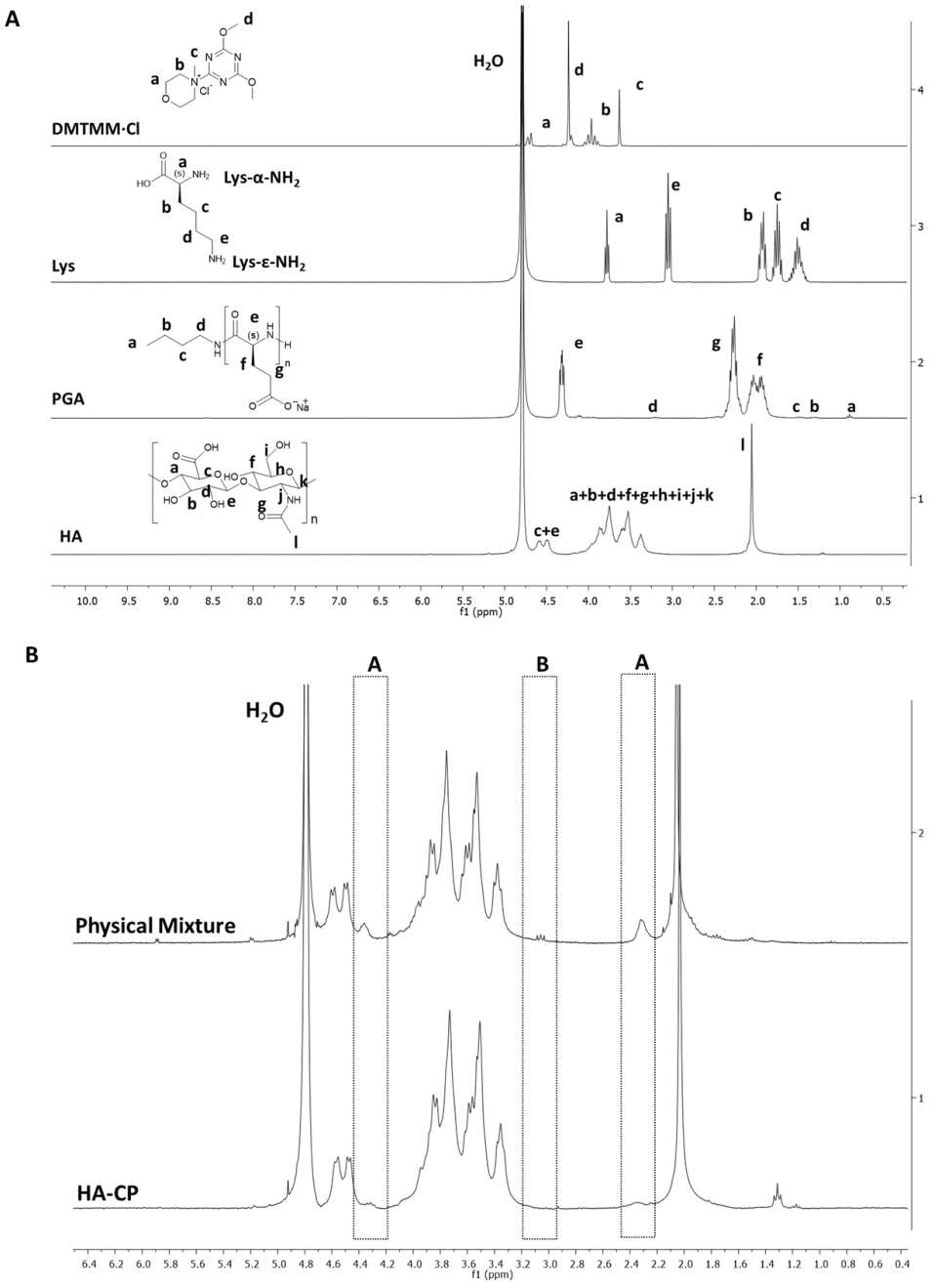

Figure III. 2: **NMR studies. (A)** ^{1}H-NMR spectra in D_2O for starting materials with assigned protons. **(B)** ^{1}H-NMR spectra in D_2O for HA-CP and the physical mixture of starting materials, showing PGA signals in the HA-CP (**A:** Signal for PGA; **B:** No signals for lysine (Lys) in HA-CP were observed).

We performed Mw distribution comparing HA-CP with the starting HA material. SEC elugrams employing a refractive index (RI) detector revealed higher Mw distribution

for HA-CP when compared to starting HA in terms of retention time, yielding a three-dimensional reticulated HA-CP network of 150 kDa (**Figure III. 3A**). Mw distribution values represented in **Table III. 1** obtained by SEC [43] indicated a Mw of our novel HA-CP cross-polymer three-times higher than the starting HA (145 kDa and 49 kDa, respectively).

Table III. 1: Mw distributions and polydispersity index (PDI) by SEC.

Compound	Mw (kDa) by SEC	PDI by SEC
Starting HA	49.1	1.119
HA-CP	145.2	1.863

We monitored the cross-linking reaction through free amine quantification by TNBSA [44, 45] and viscosity assays. Although the cross-linking reactions can produce undesired ester bond formation between carboxylic acids and alcohols of HA, the higher amine nucleophilic character when compared to the alcohol [42, 46] directs the reaction towards amide bond formation. Although NMR studies failed to find evidence for the presence of lysine in the cross-polymer, we observed a population of free amines by TNBSA assay. Of note, as the reaction progresses, free amine levels fall while viscosity increases due to amide bond formation and the promotion of cross-linking. Furthermore, the pH decreased as a consequence of the release of protons during the formation of each amide bond (**Figure III. 3B and C**).

According to the results obtained from the viscosity assay and free amine quantification by TNBSA assay, we obtained the desired cross-linked material after 500 min of reaction. At this point, HA alcohols form undesired cross-linked reactions by the formation of ester bonds in the absence of free lysine amines in the reaction media, yielding an unstable material with excessive viscosity. Excessively cross-linked HA matrices increase collagen deposition and therefore trigger some adverse effects, such as inflammatory reactions [43]. For these reasons, we terminated the cross-linked reaction time at 500 min to avoid the formation of undesired cross-linking reactions.

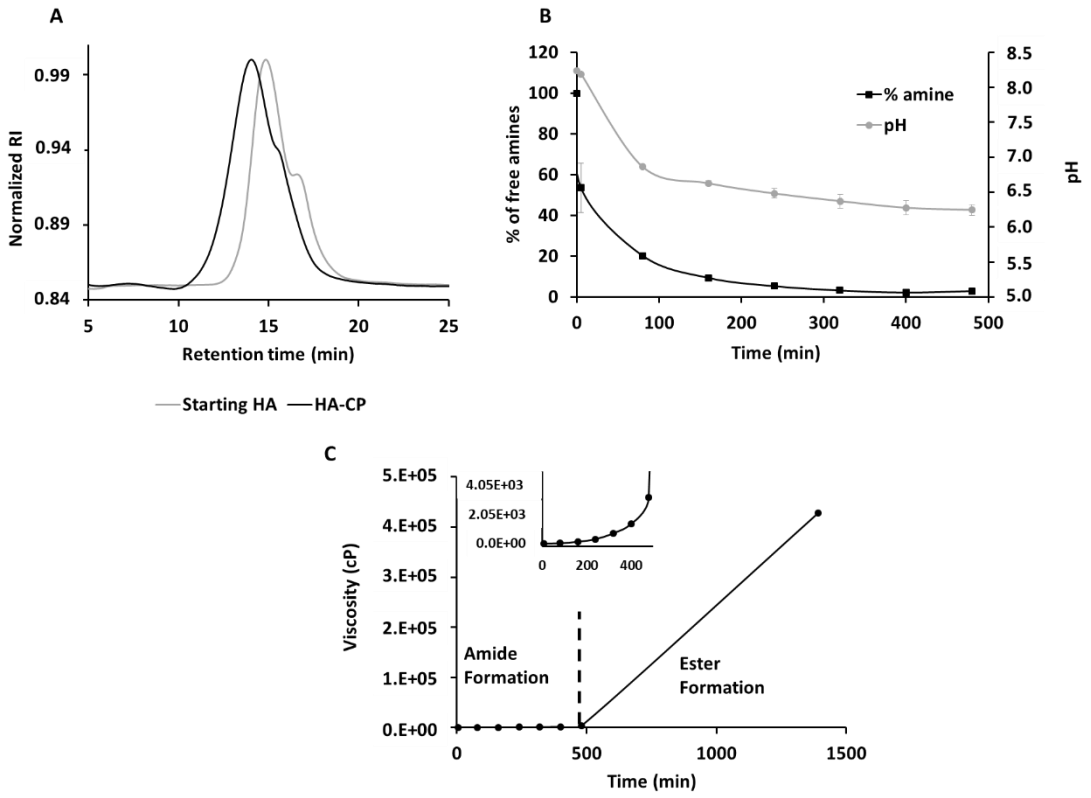

Figure III. 3: Molecular weight calculations and cross-linking reaction monitoring. **(A)** SEC-RI elugram for HA-CP and starting HA in aqueous media with 100 mM $NaNO_3$ at pH 5 demonstrating higher Mw distribution for HA-CP compared to starting HA. **(B)** Percentage (%) of free lysine amines determined by TNBSA assay in the cross-linked reaction media for 500 min, including pH values. **(C)** Viscosity in cP of the cross-linked reaction media, demonstrating an exponential increase during the first 500 min, and an excessive viscosity increase after lysine consumption.

In summary, we successfully developed a cross-linking reaction between HA and PGA through lysine moieties employing DMTMM·Cl as a coupling agent. As expected, analysis of the physico-chemical characteristics demonstrated an increase in the molecular size and viscosity of HA-CP due to the cross-linking reaction when compared to starting HA.

III.2.1.2. Development of Fluorescently-labeled HA-based Materials

To compare the skin permeation of our novel cross-polymer compared to conventional HA, we fluorescently labeled both HA-based materials with the Cyanine 5.5 (Cy5.5) fluorescent dye, generating HA-CP-Cy5.5 and HA-Cy5.5 materials. We based the synthetic strategy on peptidic coupling through DMTMM·Cl carboxylic group

activation following to Cy5.5 amine nucleophile attack and new amide bond formation. We characterized both labeled materials by UV-Vis spectroscopy to determine the loading percentage (% w/w) within the materials, and by SEC to determine Mw distributions (**Table III. 2**). Dye loading by UV-Vis quantification demonstrated an enhanced conjugation efficiency for HA-CP (0.63 % molar dye) in comparison to linear HA (0.43 % molar dye), with 1% molar the target dye loading in both cases. SEC elugrams revealed successful dye moiety conjugation to both HA-based materials, showing perfect correlation in terms of retention times, which may be attributed to the covalent union between the carboxylic acids (from HA and HA-CP) and Cy5.5 (**Figure III. 4**). We next employed the resultant labeled materials for skin permeation studies.

Table III. 2: Results of Cy5.5 loading by UV-Vis spectroscopy and Mw distributions by SEC

Compound	% w/w Cy5.5*	% Molar Cy5.5*	Conjugation Efficiency*	Mw (kDa)**	PDI**
HA-CP-Cy5.5	1.18	0.63	63%	145.2	1.863
HA-Cy5.5	0.81	0.43	43%	205.5	1.442

*Data obtained by UV-Vis spectroscopy measured at 676 nm.**Data obtained by SEC measurements.

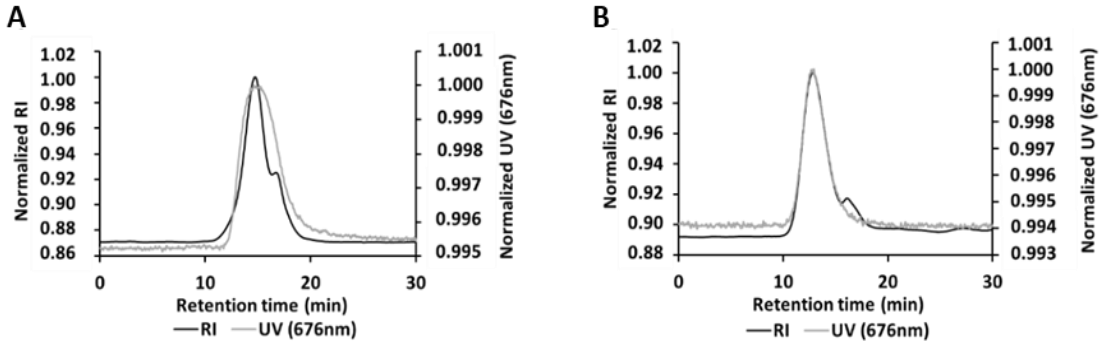

Figure III. 4: **(A)** SEC-RI-UV elugram for HA-CP-Cy5.5. **(B)** SEC-RI-UV elugram for HA-Cy5.5. SEC-RI-UV chromatograms were achieved at 3.75 mg/mL in 150 mM $NaNO_3$ adjusted to pH 5 with 5 mM PB.

III.2.2. Analysis of the HA-CP as a Biomaterial for Topical Skin Applications

To fully understand the biological behavior of our newly developed HA-CP vehicle for topical skin applications, we studied several properties in comparison to a conventional linear HA with a similar Mw distribution (PrimalHyal300; 200 kDa).

III.2.2.1. Hyaluronidase Degradation Studies

We studied the degradation of our HA-based materials by assessing Mw distribution alterations in the presence of hyaluronidase (HAase), a natural enzyme located in the skin that degrades HA [47]. We selected SEC to study the HAase-mediated degradation of our HA-based materials, due to its robustness and reproducibility in Mw determination. Furthermore, SEC also allows the study of degradation kinetics and comparison between samples. Although the effective HAase concentration depends on the Mw of the HA [47], we used 5 U/mL according to literature to mimic the concentration of HAase present within human skin [48-50]. We evaluated Mw values obtained from the kinetics per triplicate from three different degradations at 0, 1, 2, 3, 4, 6, 8, 10, and 24 h. The results obtained by SEC revealed a rapid degradation for linear HA when compared to HA-CP under the same conditions, with HA-CP presenting a more constant and sustained degradation over time (**Figure III. 5**). This effect may be explained by the different structural conformation of HA-based materials; a cross-linked conformation may possess intrinsic resistance to HAase activity due to the inaccessibility of the HA chains in solution while HAase may have free access to the linear HA chains and degrade them more rapidly, thereby promoting a rapid decrease in Mw distribution. In addition, maybe our PGA might also have some HAase inhibition activity as in the case of γ-PGA, but the complete rationale for this phenomenon lies outside the scope of the present work.

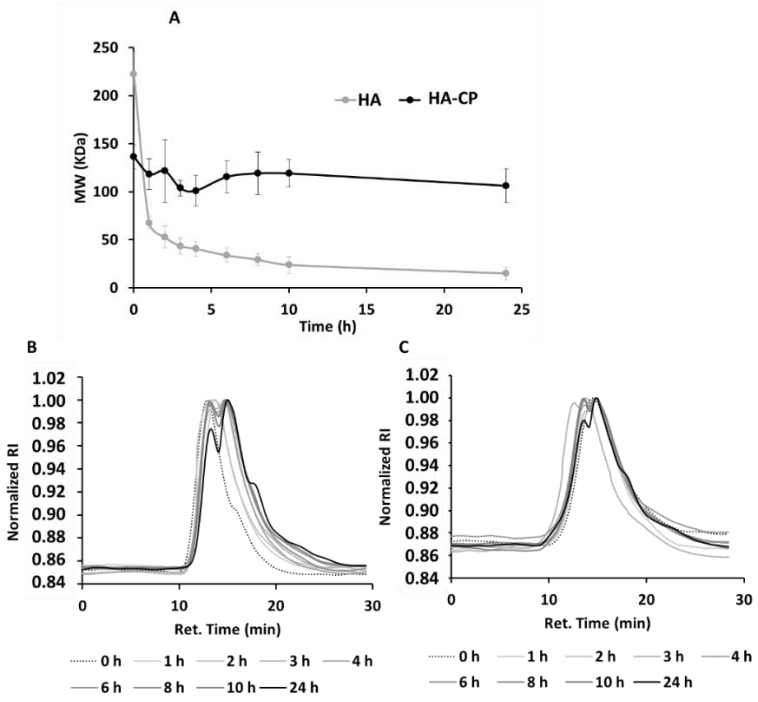

Figure III. 5: **(A)** HAase degradation of HA-CP and linear HA showing Mw values obtained by SEC. **(B)** SEC-RI elugram for linear HA. **(C)** SEC-RI elugram for HA-CP. SEC conditions employed: 100 mM $NaNO_3$ at pH 5 using 5 mM PB in the presence of bovine testicular HAase at 5 U/mL.

III.2.2.2 Cell Viability *In Vitro*

We carried out cell viability assays after 72 h of treatment to determine the toxicity of both HA-based materials in human keratinocytes (HaCaT cells) and human fibroblasts [51]. As hoped, both linear HA and the HA-CP vehicle maintained cell viability in both cell lines up to the concentrations tested (**Figure III. 6**).

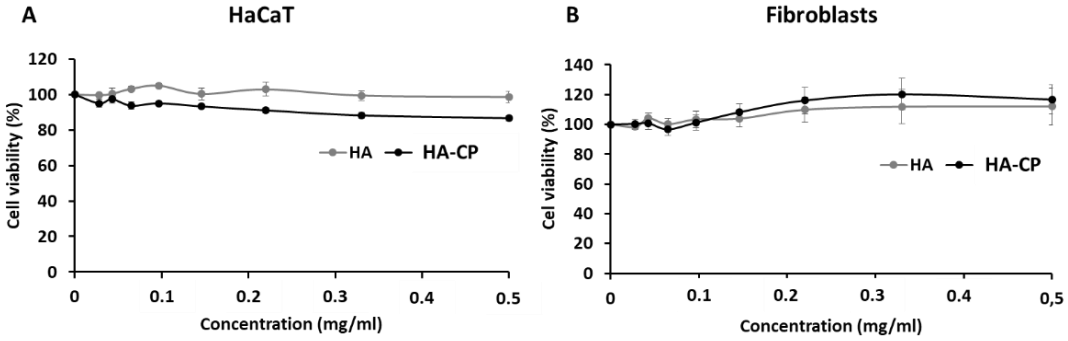

Figure III. 6: Cell viability by MTS assay of HA-CP and HA in **(A)** HaCaT keratinocytes and **(B)** human fibroblasts after 72 h of treatment (n = 3).

III.2.2.3. Tissue Viability in an *Ex Vivo* Human Skin Model

We also evaluated tissue viability in an *ex vivo* human skin model (see **Chapter II** for more details) after 24, 48, and 72 h of treatment with 3 µL of 1% w/v solution of linear HA and HA-CP. We obtained breast skin samples with informed consent from healthy women undergoing plastic surgery (Hospital la Fe, Valencia, Spain). The results shown in **Figure III. 7** demonstrate that all both treatments allowed the maintenance of tissue viability at the concentration tested. Interestingly, the HA-CP vehicle provided enhanced results when compared to linear HA at 48 h. This phenomenon may be due to an increase in the hydration of the skin after HA-CP application, given the slower degradation of HA present in the HA-CP than linear HA. These results agreed with the HAase degradation kinetics obtained by SEC.

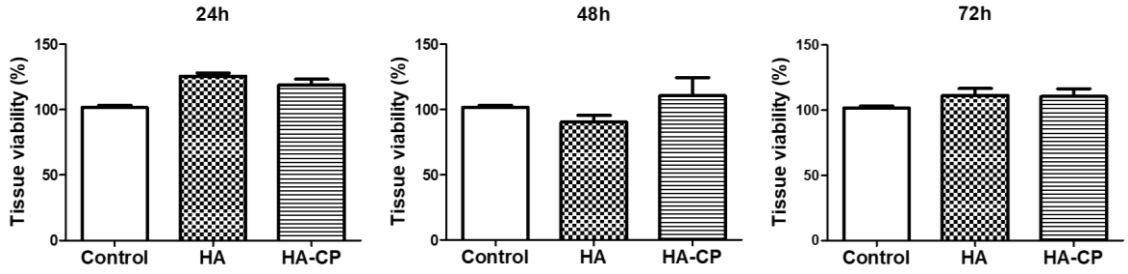

Figure III. 7: Tissue viability in an *ex vivo* human skin model after 24, 48, and 72 h of treatment with HA and HA-CP (n = 3).

III.2.2.4. *Ex Vivo* Human Skin Permeation by Franz Diffusion Cells

We next performed skin permeation studies by Franz diffusion cells using human skin [52, 53]. Again for this experiment, we obtained breast skin samples with informed consent from healthy women undergoing plastic surgery (kindly donated from Hospital la Fe, Valencia, Spain). We carefully fixed skin between the donor and the receptor chambers of the Franz cells so that the stratum corneum faced upwards; we then filled the receptor chamber with 8 mL of 0.01 M PBS pH = 7.4. We added 100 µL of 1% w/v solution of fluorescently labeled HA-based materials to the donor chamber, which is in contact with the upper part of human skin (stratum corneum), incubated the samples for 8 h, and then studied skin sections by confocal microscopy (**Figure III. 8A**).

The levels of detected fluorescence suggested that HA-based materials permeated through the stratum corneum; images for HA-CP-Cy5.5 verified successful penetration

through the stratum corneum, with a marked diffusion through to the viable epidermis. However, images captured for the linear HA-Cy5.5 revealed accumulation mainly in the stratum corneum, a finding that agrees with a previous report from Essendoubi *et al*. that employed an HA of 100-300 kDa [54]. Furthermore, pixel quantification of Cy5.5 fluorescence using Image J software analysis revealed a marked accumulation of HA-CP-Cy5.5 in the viable epidermis and lower accumulation in the stratum corneum compared to linear HA-Cy5.5 (**Figure III. 8B**).

Overall, skin permeation experiments demonstrated that HA-CP-Cy5.5 possesses an enhanced skin permeation capacity when compared to linear HA-Cy5.5, reaching deeper skin layers.

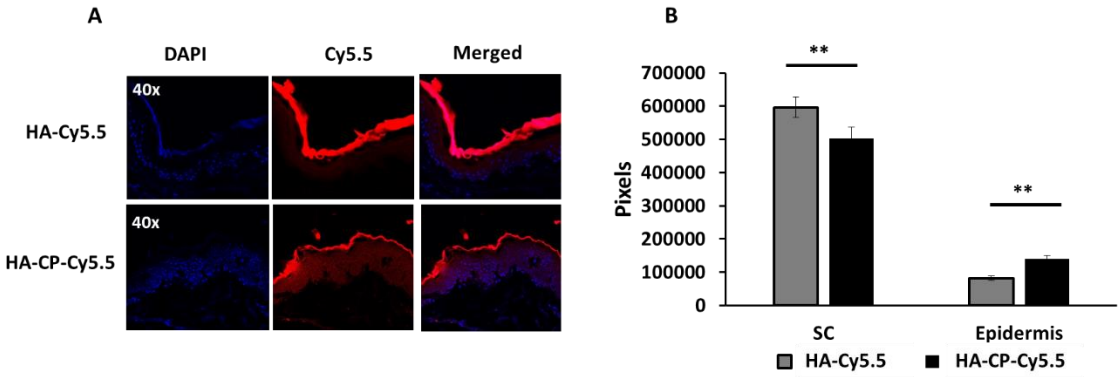

Figure III. 8: Permeation studies using Franz diffusion cells after 8 h of treatment with HA-Cy5.5 and HA-CP-Cy5.5 at 1% w/v. **(A)** Confocal microscopy images of Cy5.5-labeled HA and HA-CP after 8 h of permeation. Original magnification displayed in each image was 40x. **(B)** Quantification of Cy5.5 fluorescence intensity in the stratum corneum (SC) and the viable epidermis by Image J software. Asterisks indicate statistically significant differences after ANOVA analysis followed Bonferroni's post hoc tests, mean ± SEM. In all cases, we considered differences to be significant when p***<0.001; p**<0.01; p*<0.05.

We also studied the ability of both systems to penetrate to the deepest skin layer, the dermis, which is in contact with the liquid in the receptor chamber (representing the circulatory system for our purposes). We employed benzoic acid, a well-known drug that can penetrate through the skin [55], as a positive control for skin penetration (**Figure III. 9**). As expected, results obtained by HPLC analysis suggested that the positive control reaches the dermis, increasing in concentration in the receptor chamber as treatment time increases.

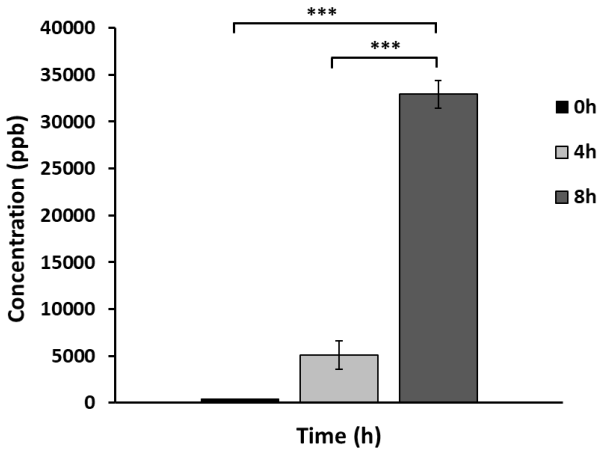

Figure III. 9: Concentration of benzoic acid in the receptor chamber of the Franz diffusion cells at different permeation times analyzed by HPLC. Asterisks indicate statistically significant differences after ANOVA analysis followed Bonferroni's post hoc tests, mean ± SEM. In all cases, we considered differences to be significant when p***<0.001; p**<0.01; p*<0.05.

However, HPLC analysis of aliquots taken from the receptor chamber (representing the circulatory system) revealed the absence of Cy5.5 signal in the case of HA-based materials (**Figure III. 10**). Therefore, the results suggest that either HA-based materials remain in the epidermis (HA-CP-Cy5.5) or the stratum corneum (HA-Cy5.5) without reaching the dermis.

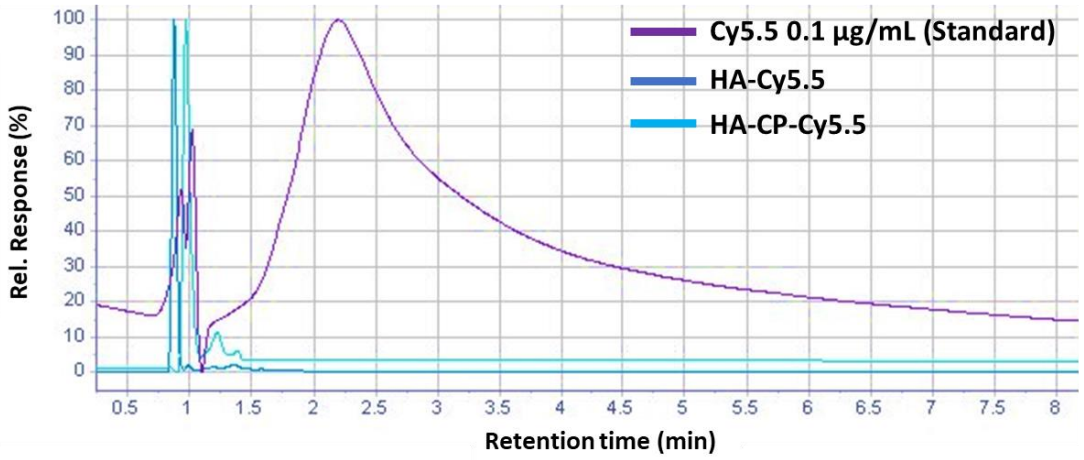

Figure III. 10: Aliquots from the receptor chamber after 8 h of permeation study in human skin by Franz diffusion cells analyzed by HPLC. Chromatograms of a standard sample of Cy5.5 at 0.1 µg/mL, HA-Cy5.5, and HA-CP-Cy5.5.

In summary, our novel HA-CP vehicle has demonstrated suitability for topical applications, and the avoidance of systemic absorption and any associated undesired systemic effects.

III.2.2.5. Hydration Assays in Human Volunteers

Finally, through a certified laboratory (Prof. Cortijo Lab. Univ. Valencia, Spain) we performed *in vivo* hydration assays with both HA-based materials in over 15 healthy volunteers (**Figure III. 11**). The zone of the cheekbone and nasolabial fold were measured using a Corneometer®, an instrument used to indicate the hydration level of the layers of the skin via measurement of the skin dielectric properties. For the experiment, we used two pharmaceutical formulations developed by the company PTS following Good Manufacturing Practice (GMP) in compliance with all regulations (ICH guidelines; https://www.ich.org/products/guidelines.html) and using as active component HA and HA-CP. The formulations were applied to the left zone, while the right zone acted as a control, and performed measurements at time 0 (before applying the product) and at 1, 3, 8, 16, 24, and 40 h post-treatment.

The results suggest that conventional linear HA provided significant higher skin hydration than HA-CP over short times. However, HA-CP administration displayed a trend (non-significant) towards prolonged and enhanced skin hydration when compared with linear HA and the control from 8 h. These results agree with the results obtained in the HAase assay, where HA-CP displayed higher resistance to HAase-mediated degradation at 24 h, supporting the hypothesis that the cross-polymer maintains its native structure and intrinsic properties for an extended period of time, providing better results in terms of total hydration, cell viability, and skin permeation than conventional linear HA.

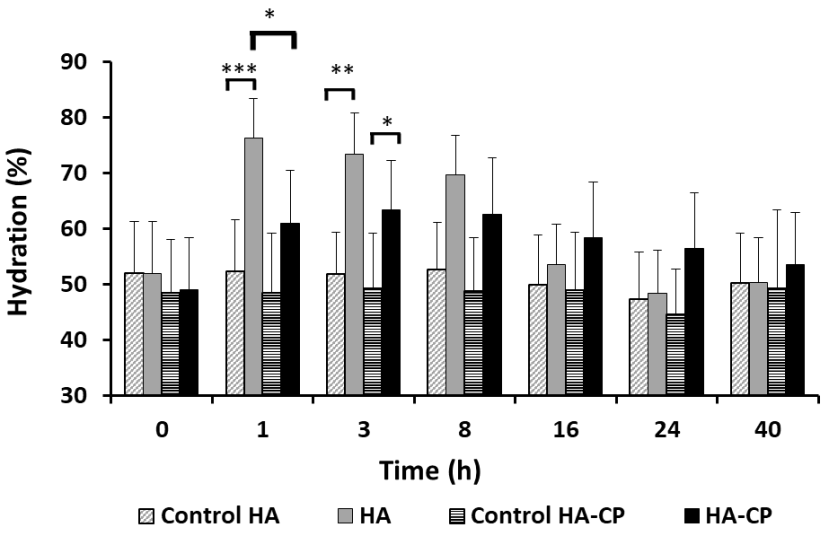

Figure III. 11: Hydration assay in human volunteers using linear HA and HA-CP over 40 h (n = 15). Asterisks indicate statistically significant differences after ANOVA analysis followed Bonferroni's post hoc tests, mean ± SEM. In all cases, we considered differences to be significant when p***<0.001; p**<0.01; p*<0.05.

III.2.3. Hybrid Material: HA-CP Vehicle Combined with Polypeptidic Micelles for Transdermal Delivery of Hydrophobic APIs

After the robust physico-chemical characterization and biological evaluation of HA-CP and in order to validate its capacity as permeation enhancer, we next analyzed a hybrid material, with polymeric micelles embedded within HA-CP, as a novel platform system for topical delivery for hydrophobic APIs. The polymeric micelles were developed via amphiphilic block copolymer formulation.

III.2.3.1. Synthesis and Characterization of Block Copolymers

Firstly, we prepared six amphiphilic PEG-amino acid block copolymers by ring-opening polymerization (ROP) of N-carboxy anhydride (NCA). Using this material, we then prepared micelles using a co-solvent methodology [56]. ROP of NCAs occurs via two mechanisms: normal amine mechanism (induced by nucleophilic substitution) and activated monomer mechanism (AMM, induced by deprotonation) [57]. The synthesis of our block copolymers proceeds by normal amine mechanism, based on the nucleophile attack of the initiator PEG (in this case). We employed hydrophilic block copolymers composed by PEG of 5 kDa (approx. 114 units of ethylene oxide), and L-phenylalanine (Phe) or benzyl-L-glutamate (BG) with different degree of polymerization (DP: 10, 20,

and 40) as the hydrophobic component. Synthesis yielded a family of six amphiphilic block copolymers: PEG-PPhe10, PEG-PPhe20, PEG-PPhe40, PEG-PBG10, PEG-PBG20, and PEG-PBG40 (**Scheme III. 2**).

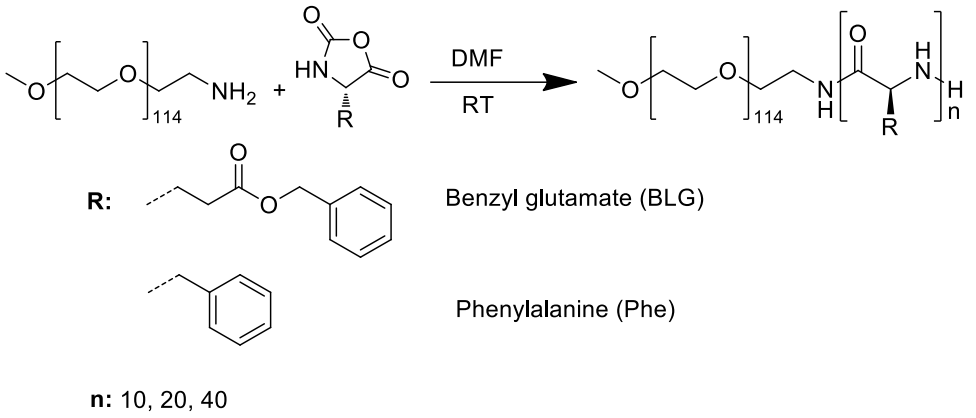

Scheme III. 2: Synthetic scheme for the preparation of the block copolymer family.

We synthesized amphiphilic block copolymers as previously described [58-60]. We employed a well-controlled polymerization reaction by modifying the initiator PEG (MeO-PEG-NH_2), as illustrated by the well-defined architecture obtained for poly-L-benzyl glutamate derivatives in terms of targeted Mw and low PDI derived from GPC analysis (**Figure III. 12A**). In the case of PPhe derivatives, we discovered the hindered growth of the polypeptide backbone for a degree of polymerization higher than 10, perhaps attributed to the increasing insolubility of the resulting polymers (as evidenced by the generation of cloudy suspensions during polymerization). We obtained further evidence of low solubility from GPC analysis, where larger aggregates appeared for all Phe derivatives as the degree of polymerization increased (**Figure III. 12C**). We employed ^{1}H-NMR spectra to assess purity, identity, and confirm the experimental degree of polymerization (**Figure III. 12B and D**). These findings agreed with data obtained by GPC, revealing a predominantly normal amine mechanism for the polymerization (**Table III. 3**).

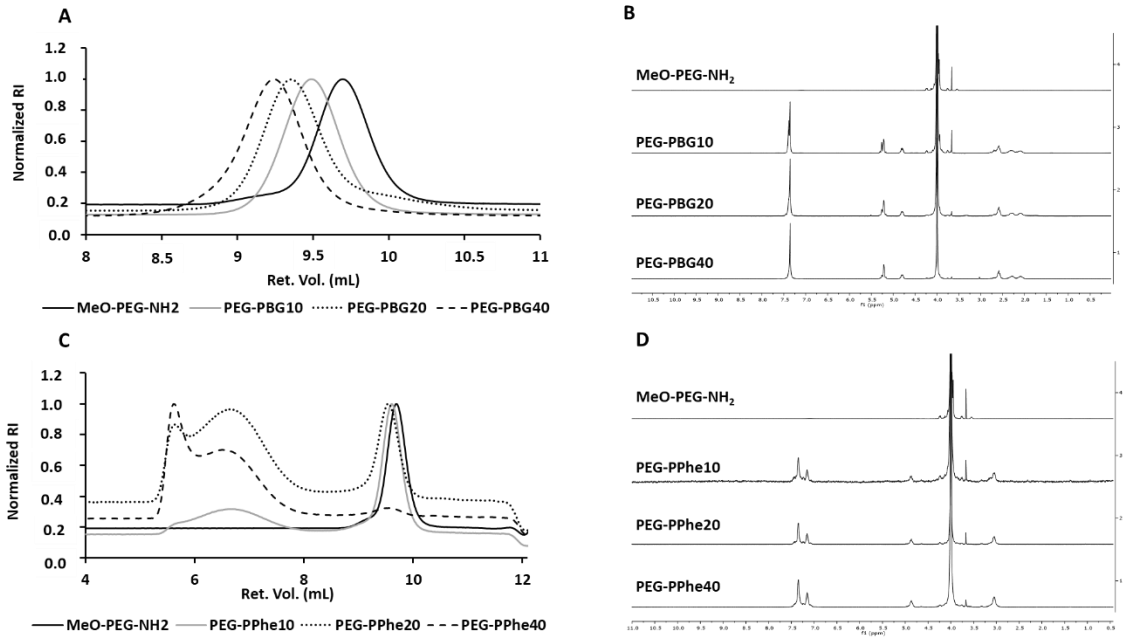

Figure III. 12: **(A)** SEC-RI elugram for PEG-PBG diblock family in DMF. **(B)** ^{1}H-NMR spectra in deuterated trifluoroacetic acid (TFA) for PEG-PBG family. **(C)** SEC-RI elugram for PEG-PPhe diblock family in DMF. **(D)** ^{1}H-NMR spectra in deuterated TFA for PEG-PPhe family.

Table III. 3: Physico-chemical characterization of the family of amphiphilic block copolymers with different degree of polymerization and amino acid backbone.

Block copolymer	Target DP	Mw[a] (kDa)	Mn[a] (kDa)	DP[a]	DP[b]	Đ[a]
MeO-PEG-NH$_2$	-	6749	--	-	-	1.187
PEG-PBG10	10	8943	7801	10	9	1.146
PEG-PBG20	20	10931	10931	19	17	1.140
PEG-PBG40	40	13863	11329	33	38	1.224
PEG-PPhe10	10	7651	7925	6	8	1.134
PEG-PPhe20[c]	20	8571	8954	13	15	1.149
PEG-PPhe40[c]	40	10759	9248	18	17	1.288

[a]Data obtained by GPC (DMF, LiBr 1 % w/w) at 8 mg/mL. [b]Data obtained by ^{1}H-NMR in deuterated TFA by integrating PEG signal of the macroinitiator to α-proton of polypeptide block. [c]Precipitation observed in the polymerization reaction, GPC data showed bimodal traces pointing to strong aggregation. DP: Degree of polymerization. Đ = polydispersity.

III.2.3.2. Characterization of Block Copolymer Micelle Formulation

We used synthesized block copolymers to create the micelles using the co-solvent method [56] developed for efficient encapsulation of hydrophobic APIs, encapsulating the fluorophore Dil as an example of a hydrophobic API. We performed a preselection of

diblock copolymers at 10 mg/mL based on their micellar formulation stability. Larger polypeptidic backbone block copolymers (PEG-PPhe40 and PEG-PBG40) precipitated within a few hours of incubation at room temperature (r.t.), probably due to an imbalance of the hydrophilic and lipophilic ratio. Therefore, we selected PEG-PBG10, PEG-PBG20, PEG-PPhe10, and PEG-PPhe20 for further evaluation. The micelles displayed a small hydrodynamic diameter by number, a narrow PDI, and a Z-potential close to 0. Of note, we observed smaller encapsulation efficiency for PEG-PPhe (~50%) than PEG-PBG (~100%) (**Table III. 4**).

Table III. 4: Characteristics of the micelles formed by block copolymers with and without encapsulated dye.

Block Copolymer	E.E[a] %	Dil Loading[a] % w/w	CMC[b] mg/mL	Conc. mg/mL	Size, I[c] nm	Size, N[d] nm	PDI	Z-pot mV
PEG-PBG10	---	---	0.04	10	28/317[e]	16	0.316	-0.695
				5	30	16	0.251	-0.111
				1	22/312[e]	12	0.312	7.243
PEG-PBG10 + Dil	114[f]	1.14[f]	---	10	32/173[e]	15	0.420	-0.781
				5	33/179[e]	17	0.373	0.230
				1	35/248[e]	18	0.338	2.040
PEG-PBG20	---	---	0.01	10	30	18	0.149	-0.269
				5	32	19	0.130	-0.157
				1	33	20	0.152	-0.039
PEG-PBG20 + Dil	105[f]	1.05[f]	---	10	32	19	0.164	0,184
				5	34	20	0.127	0.384
				1	36	19	0.254	0.771
PEG-PPhe10	---	---	0.008	10	164	25	0.363	0.052
				5	137	31	0.279	0.481
				1	110	27	0.246	1.867
PEG-PPhe10 + Dil	47	0.47	---	10	166	30	0.322	0.390
				5	145	30	0.297	1.103
				1	108	28	0.261	3.36
PEG-PPhe20	---	---	<0.004	10	143	28	0.409	2.443
				5	128	30	0.282	3.207
				1	103	21	0.232	5.143
PEG-PPhe20 + Dil	58	0.58	---	10	77/403[e]	30	0.466	2.683
				5	79/330[e]	34	0.388	3.170
				1	107	26	0.317	5.110

E.E = Encapsulation efficiency. [a] Determined by UV-Vis. [b] Critical micelle concentration (CMC) determined by fluorescence using pyrene as a hydrophobic probe. [c] Hydrodynamic diameter by intensity. [d] Hydrodynamic diameter by number. [e] Bimodal size distribution by intensity (values related to each peak by DLS). [f] PEG-PBG was found to be highly hygroscopic, deviation in the weighted mass leads to E.E. > 100%.

Moreover, PEG-PBG displayed higher critical micelle concentration (CMC) than Phe derivatives, presenting values between 0.04 - 0.01 and 0.004 - 0.008 mg/mL, respectively. These results indicate higher propensity for self-assembly of PEG-PPhe in aqueous solution, probably due to the strong hydrophobic nature of PPhe (**Figure III. 13A**). In agreement with these results, GPC analysis revealed a robust aggregation behavior for PEG-PPhe copolymers.

We next employed circular dichroism (CD) to evaluate the secondary structure of the polypeptidic block within the micellar core. As shown in **Figure III. 13B**, micellar aqueous solutions of block copolymers displayed the typical alpha-helix conformation for PB and a mixture of beta-sheet and alpha-helix conformation for Phe, both with pronounced negative bands for polymers with a larger degree of polymerization (PEG-PPhe20 and PEG-PBG20). Interestingly, the intensity and the shape of the characteristic alpha-helix band changed for PPhe to PBG copolymers, pointing to structurally different arrangements of side-chain groups. PPhe derivatives strongly form aggregates; as an example, diphenylalanine demonstrates self-assembly behavior generating nanotubes in aqueous solutions [61]. Castelletto and Hamley developed a similar system to ours (5 kDa PEG and 4 units of Phe) [62], and their CD and fluorescence analysis revealed that self-assembly behavior relied on π-π* interactions, yielding fibrils at 0.5 mg/mL. Decandio *et al.* analyzed a peptide composed by arginine (Arg) and Phe and discovered the same negative band over 200 nm [63]. The negative band for Phe derivatives was also observed for triblock PEG-PGA-PPhe micelles at pH 4.5 in aqueous solution [64]. These experiments agree with our results and confirm strong aggregation observed for the micelles containing Phe residues.

Size analysis of the micelles by DLS revealed similar mean size distribution (Dh) for the selected copolymers, ranging from 12 to 30 nm with no significant variation upon changing concentration (1 - 10 mg/mL) in good agreement with reported values for similar amphiphilic block copolymers [65-67] (**Figure III. 13C**). Transmission electron microscopy (TEM) images confirmed that micelles displayed a mainly spherical shape with a uniform diameter (**Figure III. 13D**).

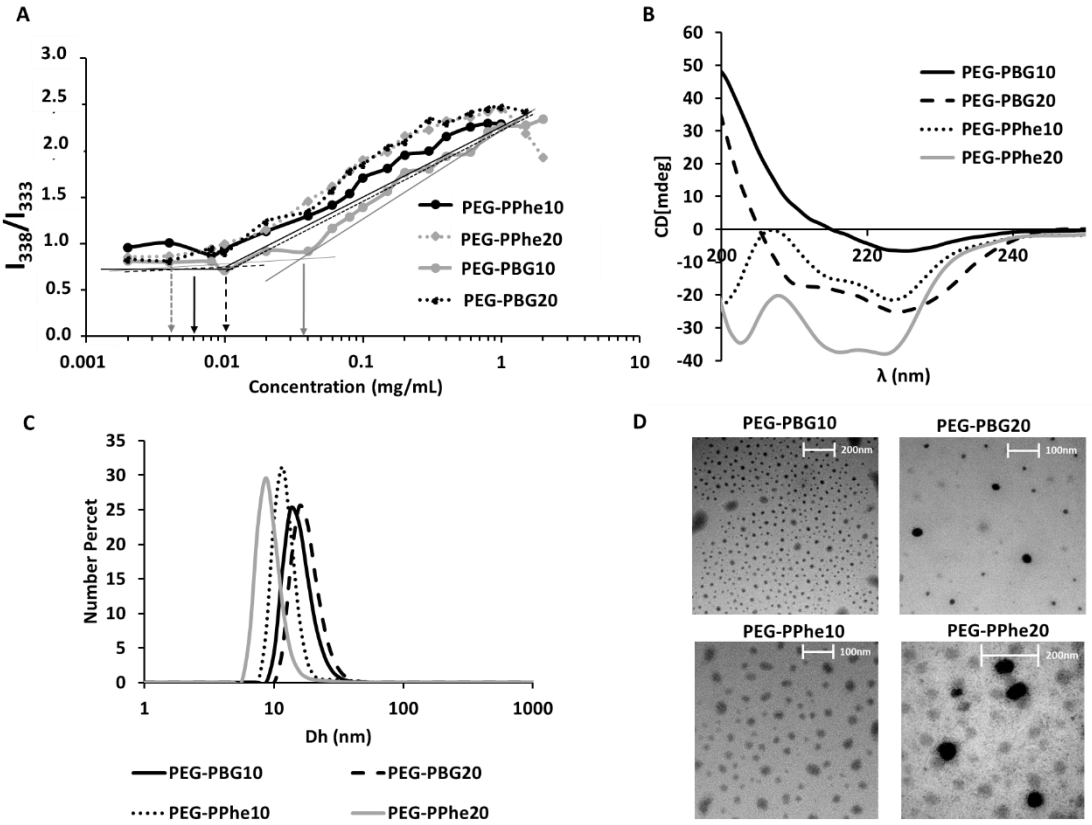

Figure III. 13: Physico-chemical characterization of micelles. **(A)** CMC obtained for aqueous micellar formulations using a fluorimeter employing an intensity ratio I_{338}/I_{333}. **(B)** CD spectra of micellar solutions at 0.5 mg/mL in water. **(C)** Size distribution by number obtained from DLS measurements at 10 mg/mL of micelles formulation. **(D)** TEM images of aqueous micellar formulations at 2 mg/mL.

In conclusion, the application of a Phe backbone promoted a more rigid inner core, probably very tightly packed. As a result, the Phe-based block copolymers possess a higher tendency to form micelles (lower CMC) and lower capacity to encapsulate the dye (Dil) than the BG-based block copolymers, as expected due to the modification of the hydrophilic-hydrophobic balance.

III.2.3.3. Cell Viability Studies *In Vitro* of Selected Micelles

We performed cell viability assays with the selected micelles (PGA-PPhe10, PGA-PPhe20, PGA-PBG10, and PGA-PBG20) to determine any toxicity in HaCaT keratinocytes and human fibroblasts by MTS assay. As shown in **Figure III. 14**, all the micelles do not diminished cell viability in both cell lines up to the concentrations tested.

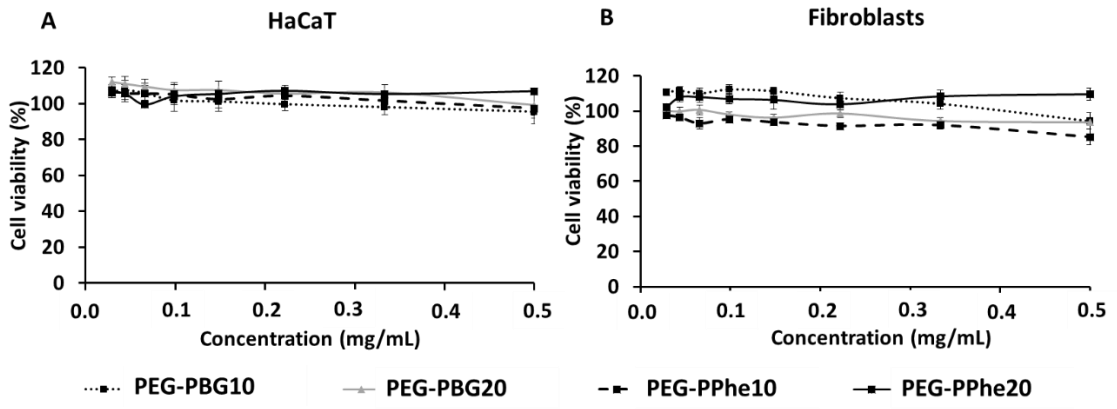

Figure III. 14: Cell viability by MTS assay of PGA-PPhe10, PGA-PPhe20, PGA-PBG10, and PGA-PBG20 in **(A)** HaCaT keratinocytes and **(B)** human fibroblasts after 72 h of treatment (n=3).

III.2.3.4. Characterization of the Hybrid Material

To study the properties of the HA-CP vehicle as a skin permeation enhancer for hydrophobic APIs, we prepared hybrid materials containing HA-CP vehicle and micelles loaded with the fluorophore Dil (PEG-PPhe10-Dil, PEG-PPhe20-Dil, PEG-PBG10-Dil, and PEG-PBG20-Dil). We dissolved each micelle at 10 mg/mL in a 1% w/v solution of HA-CP vehicle.

We characterized the resultants hybrid materials in terms of size distribution by DLS. The micelles composed by the block copolymers formed by 10 units of polypeptides (PEG-PPhe10 and PEG-PBG10), displayed lower size distribution by number, with sizes close to micelles without HA-CP (**Table III. 5**); however, the micelles embedded into HA-CP with 20 units of polypeptides (PEG-PPhe20 and PEG-PBG20) displayed a broad size distribution, maybe presenting fewer but larger aggregates, but the complete explanation requires deeper studies (**Figure III. 15**). By intensity, all the hybrid materials revealed higher size distribution, with similar values to micelles formulated in pure water (without the HA-CP).

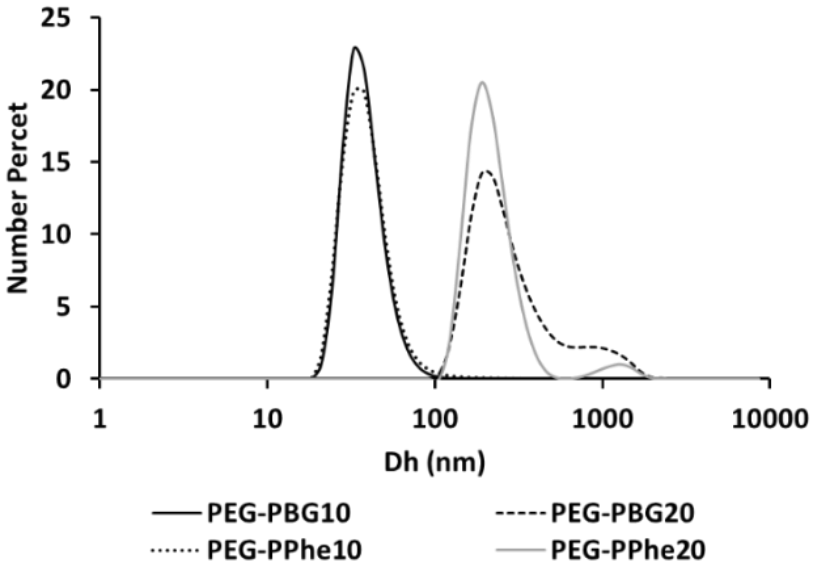

Figure III. 15: Size distribution by number obtained from DLS measurements at 10 mg/mL of micelle formulations embedded into the HA-CP vehicle at 1% w/v.

Table III. 5: Size distribution by DLS of the micelles embedded into HA-CP vehicle (1% w/v).

Hybrid System	Size, I[a] (nm)	Size, N[b] (nm)	PDI
PEG-PBG10 in HA-CP (1% w/v)	75/559[c]	38	0.521
PEG-PBG20 in HA-CP (1% w/v)	222	189	0.881
PEG-PPhe10 in HA-CP (1% w/v)	315	35	0.434
PEG-PPhe20 in HA-CP (1% w/v)	262	214	1.000

[a] Hydrodynamic diameter by intensity. [b] Hydrodynamic diameter by number. [c] Bimodal size distribution by intensity (values related to each peak by DLS). Concentration of micelles was 10 mg/mL embedded in the HA-CP vehicle (1% w/v).

III.2.3.5. *Ex Vivo* Human Skin Permeation of Hybrid Material by Franz Diffusion Cells

We next undertook skin permeation studies following 8 h of treatment using Franz diffusion cells employing human skin. To perform the permeation studies, we added 100 µL of a 10 mg/mL solution of each micelle with encapsulated Dil (PEG-PPhe10-Dil, PEG-PPhe20-Dil, PEG-PBG10-Dil, and PEG-PBG20-Dil) applied in the HA-CP (1% w/v) vehicle to the donor chamber, which is in contact with the upper part of human skin (stratum corneum). Encouragingly, all micelles formulated in the HA-CP vehicle penetrated through the stratum corneum, reaching the viable epidermis (**Figure III. 16A**).

Of note, by Image J analysis we demonstrated that the hybrid material that contained the PEG-PBG20-Dil micelle accumulated significantly in the epidermis in comparison to the other micelles composed by different block copolymers, perhaps due to the physico-chemical differences of each micelle stated above, such as the conformation (PEG-PBG20 presented alpha-helix conformation in solution) and a less rigid inner core compared to Phe-based micelles (**Figure III. 16B**).

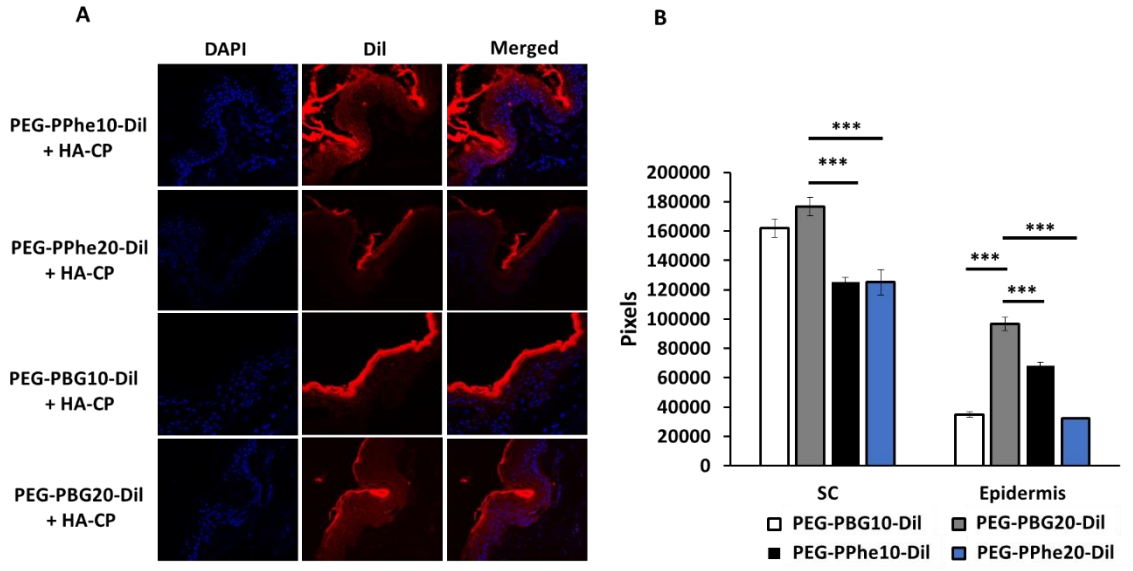

Figure III. 16: Permeation studies with polypeptide-based micelles formulated in HA-CP (1% w/v) after 8 h of permeation using Franz diffusion cells. **(A)** Confocal microscopy images of Dil-labeled micelles formulated in HA-CP. Original magnification displayed in each image was 40x. **(B)** Dil fluorescence intensity quantification by Image J software in the stratum corneum (SC) and the viable epidermis. Asterisks indicate statistically significant differences after ANOVA analysis followed Bonferroni's post hoc tests, mean ± SEM. In all cases, we considered differences to be significant when p***<0.001; p**<0.01; p*<0.05.

Additionally, HPLC analysis of aliquots taken from the receptor chamber following permeation studies demonstrated the absence of Dil signal for all the micelles studied after 8 h of treatment (**Figure III. 17**). Therefore, these findings confirm the potential of our novel HA-CP vehicle as a penetration enhancer for topical applications, transporting the micelles to the epidermis without reaching the dermis, thereby avoiding systemic absorption and further diffusion.

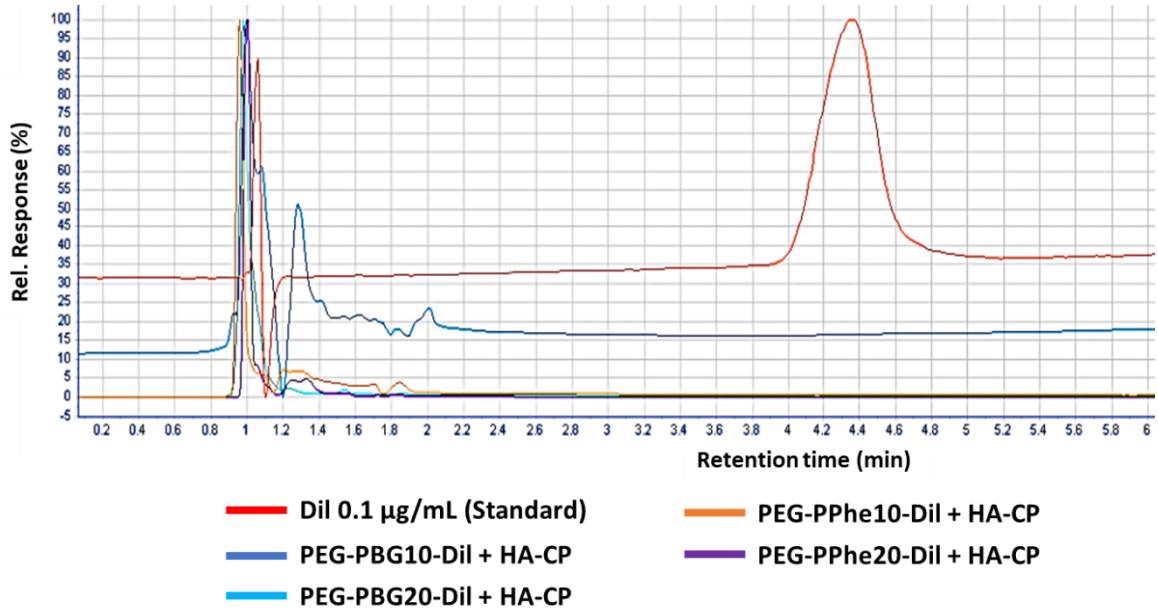

Figure III. 17: Aliquots from the receptor chamber after 8 h of permeation study in human skin by Franz diffusion cells analyzed by HPLC. Chromatograms of a standard sample of Dil at 0.1 µg/mL and the four formulations PEG-PPhe10-Dil, PEG-PPhe20-Dil, PEG-PBG10-Dil, and PEG-PBG20-Dil applied in the HA-CP (1% w/v) vehicle.

Finally, due to the higher capacity of the hybrid material composed by PEG-PBG20-Dil and HA-CP to permeate through the epidermis, we selected this formulation to carry out comparative permeation studies when the system is applied in water, linear HA, and HA-CP vehicle. Confocal microscopy images revealed that HA-CP enhanced the permeation of the PEG-PBG20-Dil compared to linear HA or water formulation, accumulating mainly in the viable epidermis (**Figure III. 18A**). Quantification of Dil intensity by Image J software suggested that the micelle applied in HA-CP penetrated significantly through the epidermis, with an almost two-fold higher intensity when compared to the formulations in water or linear HA (**Figure III. 18B**). The intensity in the stratum corneum for the formulation with HA-CP remains low, suggesting that the micelle penetrates across the stratum corneum barrier and reaches deeper skin layers. This enhancement relates to the resistance of HA-CP vehicle against the HAase degradation, which maintains an intact structure over time, thereby permitting sustained activity over a longer time.

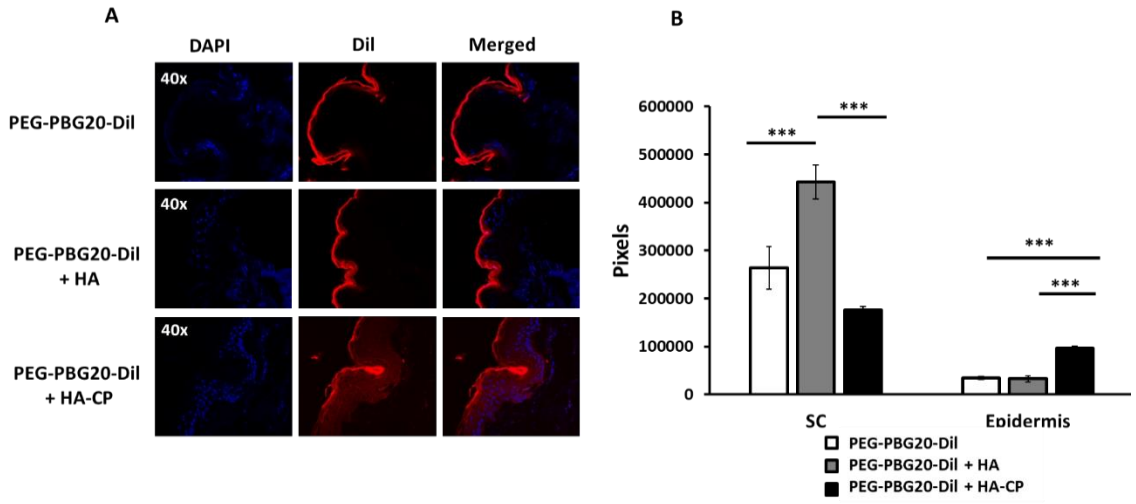

Figure III. 18: Permeation studies of PEG-PBG20-Dil applied in water, HA (1% w/v), and HA-CP (1% w/v) after 8 h of permeation using Franz diffusion cells. **(A)** Confocal microscopy images of Dil-labeled micelle PEG-PBG20 in the three formulations. Original magnification displayed in each image was 40x. **(B)** Dil fluorescence intensity quantification by Image J software in the stratum corneum (SC) and the viable epidermis. Asterisks indicate statistically significant differences after ANOVA analysis followed Bonferroni's post hoc tests, mean ± SEM. In all cases, we considered differences to be significant when p***<0.001; p**<0.01; p*<0.05.

III.2.3.6. Tissue Viability of Hybrid Material in an *Ex Vivo* Human Skin

We also evaluated tissue viability in an *ex vivo* human skin model (see **Chapter II** for more details) after 24, 48, and 72 h of treatment with 3 µL of a 10 mg/mL solution of the three selected formulations due to its higher permeation through the skin: (i) PEG-PBG20 in water, (ii) PEG-PBG20 applied in linear HA (1% w/v), and (iii) PEG-PBG20 applied in HA-CP (1% w/v). The results shown in **Figure III. 19** demonstrate that all treatments did not diminish tissue viability at the concentration tested.

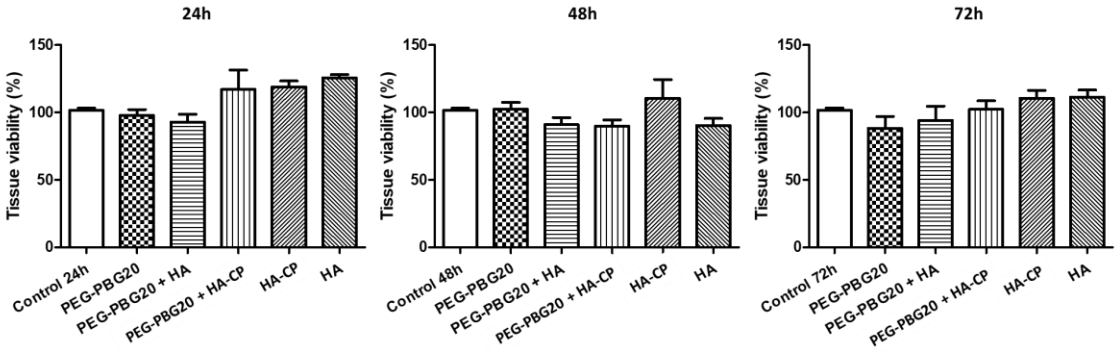

Figure III. 19: Tissue viability in an *ex vivo* human skin model after 24, 48, and 72 h of treatment with the selected formulations: (i) PEG-PBG20 in water, (ii) PEG-PBG20 applied in linear HA, (iii) PEG-PBG20 applied in HA-CP, with HA and HA-CP as controls.

III.3. Conclusions

Encouraged by previous studies that employed polypeptides in skincare products, we proposed a novel transdermal drug delivery platform based on a cross-linked hyaluronic acid and polyglutamic acid (HA-CP). In close collaboration with the company Polypeptide Therapeutic Solution S.L., we synthesized a biodegradable and biocompatible cross-polymer composed by cross-linked HA and PGA through lysine moieties. We demonstrated the enhanced properties of HA-CP vehicle compared to linear HA, including HAase activity resistance and higher long-term hydration skin capacity in human volunteers, which promotes human skin tissue compatibility. Permeation studies in human skin established that our novel HA-CP vehicle exhibited a marked penetrative capacity to the viable epidermis when compared to linear HA.

To further demonstrate the penetration properties of our vehicle, we developed a family of amphiphilic block copolymers of different nature, using PPhe and PBG with different degree of polymerization carrying a hydrophobic fluorescent dye (Dil) as a hydrophobic API model, and we studied their skin penetration in the presence of HA-CP vehicle. We demonstrated that changes in the solution conformation of the nanocarrier were driven by the presence of Phe as aminoacid in the polymeric chain. Moreover, the type of polypeptide modifies other physico-chemical characteristics of the micelles such as the critical micelle concentration (CMC) and the encapsulation efficiency (E.E) of Dil; Phe-based block copolymers micelles possess lower CMC and capacity to encapsulate

the dye than the BG-based micelles. We observed the enhanced penetration of micelles into the viable epidermis, with a marked accumulation in the case of PEG-PBG20-Dil, demonstrating the ability of the cross-polymer to enhance the penetration through the skin. Of note, all micelles accumulated in the epidermis without reaching the dermis, therefore avoiding the possible undesirable adverse effects observed at the systemic level.

Finally, using the PEG-PBG20-Dil micelle as an example, we studied skin penetration when applied alone, in linear HA, or in the HA-CP vehicle. This study demonstrated the utility of our HA-CP vehicle to promote the penetration of micelles in comparison with linear HA. Also, our HA-CP vehicle revealed enhanced tissue viability compared to control in an *ex vivo* human skin model.

III.4. Materials and Methods

III.4.1. Materials

All reagent grade chemicals were obtained from Sigma Aldrich (Spain) and used without further purification unless otherwise indicated. H-L-Glu(OBzl)-OH, L-Phenylalanine (Phe) and MeO-PEG-NH_2 (Mw = 5 kDa, 114 ethylene glycol units) were obtained from Iris Biotech (Germany). Sodium hyaluronate PrimalHyal300 (Mw = 200 kDa) was supplied by Comercial Química Massó S.A. (Spain) and sodium hyaluronate (Mw = 50 kDa) by Principium S.A. (Switzerland). Dil dye fluorophore (1,1'-dioctadecyl-3,3,3',3'-tetramethylindocarbocyanine perchlorate (Dil; DilC18(3)) was purchased from Thermo Fisher Scientific (Spain). Cyanine5.5 amine dye fluorophore was purchased from Lumiprobe GmbH (Germany). Bovine testicular HAase (Type IV-S) with a specific activity of 999 units per milligram was obtained from Sigma Aldrich (Spain). HAase was weighed before each experiment because activity in frozen solution did not remain constant [47]. Pyrene was obtained from Fluka Analytical (Spain). Deuterated trifluoroacetic acid (TFA-d_1), chloroform-d_1, dimethylsulfoxide-d_6, and deuterium oxide (D_2O) were purchased from Deutero GmbH (Germany). Dialysis was performed in a Millipore ultrafiltration device fitted with a 1, 3, 10 or 30 kDa MWCO regenerated cellulose membrane (Vivaspin®).

The human immortalized non-tumorigenic keratinocyte cell line (HaCaT) was supplied by CLS Cell Lines Service (Eppelheim, Germany) and human fibroblasts were

supplied by Hospital La Fe (Valencia, Spain). High glucose DMEM Glutamax and Dulbecco's Modified Eagle's Medium-high glucose were purchased from Fisher (Spain) and Sigma Aldrich (Spain), respectively. Phosphate buffer saline (PBS) and fetal bovine serum (FBS) Medium 200 were provided from Gibco (Spain). (3-(4,5-dimethylthiazol-2-yl)-5-(3-carboxymethoxyphenyl)-2-(4-sulfophenyl)-2H-tetrazolium) (MTS) was supplied by Promega (Spain). All solvents were of analytical grade and dried and freshly distilled. Ultrapure water (MilliQ water) with a resistivity of 18 MΩ.cm was used in all aqueous preparations.

III.4.2. Physico-Chemical Characterization Methods

III.4.2.1. Nuclear Magnetic Resonance (NMR) Spectroscopy

NMR spectra were recorded at 27°C (300 K) on a 300 UltrashieldTM from Bruker (Billerica MA, USA). Data were processed with the software Topspin (Bruker GmbH, Karlsruhe, Germany). Samples were prepared at a concentration of 5 mg/mL in the required solvent.

III.4.2.2. Gel Permeation Chromatography (GPC) in DMF

For SEC measurements in DMF containing 1 g/L of lithium bromide as an additive, a GPC max (Malvern Instruments, Spain) autosampler was used with a flow rate of 0.7 mL/min at 60°C as an integrated instrument, including two columns (105/103/102Å porosity) from Tosoh. Viscotec TDATM 302 triple detector was used as an integrated detection system (Refractive index and Light Scattering), and the calibration curve was obtained with PEG analytical standards kit (Sigma Aldrich, Spain), ReadyCal set Mp 200-1.200.000 for GPC.

III.4.2.3. Gel Permeation Chromatography (GPC) in Aqueous Media

For SEC measurements in aqueous media containing 150 mM $NaNO_3$, 5 mM phosphate buffer (PB) at pH 5, and 0.005 % (w/w) sodium azide as an additive were used in an AF2000 system from Postnova Analytics (Landsberg, Germany). The system was configured to work on SEC mode with an isocratic pump (PN1130) an autosampler (PN5300), a refractive index (RI, PN3150), 21 angle-multi angle light scattering (MALS, PN3621), and an ultraviolet-visible (UV-Vis) (PN3211) detectors. A working flow rate

of 0.8 mL/min at 30°C was employed with one TSKgel G6000PWXL column. Refractive index (RI) and multi-angle light scattering (MALS) were used for detection and Mw determination, calibration of both RI and MALS detectors was achieved with well-defined Pullulan (50 kDa) and validation with polymethacrylic acid sodium salt (62.5 kDa PMASS) standards, purchased from Polymer Standards Service (PSS, Mainz, Germany). dn/dc values for cross-linked sodium hyaluronates were determined from recovered mass assuming 95 - 100% recovery from the chromatographic column and found to be within 0.125 - 0.150 mL/g. 30 μL of a 3.75 mg/mL polymer solution was injected each time. For linear sodium hyaluronates, 0.150 mL/g as dn/dc value was used according to the values reported in the literature [47].

Hyaluronidase Degradation Studies by Gel Permeation Chromatography (GPC) in Aqueous Media: HA-based materials were degraded by HAase at 37ºC employing the thermo conditioning autosampler of AF2000 system from Postnova Analytics (Landsberg, Germany). GPC measurements were carried out as described previously in the previous point. Concentration for HA materials was 3.75 mg/mL and for HAase was 5 U/mL. Mw distributions values were achieved per triplicate and represented as the average of Mw.

III.4.2.4. Circular Dichroism (CD)

CD Spectroscopy was performed with a J-815 CD Spectrometer using a Peltier thermostated cell holder (PTC-4230) with a recirculating cooler (JULABO F250) (JASCO Corporation, Spain). A nitrogen flow (~2.7 L/min) was led through the spectrometer and controlled with a nitrogen flow monitor (Afriso Euro-Index, Germany). The samples were dissolved under different conditions at different concentrations in MilliQ water. Samples were measured in triplicate in a quartz cuvette with d = 0.1 cm.

III.4.2.5. Dynamic Light Scattering (DLS)

DLS measurements were performed using a Malvern Zetasizer NanoZS instrument, equipped with a 532 nm laser at a fixed scattering angle of 173° (Malvern Instruments Ltd., UK). Polymer solutions were prepared in MilliQ water or 1 mM KCl at different concentrations and temperatures, and then solutions were sonicated for 10 min and allowed to equilibrate for the required time, filtered through a 0.45 μm cellulose membrane filter, and finally measured. Size distribution was measured (radius, nm) for

each polymer sample in triplicate and automatic optimization of beam focusing and attenuation was applied for each sample.

Z-potential measurements were performed at 20°C using a Malvern ZetaSizer NanoZS instrument, equipped with a 532 nm laser using disposable folded capillary cells (Malvern Instruments Ltd., UK). Polymer solutions were prepared in 1 mM KCl in MilliQ water. The solutions were filtered through a 0.45 μm cellulose membrane filter. Z-potential was measured for each sample in triplicate.

III.4.2.6. Fluorescence Spectroscopy

Critical micelle concentration (CMC) determination was carried out through fluorescence experiments performed using a JASCO FP-6500 spectrofluorimeter (JASCO Corporation, Spain) at 25ºC with 1 cm quartz cells. The pyrene assay was performed as published elsewhere [68]. In brief, several solutions of the compounds were prepared to cover a wide range of polymer concentrations (between 2 - 0.004 mg/mL) to which 3 μL of the pyrene stock solution (0.02 mg/mL) in acetone were added. Then, all solutions were placed in vials and are incubated at 37ºC for 2 h to evaporate the acetone. After storing the samples for 24 h, measurements were carried out. Each excitation spectrum is recorded from 300 to 360 nm with an emission wavelength of 390 nm. The excitation and emission band slits are 5 and 2.5 nm, respectively. Finally, data were expressed by plotting the intensity ratio I_{338}/I_{333} against the polymer concentration in order to determine the CMC value.

III.4.2.7. Ultraviolet-Visible (UV-Vis) Spectroscopy

UV-Vis measurements were performed using JASCO V-630 spectrophotometer (JASCO Corporation, Spain) at 25°C with 1.0 cm matched quartz cells and with a spectral bandwidth of 0.5 nm.

Quantification of Dil Loading: Dye loading was determined by recording the absorbance band at 548 nm using a calibration curve in MeOH, giving a concentration range between 0.00001 - 0.00014 mg/mL.

Quantification of Cy5.5 Loading: Dye loading was determined by recording the absorbance band at 676 nm using a calibration curve in water containing 0.001% of

DMSO to improve the Cy5.5 solubility, giving a concentration range between 0.00005 - 0.00025 mg/mL.

III.4.2.8. Transmission Electron Microscopy (TEM)

TEM images were recorded in a transmission electron microscope EM 410, Philips operating at 60 - 80 kV. Block copolymers samples (1 - 2 mg/mL) were applied directly onto carbon film on 200 mesh copper grids. Any excess of sample was carefully removed by capillary action, and the grids were immediately stained with one drop of 0.1% phosphotungstic acid for 30 s. Excess stain was also removed by capillary action.

III.4.2.9. Amine Quantification by TNBSA Assay

0.01% (w/v) solution of TNBSA (2,4,6-trinitrobenzene sulfonic acid) was prepared using 0.1 M sodium bicarbonate buffer at pH 8.5 as a diluent (prepared fresh for each measurement). A calibration curve was constructed with lysine from 10 to 250 µM. HA-CP aliquots were taken at different times and diluted in the sodium bicarbonate buffer and then measured. The levels of amine were obtained via interpolation of the calibration curve. Measurements were performed with UV-Vis spectrophotometer plate reader for 96 well plates SPECTROstar^{NANO} (Biogen, Spain) at 335 nm.

III.4.2.10. High-Performance Liquid Chromatography (HPLC)

Analytical determination of Dil content in the receptor chamber after permeation studies by Franz diffusion cells was performed on a system comprising an Agilent 1260 Infinity III Quaternary Pump solvent delivery module, a G7115A Diode Array Detector WR (Santa Clara, CA, USA), a InfinityLab Poroshell 120 C18 RP-HPLC column (EC-C18, 4.6 x 100 mm, 4 µm) (Santa Clara, CA, USA), and an Open Lab (Agilent) workstation. The composition of the mobile phase was methanol: tetrahydrofuran (8:2) with a flow rate of 1.0 mL/min and a column temperature of 25ºC. The injected sample volume was 10 µL at a concentration of 0.1 mg/mL of Dil standard, with a retention time between 4.5 and 7.5 min. The dye was monitored at 552 nm.

III.4.2.11. Viscosity Measurements

Viscosity values of the HA-based materials were obtained using a Fungilab rotational viscosimeter Visco Smart LT20 (Fisher Scientific, Spain) composed by (i)

viscometer head, (ii) adapter for small samples and (iii) a spindle. The concentration of HA-CP in aqueous solution was 3.4%, and the temperature employed was 25ºC. A starting rpm of 100 was fixed until the system stabilized. Then, rpm values were varied until reaching a percentage of base scale 40 ± 3 %. When the percentage was stable to 40, the value was obtained as long as values remained constant ± 10 cP.

III.4.3. Synthetic Protocols

III.4.3.1. Synthesis of Hyaluronic Acid-poly-L-Glutamate Cross-Polymer

Synthesis of 4-(4,6-Dimethoxy-1,3,5-triazin-2-yl)-4-methylmorpholinium chloride (DMTMM·Cl): This coupling agent was obtained according to synthetic procedures plentifully described [69]. Yield: 80%. ^{1}H-NMR (300 MHz, D_2O) δ 4.70 (d, J = 11.4 Hz, 2H), 4.22 (d, J = 8.7 Hz, 8H), 4.06 – 3.87 (m, 4H), 3.63 (s, 3H).

Synthesis of Cross-Linked Hyaluronic-Polyglutamate Vehicle: HA-CP was obtained by peptidic amide bond formation between carboxylic glutamate groups and both amine of lysine using DMTMM·Cl as coupling agent [41]. HA-CP was synthesized using hyaluronic acid (Mw = 50 kDa). Four solutions were prepared in parallel: (A) sodium hyaluronate (100 mg, 0.249 mmol, 1 eq.) was dissolved in distilled water; (B) sodium poly-L-glutamate (2.6 mg, 0.017 mmol, 0.07 eq.) was dissolved in distilled water; (C) DMTMM·Cl (44 mg, 0.159 mmol, 0.6 eq. to total carboxylic acids) was dissolved in distilled water. (D) Lysine hydrochloride salt (1.5 mg, 0.008 mmol, 0.03 eq. to total carboxylic acids) was dissolved in distilled water. B solution was added into A, and then, C was added and mixed, and the pH was adjusted to 7 with a few microliters of 1 M NaOH. The solution was stirred for 15 min before D was added, and the pH adjusted to 8.5 with a few microliters of 1 M NaOH. The reaction was carried out overnight at r.t. Then, the product was purified by dialysis using a Vivaspin® centrifugal concentrators containing an MWCO membrane of 30 kDa. The product was washed with 5 mM PB at pH 7.5 and was then washed with distilled water. The solution was lyophilized, and a white powder obtained.

III.4.3.2. Cyanine5.5 Labeling of HA-based Materials

Synthesis of Fluorescently Labeled HA-CP with Cy5.5 (HA-CP-Cy5.5): A fluorescent HA-CP was obtained through the formation of an amide bond between

carboxylic HA groups and Cyanine 5.5 amine, using DMTMM·Cl as a coupling agent. HA-CP (100 mg; 0.249 mmol, 1 eq.) was dissolved in distilled water. In parallel, coupling agent DMTMM·Cl (3.4 mg; 0.012 mmol, 0.05 eq.) was dissolved in water. The DMTMM·Cl solution was added to HA-CP solution, and the pH was adjusted to 7 with a few microliters of 1 M NaOH. The coupling activation of carboxylic acid through DMTMM·Cl was allowed to proceed for 30 min. After that, a solution of Cy5.5 amine (1.8 mg, 0.003 mmol, 0.01 eq.) previously prepared in a mixture of water:DMSO (1:1) was added, and the pH was adjusted at 8.5 with a few microliters of 1 M NaOH. The resultant blue solution of conjugation reaction was allowed to proceed for 72 h at r.t. Then, the product was purified by dialysis using a Vivaspin® centrifugal concentrators containing an MWCO membrane of 30 kDa. The product was washed with 5 mM PB at pH 7.5 and then was washed with distilled water. The solution was lyophilized, and a blue powder was obtained.

Synthesis of Fluorescently Labeled HA with Cy5.5 (HA-Cy5.5): Fluorescent HA was obtained through the same procedure described previously for HA-CP-Cy5.5 using a PrimalHyal300 HA (Mw = 200 kDa).

III.4.3.3. Synthesis of Amphiphilic Block Copolymers

General Synthesis of Block Copolymers: Synthesis of PEG-polyamino acid block copolymers was achieved following well-established protocols described elsewhere [59, 60], adjusting the feeding ratio [monomer]/[initiator] to obtain the target degree of polymerization. The NCA monomer (3.923 mmol, 10 equivalents (eq.)) was weighed in a Schlenk tube, which was fitted with a stir bar and dried at 80ºC for at least 24 h before starting the reaction. The tube was purged with Argon/vacuum cycles, and the monomer was dissolved in 4 mL of dry DMF. The MeO-PEG-NH_2 macroinitiator was weighed in a vial, purged with argon and dissolved in 1 mL of dry DMF. The initiator solution was added to monomer solution under an argon atmosphere, and the polymerization media was placed at 4ºC under vigorous stirring for three to four days. The reaction mixture was poured over 50 mL diethyl ether, and the white precipitate was filtered and washed with additional diethyl ether. Further purification was carried out by suspension in THF and precipitation over excess diethyl ether. Finally, the product was filtered and dried under an N_2 stream.

III.4.3.4. Preparation of the Micelles using the Block Copolymers

Co-solvent Method: This method was adapted from the literature [56]. The block copolymer (20 mg/mL) was dissolved in THF and added dropwise into MilliQ water with continuous stirring at r.t. until the evaporation of the organic solvent. The formulations were allowed to equilibrate at r.t. for 24 h, followed by centrifugation at 1000 rpm for 10 min, and the supernatant was dialyzed against MilliQ water, MWCO = 1 kDa. The polymers were studied at concentrations of 1, 5, and 10 mg/mL.

Synthesis of Fluorescently Labeled Micelles with Dil: For the preparation of fluorescently labeled micelles, 1% w/w of Dil loading was aimed for by dissolving the block copolypeptides and the dye in THF and following the same procedures described above.

III.4.4. Biological Evaluation

III.4.4.1. *In Vitro* Evaluation

III.4.4.1.1. Cell Viability

To carry out the cytotoxicity studies *in vitro* two cell lines were used: a human immortalized non-tumorigenic keratinocyte cell line (HaCaT) was supplied by CLS Cell Lines Service (Eppelheim, Germany) and human fibroblasts were supplied by Hospital La Fe (Valencia, Spain). The culture media used was high glucose DMEM Glutamax (Fisher, Spain) for HaCaT keratinocytes and DMEM (Sigma-Aldrich Chemical Co., Spain) for fibroblasts; both were supplemented with 2% penicillin/streptomycin and 50 mL of FBS in a humidified incubator (Hucoa-Erlöss S.A., Spain) at 5% CO_2 and 37°C. Briefly, 50 μL of cells were seeded in 96-well plates at a concentration of 4,000 cells/well in the case of HaCaT and 2,000 cells/well for fibroblasts. After 24 h, 50 μL of each treatment were added, reaching a final volume of 100 μL in the well. All treatments were filtered before adding to the well (pore size 0.45 μm). Cells were incubated with samples or controls for 72 h, and then the MTS assay was performed. For this assay, 20 μL of a 90% phenazine methosulfate minimum (PMS, Sigma, Spain) solution and salt of 3-(4,5-dimethylthiazol-2-yl)-5-(3-carboxymethylphenyl)-2-(4-sulfophenyl)-2H tetrazolium), (MTS, Promega, Spain) were added in a ratio 1:20. After 3 h of incubation, the absorbance was read at 490 nm using Victor^{2}Wallac™ plate reader (Perkin Elmer, Spain). The

concentrations tested were in a range from 0.029 to 0.5 mg/mL for PEG-PPhe10, PEG-PPhe20, PEG-PBG10, and PEG-PBG20.

III.4.4.2. *Ex Vivo* Evaluation

III.4.4.2.1. Permeation Studies by Franz Diffusion Cells

Breast skin samples were obtained from healthy women undergoing plastic surgery after written informed consent (kindly donated by Hospital la Fe, Valencia, Spain). Immediately after excision, the subcutaneous fatty tissue was carefully removed using a scalpel. The skin was cut into 4 cm^2 pieces, wrapped in aluminum foil and stored at -20ºC until use. To reduce inter-individual variability and afford a better comparison of results, skin from only one donor was used in all experiments. Before starting each experiment, the skin was allowed to equilibrate at r.t.

Permeation studies employed the modified Franz diffusion cells (Logan Instruments Corp., EE. UU) with a diffusional area of 0.95 cm^2. The skin was fixed carefully between the donor and the receptor chamber, so that stratum corneum was placed upwards. The receptor chamber was filled with 8 mL of 0.01 M PBS pH = 7.4 and stirred with a magnetic stirring bar at 600 rpm with a thermostated temperature of 37ºC. After an equilibration time of 30 min, 100 µL of the formulations using a fixed concentration (10 mg/mL) were introduced into the donor chamber using a standard pipette. The formulations studied were HA-Cy5.5 (1% w/v), HA-CP-Cy5.5 (1% w/v), four types of micelles with encapsulated Dil applied in HA-CP (1% w/v) (PEG-PPhe10-Dil, PEG-PPhe20-Dil, PEG-PBG10-Dil, and PEG-PBG20-Dil), and finally the PEG-PBG20-Dil micelle in water and linear HA (1% w/v). Also, benzoic acid as a positive control at the same concentration was employed. The donor chamber was then sealed with Parafilm®, and aluminum foil and the experiments ran for 8 h. Samples from the receptor chamber were taken at times 0, 4, and 8 h and was immediately refilled with fresh solution. After the permeation study, skin samples were washed twice with 0.1% PBS-BSA and kept in 4% paraformaldehyde (PFA) for 24 h at r.t. Then, the samples were washed with 30% sucrose in PBS solution and retained for 24 h at 4ºC. Finally, skin samples were washed twice with PBS and preserved in a cryopreservation solution (40% 0.1 M PB, 30% ethylene glycol and 30% glycerol) at 4ºC until use. Then, skin samples were included in the optimum cutting temperature inclusion medium and slides of 5 µm

were acquired with the cryostat (version CM1850 UV, Leica, Germany), and samples were analyzed by confocal microscopy. Images were captured with an inverted DM IRE2 microscope equipped with a λ-blue 40x oil immersion objective and handled with a TCS SP2 system, equipped with an Acoustic Optical Beam Splitter (AOBS). Dil C18(3) was excited at 549 nm, Cy5.5 at 675 nm and DAPI at 405 nm. Images were captured at an 8-bit greyscale and processed with LCS software (version 2.5.1347a, Leica, Germany) containing multicolor, macro and 3D components. Control tissue that follows the same incubation time with MilliQ water was also analyzed to establish the autofluorescence. Cy5.5 or Dil intensity was quantified five times per sample using Image J software and expressed as pixels versus the thickness of the skin (µm). The control intensity was subtracted in each case.

III.4.4.2.2. Evaluation of Tissue Viability in an *Ex Vivo* Human Skin Model

Breast skin samples were obtained from healthy women undergoing plastic surgery after written informed consent (kindly donated from Hospital la Fe, Valencia, Spain). The skin was cut to approximately 1 cm^2 and placed in 6-well plates so that the dermal side was in contact with DMEM supplemented with 50 mL FBS, 5.5 mL penicillin/streptomycin, and 50 µL amphotericin B, and the epidermis was exposed to the air. The *ex vivo* human skin model was incubated at 37ºC under 5% CO_2 (see **Chapter II** for more details). After 24 h in culture, the treatments were applied. Tissue viability of 3 µL of a 10 mg/mL solution of PEG-PBG20 applied in water, applied in linear HA (1% w/v), and in the HA-CP (1% w/v) vehicle was evaluated after 24, 48 and 72 h of treatment. HA (1% w/v) and HA-CP (1% w/v) vehicles were applied as controls. Tissue viability after each treatment was evaluated by MTT assay. Briefly, skin pieces were washed twice with PBS and were added to 4 mL of MTT solution (2 mg/mL). After 4 h of incubation at 37ºC, skin samples were washed twice with PBS and added to 4 mL of DMSO to extract formazan from the skin. After 15 h of extraction, the absorbance was read at 490 nm using Victor^{2}Wallac™ plate reader (Perkin Elmer, Spain).

III.4.4.3. *In Vivo* Evaluation

III.4.4.3.1. Hydration Assays

To determine the hydration percent, the Corneometer® CM 825 probe of the Cutometer dual MPA 580 (Microcraya S.L., Spain) was used showing the arithmetic

mean of five determinations, under the conditions of 22°C ± 2 with relative humidity between 40 - 60%. Two pharmaceutical formulations developed following Good Manufacturing Practice (GMP) using as active component HA and HA-CP were used. The measurement was performed in the corresponding zone between cheekbone and nasolabial fold in over 15 human volunteers. HA and HA-CP formulations were applied in the left zone, while the right zone was used to carry out the control measures. Measurements were performed at time 0 (before applying the product) and at 1, 3, 8, 16, 24, and 40 h after applying the HA-based materials. Finally, reference values for the degree of hydration were collected.

III.5. References

[1] M. Kong, X.G. Chen, D.K. Kweon, H.J. Park, Investigations on skin permeation of hyaluronic acid based nanoemulsion as transdermal carrier, Carbohyd Polym 86(2) (2011) 837-843.
[2] K.A. Kosakowska, B.K. Casey, S.L. Kurtz, L.B. Lawson, S.M. Grayson, Evaluation of Amphiphilic Star/Linear-Dendritic Polymer Reverse Micelles for Transdermal Drug Delivery: Directing Carrier Properties by Tailoring Core versus Peripheral Branching, Biomacromolecules 19(8) (2018) 3163-3176.
[3] L. Gao, F. Zabihi, S. Ehrmann, S. Hedtrich, R. Haag, Supramolecular nanogels fabricated via host-guest molecular recognition as penetration enhancer for dermal drug delivery, J Control Release 300 (2019) 64-72.
[4] K. Xu, F. Lee, S. Gao, M.-H. Tan, M. Kurisawa, Hyaluronidase-incorporated hyaluronic acid–tyramine hydrogels for the sustained release of trastuzumab, J Control Release 216 (2015) 47-55.
[5] C. Loebel, M. D'Este, M. Alini, M. Zenobi-Wong, D. Eglin, Precise tailoring of tyramine-based hyaluronan hydrogel properties using DMTMM conjugation, Carbohyd Polym 115 (2015) 325-333.
[6] S. Khunmanee, Y. Jeong, H. Park, Crosslinking method of hyaluronic-based hydrogel for biomedical applications, J Tissue Eng 8 (2017) 2041731417726464.
[7] R. Parhi, Cross-Linked Hydrogel for Pharmaceutical Applications: A Review, Adv Pharm Bull 7(4) (2017) 515-530.
[8] L. Kenne, S. Gohil, E.M. Nilsson, A. Karlsson, D. Ericsson, A. Helander Kenne, L.I. Nord, Modification and cross-linking parameters in hyaluronic acid hydrogels—Definitions and analytical methods, Carbohyd Polym 91(1) (2013) 410-418.
[9] K.Y. Lee, D.J. Mooney, Hydrogels for Tissue Engineering, Chem Rev 101(7) (2001) 1869-1880.
[10] K. Meyer, J.W. Palmer, The polysaccharide of the vitreous humor, J Biol Chem 107(3) (1934) 629-634.
[11] C.C. Zouboulis, R. Ganceviciene, A.I. Liakou, A. Theodoridis, R. Elewa, E. Makrantonaki, Aesthetic aspects of skin aging, prevention, and local treatment, Clin Dermatol 37(4) (2019) 365-372.

[12] L. Genovese, S. Sibilla, Innovative Nutraceutical Approaches to Counteract the Signs of Aging, in: M.A. Farage, K.W. Miller, H.I. Maibach (Eds.), Textbook of Aging Skin, Springer Berlin Heidelberg, Berlin, Heidelberg, 2017, pp. 1967-1991.
[13] G. Kogan, L. Šoltés, R. Stern, P. Gemeiner, Hyaluronic acid: a natural biopolymer with a broad range of biomedical and industrial applications, Biotechnol Lett 29(1) (2007) 17-25.
[14] R.D. Price, M.G. Berry, H.A. Navsaria, Hyaluronic acid: the scientific and clinical evidence, J Plast Reconstr Aesthet 60(10) (2007) 1110-1119.
[15] Y. Luo, K.R. Kirker, G.D. Prestwich, Cross-linked hyaluronic acid hydrogel films: new biomaterials for drug delivery, J Control Release 69(1) (2000) 169-184.
[16] M.B. Brown, S.A. Jones, Hyaluronic acid: a unique topical vehicle for the localized delivery of drugs to the skin, J Eur Acad Dermatol 19(3) (2005) 308-318.
[17] S. Kumar, M. Zakrewsky, M. Chen, S. Menegatti, J.A. Muraski, S. Mitragotri, Peptides as skin penetration enhancers: mechanisms of action, J Control Release 199 (2014) 168-78.
[18] A. Bolhassani, Improvements in chemical carriers of proteins and peptides, Cell Biol Int 43(4) (2019) 437-452.
[19] P.C. DeMuth, X. Su, R.E. Samuel, P.T. Hammond, D.J. Irvine, Nano-Layered Microneedles for Transcutaneous Delivery of Polymer Nanoparticles and Plasmid DNA, Adv Mater 22 (2010) 4851-4856.
[20] I. Bajaj, R. Singhal, Poly (glutamic acid) – An emerging biopolymer of commercial interest, Bioresour Technol 102 (2011) 5551-5561.
[21] A. Ogunleye, A. Bhat, V.U. Irorere, D. Hill, C. Williams, I. Radecka, Poly-gamma-glutamic acid: production, properties and applications, Microbiology 161(Pt 1) (2015) 1-17.
[22] N. Ben-Zur, γ-poly glutamic acid : a novel peptide for skin care, Cosmet Toilet 122(4) (2007) 65-74.
[23] M.H. Sung, Park, C., Choi, J. C., Uyama, H. & Park, S. L. (2005). Hyaluronidase inhibitor containing poly-gamma-glutamic acid as an effective component. US Patent 12/090,678.
[24] M.C. Chen, M.H. Ling, S.J. Kusuma, Poly-γ-glutamic acid microneedles with a supporting structure design as a potential tool for transdermal delivery of insulin, Acta Biomaterialia 24 (2015) 106-116.
[25] A. Duro-Castano, I. Conejos-Sánchez, J.M. Vicent, Peptide-Based Polymer Therapeutics, Polymers (Basel) 6 (2014) 515-551.
[26] R. Duncan, Polymer conjugates as anticancer nanomedicines, Nat Rev Cancer 6 (2006) 688-701.
[27] A. Duro-Castano, R.M. England, D. Razola, E. Romero, M. Oteo-Vives, M.A. Morcillo, M.J. Vicent, Well-Defined Star-Shaped Polyglutamates with Improved Pharmacokinetic Profiles As Excellent Candidates for Biomedical Applications, Mol Pharm 12(10) (2015) 3639-3649.
[28] S. Wang, X. Cao, M. Shen, R. Guo, I. Bányai, X. Shi, Fabrication and morphology control of electrospun poly(γ-glutamic acid) nanofibers for biomedical applications, Colloids Surf B Biointerfaces 89 (2012) 254-264.
[29] Y. Otani, Y. Tabata, Y. Ikada, Rapidly curable biological glue composed of gelatin and poly(l-glutamic acid), Biomaterials 17(14) (1996) 1387-1391.
[30] R. Wang, B. Zhou, D.-l. Xu, H. Xu, L. Liang, X.-h. Feng, P.-k. Ouyang, B. Chi, Antimicrobial and biocompatible ε-polylysine–γ-poly(glutamic acid)–based hydrogel system for wound healing, J Bioact Compat Pol 31(3) (2016) 242-259.

[31] C.T. Tsao, C.H. Chang, Y.Y. Lin, M.F. Wu, J.L. Wang, T.H. Young, J.L. Han, K.H. Hsieh, Evaluation of chitosan/γ-poly(glutamic acid) polyelectrolyte complex for wound dressing materials, Carbohyd Polym 84(2) (2011) 812-819.
[32] X. Ma, S. Liu, H. Tang, R. Yang, B. Chi, Z. Ye, In situ photocrosslinked hyaluronic acid and poly (γ-glutamic acid) hydrogels as injectable drug carriers for load-bearing tissue application, J Biomater Sci Polym Ed 29(18) (2018) 2252-2266.
[33] X. Ma, T. Xu, W. Chen, H. Qin, B. Chi, Z. Ye, Injectable hydrogels based on the hyaluronic acid and poly (γ-glutamic acid) for controlled protein delivery, Carbohyd Polym 179 (2018) 100-109.
[34] Z. Fan, P. Cheng, M. Liu, D. Li, G. Liu, Y. Zhao, Z. Ding, F. Chen, B. Wang, X. Tan, Z. Wang, J. Han, Poly(glutamic acid) hydrogels crosslinked via native chemical ligation, New J Chem 41(16) (2017) 8656-8662.
[35] C. Fetsch, J. Gaitzsch, L. Messager, G. Battaglia, R. Luxenhofer, Self-Assembly of Amphiphilic Block Copolypeptoids - Micelles, Worms and Polymersomes (vol 6, 33491, 2016), Sci Rep 6 (2016) 1.
[36] M. Lapteva, V. Santer, K. Mondon, I. Patmanidis, G. Chiriano, L. Scapozza, R. Gurny, M. Möller, Y.N. Kalia, Targeted cutaneous delivery of ciclosporin A using micellar nanocarriers and the possible role of inter-cluster regions as molecular transport pathways, J Control Release 196 (2014) 9-18.
[37] M. Lapteva, K. Mondon, M. Moller, R. Gurny, Y.N. Kalia, Polymeric micelle nanocarriers for the cutaneous delivery of tacrolimus: a targeted approach for the treatment of psoriasis, Mol Pharm 11(9) (2014) 2989-3001.
[38] X. Meng, K.J. Edgar, "Click" reactions in polysaccharide modification, Prog Polym Sci 53 (2016) 52-85.
[39] D. Petta, D. Eglin, D.W. Grijpma, M. D'Este, Enhancing hyaluronan pseudoplasticity via 4-(4,6-dimethoxy-1,3,5-triazin-2-yl)-4-methylmorpholinium chloride-mediated conjugation with short alkyl moieties, Carbohyd Polym 151 (2016) 576-583.
[40] J.J. Arroyo-Crespo, A. Armiñán, D. Charbonnier, L. Balzano-Nogueira, F. Huertas-López, C. Martí, S. Tarazona, J. Forteza, A. Conesa, M.J. Vicent, Tumor microenvironment-targeted poly-L-glutamic acid-based combination conjugate for enhanced triple negative breast cancer treatment, Biomaterials 186 (2018) 8-21.
[41] I. Conejos-Sanchez, A. Duro-Castano, A. Birke, M. Barz, M.J. Vicent, A controlled and versatile NCA polymerization method for the synthesis of polypeptides, Polym Chem 4(11) (2013) 3182-3186.
[42] P. Perdih, S. Cebasek, A. Mozir, E. Zagar, Post-polymerization modification of poly(L-glutamic acid) with D-(+)-glucosamine, Molecules 19(12) (2014) 19751-68.
[43] C. Guarise, M. Pavan, L. Pirrone, D. Renier, SEC determination of cross-link efficiency in hyaluronan fillers, Carbohyd Polym 88(2) (2012) 428-434.
[44] W.A. Bubnis, C.M. Ofner, The determination of ϵ-amino groups in soluble and poorly soluble proteinaceous materials by a spectrophotometrie method using trinitrobenzenesulfonic acid, Anal Biochem 207(1) (1992) 129-133.
[45] R.B. Sashidhar, A.K. Capoor, D. Ramana, Quantitation of ϵ-amino group using amino acids as reference standards by trinitrobenzene sulfonic acid: A simple spectrophotometric method for the estimation of hapten to carrier protein ratio, J Immunol Methods 167(1) (1994) 121-127.
[46] X. Tao, B. Zheng, T. Bai, B. Zhu, J. Ling, Hydroxyl Group Tolerated Polymerization of N-Substituted Glycine N-Thiocarboxyanhydride Mediated by Aminoalcohols: A Simple Way to α-Hydroxyl-ω-aminotelechelic Polypeptoids, Macromolecules 50(8) (2017) 3066-3077.

[47] F. Tranchepain, B. Deschrevel, M.N. Courel, N. Levasseur, D. Le Cerf, C. Loutelier-Bourhis, J.C. Vincent, A complete set of hyaluronan fragments obtained from hydrolysis catalyzed by hyaluronidase: Application to studies of hyaluronan mass distribution by simple HPLC devices, Anal Biochem 348(2) (2006) 232-242.
[48] X. Li, Z. Zhou, Y. Tang, C. Cheng Zhang, Y. Zheng, J. Gao, Q. Wang, Modulation of assembly and disassembly of a new tetraphenylethene based nanosensor for highly selective detection of hyaluronidase, Sensor Actuat B-Chem 276 (2018) 95-100.
[49] J. Baier Leach, K.A. Bivens, C.W. Patrick Jr, C.E. Schmidt, Photocrosslinked hyaluronic acid hydrogels: Natural, biodegradable tissue engineering scaffolds, Biotechnol Bioeng 82(5) (2003) 578-589.
[50] J.B. Leach, K.A. Bivens, C.N. Collins, C.E. Schmidt, Development of photocrosslinkable hyaluronic acid-polyethylene glycol-peptide composite hydrogels for soft tissue engineering, J Biomed Mater Res A 70A(1) (2004) 74-82.
[51] A.M. Wojtowicz, S. Oliveira, M.W. Carlson, A. Zawadzka, C.F. Rousseau, D. Baksh, The importance of both fibroblasts and keratinocytes in a bilayered living cellular construct used in wound healing, Wound Repair Regen 22(2) (2014) 246-55.
[52] S.S. Kwon, S.Y. Kim, B.J. Kong, K.J. Kim, G.Y. Noh, N.R. Im, J.W. Lim, J.H. Ha, J. Kim, S.N. Park, Cell penetrating peptide conjugated liposomes as transdermal delivery system of Polygonum aviculare L. extract, Int J Pharm 483(1-2) (2015) 26-37.
[53] A.L.M. Ruela, E.C. Figueiredo, G.R. Pereira, Molecularly imprinted polymers as nicotine transdermal delivery systems, Chem Eng J 248 (2014) 1-8.
[54] M. Essendoubi, C. Gobinet, R. Reynaud, J.F. Angiboust, M. Manfait, O. Piot, Human skin penetration of hyaluronic acid of different molecular weights as probed by Raman spectroscopy, Skin Res Technol 22(1) (2016) 55-62.
[55] S. Bode, B. Baert, M. Vangele, J. Lambert, C. Burvenich, G. Slegers, B. De Spiegeleer, Stability of the OECD model compound benzoic acid in receptor fluids of Franz diffusion cells, Pharmazie 62(6) (2007) 470-1.
[56] G. Gaucher, M.H. Dufresne, V.P. Sant, N. Kang, D. Maysinger, J.C. Leroux, Block copolymer micelles: preparation, characterization and application in drug delivery, J Control Release 109(1-3) (2005) 169-188.
[57] J. Huang, A. Heise, Stimuli responsive synthetic polypeptides derived from N-carboxyanhydride (NCA) polymerisation, Chem Soc Rev 42(17) (2013) 7373-7390.
[58] A.V. Hubina, A.A. Pogodaev, V.V. Sharoyko, E.G. Vlakh, T.B. Tennikova, Self-assembled spin-labeled nanoparticles based on poly(amino acids), React Funct Polym 100 (2016) 173-180.
[59] J. Cheng, T.J. Deming, Synthesis of polypeptides by ring-opening polymerization of alpha-amino acid N-carboxyanhydrides, Top Curr Chem 310 (2012) 1-26.
[60] D. Huesmann, A. Sevenich, B. Weber, M. Barz, A head-to-head comparison of poly(sarcosine) and poly(ethylene glycol) in peptidic, amphiphilic block copolymers, Polymer J 67 (2015) 240-248.
[61] M. Reches, E. Gazit, Casting Metal Nanowires Within Discrete Self-Assembled Peptide Nanotubes, Science 300(5619) (2003) 625.
[62] V. Castelletto, I.W. Hamley, Self assembly of a model amphiphilic phenylalanine peptide/polyethylene glycol block copolymer in aqueous solution, Biophys Chem 141(2) (2009) 169-174.
[63] C.C. Decandio, E.R. Silva, I.W. Hamley, V. Castelletto, M.S. Liberato, V.X. Oliveira, Jr., C.L. Oliveira, W.A. Alves, Self-Assembly of a Designed Alternating Arginine/Phenylalanine Oligopeptide, Langmuir 31(15) (2015) 4513-23.

[64] X. Liu, R. Fan, B. Lu, Y. Le, Polypeptides Micelles Composed of Methoxy-Poly(Ethylene Glycol)-Poly(l-Glutamic Acid)-Poly(l-Phenylalanine) Triblock Polymer for Sustained Drug Delivery, Pharmaceutics 10(4) (2018).
[65] K. Prompruk, T. Govender, S. Zhang, C.D. Xiong, S. Stolnik, Synthesis of a novel PEG-block-poly(aspartic acid-stat-phenylalanine) copolymer shows potential for formation of a micellar drug carrier, Int J Pharm 297(1) (2005) 242-253.
[66] Z. Ahmad, Z. Tang, A. Shah, S. Lv, D. Zhang, Y. Zhang, X. Chen, Cisplatin loaded methoxy poly (ethylene glycol)-block-Poly (L-glutamic acid-co-L-Phenylalanine) nanoparticles against human breast cancer cell, Macromol Biosci 14(9) (2014) 1337-45.
[67] B. Weber, C. Kappel, M. Scherer, M. Helm, M. Bros, S. Grabbe, M. Barz, PeptoSomes for Vaccination: Combining Antigen and Adjuvant in Polypept(o)ide-Based Polymersomes, Macromol Biosci 17(10) (2017).
[68] A. Duro-Castano, V.J. Nebot, A. Nino-Pariente, A. Arminan, J.J. Arroyo-Crespo, A. Paul, N. Feiner-Gracia, L. Albertazzi, M.J. Vicent, Capturing "Extraordinary" Soft-Assembled Charge-Like Polypeptides as a Strategy for Nanocarrier Design, Adv Mater 29 (2017) 12.
[69] M. Kunishima, C. Kawachi, J. Morita, K. Terao, F. Iwasaki, S. Tani, 4-(4,6-dimethoxy-1,3,5-triazin-2-yl)-4-methyl-morpholinium chloride: An efficient condensing agent leading to the formation of amides and esters, Tetrahedron 55(46) (1999) 13159-13170.

CHAPTER IV

POLYMER THERAPEUTICS FOR THE TREATMENT OF SKIN DISEASES. PSORIASIS TREATMENT AS PROOF OF CONCEPT

IV.1. Antecedents and Background

Approaches involving nanosized drug delivery systems represent an efficient means to treat skin diseases such as psoriasis, a molecularly complex autoimmune disease.

Pharmacotherapy for psoriasis disease is generally divided into systemic or topical treatment approaches. The primary topical treatments used in the clinics are corticosteroids, which exhibit anti-inflammatory, immunosuppressive, anti-proliferative, and vasoconstrictive activities [1]. Corticosteroids act by binding to the α-isoform of the nuclear glucocorticoid receptor, which modulates the transcription of anti-inflammatory proteins. Glucocorticoid receptors are found in most cells of the human body; in the skin, these receptors are located in epidermal keratinocytes and dermal fibroblasts [2, 3]. Binding of corticosteroids to their receptor, following uptake via passive diffusion, leads to the dissociation of the heat-shock proteins and immunophilins that keep the receptor in an inactive form in the cytoplasm, allowing the translocation of the corticosteroid-receptor complex to the nucleus [4]. In the nucleus, this complex binds to a specific sequence of DNA (glucocorticoid-response element) and induces the synthesis of anti-inflammatory and regulatory proteins.

While the topical corticosteroids display great potential as anti-inflammatory and immunomodulatory drugs, several studies have reported that these drugs can trigger immediate and delayed hypersensitivity reactions with continued application, as they can behave as allergens [5, 6]. Moreover, cross-reactivity between different topically-administered corticosteroids has also been reported [7].

Fluocinolone acetonide (FLUO), 6-alpha, 9-alpha-difluoro-16-alpha, 17 alpha-acetonide, is classified by the FDA as a class 6 (mild) topical corticosteroid [8] and is currently widely applied in the treatment of eye diseases [9-12]. Several FLUO-containing implants approved by the FDA are currently on the market, including Retisert® for the treatment of uveitis [13] and Iluvien® for the treatment of diabetic macular edema [14, 15]. Furthermore, several studies have demonstrated the potential of FLUO as an anti-inflammatory and anti-psoriatic drug [16-18]. The anti-psoriatic activity of this drug was initially studied by Scholtz *et al.*, in 1961, who revealed its ability to reduce psoriatic skin lesions in a study with twelve patients [19]. Since then, many studies have tried to

improve the effectiveness of FLUO by modifying the optimal concentration and the type of vehicle used (e.g., cream, gel, foam) to enhance the penetration into the skin [20].

Therefore, the development of new formulations that improve the effectiveness of FLUO and increase its concentration in the required skin layer, via a more controlled and targeted release, continues as an unmet clinical need. Of note, any formulation developed should also aim to diminish the adverse effects caused by the continual topical application of corticosteroids, such as stinging, irritation, and photosensitivity, among others [21].

Our proposal to overcome these challenges is the conjugation of FLUO to a polymeric backbone using rationally designed covalent bonds to promote sustained drug release at the desired site of action in response to specific triggers, such as pH or the presence of specific enzymes. Furthermore, control and modification of the specific physico-chemical characteristics will allow the synthesis of polymer-drug conjugates that can penetrate through the skin via selective pathways of penetration. Polymer conjugation will also inhibit the degradation of FLUO, thereby ensuring elevated levels of the drug at the desired target cell or tissue. The use of biodegradable polymers such as polypeptides, in particular poly-glutamic acid (PGA) [22, 23], can reduce the side-effects derived from the continued use of non-degradable polymeric carriers [24].

Therefore, in the present study, we proposed giving FLUO a "new breath of life" by developing a PGA-conjugated form (PGA-FLUO) that we hoped would improve penetration to specific skin layer as well as its anti-inflammatory activity. The use of an ester as covalent bond between the polymer and the drug allows FLUO release in a pH-responsive manner that could permit selective intracellular release of FLUO allowing its binding to the glucocorticoid receptor. Furthermore, the abundant esterase activity observed within viable skin (epidermis and dermis) will also facilitate the hydrolysis of the ester linker and the release of the drug [25-27]. Additionally, in **Chapter III** of this thesis, the hyaluronic-poly-L-glutamate cross-polymer (HA-CP) vehicle demonstrated the improvement of the penetration of several micelles through the skin and provided a considerable increase in skin hydration. Therefore, we aimed to improve the topical administration of PGA-FLUO conjugate in the skin by embedding the conjugate within the HA-CP vehicle.

In this chapter, we present the PGA-FLUO conjugate as a promising treatment for psoriasis, highlighting the importance of linker design that would secure a sustained drug release. We also emphasize the importance of the use of an adequate vehicle for the topical application of the conjugate in order to enhance skin penetration. The use of HA-CP as vehicle provides additional advantages such as skin hydration (**Chapter III**). Therefore, the improvement of the physiological characteristics of the skin could also improve the effectiveness of our conjugate in the psoriasis treatment, expecting a synergism of PGA-FLUO conjugate and HA-CP combination.

IV.2. Results

IV.2.1. Safety and Skin Penetration of Linear and Star PGAs

As described in **Chapter I**, the inherent versatility of the polymers based on polypeptides, as poly-glutamic acid (PGA), allows the synthesis of different architectures, including simple linear or more complex branched polymers (e.g., star polymers) [28]. We first assessed the suitability of linear polymer (PGA) and star polymer (ST-PGA) for topical applications. *In vitro* cell viability assays on keratinocytes (HaCaT cells) and human fibroblasts after 72 h of treatment confirmed that both polymers maintained or increased cell viability up to the concentration tested (**Figure IV. 1**).

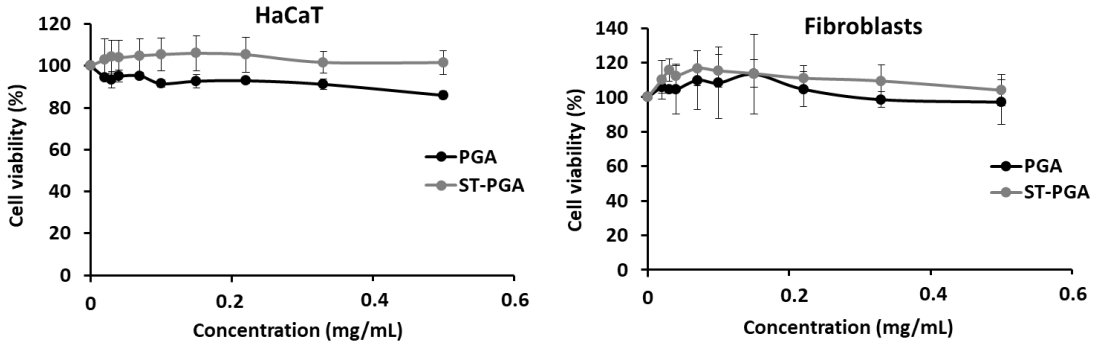

Figure IV. 1: Cell viability assays in HaCaT cells (left) and human fibroblasts (right) after 72 h of treatment of PGA and ST-PGA (n=3).

After confirming the absence of toxicity in cell lines, we evaluated the penetration of 10 mg/mL Oregon Green-labeled PGA (PGA-OG) and ST-PGA (ST-PGA-OG) both formulated in water in human skin explants by Franz diffusion cells after 24 h of

treatment. After fixation and tissue processing, we took confocal images to evaluate skin penetration. The results suggest that both polymers reached the epidermis, although they mainly accumulated within the stratum corneum (SC) (**Figure IV. 2A**). We quantified the intensity of OG using Image J software, discovering a slightly higher intensity in the SC and viable epidermis for the linear PGA (**Figure IV. 2B**). Considering these preliminary results, we decided to conjugate FLUO to the linear PGA for further studies.

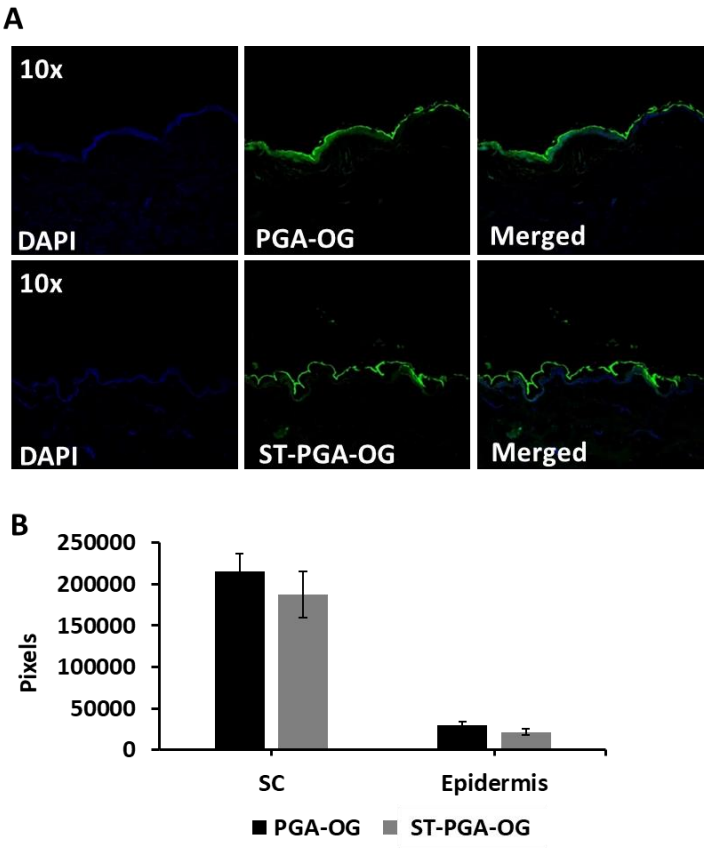

Figure IV. 2: Skin penetration of linear and star polymers labeled with OG. **(A)** Confocal microscopy images of PGA-OG and ST-PGA-OG polymers after 24 h of penetration by Franz diffusion cells. **(B)** Quantification of OG intensity by Image J in the stratum corneum (SC) and the viable epidermis (n=5).

IV.2.2. Synthesis and Characterization of Poly-L-Glutamate Fluocinolone Acetonide Conjugates

Herein we aimed to conjugate the poorly water-soluble corticosteroid fluocinolone acetonide (FLUO) to a water-soluble PGA carrier via an ester bond, aiming to improve FLUO bioavailability after topical administration in the skin while providing a modulated release rate of the drug in the specific skin layer. We chose PGA based on

its successful application in the synthesis of polymer-drug conjugates in terms of cargo loading capacity due to its multivalcency (carboxylic acid groups in the side chains) [29], high hydrophilicity, elevated biodegradability of the polyaminoacid backbone under physiologically relevant conditions [30], and the ability of PGA-based nanomedicines to bypass biological barriers with a non-toxic and safe biodistribution profile [31-33]. Furthermore, PGA is composed of repeating units of glutamic acid, an essential amino acid that can provide the skin with the necessary nutrition for proper cellular function, and hence, enhances skin hydration, thereby exhibiting a soothing effect on damaged skin [34].

We prepared PGA-FLUO conjugates following well-established synthetic procedures [35], attaching FLUO to the polypeptidic backbone through an ester linker (**Figure IV. 3**) by means of a carbodiimide coupling using EDC and 4-dimethylaminopyridine (DMAP) as a catalyst.

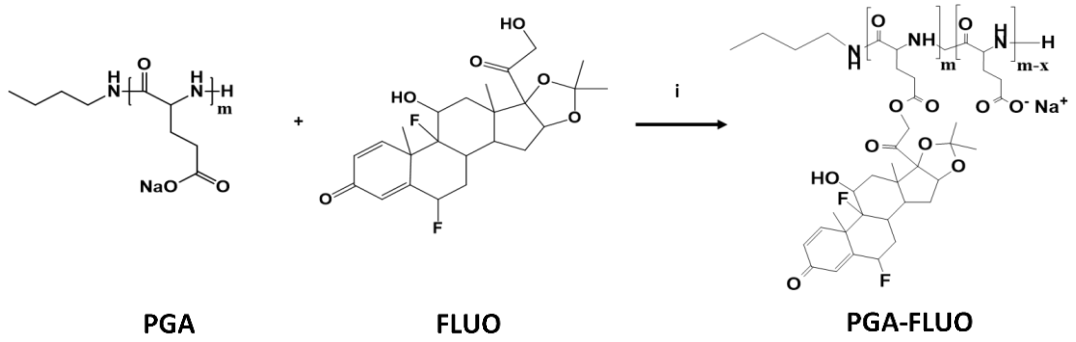

Figure IV. 3: Synthetic route for the preparation of PGA-FLUO conjugates through an ester linker: i) EDC, DMAP, DMF, 0ºC, N_2 (see synthetic methods section for more details).

The molecular weight for PGA backbone was determined as 15 kDa by size-exclusion chromatography (SEC) (100 units of glutamic acid, see **Figure IV. 4**), and a targeted drug molar content of ~8 mol% as determined via ^{1}H-NMR (**Figure IV. 5**).

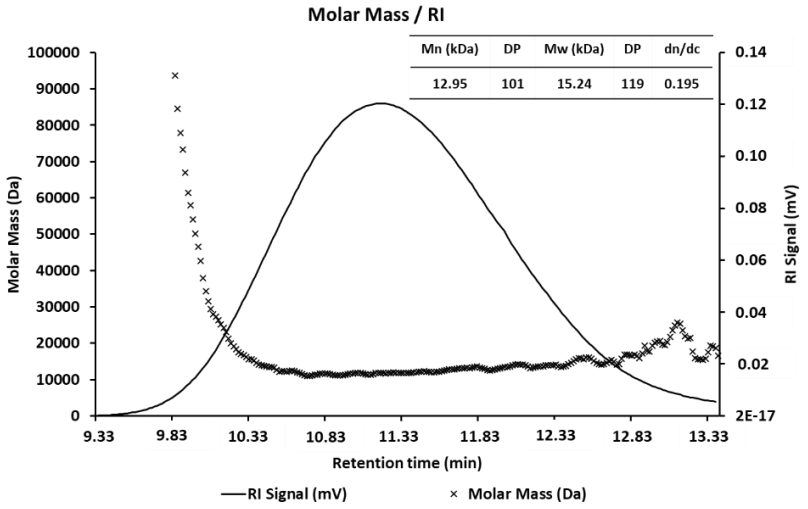

Figure IV. 4: SEC in aqueous conditions (refractive index channel (crosses) vs. molar mass (line)) of PGA.

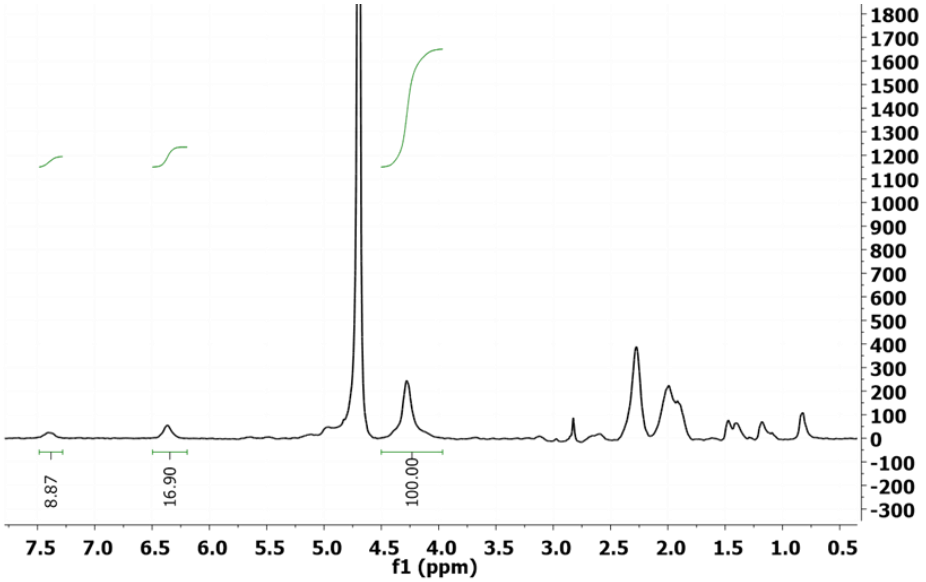

Figure IV. 5: ^{1}H-NMR quantification (mol%) of FLUO (aromatic signals) in the PGA-FLUO conjugate in 500 µL of 5 mg/mL solution in D_2O. The efficient conjugation was demonstrated by achieving around 8 mol% drug loading in all the conjugates.

We characterized the synthesized conjugates through a battery of techniques to ensure identity, purity, total drug loading, and free drug content. The synthetic strategy yielded the desired conjugates with excellent purity as revealed via NMR spectroscopy. After the conjugation of FLUO to PGA, a broadening of the bands can be observed although still retaining the characteristic peaks of the parent drug derivative at 6.5 - 7.5 ppm. Indeed, the integrity of the acetonide moiety was proven along with the conjugate

as shown by the prevalence of the associated peaks at 0.5 and 1.5 ppm respectively within the conjugate (**Figure IV. 6**).

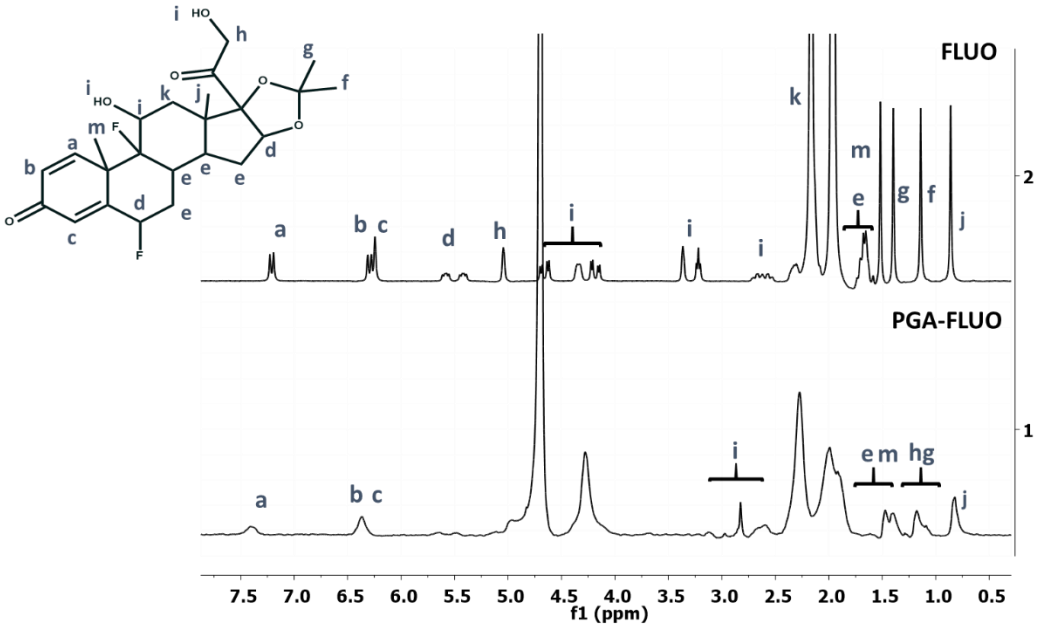

Figure IV. 6: ^{1}H-NMR assignment of FLUO signals in the PGA-FLUO conjugate in D_2O and FLUO in deuterated acetonitrile (5 mg/mL). Aromatic signals that allow the quantification of FLUO (6.5 - 7.5 ppm) were maintained after conjugation to PGA. The signals of the acetonide group, between 0.5 - 1.5 ppm, were also maintained after conjugation to the polymeric backbone.

As shown in **Figure IV. 7**, UV-Vis spectra of PGA-FLUO shows the preservation of the characteristic maximum absorbance of the parent drug (239 nm). However, the signals of PGA and FLUO overlap at the maximum absorbance, and so we quantified total drug loading at 260 nm. UV-Vis analysis allowed us to determine total drug loading (TDL) by weight of 16 - 24 wt%, which agreed with the estimated value obtained from NMR analysis (6.5 to 8.9 mol%) for the different batches**.** In the case of the OG-labeled conjugates, we also analyzed the loading of OG by UV-Vis spectroscopy, yielding a result of ~0.3 mol% of modification of the PGA backbone (**Figure IV. 8**).

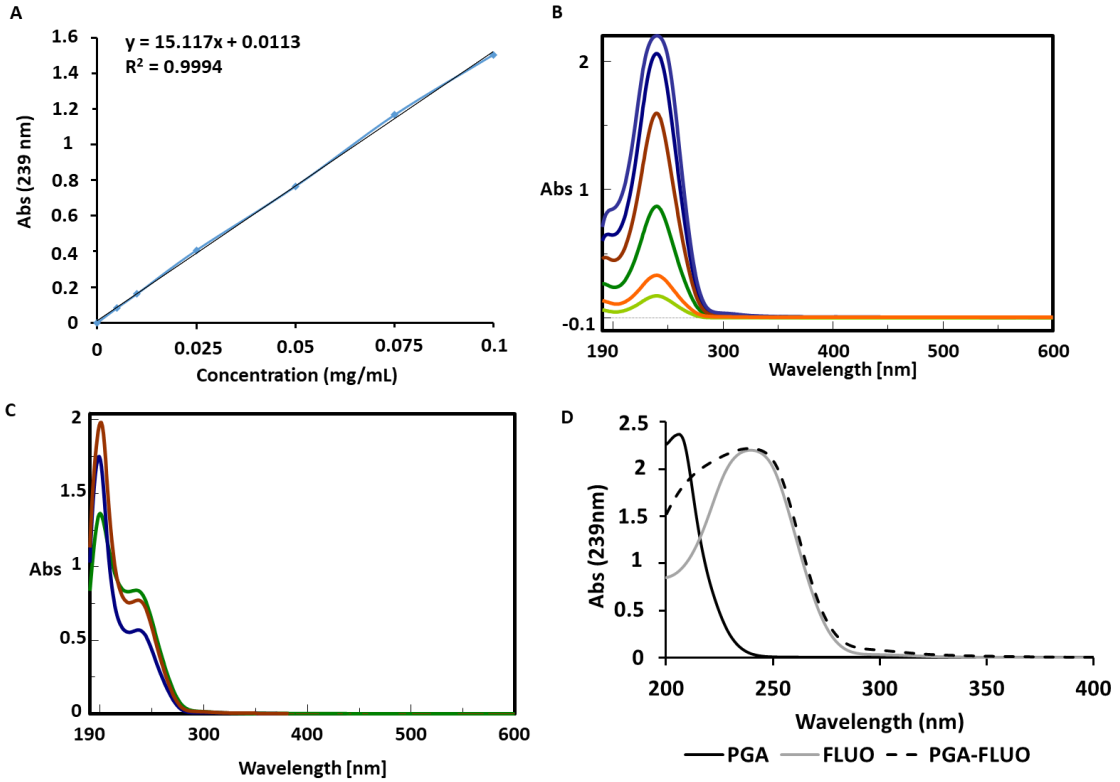

Figure IV. 7: UV-Vis spectra of PGA-FLUO and PGA-FLUO-OG conjugates. **(A)** Calibration curve of FLUO at 239 nm. **(B)** Spectra of the calibration curve of FLUO. **(C)** Spectra of PGA-FLUO conjugates. **(D)** Spectra of PGA, FLUO and PGA-FLUO conjugate.

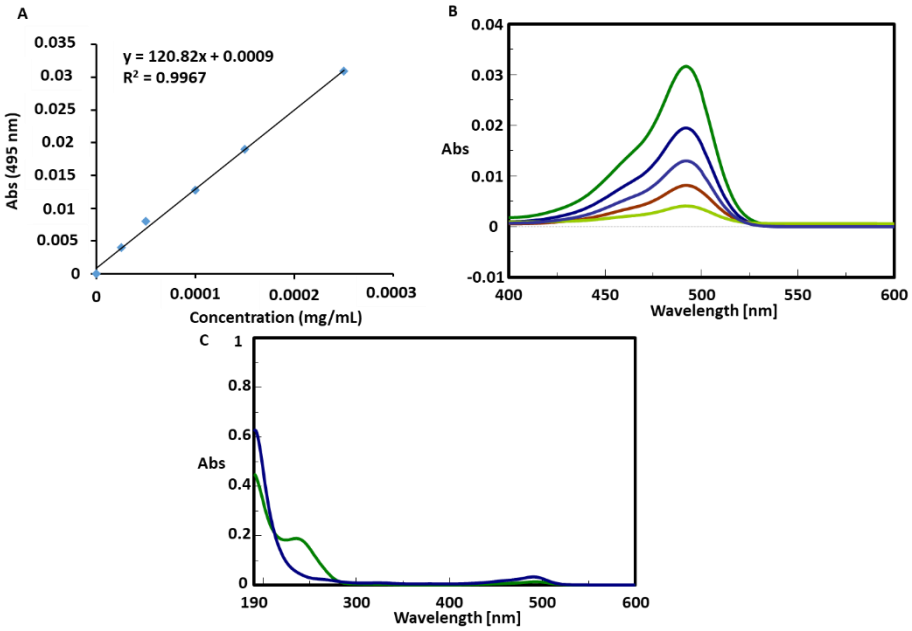

Figure IV. 8: UV-Vis spectra of OG-labeled PGA-FLUO conjugates. **(A)** Calibration curve of OG at 495 nm. **(B)** Spectra of the calibration curve of OG. **(C)** Spectra of PGA-FLUO-OG conjugates.

We established the homogenous conjugation of the drug throughout the polypeptidic backbone, as evidenced by SEC chromatograms obtained from the parent PGA and the conjugates, detected by UV-Vis at the absorbance peak of FLUO (260 nm) in good agreement with the refractive index chromatograms (note that the peak at 17 min comes from the Na^+ counter ion from PGA backbone) (**Figure IV. 9**).

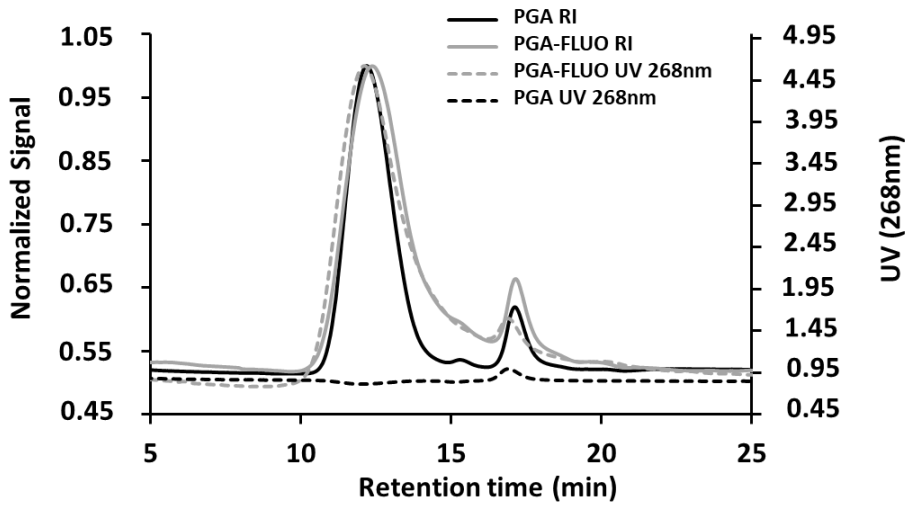

Figure IV. 9: SEC in aqueous conditions (refractive index and UV channel) of PGA and PGA-FLUO.

Then, we optimized the synthetic methodology for robust reproducibility and scalability (up to multigram scale), yielding the desired products with high purity. **Table IV. 1** summarizes the most relevant parameters for the physico-chemical characterization of our polymer-drug conjugates from three different batches and scales, demonstrating batch to batch reproducibility together with the robustness of the synthetic methodology followed (**Figure IV. 10**).

Table IV. 1: Physico-chemical characterization of PGA-FLUO conjugates. [a] Determined by UV-Vis. [b] Determined by HPLC. [c] Determined by ^{1}H-NMR. [d] Hydrodynamic radius (1 mg/mL and intensity) and Z-potential measured via DLS instrument in 1 mM KCl.

Conjugate	Amount	Linker	Yield (%)	Conj.Eff. (%)	TDL[a] (wt%)	FD[b] (wt%)	TDL[c] (mol%)	R_h[d] (nm)	Z-pot (mV)
PGA-FLUO (batch 1)	200 mg	Ester	49.80	41.90	16.23	0.12	6.57	93.27	-44.7
PGA-FLUO (batch 2)	200 mg	Ester	34.32	52.90	20.50	0.11	8.53	91.32	-53.7
PGA-FLUO (batch 3)	1 g	Ester	59.48	99.80	23.80	0.10	8.87	88.82	-49.5

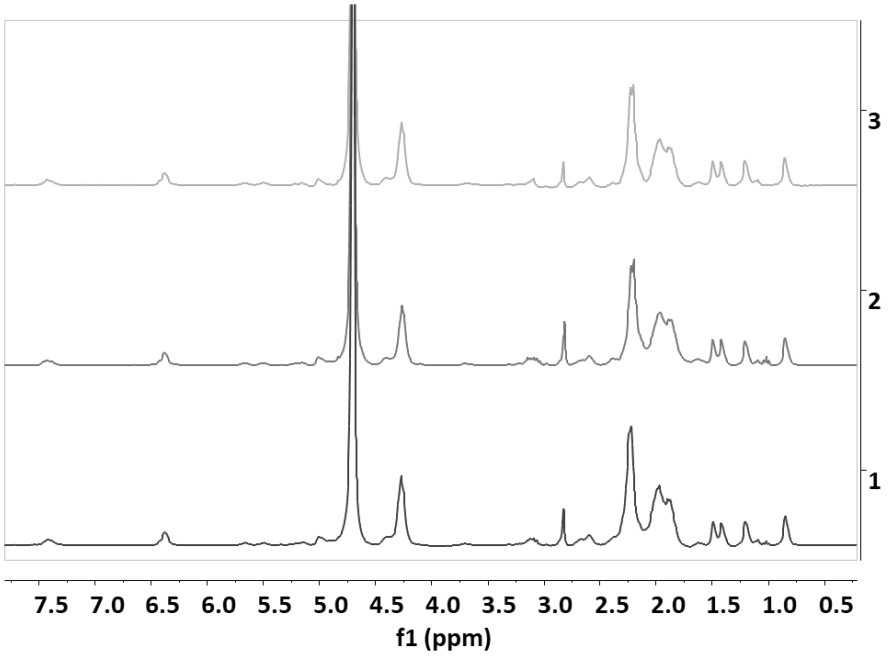

Figure IV. 10: ^{1}H-NMR spectra in D_2O of three different batches of PGA-FLUO demonstrating batch-to-batch reproducibility.

Furthermore, we found a free drug (FD) content of 0.10 - 0.12 wt% in relation to the total drug loading in all studied conjugates as determined by high-performance liquid chromatography (HPLC). The results obtained demonstrated free drug content below 2 wt% (relative to total drug loading) after the exhaustive purification of the conjugate, thereby providing evidence for the purity and high drug loading of the conjugate (**Figure IV. 11**). We employed Batch 3 for the subsequent complete physico-chemical and biological evaluation.

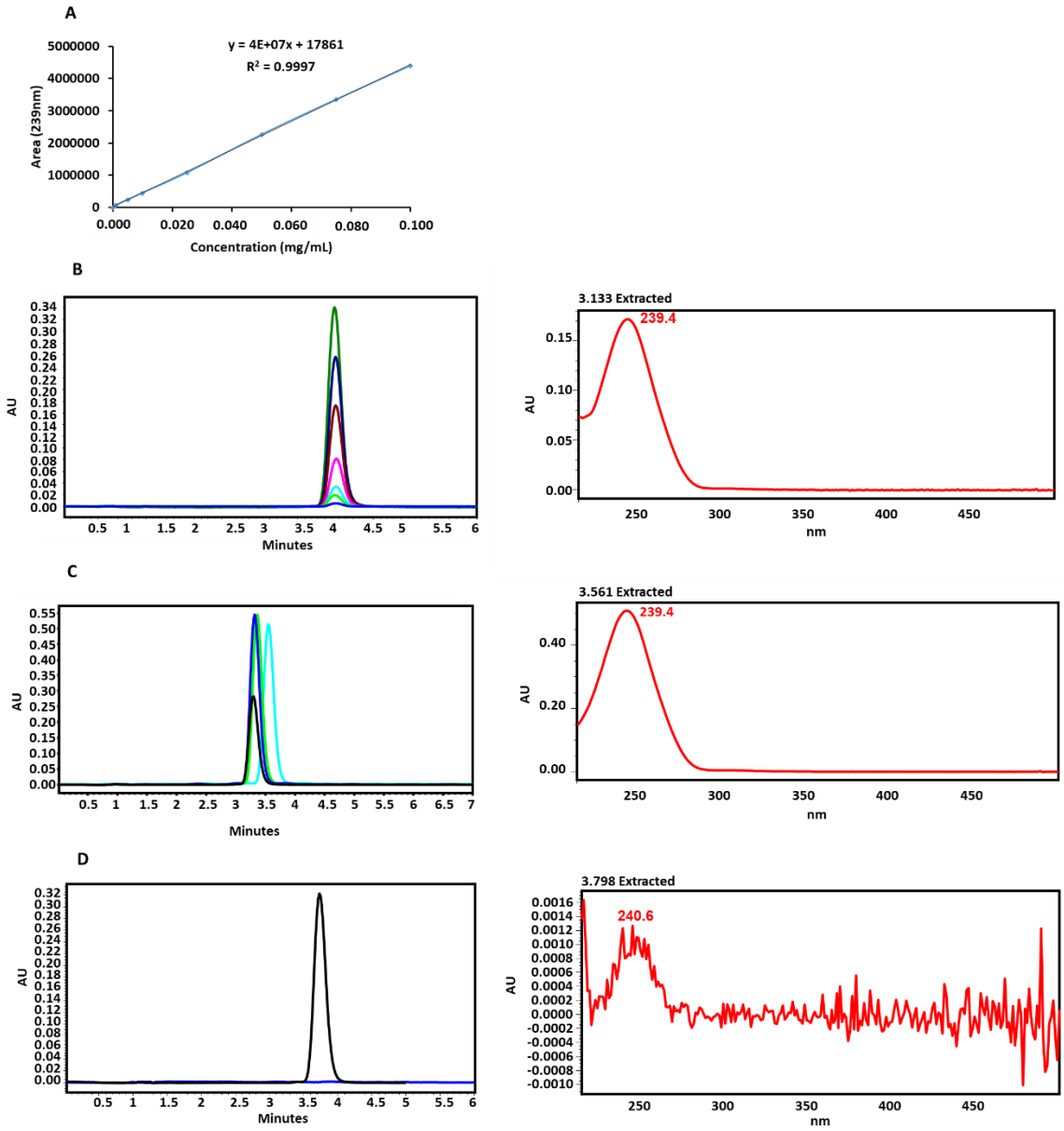

Figure IV. 11: **(A)** Calibration curve of FLUO at 239 nm. **(B)** HPLC chromatograms of the calibration curve of FLUO. **(C)** HPLC chromatogram of liquid-liquid extraction of FLUO, FLUO + PGA, FLUO + PGA-FLUO conjugate, and FLUO + PGA-FLUO + HA-CP vehicle. **(D)** HPLC chromatogram of free FLUO from PGA-FLUO conjugate (blue) in comparison with a standard sample of FLUO at 0.075 mg/mL (black).

IV.2.3. Self-assembling Behavior of PGA-FLUO

We next studied the behavior of the PGA-FLUO conjugates in an aqueous environment as the conjugation of the corticoid motifs into the hydrophilic PGA backbone may result in the generation of an amphiphilic system with appropriate hydrophobic-hydrophilic balance, enabling the self-assembly into larger nanometer-sized

objects [36]. At the molecular level, we found evidence that the self-assembly of the PGA-FLUO proceeded primarily via hydrophobic effect, as evidenced by the pyrene assay performed to determine the critical aggregation concentration (CAC) [37]. The presence of hydrophobic pockets within the assemblies allowed us to determine the CAC via pyrene probe resulting in a low value of 0.06 mg/mL, in close agreement with other anionic polymer amphiphiles reported in the literature [38] (**Figure IV. 12A**).

We then employed circular dichroism (CD) to determine the conformation of the conjugates as a function of PGA-FLUO conjugate concentration and at different pHs that would mimic the different environments to which the conjugates will be exposed after topical administration (**Figure IV. 12B**). At pH 7.4, PGA-FLUO took on a predominantly random coil conformation, as revealed by the absolute minimum ellipticity value at 200 nm. We also recorded a significant redshift evolution of the random coil negative band below and above the CAC threshold value, together with the appearance of a cotton effect in the 270 - 300 nm region, which is a characteristic change in optical rotatory dispersion in the vicinity of an absorption band of a substance, and in this case such bands are attributed to the ketones within the FLUO molecules [39]. The increase in the cotton band intensity is most likely related to the increasing concentration of the FLUO content rather than a supramolecular organization of the inner core of the assembled conjugates, as derived by the flat shape of the CD spectra when representing the molar ellipticity and hence correcting the concentration effect (**Figure IV. 13**).

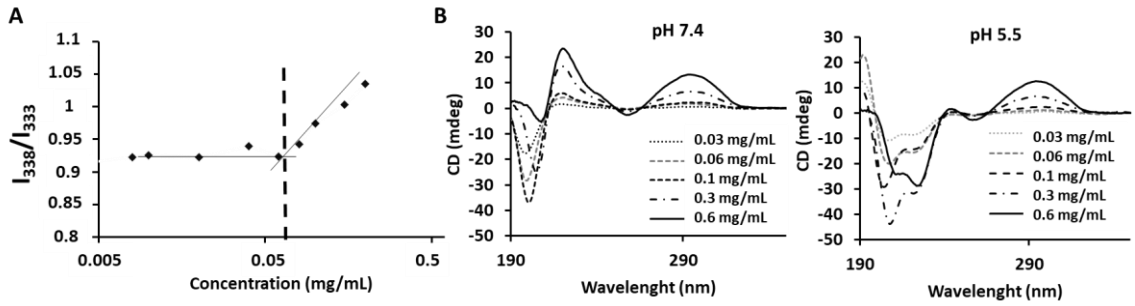

Figure IV. 12: Self-assembly behavior of PGA-FLUO conjugates. **(A)** Pyrene assay of PGA-FLUO conjugates by fluorescence spectroscopy. **(B)** Secondary structure of the conjugates by CD at pH 7.4 and 5.5 at different concentrations.

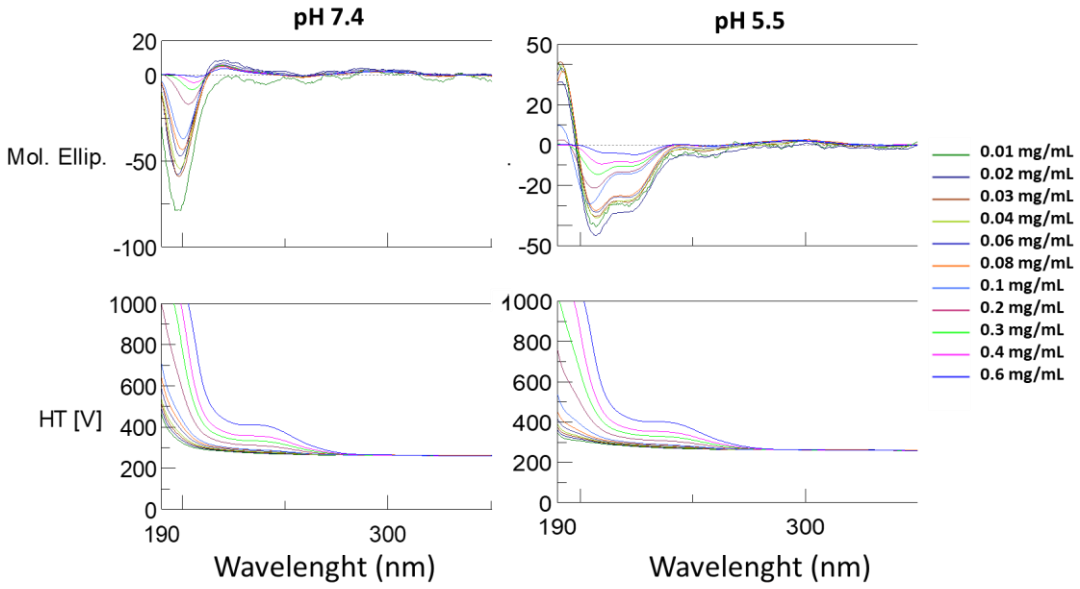

Figure IV. 13: Molar ellipticity of PGA-FLUO at different concentrations at pH 7.4 and 5.5.

At pH 5.5, in contrast, we found a partial alpha-helix characteristic conformation that evolved when increasing the concentration above the CAC. Under this condition, the random coil to alpha-helix transition is expected to be partial according to the pKa values (which indicated the strength of an acid) reported in literature around 4.9 (roughly 50% of side chains are protonated at pH 5.5) [28], and the fact that we failed to observe precipitation or cloudiness at pH 5.5 [40] as can be observed at pH 3 (**Figure IV. 14**).

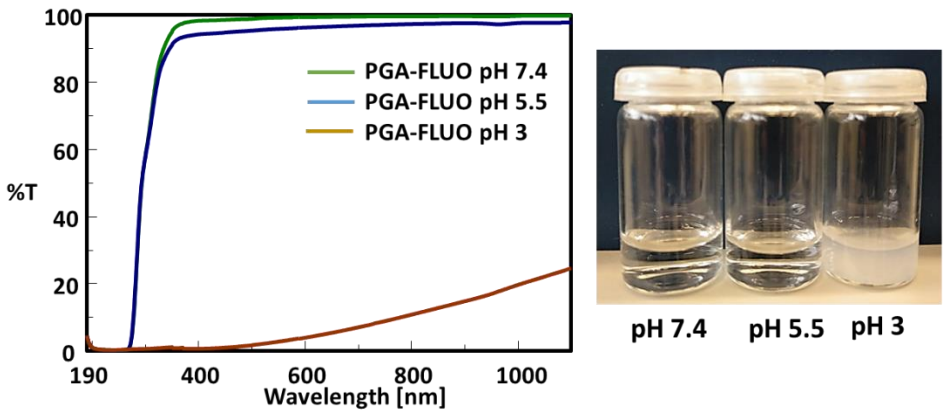

Figure IV. 14: Transmittance measurements by UV-Vis of PGA-FLUO at pH 7.4, 5.5, and 3.

TEM micrographs confirmed the spherical aspect of the self-assembled carriers with geometrical sizes in the range of 50 - 100 nm with no particular evidence for core-shell morphologies (**Figure IV. 15A**). The conjugates exhibited a hydrodynamic radius

(Rh) of 40 - 100 nm in aqueous solutions at different pHs and ionic strengths, confirming the assembly of multiple PGA-FLUO conjugates molecules within the globular nanoassembly (**Figure IV. 15B**). Z-potential measurements resulted in a highly negative value of -50 mV, confirming the assembly of multiple PGA-FLUO molecules within the globular nanoassembly. The compaction of the assembled conjugates upon increasing ionic strength reinforces the critical character of hydrophobic interactions. These interactions can drive the self-assembly process exposing the polyglutamate anionic backbone to the surface, and hence experiencing a screening of anionic repulsions upon increasing ionic strength and leading to the recorded decrease in Rh [41].

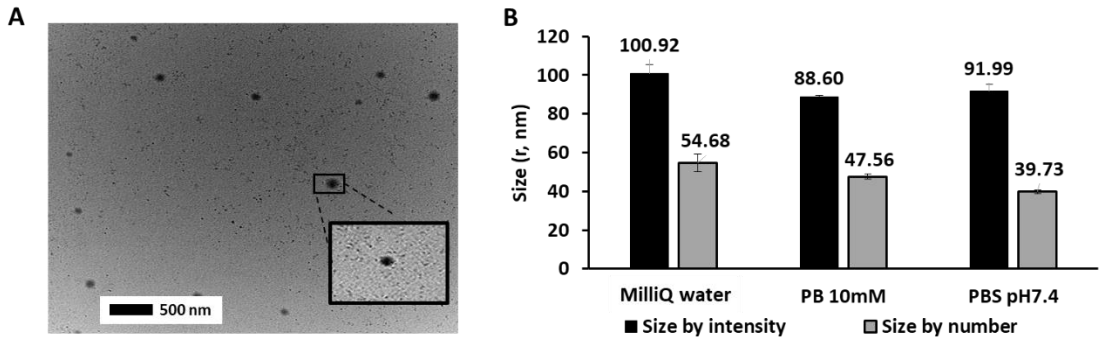

Figure IV. 15: **(A)** TEM micrographs of PGA-FLUO from a sample prepared in MilliQ water at 2 mg/mL. **(B)** Hydrodynamic radius by DLS in different solvents (MilliQ water, PB 10 mM, and PBS pH 7.4) with a constant size close to 100 nm.

In summary, the conjugation of the highly hydrophobic corticoid FLUO to PGA results into an amphiphilic PGA-FLUO conjugate that self-assembles into spherical nanosized objects driven by the hydrophobic interactions of the FLUO motifs. Although we found no clear evidence for a core-shell structure by TEM, spectroscopic analyses suggest an unordered arrangement of FLUO within an inner hydrophobic core. At the outer layer of the constructs, CD analysis and z-potential values indicate a PGA backbone composition with a high anionic carboxylate form at pH 7.4 in a relatively constrained random coiled conformation, probably due to electrostatic repulsions, which might transition to partial alpha-helix conformation at pH 5.5 without altering the solubility of the system.

IV.2.4. FLUO Release Kinetics as a Crucial Feature Driving Sustained Release into the Skin

We subsequently studied drug release kinetics under hydrolytic and proteolytic conditions owing to the pH-labile nature of the ester bond and cathepsin B-mediated degradation of the polymer backbone. We incubated samples of PGA-FLUO at 37ºC at different pHs including 5.5 (lysosome, in presence and absence of cathepsin B) and 7.4 (blood) up to 72 h. In addition, as we use the HA-CP hydrogel (see **Chapter III** for more details) as a vehicle to administer the conjugate into the skin, we performed drug release kinetics in the presence of the HA-CP vehicle. Overall, the data collected suggests a small but sustained FLUO release in all the cases (**Figure IV. 16 and Figure IV. 17**).

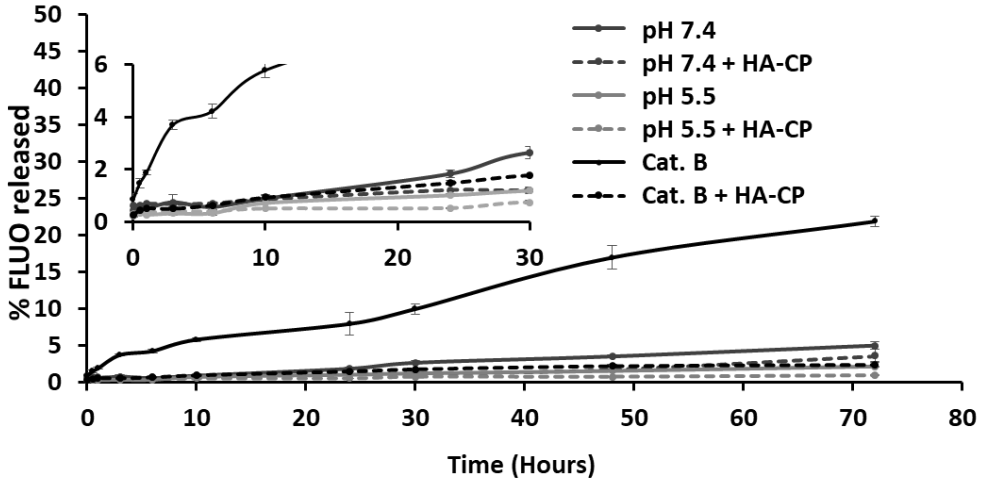

Figure IV. 16: Drug release profiles by HPLC at different pH (5.5 and 7.4) and under proteolytic conditions (Cat. B) of PGA-FLUO alone and applied in the HA-CP vehicle. Experiments were carried out per triplicate, mean ± SEM.

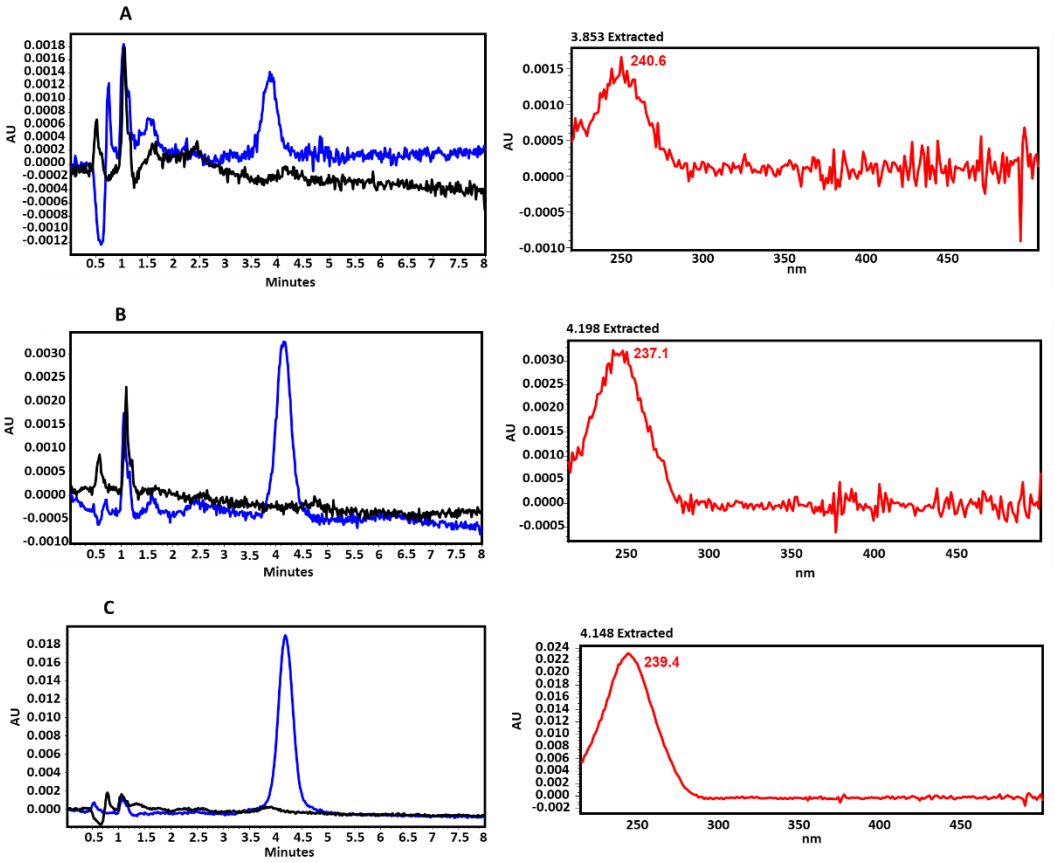

Figure IV. 17: Drug release chromatograms by HPLC. **(A)** Release of FLUO at pH 5.5 at time 0 (black) and after 72 h (blue) **(B)** Release of FLUO at pH 7.4 at time 0 (black) and after 72 h (blue) **(C)** Release of FLUO in presence of cathepsin B at time 0 (black) and after 72 h (blue).

The results suggest that drug release kinetics from the conjugate at 72 h is 2-fold faster at pH 7.4 (5 wt% of free FLUO) than at pH 5.5 (2.4 wt% of free FLUO). Although these results might seem counterintuitive, we must consider the conformational and spatial arrangement of the drug within the polymer-drug conjugate and the resulting assembled nanocarrier. Although acids or bases chemically catalyze ester-bond hydrolysis [42-44], these results might be explained in terms of a PGA backbone response to pH. At pH 5.5, protonation of PGA side chains represents roughly 50% molar of the overall carboxylates as derived from the pKa of linear PGA reported in literature [28]. These effects induce a partial random coil to alpha-helix conformation transition as shown above, although the system remains fully soluble according to turbidimetric data. At pH 7.4, 100% molar side chains in PGA are carboxylates, yielding a full random coil conformation. Whether the observed change in release kinetics derives from conformational aspects (i.e., rigidity, compactness, accessibility to PGA-FLUO bonds) or auxiliary effect of vicinal carboxylates, the result observed represents an inverse

release profile to that expected. Unfortunately, the complete rationale for this phenomenon lies outside the scope of the present work. We also studied drug release in the presence of cathepsin B (5 U), a lysosomal cysteine protease that forms a major part of the proteolytic conditions faced by the polymer-drug conjugates following cell uptake. We found the release of FLUO to be significantly higher following the addition of cathepsin B when compared to hydrolytic conditions, with 20 wt% drug released within 72 h (**Figure IV. 16**). This significant increase in drug release can be ascribed to the digestion of PGA backbone, enabling the heightened accessibility of the PGA-FLUO bond to hydrolytic conditions [45].

Additionally, the incorporation of the PGA-FLUO conjugate within the HA-CP vehicle caused a marked decrease in the release of FLUO under hydrolytic conditions, obtaining half of the free FLUO released at pH 7.4 (~2.5 wt% of free FLUO) and pH 5.5 (~1.2 wt% of free FLUO). However, more importantly, we observed a marked decrease under proteolytic conditions, obtaining ~2.5 - 3 wt% of free FLUO in comparison with the 20 wt% drug release without the HA-CP vehicle.

IV.2.5. Compatibility of PGA-FLUO with the HA-CP Vehicle

As PGA-FLUO will be delivered topically using the HA-CP vehicle (previously reported to enhance permeation to the epidermis in **Chapter III**), we studied the compatibility of the intended formulations. The incorporation of PGA-FLUO at a working concentration of 10 mg/mL within 1% w/v of HA-CP vehicle established the complete solubility and stability of the conjugate in the vehicle. Furthermore, the vehicle displayed no effect over nanosized PGA-FLUO in terms of homogenous globular shape nanoparticles and an expected size of about 80 - 100 nm, as evidenced in TEM micrographs (**Figure IV. 18**).

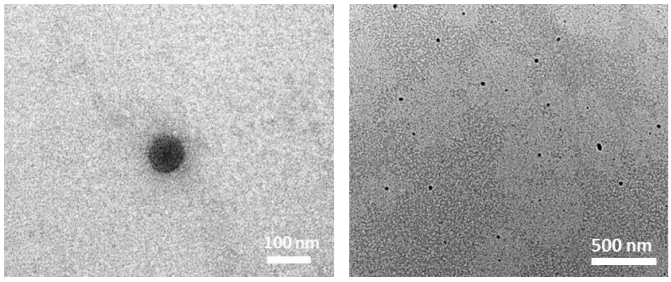

Figure IV. 18: Representatives TEM images of PGA-FLUO conjugates in the HA-CP (1% w/v) vehicle at 10 mg/mL, scale bar is 100 nm (left) and 500 nm (right).

In order to explain the reduction of drug release observed from the PGA-FLUO under proteolytic conditions in the presence of the HA-CP, we studied the activity of the cathepsin B *in vitro* with and without the vehicle. We used medium (80 µL of acetate buffer 20 mM pH=5, 10 µL of EDTA 2 mM and 10 µL of DTT 5 mM), medium with the substrate (Z-Arg-Arg-AMC), and negative control (leupeptin) as controls (**Figure IV. 19**). The increase in the viscosity caused sequestering of the nanocarrier structure within the gel network contributing to the delayed release of FLUO compared to the aqueous dispersion. The decrease of the drug release is more evident under proteolytic conditions, where the reduction in the release kinetics is most likely related to the lower mobility of enzyme and substrate. Indeed, we discovered a significant decrease of cathepsin B activity in the presence of HA-CP vehicle. These results suggest a protective effect of the HA-CP vehicle on PGA-FLUO.

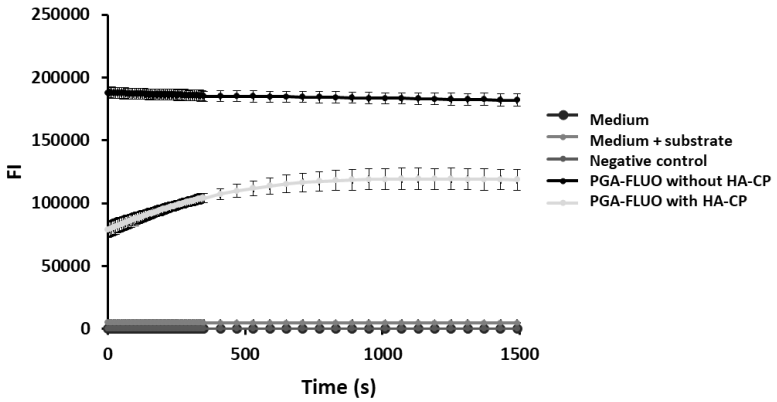

Figure IV. 19: Cathepsin B activity *in vitro* with or without HA-CP vehicle by the quantification of the fluorescence intensity.

IV.2.6. *In Vitro* Skin Compatibility and Cell Trafficking Studies of PGA-FLUO Conjugates

Cell viability assays performed on HaCaT cells and human fibroblasts after 72 h of treatment with increasing doses of free FLUO or PGA-FLUO at the same drug equivalents revealed the absence of cell toxicity up to the concentrations tested, demonstrating the safety of the conjugation strategy for dermal applications (**Figure IV. 20A and 20B**).

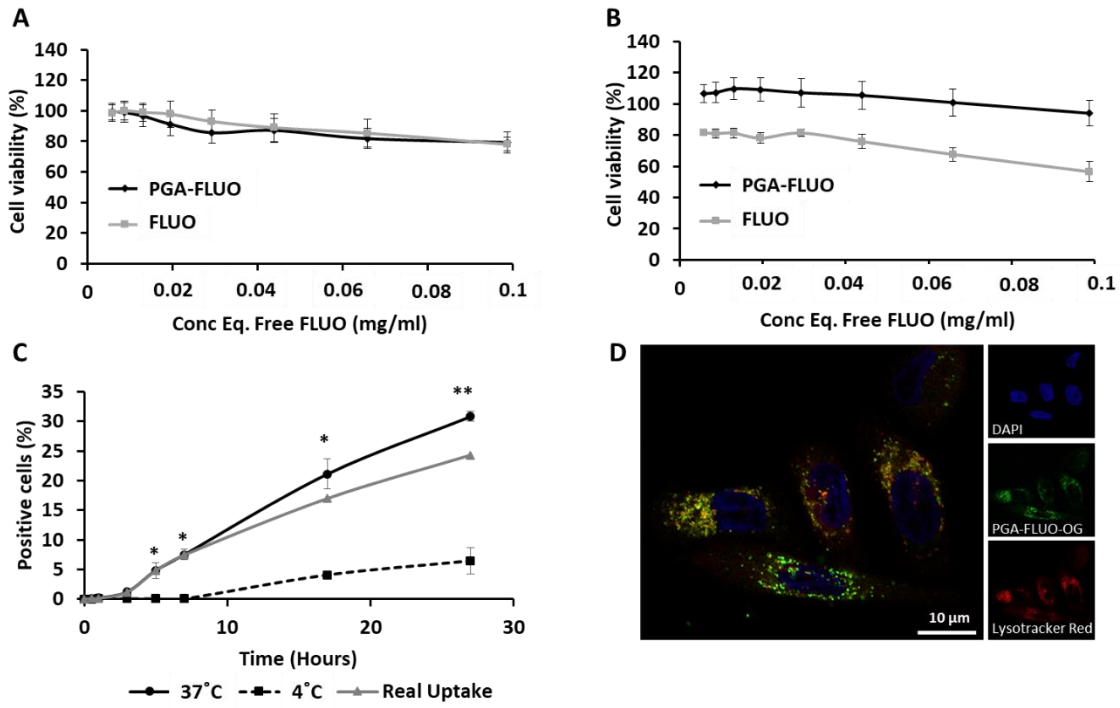

Figure IV. 20: *In vitro* evaluation of PGA-FLUO conjugates. Cell viability assays in **(A)** HaCaT cells and **(B)** human fibroblasts after 72 h of treatment with FLUO or PGA-FLUO conjugate (n=3). **(C)** Uptake study by flow cytometry of PGA-FLUO conjugates fluorescently labeled with OG in HaCaT cells. Results represented as the average of positive cells (%) ± SEM. t-student, comparison of pair of data with control condition, ***p<0.001, **p<0.01, *p<0.05 (n=3). **(D)** Confocal images from the uptake of OG-labeled PGA-FLUO conjugates at 24 h post-treatment in HaCaT cells, in which a colocalization with lysotracker red was observed (yellow).

In addition, we performed flow cytometry (**Figure IV. 20C**) and fluorescence confocal microscopy (**Figure IV. 20D**) at non-toxic concentrations in keratinocytes as our target cell to understand the cell internalization of OG-labeled PGA-FLUO. As expected for these macromolecular systems [46, 47], we observed energy-dependent endocytic uptake, reaching 30% of positive cells at 24 h post-treatment. In agreement with these results, we obtained confocal images to identify the subcellular localization of the PGA-FLUO-OG conjugate inside the keratinocytes after 24 h of uptake, demonstrating a clear co-localization with the lysosomal marker Lysotracker red. These findings indicate the suitability of our polypeptidic nanocarriers for lysosomotropic drug delivery [48].

IV.2.7. PGA-FLUO Reduces the Release of Pro-Inflammatory Cytokines *In Vitro*

Additionally, we evaluated cell viability of murine macrophages (Raw264.7 cell line) in response to FLUO after 72 h of treatment, allowing us to select 0.49 ng/mL as FLUO concentration for any subsequent pharmacological study in this cell line (**Figure IV. 21A**).

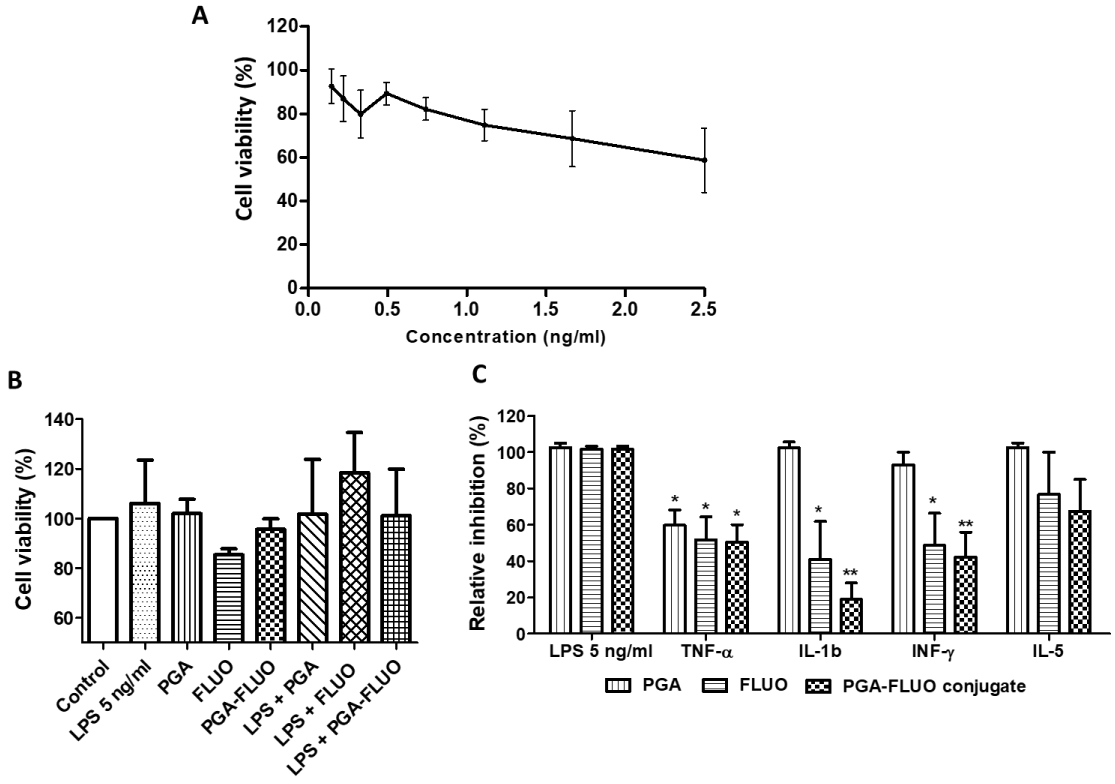

Figure IV. 21: *In vitro* PGA-FLUO evaluation in macrophages. **(A)** Cell viability assay in Raw264.7 macrophages following treatment with varying concentrations of FLUO for 72 h (n=3, mean±SEM). **(B)** Cell viability assay after 72 h of treatment with FLUO, PGA-FLUO conjugate, and vehicles at 0.49 ng/mL FLUO eq. **(C)** Reduction of pro-inflammatory cytokines release after treatment for 72 h in macrophages stimulated with bacterial LPS (n=3). Asterisks indicate statistically significant differences after ANOVA analyses followed Tukey's post hoc tests mean ± SEM. In all cases, we considered differences to be significant when p***<0.0001; p**<0.01; p*<0.05.

We then assessed cell viability after the treatments with FLUO, PGA-FLUO, and vehicles by MTS assay at the selected concentration of FLUO, revealing a non-toxic profile when tested at 72 h of incubation (**Figure IV. 21B**). Finally, we tested the anti-inflammatory activity of the FLUO derivatives by assessing the reduction of the pro-inflammatory cytokines release to the culture media from the macrophages treated with

5 ng/mL of bacterial LPS from *E. coli*, using a LUMINEX multiplex immunoassay for the quantification of the cytokines. The results obtained suggested that FLUO not only retains its anti-inflammatory activity following incorporation into the polypeptidic backbone, but also that the conjugation to PGA promotes the inhibitory effect of FLUO on the release of pro-inflammatory cytokines IL-1b and INF-γ (**Figure IV. 21C**).

IV.2.8. PGA-FLUO Biocompatibility and Anti-Inflammatory Effect in an Inflammatory Skin Equivalents Model and an Inflammatory *Ex Vivo* Human Skin Model

Ex vivo models represent valuable research tools for investigations into different skin diseases such as psoriasis, and are considered more relevant than *in vitro* research involving cell lines. We employed two *ex vivo* models, from which we can obtain complementary information, to evaluate the safety and the anti-inflammatory activity of the synthesized conjugates. We explored two *ex vivo* models to corroborate the data obtained in the cell studies: (i) an *ex vivo* human skin model (**Figure IV. 22A**) and (ii) a skin equivalent model (**Figure IV. 22B**).

In an *ex vivo* human skin model (**Figure IV. 22C**), tissue viability after the treatment with 3 µL of a solution of 10 mg/mL of PGA, FLUO, PGA-FLUO applied in water or in the HA-CP vehicle (1% w/v), and the HA-CP (1% w/v) during 24 h revealed that all the treatments maintain tissue viability. Additionally, in a skin equivalents model the application of two doses of 5 mg/mL of the same treatments on day 11 and 13 of culture also demonstrated excellent biocompatibility, as indicated by the absence of significant cytotoxic effects (**Figure IV. 22D**).

Additionally, we developed inflammatory models to assess the anti-inflammatory potential of the FLUO derivatives at the same concentration evaluated in the viability assays. We studied IL-6 secretion by ELISA assay in an optimized inflammatory *ex vivo* human skin model after inflammatory insult via the combined treatment with bacterial lipopolysaccharide (LPS; 15 µg/mL) and epidermal growth factor (EGF; 2.5 ng/mL) for 24 h in the culture media (see **Chapter II** for more details).

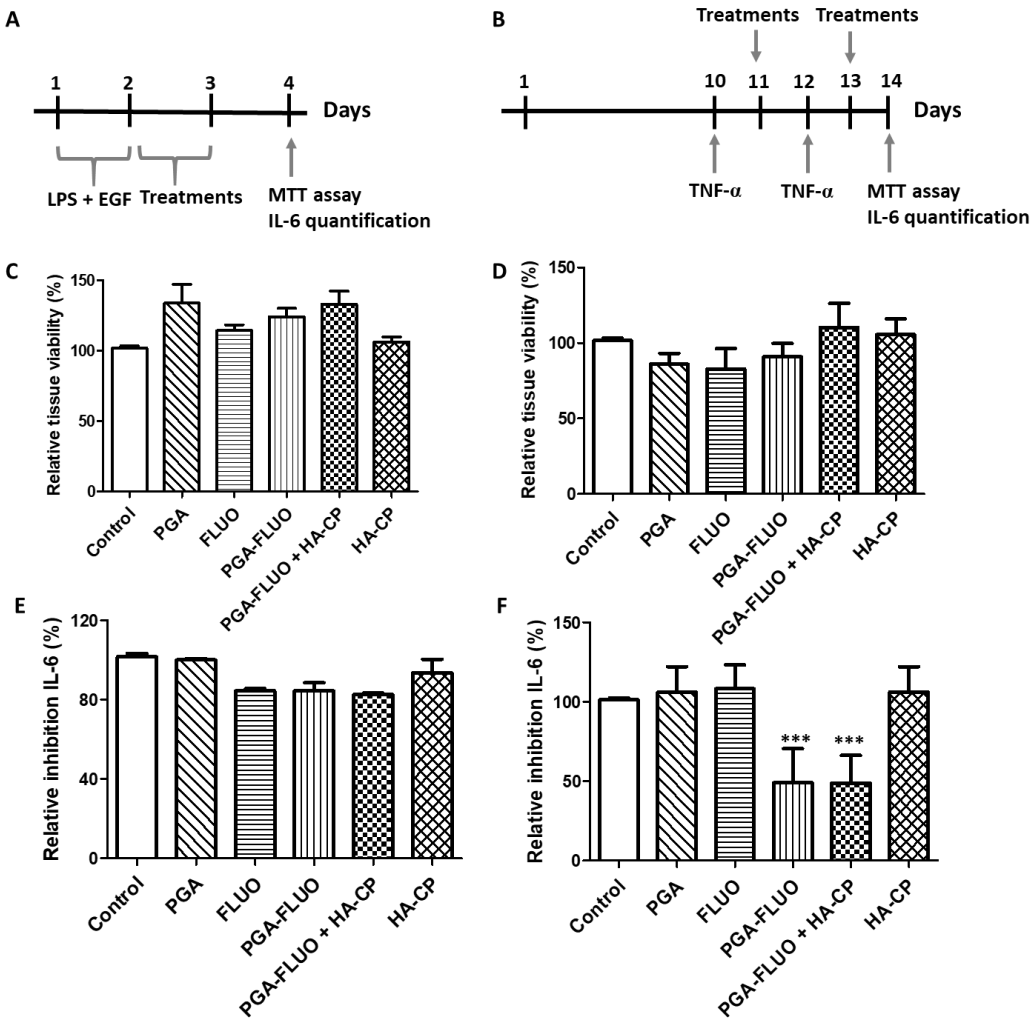

Figure IV. 22: Evaluation of tissue viability and anti-inflammatory activity of FLUO derivatives in inflammatory skin models. **(A)** Establishment on the inflammatory *ex vivo* human skin model. **(B)** Establishment of the inflammatory skin equivalents model. **(C)** Tissue viability in an inflammatory *ex vivo* human skin model after 24 h of treatment (10 mg/mL of PGA, FLUO, PGA-FLUO in water and HA-CP vehicle (1% w/v), and HA-CP (1% w/v)) by MTT assay. **(D)** Tissue viability in the inflammatory skin equivalents model after 2 doses of treatment (5 mg/mL of PGA, FLUO, PGA-FLUO in water and HA-CP vehicle (1% w/v), and HA-CP (1% w/v)) by MTT assay. **(E)** IL-6 levels in the inflammatory *ex vivo* human skin model after the induction with the combination of bacterial LPS (15 µg/mL) and EGF (2.5 ng/mL), following treatment (10 mg/mL of PGA, FLUO, PGA-FLUO in water and HA-CP vehicle (1% w/v), and HA-CP (1% w/v)) for 24 h. Values expressed as relative inhibition of IL-6 (%). **(F)** IL-6 levels in the inflammatory skin equivalents model stimulated with TNF-α (20 ng/mL), following two doses of treatment (5 mg/mL of PGA, FLUO, PGA-FLUO in water and HA-CP vehicle (1% w/v), and HA-CP (1% w/v)). Values are expressed as relative inhibition of IL-6 (%). Asterisks indicate statistically significant differences after ANOVA analyses followed Bonferroni's post hoc tests, mean ± SEM. In all cases, we considered differences to be significant when p***<0.001; p**<0.01; p*<0.05.

Treatment for 24 h revealed that the reduction in IL-6 release following FLUO administration was similar to PGA-FLUO treatment (both applied in water or in the HA-CP vehicle). All treatments reduced IL-6 levels by around 20% compared to the corresponding untreated control (**Figure IV. 22E**). To ratify this data, we also studied IL-6 secretion in the second inflammatory skin equivalents model induced by the application of 20 ng/mL of recombinant TNF-α in the culture media on days 10 and 12 of culture [49-52]. Of note, this model provides a more permeable stratum corneum than the *ex vivo* human skin model, given the reconstitution of this skin model from cells. On day 11 and 13, we topically applied the same treatments at 5 mg/mL (35 μg/cm^2) and evaluated the release of IL-6 by ELISA assay. We discovered a significant reduction in IL-6 secretion (almost 50%) in the case of PGA-FLUO treatment applied in water or the HA-CP vehicle when compared to the free drug, most probably due to the lower amount of model variance when compared to the higher variation observed among the human skin samples (**Figure IV. 22F**).

IV.2.9. FLUO Conjugation and the Use of HA-CP as Vehicle Enhances Skin Permeation

To visualize skin penetration of PGA-FLUO and explore the role of the HA-CP on the extent of skin permeation, we performed a qualitative study on human skin using Franz diffusion cells comparing the permeation of 100 μL from 10 mg/mL solution of OG-labeled PGA-FLUO applied in water or embedded in Cy5.5-labeled HA-CP vehicle (1% w/v) for 24 h. After fixation and tissue process, we acquired confocal microscopy images that revealed the significant accumulation of the PGA-FLUO within the stratum corneum, and a lower accumulation in the epidermis (**Figure IV. 23A**). However, PGA-FLUO within the HA-CP vehicle displayed enhanced penetration through the epidermal layer (**Figure IV. 23B**). The quantification of OG intensity in the different skin layers by Image J software revealed that the presence of the HA-CP vehicle significantly enhanced the epidermal accumulation of PGA-FLUO, proven by the higher fluorescence intensity detected in both, the stratum corneum and the viable epidermis (**Figure IV. 23C**).

Furthermore, we extracted FLUO from the whole skin at 24 h post-treatment with PGA-FLUO (10 mg/mL) in water or embedded in the HA-CP vehicle (1% w/v) and analyzed the samples by HPLC (**Figure IV. 24**). We normalized HPLC data considering the amount of FLUO released determined from the release kinetics studies under similar

conditions (with or without HA-CP), demonstrating that the amount of FLUO was almost two-fold higher in presence of HA-CP as vehicle (**Figure IV. 23D**). These findings prove the ability of the HA-CP vehicle to act as penetration enhancer, being able to promote the accumulation of the conjugate in the epidermal layer, thereby creating a source for the sustained release of the drug that could reduce the need for the repeated skin administration.

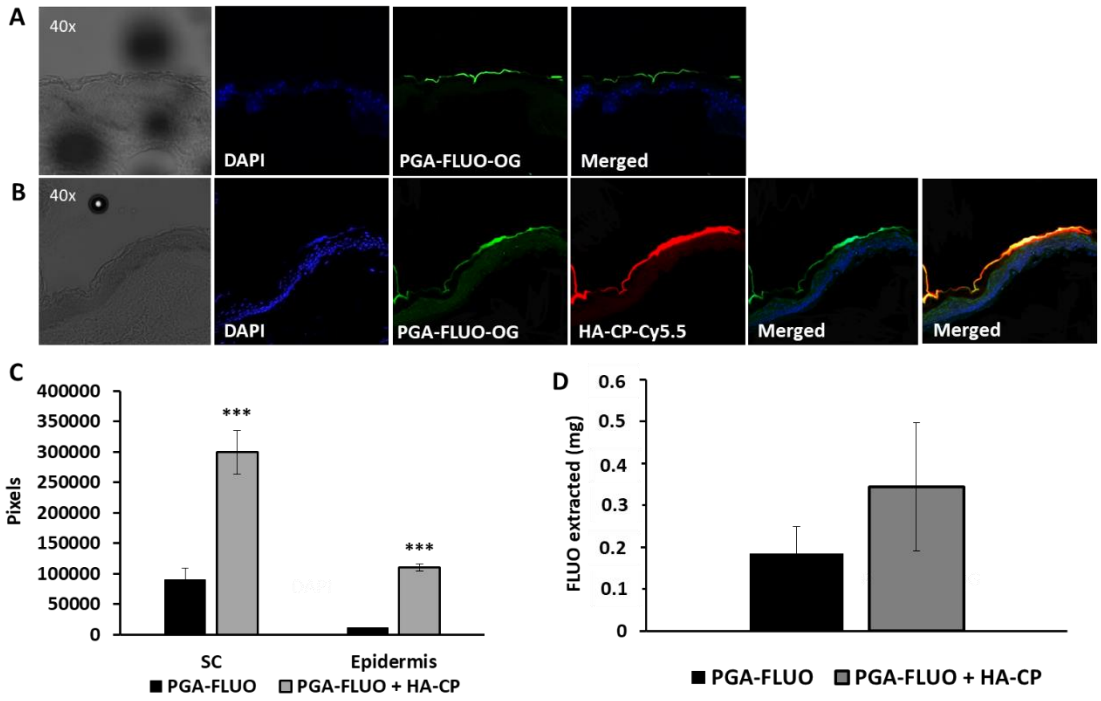

Figure IV. 23: Evaluation of skin permeation of PGA-FLUO and FLUO quantification in whole skin. **(A)** Confocal images after permeation studies of OG-labeled conjugates formulated in water. **(B)** Confocal images after permeation studies of OG-labeled conjugates formulated in the HA-CP vehicle (1% w/v). **(C)** Quantification of OG intensity by Image J software in the stratum corneum (SC) and the viable epidermis (n=5) after permeation studies. **(D)** Quantification of FLUO extracted from the whole skin (see material and methods for details) analyzed by HPLC after the permeation studies of PGA-FLUO with and without the HA-CP vehicle (n=3). Asterisks indicate statistically significant differences after ANOVA analyses followed Bonferroni's post hoc tests, mean ± SEM. In all cases, we considered differences to be significant when p***<0.001; p**<0.01; p*<0.05.

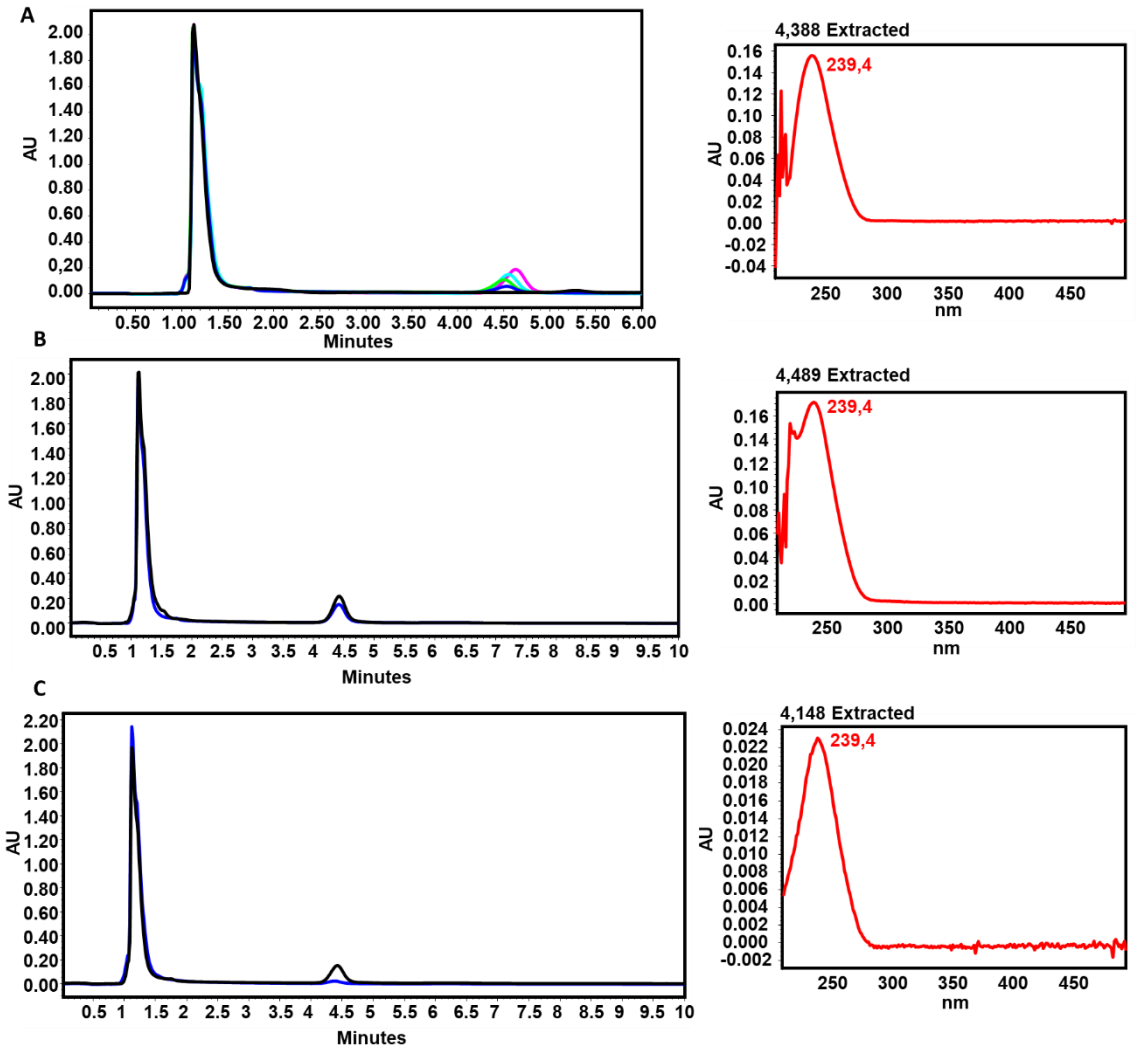

Figure IV. 24: HPLC chromatograms of FLUO extracted from the skin after the permeation studies in Franz diffusion cells for 24 h. **(A)** Calibration curve of FLUO at 239 nm in DMSO. **(B)** Chromatogram of FLUO extracted when the PGA-FLUO conjugate was applied in water (blue) in comparison with a standard sample at 0.075 mg/mL (black) **(C)** Chromatogram of FLUO extracted when the PGA-FLUO conjugate was applied in the HA-CP vehicle (blue) in comparison with a standard sample at 0.075 mg/mL (black).

Additionally, we analyzed the aliquots extracted from the receptor chamber obtained during the permeation studies by UV-Vis spectroscopy, in order to detect any signal from OG that would suggest the capability of the specific formulation to reach systemic circulation, feature to be avoided with corticosteroids in order to prevent systemic toxicities. MilliQ water as well as the use of HA-CP-Cy5.5 without the conjugate were used as controls. The results revealed the absence of OG signal at 495 nm and Cy5.5 at 676 nm (as already demonstrated in **Chapter III**) at 8 and 24 h of study,

suggesting that the conjugate is not capable to reach the dermis, and therefore the receptor chamber in contact with the dermis (**Figure IV. 25**). As the receptor chamber simulates the bloodstream, this finding would indicate that the conjugate would not reach the systemic circulation avoiding the possible corticosteroids adverse effects and focusing its action on the desired epidermis.

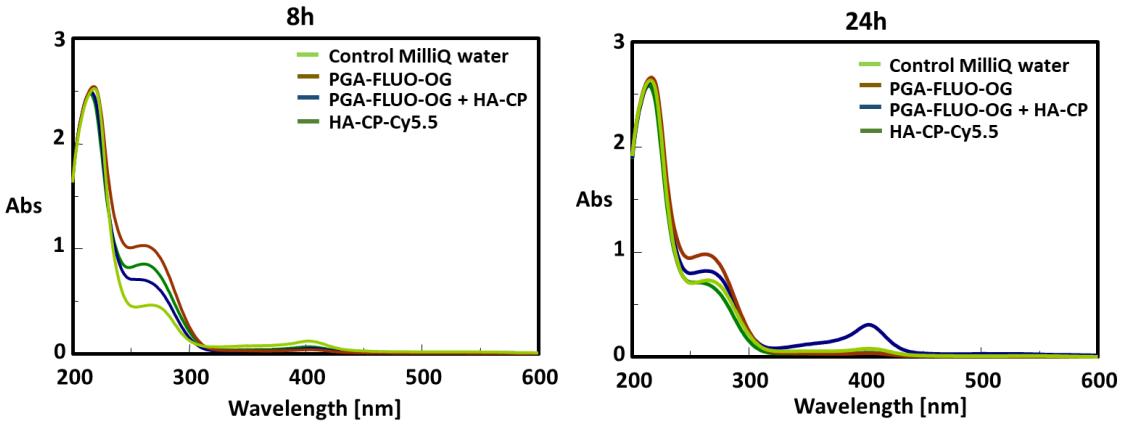

Figure IV. 25: UV-Vis spectra of the aliquots extracted from the receptor chamber after 8 (left) and 24 h (right) after Franz diffusion cell permeation studies in human skin by using PGA-FLUO-OG applied in water or in the HA-CP vehicle and HA-CP-Cy5.5 as control.

IV.2.10. Optimization of *In Vivo* Experiments

Several reports have demonstrated that imiquimod (IMQ) can activate immune cells via a toll-like receptor to induce psoriasis-like inflammation [53-55]. In **Chapter II**, we optimized our IMQ-psoriasis induced model in order to evaluate the anti-psoriatic activity of the conjugates compared to the free drug.

Firstly, *in vivo* experiments were conducted to optimize the optimal concentration of FLUO equivalents that trigger the maximum anti-psoriatic activity, in order to select the adequate therapeutic window. After seven days of application of IMQ cream in the back and the right ear, we split mice into representative groups. We employed healthy and untreated mice as controls (negative and positive control). Conjugate-based treatments at different FLUO equivalents (0.01, 0.15 and 0.3 wt% FLUO eq.) were studied, based on the commonly marketed dose of FLUO in the formulations (0.01% w/w) [20]. The conjugates were dissolved in the HA-CP vehicle (1% w/v) and immediately applied topically in the back and the right ear for five consecutive days. We also applied HA-CP vehicle (1% w/v) as control following the same methodology. The safety of the

treatments was evaluated by tracking body weight every two days, demonstrating that after a slightly decrease in body weight during the application of IMQ, the animals maintain and recover body weight during the application of the treatments (**Figure IV. 26**).

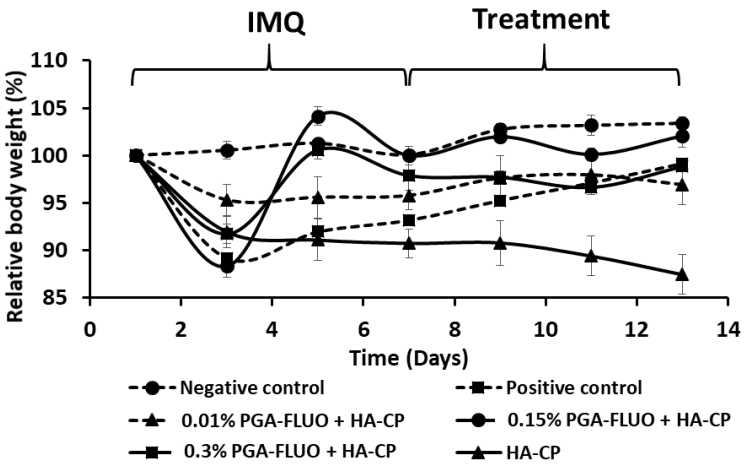

Figure IV. 26: Relative body weight of the mice during the treatment showing no significant alterations, which displayed a 100% survival rate.

IV.2.10.1. Reduction of Skin Inflammation, Ear Thickness, and Splenomegaly

We evaluated the evolution and progression of the disease for five days of treatment after the last application of IMQ cream. PASI score allowed the assessment of several features of psoriasis disease, such as erythema, scaling and thickness (skin induration) of the back of the mice after the treatment with the different concentrations of PGA-FLUO conjugates (0.01, 0.15, and 0.3 wt% FLUO eq.) (**Figure IV. 27A**). Examination of the back every two days revealed that the groups treated with the different concentrations of PGA-FLUO conjugate showed a significant reduction in the studied features. In the three parameters evaluated, we observed a progressive improvement by increasing the concentration of PGA-FLUO conjugate used, obtaining values close to 0 in the case of the 0.15 and 0.3 wt% FLUO eq. In addition, in those animals treated with HA-CP vehicle, we observed a marked reduction of erythema and scaling at day 13, as a possible consequence of the general improvement of the skin features, specifically skin hydration.

Ear thickness was also evaluated every two days using a caliper in comparison with the positive control. The results obtained at day 13 revealed that the group treated

with 0.01 wt% FLUO eq. reduces ear thickness by 10% compared with the positive control. Importantly, a significant decrease in the ear thickness was observed using 0.15 and 0.3 wt% FLUO eq. reducing ear thickness by almost 20% (**Figure IV. 27B**).

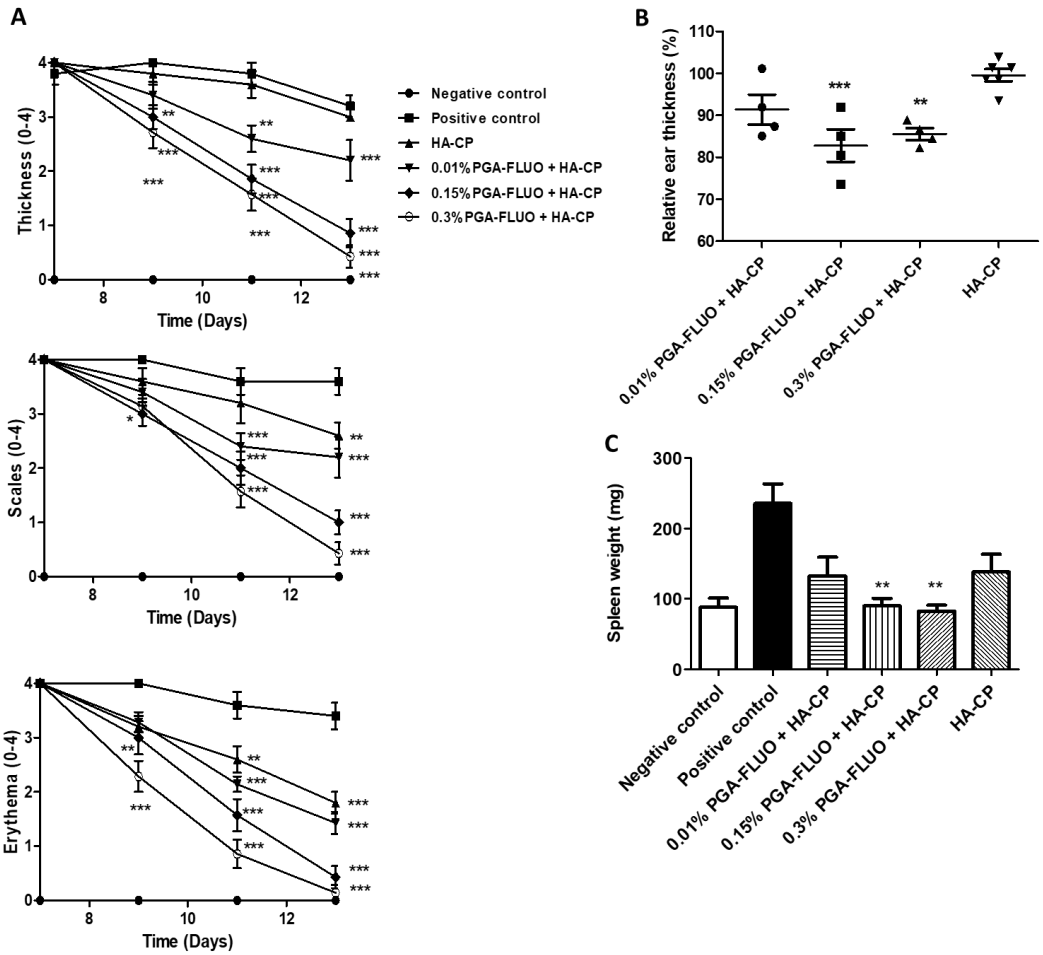

Figure IV. 27: Reduction of skin inflammation, ear thickness, and splenomegaly in an IMQ-induce in vivo psoriasis model. **(A)** Scoring severity of skin inflammation in the dorsal skin with PASI score (erythema, scaling, and thickness) every two days during the treatment, scale from 0 to 4. **(B)** Relative reduction of ear thickness after the treatments compared to the positive control. **(C)** Spleen weight (mg) determination after five days of treatment. Asterisks indicate statistically significant differences after ANOVA analyses followed Bonferroni's post hoc tests, mean ± SEM. In all cases, we considered differences to be significant when p***<0.001; p**<0.01; p*<0.05.

Of note, as explained in **Chapter II**, the topical application of IMQ cream for seven consecutive days has been reported to induce a significant increase in spleen weight [56]. This splenomegaly is correlated with the increment of the synthesis of pro-inflammatory cytokines which are involved in the onset of the disease. After five days of treatment application, we observed a marked reduction in the animals spleen weight with

the three concentrations tested. The groups treated with 0.01, 0.15 and 0.3 wt% FLUO eq. presented a value of spleen weight around 150, 90 and 85 mg, respectively, reaching up to a splenomegaly reduction >70% compared with the positive control (**Figure IV. 27C**). These results showed that there is a decrease in the immune response not only at the local level but also at the systemic level. Therefore, the reduction in spleen weight may be closely related to the decrease of the localized inflammation in the skin and the synthesis of pro-inflammatory cytokines. Of note, the group treated with the HA-CP vehicle also revealed a reduction in spleen weight, which could be related to an improvement of the skin properties at a local level triggering a decrease of the local inflammation, which also results in a decrease of the systemic inflammation.

IV.2.10.2. Reduction of Epidermal Thickness

We also assessed the reduction of the epidermal thickness of the ear and the back by histological examination. Firstly, H&E staining of the right ear treated with IMQ cream revealed a marked difference in epidermal thickness when compared to the contralateral healthy ear, mimicking the pathophysiology of the psoriasis (**Figure IV. 28**).

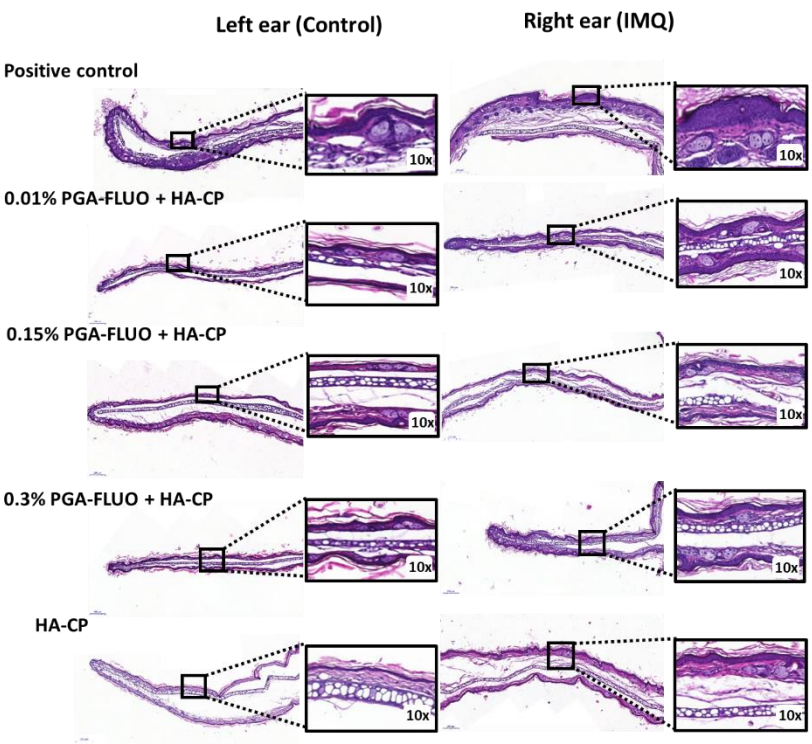

Figure IV. 28: H&E staining of the ears after five days of treatment in the IMQ-induced skin inflammation model. Original magnification displayed in each image was 10x. One representative picture is shown for each treatment regimen.

Although with the three concentrations of FLUO eq. tested we can observe a decrease in the epidermal thickness, a more pronounced decrease was revealed in the groups treated with 0.15 and 0.3 wt% FLUO eq., even resembling the results of the control healthy ear. The control group treated with HA-CP vehicle showed a decrease in epidermal thickness, as a possible consequence of improved skin hydration and a decrease in the scaling process.

In addition, we observed the same trend via H&E staining in mouse backs in a concentration dependent manner recovering almost completely the skin structure with the highest concentration used (**Figure IV. 29**). Of note, the group treated with the HA-CP vehicle also presents a reduction in the epidermal thickness, similar to which occurs with the lowest concentration tested (0.01 wt% FLUO eq.). This fact, also observed in the right ear, may be explained due to improved dryness and desquamation of the skin, and therefore, the improvement of these properties leads to a reduction of the local inflammation and the epidermal thickness.

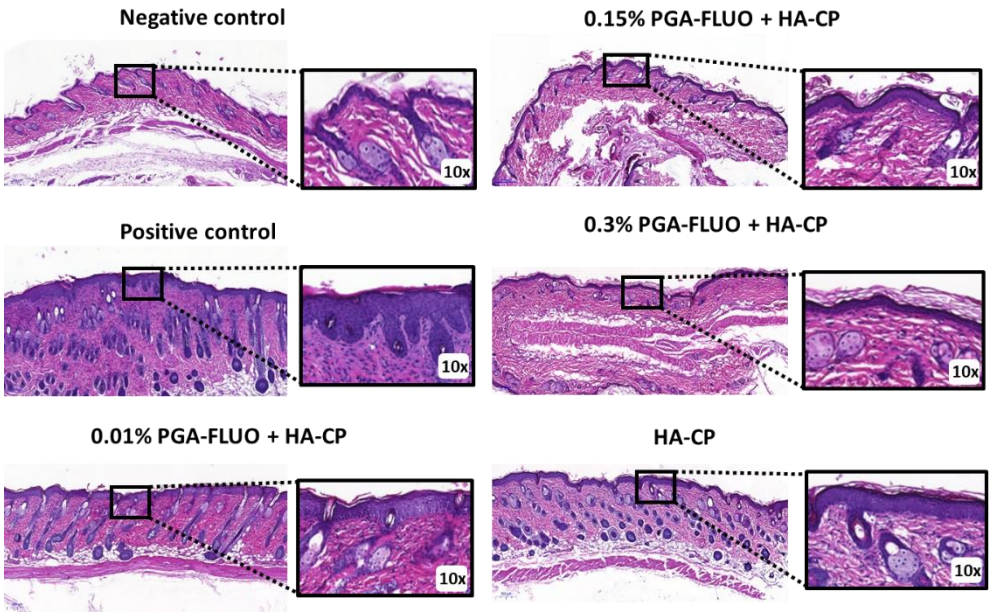

Figure IV. 29: H&E staining of the back of the mice after five days of treatment in the IMQ-induced skin inflammation model. Original magnification displayed in each image was 10x. One representative picture is shown for each treatment regimen.

IV.2.10.3. Reduction of Pro-Inflammatory Cytokines Levels in Serum

IL-23, IL-17, INF-γ, and TNF-α act as major pro-inflammatory mediators of psoriasis in serum and tissue, and could be induced upon IMQ treatment [56-58]. In this

optimization, we will focus on the quantification of pro-inflammatory cytokines in serum (specifically IL-1b, IL-23, and INF-γ) detected by LUMINEX assay.

After five days of treatment with different FLUO eq., the expression of IL-1b, IL-23, and INF-γ in serum were measured and values compared with controls (**Figure IV. 30**). All the concentrations tested and also the HA-CP vehicle revealed a notable decrease of the pro-inflammatory cytokine levels compared to the positive control. In the case of the IL-1b levels a decrease of 20% respect to the positive control was observed with no marked differences between the treatments. For IL-23 levels, the group treated with 0.01 wt% FLUO eq. showed around a 20% reduction, however, the groups treated with 0.15 and 0.3 wt% FLUO eq. revealed a higher significant reduction (~55%) compared to the positive control. Finally, in the case of INF-γ levels, the best results (40% decrease) was obtained with 0.15 wt% FLUO eq. Hence, in general, the group treated with 0.15 wt% FLUO eq. exhibited the best results.

Moreover, the treatment with the HA-CP vehicle also displayed a marked reduction of the IL-1b, IL-23, and INF-γ levels. As explained in previous sections, this fact is related to the reduction of the systemic inflammation triggered by the reduction of the local inflammation present in the skin.

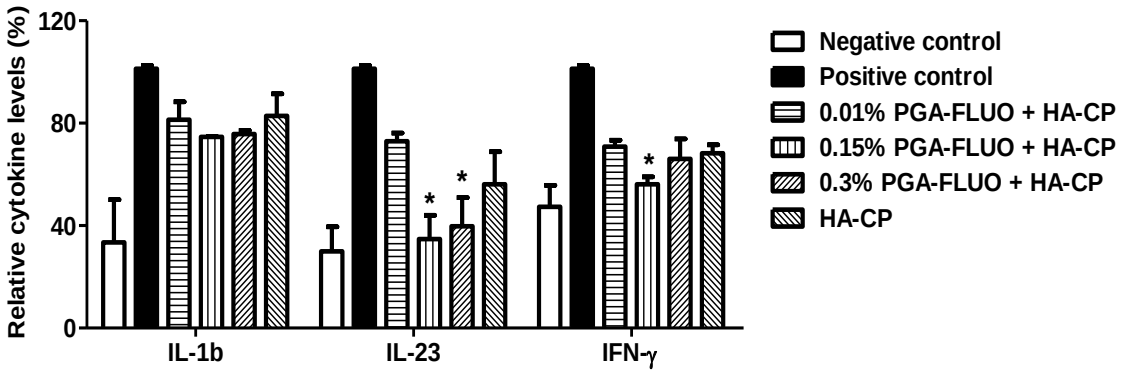

Figure IV. 30: Reduction of pro-inflammatory cytokines IL-1b, IL-23, and INF-γ in serum post-treatment measured by LUMINEX assay. Asterisks indicate statistically significant differences after ANOVA analyses followed Bonferroni's post hoc tests, mean ± SEM. In all cases, we considered differences to be significant when p***<0.001; p**<0.01; p*<0.05.

Based on these results, further studies *in vivo* were conducted using the intermediate concentration tested, 0.15 wt% FLUO eq. applied in the HA-CP vehicle. Therefore, next section describes a final evaluation of the anti-psoriatic activity of our

formulation (0.15 wt% FLUO eq. in the HA-CP vehicle) in comparison with the same concentration of the conjugate and the free FLUO both applied in a commercially-available cream used with current marketed corticosteroids.

IV.2.11. PGA-FLUO in HA-CP Reduces Imiquimod-Induced Skin Inflammation *In Vivo*

After the optimization of the experimental condition to perform the *in vivo* experiments (0.15 wt% FLUO eq. applied during 5 days) we carried out the final benchmark experiment. We used this concentration to compare the anti-psoriatic activity of FLUO applied in a commercially-available cream used for current corticosteroids (due to its hydrophobicity and poor water solubility) with PGA-FLUO in the same cream and also applied in the HA-CP vehicle due to its adequate hydrophilicity. We applied treatments to the back and the right ear of IMQ-treated 6-week-old male BALB/c mice for five days. We also applied the cream and the HA-CP vehicle alone as controls. Treatment safety was evaluated by tracking body weight every two days and comparing results to healthy animals. Encouragingly, we discovered that treatments failed to significantly alter body weight (**Figure IV. 31**).

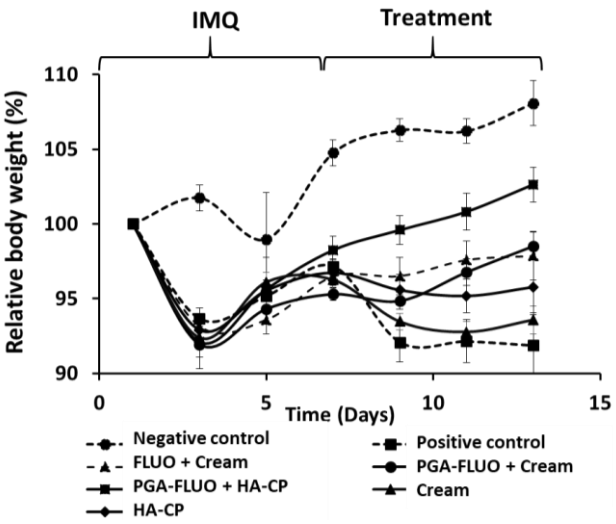

Figure IV. 31: Relative body weight of the mice measured every two days. During treatments, the animals recover body weight and we observed no significant alterations.

Histological examination of the mouse ears and back sections revealed a marked difference in the extent of epidermal thickening and elongation of epidermal ridges between the treated groups. PGA-FLUO treatment resulted in a more significant

diminishment of ear thickness and epidermal ridges and, remarkably, the choice of the vehicle employed for the administration also influenced overall effects, with the group treated with PGA-FLUO in HA-CP providing similar results to those observed in healthy control animals. Overall, PGA-FLUO in HA-CP exhibited significant differences compared to all other groups, presenting minimal epidermal thickening, an intact stratum corneum, and histological features compared to the negative control (**Figure IV. 32**). Importantly, following analysis of the control groups treated with the vehicles, we discovered that the group treated with the HA-CP presented a decrease in the epidermis thickness, whereas treatment with the commercially available cream failed to elicit any anti-psoriatic effect. This finding suggests that the probable increase in skin hydration via HA-CP treatment can lead to an improvement in the symptoms (dryness, scaling) produced by IMQ application.

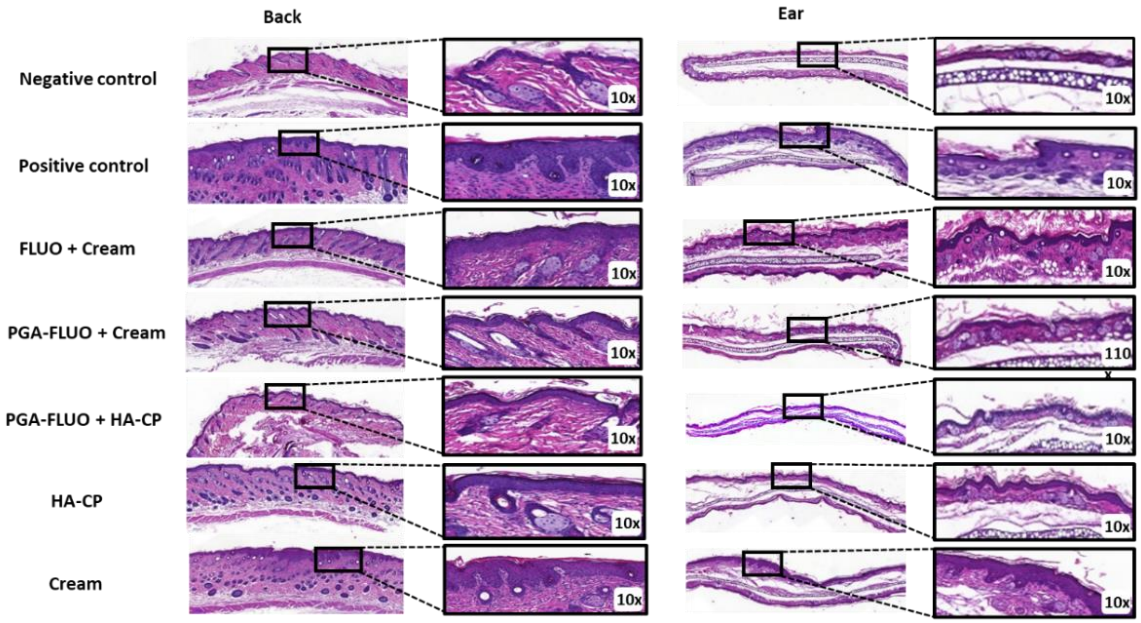

Figure IV. 32: H&E staining of the back and right ear of the mice after five days of treatments in an IMQ-induced skin inflammation model. Original magnification displayed in each image was 10x. One representative picture is shown for each treatment regimen.

Therefore, the use of this HA-CP vehicle offers a synergistic effect with the conjugated corticosteroids triggering an enhanced cutaneous anti-psoriatic effect. Signs of epidermal thickening due to inflammation were not only evident in the back but also by microscopical examination of the ear sections.

IV.2.12. Reduction of Skin Inflammation, Ear Thickness, and Splenomegaly

We also evaluated erythema, scaling, and thickness of the dorsal skin by PASI score after five days of treatment (**Figure IV. 33A**). Whereas examination of the back every two days revealed that the group treated with FLUO displayed a reduction in all the parameters, this was not enough to restore typical values. Again, FLUO conjugation to PGA prompted an enhanced effect when applied in cream and a more marked effect when administered in the HA-CP vehicle, presenting significant morphological tissue recovery (similar to the negative control, a value of 0 in the PASI score at the end of the experiment in the three measured parameters). The group treated with the HA-CP vehicle also exhibited a reduction in PASI score, due to its ability to hydrate the skin and diminish IMQ-induced skin dryness. Regarding the ear thickness measured every two days during the treatments with a caliper, the results corroborate the findings observed by H&E staining; all treated groups showed a decrease compared to the positive control group, with a maximum reduction (20%) of thickness observed in the group treated with PGA-FLUO within the HA-CP vehicle (**Figure IV. 33B**).

Finally, several studies have reported that IMQ can produce a significant spleen enlargement with a weight increase, which is attributed to the release of inflammatory cytokines [56]. In our IMQ-induced model, we established an average spleen weight in the positive control of 250 mg compared to 100 mg in the negative control (**Figure IV. 33C**). All treated groups exhibited a marked decreased in the spleen weight (FLUO 125 mg and PGA-FLUO applied in cream 100 mg), which was maximal for the group treated with PGA-FLUO within the HA-CP vehicle. There was no significant difference in the spleen weights between the negative control and the group treated with PGA-FLUO in HA-CP, confirming the ability of the vehicle embedded conjugate to reach the epidermal layers of the skin and reduce inflammation.

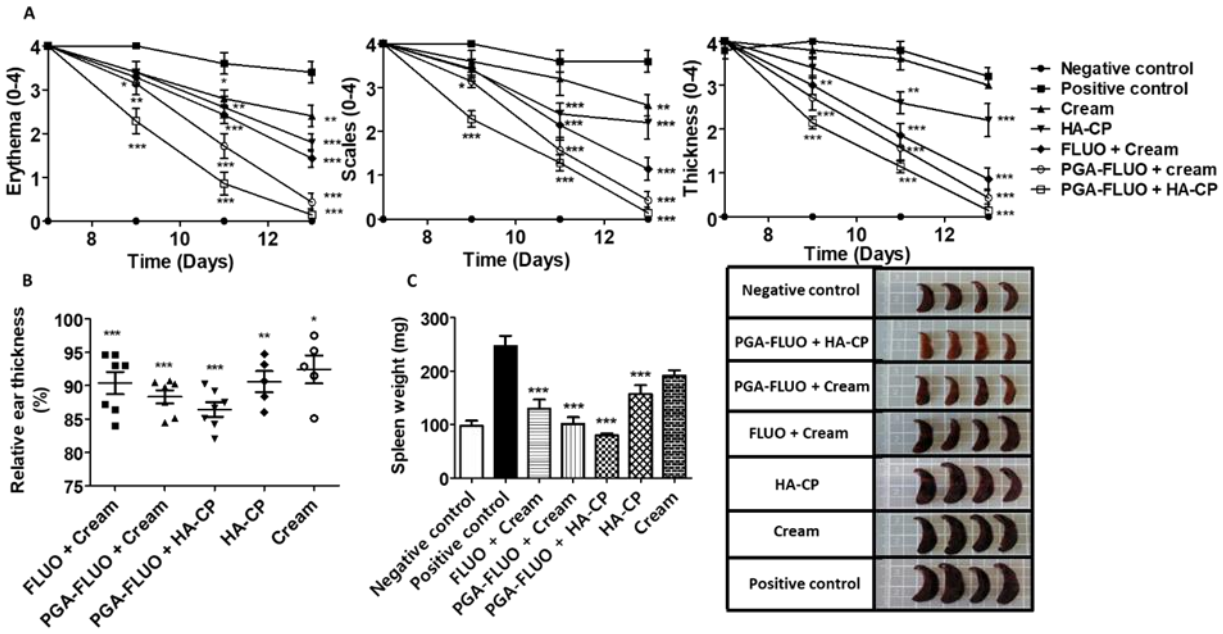

Figure IV. 33: Reduction of skin inflammation, ear thickness, and splenomegaly. **(A)** Scoring severity of skin inflammation in the dorsal skin with PASI score (erythema, scaling, and thickness) every two days during the treatments using a scale from 0 to 4. **(B)** Relative reduction of ear thickness after the treatments compared to the positive control. **(C)** Spleen weight (mg) determination after five days of treatment. Asterisks indicate statistically significant differences after ANOVA analyses followed Bonferroni's post hoc tests, mean ± SEM. In all cases, we considered differences to be significant when p***<0.001; p**<0.01; p*<0.05.

IV.2.13. PGA-FLUO Conjugates Reduce Pro-Inflammatory Cytokines Levels in Serum and Tissue

TNF-α, IL-17, IL-23, and INF-γ act as major mediators of psoriasis as they mark the onset of the IMQ induced psoriasis [56-58]. We discovered the significantly higher expression of INF-γ and IL-23 for the positive control compared to the negative control in tissue and INF-γ in serum, which confirmed adequate *in vivo* psoriatic model development (**Figure IV. 34**). In tissue, the levels of INF-γ were reduced by 31% and 51% in the groups treated with PGA-FLUO in cream and PGA-FLUO in HA-CP, respectively, compared to 6% for the free FLUO group. Furthermore, IL-23 levels were reduced by 21% and 34% for PGA-FLUO in cream and PGA-FLUO in the HA-CP vehicle, respectively, as compared to the free FLUO (24%). Similar reduction values and differences among groups were observed when INF-γ levels were studied in serum, establishing that PGA-FLUO within the HA-CP vehicle displayed the highest anti-inflammatory capacity. Of note, the group treated with HA-CP vehicle displayed a

reduction in INF-γ levels in tissue and serum by 28% and 27%, respectively. The possible explanation can be ascribed to the intrinsic nature of HA-CP as it results from cross-linking of HA with amino acids which protect its enzymatic degradation by hyaluronidases and consequently allows a prolonged moisturizing effect that could trigger its impact in reducing inflammation (see **Chapter III**).

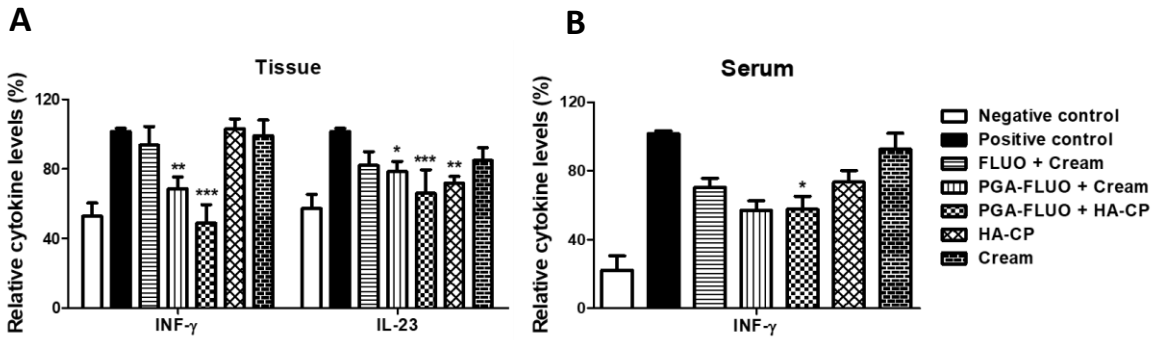

Figure IV. 34: Reduction of pro-inflammatory cytokines levels related to the disease in **(A)** tissue and **(B)** serum. Asterisks indicate statistically significant differences after ANOVA analyses followed Bonferroni's post hoc tests, mean ± SEM. In all cases, we considered differences to be significant when p***<0.001; p**<0.01; p*<0.05.

In summary, the topical application of PGA-FLUO within an HA-CP vehicle ameliorated IMQ-induced psoriasis, returning indicators of disease back to basal levels. We believe that the synergism observed derives from the conjugation of the corticosteroid to a polypeptidic carrier and from the application of a highly hydrating vehicle for topical administration as a permeation enhancer. The application of FLUO as a water-soluble PGA conjugate resulted in higher drug concentration available at the site of application, while the inclusion of PGA-FLUO within the HA-CP vehicle results in higher uptake by dermal cells and improved skin permeation, leading a deeper penetration of PGA-FLUO into the viable epidermis. Furthermore, the incorporation of PGA-FLUO in HA-CP might increase skin hydration, an additional factor required for treatment success, while HA-CP may also protect the conjugate from enzymatic degradation, thereby allowing it to reach the target epidermal layer. We believe that the combination of a polymer-corticosteroid conjugate and HA-CP vehicle provides a synergistic effect that may make corticosteroid treatments more efficient and safer for the treatment of psoriasis.

IV.3. Conclusions

Herein, we have demonstrated that the polypeptide conjugation of a corticosteroid used for the topical treatment of psoriasis (PGA-FLUO) provides a significant improvement in the pharmacological activity due to greater bioavailability in the require skin layer. Polypeptide conjugation may contribute to improve the penetration and drug exposure, thereby increasing the amount of corticosteroid in the viable epidermis, and therefore, increasing the effectiveness of the treatment. An adequate drug release kinetic profile represents a crucial parameter for the achievement of a suitable drug concentration in the epidermis, and therefore, polymer-drug linker design represents an essential feature. However, the mode of conjugate administration also plays a vital role, as the application of the polypeptide-conjugated corticosteroid within a polymeric vehicle (HA-CP) protected the conjugate, resulting in the slower and sustained release of the drug in the epidermis and allowing for sustained residence time.

In conclusion, the synergistic combination of PGA-FLUO and HA-CP provides an elevated reduction in inflammation and, therefore, represents a possible palliative treatment of inflammatory skin diseases. Our strategy opens a new horizon in the field of localized dermal delivery that can be extended to the conjugation of other therapeutic moieties implemented for other aggressive skin diseases, such as cancer. The use of polymer/polypeptide therapeutic-based formulations for various skin diseases could revolutionize current therapeutic strategies of dermatology, overcoming old challenges, and offering new perspectives for the treatment and prevention of dermatological conditions.

IV.4. Materials and Methods

IV.4.1. Materials

All organic solvents were of analytical grade purchased from Scharlab and used without further purification. All chemicals were of reagent grade and used without further purification, purchased from Sigma-Aldrich otherwise stated. Poly-(alpha-L-glutamic acid) (Mw: 12,9 kDa, PDI: 1.2, 100 subunits per polymer, PGA100 u) was obtained from Polypeptide Therapeutic Solutions SL (Valencia, Spain). Fluocinolone acetonide was

purchased from Cymit Quimica S.L. (Barcelona, Spain). Anhydrous N,N-Dimethylformamide (DMF, ≥99.8% anhydrous) was purchased from Scharlab SL (Sentmenat, Spain). Oregon Green 488 cadaverine and Cyanine5.5 were purchased from Invitrogen (Spain). Ultrapure water with a resistivity of 18 MΩ cm was used in all aqueous preparations (MilliQ water ultrapure). Preparative SEC was performed using either Sephadex® G-25 or Sephadex® LH-20, purchased from GE Healthcare Bio-Sciences AB (Uppsala, Sweden).

Phenazinemethosulfate (PMS), amphotericin B, and leupeptin were supplied by Sigma (Spain). Dulbecco's Modified Eagle's Medium (DMEM) with Glutamax was purchased from Fisher (Spain). DMEM, phosphate buffer saline (PBS), fetal bovine serum (FBS) Medium 200, trypsin, and penicillin/streptomycin were provided from Gibco (Spain). 3-(4,5-dimethylthiazol-2-yl)-5- (3-carboxymethoxyphenyl)-2-(4-sulfophenyl)-2H-tetrazolium (MTS) was supplied by Promega (Spain). Cathepsin B from bovine spleen (25 units) was supplied by Sigma Aldrich (Spain). The Raw267.4 macrophages cell line was supplied by CLS Cell Lines Service (Germany).

IV.4.2. Physico-Chemical Characterization Methods

IV.4.2.1. Nuclear Magnetic Resonance (NMR) Spectroscopy

NMR spectra were recorded at 27°C (300 K) on an Avance III 300 MHz Bruker spectrometer equipped with a 5 mm TBI broadband probe or a 300 Ultrashield™ from Bruker (Billerica MA, USA). Data were processed with the software Mestrenova (Bruker GmbH, Karlsruhe, Germany). Samples were prepared typically at 5 mg/mL in deuterated solvents.

IV.4.2.2. Ultraviolet-Visible (UV-Vis) Spectroscopy

UV-Vis measurements were performed using V-630 spectrophotometer (JASCO Corporation, Spain) at 25°C with 1.0 cm matched quartz cells and with a spectral bandwidth of 0.5 nm. The determination of total FLUO content was measured by UV-Vis spectroscopy. First, a stock solution of FLUO in MilliQ water/ACN (60:40) was prepared at 1 mg/mL, to prepare a calibration curve. Samples were diluted using the same solution to give a concentration range of 0.1-0.005 mg/mL. Total drug loading of the conjugates at different concentrations (0.5, 0.25, 0.1 mg/mL) was determined by

measuring the absorbance at 260 nm in a solution of MilliQ water/ACN (60:40). PGA at the same concentration range was used as blank.

IV.4.2.3. Size Exclusion Chromatography (SEC) in Aqueous Media

For SEC measurements in aqueous media containing 0.1 M $NaNO_3$ and 0.005% (w/w) azide as an additive was performed in an AF2000 system from Postnova Analytics (Landsberg, Germany). The system was configured to work on SEC mode with an isocratic pump (PN1130), an autosampler (PN5300), a refractive index (RI, PN3150), 21 angle-multi angle light scattering (MALS, PN3621), and an UV-Vis detectors (PN3211). A working flow rate of 0.7 mL/min at 30°C was employed with one TSKgel G3000PWXL column. Refractive index and Multi-Angle Light Scattering were used for detection and Mw determination, calibration of both RI and MALS detectors was achieved with well-defined Pullulan (50 kDa) and validation with polymethacrylic acid sodium salt (PMASS, 62.5 kDa) standards, purchased from Polymer Standards Service (PSS)/Mainz Germany. Dn/dc values for polyglutamates were determined from recovered mass, assuming 95 - 100% recovery from the chromatographic column and found to be within 0.185 - 0.195. The wavelength used was 268 nm for the polyglutamates containing FLUO, and 512 nm for OG-labeled polyglutamates. Finally, 30 µL of a polymer solution of 5 mg/mL was injected each time.

IV.4.2.4. Fluorescence Spectroscopy

Fluorescence experiments were performed using a FP-6500 spectrofluorometer (JASCO Corporation, Spain) at 25ºC with 1 cm quartz cells. Pyrene assay was performed as published elsewhere in order to determine the critical aggregation concentration (CAC) [28]. In brief, several solutions of the compounds were prepared to cover a wide range of concentrations (from 0.004 to 2 mg/mL) to which 3 µL of the pyrene stock solution (0.02 mg/mL) in acetone was added. Then, all the solutions were placed in vials and were incubated in an oven at 37ºC for 2 h in order to evaporate the acetone. After storing the samples for 24 h, measurements were carried out. Each excitation spectra was recorded from 300 to 360 nm with an emission wavelength of 390 nm. The excitation and emission band slits are 5 and 2.5 nm, respectively. Finally, data were expressed by plotting the intensity ratio I_{338}/I_{333} against the concentration to determine CAC value.

IV.4.2.5. Transmission Electron Microscopy (TEM)

TEM images were recorded using a JOEL 2100 transmission electron microscope. Samples were applied directly onto carbon film on 200 mesh copper grids. Excess of the samples was carefully removed by capillarity, and the grids were immediately stained with one drop of 0.1% phosphotungstic acid for 30 s. Excess stain was removed by capillary action.

IV.4.2.6. Dynamic Light Scattering (DLS)

DLS measurements were performed using a Malvern Zetasizer NanoZS instrument (Malvern Instruments Ltd., Worcestershire, UK), equipped with a 532 nm laser at a fixed scattering angle of 173°. Solutions were sonicated for 10 min, allowed to age for the required time, filtered through a 0.45 μm cellulose membrane filter and measured. The samples were dissolved under different conditions (MilliQ water, PBS, PB 10 mM) and different concentrations (from 0.02 to 2 mg/mL). Size distribution was measured (radius, nm) per triplicate with n > 3 measurements.

Z-potential measurements were performed at 20ºC using a Malvern Zetasizer NanoZS instrument, equipped with a 532 nm laser using disposable folded capillary cells, provided by Malvern Instruments Ltd. (Worcestershire, UK). Polymer solutions were prepared in 1 mM KCl in MilliQ water. The solutions were filtered through a 0.45 μm cellulose membrane filter. Z-potential was measured for each simple per triplicate with n >3 measurements.

IV.4.2.7. High-Performance Liquid Chromatography (HPLC)

Analytical determination of free drug was performed on a Waters HPLC system provided with 2 x 515 binary pumps, autosampler 717 Plus, FLD 2475 and PDA 2996 (Waters Corporation, S.A, Spain). The measurements were performed using an RP C-18 Lichrospher analytical column (125 x 4.0 mm) (Scharlab S.L., Barcelona, Spain), with a flow rate of 1 mL/min, the volume of injection was 20 μL and using a mobile phase of H_2O (1% orthophosphoric acid)/ACN (60/40). Detection of FLUO absorbance was measured at $\lambda = 239$ nm with a retention time between 3.5 - 4.5 min. The calibration curve was performed using commercial FLUO, showing a linear response within the

concentration range employed (0.001 - 0.1 mg/mL). Chromatograms were treated with Empower 2.0 software (Waters Corporation, S.A, Spain).

IV.4.2.7.1. Recovery of FLUO in a Polymeric Matrix: Liquid-liquid Extraction

Recovery studies were performed to understand the behavior of the drug in the presence of the PGA, in order to evaluate the adequate method of extraction to quantify the free FLUO. In the study, four calibration curves were used using the extraction treatment: FLUO without treatment (control), FLUO with extraction treatment, FLUO with PGA treated, and FLUO and the PGA-FLUO conjugate treated. Liquid-liquid extraction was the treatment used to determine the recovery of FLUO content in the polymeric matrix.

PGA-FLUO conjugate was dissolved in PBS/ACN (60:40) solution and extracted with 5 mL of isopropanol (IPA)-dichloromethane (DCM) (5:95) solution by mechanical stirring with the vortex (3 x 30 s). The upper aqueous layer was carefully removed, and the solvent was evaporated under reduced pressure using the speedvac (1:30 h, 80ºC, 0.01 vacuum). The residue was resuspended in 500 µL of ACN, and the suspension was filtered (0.45 µm) into HPLC vials for analysis. Samples were measured per triplicate.

- **Determination of Free FLUO in the Conjugates**

Liquid-liquid extraction was used to determine free drug content; the concentration of PGA-FLUO conjugate used was 1 mg/mL.

- **Drug Release Kinetics**

Drug release kinetics of PGA-FLUO conjugates was performed at two different pHs (5.5 and 7.4) and also in the presence of cathepsin B. A stock solution was prepared in the PBS buffers (2 mg/mL), and in the case of cathepsin B the solution was a mixture of 700 µL acetate buffer 20 mM pH=5, 100 µL EDTA 2 mM, 100 µL DTT 5 mM and 100 µL cathepsin B. The stock was divided into aliquots (50 µL) and were incubated at 37ºC at different time points (from 0 to 72 h). After the incubation, 10 µL of PBS buffers and 40 µL of ACN were added to each sample, in order to have a PBS/ACN (60:40) solution. Then, we followed the same methodology for the recovery of FLUO, using the liquid-liquid extraction. Finally, the residue was resuspended in 500 µL of ACN, and the suspension was filtered (0.45 µm) into HPLC vials for analysis. Samples were measured repeatedly (n= 3).

IV.4.2.7.2. Extraction and Quantification of FLUO in the Skin

The permeation of PGA-FLUO conjugate (100 µL of 10 mg/mL solution in water and in the HA-CP (1% w/v)) in the skin was evaluated over 24 h in Franz diffusion cells. Whole skin was then washed twice with 0.1% PBS-BSA (PBS supplemented with bovine serum albumin (BSA)), cut into small pieces and added to 4 mL of DMSO for FLUO extraction for 24 h with stirring. Skin samples were then removed and DMSO evaporated under reduced pressure using a speedvac (3 h, 80ºC, 0.01 vacuum). Next, the residue was resuspended in 500 µL of ACN and sonicated (15 min). Finally, the suspension was filtered (0.45 µm) into HPLC vials for analysis. Samples were measured repeatedly (n= 3).

IV.4.2.8. Circular Dichroism (CD)

CD spectroscopy was performed with a J-815 CD spectrometer (JASCO Corporation, Spain) using a Peltier thermostated cell holder (PTC-423, JASCO Corporation, Spain) with a recirculating cooler (JULABO F250, JASCO Corporation, Spain). A nitrogen flow (~2.7 L·min-1) was led through the spectrometer and controlled with a nitrogen flow monitor (Afriso Euro-Index, Germany). The samples were dissolved under different conditions (MilliQ water or 10 mM PB) at different concentrations (from 0.1 to 0.6 mg/mL). Samples were measured repeatedly (n=3) in a quartz cuvette with d= 0.1 cm.

IV.4.3. Synthetic Protocols

IV.4.3.1 Synthesis of Poly-L-glutamate Fluocinolone Acetonide Conjugates

We aimed to conjugate around 8% molar of FLUO relative to glutamate residues as a general synthetic procedure. As an example, to describe the synthesis, we used 200 mg of PGA.

PGA_{100}-OH (200 mg, 1.55 mmol) in DMF (5 mL) was added to a two necked flask equipped with a stir bar under N_2 flow and heated until dissolved. FLUO dissolved in 1 mL of DMF was added (140.27 mg, 0.3 mmol, 0.2 eq. to glutamic acid units (GAU)) to this solution, and the mixture was allowed to stir for ten min. The reaction mixture was then cooled in an ice bath and, finally, 1 mL of DMF with DMAP (1.9 mg, 0.0155 mmol, 0.01 eq. to GAU) and 4 mL DMF with EDAC (89.22 mg, 0.465 mmol, 0.3 eq. to GAU)

were added. The mixture was stirred for 72 h under N_2 flow at room temperature (r.t.). Thin-layer chromatography (MeOH) confirmed the consumption of FLUO. The solution was purified by size exclusion chromatography employing either Sephadex® LH-20 (DMF) and after evaporating the DMF (under vacuum conditions) the residue was dissolved with 0.5 M $NaHCO_3$ and repurified using Sephadex® G-25 (MilliQ water). Finally, the resulting aqueous suspension was freeze-dried and the white powder characterized (Yield = 60%).

^{1}H-NMR (300 MHz, D_2O) δ 7.42 (s, 1H), 6.38 (s, 2H), 5.58 (d, *J* = 52.2 Hz, 1H), 5.26 – 5.07 (m, 1H), 5.01 (s, 1H), 4.33 (d, *J* = 40.9 Hz, 10H), 3.68 (d, *J* = 13.9 Hz, 1H), 2.89 (td, *J* = 70.7, 29.2 Hz, 4H), 2.26 (t, *J* = 21.5 Hz, 16H), 2.05 – 1.81 (m, 15H), 1.63 (s, 1H), 1.46 (d, *J* = 23.3 Hz, 3H), 1.30 – 1.09 (m, 2H), 0.81 (d, *J* = 24.5 Hz, 2H).

IV.4.3.2 Oregon Green Labeling of PGA-FLUO Conjugates

70 mg of PGA-FLUO conjugate (0.4183 mmol GAU, 1 eq.) was dissolved in 12 mL of dry DMF under N_2 flow in a round two necked bottom flask fitted with a stirrer bar. Then, 2.745 mg of DMTMM·BF_4 (8.366×10^{-3} mmol, 0.02 eq. to GAU) was added to the solution and incubated for 10 min at r.t. Finally, 0.01 eq. of the amino dye OG was added. The pH was adjusted to 8 by adding ~100 µL of DIEA. The mixture was left stirring for 48 h at r.t. and protected from light. The solution was purified by size exclusion chromatography employing either Sephadex® LH-20 (DMF) and then the DMF was evaporated under vacuum conditions, and then the residue was dissolved with 0.5 M $NaHCO_3$ and repurified using Sephadex® G-25 (MilliQ water). Finally, the resulting aqueous suspension was freeze-dried, and the powder characterized. (Yield = 40%).

The percentage of dye loading in the conjugate was determined by UV-Vis spectroscopy. A calibration curve of free dye was performed under the same conditions (MilliQ water). To obtain a calibration curve, the free dye was diluted to give a concentration range of 0.000025 - 0.000250 mg/mL. The total dye loading of the conjugates was determined by measuring the absorbance of the samples at 495 nm in MilliQ water.

IV.4.4. Biological Evaluation of Polymer-Drug Conjugates

IV.4.4.1. *In Vitro* Evaluation

IV.4.4.1.1. Cell Viability

To perform the cytotoxicity studies *in vitro* two cell lines were used: Human immortalized non-tumorigenic keratinocyte cell line (HaCaT) was supplied by CLS Cell Lines Service (Eppelheim, Germany) and human fibroblasts were supplied by Hospital La Fe (Valencia, Spain). The culture media used was high glucose DMEM Glutamax (Fisher, Spain) for HaCaT cells and Dulbecco's Modified Eagle's Medium-high glucose (Sigma-Aldrich Chemical Co., Spain) for human fibroblasts, both supplemented with 2% penicillin/streptomycin and 50 mL of fetal bovine serum (FBS) in a humidified incubator (Hucoa-Erlöss S.A., Spain) 5% CO_2 and 37°C. 50 μL of cells were seeded in 96-well plates at a concentration of 4,000 cells/well in the case of HaCaT cells and 2,000 cells/well for human fibroblasts. After 24 h, 50 μL of each treatment were added reaching a final volume of 100 μL in the well. All the treatments were filtered before adding to the well (pore size 0.22 μm). Cells were incubated with samples or controls for 72 h and then was performed the MTS assay. For that, 20 μL of the solution of Phenazine Methosulfate Minimum 90% (PMS) and the salt of 3-(4,5-dimethylthiazol-2-yl)-5-(3-carboxymethylphenyl)-2-(4-sulfophenyl)-2H tetrazolium (MTS) were added, with a dilution 1:20, respectively. After 3 h of incubation, the absorbance was read at 490 nm using a Victor^{2}Wallac™ plate reader (Perkin Elmer, Spain). The absorbance values were represented as the percentage of cell viability taken as 100% cell viability of untreated control cells. The concentrations of linear and star PGA were in a range from 0.02 to 0.5 mg/mL of polymer, and the concentrations of PGA, FLUO, and PGA-FLUO conjugate from 0.0057 to 0.0987 mg/mL FLUO eq.

IV.4.4.1.2. Cellular Uptake by Flow Cytometry

Flow cytometry (cell uptake and binding) together with live cell confocal microscopy analysis were used to study cellular trafficking of the OG-labeled polymers in HaCaT cells. HaCaT cells were seeded in 6-well plates at a density of ~120,000 cells/cm^2 (1 mL cell suspension per well) and allowed to adhere for 24 h. In binding experiments conducted at 4ºC, cells were pre-incubated at this temperature for 30 min prior to start the experiment. For both experiments, 4ºC and 37ºC, the cathepsin B

inhibitor CA-074 (0.4 µL from a solution of 5 µM to reach a final concentration of 2 µM) was added 30 min before the addition of PGA-FLUO-OG. Then, 15 µL of OG-labeled polymer (were added at different time points from 0 to 27 h) while cells were incubated either at 37ºC or 4ºC for each experiment. Finally, cells were placed on ice to inhibit energy dependent mechanism and washed twice with cold 0.1% PBS-BSA. Then, 400 µL of trypsin was added to detach the cells and 600 µL of culture media was added, and the cell pellet was placed in flow cytometer tubes. The fluorescence was then analyzed using a fluorescence-activated cell sorting (FACS) caliber cytometer (Becton Dickinson, California, USA) equipped with an argon laser (488 nm) and emission filter for 550 nm. Data collection involved 10,000 counts per sample, and were analyzed using CELLQuest^{TM} version 3.3 software. Data are expressed as a percentage of positive cells. Cells incubated without the polymer were used to detect background fluorescence.

IV.4.4.1.3. Uptake Studies by Confocal Microscopy

HaCaT cells were seeded in glass in 6-well plates at a density of ~120,000 cells/cm^2 (1 mL cell suspension per well) and allowed to adhere for 24 h at 37ºC. First, cathepsin B inhibitor CA-074 (0.4 µL from a solution of 5 µM to reach a final concentration of 2 µM) was added 30 min before the addition of the conjugate PGA-FLUO-OG. Then, 15 µL of OG-labeled polymer was added at different time points from 0 to 72 h while cells were incubated at 37ºC. 30 min before washing the cells with PBS-BSA 0.1%, the nuclear marker Hoechst (1 µL from a solution of 5 mM) and the lysosomal marker Lysotracker Red (0.75 µL from a solution of 100 mM) were added and incubated 20 min in order to identify possible co-localizations and therefore establish an endocytic pathway. Finally, cells were washed with 0.1% PBS-BSA, and the glass was removed and placed on the microscope chamber with 1 mL of fresh media containing 2 µM of CA-074 inhibitor. Samples were analyzed under the microscope. Images were captured with an inverted DM IRE2 microscope equipped with a λ-blue 60 x oil immersion objective and handled with a TCS SP2 system, equipped with an Acoustic Optical Beam Splitter (AOBS). Excitations were performed with an argon laser ((OG 496 nm), and HeNe laser (Lysotracker red 594 nm), and blue diode (Hoechst 405 nm). Images were captured at an 8-bit greyscale and processed with LCS software (version 2.5.1347a, Leica Germany) containing multicolor, macro and 3D components. Control cells that follow the same incubation time were also analyzed to establish the autofluorescence, as well as cells treated only with Hoechst or Lysotracker red.

IV.4.4.1.4. Anti-Inflammatory Activity

To perform the activity studies *in vitro*, we used macrophages (Raw264.7 cell line), which was supplied by CLS Cell Lines Service (Eppelheim, Germany). The culture media used was high glucose DMEM (Fisher, Spain), supplemented with 2% penicillin/streptomycin and 50 mL of FBS in a humidified incubator (Hucoa-Erlöss S.A., Spain) 5% CO_2 and 37°C.

50 µL of cells were seeded in 96-well plates at a concentration of 6,000 cells/well. After 24 h, 50 µL of each individual treatment (LPS from *E. coli* (5 ng/mL), FLUO (0.49 ng/mL), PGA-FLUO conjugate (0.49 ng/mL FLUO eq.), and PGA) were added, reaching a final volume of 100 µL in the well to evaluate cell viability by MTS assay. At the same time, the combination of LPS with FLUO, PGA-FLUO conjugate, and PGA was evaluated to assess the anti-inflammatory activity by LUMINEX assay, adding 25 µL of each treatment. All the treatments were filtered before adding to the well (pore size 0.22 µm). Cells were incubated with samples or controls for 72 h and then performed the MTS assay. For the subsequent MTS assay, 20 µL of the solution of phenazine methosulfate minimum 90% (PMS, Sigma, Spain) and 3-(4,5-dimethylthiazol-2-yl)-5-(3-carboxymethylphenyl)-2-(4-sulfophenyl)-2H tetrazolium salt (MTS, Promega, Spain) were added, using a dilution 1:20. After 2 h of incubation, the absorbance was read at 490 nm using Victor^{2}Wallac™ plate reader (Perkin Elmer, Spain).

Next, for the quantification of the pro-inflammatory cytokines released to the culture media by LUMINEX assay, the 96-well plates were centrifuged 5 min, 22°C, 400 rcf, and 90 µL of supernatant were collected and frozen until use. Pro-inflammatory cytokines levels were measured by LUMINEX multiplex immunoassay (Affymetrix m Th1/2/9/17/22/Treg 17plex, eBioscience, Spain). This study was performed using LUMINEX 200 equipment (LUMINEX Corporation, USA) and results expressed as a percentage of inhibition of each cytokine.

IV.4.4.1.5. Cathepsin B Activity

The enzymatic activity of cathepsin B was measured by means of a fluorescence reader CLARIOstar®, software version 5.21 R2 from BMH LABTECH (Offenburg, Germany). The activity was analyzed using specific fluorescent substrate for this type of enzyme, N-CBZ-l-arginyl-l-arginine 7-amido-4-methyl-coumarin (Z-Arg-Arg-AMC) 0.05 mM. The buffer used was 80 µL of acetate buffer 20 mM pH=5, 10 µL of EDTA 2

mM and 10 µL of DTT 5 mM (final volume of 100 µL). Leupeptin (50 µM) was used as a negative control. Buffer, buffer with the substrate, and negative control were used as controls. Cathepsin B solution (6.25 units) was a mixture of 700 µL acetate buffer 20 mM pH=5, 100 µL EDTA 2 mM, 100 µL DTT 5 mM and 100 µL cathepsin B. 10 µL of this stock were added to the samples with or without the HA-CP vehicle (1% w/v). The reaction mixture (100 µL) was placed in a 96-well fluorescence plate and incubated at 37°C. The fluorescence was read at time 0 and at 25 min, using excitation and emission wavelengths of 360 nm and 460 nm, respectively. Samples were measured repeatedly (n=3).

IV.4.4.2. *Ex Vivo* Evaluation

IV.4.4.2.1. Permeation Studies by Franz Diffusion Cells

Breast skin samples were obtained from healthy women undergoing plastic surgery after written informed consent (kindly donated from Hospital La Fe, Valencia, Spain). Immediately after excision, the subcutaneous fatty tissue was removed using a scalpel. The skin was cut into 4 cm^2 pieces, wrapped in aluminum foil and stored at -20ºC until use. Permeation study was developed using Franz diffusion cells (Logan Instruments Corp., USA).

Skin samples were fixed between the donor and the receptor chamber, so that stratum corneum was placed upwards. The receptor chamber was filled with 8 mL of 0.01 M PBS pH 7.4, and mixed with a magnetic stirring bar, while the temperature was kept at 37ºC. Treatments with 100 µL of 10 mg/mL of linear or star PGA labeled with OG applied in water, and PGA-FLUO-OG applied in water or in the HA-CP vehicle labeled with Cy5.5 (1% w/v), were applied on the upper area of the skin. Aliquots from the receptor chamber (2 mL) were taken at 8 and 24 h, and the liquid was immediately refilled with fresh solution. After the permeation study, skin samples were washed twice with 0.1% PBS-BSA and kept in 4% paraformaldehyde (PFA) for 24 h at r.t. Then, samples were washed with 30% sucrose in PBS solution for 24 h at 4ºC. After that, skin samples were washed twice with PBS and preserved in a cryopreservation solution (40% 0.1 M PB, 30% ethylene glycol, and 30% glycerol) at 4ºC until use. Finally, the samples were placed in the optimum cutting temperature (OCT) inclusion medium, and slides of 5 µm

were generated via cryostat (version CM1850 UV, Leica, Germany) and samples were analyzed by confocal microscopy.

Images were captured with an inverted DM IRE2 microscope equipped with a λ-blue 40x oil immersion objective and handled with a TCS SP2 system, equipped with an Acoustic Optical Beam Splitter (AOBS). Excitation was performed with an argon laser (OG, 496 nm), a blue diode (DAPI, 405 nm), and red diode (Cy5.5, 675 nm). Images were captured at an 8-bit greyscale and processed with LCS software (version 2.5.1347a, Leica Germany) containing multicolor, macro and 3D components. Control tissue that followed the same incubation time with MilliQ water was also analyzed to establish the autofluorescence. OG intensity was quantified five times per sample using Image J software and expressed as pixels versus the thickness of the skin (μm). Control intensity was subtracted in each case.

IV.4.4.2.2. Tissue Viability and Evaluation of the Anti-Inflammatory Activity of PGA-FLUO Conjugates in an Inflammatory *Ex Vivo* Human Skin Model

Breast skin samples were obtained from healthy women undergoing plastic surgery after written informed consent (kindly donated from Hospital La Fe, Valencia, Spain). The skin was cut to approximately 1 cm^2 and placed in 6-well plates so that the epidermis was exposed to the air and the dermal side was in contact with DMEM medium supplemented with 50 mL fetal bovine serum, 5.5 mL penicillin/streptomycin, and 50 μL amphotericin B, and the skin was incubated at 37ºC under 5% CO_2. The inflammatory model was induced by the addition of a combination of a constant concentration of EGF (2.5 ng/mL) and 15 μg/mL of LPS from *E.coli* (InvivoGen, USA) to the culture media, and further incubation for 24 h at 37ºC under 5% CO_2. The exhaustive characterization of the model was explained in **Chapter II**.

After inflammatory insult via combined treatment with bacterial LPS and EGF for 24 h, 3 μL of a solution at 10 mg/mL of PGA, FLUO, PGA-FLUO conjugate applied and in the HA-CP vehicle (1% w/v) and HA-CP (1% w/v) were applied topically. After 24 h, skin pieces were washed twice with PBS and were introduced in 4 mL of MTT solution (2 mg/mL) at 37ºC. MTT assay is a colorimetric assay for assessing cell metabolic activity. After 4 h of incubation, skin samples were washed twice with PBS and introduced in 4 mL of DMSO, in order to extract the formazan from the skin. After 15 h

of extraction, the absorbance was read at 490 nm using Victor^{2}Wallac™ plate reader (Perkin Elmer, Spain).

In addition, culture medium was collected under standardized conditions after 24 h of incubation with the treatments and kept at -80ºC until use. IL-6 concentrations in the culture medium were measured by ELISA assay (Invitrogen, Spain). Cytokine concentrations were determined according to standard solutions.

IV.4.4.2.3. Development of a Skin Equivalents Construction Model and Cell Viability Assays

Human skin equivalents were prepared from primary human keratinocytes and fibroblasts from juvenile foreskin following circumcision from three different donors (EA: 1/081/13, written consent was obtained) as previously described [52, 59]. Negative control (solvent control), untreated control, and positive control (sodium dodecyl sulfate (SDS) 1%) were studied to ensure the development of the model. PGA, FLUO, PGA-FLUO conjugate applied in water or in the HA-CP vehicle (1% w/v) and HA-CP vehicle (1% w/v) at 5 mg/mL (35 μg/cm^2) were applied topically at days 11 and 13. At day 14, tissue viability was evaluated by MTT assay. Human skin equivalents were introduced in 1.8 mL of MTT solution (0.5 mg/mL), and after 4 h of incubation at 37ºC, samples from the human skin equivalents were cut and introduced in 1.5 mL of acidic isopropanol shaking 3 h in the dark, in order to extract the formazan from the skin. After 3 h of extraction, the absorbance was read at 450 nm using Victor^{2}Wallac™ plate reader (Perkin Elmer, Spain).

IV.4.4.2.4. Development of an Inflammatory Skin Equivalents Construction Model and Anti-Inflammatory Activity of PGA-FLUO conjugates

Human skin equivalents were prepared from primary human keratinocytes and fibroblasts as previously described [52, 59]. To develop an inflammatory phenotype in the skin equivalents emulating characteristics of psoriatic skin *in vitro*, such as hyperproliferation, 20 ng/mL of recombinant TNF-α (eBioscience, Hatfield, UK) were added to the culture media on day 10 and 12 to induce skin inflammation. Negative control and untreated control were studied to ensure the development of the model. PGA, FLUO, PGA-FLUO conjugate applied in water or in the HA-CP vehicle (1% w/v) and HA-CP vehicle (1% w/v) at 5 mg/mL (35 μg/cm^2) were applied topically at days 11 and

13. At day 14, culture media was collected for quantification of IL-6 levels using an ELISA assay (Invitrogen, Spain). Cytokines concentrations were determined according to standard solutions. The absorbance was read at 450 nm using Victor^{2}Wallac™ plate reader (Perkin Elmer, Spain). Cytokine concentrations were determined according to standard solutions.

IV.4.4.3. *In Vivo* Evaluation

IV.4.4.3.1. Ethical Considerations

Animal experiments were performed in accordance with the European Communities Council Directive (86/609/ECC) guidelines and by the Spanish Royal Decree 1201/2005. All the experimental procedures were approved by the Institutional Animal Care and Use Committee and accomplished by accredited and trained staff, meeting the animal care rules. All mice were maintained in a specific pathogen free facility, under temperature, humidity, and using a 12 h light-dark cycle. Food pellets and water were provided ad-libitum during the whole experiments in all cases, and general aspect, body weight, grooming conduct, and behavior were evaluated daily from the beginning of the experiment to ensure animal wellness.

IV.4.4.3.2. Optimization of Optimal FLUO Concentration for Psoriatic Mice Model

IV.4.4.3.2.1. Establishment of Psoriatic Model

6-week-old male BALB/c mice used for all experimental procedures were purchased from Envigo Laboratories Inc. (Spain, EU). One day before the first IMQ application, approximately 2x3 cm of the back of the mice was shaved. Psoriasis-like symptoms were induced by the daily application of 62.5 mg of commercially available IMQ cream (5%) (Imunocare®; Industrial Farmacéutica Cantabria, S.A., Spain) on the back and the right ear for seven consecutive days, translating in a daily dose of 3.125 mg of the active compound. This dose was empirically determined to cause the most optimal and reproducible skin inflammation in mice [60-62].

IV.4.4.3.2.1. Safety Evaluation of Treatments

Seven days after the induction of the disease, mice were split into representative groups. Healthy and untreated mice were used as controls (negative and positive control,

respectively). Conjugate-based treatments at different FLUO equivalents (0.01, 0.15, and 0.3 wt% FLUO eq.) were dissolved in the HA-CP vehicle (1% w/v) and immediately applied topically in the back and the right ear during five consecutive days. HA-CP vehicle was applied as control, following the same methodology. Treatments safety was evaluated by tracking body weight every two days compared to the positive control and healthy animals. After five days of treatment, mice were sacrificed using a CO_2 atmosphere, and major organs, skin, ears, and blood were extracted for further analysis.

IV.4.4.3.2.2. Scoring Severity of Skin Inflammation: PASI score

The anti-psoriatic potential of the formulations was evaluated using an objective scoring system based on the clinical Psoriasis Area and Severity Index (PASI). Erythema, scaling, and thickening (induration of the skin) were assigned independently on a scale from 0 to 4: 0, none; 1, slight; 2, moderate; 3, marked; 4, very marked.

IV.4.4.3.2.3. Spleen Weight

After five days of treatments, mice were sacrificed using a CO_2 atmosphere, and spleen weight was measured, comparing treatments with positive control and healthy animals.

IV.4.4.3.2.4. Ear Thickness

Ear thickness was measured using a caliper every two days during the treatments in comparison with positive control and healthy animals.

IV.4.4.3.2.5. Histology

H&E staining was performed in both ears and the back of the mice. After the sacrifice, tissues were washed with fresh PBS, carefully dried, weighed, and fixed in 4% of PFA for 24 h. Then, PFA was eliminated by successive washing with PBS, and common dehydration and paraffin inclusion procedures were performed, leading to blocks that were sliced into 5 μm sections. The staining was performed as required (Dako Autostainer 48, US), and the slides were assembled with Eukitt. Finally, the slides were observed under the microscope, scanned with a Panoramic 250 Flash III slide scanner and processed with CaseViewer software (both from (3DHISTECH Ltd, Budapest, Hungary).

IV.4.4.3.2.6. Pro-Inflammatory Interleukin Levels in Serum

The pro-inflammatory interleukin levels were measured in serum. Fresh serum was isolated from the blood through centrifugation (4000 rpm, 10 min, 4ºC) and was stored at -80ºC until use. The quantification of IL-23, INF-γ, and IL-1b levels were performed by LUMINEX assay, using a ProcartaPlex™ Multiplex Immunoassay according to the manufacturer's instructions (Invitrogen, Spain).

IV.4.4.3.3. Evaluation of Anti-Inflammatory Activity of PGA-FLUO Conjugates in Psoriatic Mice Model

IV.4.4.3.3.1. Establishment of Psoriatic Model

6-week-old male BALB/c mice used for all experimental procedures were purchased from Envigo Laboratories Inc. (Spain, EU). One day before the first IMQ application, approximately 2x3 cm of the back of the mice was shaved. Psoriasis-like symptoms were induced by the daily application of 62.5 mg of commercially available IMQ cream (5%) (Imunocare®; Industrial Farmacéutica Cantabria, S.A., Spain) on the back and the right ear for seven consecutive days, translating in a daily dose of 3.125 mg of the active compound. This dose was empirically determined to cause the most optimal and reproducible skin inflammation in mice [60, 62].

IV.4.4.3.3.2. Safety Evaluation of Treatments

Seven days after the induction of the disease, mice were split into representative groups. Healthy and untreated mice were used as controls (negative and positive control, respectively). Previous studies were conducted to optimize the optimal concentration of FLUO, demonstrating that the concentration of 0.15 wt% FLUO eq. had the maximum therapeutic potential. Therefore, conjugate-based treatments with 0.15% FLUO eq. were applied in the HA-CP vehicle (1% w/v) and in a commercial base cream used for current corticosteroids (Cold cream®, Farmacia BOIX, Spain). Free FLUO was dissolved with 0.5 mL of Hydrolite® (Guinama S.L., Spain) and incorporated in the base cream. HA-CP vehicle (1% w/v) and the base cream were applied as controls, following the same methodology. All the treatments were immediately applied topically in the back and the right ear for five consecutive days. Treatments safety was evaluated by tracking body weight every two days compared to the positive control and healthy animals. After five

days of treatment, mice were sacrificed using a CO_2 atmosphere and major organs, skin, ears, and blood were extracted for further analysis.

IV.4.4.3.3.3. Scoring Severity of Skin Inflammation: PASI score

The anti-psoriatic potential of the formulations was evaluated using an objective scoring system based on the clinical Psoriasis Area and Severity Index (PASI). Erythema, scaling, and thickening (induration of the skin) were assigned independently on a scale from 0 to 4: 0, none; 1, slight; 2, moderate; 3, marked; 4, very marked.

IV.4.4.3.3.4. Spleen Weight

After five days of treatment, mice were sacrificed using a CO_2 atmosphere, and spleen weight was measured comparing the treatments with positive control and healthy animals.

IV.4.4.3.3.5. Ear Thickness

Ear thickness was measured using a caliper every two days during the treatments in comparison with positive control and healthy animals.

IV.4.4.3.3.6. Histology

H&E staining was performed in both ears and the back of the mice. After the sacrifice, tissues were washed with fresh PBS, carefully dried, weighed, and fixed in 4% of PFA for 24 h. Then, PFA was eliminated by successive washing with PBS, and common dehydration and paraffin inclusion procedure were performed, leading to blocks that were sliced into 10 μm sections. The staining was performed as required (Dako Autostainer 48, US), and the slides were assembled with Eukitt. Finally, the slides were observed under the microscope, scanned with a Panoramic 250 Flash III slide scanner and processed with CaseViewer software (both from (3DHISTECH Ltd, Budapest, Hungary).

IV.4.4.3.3.7. Pro-Inflammatory Interleukin Levels in Serum and Tissue

The pro-inflammatory interleukin levels were measured both in serum and in the tissue from the back of the mice. Fresh serum was isolated from the blood through centrifugation (4000 rpm, 10 min, 4ºC) and stored at -80ºC until use. To performed

protein extraction from frozen tissue, the skin was mixed with PBS (pH 7.4) with a protease and phosphatase inhibitor cocktail and then treated in an ice bath by Ultra Turrax Scatter at 10000 ref/min for 20 min. Immediately after the incubation, the tube was centrifuged at 4000 rpm for 20 min at 4°C and supernatants were collected and stored at -80ºC until use. For LUMINEX assays, IL-23 and INF-γ protein expression in skin lysates and serum were quantified with ProcartaPlex™ Multiplex Immunoassay according to the manufacturer's instructions (Invitrogen, Spain).

IV.5. References

[1] G. Kwatra, S. Mukhopadhyay, Topical Corticosteroids: Pharmacology, in: K. Lahiri (Ed.), A Treatise on Topical Corticosteroids in Dermatology: Use, Misuse and Abuse, Springer Singapore, Singapore, 2018, pp. 11-22.
[2] M. Ponec, J.A. Kempenaar, E.R. De Kloet, Corticoids and Cultured Human Epidermal Keratinocytes: Specific Intracellular Binding and Clinical Efficacy, J Invest Dermatol 76(3) (1981) 211-214.
[3] R. Marks, J.W. Barlow, J.W. Funder, Steroid-induced vasoconstriction: glucocorticoid antagonist studies, J Clin Endocrinol Metab 54(5) (1982) 1075-7.
[4] R.A. Sarabdjitsingh, O.C. Meijer, M.J.M. Schaaf, E.R. de Kloet, Subregion-specific differences in translocation patterns of mineralocorticoid and glucocorticoid receptors in rat hippocampus, Brain Research 1249 (2009) 43-53.
[5] I.M. Otani, A. Banerji, Immediate and Delayed Hypersensitivity Reactions to Corticosteroids: Evaluation and Management, Curr Allergy Asthma Rep 16(3) (2016) 18.
[6] L. Berbegal, F.J. DeLeon, J.F. Silvestre, Hipersensitivity Reactions to Corticosteroids, Actas Dermosifiliogr 107(2) (2016) 107-15.
[7] A. Patel, S.L. Bahna, Immediate hypersensitivity reactions to corticosteroids, Ann Allergy Asthma Immunol 115(3) (2015) 178-182.e3.
[8] T.S. Wang, T.F. Tsai, Managing Scalp Psoriasis: An Evidence-Based Review, Am J Clin Dermatol 18(1) (2017) 17-43.
[9] A.J. Abd, R.K. Kanwar, Y.V. Pathak, M. Al Mohammedawi, J.R. Kanwar, Nanomedicine-Based Delivery to the Posterior Segment of the Eye: Brighter Tomorrow, in: J.K. Patel, V. Sutariya, J.R. Kanwar, Y.V. Pathak (Eds.), Drug Delivery for the Retina and Posterior Segment Disease, Springer International Publishing, Cham, 2018, pp. 195-212.
[10] H. Kaji, N. Nagai, M. Nishizawa, T. Abe, Drug delivery devices for retinal diseases, Adv Drug Deliv Rev 128 (2018) 148-157.
[11] A. Haesslein, H. Ueda, M.C. Hacker, S. Jo, D.M. Ammon, R.N. Borazjani, J.F. Kunzler, J.C. Salamone, A.G. Mikos, Long-term release of fluocinolone acetonide using biodegradable fumarate-based polymers, J Control Release 114(2) (2006) 251-60.
[12] A.H. Salama, A.A. Mahmoud, R. Kamel, A Novel Method for Preparing Surface-Modified Fluocinolone Acetonide Loaded PLGA Nanoparticles for Ocular Use: In Vitro and In Vivo Evaluations, AAPS PharmSciTech 17(5) (2016) 1159-72.
[13] G.J. Jaffe, D. Martin, D. Callanan, P.A. Pearson, B. Levy, T. Comstock, Fluocinolone Acetonide Implant (Retisert) for Noninfectious Posterior Uveitis: Thirty-

Four–Week Results of a Multicenter Randomized Clinical Study, Ophthalmology 113(6) (2006) 1020-1027.
[14] M. Sanford, Fluocinolone Acetonide Intravitreal Implant (Iluvien®), Drugs 73(2) (2013) 187-193.
[15] J. Wang, A. Jiang, M. Joshi, J. Christoforidis, Drug delivery implants in the treatment of vitreous inflammation, Mediators Inflamm 2013 (2013) 780634.
[16] L.T.H. Nguyen, A. Muktabar, J. Tang, Y.S. Wong, C.S. Thaxton, S.S. Venkatraman, The Potential of Fluocinolone Acetonide to Mitigate Inflammation and Lipid Accumulation in 2D and 3D Foam Cell Cultures, Biomed Res Int 2018 (2018) 3739251.
[17] M. Pauporte, H. Maibach, N. Lowe, M. Pugliese, D.J. Friedman, H. Mendelsohn, I. Cargill, R. Ramirez, Fluocinolone acetonide topical oil for scalp psoriasis, J Dermatolog Treat 15(6) (2004) 360-4.
[18] A.S. Paller, S. Nimmagadda, L. Schachner, S.B. Mallory, T. Kahn, I. Willis, L.F. Eichenfield, Fluocinolone acetonide 0.01% in peanut oil: therapy for childhood atopic dermatitis, even in patients who are peanut sensitive, J Am Acad Dermatol 48(4) (2003) 569-77.
[19] J.R. Scholtz, A new corticoid for topical therapy. Fluocinolone acetonide, California medicine 95(4) (1961) 224-226.
[20] B.A. Price, J.B. Jackson, Psoriasis, in: S.J. Enna, D.B. Bylund (Eds.), xPharm: The Comprehensive Pharmacology Reference, Elsevier, New York, 2007, pp. 1-6.
[21] A.B. Mehta, N.J. Nadkarni, S.P. Patil, K.V. Godse, M. Gautam, S. Agarwal, Topical corticosteroids in dermatology, Indian J Dermatol Venereol Leprol 82(4) (2016) 371-8.
[22] S. Hehir, N.R. Cameron, Recent advances in drug delivery systems based on polypeptides prepared from N-carboxyanhydrides, Polym Int 63(6) (2014) 943-954.
[23] O. Zagorodko, J.J. Arroyo-Crespo, V.J. Nebot, M.J. Vicent, Polypeptide-Based Conjugates as Therapeutics: Opportunities and Challenges, Macromol Biosci 17 (2017) 1600316.
[24] R. Duncan, Polymer therapeutics at a crossroads? Finding the path for improved translation in the twenty-first century, J Drug Target 25(9-10) (2017) 759-780.
[25] X. Pang, X. Yang, G. Zhai, Polymer-drug conjugates: recent progress on administration routes, Expert Opin Drug Deliv 11(7) (2014) 1075-86.
[26] T. Ngawhirunpat, P. Opanasopit, T. Rojanarata, S. Panomsuk, L. Chanchome, Evaluation of Simultaneous Permeation and Metabolism of Methyl Nicotinate in Human, Snake, and Shed Snake Skin, Pharm Dev Technol 13(1) (2008) 75-83.
[27] T. Ngawhirunpat, N. Kawakami, T. Hatanaka, J. Kawakami, I. Adachi, Age Dependency of Esterase Activity in Rat and Human Keratinocytes, Biol Pharm Bull 26(9) (2003) 1311-1314.
[28] A. Duro-Castano, V.J. Nebot, A. Nino-Pariente, A. Arminan, J.J. Arroyo-Crespo, A. Paul, N. Feiner-Gracia, L. Albertazzi, M.J. Vicent, Capturing "Extraordinary" Soft-Assembled Charge-Like Polypeptides as a Strategy for Nanocarrier Design, Adv Mater 29 (2017) 12.
[29] A. Duro-Castano, I. Conejos-Sánchez, J.M. Vicent, Peptide-Based Polymer Therapeutics, Polymers (Basel) 6 (2014) 515-551.
[30] R. Duncan, M.J. Vicent, Polymer therapeutics-prospects for 21st century: the end of the beginning, Adv Drug Deliv Rev 65 (2013) 60-70.
[31] X. Xu, W. Ho, X. Zhang, N. Bertrand, O. Farokhzad, Cancer nanomedicine: from targeted delivery to combination therapy, Trends Mol Med 21 (2015) 223-232.
[32] B.L. Banik, P. Fattahi, J.L. Brown, Polymeric nanoparticles: the future of nanomedicine, Wiley Interdiscip Rev Nanomed Nanobiotechnol 8 (2016) 271-299.

[33] W.R. Sanhai, J.H. Sakamoto, R. Canady, M. Ferrari, Seven challenges for nanomedicine, Nat Nanotechnol 3 (2008) 242.
[34] I. Bajaj, R. Singhal, Poly (glutamic acid) – An emerging biopolymer of commercial interest, Bioresour Technol 102 (2011) 5551-5561.
[35] C. Li, S. Wallace, Polymer-drug conjugates: Recent development in clinical oncology, Adv Drug Deliv Rev 60 (2008) 886-898.
[36] J.J. Arroyo-Crespo, et al., *Anticancer activity driven by drug linker modification in a polyglutamic acid-based combination-drug conjugate*. Adv. Funct. Mater, 2018. **28**: 13.
[37] (!!! INVALID CITATION !!!).
[38] Y. Bakkour, V. Darcos, S. Li, J. Coudane, Diffusion ordered spectroscopy (DOSY) as a powerful tool for amphiphilic block copolymer characterization and for critical micelle concentration (CMC) determination, Polym Chem 3 (2012) 2006-2010.
[39] W. Moffitt, R.B. Woodward, A. Moscowitz, W. Klyne, C. Djerassi, Structure and the Optical Rotatory Dispersion of Saturated Ketones, J Am Chem Soc 83 (1961) 4013-4018.
[40] J. Lai, Y. Huang, Fibril aggregates of the poly(glutamic acid)–drug conjugate, RSC Advances 5 (2015) 48856-48860.
[41] A.S. Lee, V. Bütün, M. Vamvakaki, S.P. Armes, J.A. Pople, A.P. Gast, Structure of pH-Dependent Block Copolymer Micelles: Charge and Ionic Strength Dependence, Macromolecules 35 (2002) 8540-8551.
[42] L. Hu, P. Zhang, X. Wang, X. Cheng, J. Qin, R. Tang, pH-sensitive carboxymethyl chitosan hydrogels via acid-labile ortho ester linkage for potential biomedical applications, Carbohydr Polym 178 (2017) 166-179.
[43] J. Tian, V.J. Stella, Degradation of paclitaxel and related compounds in aqueous solutions III: Degradation under acidic pH conditions and overall kinetics, J Pharm Sci 99 (2010) 1288-98.
[44] P.T. Wong, S.K. Choi, Mechanisms of drug release in nanotherapeutic delivery systems, Chem Rev 115 (2015) 3388-432.
[45] J.J. Arroyo-Crespo, A. Armiñán, D. Charbonnier, L. Balzano-Nogueira, F. Huertas-López, C. Martí, S. Tarazona, J. Forteza, A. Conesa, M.J. Vicent, Tumor microenvironment-targeted poly-L-glutamic acid-based combination conjugate for enhanced triple negative breast cancer treatment, Biomaterials 186 (2018) 8-21.
[46] R. Duncan, S.C. Richardson, Endocytosis and intracellular trafficking as gateways for nanomedicine delivery: opportunities and challenges, Mol Pharm 9 (2012) 2380-402.
[47] I. Canton, G. Battaglia, Endocytosis at the nanoscale, Chem Soc Rev 41(7) (2012) 2718-2739.
[48] R. Duncan, Polymer conjugates as anticancer nanomedicines, Nat Rev Cancer 6 (2006) 688-701.
[49] M. Giulbudagian, G. Yealland, S. Honzke, A. Edlich, B. Geisendorfer, B. Kleuser, S. Hedtrich, M. Calderon, Breaking the Barrier - Potent Anti-Inflammatory Activity following Efficient Topical Delivery of Etanercept using Thermoresponsive Nanogels, Theranostics 8 (2018) 450-463.
[50] M.O. Danso, V. van Drongelen, A. Mulder, J. van Esch, H. Scott, J. van Smeden, A. El Ghalbzouri, J.A. Bouwstra, TNF-α and Th2 cytokines induce atopic dermatitis-like features on epidermal differentiation proteins and stratum corneum lipids in human skin equivalents, J Invest Dermatol 134 (2014) 1941-1950.
[51] G. Tjabringa, M. Bergers, D. van Rens, R. de Boer, E. Lamme, J. Schalkwijk, Development and validation of human psoriatic skin equivalents, Am J Pathol 173 (2008) 815-23.

[52] S. Hönzke, L. Wallmeyer, A. Ostrowski, M. Radbruch, L. Mundhenk, M. Schäfer-Korting, S. Hedtrich, Influence of Th2 Cytokines on the Cornified Envelope, Tight Junction Proteins, and ß-Defensins in Filaggrin-Deficient Skin Equivalents, J Invest Dermatol 136 (2015) 631-639.
[53] V. Avasatthi, H. Pawar, C.P. Dora, P. Bansod, M.S. Gill, S. Suresh, A novel nanogel formulation of methotrexate for topical treatment of psoriasis: optimization, in vitro and in vivo evaluation, Pharm Dev Technol 21 (2015) 554-62.
[54] A. Walter, M. Schäfer, V. Cecconi, C. Matter, M. Urosevic-Maiwald, B. Belloni, N. Schönewolf, R. Dummer, W. Bloch, S. Werner, H.D. Beer, A. Knuth, M. van den Broek, Aldara activates TLR7-independent immune defence, Nat Commun 4 (2013) 1560.
[55] H. Vinter, K. Kragballe, T. Steiniche, M. Gaestel, L. Iversen, C. Johansen, Tumour necrosis factor-alpha plays a significant role in the Aldara-induced skin inflammation in mice, Br J Dermatol 174(5) (2016) 1011-21.
[56] L. van der Fits, S. Mourits, J.S. Voerman, M. Kant, L. Boon, J.D. Laman, F. Cornelissen, A.M. Mus, E. Florencia, E.P. Prens, E. Lubberts, Imiquimod-induced psoriasis-like skin inflammation in mice is mediated via the IL-23/IL-17 axis, J Immunol 182 (2009) 5836-45.
[57] H.L. Ma, S. Liang, J. Li, L. Napierata, T. Brown, S. Benoit, M. Senices, D. Gill, K. Dunussi-Joannopoulos, M. Collins, C. Nickerson-Nutter, L.A. Fouser, D.A. Young, IL-22 is required for Th17 cell-mediated pathology in a mouse model of psoriasis-like skin inflammation, J Clin Invest 118 (2008) 597-607.
[58] S. Shibata, Y. Tada, Y. Asano, K. Yanaba, M. Sugaya, T. Kadono, N. Kanda, S. Watanabe, S. Sato, IL-27 activates Th1-mediated responses in imiquimod-induced psoriasis-like skin lesions, J Invest Dermatol 133 (2012) 479-88.
[59] S. Kuchler, D. Henkes, K.M. Eckl, K. Ackermann, J. Plendl, H.C. Korting, H.C. Hennies, M. Schafer-Korting, Hallmarks of atopic skin mimicked in vitro by means of a skin disease model based on FLG knock-down, Altern Lab Anim 39(5) (2011) 471-80.
[60] A.B. Van Belle, M. de Heusch, M.M. Lemaire, E. Hendrickx, G. Warnier, K. Dunussi-Joannopoulos, L.A. Fouser, J.C. Renauld, L. Dumoutier, IL-22 is required for imiquimod-induced psoriasiform skin inflammation in mice, J Immunol 188 (2011) 462-9.
[61] S.J. Kim, Y.W. Jang, K.E. Hyung, D.K. Lee, K.H. Hyun, S.Y. Park, E.S. Park, K.W. Hwang, Therapeutic Effects of Methanol Extract from, J Immunol Res 2017 (2017) 7052560.
[62] S.P. Jin, S.J. Koh, D.A. Yu, M.W. Kim, H.T. Yun, D.H. Lee, H.S. Yoon, S. Cho, H.S. Park, Imiquimod-applied Interleukin-10 deficient mice better reflects severe and persistent psoriasis with systemic inflammatory state, Exp Dermatol 27 (2017) 43-49.

CHAPTER V:

DEVELOPMENT OF POLYMER CONJUGATES FOR TISSUE HEALING

V.1. Antecedents and Background

The wound healing process aims to re-establish the normal architecture and biological activity of damaged tissue [1]. Due to the high incidence rate and the exponential increase in the aged population, wound healing has a substantial socioeconomic impact worldwide [2]. During the development of this chapter, we focus on the treatment of skin wounds and ischemia-reperfusion injury in the heart with polymer-drug conjugates as examples of tissue healing therapeutic approaches.

V.1.1. Skin Wound Healing

As we have shown throughout this thesis, PGA-drug conjugates can penetrate and permeate through the different layers of the skin, even in cases where the skin barrier is modified or altered (such as psoriasis, **Chapter IV**); therefore, they may be used in the enhancement of skin regeneration and repair, thereby contributing towards wound healing. Wound healing represents a common medical challenge, and exists a rising incidence of wound healing-related problems associated with metabolic syndrome (e.g., obesity and type II diabetes patients), and aging [3]. The main physiological events in wound repair can be classified into three stages that overlap the repair process: the inflammatory stage, the proliferative stage, and the remodeling stage [4, 5] (**Figure V. 1**).

Wound healing involves the complex interaction of several biological and molecular processes associated with tissue regeneration. Tissue damage triggers the onset of the inflammatory stage of wound repair; at this stage, components of the coagulation cascade, inflammatory pathways, and immune system become activated to minimize blood/fluid losses and infection. Meanwhile, a platelet plug composed of platelets, fibronectin, vitronectin, and thrombospondins forms at the injury site to create a scaffold-like structure into which various cells types, such as leukocytes, neutrophils, keratinocytes, fibroblasts, and endothelial cells, infiltrate [4]. Two to three days after the onset of tissue damage, monocytes migrate from the blood vessels to the lesion area and differentiate into macrophages. These cells act as antigen-presenting cells and collaborate with the neutrophils in the phagocytosis process to eliminate foreign materials and damaged cells, and also participate in the synthesis and release of pro-inflammatory cytokines [6, 7].

The proliferative stage occurs between two to ten days after tissue damage and reduces the injured tissue area by creating a viable epithelial barrier to the epithelialization process by stimulated keratinocytes. The closure of the wound and restoration of the vascular system (via angiogenesis) also occurs during this stage, with macrophage-stimulated differentiation of fibroblasts into myofibroblasts [8] facilitating wound closure.

The remodeling stage begins after two to three weeks of tissue damage and can last for over a year. During this stage, endothelial cells, macrophages, and myofibroblasts apoptosis halts the wound healing processes [9], thereby creating an avascular and acellular mature wound [10]. After six to twelve months, matrix metalloproteinases excreted by different cells promote the replacement of the collagen III component of the acellular matrix synthesized in the proliferative stage with the more robust collagen I [11]. Additionally, a marked decrease of angiogenesis, blood flow, and metabolic activity in the wound is also observed.

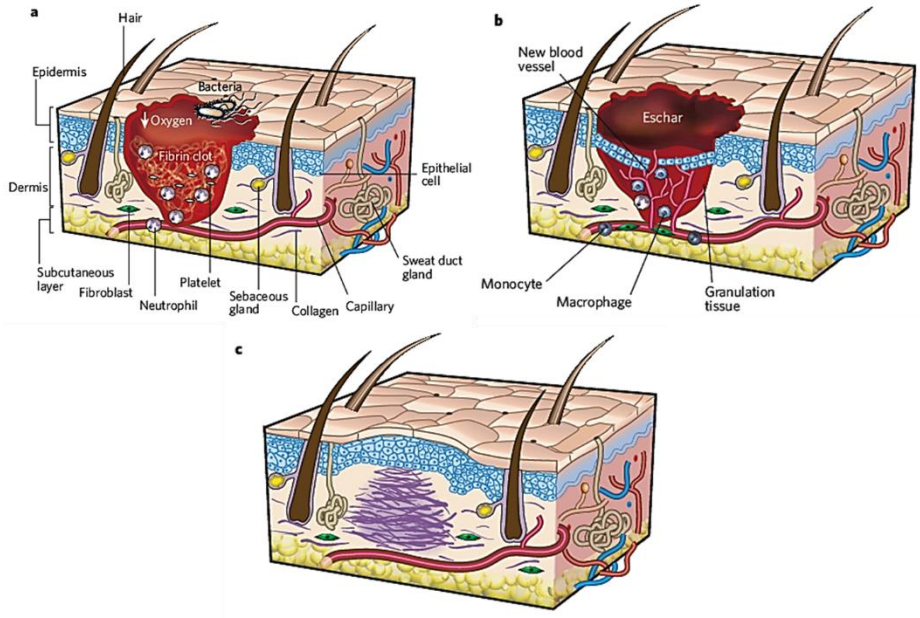

Figure V. 1: Stages of wound repair: **(a)** inflammatory stage, **(b)** proliferative stage, and **(c)** remodeling stage. Adapted from [9].

Traditional therapies for wound healing treatment have included naturally occurring products such as plants or animal-derived products (such as honey) due to their anti-inflammatory, antimicrobial, and cell-stimulating properties [12]. However, more recently developed therapies (e.g., the use of skin substitutes, growth factors, or

dressings) have significantly improved wound treatment [13]. The avoidance of wound contamination represents the primary function of wound dressings [14]; however, they can also act as platforms to deliver bioactive molecules to the wound site and promote tissue regeneration. Incorporated bioactive drugs can enhance the wound healing process directly by promoting the removal of necrotic tissue or indirectly by avoiding/treating infections in the wound area and dampening inflammatory responses [3].

Bioactive molecules that modulate inflammatory responses and promote skin wound healing include the family of omega-3 polyunsaturated fatty acids (PUFA) [15-19]. Docosahexaenoic acid (DHA), a 22-carbon omega-3 fatty acid with six *cis*-double bonds, represents the most abundant and highly unsaturated PUFA in tissues (primarily in the brain and retina) [20, 21]. DHA is commonly obtained from fish oil, in particular from plasma, tissue, and cellular membranes [22].

Dietary studies positively associated DHA with the prevention of numerous human diseases, including cancer [23-25], cardiovascular diseases [26-29], and Alzheimer's disease [30, 31], amongst others [32]. In terms of wound repair, a range of studies have reported the beneficial role of DHA [16, 33]. Lu *et al*. revealed that endogenous DHA accelerated tissue repair by acting as a substrate for the synthesis of 14S,21R-dihydroxy-DHA, a compound that enhances both reepithelization and wound area closure. Wound-resident activated macrophages promote the activity of 12-lipoxygenase and p450, catalyzing the conversion of DHA into 14S,21R-dihydroxy-DHA [34]. In 2011, a study confirmed deficiency in 14S,21R-dihydroxy-DHA production in a diabetic wound healing mouse model, increasing the importance of the topical application of DHA to chronic skin wounds [33].

Importantly, DHA exhibits anti-inflammatory activity through various mechanisms of action and, therefore, could also represent a potential therapeutic for psoriasis [35-37] (to be further explored in our models, **Chapter IV**, in a near future). DHA can act as a substrate for the production of some anti-inflammatory molecules, such as the resolvins (metabolic byproducts of omega-3 fatty acids) [38-40]. DHA also modifies the expression of some pro-inflammatory cytokines and mediators, such as cyclooxygenase-II (COX-2) and TNF [22, 38, 41, 42]. Interestingly, recent studies have discovered the presence of a membrane receptor for DHA, G-protein-coupled receptor 120 (GPR120), which inhibits TLR4 and TNF receptor 1 (TNFR1)-induced activation of

the IkB kinase (IKK) [43]. As these factors represent potential enhancers of metabolic inflammation [44], DHA may promote a general reduction in inflammatory activity.

Recent studies have also described an effect of DHA on endothelial cell function. De Caterina *et al*. employed cultured human endothelial cells activated by pro-inflammatory cytokines to evaluate DHA-modulated endothelial activation. Interestingly, DHA treatment resulted in the reduced expression of vascular cell adhesion molecule 1 (VCAM-1), intercellular adhesion molecule 1 (ICAM-1), E-selectin, and pro-inflammatory cytokines such as IL-6 and IL-8 [45, 46]. DHA also modifies cell membrane features [47] and the organization and composition of the membrane microdomains [48-50], specifically in lipid rafts (areas with high concentrations of cholesterol and sphingolipids) [51].

Of note, several factors, including oxygen, light, elevated temperatures, and irradiation can provoke lipid oxidation, structure destabilization, and reduced activity of PUFAs [52]. Lipid oxidation gives rise to various unstable products, creating a mixture of intermediate and secondary products that include free radicals and hydroperoxides. These products also can be oxidized into aldehydes and ketones, for example, which can produce several adverse effects [53]. Furthermore, PUFAs display some limitations regarding their incorporation into various formulations, as they can only be completely solubilized into formulations with at least one oil phase. Therefore, there exists a growing effort to improve stability and overcome the limitations associated with PUFAs through innovative delivery methods.

The use of nanoemulsions and liposomes represent the most commonly employed methods to include fatty acids such as PUFAs in topical treatments. As an example, Marinosomes® are liposomes composed of polyunsaturated fatty acids such as eicosapentaenoic acid (EPA) and DHA obtained from natural marine lipid extracts [54]. Jung *et al*. used a newly developed emulsification method, layer-by-layer (LbL) deposition, to encapsulate the omega-3 fatty acids present in fish oil. Excitingly, this study established improved skin permeability of LbL emulsions compared to free fatty acids by Franz diffusion cells using a method described by Sonavane *et al*. [55] with some modifications [56]. Yang *et al*. developed a nanoemulsion loaded with algae oil (rich in DHA) and coffee oil, to study the inhibitory effect on UVA-radiation induced skin damage in mice and melanoma cell growth. *In vitro* cytotoxicity assay of nanoemulsions

in melanoma cells revealed effective inhibition of cell growth with an IC_{50} value of 26.5 µg/mL and cell cycle arrest at the G2/M phase. Moreover, *in vivo* results demonstrated that a nanoemulsion dose of 0.1% coffee oil-algae oil reduced several characteristics parameters after UVA-damaged skin, such as trans-epidermal water loss, skin erythema, melanin formation, and subcutaneous blood flow [57].

However, topical application presents with certain limitations, including a requirement for aqueous and oily phases to incorporate fatty acids. To overcome these limitations, we proposed the application of polymer conjugation.

In this project, we used a type of DHA composed of two chains containing 12 double bonds, called didocosahexaenoic acid (diDHA), in order to achieve adequate bioresponsive linking chemistry with our carriers. Specifically, we assessed the potential for a PGA-conjugated form of diDHA using an ester linker (PGA-diDHA conjugates) that promotes stability, solubility in water and allows its incorporation in aqueous formulations, such as hydrogels.

V.1.2. Heart Tissue Damage by Induced Ischemia-Reperfusion Injury

Cardiovascular diseases (CVD) currently represent a significant cause of mortality across the world; an estimated 22 million people will die from CVD in 2030 [58]. Interestingly, the use of PUFAs as therapeutic agents to treat CVD has grown exponentially in recent years. Specifically, DHA protects the heart against myocardial ischemia-reperfusion (I/R)-induced injury [59], entailing both morbidity and loss of quality of life in patients [60]. Ischemia, or the lack of oxygen in the myocardial vascular territory, cause irreversible damage to the myocardium by inducing necrosis and apoptosis of cardiomyocytes [61]. However, subsequent reperfusion with oxygenated blood provokes tissue damage, inflammation, and oxidative stress in the area, leading to cardiomyocyte death. This process decreases contractile activity and induces alterations to the heart wall, thereby generating cardiac dysfunction [62, 63]. Preventing cell death during the reperfusion process represents a promising approach for the reduction of secondary effects following the implementation of treatment after an ischemic heart disease. Of note, recent studies have demonstrated that dietary supplementation with fish oil or direct intravenous DHA infusion can reduce arrhythmias in I/R animal models [64, 65], myocardial infarct size [66-68], and cardiac dysfunction [69-71].

For this reason, after exploring skin wound healing application, in the second part of this chapter we also studied the ability of the PGA-diDHA conjugates to reduce and prevent damage caused by I/R during the cardiac ischemic process, through a collaboration with the laboratory of Dr. Pilar Sepúlveda (Hospital La Fe, Valencia, Spain). We aimed to enhance the already known properties of diDHA upon polymer conjugation by decreasing the damage associated with the I/R process. Mainly, by diminishing the effect of blood flow during the reperfusion process not only by a physical effect (adhesion of PGA-diDHA to the endothelium) but also by enhancing the anti-inflammatory and healing properties of diDHA triggering its controlled and sustained release at the injury site.

IV.2. Results and Discussion

V.2.1. Synthesis and Characterization of Poly-L-Glutamate-Didocosahexaenoic Acid Conjugates

We prepared a family of PGA-diDHA conjugates following well-established synthetic procedures [72]. We attached diDHA to the polypeptidic backbone employing an ester linker through an esterification reaction using DMTMM·BF_4 [73] and DMAP as a catalyst (**Scheme V. 1**). We conjugated different diDHA loadings to PGA, creating a broad family of conjugates that exhibit different physico-chemical properties.

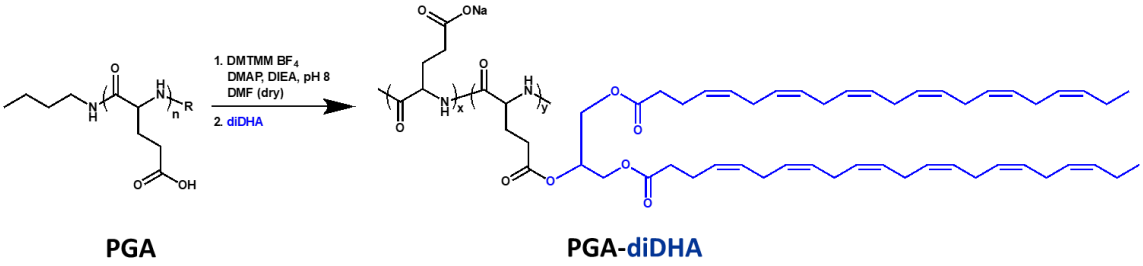

Scheme V. 1: Synthetic procedures for PGA-diDHA conjugate synthesis.

We started from a PGA of an average molecular weight of 41.3 kDa (273 units of glutamic acid) and proceed with the conjugation of diDHA achieving the desired family of PGA-diDHA conjugates with mol% loading ranging from 2 to 9 mol%, as determined via ^{1}H-NMR (namely, PGA-diDHA2.2, PGA-diDHA6.4, and PGA-diDHA9.1 conjugates). We optimized the synthetic methodology, which proved reproducible and

yielded the desired products with high purity as also revealed via ^{1}H-NMR (60% yield). While we observed a broadening of the bands after diDHA conjugation to PGA, the characteristic peaks of the parent drug at 5.5 - 5 ppm were retained (**Figure V. 1A**). We calculated the backbone modification by ^{1}H-NMR, comparing the integration for the alkenyl diDHA protons (5.5 - 5 ppm) to that of the PGA backbone (4.5 - 4 ppm). Indeed, we revealed the integrity of the diDHA signals throughout the conjugate, as evidenced by the prevalence of the associated peaks at 5.5 - 5 ppm, 3 - 2.5 ppm, and 1 - 0.5 ppm within the conjugate (**Figure V. 1B**).

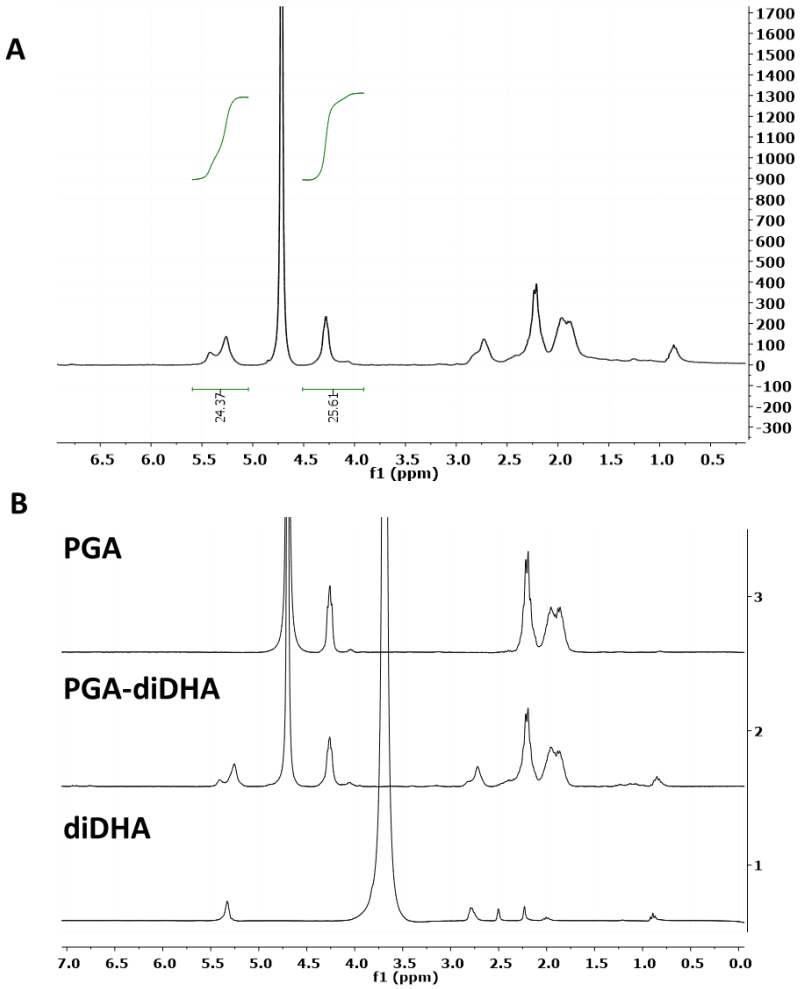

Figure V. 1: **(A)** ^{1}H-NMR approach to diDHA loading quantification (mol%) by means of relative integration (alkenyl diDHA protons 5.5 - 5 ppm *vs*. -CH at PGA backbone 4.5 – 4 ppm) in the PGA-diDHA conjugate (5 mg/mL D_2O). **(B)** diDHA signals were maintained after the conjugation to the polymeric backbone, ensuring the protection of the drug during the synthesis of the conjugate.

In order to achieve the different diDHA loading in the conjugates the same synthetic methodology was implemented demonstrating the robustness of the synthesis (**Figure V. 2**).

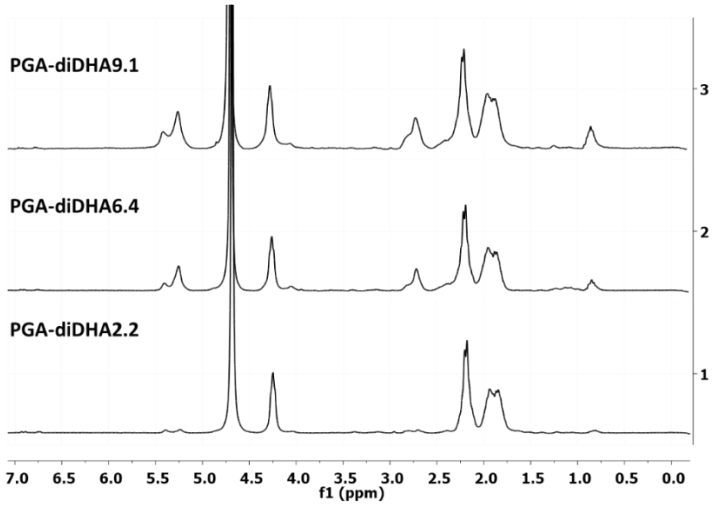

Figure V. 2: ^{1}H-NMR spectra in D_2O of PGA-diDHA conjugates with different loading demonstrating conjugation efficiency and purity.

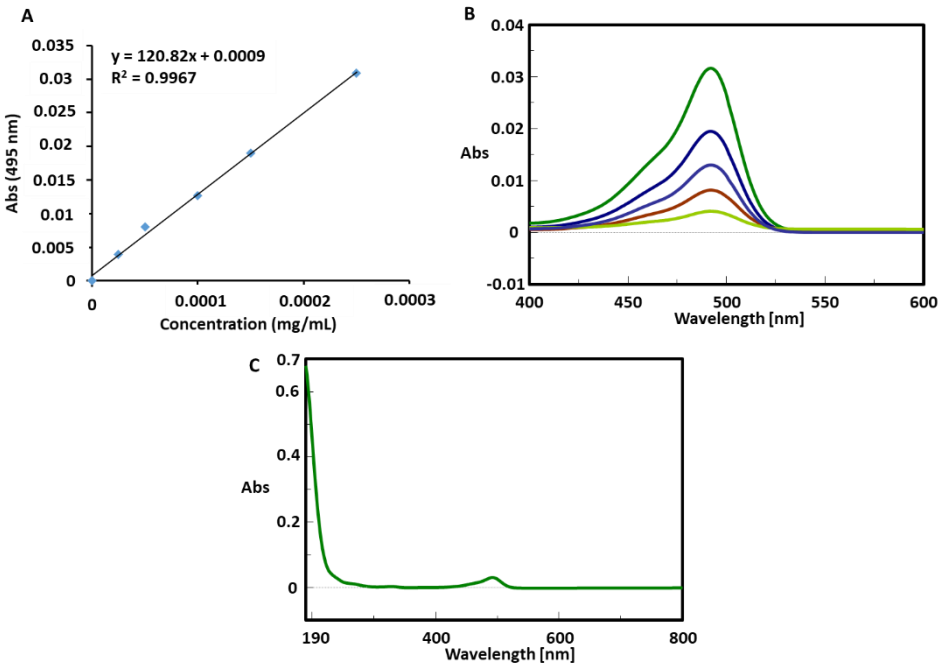

Figure V. 3: UV-Vis spectra of OG labeled PGA-diDHA conjugates. **(A)** Calibration curve of OG at 495 nm. **(B)** UV-Vis spectra of the OG calibration curve. **(C)** UV-Vis spectra of PGA-diDHA6.4-OG conjugate as representative example.

In the case of the conjugates labeled with Oregon Green (OG), we also calculated the backbone modification by ^{1}H-NMR (integration of the PGA -CH at 4.5 - 4 ppm *vs.* aromatic OG protons from 6.7 to 8.1 ppm) yielding as result 1.9 mol% OG in all the conjugates. We further verified loading efficiency by assessing the UV-Vis absorbance at 495 nm compared to a standard curve of free OG, which provided a similar result (2 mol% OG) (**Figure V. 3**).

Table V. 1 summarizes the most relevant physico-chemical parameters of the synthesized PGA-diDHA conjugates. We further confirmed diDHA loading determined by ^{1}H-NMR using the triglyceride assay, finding diDHA loadings of 1.6, 9.5, and 14.7 diDHA/PGA for PGA-diDHA2.2, 6.4, and 9.1, respectively. The differences compared with the results by ^{1}H-NMR could derive from the degradation of the alkene bonds by means of several factors, including peroxidation or hydrolysis. Of note, the size assessments of the conjugates by DLS measurements (in number) revealed that diDHA loading plays an important role: higher diDHA loading generated conjugates with smaller sizes. The measurements by DLS in terms of intensity reflects the different aggregation behavior for the synthesized conjugates revealing much larger aggregates for the intermediate diDHA loading. Deeper physico-chemical studies on conjugate conformation by SAXS and/or SANS techniques are required to fully understand this behavior (for preliminary data in this direction see **section V.2.3.**).

Table V. 1: Physico-chemical characterization of PGA-diDHA conjugates. **a.** Diameter by DLS in MilliQ water by number (2 mg/mL) **b.** Diameter by DLS in MilliQ water by intensity (2 mg/mL) **c.** Polydispersity index (PDI) as determined by DLS **d.** Critical concentration of aggregation (CAC) by pyrene assay **e.** diDHA loading (mol%) by ^{1}H-NMR **f.** diDHA loading (mol%) by triglyceride assay **g.** Free diDHA (wt% of the total drug loading) by FPLC.

Conjugate	Mw (Da)	Rh[a] (nm) Number	Rh[b] (nm) Intensity	PDI[c]	CAC[d] (µM)	Z-Potential (mV)	diDHA[e] (mol%)	diDHA[f] (mol%)	Free diDHA[g]
PGA-diDHA$_{2.2}$	43000	66.86	175.2	0.245	28.87	-55.4	2.2	1.59	0.02
PGA-diDHA$_{6.4}$	45900	36.42	308.7	0.273	3.96	-57.2	6.4	9.48	0.02
PGA-diDHA$_{9.1}$	47800	16.43	223	0.518	2.84	-55.4	9.1	14.67	0.15

All conjugates displayed a negative Z-potential close to -50 mV, in good agreement with reported data in the literature for similar systems [74], due to the contribution of PGA. Moreover, we detected free diDHA content of <0.15 wt% of the

total drug loading in all the conjugates tested, as determined by FPLC, demonstrating the purity of the conjugates.

V.2.2. Enhanced Solubility and Stability upon diDHA Conjugation

diDHA displays very low aqueous solubility (forming a solid gel visible at the tip of the Eppendorf tube), likely due to diDHA autopolymerization upon contact with water. However, conjugation of diDHA to PGA significantly increases water solubility, as shown for PGA-diDHA-OG conjugate in **Figure V. 4A**. Conjugation also protects diDHA from oxidative damage, as evidenced by a ^{1}H-NMR degradation study that compared the depletion of signal from the alkene groups to an internal standard over 28 days (**Figure V. 4B**).

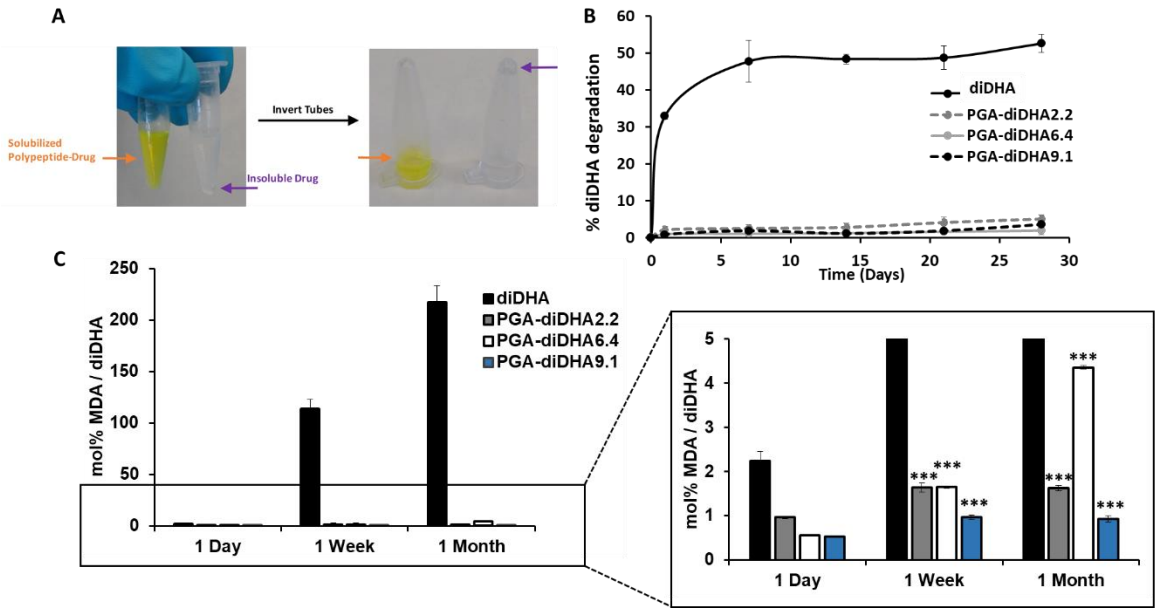

Figure V. 4: Increased stability and solubility of PGA-diDHA. **(A)** Increased solubility in water of PGA-diDHA conjugates (yellow staining = OG labeled PGA-diDHA). Free diDHA forms gels on contact with water, creating an insoluble mass stuck to the bottom of the tube (clear gel). **(B)** Degradation over time of diDHA and PGA-diDHA conjugates as assessed by ^{1}H-NMR for 28 days (n=3). **(C)** Degradation over time of diDHA and PGA-diDHA conjugates by MDA assay (n=3). Asterisks indicate statistically significant differences after ANOVA analyses followed by Bonferroni's post hoc tests, mean ± SEM. In all cases, we considered differences to be significant when p***<0.001; p**<0.01; p*<0.05.

After one day, free diDHA degraded by 30 - 40%, while PGA-diDHA conjugates maintained their alkene bond integrity and degraded by less than 5%. Encouragingly, at

day 28, diDHA degraded by 50%, while PGA-diDHA displayed only 10% degradation, demonstrating that PGA conjugation stabilizes and protects diDHA.

We confirmed the stabilizing effect through the malondialdehyde (MDA) lipid peroxidation assay (**Figure V. 4C**). Independently of the diDHA loading in the conjugates, we detected <5 mol% MDA/diDHA for all PGA-diDHA conjugates at room temperature (r.t.) after one month, while free diDHA samples provided >100 mol% MDA/diDHA after only one week, and >200 mol% MDA/diDHA after one month. Overall, these findings suggest that PGA conjugation could significantly enhance the shelf-life of diDHA and the stabilization of the molecule. The differences between the results of the MDA assay and ^{1}H-NMR assays could derive from the various means of degrading alkene bonds, including peroxidation, hydrolysis, and polymerization, therefore deeper studies should be performed to fully understand the cause of the differences.

V.2.3. Self-assembling Behavior of PGA-diDHA Conjugates

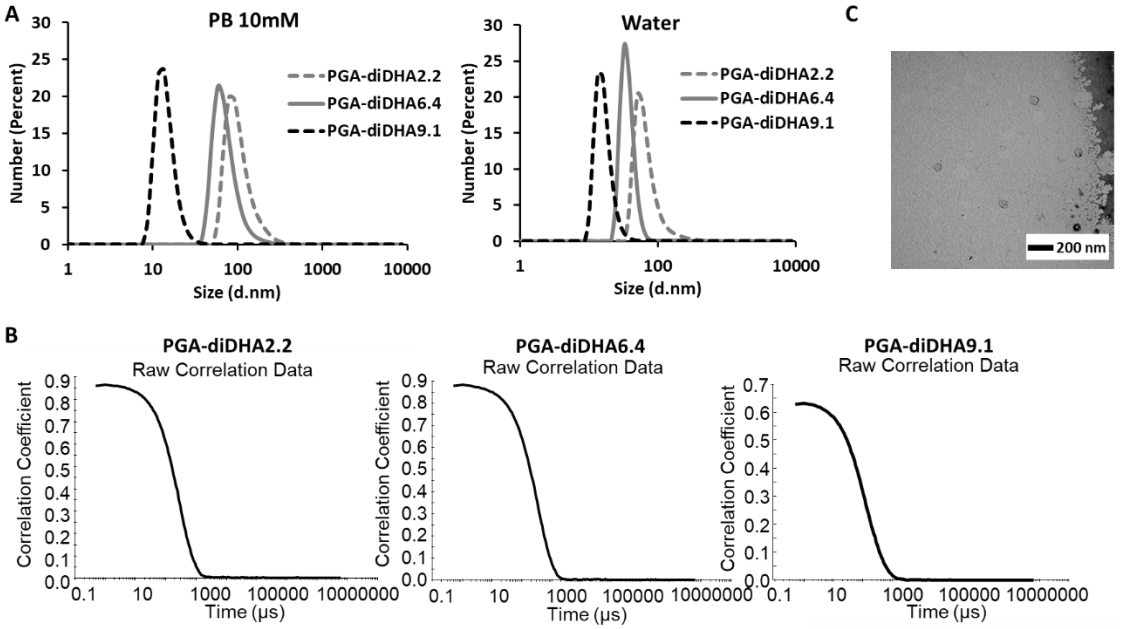

Figure V. 5: Physico-chemical characterization of PGA-diDHA conjugates. **(A)** Size measurements of PGA-diDHA by DLS in PB 10 mM and water. **(B)** Correlation coefficients of each PGA-diDHA by DLS. **(C)** TEM images of PGA-diDHA at 2 mg/mL.

We studied the behavior of the PGA-diDHA conjugates in solution, creating an amphiphilic system with appropriate hydrophobic-hydrophilic (diDHA-PGA) balance,

enabling the self-assembly behavior into larger nanometer-sized objects [74]. We characterized the synthesized conjugates using a battery of techniques. First, we measured the sizes of selected PGA-diDHA conjugates in PB 10 mM and water by DLS (**Figure V. 5A**), discovering adequate quality criteria and correlation coefficients (**Figure V. 5B**). In both media, we observed a relationship between diDHA loading and the size of the conjugates; the size decreases as diDHA loading increases, with values of 100 nm to 20 nm for PGA-diDHA9.1 and PGA-diDHA2.2, respectively. In agreement with the above-mentioned data (**Table V.1**). This phenomenon may be intimately related to the hydrophilic-lipophilic ratio in the conjugates. As expected, looking at solution conformation of our nanoconjugates, as the lipophilic part (diDHA) increases, elevated compaction occurs, thereby causing a reduction in size. This finding agrees with the results obtained by TEM images that confirmed the existence of nanosized spherical aggregates (**Figure V. 5C**).

We next performed a pyrene assay to determine the critical aggregation concentration (CAC) of the conjugates, which suggested that the self-assembly of PGA-diDHA conjugates was triggered mainly due to hydrophobic interactions. As shown in **Figure V. 6**, the presence of hydrophobic pockets within the assemblies allowed the determination of the CAC using a pyrene probe. Of note, diDHA loading modifies the capacity of nanoconjugate self-assembly; PGA-diDHA9.1, 6.4, and 2.2 exhibit CACs of 2.84 µM, 3.96 µM, and 28.87 µM, respectively. This difference in the self-assembly capacity of the conjugates directly relates to the range of sizes obtained according to diDHA loading.

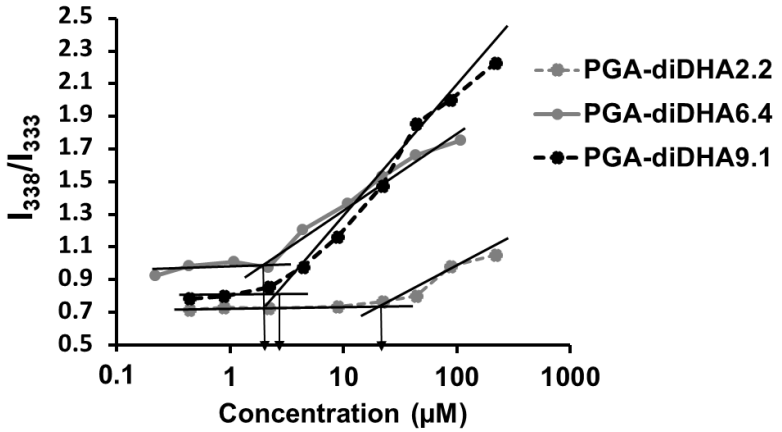

Figure V. 6: CAC determination for PGA-diDHA conjugates by pyrene assay.

We next determined free diDHA content by FPLC to ensure the safety and purity of the synthesized conjugates (**Figure V. 7**). The presence of free diDHA in the conjugates can trigger adverse reactions, as well as undesirable biological activity. For this reason, after the optimization of the synthesis of the PGA-diDHA conjugates, the purification process plays an essential role. After an exhaustive purification by means of dialysis, free diDHA content was determined up to a maximum of 0.15 wt% of the total diDHA loading in all the conjugates, thereby proving the purity and overall drug loading to secure further biological evaluations (see also **Table V.1**).

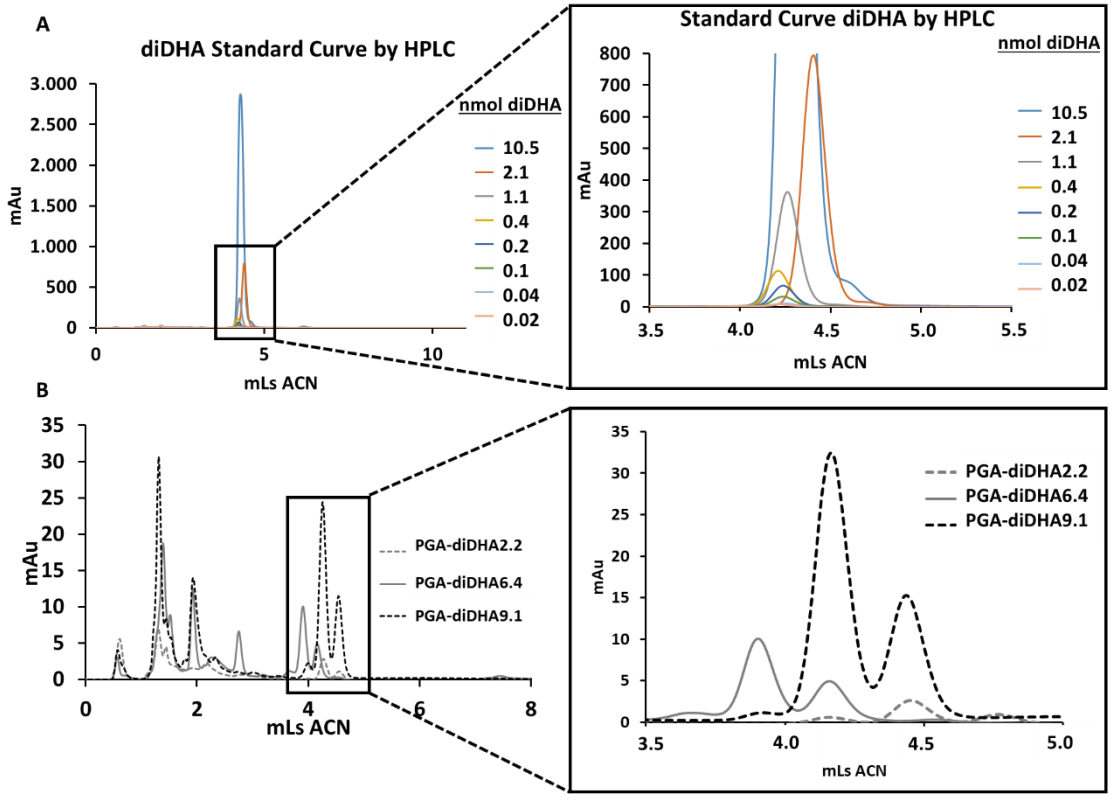

Figure V. 7: Free diDHA content in the PGA-diDHA conjugates by FPLC. **(A)** Chromatograms of the diDHA calibration curve. **(B)** Chromatogram of free diDHA from PGA-diDHA conjugates.

In summary, conjugation of the highly hydrophobic fatty acid diDHA to PGA results in amphiphilic PGA-diDHA conjugates that self-assemble into spherical nanosized objects driven by hydrophobic interactions among diDHA residues, therefore, diDHA loading drives nanoconjugate solution conformation with the greatest core compaction and consequently the smallest size with the highest diDHA loading.

V.2.4. Drug Release Kinetics and Conformation of PGA-diDHA Conjugates

In order to demonstrate diDHA sustained release from the polymeric carrier, we studied drug release kinetics by FPLC under hydrolytic conditions, given the pH-labile nature of the ester bond. We performed this study only for those conjugates that presented promising results in the *in vitro/in vivo* biological evaluation in both the skin and the I/R-cardio models (see **section V.2.5 and V.2.6**). The selected conjugates will be evaluated in an *in vivo* wound healing model in the near future and from the I/R model are currently being tested in a swine model (Dr. Sepúlveda, Hospital La Fe, Valencia, Spain).

We incubated the selected conjugates (PGA-diDHA6.4 and PGA-diDHA2.2) at 37ºC in hydrolytic conditions: pH 5.5 (lysosome) and 7.4 (blood) up to 72 h, discovering a small but sustained diDHA release, with values around 5% and 3% for PGA-diDHA6.4 and PGA-diDHA2.2, respectively. Unexpectedly considering our physico-chemical characterization regarding CAC and size, diDHA release from the PGA-diDHA6.4 conjugate was found to be two-fold faster than that from PGA-diDHA2.2 conjugate, both at pH 5.5 and pH 7.4, most probably due to the different aggregation behavior seen in both conjugates. Furthermore, our data indicates a faster drug release at pH 7.4 (as in the case of PGA-FLUO conjugates - see **Chapter IV** for more details) compared to the acidic pH. In the case of PGA-diDHA6.4, we obtained 5 and 4.5% of free diDHA, and for PGA-diDHA2.2 we obtained a 3 and 2.5% of free diDHA at pH 7.4 and 5.5, respectively (**Figure V. 8A**). In the case of the PGA-diDHA2.2 at both pHs, we observed a sustained diDHA release over the first 24 h of incubation after a rapid diDHA release, followed by an increased release up to 72 h. This plateau may be explained in terms of size, the presence of different species (aggregates) in solution, and the exposure of the drug; the conjugate PGA-diDHA6.4 presents smaller size by number but higher size by intensity (analyzed by DLS) than PGA-diDHA2.2 conjugate, indicating that PGA-diDHA6.4 displays different species in solution, presenting larger aggregates. Thereby, in the PGA-diDHA2.2 conjugate the drug could be found in a more compressed form within the polypeptidic system, provoking a more impeded exposure of the drug and therefore a more sustained release would be obtained over time. As mentioned above, a deeper understanding on solution conformation for PGA-diDHA conjugates by SAXS, SANS, or even AF4 techniques would help to elucidate the reason for such differences on drug release kinetics.

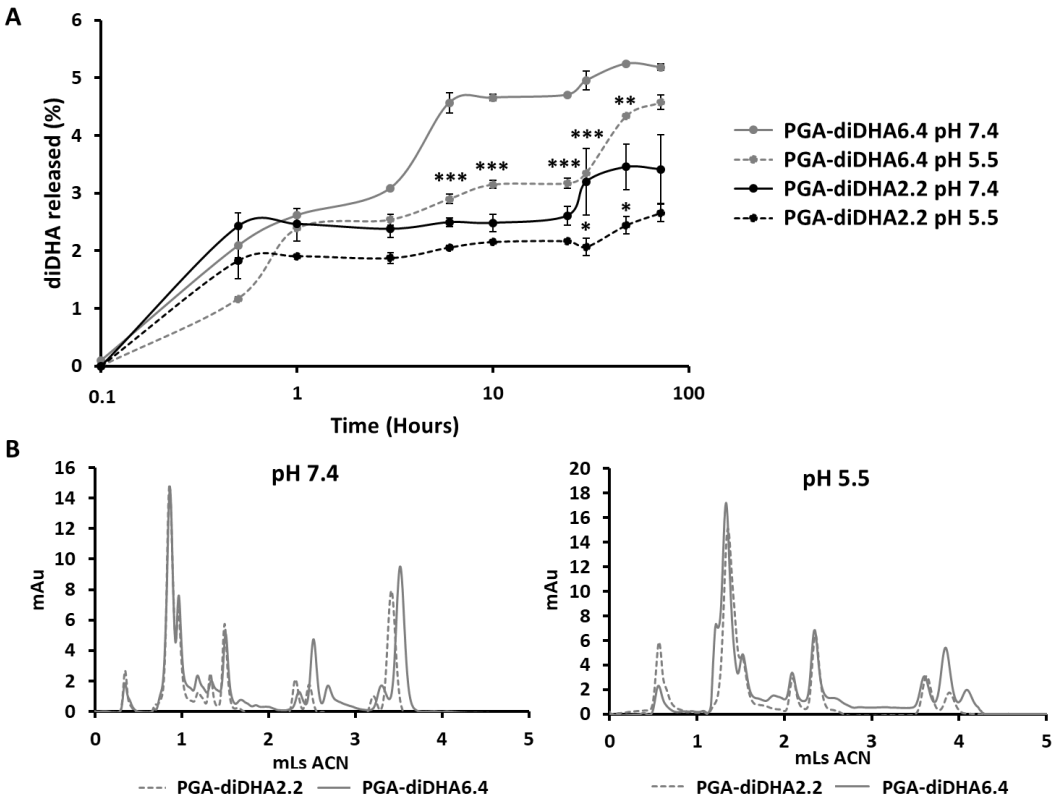

Figure V. 8: Drug release kinetics of PGA-diDHA2.2 and PGA-diDHA6.4 conjugates by FPLC. **(A)** diDHA release kinetics at pH 5.5 and 7.4. **(B)** Chromatograms of released diDHA from PGA-diDHA conjugates (n=3). Asterisks indicate statistically significant differences after ANOVA analyses followed Bonferroni's post hoc tests, mean ± SEM. In all cases, we considered differences to be significant when p***<0.001; p**<0.01; p*<0.05.

To understand these results for a pH labile ester linker, we next sought to analyze the spatial arrangement of the drug within the polymer-drug conjugate and the resulting assembled nanocarrier to further explore drug release characteristics. We analyzed the conjugates by circular dichroism (CD) as a function of PGA-diDHA conjugate concentration and different pHs that mimic the different environments that conjugates encounter following topical administration (**Figure V. 9**).

At pH 7.4, 100% molar side chains in PGA are presented as carboxylates, yielding a full random coil conformation - a more accessible and flexible structure that favors the access to cleavable linker and release the drug. However, at pH 5.5, protonation of PGA side chains represents roughly 50% molar of the overall carboxylates, as derived from the pKa of linear PGA reported in the literature [75]. The protonation induces a partial random coil to alpha-helix conformation transition, thereby generating a much more rigid

and compact structure that inhibits access to the linker and drug release. This pH-dependent secondary structure transition could explain the kinetics of diDHA release in both conjugates.

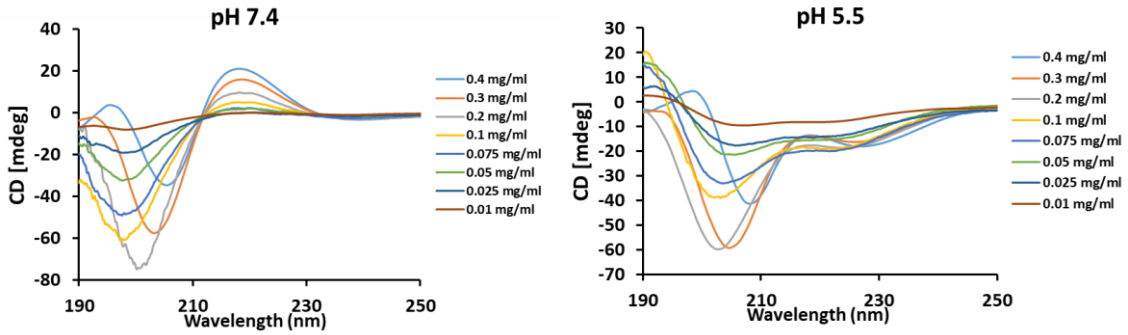

Figure V. 9: Secondary structure of PGA-diDHA6.4 conjugates at pH 7.4 and 5.5 as determined by circular dichroism.

V.2.5. PGA-diDHA Treatment of Skin Wound Healing

V.2.5.1. Cell Viability Studies with PGA-diDHA Conjugates

We performed cell viability assays using immortalized human keratinocytes (HaCaT cells) and human dermal fibroblasts after 72 h of treatment with increasing doses of free diDHA or PGA-diDHA conjugates (0.37 - 23.75 ng/mL diDHA equivalents (eq.)) (**Figure V. 10**). While we failed to observe cell toxicity with PGA-diDHA conjugates at the concentrations used, treatment with free diDHA from 2.97 ng/mL led to significant decreases in cell viability in both cell types.

These results revealed that in addition to providing stability and protection against diDHA degradation, conjugation also minimizes the toxicity of diDHA *in vitro*.

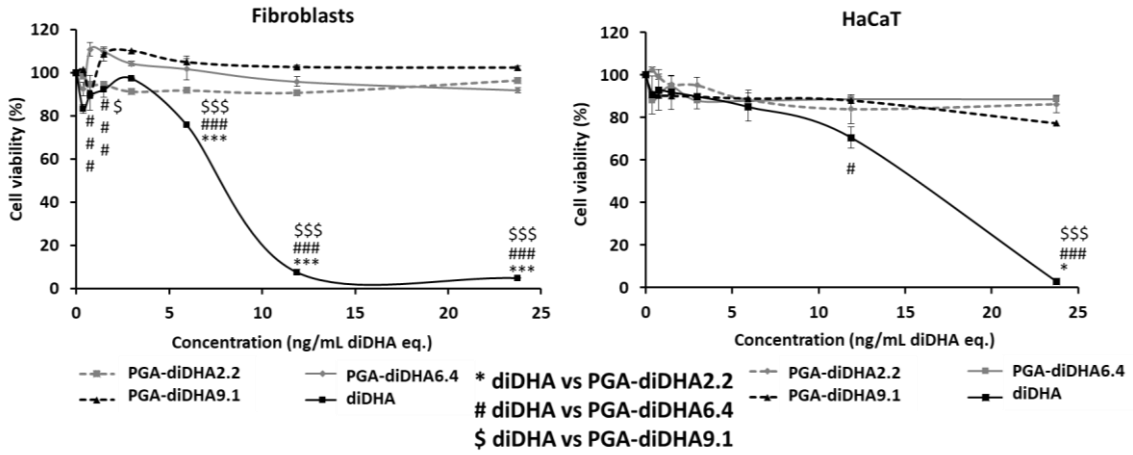

Figure V. 10: Cell viability assays in human fibroblasts (left) and keratinocytes (HaCaT) cells (right) after 72 h of treatment with diDHA or PGA-diDHA conjugates (n=3). Asterisks indicate statistically significant differences after ANOVA analyses followed by Bonferroni's post hoc tests, mean ± SEM. In all cases, we considered differences to be significant when p***<0.001; p**<0.01; p*<0.05.

V.2.5.2. Enhanced Cell Migration by PGA-diDHA Conjugates

The scratch assay evaluates the capacity of compounds to modulate cell migration, acting as a proxy for wound healing potential [76, 77]. Following scratch formation in a human dermal fibroblast cell culture, we directly added the treatments (diDHA and PGA-diDHA conjugates) to the cell culture medium and compared the capacity of free diDHA compared to PGA-diDHA conjugates to enhance the migration of the cells at 24 h post-treatment (**Figure V. 11**). For this study, we used the highest non-toxic concentrations from cell viability assays (2.97 ng/mL diDHA eq.). As controls we included an untreated sample and PGA for better comparison. Interestingly, while diDHA, PGA-diDHA2.2, and PGA-diDHA9.1 treatment failed to significantly alter cell migration and proliferation compared to controls, treatment with PGA-diDHA6.4 induced ~20% increase in fibroblast migration, suggesting that diDHA loading significantly influences conjugate biological activity.

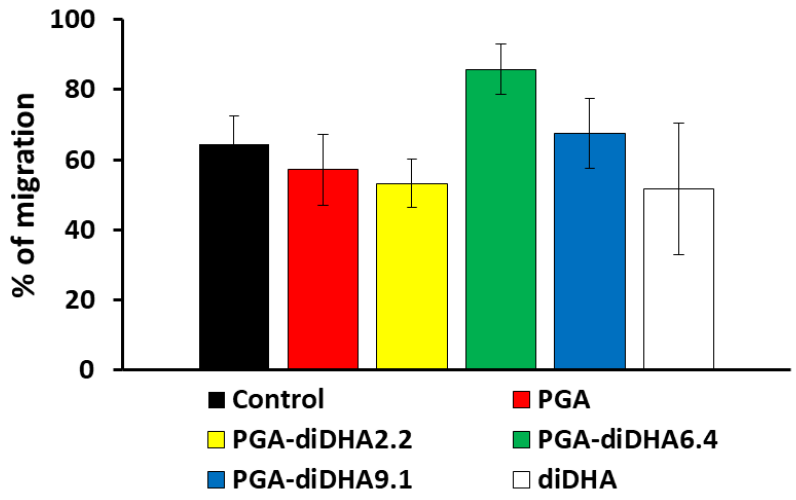

Figure V. 11: Scratch assay using human dermal fibroblasts. Quantification of the percentage of migration of the fibroblasts after 24 h of treatment with PGA, PGA-diDHA conjugates, and diDHA (n=3).

V.2.5.3. PGA-diDHA Permeation into the Epidermis

We evaluated the penetration of PGA-diDHA-OG labeled after 24 h of incubation in human skin explants using Franz diffusion cells. For this study, we used the maximum and minimum diDHA loading in the conjugates (PGA-diDHA9.1-OG and PGA-diDHA2.2-OG) to explore the differences in skin penetration upon diDHA loading. After fixation and tissue processing, we captured confocal images to assess skin penetration. The results suggest that the conjugate with low diDHA loading (PGA-diDHA2.2-OG) can reach the viable epidermis, although the PGA-diDHA9.1-OG conjugate mainly accumulated in the stratum corneum (**Figure V. 12A**). We next quantified OG intensity by Image J software after the permeation studies, corroborating the results obtained by confocal microscopy. In general, the data obtained revealed significantly higher PGA-diDHA2.2-OG intensity compared to the PGA-diDHA9.1-OG in all skin layers, encountering the most remarkable difference in the viable epidermis (**Figure V. 12B**). It was clear that diDHA loading determines skin penetration, whereas PGA-diDHA9.1-OG mainly remains in the stratum corneum, PGA-diDHA2.2-OG efficient found her path up to the viable epidermis, our desired skin layer to trigger the therapeutic response. Most probably due to the greater exposure of diDHA to the cells due to a less compact conjugate solution conformation with lower diDHA loading.

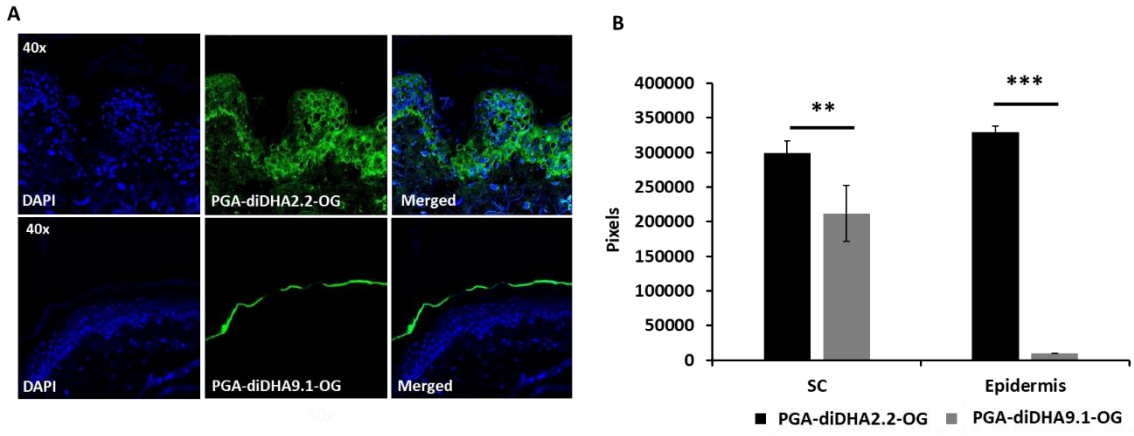

Figure V. 12: Permeation studies of PGA-diDHA-OG conjugates in human skin by Franz diffusion cells. **(A)** Confocal images of PGA-diDHA2.2-OG and PGA-diDHA9.1-OG conjugates after 24 h of permeation. **(B)** Quantification of OG intensity by Image J software in the stratum corneum (SC) and the viable epidermis (n=5). Asterisks indicate statistically significant differences after ANOVA analyses followed by Bonferroni's post hoc tests, mean ± SEM. In all cases, we considered differences to be significant when p***<0.001; p**<0.01; p*<0.05.

Moreover, we studied the capacity of PGA-diDHA-OG conjugates to cross the whole skin, quantifying the signal of OG in the receptor chamber acting as a proxy for the passage of our conjugates/drugs into the circulatory system. We analyzed 2 mL from the receptor chamber at 8 and 24 h of study by Franz diffusion cells and quantified the OG signal at 495 nm in the UV-Vis spectrophotometer (**Figure V. 13**). When we compared results with a negative control using MilliQ water, we failed to observe any OG signal, indicating that conjugates failed to penetrate through the skin and therefore could be unlikely to reach the circulatory system and induce undesirable side effects.

Thus, these data provide evidence regarding the safety for topical application of our PGA-diDHA conjugates.

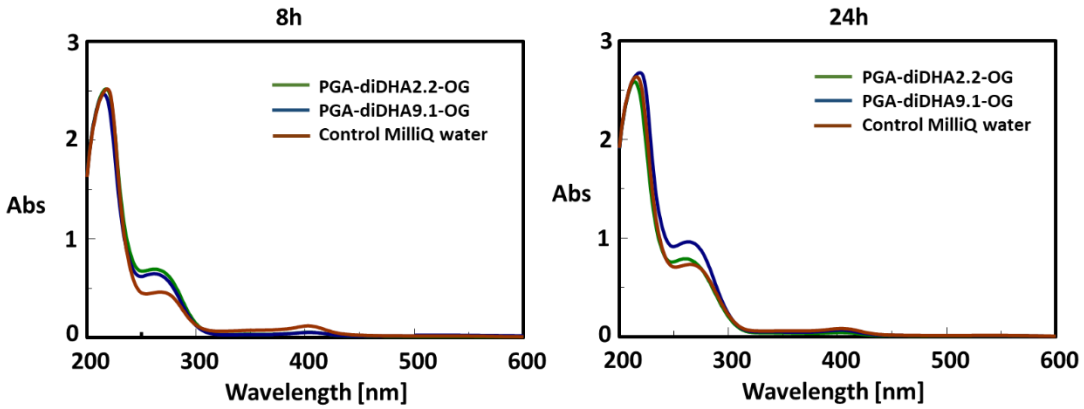

Figure V. 13: UV-Vis spectra of the aliquots from the receptor chamber after 8 and 24 h of permeation in human skin using PGA-diDHA-OG conjugates by Franz diffusion cells.

V.2.6. PGA-diDHA Treatment of Ischemia-Reperfusion (I/R) Injury

As mentioned previously, several studies have demonstrated a role for DHA in the protection of the heart against myocardial ischemia-reperfusion (I/R)-induced injury. Hence, we studied the ability of our PGA-diDHA conjugates to reduce and prevent damage caused by I/R. For this purpose, we employed the family of PGA-diDHA conjugates following well-established synthetic procedures, described above, which we subsequently biologically evaluated *in vitro* and *in vivo*.

V.2.6.1. Enhanced Cell Viability after diDHA Conjugation *In Vitro*

We evaluated cell viability and the capacity of the PGA-diDHA conjugates to reduce damage caused by I/R *in vitro* using murine H9C2 cell line (myoblasts). We assessed the effect of PGA-diDHA conjugates on cell viability by MTS assay to determine the optimum concentration for our cell models. We added PGA, PGA-diDHA2.2, PGA-diDHA6.4, PGA-diDHA9.1, and diDHA at 0.2, 2, 10, and 20 µg/mL diDHA eq. for 72 h (**Figure V. 14**). PGA, PGA-diDHA2.2, and PGA-diDHA6.4 did not exhibit adverse effects on cell viability; however, PGA-diDHA9.1 decreased cell viability by 30% at 10 and 20 µg/mL. Additionally, free diDHA revealed a cytotoxic effect at 2, 10, or 20 µg/mL, but not at 0.2 µg/mL. These data confirmed that conjugation of diDHA to PGA has a positive effect on the cellular model, diminishing the toxicity of diDHA.

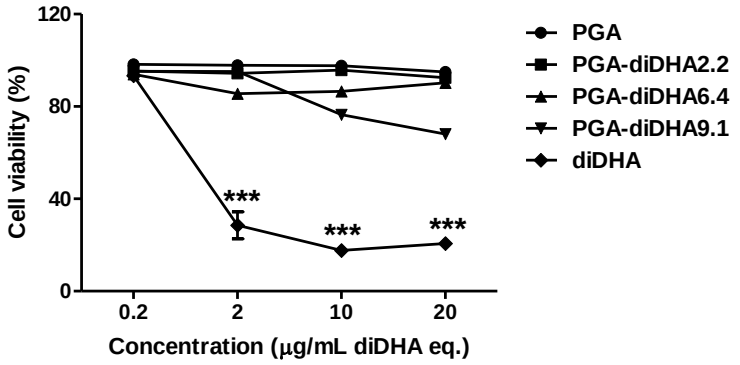

Figure V. 14: Cell viability assays in H9C2 cells after 72 h of treatment with PGA, diDHA, or PGA-diDHA conjugates. Asterisks indicate statistically significant differences after ANOVA analyses followed by Bonferroni's post hoc tests, mean ± SEM. In all cases, we considered differences to be significant when p***<0.001; p**<0.01; p*<0.05.

We next assessed the capacity of PGA-diDHA conjugates to reduce the damage caused by I/R injury *in vitro* using the lactate dehydrogenase (LDH) assay, which is widely used to study cell damage (higher amounts of LDH secretion correlates with more severe cellular damage). In this study, we assessed the amount of LDH in the culture medium after 72 h of exposition to PGA, PGA-diDHA2.2, PGA-diDHA6.4, PGA-diDHA9.1, and free diDHA at the same concentrations used for cell viability assays, compared to control cells (1% LDH release). This experiment reflects the importance of the diDHA availability, as although non-significant differences were observed, there is a clear trend on possible cell damage recovery at 0.2 µg/mL for free diDHA although an increase in concentration reverts such effect due to possible cytotoxicity as shown before (**Figure V.14**). In the case of the conjugates, the same effect is observed but at different drug concentration as it is clearly correlated with the drug release kinetics profile (**Figure V. 15**). Apoptosis and autophagy studies as mean of cell death/recovery with these diDHA derivatives have been also performed with much more significant results than those obtained with LDH, as it seems mitochondria-mediated cell death is the molecular mechanism followed. PGA-diDHA6.4 conjugate revealed the higher prevention of cell death *in vitro* after an I/R injury (data included in the PhD thesis of Sandra Tejedor, Dr. Sepúlveda Lab., Hospital La Fe, Valencia, Spain), and also the presence of PGA-diDHA2.2 triggered a recovery trend.

Based on the promising results *in vitro*, we moved to the *in vivo* experiments with the conjugates that revealed the best therapeutic potential: PGA-diDHA2.2 and PGA-

diDHA6.4. As PGA-diDHA9.1 clearly displayed cytotoxic effects at high concentration against H9C2 cells we did not further consider it for *in vivo* experiments.

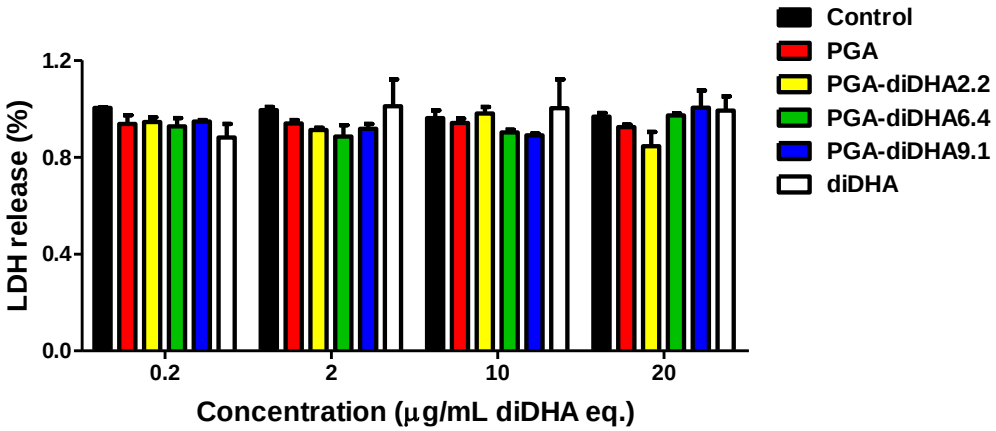

Figure V. 15: LDH release to the culture medium in H9C2 cells after 72 h of treatment with PGA, diDHA, or PGA-diDHA conjugates. Results obtained were normalized with values obtained from control cells. Data were obtained from three independent experiments by triplicate and presented as mean ± SEM.

V.2.6.2. PGA-diDHA6.4 Treatment Decreases Myocardial Infarct Size in an I/R Model *In Vivo*

We evaluated the selected PGA-diDHA conjugates *in vivo* in a rat I/R model to assess the protective capacity of conjugates on cardiomyocytes. We split rats into different groups and induced acute myocardial infarction (AMI) as described in the materials and methods. We treated the control group with PBS, and we used a negative group without I/R-induced injury (sham or placebo surgery). Based on previous results *in vitro*, we decided to test PGA-diDHA2.2 and PGA-diDHA6.4 conjugates at 10 µg/mL diDHA eq. We stained representative pictures of heart slices with the redox indicator 2,3,5 triphenyl tetrazolium chloride (TTC) after the surgical procedure (**Figure V. 16A**). **Figure V. 16B** depicts the differences between infarct sizes observed. Following the I/R procedure and PBS injection as control, we observed an infarct size of 28.32 ± 5.57%. We observed a non-significant reduction in infarct size in the group treated with PGA-diDHA2.2, obtaining values similar to the control (23.43 ± 1.91%); however, we discovered significantly lower tissue damage in the group treated with PGA-diDHA6.4 conjugate (11.99 ± 3.75%). These data suggest that PGA conjugation of diDHA has beneficial effects regarding the treatment of AMI through a reduction in the required dose of diDHA and an increase in its therapeutic efficiency. Also, this effect is concentration

dependent, and in this case a higher loading resulted in a greater therapeutic output most probably due to the higher diDHA bioavailability at the site of action (see drug release kinetics studies, **section V.2.4**).

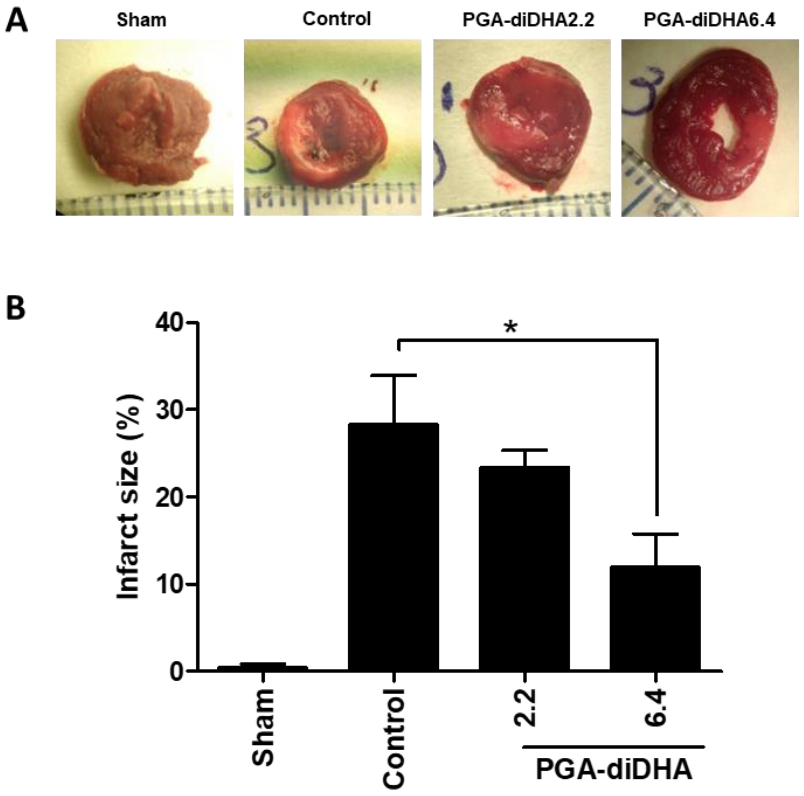

Figure V. 16: PGA-diDHA6.4 conjugate decreases myocardial infarct size in an I/R model *in vivo*. **(A)** Representative pictures of TTC staining in heart slices determined the effect of the different experimental procedures on myocardial infarct size. **(B)** Myocardial infarct size expressed as the percentage of area at risk. Sham group without I/R (n=4), control group treated with PBS (n=4), PGA-diDHA2.2 (n=6), and PGA-diDHA6.4 (n=5). Results were presented as mean ± SEM and analyzed by ANOVA. All groups are compared with the I/R condition (*$p<0.05$).

V.3. Conclusions

The use of diDHA provides several advantages in the tissue healing due to its ability to promote the reepithelization and closure of the wound area and its anti-inflammatory activity. To improve the physico-chemical characteristics of diDHA and, therefore, the effectiveness of the treatment, we successfully synthesized and characterized a new family of PGA-diDHA conjugates. We discovered that diDHA

loading determines the final conjugate solution conformation, including size and the critical concentration of aggregation giving a more compact constructs upon increasing drug loading, which is also a key feature modulating drug release kinetics. Our analyses demonstrated that PGA conjugation enhanced diDHA stability by protecting the lipid and reducing degradation over time while also increasing its aqueous solubility.

Moreover, PGA conjugation to diDHA led to a marked improvement in dermal cell viability when compared to the free drug, most probably due to the reduction of the diDHA degradation subproducts. Of note, diDHA loading also represents a crucial parameter towards achieving an adequate biological activity; migration and skin penetration studies revealed that lower diDHA loadings prompted better therapeutic activity, thereby promoting enhanced closure of the wound and skin penetration.

These results lay the groundwork for polymer conjugation as an effective means to diminish or avoid drug degradation and adverse effects. Moreover, the use of polyglutamates as a carrier enhances the skin penetration of conjugated drugs, as has been demonstrated in previous chapters of this Thesis, which also contributes to the effectiveness of the treatment. Future studies will focus on developing a diabetic rat model to evaluate the proliferative and anti-inflammatory activity of conjugates with the low-medium diDHA loading.

Looking at I/R-induced damage applications, our results showed that diDHA loadings in the conjugate play a key role in the final biological activity and more importantly, PGA-diDHA6.4 conjugate has the best therapeutic effects under I/R condition *in vitro* and *in vivo* in comparison with free diDHA in terms of safety as well as therapeutic efficiency.

Infusion of nanoconjugates and free diDHA in an *in vivo* I/R rat model showed that heart infarct size was significantly reduced when PGA-diDHA6.4 was administrated before reperfusion in comparison with free diDHA at the same dose. Collectively, our data showed that PGA-diDHA6.4 could be effective in mitigating I/R-induced injury thereby providing a new therapeutic agent for future clinical studies.

V.4. Materials and Methods

V.4.1. Materials

All analytical grade organic solvents and anhydrous N,N-Dimethylformamide (DMF, ≥99.8% anhydrous) were purchased from Scharlab S.L. (Spain) and used without further purification. Poly-(alpha-L-glutamic acid) (Mw: 41.3 kDa, PDI: 1.2, 273 subunits per polymer) was obtained from Polypeptide Therapeutic Solutions S.L. (Spain). D*idocosahexaenoic* acid (diDHA) was purchased from Nu-Chek Prep, Inc. (Elysian, MN, USA). Oregon Green 488 cadaverine was purchased from Invitrogen (Spain). Ultrapure water with a resistivity of 18 MΩ cm was used in all aqueous preparations (MilliQ water). Phenazine methosulfate (PMS) was supplied by Sigma (Spain). Dulbecco's Modified Eagle's Medium (DMEM) with Glutamax was purchased from Fisher (Spain). DMEM, phosphate buffer saline (PBS), fetal bovine serum (FBS) Medium 200, trypsin, and penicillin/streptomycin were provided from Gibco (Spain). (3-(4,5-dimethylthiazol-2-yl)-5-(3-carboxymethoxyphenyl)-2-(4-sulfophenyl)-2H-tetrazolium) (MTS) was supplied by Promega (Spain).

V.4.2. Physico-Chemical Characterization Methods

V.4.2.1. Nuclear Magnetic Resonance (NMR) Spectroscopy

NMR spectra were recorded at 27°C (300 K) on a 500 MHz Bruker spectrometer (Billerica, US). Data were processed with the software Mestrenova (Bruker GmbH, Germany). Samples were typically prepared at 5 mg/mL in deuterated solvents.

V.4.2.2. Ultraviolet-Visible (UV-Vis) Spectroscopy

UV-Vis measurements were performed using V-630 spectrophotometer (JASCO Corporation, Spain) at 25°C with 1.0 cm matched quartz cells and with a spectral bandwidth of 0.5 nm. Determination of total OG content was measured by UV-Vis spectroscopy. To obtain a calibration curve, free dye was diluted in MilliQ water to give a concentration range of 0.000250 – 0.000025 mg/mL. The total dye loading of the conjugates at different concentrations (0.5, 0.25, 0.1 mg/mL) was determined by measuring the absorbance of the samples at 495 nm in MilliQ water.

V.4.2.3. Fluorescence Spectroscopy

Fluorescence experiments were performed using a JASCO FP-6500 spectrofluorimeter (JASCO Corporation, Spain) at 25ºC with 1cm quartz cells. Pyrene assay was performed as published elsewhere to determine the critical concentration of aggregation (CAC) [78]. In brief, polymers were dissolved and diluted ranging from 0.44 - 240 μM in PBS with a final volume of 1 mL, to which 3 μL of the pyrene stock solution (0.02 mg/mL) in acetone was added. Then, all solutions were placed in vials and were incubated at 37ºC for 2 h to evaporate acetone. The solutions were then allowed to rest overnight at r.t. and then transferred into a 1 mL quartz cuvette, and the excitation spectra from 300 - 360 were recorded with emission set to 390 nm on the spectrofluorometer. Excitation and emission band slits were set to 5 and 2.5 nm. The I_{338}/I_{333} fluorescence intensity was plotted as a function of logarithmic polymer concentration. The I_{338}/I_{333} ratio increased steadily with increasing polymer concentration and became sigmoidal in the crossover region. The CAC was determined at the intersection of the horizontal tangent line through points of low polymer concentration and the tangent line of the curve at the inflection point.

V.4.2.4. Transmission Electron Microscopy (TEM)

TEM images were recorded using a JOEL 2100 transmission electron microscope. Samples were applied directly onto carbon film on 200 mesh copper grids at 2 mg/mL. Any excess of the sample was carefully removed by capillary action, and the grids were immediately stained with one drop of 0.1% phosphotungstic acid for 30 s. Excess stain was removed by capillary action.

V.4.2.5. Dynamic Light Scattering (DLS)

DLS measurements were performed using a Malvern ZetaSizer NanoZS instrument (Malvern Instruments Ltd., UK), equipped with a 532 nm laser at a fixed scattering angle of 173°. Solutions were sonicated for 10 min and allowed to equilibrate for the required time, filtered through a 0.45 μm cellulose membrane filter, and then measured. The samples were dissolved in MilliQ water and 10 mM PB. Size distribution by number and intensity (diameter, nm) were measured in triplicate.

Z-potential measurements were performed at 20ºC using a Malvern ZetaSizer NanoZS instrument (Malvern Instruments Ltd., UK), equipped with a 532 nm laser using disposable folded capillary cells. Z-potential was measured for the highest concentration of each polymer (2 mg/mL) in 1 mM KCl in MilliQ water. The solutions were filtered through a 0.45 µm cellulose membrane filter. Z-potential was measured for each sample in triplicate.

V.4.2.6. Fast Protein Liquid Chromatography (FPLC)

Analytical determination of the free drug was performed on an ETTAN LC equipment (Amersham Biosciences, Spain). The measurements were performed using a C-18 LiChrospher analytical column (125 x 4.0 mm) (Scharlab S.L., Spain), with a flow rate of 0.7 mL/min, a 15 µL loop, and isocratic conditions with 100% acetonitrile (ACN). Detection of the alkene bonds of diDHA absorbance was measured at λ = 200 nm. The calibration curve was constructed using commercial diDHA, showing a linear response within the concentration range employed (0.001 - 0.5 mg/mL).

- **Free Drug Content**

PGA-diDHA conjugates were dissolved in water at 1 mg/mL and lyophilized to form a thin film at the bottom of glass vials, protected from light. Then, 300 µL of ACN was added slowly over the films, and the vials sealed for 30 min. The contents were then physically mixed via a glass pipette and vortex to ensure thorough washing of the solid polymers. The liquid was then transferred to a new glass container for centrifugation, and 80 µL of the supernatant was filtered (0.45 µm) and injected in the FPLC system. Samples were measured repeatedly (n=3). The area for peak(s) from 3.5 - 4 mL were used against a standard curve of diDHA to determine the free diDHA in the conjugates.

- **Drug Release Kinetics**

Drug release kinetics of PGA-diDHA2.2 and PGA-diDHA6.4 conjugates were performed at two different pHs (5.5 and 7.4). A stock solution of the conjugates was prepared in PBS buffer (5 mg/mL) and was divided into 100 µL aliquots; each aliquot was then incubated at 37ºC over times ranging from 0 to 72 h. After incubation, the samples were lyophilized, the residue resuspended in 500 µL of ACN, and then centrifuged 5 min at 10,000 rpm to separate the free drug from the polymer. Finally, the

supernatant was evaporated under reduced pressure using the speedvac (1:30 h, 80ºC, 0.01 vacuum). The final residue was resuspended in 300 µL of ACN and filtered (0.45 µm) for analysis. Samples were measured in triplicate. The area for peak(s) from 3.5 - 4 mL were used against a standard curve of diDHA to determine the final free diDHA released.

V.4.2.7. Circular Dichroism (CD)

CD spectroscopy was performed with a J-815 CD Spectrometer using a PTC-423 Peltier thermostated cell holder with a JULABO F250 recirculating cooler (All JASCO Corporation, Spain). A nitrogen flow (~2.7 L/min) was led through the spectrometer and controlled with a nitrogen flow monitor (Afriso Euro-Index, Germany). Samples were dissolved in MilliQ water or 10 mM PB, and employed at different concentrations (0.01-0.4 mg/mL). Samples were measured in triplicate in a quartz cuvette with d = 0.1 cm.

V.4.2.8. Stability Over Time by NMR Analysis

^{1}H-NMR was used to track the oxidation of fatty acids. Samples were prepared as follows: PGA-diDHA conjugates (PGA-diDHA2.2, PGA-diDHA6.4 and PGA-diDHA9.1) were dissolved at 10 mg/mL in D_2O and transferred to an NMR tube. To these, an insert with 1 mg/mL of 4,4-dimethyl-4-silapentane-1-sulfonic acid (DSS) in D_2O was added. Free diDHA was dissolved at 10 mg/mL in MeOD with 0.03% of tetramethylsilane (TMS) as the internal standard. The NMR tubes were capped, sealed with parafilm to prevent evaporation, and placed in the dark, wrapped in foil. At each time point, samples were analyzed by ^{1}H-NMR on a Bruker 500 MHz spectrometer (relaxation delay time = 10 seconds, 500 scans) and the spectra analyzed using TopSpin 3.5 pl 7 software. To calculate the percentage of degradation, the integration of the internal standard was set to 1, and then the alkenyl peaks for diDHA from 5.66 - 5.17 ppm at each time point were compared to the integration in the same region at day 0.

V.4.2.9. Stability Over Time by Malondialdehyde Colorimetric Assay

Malondialdehyde (MDA) formation was evaluated over time to assess the protective function of PGA conjugation on the prevention of lipid peroxidation by diDHA. PGA-diDHA conjugates were dissolved at 4 mg/mL in 10 mM PB pH 7.4 (-NaCl, -Mg^{2+}, -Ca^{2+}) and free diDHA in ethanol. Both were allowed to incubate at r.t.,

capped and sealed with parafilm, and protected from light. At each time point (one day, one week, two weeks, and one month), an aliquot was taken from each sample, and MDA levels were quantified via the TBARS (thiobarbituric acid reactive substance) Lipid Peroxidation Assay Kit (Sigma Aldrich, Spain). Briefly, 50 μL of sample or standard were mixed with 300 μL TBA solution and heated at 95ºC for 1 h, the solutions were then cooled for 5 min, and fluorescence monitored at 530/590 (Ex/Em) using a Victor^{2}Wallac™ plate reader (Perkin Elmer, Spain).

V.4.2.10. Quantitative Determination of the Triglyceride Content in the PGA-diDHA Conjugates

Total triglyceride (TG) content in the conjugates was quantified using a LabAssay^{TM} Triglyceride kit (Wako Chemicals GmbH, Germany), which is based on the enzymatic GPO-DAOS method [79]. Briefly, a calibration curve was constructed using concentrations of glycerol ranging from 0 to 134.62 nmol. PGA-diDHA conjugates were dissolved at 15 mg/mL in MilliQ water and 50 μL of the samples were added to 250 μL of color reagent containing chromogen substrate (prepared according to the assay kit instructions). The mixture was incubated at 37ºC for 5 min, and the absorbance was measured at 590 nm using a Victor^{2}Wallac™ plate reader (Perkin Elmer, Spain). TG content was determined according to standard solutions.

V.4.3. Synthetic Protocols

V.4.3.1 Synthesis of Poly-L-Glutamate Didocosahexaenoic Acid Conjugates

PGA (100 mg, 3 μmol, 273 eq. GAU, 1 eq.) was dissolved in 10 mL dry DMF in a 100 mL round bottom under an inert atmosphere. DMTMM·BF_4 (19.0 mg, 0.06 mmol, 20.0 eq.) was dissolved in 1 mL dry DMF under nitrogen and added dropwise to the PGA solution. A catalytic amount of DMAP was added in 1 mL dry DMF, and the solution was stirred for 30 min. diDHA (27.6 mg, 0.04 mmol, 13.6 eq.) was dissolved in 1 mL dry DMF (0.3 ppm BHT added) and the pH adjusted to 8 with N,N-Diisopropylethylamine (DIEA). The solution was protected from light and allowed to stir at r.t. for 3 days until all diDHA had reacted, as visualized by *thin-layer chromatography (*TLC) (80:20:1 hexanes:ether:acetic acid, retention factor (R_f): R_f (diDHA) = 0.2 and R_f (PGA) = 0.1). The pH was adjusted as necessary to pH 8, and the solution precipitated into cold diethyl

ether. The precipitate was then rinsed (with vortexing) three times with ether. Then, the precipitate was suspended in water, and the pH was adjusted to 8 with sodium carbonate/bicarbonate buffer pH 10. This solution was then dialyzed (MWCO 3000) protected from light against sodium carbonate/bicarbonate buffer pH 10 for 12 h followed by MilliQ water to remove salts. The purified product was then lyophilized and stored under an inert atmosphere at -20°C protected from light.

V.4.3.2 Oregon Green Labeling of PGA-diDHA Conjugates

PGA (600 mg, 0.02 mmol, 273 eq. GAU, 1 eq.) was dissolved in 100 mL dry DMF in a two-neck round bottom flask under nitrogen atmosphere. DMTMM·BF_4 (23 mg, 0.07 mmol, 4.1 eq.) and a catalytic amount of DMAP were added in 10 mL additional dry DMF and the solution allowed to stir for 30 min. OG (23 mg, 0.05 mmol, 2.7 eq.) was added to the reaction mixture in 10 ml dry DMF, protected from light. The pH was adjusted to 8 with DIEA and stirred for three days. The reaction mixture was then either purified or further modified with diDHA. For example, for 5 mol% diDHA modification, additional DMTMM·BF_4 (38 mg, 0.12 mmol, 20.5 eq.) and catalytic DMAP in 10 mL DMF were added to one third of the crude reaction mixture for 30 min, followed by the addition of diDHA (55 mg, 0.08 mmol, 13.6 eq.). The pH was again adjusted to 8 with DIEA and allowed to react for three days. At the end of the reaction, the pH was adjusted to pH 8, and the solution precipitated into cold diethyl ether. The precipitate was then rinsed (with vortexing) three times with ether. Then, the precipitate was suspended in water, and the pH was adjusted to 8 with sodium carbonate/bicarbonate buffer pH 10. This solution was then dialyzed (MWCO 3000) protected from light against sodium carbonate/bicarbonate buffer pH 10 for 12 h followed by MilliQ water to remove salts. The purified product was then lyophilized and stored under an inert atmosphere at -20°C protected from light.

V.4.4. Biological Evaluation of PGA-diDHA Conjugates

V.4.4.1. Skin Wound Healing

V.4.4.1.1. *In Vitro* Evaluation

V.4.4.1.1.1. Cell Viability

To carry out the *in vitro* cytotoxicity studies, two cell lines were used: human immortalized non-tumorigenic keratinocytes (HaCaT cells), supplied by CLS Cell Lines Service (Germany), and human fibroblasts supplied by Hospital La Fe (Valencia, Spain). High glucose DMEM Glutamax (Fisher, Spain) was used for keratinocyte culture and DMEM (Gibco, Spain) for fibroblast culture; both were supplemented with 2% penicillin/streptomycin and 50 mL of FBS in a humidified incubator (Hucoa-Erlöss S.A., Spain) at 5% CO_2 and 37°C.

For the cell viability assays, 50 µL of cells were seeded in 96-well plates at a concentration of 4,000 cells/well for HaCaT cells and 2,000 cells/well for human fibroblasts. After 24 h, 50 µL of each treatment was added, reaching a final volume of 100 µL. All treatments were previously filtered (pore size 0.22 µm). Cells were incubated with samples or controls for 72 h before performing MTS assay. For this assay, 20 µL of PMS and MTS (1:20) solution were added. After 3 h of incubation, absorbance values were captured at 490 nm using a Victor^{2}Wallac™ plate reader (Perkin Elmer, Spain). The absorbance values were represented as the percentage of cell viability relative to the 100% cell viability of untreated control cells. The concentrations of PGA, diDHA, and PGA-diDHA conjugates were in a range from 0.37 to 23.75 ng/mL diDHA eq.

V.4.4.1.1.2. Scratch Assays

Human fibroblasts were seeded in a 24-well plate at a concentration of 75,000 cells/well. After 24 h, simple scratch wounds were made with a white Gilson pipette tip in all wells, culture media was removed, and treatments were applied at a 2.97 ng/mL diDHA eq. in 400 µL of media. All treatments were previously filtered (pore size 0.22 µm). A Leica DMI6000 automatic inverted microscope (Leica, Germany) was used to follow the migration of the cells, taking pictures every half hour for 24 h. Finally, the reduction in scratch wound area compared to time 0 was calculated.

V.4.4.1.2. *Ex Vivo* Evaluation

V.4.4.1.2.1. Visualization of Dermal Penetration

Breast skin samples were obtained with informed consent from healthy women undergoing plastic surgery (kindly donated by Hospital la Fe, Valencia, Spain). Immediately after excision, the subcutaneous fatty tissue was removed using a scalpel. The skin was cut into 4 cm^2 pieces, wrapped in aluminum foil and stored at -20ºC until use. Permeation study was developed using Franz diffusion cells (Logan Instruments Corp., USA). The skin was fixed between the donor and the receptor chamber, so that stratum corneum faced upwards. The receptor chamber was filled with 8 mL of 0.01 M PBS pH 7.4 and mixed with a magnetic stirring bar while the temperature was kept at 37ºC. The skin was placed between the chambers and 100 µL of a solution of 10 mg/mL of PGA-diDHA2.2-OG and PGA-diDHA9.1-OG in water were topically applied to the skin surface. 2 mL sample were taken from the receptor chamber at 8 and 24 h for further analysis by UV-Vis and immediately refilled with fresh solution. After 24 h, skin samples were gently rinsed twice with 0.1% PBS-BSA and incubated in 4% paraformaldehyde (PFA) for 24 h at r.t. Then samples were washed with 30% sucrose in PBS and retained in said solution for 24 h at 4ºC. Finally, skin samples were washed twice with PBS and preserved in a cryopreservation solution (40% 0.1 M PB, 30% ethylene glycol and 30% glycerol) at 4ºC until use. Finally, skin samples were included in the optimum cutting temperature inclusion medium, and slides of 5 µm were performed with the cryostat version CM1850 UV (Leica, Germany).

V.4.4.1.2.2. Confocal Microscopy

The permeation of the fluorescent labeled-conjugates by Franz diffusion cells was evaluated by confocal microscopy. Excitation was performed with an argon laser ((OG, 496 nm) and blue diode (Hoechst, 405 nm). Images were captured at an 8-bit greyscale and processed with LCS software version 2.5.1347a (Leica Germany) containing multicolor, macro, and 3D components. Control tissue that follows the same incubation time with MilliQ water was also analyzed to establish the autofluorescence. OG intensity was quantified five times per sample using Image J software and expressed as pixels versus the thickness of the skin (µm). The controlled intensity was subtracted in each case.

V.4.4.2. Ischemia-Reperfusion Injury

V.4.4.2.1. *In Vitro* Evaluation

H9C2 cells were seeded on 96-well plates and were treated with increasing concentrations of PGA, diDHA, and PGA-diDHA conjugates, using 0.2, 2, 10, and 20 µg/mL diDHA eq. for 72 h in 190 µL of culture medium. Then, 100 µl of the culture medium were taken for LDH activity measurement, following the recommended protocol (Roche, Spain). Triton-treated cells were used as a positive control of the assay. The absorbance of LDH activity was measured at 490 nm using a Victor^{2}Wallac™ plate reader (Perkin Elmer, Spain).

Cell viability was determined using the MTS assay (CellTiter 96® AQ_{ueous} Non-Radioactive Cell Proliferation Assay, Promega, USA). Cells were supplemented with MTS solution (10 µL/well) and incubated for 3 h at 37°C. Then, the absorbance was recorded at 490 nm using a Victor^{2}Wallac™ plate reader (Perkin Elmer, Spain).

V.4.4.2.2. *In Vivo* Evaluation

Adult male Wistar rats (Charles River Laboratories, Inc., US) weighing 350 – 400 g were housed in a standard vivarium with free access to food and water. All procedures were approved by institutional ethical and animal care committees. Before experiments, animals were randomized into experimental groups. Rats were anesthetized intraperitoneally with fentanyl (Acost-Comercial Generis Pharma, S.L., Spain) at 0.05 mg/kg and by inhalation with Sevorane (Abbot, Spain). Once animals were anesthetized, intubation was carried out to ensure proper anesthesia during the procedure. Later, the left paw was tied to feel the heart beating. The left chest area was sterilized, and a thoracotomy was performed. For myocardial ischemia, the left anterior descending coronary artery was occluded with a silk suture as previously described [80]. Different treatments at 10 µg/mL diDHA eq. (PGA-diDHA2.2 and PGA-diDHA6.4) were prepared in PBS and were injected after 15 min of ischemia. PBS alone was injected in control rats, and the sham group was used as a negative control.

V.5. References

[1] N. Meschi, A.B. Castro, K. Vandamme, M. Quirynen, P. Lambrechts, The impact of autologous platelet concentrates on endodontic healing: a systematic review, Platelets 27(7) (2016) 613-633.
[2] T. Velnar, T. Bailey, V. Smrkolj, The Wound Healing Process: An Overview of the Cellular and Molecular Mechanisms, J Int Med Res 37(5) (2009) 1528-1542.
[3] J. Boateng, O. Catanzano, Advanced Therapeutic Dressings for Effective Wound Healing--A Review, J Pharm Sci 104(11) (2015) 3653-80.
[4] J.M. Reinke, H. Sorg, Wound repair and regeneration, Eur Surg Res 49(1) (2012) 35-43.
[5] M.P. Rowan, L.C. Cancio, E.A. Elster, D.M. Burmeister, L.F. Rose, S. Natesan, R.K. Chan, R.J. Christy, K.K. Chung, Burn wound healing and treatment: review and advancements, Crit Care 19 (2015) 243.
[6] A.C. Gonzalez, T.F. Costa, Z.A. Andrade, A.R. Medrado, Wound healing - A literature review, An Bras Dermatol 91(5) (2016) 614-620.
[7] S.A. Eming, T. Krieg, J.M. Davidson, Inflammation in wound repair: molecular and cellular mechanisms, J Invest Dermatol 127(3) (2007) 514-25.
[8] S.R. Opalenik, J.M. Davidson, Fibroblast differentiation of bone marrow-derived cells during wound repair, FASEB J 19(11) (2005) 1561-3.
[9] G.C. Gurtner, S. Werner, Y. Barrandon, M.T. Longaker, Wound repair and regeneration, Nature 453(7193) (2008) 314-21.
[10] D.G. Greenhalgh, The role of apoptosis in wound healing, Int J Biochem Cell Biol 30(9) (1998) 1019-30.
[11] H.N. Lovvorn, D.T. Cheung, M.E. Nimni, N. Perelman, J.M. Estes, N.S. Adzick, Relative distribution and crosslinking of collagen distinguish fetal from adult sheep wound repair, J Pediatr Surg 34(1) (1999) 218-23.
[12] R.F. Pereira, P.J. Bártolo, Traditional Therapies for Skin Wound Healing, Adv Wound Care 5(5) (2014) 208-229.
[13] G. Han, R. Ceilley, Chronic Wound Healing: A Review of Current Management and Treatments, Adv Therapy 34(3) (2017) 599-610.
[14] V. Jones, J.E. Grey, K.G. Harding, Wound dressings, BMJ 332(7544) (2006) 777-80.
[15] E.L. Arantes, N. Dragano, A. Ramalho, D. Vitorino, G.F. de-Souza, M.H. Lima, L.A. Velloso, E.P. Araújo, Topical Docosahexaenoic Acid (DHA) Accelerates Skin Wound Healing in Rats and Activates GPR120, Biol Res Nurs 18(4) (2016) 411-9.
[16] C.R. Cardoso, M.A. Souza, E.A. Ferro, S. Favoreto, J.D. Pena, Influence of topical administration of n-3 and n-6 essential and n-9 nonessential fatty acids on the healing of cutaneous wounds, Wound Repair Regen 12(2) (2004) 235-43.
[17] E. Hatanaka, A. Dermargos, A.E. Hirata, M.A. Vinolo, A.R. Carpinelli, P. Newsholme, H.A. Armelin, R. Curi, Oleic, linoleic and linolenic acids increase ros production by fibroblasts via NADPH oxidase activation, PLoS One 8(4) (2013) e58626.
[18] K.I. Shingel, M.P. Faure, L. Azoulay, C. Roberge, R.J. Deckelbaum, Solid emulsion gel as a vehicle for delivery of polyunsaturated fatty acids: implications for tissue repair, dermal angiogenesis and wound healing, J Tissue Eng Regen Med 2(7) (2008) 383-93.
[19] L.M. Pereira, E. Hatanaka, E.F. Martins, F. Oliveira, E.A. Liberti, S.H. Farsky, R. Curi, T.C. Pithon-Curi, Effect of oleic and linoleic acids on the inflammatory phase of wound healing in rats, Cell Biochem Funct 26(2) (2008) 197-204.
[20] A.A. Spector, Essentiality of fatty acids, Lipids 34 Suppl (1999) S1-3.

[21] J. Lengqvist, A. Mata De Urquiza, A.C. Bergman, T.M. Willson, J. Sjövall, T. Perlmann, W.J. Griffiths, Polyunsaturated fatty acids including docosahexaenoic and arachidonic acid bind to the retinoid X receptor alpha ligand-binding domain, Mol Cell Proteomics 3(7) (2004) 692-703.
[22] J.C. McDaniel, M. Belury, K. Ahijevych, W. Blakely, Omega-3 fatty acids effect on wound healing, Wound Repair Regen 16(3) (2008) 337-45.
[23] E. Theodoratou, G. McNeill, R. Cetnarskyj, S.M. Farrington, A. Tenesa, R. Barnetson, M. Porteous, M. Dunlop, H. Campbell, Dietary fatty acids and colorectal cancer: a case-control study, Am J Epidemiol 166(2) (2007) 181-95.
[24] K. Kuriki, K. Wakai, K. Hirose, K. Matsuo, H. Ito, T. Suzuki, T. Saito, Y. Kanemitsu, T. Hirai, T. Kato, M. Tatematsu, K. Tajima, Risk of colorectal cancer is linked to erythrocyte compositions of fatty acids as biomarkers for dietary intakes of fish, fat, and fatty acids, Cancer Epidemiol Biomarkers Prev 15(10) (2006) 1791-8.
[25] M.C. Balcos, S.Y. Kim, H.S. Jeong, H.Y. Yun, K.J. Baek, N.S. Kwon, K.C. Park, D.S. Kim, Docosahexaenoic acid inhibits melanin synthesis in murine melanoma cells in vitro through increasing tyrosinase degradation, Acta Pharmacol Sin 35(4) (2014) 489-95.
[26] M.H. Davidson, Mechanisms for the hypotriglyceridemic effect of marine omega-3 fatty acids, Am J Cardiol 98(4A) (2006) 27i-33i.
[27] A. König, C. Bouzan, J.T. Cohen, W.E. Connor, P.M. Kris-Etherton, G.M. Gray, R.S. Lawrence, D.A. Savitz, S.M. Teutsch, A quantitative analysis of fish consumption and coronary heart disease mortality, Am J Prev Med 29(4) (2005) 335-46.
[28] J.D. Buckley, S. Burgess, K.J. Murphy, P.R. Howe, DHA-rich fish oil lowers heart rate during submaximal exercise in elite Australian Rules footballers, J Sci Med Sport 12(4) (2008) 503-7.
[29] E.M. Roth, W.S. Harris, Fish oil for primary and secondary prevention of coronary heart disease, Curr Atheroscler Rep 12(1) (2010) 66-72.
[30] S. Kotani, E. Sakaguchi, S. Warashina, N. Matsukawa, Y. Ishikura, Y. Kiso, M. Sakakibara, T. Yoshimoto, J. Guo, T. Yamashima, Dietary supplementation of arachidonic and docosahexaenoic acids improves cognitive dysfunction, Neurosci Res 56(2) (2006) 159-64.
[31] L.S. Honig, Inflammation in neurodegenerative disease: good, bad, or irrelevant?, Arch Neurol 57(6) (2000) 786-8.
[32] N.D. Riediger, R.A. Othman, M. Suh, M.H. Moghadasian, A systemic review of the roles of n-3 fatty acids in health and disease, J Am Diet Assoc 109(4) (2009) 668-79.
[33] H. Tian, Y. Lu, S.P. Shah, S. Hong, 14S,21R-dihydroxydocosahexaenoic acid remedies impaired healing and mesenchymal stem cell functions in diabetic wounds, J Biol Chem 286(6) (2010) 4443-53.
[34] Y. Lu, H. Tian, S. Hong, Novel 14,21-dihydroxy-docosahexaenoic acids: structures, formation pathways, and enhancement of wound healing, J Lipid Res 51(5) (2009) 923-32.
[35] M. Rahman, S. Beg, M.Z. Ahmad, I. Kazmi, A. Ahmed, Z. Rahman, F.J. Ahmad, S. Akhter, Omega-3 fatty acids as pharmacotherapeutics in psoriasis: current status and scope of nanomedicine in its effective delivery, Curr Drug Targets 14(6) (2013) 708-22.
[36] V.A. Ziboh, C.C. Miller, Y. Cho, Metabolism of polyunsaturated fatty acids by skin epidermal enzymes: generation of antiinflammatory and antiproliferative metabolites, Am J Clin Nutr 71(1 Suppl) (2000) 361S-6S.
[37] M.H. Zulfakar, L.M. Chan, K. Rehman, L.K. Wai, C.M. Heard, Coenzyme Q10-Loaded Fish Oil-Based Bigel System: Probing the Delivery Across Porcine Skin and

Possible Interaction with Fish Oil Fatty Acids, AAPS PharmSciTech 19(3) (2017) 1116-1123.
[38] C.N. Serhan, N. Chiang, T.E. Van Dyke, Resolving inflammation: dual anti-inflammatory and pro-resolution lipid mediators, Nat Rev Immunol 8(5) (2008) 349-61.
[39] K.H. Weylandt, C.Y. Chiu, B. Gomolka, S.F. Waechter, B. Wiedenmann, Omega-3 fatty acids and their lipid mediators: towards an understanding of resolvin and protectin formation, Prostaglandins Other Lipid Mediat 97(3-4) (2012) 73-82.
[40] B. Dangi, M. Obeng, J.M. Nauroth, M. Teymourlouei, M. Needham, K. Raman, L.M. Arterburn, Biogenic synthesis, purification, and chemical characterization of anti-inflammatory resolvins derived from docosapentaenoic acid (DPAn-6), J Biol Chem 284(22) (2009) 14744-59.
[41] H. Grimm, K. Mayer, P. Mayser, E. Eigenbrodt, Regulatory potential of n-3 fatty acids in immunological and inflammatory processes, Br J Nutr 87 Suppl 1 (2002) S59-67.
[42] M. Rahman, J.K. Kundu, J.W. Shin, H.K. Na, Y.J. Surh, Docosahexaenoic acid inhibits UVB-induced activation of NF-κB and expression of COX-2 and NOX-4 in HR-1 hairless mouse skin by blocking MSK1 signaling, PLoS One 6(11) (2011) e28065.
[43] D.Y. Oh, S. Talukdar, E.J. Bae, T. Imamura, H. Morinaga, W. Fan, P. Li, W.J. Lu, S.M. Watkins, J.M. Olefsky, GPR120 Is an Omega-3 Fatty Acid Receptor Mediating Potent Anti-inflammatory and Insulin-Sensitizing Effects, Cell 142(5) (2010) 687-698.
[44] L.A. Velloso, F. Folli, M.J. Saad, TLR4 at the Crossroads of Nutrients, Gut Microbiota, and Metabolic Inflammation, Endocr Rev 36(3) (2015) 245-71.
[45] R. De Caterina, M.I. Cybulsky, S.K. Clinton, M.A. Gimbrone, P. Libby, The omega-3 fatty acid docosahexaenoate reduces cytokine-induced expression of proatherogenic and proinflammatory proteins in human endothelial cells, Arterioscler Thromb 14(11) (1994) 1829-36.
[46] R. De Caterina, J.K. Liao, P. Libby, Fatty acid modulation of endothelial activation, Am J Clin Nutr 71(1 Suppl) (2000) 213S-23S.
[47] E.E. Williams, L.J. Jenski, W. Stillwell, Docosahexaenoic acid (DHA) alters the structure and composition of membranous vesicles exfoliated from the surface of a murine leukemia cell line, Biochim Biophys Acta 1371(2) (1998) 351-62.
[48] S.R. Shaikh, V. Cherezov, M. Caffrey, W. Stillwell, S.R. Wassall, Interaction of cholesterol with a docosahexaenoic acid-containing phosphatidylethanolamine: trigger for microdomain/raft formation?, Biochemistry 42(41) (2003) 12028-37.
[49] R.S. Chapkin, N. Wang, Y.Y. Fan, J.R. Lupton, I.A. Prior, Docosahexaenoic acid alters the size and distribution of cell surface microdomains, Biochim Biophys Acta 1778(2) (2007) 466-71.
[50] D.W. Ma, J. Seo, K.C. Switzer, Y.Y. Fan, D.N. McMurray, J.R. Lupton, R.S. Chapkin, n-3 PUFA and membrane microdomains: a new frontier in bioactive lipid research, J Nutr Biochem 15(11) (2004) 700-6.
[51] K.R. Rogers, K.D. Kikawa, M. Mouradian, K. Hernandez, K.M. McKinnon, S.M. Ahwah, R.S. Pardini, Docosahexaenoic acid alters epidermal growth factor receptor-related signaling by disrupting its lipid raft association, Carcinogenesis 31(9) (2010) 1523-30.
[52] E. Arab-Tehrany, M. Jacquot, C. Gaiani, M. Imran, S. Desobry, M. Linder, Beneficial effects and oxidative stability of omega-3 long-chain polyunsaturated fatty acids, Trends Food Sci Tech 25(1) (2012) 24-33.
[53] E. Valero, M. Villamiel, B. Miralles, J. Sanz, I. Martínez-Castro, Changes in flavour and volatile components during storage of whole and skimmed UHT milk, Food Chem 72(1) (2001) 51-58.

[54] N. Moussaoui, M. Cansell, A. Denizot, Marinosomes®, marine lipid-based liposomes: physical characterization and potential application in cosmetics, Int J Pharm 242(1) (2002) 361-365.
[55] G. Sonavane, K. Tomoda, A. Sano, H. Ohshima, H. Terada, K. Makino, In vitro permeation of gold nanoparticles through rat skin and rat intestine: Effect of particle size, Colloids Surf B Biointerfaces 65(1) (2008) 1-10.
[56] E.Y. Jung, K.B. Hong, H.S. Son, H.J. Suh, Y. Park, Effect of Layer-by-Layer (LbL) Encapsulation of Nano-Emulsified Fish Oil on Their Digestibility Ex Vivo and Skin Permeability In Vitro, Prev Nutr Food Sci 21(2) (2016) 85-9.
[57] C.C. Yang, C.F. Hung, B.H. Chen, Preparation of coffee oil-algae oil-based nanoemulsions and the study of their inhibition effect on UVA-induced skin damage in mice and melanoma cell growth, Int J Nanomedicine 12 (2017) 6559-6580.
[58] S. Di Franco, C. Amarelli, A. Montalto, A. Loforte, F. Musumeci, Biomaterials and heart recovery: cardiac repair, regeneration and healing in the MCS era: a state of the "heart", J Thorac Dis 10(Suppl 20) (2018) S2346-S2362.
[59] M. Burban, G. Meyer, A. Olland, F. Séverac, B. Yver, F. Toti, V. Schini-Kerth, F. Meziani, J. Boisramé-Helms, An Intravenous Bolus of Epa: Dha 6: 1 Protects Against Myocardial Ischemia-Reperfusion-Induced Shock, Shock 46(5) (2016) 549-556.
[60] D. Garcia-Dorado, A. Rodríguez-Sinovas, M. Ruiz-Meana, J. Inserte, Protection against myocardial ischemia-reperfusion injury in clinical practice, Rev Esp Cardiol (Engl Ed) 67(5) (2014) 394-404.
[61] D.M. Yellon, D.J. Hausenloy, Myocardial reperfusion injury, N Engl J Med 357(11) (2007) 1121-35.
[62] H.N. Sabbah, S. Goldstein, Ventricular remodelling: consequences and therapy, Eur Heart J 14 Suppl C (1993) 24-9.
[63] J.J. Gajarsa, R.A. Kloner, Left ventricular remodeling in the post-infarction heart: a review of cellular, molecular mechanisms, and therapeutic modalities, Heart Fail Rev 16(1) (2011) 13-21.
[64] C. Pignier, C. Revenaz, I. Rauly-Lestienne, D. Cussac, A. Delhon, J. Gardette, B. Le Grand, Direct protective effects of poly-unsaturated fatty acids, DHA and EPA, against activation of cardiac late sodium current: a mechanism for ischemia selectivity, Basic Res Cardiol 102(6) (2007) 553-64.
[65] Y.F. Xiao, D.C. Sigg, M.R. Ujhelyi, J.J. Wilhelm, E.S. Richardson, P.A. Iaizzo, Pericardial delivery of omega-3 fatty acid: a novel approach to reducing myocardial infarct sizes and arrhythmias, Am J Physiol Heart Circ Physiol 294(5) (2008) H2212-8.
[66] R.L. Castillo, C. Arias, J.G. Farías, Omega 3 chronic supplementation attenuates myocardial ischaemia-reperfusion injury through reinforcement of antioxidant defense system in rats, Cell Biochem Funct 32(3) (2013) 274-81.
[67] D. Richard, F. Oszust, C. Guillaume, H. Millart, D. Laurent-Maquin, C. Brou, P. Bausero, F. Visioli, Infusion of docosahexaenoic acid protects against myocardial infarction, Prostaglandins Leukot Essent Fatty Acids 90(4) (2014) 139-43.
[68] S. Zeghichi-Hamri, M. de Lorgeril, P. Salen, M. Chibane, J. de Leiris, F. Boucher, F. Laporte, Protective effect of dietary n-3 polyunsaturated fatty acids on myocardial resistance to ischemia-reperfusion injury in rats, Nutr Res 30(12) (2010) 849-57.
[69] C. Chrysohoou, G. Metallinos, G. Georgiopoulos, D. Mendrinos, A. Papanikolaou, N. Magkas, C. Pitsavos, G. Vyssoulis, C. Stefanadis, D. Tousoulis, Short term omega-3 polyunsaturated fatty acid supplementation induces favorable changes in right ventricle function and diastolic filling pressure in patients with chronic heart failure; A randomized clinical trial, Vascul Pharmacol 79 (2016) 43-50.

[70] C. Cipollina, S.R. Salvatore, M.F. Muldoon, B.A. Freeman, F.J. Schopfer, Generation and dietary modulation of anti-inflammatory electrophilic omega-3 fatty acid derivatives, PLoS One 9(4) (2014) e94836.
[71] K.M. O'Shea, R.J. Khairallah, G.C. Sparagna, W. Xu, P.A. Hecker, I. Robillard-Frayne, C. Des Rosiers, T. Kristian, R.C. Murphy, G. Fiskum, W.C. Stanley, Dietary omega-3 fatty acids alter cardiac mitochondrial phospholipid composition and delay Ca2+-induced permeability transition, J Mol Cell Cardiol 47(6) (2009) 819-27.
[72] C. Li, S. Wallace, Polymer-drug conjugates: Recent development in clinical oncology, Adv Drug Deliv Rev 60 (2008) 886-898.
[73] M. Barz, A. Duro-Castano, M.J. Vicent, A versatile post-polymerization modification method for polyglutamic acid: synthesis of orthogonal reactive polyglutamates and their use in “click chemistry”, Polym Chem 4(10) (2013) 2989-2994.
[74] J.J. Arroyo-Crespo, et al., *Anticancer activity driven by drug linker modification in a polyglutamic acid-based combination-drug conjugate*. Adv. Funct. Mater, 2018. **28**: 13.
[75] A. Duro-Castano, V.J. Nebot, A. Nino-Pariente, A. Arminan, J.J. Arroyo-Crespo, A. Paul, N. Feiner-Gracia, L. Albertazzi, M.J. Vicent, Capturing "Extraordinary" Soft-Assembled Charge-Like Polypeptides as a Strategy for Nanocarrier Design, Adv Mater 29 (2017) 12.
[76] R. van Horssen, N. Galjart, J.A. Rens, A.M. Eggermont, T.L. ten Hagen, Differential effects of matrix and growth factors on endothelial and fibroblast motility: application of a modified cell migration assay, J Cell Biochem 99(6) (2006) 1536-52.
[77] C.C. Liang, A.Y. Park, J.L. Guan, In vitro scratch assay: a convenient and inexpensive method for analysis of cell migration in vitro, Nat Protoc 2(2) (2007) 329-33.
[78] A. Duro-Castano, V.J. Nebot, A. Niño-Pariente, A. Armiñán, J.J. Arroyo-Crespo, A. Paul, N. Feiner-Gracia, L. Albertazzi, M.J. Vicent, Capturing "Extraordinary" Soft-Assembled Charge-Like Polypeptides as a Strategy for Nanocarrier Design, Adv Mater 29(39) (2017).
[79] R.W. Spayd, B. Bruschi, B.A. Burdick, G.M. Dappen, J.N. Eikenberry, T.W. Esders, J. Figueras, C.T. Goodhue, D.D. LaRossa, R.W. Nelson, R.N. Rand, T.W. Wu, Multilayer film elements for clinical analysis: applications to representative chemical determinations, Clin Chem 24(8) (1978) 1343.
[80] C. Gandia, A. Arminan, J.M. Garcia-Verdugo, E. Lledo, A. Ruiz, M.D. Minana, J. Sanchez-Torrijos, R. Paya, V. Mirabet, F. Carbonell-Uberos, M. Llop, J.A. Montero, P. Sepulveda, Human dental pulp stem cells improve left ventricular function, induce angiogenesis, and reduce infarct size in rats with acute myocardial infarction, Stem Cells 26(3) (2008) 638-45.

GENERAL DISCUSSION

GENERAL DISCUSSION

Topical administration represents the main route to attain local therapeutic activity of bioactive agents due to its affordability compared to other administration routes (e.g., intravenous and intramuscular administration) enhancing patient compliance and clinician acceptance [1]. The principal body sites explored that benefit from topical drug administration include the skin, vagina, eyes and nose, but also other organs, as the heart, could be reach by means of devices that act as a reservoir and are capable to enhance drug transport through the endothelium.The main challenge of the topical administration of various therapeutics is the requirement to bypass specific biological barriers to achieve a required concentration of a given therapeutic agent at the desired site of action for a duration that would allow optimal pharmacological activity [2].

The skin represents the main biological barrier present in the human body, controlling the exchange of molecules between the body and the environment; however, this protective system also diminishes the penetration of therapeutic agents [3]. In particular, the nanoporosity and composition of the stratum corneum represent the most significant obstacles for therapeutics to surpass [4] leading to low drug bioavailability and efficacy. These deficiencies have led to the administration of higher concentrations of therapeutic agents to achieve a desired level of activity, but also to the development of complex formulations that enhance skin penetration of the therapeutic to the required skin layer. Nanosized drug delivery systems represent an exciting means to safely increase drug penetration into the skin [5-7] and maintain a prolonged and constant drug release rate at the desired site of action [8].

In this thesis we focused on the topical administration of advanced therapeutics mainly for skin pathologies (**Chapter III and IV**), but we have also begun to explore a local administration approach that aims to diminish the consequences of ischemia/reperfusion (I/R) injury in the heart (**Chapter V**). We developed our new advanced therapeutics using a polymer therapeutics-based approach: the conjugation of active agents to a biodegradable and biocompatible polypeptide scaffold to create novel nanosized drug delivery systems that improve drug penetration through the skin or promote endothelial transport to reach cardiac tissue.

To this end, we followed the strategies described below:

(1) The use of biodegradable and biocompatible polymeric carriers, mainly polypeptide-based derivatives that permit chronic treatment via topical application while avoiding bioaccumulation and any undesirable side-effects.

(2) The rational design of the final polypeptide-drug conjugates alone and in combination with polypeptide-base penetration enhancers, to enhance the activity and promote the attainment of therapeutic drug concentrations at the desired place of action.

(3) An exhaustive physico-chemical characterization of the synthesised conjugates to correlate features with the biological activity.

(4) The use of preclinically relevant models of disease, including *ex vivo* human skin models and an *in vivo* psoriatic model.

Polymer-drug conjugates, a subtype of polymer therapeutics, offer advantages when compared to other nanomedicines that favor drug skin penetration [9-11]. These properties include: (1) chemical stability and controlled physico-chemical features due to the presence of a covalent linker between the drug and the polymer carrier, (2) solubility of hydrophobic drugs in aqueous media, (3) sustained and site-specific release of drugs via rationally designed bioresponsive linkers, and (4) the capacity to load drug combinations or add targeting moieties due to polymer multivalency [12]. Herein, we have achieved proof of concept regarding the benefits of the implementation of polymer therapeutics-based approaches for topical administration in pathologies such as psoriasis or wound healing.

Psoriasis is a common inflammatory chronic disease mediated by the immune system with a predominantly cutaneous involvement [13]. There are several clinical phenotypes of psoriasis that are classified based on the characteristics of the disease, including patient age at disease onset, degree of skin involvement, morphologic pattern, and anatomical location [14]. Scaly skin, erythematous plaques, and inflammatory cell infiltration characterize plaque psoriasis, the most prevalent type of psoriasis [15, 16]. In recent years, the immune response involved in the onset of the disease has been extensively investigated, uncovering the relative importance of the Interleukin (IL)-

23/IL-17 axis [16, 17]. The current development of anti-psoriatic therapeutics, mainly IL-17 and IL-23 inhibitors, focuses on systemic treatments that target the immune system [17]. However, topical treatment with corticosteroids remains one of the most widely employed treatments for approximately 80% of patients affected with mild to moderate psoriasis [18]. Corticosteroids induce anti-inflammatory, antiproliferative, immunosuppressive, and vasoconstrictive effects through binding to intracellular corticosteroid receptors and the modulation of pro-inflammatory cytokine gene transcription [19].

However, many topical corticosteroids that are currently employed or under assessment in clinical trials lack adequate physico-chemical properties (e.g., solubility) and suffer from local cutaneous (e.g., skin atrophy and acne) and systemic side effects (e.g., osteoporosis, diabetes and weight gain) that limit their clinical use [20]. These effects correlate with the high doses required and the elevated frequency of applications and have been noted for both high and reduced potency corticosteroids. Therefore, any advanced therapeutic approaches that allow a reduction in dose and the avoidance of systemic circulation of corticosteroids could significantly enhance treatment efficacy and patient compliance.

The application of nanomedicines as advanced therapeutics in the field of topical and transdermal delivery of active compounds [21-25] and immunotherapy [26] is currently in exponential growth. Liposomes have been the most used carriers for skin delivery, although their large sizes and heterogeneous size distribution limit their efficiency when acting as skin permeation enhancers [27, 28]. The application of controlled polymerization techniques and the tailoring of critical nanocarrier parameters, such as size and Z-potential, can significantly enhance the penetration of active substances into the skin, as has been demonstrated for polypeptide-based nanostructures [29, 30]. Furthermore, the mode of the drug encapsulation/entrapment [31] or polypeptide carrier-conjugation [32, 33] significantly influences the site of drug release and kinetic profile of drug release. Although currently underexplored for skin delivery, rationally-designed bioresponsive linkers as part of a nonmedicinal approach can optimize the therapeutic output of topical treatment by enhancing efficiency and reducing side effects [34, 35]. Finally, the vehicle used for the administration of a given therapeutic may also have an essential synergistic effect; formulations with an optimal interaction between the vehicle and the therapeutic agent can enhance penetration and hydration of the skin [36].

We developed healthy and inflammatory *ex vivo* human skin models and establish an *in vivo* psoriatic murine model with the hope of understanding the complex pathology and histological features of psoriasis (**Chapter II**). These models also provide a useful platform to confirm advanced anti-inflammatory and anti-psoriatic therapeutics. Moreover, the *ex vivo* human skin model allows the evaluation of therapeutics in a more realistic setting than those in *in vitro* assays.

During the development of the inflammatory *ex vivo* skin model, we assessed tissue viability after the induction of inflammation by treatment with LPS and EGF, finding maintained tissue viability at each time and concentration evaluated. Histomorphologic analysis of the skin samples with H&E staining and the Ki67 and Ck5/6 markers confirmed that treated skin maintained its structure, viability, and proliferation capacity in response to the inflammatory insult. Of note, the skin mimicked certain features of the psoriasis, including induced epidermal thickness and acanthosis, in good agreement with other reports [37, 38]. We also assessed the inflammatory model through the quantification of pro-inflammatory cytokines released into the culture media (e.g., IL-1b, TNF-α, INF-γ, and IL-6), and then employed this model to evaluate the safety and the anti-inflammatory activity of our newly developed family of drug conjugates in **Chapter IV**. However, the absence of a full immune response in this *ex vivo* human skin represents a significant limitation in the modeling of autoimmune diseases, such as psoriasis. Therefore, the information from *in vivo* preclinical mouse models can complement the *ex vivo* models with regards to the understanding of the immune mechanisms contributing to disease development and reflect the critical features of the human disease [39].

With this in mind, we subsequently developed an imiquimod (IMQ)-induced model of skin inflammation in immunocompetent (BALB/c) mice for the preclinical study of psoriasis. Although the main limitation of the IMQ model relates to the duration, this acute model does not represent a chronic disease [40], this model remains relevant and widely employed as it mimics the histopathological characteristics of inflamed skin and induces a systemic inflammatory response [41]. We developed this model by applying IMQ cream daily to the mouse back and ear for seven consecutive days, following the timing reported in other studies [41-43]. After this point, we evaluated the histological characteristics of the mice for ten days to determine the best time for further studies into the application of anti-psoriatic treatments.

We employed different methodologies to assess disease progression. We monitored mouse body weight measurements to ensure the safety of the treatment, demonstrating that after the application of the treatments the animals maintain and even recover weight. At the gross morphological level, we used the PASI score [44] to evaluate itching, erythema, scaling, and skin thickness on the back of the mice, revealing a maximum level at day seven which remained for up to five days later. We also assessed the increase in epidermal thickness by H&E staining on the back and treated ear, revealing marked epidermal hyperplasia and hyperkeratosis compared to the control group at day seven that was maintained up to five days after. In the case of the treated mouse ear, we corroborated the increase in epidermal thickness via caliper measurements every two days. Therefore, our mouse model demonstrated the same histopathologic changes as observed in human psoriasis [45]. Of note, we discovered a significant enlargement of the spleen after the application of IMQ cream, corroborating the results of previous studies [41, 46, 47]. The enlargement was maintained for five days after the last application of IMQ, correlating this phenomenon with the increase in pro-inflammatory cytokine synthesis observed in tissue and serum. In both cases, we observed a significant induction of the pro-inflammatory cytokines that play a crucial role in the onset of psoriasis such as IL-23, INF- γ, and TNF-α [48]. These findings corroborated the results obtained by other authors using the topical administration of IMQ as a trigger for the disease [41, 43, 49].

We also discovered the importance of the appropriate vehicle to transport polymer-drug conjugates into the skin during the development of this thesis [50]. Of note, penetration through the skin relies on the combination of the three factors: skin features, the physico-chemical characteristics of the polymer-drug conjugate (in this case), and the vehicle. Vehicles should possess sufficient residence time on the skin to allow a controlled and sustained release of the drug to provide a therapeutic dose, and also should enhance patient compliance [51-53]. Importantly, a universal vehicle does not exist, and so, vehicle formulation should consider the specific physico-chemical properties of the nanomaterial employed to maximize drug release across the skin.

For this reason, we used a novel biodegradable hyaluronic acid-poly-L-glutamate cross-polymer vehicle (HA-CP; Yalic®) as a penetration enhancer (developed in collaboration with Polypeptide Therapeutic Solutions S.L.). The rationale for the development of this penetration enhance lies in the properties of hyaluronic acid (HA),

whose use in dermal applications has increased in recent years [54-56] (**Chapter III**). We implemented a synthetic methodology to synthesize the cross-linked HA using PGA and lysines as cross-linkers, following well-established methodologies [57, 58]. The degradation of the HA-based materials in the presence of hyaluronidase revealed a more rapid degradation for linear HA compared to the cross-linked vehicle. These findings support the results obtained in a hydration study in human volunteers, in which the HA-CP vehicle prolonged and improved the skin hydration over time compared to linear HA.

The biological evaluation *in vitro* in keratinocytes and fibroblasts cells demonstrated that the cross-polymer maintained cell viability when compared to linear HA. Moreover, safety assessments of HA-CP in an *ex vivo* human skin model (see **Chapter II** for more details) revealed the maintainance and even improvement of tissue viability after 72 h of treatment, thereby demonstrating suitability for topical applications. We also studied the capacity of a fluorescently-labeled HA-CP cross-polymer to penetrate the skin by Franz diffusion cells, demonstrating that the HA-CP can significantly penetrate the viable epidermis when compared to linear HA, which remains mainly in the stratum corneum, in good agreement with previous studies [59, 60]. Also, we evaluated the properties of HA-CP as a skin penetration enhancer by evaluating its role as a vehicle for the delivery of a family of amphiphilic block copolymers of different nature, using PPhe and PBG with different degree of polymerization. We demonstrated that the presence of Phe as an amino acid in the polymer chain, as well as the critical micelle concentration (CMC) and the encapsulation efficiency (E.E) of a fluorophore (Dil) as a model hydrophobic drug drove changes in the nanocarrier solution conformation. Micelles composed by the Phe-based block copolymers possessed a higher tendency to form micelles (lower CMC) and a lower capacity to encapsulate Dil than the BG-based block copolymers. Finally, we confirmed the ability of the HA-CP cross-polymer to enhance the penetration of all the micelles through to the viable epidermis while avoiding problems related to systemic exposure.

Therefore, we have demonstrated the suitability of a novel biodegradable cross-polymer (HA-CP) for topical applications as a vehicle to increase the penetration of nanocarriers. Encouraged by this approach, we used this vehicle for the application of the PGA-FLUO conjugate as a treatment for psoriasis, aiming to improve the penetration of PGA-FLUO into the skin. Within **Chapter IV** of this thesis, we conjugated the poorly water-soluble corticosteroid, fluocinolone acetonide (FLUO), to a water-soluble poly-L-

glutamic acid (PGA) polymer via an ester bond (PGA-FLUO), to bypass the noted limitations of drug treatment and provide more controlled and sustained release of FLUO within the epidermis. We also validated the anti-psoriatic activity of PGA-FLUO using both preclinically-relevant *ex vivo* (including human-derived models) and an *in vivo* psoriatic model (described in **Chapter II**).

We synthesized PGA-FLUO conjugates using well-established methodologies [61] and then characterized them using a full battery of physico-chemical techniques, ensuring identity and purity. We discovered self-assembly behavior of the conjugates in aqueous environments, creating assemblies with a hydrodynamic radius of 40 - 100 nm and a highly negative Z-potential value (-50 mV) by DLS measurements. We corroborated a globular nanoassembly for PGA-FLUO by TEM, in agreement with other systems based on PGA with similar structures which revealed spherical shapes around 100 nm [62]. Drug release kinetics at relevant pHs (7.4 and 5.5) revealed higher drug release at pH 7.4 than a pH 5.5, an unexpected result due to higher degradability of the ester bond under acidic conditions, as previously reported [63-65]. However, this phenomenon could be explained by the different solution conformation of the conjugate at different pHs, which at pH 7.4 presented a random coil structure meanwhile at pH 5.5 a alpha-helix structure, more compact and less accessible than the random coil. We also studied the physico-chemical characteristics as well as the drug release kinetics of the conjugate in the HA-CP vehicle; the conjugate maintained the same size and globular shape and displayed a slower and more sustained release compared to the conjugate in PBS buffer. These results suggested that the application of the conjugate in the HA-CP vehicle promotes a more controllable and sustained release at the desired place of action, spacing the necessary doses to achieve the desired therapeutic effect.

Biological evaluation *in vitro* revealed that our newly developed PGA-FLUO conjugate maintained/enhanced skin cell viability (keratinocytes and fibroblasts) when compared to the unconjugated drug. Moreover, cell internalization of a fluorescently-labeled conjugate in keratinocytes studied by flow cytometry and confocal microscopy demonstrated an energy-dependent endocytic uptake and a clear colocalization with lysosomes. We also studied the anti-inflammatory activity of the conjugate in LPS-induced macrophages to evaluate alterations in the secretion of pro-inflammatory cytokines. Unexpectedly, we discovered that conjugation enhanced the anti-inflammatory capacity of free FLUO. Importantly, during permeation studies in human skin by Franz

diffusion cells, we observed a considerable increment in the amount of the fluorescently-labeled conjugate that reached deeper epidermal layers when applied within the HA-CP vehicle than applied in water.

We corroborated the *in vitro* findings in two *ex vivo* models: an optimized inflammatory *ex vivo* human skin model and a reconstructed inflammatory skin equivalent model [66]. In both models, we demonstrated the safety of PGA-FLUO and the improved ability to reduce the secretion of the pro-inflammatory cytokine IL-6 from the skin when compared to the free FLUO.

Moreover, *in vivo* proof of concept of the anti-psoriatic activity of our conjugate has been achieved in our preclinical IMQ-induced psoriatic mouse model (details in **Chapter II**). Histological comparisons with free FLUO in cream demonstrated that PGA-FLUO applied in cream produced a more significant reduction in epidermal thickness, both in the IMQ-treated back and ear of the mouse model. Remarkable, the group treated with PGA-FLUO in the HA-CP vehicle revealed a marked reduction of epidermal thickness, compared with healthy animals. These results could be explained due to a synergistic effect between the conjugate and the vehicle, promoting an improvement in the controlled release of the drug and its permanence in the viable epidermis while also improving skin hydration in healthy volunteers (see **Chapter III** for more details). Systemic analyses provided similar results to the localized histological analyses: PGA-FLUO applied in cream provided a more significant reduction of the release of pro-inflammatory cytokines related to psoriasis disease (IL-23 and IFN-γ) in serum and tissue compared to free FLUO. Of note, treatment with PGA-FLUO within HA-CP provided the best results compared to all other treatment modalities. In agreement with these results, we observed the same trend in spleen weight reduction, perhaps due to the decrease in the synthesis of pro-inflammatory cytokines [41]. Importantly, treatment with PGA-FLUO within HA-CP returned spleen weight in psoriatic model mice to that of healthy controls.

In conclusion, the rationally designed PGA-FLUO conjugate combined with an optimized HA-CP vehicle may represent an effective strategy for the treatment of psoriasis. This combination provides specific characteristics and advantages compared to other nanocarriers; firstly, the conjugation of the drug allows the better controlled of the drug release kinetics in the specific skin layer, and secondly, the use of the HA-CP vehicle

promotes the penetration of the conjugate into the skin, as well as improves the characteristics of the psoriatic skin, such as hydration and dryness. These results lay the groundwork for future studies and development of new anti-psoriatic treatments, using other types of drugs or drug combination.

As we have demonstrated during this thesis, PGA-drug conjugates can penetrate and permeate through the different layers of the skin, even in cases where the skin barrier is altered, such as in the case of psoriasis; therefore, they may find use in the enhancement of skin regeneration and repair, thereby contributing towards wound healing. Encouraged by these results, we also studied the potential of polymer-drug conjugates to enhance the treatment of skin wounds and ischemia-reperfusion injury in the heart.

Chronic wounds are considered a silent epidemic that affects between 1 - 2% of the population in developed countries [67, 68]. Several therapeutic agents have demonstrated the capacity to promote skin wound healing, including the family of omega-3 polyunsaturated fatty acids (PUFAs), especially docosahexaenoic acid (DHA), due to its anti-inflammatory properties [69, 70] and the capacity to modify endothelial cell function [71, 72]. In **Chapter V**, we implemeneted a type of DHA composed of two chains containing 12 double bonds called diDHA, to develop advanced therapeutics towards the treatment of chronic wounds.

Lipid oxidation of these fatty acids can compromise the implementation of these compounds by destabilizing the molecule and decreasing the intrinsic activity [73]. To enhance the stability of diDHA, we proposed the generation of a family of PGA-diDHA conjugates formed through an ester bond in the hope of protecting the drug from degradation and increasing skin wound healing activity. To this end, we synthesized, characterized, and biologically evaluated a family of PGA-diDHA conjugates with different diDHA loadings (2.2, 6.4, and 9.1 mol%) (**Chapter V**). diDHA conjugation led to increased solubility in water, stability (as evidenced by ^{1}H-NMR), and decreased lipid peroxidation of diDHA over time (as evidenced by the malondialdehyde colorimetric assay). We also discovered a self-assembly behavior of the conjugates in aqueous environments, as occurred with other polymer-drug conjugates developed in this thesis due to the hydrophilic-lipophilic ratio. PGA-diDHA conjugates possessed a hydrodynamic radius between 20 and 100 nm, in good agreement with the results obtained by TEM images, thereby confirming the existence of a globular nanoassembly

[62]. Of note, we observed smaller conjugate sizes with higher diDHA loading, results related to the critical concentration of aggregation values, which are smaller in conjugates with higher diDHA loadings. Moreover, as in the case of the PGA-FLUO conjugates (**Chapter IV**), we discovered a slightly higher drug release kinetics at pH 7.4 than at pH 5.5 – an unexpected phenomenon that again could be explained by the different conformation of the conjugate at different pHs, with overall accessibility higher at pH 7.4.

Concerning the biological evaluation, cell viability assays *in vitro* revealed that PGA-diDHA conjugates enhanced skin cell viability (keratinocytes and fibroblasts) and maintained nearly complete viability in response to the concentrations evaluated. Of note, unconjugated diDHA causes cellular toxicity at higher concentrations, demonstrating that diDHA conjugation improved drug stability and decreased cell toxicity *in vitro*. Moreover, in an *in vitro* scratch assay in fibroblasts, to evaluate the capacity of the conjugates to enhance the migration and proliferation into the wounded monolayer, only the conjugate with medium diDHA loading (PGA-diDHA6.4) showed a 20% of improvement in cell migration compared to control.

As a topical application, we also assessed the capacity of fluorescently labelled PGA-diDHA conjugates with different diDHA loadings (2.2 and 9.1 mol%) to penetrate into the human skin by Franz diffusion cells, revealing that the conjugate with lower diDHA loading can penetrate deeper into the viable skin, a finding that could be explained by saturation of the skin with higher diDHA loadings. Of note, we failed to observe any signal in the receptor chamber that could indicate that the conjugate remains in the epidermis without reaching the bloodstream and allowing adverse effects on a systemic level.

Encouraged by the successful application of PGA-diDHA conjugates *in vitro*, further studies will be focused on the *in vivo* evaluation of the selected conjugates in diabetic rats, since the biological evaluation revealed that the diDHA loading in the conjugate determines the final biological activity.

Finally, we also demonstrated the ability of the PGA-diDHA conjugates to enhance the healing process following damage to the heart produced by I/R associated with acute myocardial infarction (AMI) in collaboration with the group of Dr. P.

Sepúlveda (Hospital La Fe, Valencia, Spain). *In vitro* evaluation using a lactate dehydrogenase assay revealed that PGA-diDHA6.4 conjugate reduced heart cell damage in comparison with free diDHA. Infusion of nanoconjugates and free diDHA in an *in vivo* I/R rat model showed a significant reduction in infarct size following PGA-diDHA6.4 administration before reperfusion in comparison with free diDHA at the same dose (12 % *vs.* 28% infarcted area with or without treatment, respectively). Moreover, intracoronary infusion of PGA-diDHA6.4 nanoconjugate after 90 min of ischemia in a swine model before reperfusion limited edema and decreased the area in risk seven days after experimental infarction as assessed by cardiac magnetic resonance and histological analysis (data included in the Ph.D. thesis of Sandra Tejedor at the laboratory of Dr. Pilar Sepúlveda). Collectively, our data established the potential use of PGA-diDHA6.4 in mitigating I/R-induced injury, thereby providing a new therapeutic agent for future clinical studies.

In summary, we believe that the results reported in this thesis support the development of polypeptide-based conjugates as an effective strategy for the local delivery of therapeutic agents and the treatment of a range of conditions.

References

[1] H.-Y. Chen, J.-Y. Fang, Therapeutic patents for topical and transdermal drug delivery systems, Expert Opin Ther Pat 10(7) (2000) 1035-1043.
[2] D. Singh Malik, N. Mital, G. Kaur, Topical drug delivery systems: a patent review, Expert Opin Ther Pat 26(2) (2016) 213-28.
[3] K.W. Ng, Penetration Enhancement of Topical Formulations, Pharmaceutics 10(2) (2018).
[4] B. Baroli, Penetration of nanoparticles and nanomaterials in the skin: Fiction or reality?, J Pharm Sci 99(1) (2010) 21-50.
[5] H. Chen, X. Chang, D. Du, W. Liu, J. Liu, T. Weng, Y. Yang, H. Xu, X. Yang, Podophyllotoxin-loaded solid lipid nanoparticles for epidermal targeting, J Control Release 110(2) (2006) 296-306.
[6] S. Lombardi Borgia, M. Regehly, R. Sivaramakrishnan, W. Mehnert, H.C. Korting, K. Danker, B. Röder, K.D. Kramer, M. Schäfer-Korting, Lipid nanoparticles for skin penetration enhancement—correlation to drug localization within the particle matrix as determined by fluorescence and parelectric spectroscopy, J Control Release 110(1) (2005) 151-163.
[7] M.P. Alves, A.L. Scarrone, M. Santos, A.R. Pohlmann, S.S. Guterres, Human skin penetration and distribution of nimesulide from hydrophilic gels containing nanocarriers, Int J Pharm 341(1) (2007) 215-220.
[8] C.N. Lemos, F. Pereira, L.F. Dalmolin, C. Cubayachi, D.N. Ramos, R.F.V. Lopez, Chapter 6 - Nanoparticles influence in skin penetration of drugs: In vitro and in vivo

characterization, in: A.M. Grumezescu (Ed.), Nanostructures for the Engineering of Cells, Tissues and Organs, William Andrew Publishing2018, pp. 187-248.
[9] A. Vogt, C. Wischke, A.T. Neffe, N. Ma, U. Alexiev, A. Lendlein, Nanocarriers for drug delivery into and through the skin — Do existing technologies match clinical challenges?, J Control Release 242 (2016) 3-15.
[10] M.S. Roberts, Y. Mohammed, M.N. Pastore, S. Namjoshi, S. Yousef, A. Alinaghi, I.N. Haridass, E. Abd, V.R. Leite-Silva, H.A.E. Benson, J.E. Grice, Topical and cutaneous delivery using nanosystems, J Control Release 247 (2017) 86-105.
[11] A.H. Mota, P. Rijo, J. Molpeceres, C.P. Reis, Broad overview of engineering of functional nanosystems for skin delivery, Int J Pharm 532(2) (2017) 710-728.
[12] R. Duncan, Polymer therapeutics as nanomedicines: new perspectives, Curr Opin Biotech 22(4) (2011) 492-501.
[13] B.J. Nickoloff, F.O. Nestle, Recent insights into the immunopathogenesis of psoriasis provide new therapeutic opportunities, J Clin Invest 113 (2004) 1664-75.
[14] S.K. Raychaudhuri, E. Maverakis, S.P. Raychaudhuri, Diagnosis and classification of psoriasis, Autoimmun Rev 13 (2014) 490-5.
[15] F.O. Nestle, D.H. Kaplan, J. Barker, Psoriasis, N Engl J Med 361 (2009) 496-509.
[16] J.E. Hawkes, T.C. Chan, J.G. Krueger, Psoriasis pathogenesis and the development of novel targeted immune therapies, J Allergy Clin Immunol 140 (2017) 645-653.
[17] J. Kim, J.G. Krueger, Highly Effective New Treatments for Psoriasis Target the IL-23/Type 17 T Cell Autoimmune Axis, Annu Rev Med 68 (2016) 255-269.
[18] L. Iversen, E. Dauden, S. Segaert, K. Freeman, S. Magina, D. Rigopoulos, D. Thaci, Reformulations of well-known active ingredients in the topical treatment of psoriasis vulgaris can improve clinical outcomes for patients, J Eur Acad Dermatol Venereol 31 (2017) 1271-1284.
[19] L. Uva, D. Miguel, C. Pinheiro, J. Antunes, D. Cruz, J. Ferreira, P. Filipe, Mechanisms of Action of Topical Corticosteroids in Psoriasis, Int J Endocrinol 2012 (2012) 16.
[20] A. Bewley, Expert consensus: time for a change in the way we advise our patients to use topical corticosteroids, Br J Dermatol 158 (2008) 917-920.
[21] V. Campani, M. Biondi, L. Mayol, F. Cilurzo, S. Franzé, M. Pitaro, G. De Rosa, Nanocarriers to Enhance the Accumulation of Vitamin K1 into the Skin, Pharm Res 33 (2015) 893-908.
[22] R.H. Neubert, Potentials of new nanocarriers for dermal and transdermal drug delivery, Eur J Pharm Biopharm 77 (2010) 1-2.
[23] M.B. Pierre, I. Dos Santos Miranda Costa, Liposomal systems as drug delivery vehicles for dermal and transdermal applications, Arch Dermatol Res 303 (2011) 607-21.
[24] K. Thakur, G. Sharma, B. Singh, S. Chhibber, O.P. Katare, Current State of Nanomedicines in the Treatment of Topical Infectious Disorders, Recent Pat Antiinfect Drug Discov 13 (2018) 127-150.
[25] Z. Gu, X. Chen, Towards Enhancing Skin Drug Delivery, Adv Drug Deliv Rev 127 (2018) 1-2.
[26] Z. Zhao, A. Ukidve, A. Dasgupta, S. Mitragotri, Transdermal immunomodulation: Principles, advances and perspectives, Adv Drug Deliv Rev 127 (2018) 3-19.
[27] N. Belhaj, E. Arab-Tehrany, E. Loing, C. Bézivin, Skin delivery of hydrophilic molecules from liposomes and polysaccharide-coated liposomes, Int J Cosmet Sci 39 (2017) 435-441.
[28] N.M. Saidin, N.K. Anuar, M. Redzuan, Roles of Polysaccharides in Transdermal Drug Delivery System and Future Prospects, J Appl Pharm Sci 8 (2018) 141-157.

[29] A. Bolhassani, Improvements in chemical carriers of proteins and peptides, Cell Biol Int 43 (2019) 437-452.
[30] S. Kumar, M. Zakrewsky, M. Chen, S. Menegatti, J.A. Muraski, S. Mitragotri, Peptides as skin penetration enhancers: mechanisms of action, J Control Release 199 (2014) 168-78.
[31] P.C. DeMuth, X. Su, R.E. Samuel, P.T. Hammond, D.J. Irvine, Nano-Layered Microneedles for Transcutaneous Delivery of Polymer Nanoparticles and Plasmid DNA, Adv Mater 22 (2010) 4851-4856.
[32] A. Duro-Castano, I. Conejos-Sánchez, J.M. Vicent, Peptide-Based Polymer Therapeutics, Polymers (Basel) 6 (2014) 515-551.
[33] O. Zagorodko, J.J. Arroyo-Crespo, V.J. Nebot, M.J. Vicent, Polypeptide-Based Conjugates as Therapeutics: Opportunities and Challenges, Macromol Biosci 17 (2017) 1600316.
[34] R.V. Contri, L.A. Fiel, A.R. Pohlmann, S.S. Guterres, R.C.R. Beck, Transport of Substances and Nanoparticles across the Skin and in Vitro Models to Evaluate Skin Permeation and/or Penetration, in: R. Beck, S. Guterres, A. Pohlmann (Eds.), Nanocosmetics and Nanomedicines: New Approaches for Skin Care, Springer Berlin Heidelberg, Berlin, Heidelberg, 2011, pp. 3-35.
[35] R. Duncan, The dawning era of polymer therapeutics, Nat Rev Drug Discov 2 (2003) 347-60.
[36] K. Khezri, M. Saeedi, S. Maleki Dizaj, Application of nanoparticles in percutaneous delivery of active ingredients in cosmetic preparations, Biomed Pharmacother 106 (2018) 1499-1505.
[37] A.R. Companjen, L.I. van der Wel, L. Wei, J.D. Laman, E.P. Prens, A modified ex vivo skin organ culture system for functional studies, Arch Dermatol Res 293(4) (2001) 184-90.
[38] S. Kondo, Maintenance of epidermal structures of psoriatic skin in organ culture, J Dermatol 13(4) (1986) 242-9.
[39] J.E. Gudjonsson, A. Johnston, M. Dyson, H. Valdimarsson, J.T. Elder, Mouse Models of Psoriasis, J Invest Dermatol 127(6) (2007) 1292-1308.
[40] B. Flutter, F.O. Nestle, TLRs to cytokines: mechanistic insights from the imiquimod mouse model of psoriasis, Eur J Immunol 43(12) (2013) 3138-46.
[41] L. van der Fits, S. Mourits, J.S. Voerman, M. Kant, L. Boon, J.D. Laman, F. Cornelissen, A.M. Mus, E. Florencia, E.P. Prens, E. Lubberts, Imiquimod-induced psoriasis-like skin inflammation in mice is mediated via the IL-23/IL-17 axis, J Immunol 182 (2009) 5836-45.
[42] J.K. Wu, G. Siller, G. Strutton, Psoriasis induced by topical imiquimod, Australas J Dermatol 45(1) (2004) 47-50.
[43] U. Patel, N.M. Mark, B.C. Machler, V.J. Levine, Imiquimod 5% cream induced psoriasis: a case report, summary of the literature and mechanism, Br J Dermatol 164(3) (2011) 670-2.
[44] R.G. Langley, C.N. Ellis, Evaluating psoriasis with Psoriasis Area and Severity Index, Psoriasis Global Assessment, and Lattice System Physician's Global Assessment, J Am Acad Dermatol 51(4) (2004) 563-569.
[45] M. Murphy, P. Kerr, J.M. Grant-Kels, The histopathologic spectrum of psoriasis, Clin Dermatol 25(6) (2007) 524-8.
[46] H. Vinter, K. Kragballe, T. Steiniche, M. Gaestel, L. Iversen, C. Johansen, Tumour necrosis factor-alpha plays a significant role in the Aldara-induced skin inflammation in mice, Br J Dermatol 174(5) (2016) 1011-21.

[47] A. Ueyama, M. Yamamoto, K. Tsujii, Y. Furue, C. Imura, M. Shichijo, K. Yasui, Mechanism of pathogenesis of imiquimod-induced skin inflammation in the mouse: a role for interferon-alpha in dendritic cell activation by imiquimod, J Dermatol 41(2) (2014) 135-43.
[48] J. Baliwag, D.H. Barnes, A. Johnston, Cytokines in psoriasis, Cytokine 73(2) (2015) 342-350.
[49] A. Walter, M. Schäfer, V. Cecconi, C. Matter, M. Urosevic-Maiwald, B. Belloni, N. Schönewolf, R. Dummer, W. Bloch, S. Werner, H.D. Beer, A. Knuth, M. van den Broek, Aldara activates TLR7-independent immune defence, Nat Commun 4 (2013) 1560.
[50] U.M. Musazzi, B. Santini, F. Selmin, V. Marini, F. Corsi, R. Allevi, A.M. Ferretti, D. Prosperi, F. Cilurzo, M. Colombo, P. Minghetti, Impact of semi-solid formulations on skin penetration of iron oxide nanoparticles, J Nanobiotechnology 15(1) (2017) 14.
[51] J. Wohlrab, Topical preparations and their use in dermatology, J Dtsch Dermatol Ges 14(11) (2016) 1061-1070.
[52] M.R. Prausnitz, et al. Skin barrier and transdermal drug delivery. In: Bolognia JL, Jorizzo JL, Schaffer JV, editors. Dermatology, 3rd edn. Philadelphia, PA: Elsevier Saunders; 2012. pp. 2065–74.
[53] R. Daniels, U. Knie, Galenics of dermal products--vehicles, properties and drug release, J Dtsch Dermatol Ges 5(5) (2007) 367-83.
[54] S. Khunmanee, Y. Jeong, H. Park, Crosslinking method of hyaluronic-based hydrogel for biomedical applications, J Tissue Eng 8 (2017) 2041731417726464.
[55] S.S. Kwon, B.J. Kong, S.N. Park, Physicochemical properties of pH-sensitive hydrogels based on hydroxyethyl cellulose–hyaluronic acid and for applications as transdermal delivery systems for skin lesions, Eur J Pharm Biopharm 92 (2015) 146-154.
[56] N.M. Salwowska, K.A. Bebenek, D.A. Zadlo, D.L. Wcislo-Dziadecka, Physiochemical properties and application of hyaluronic acid: a systematic review, J Cosmet Dermatol 15(4) (2016) 520-526.
[57] D. Petta, D. Eglin, D.W. Grijpma, M. D'Este, Enhancing hyaluronan pseudoplasticity via 4-(4,6-dimethoxy-1,3,5-triazin-2-yl)-4-methylmorpholinium chloride-mediated conjugation with short alkyl moieties, Carbohyd Polym 151 (2016) 576-583.
[58] P. Perdih, S. Cebasek, A. Mozir, E. Zagar, Post-polymerization modification of poly(L-glutamic acid) with D-(+)-glucosamine, Molecules 19(12) (2014) 19751-68.
[59] M. Essendoubi, C. Gobinet, R. Reynaud, J.F. Angiboust, M. Manfait, O. Piot, Human skin penetration of hyaluronic acid of different molecular weights as probed by Raman spectroscopy, Skin Res Technol 22(1) (2016) 55-62.
[60] S. Berkó, M. Maroda, M. Bodnár, G. Erős, P. Hartmann, K. Szentner, P. Szabó-Révész, L. Kemény, J. Borbély, E. Csányi, Advantages of cross-linked versus linear hyaluronic acid for semisolid skin delivery systems, Eur Polym J 49(9) (2013) 2511-2517.
[61] C. Li, S. Wallace, Polymer-drug conjugates: Recent development in clinical oncology, Adv Drug Deliv Rev 60 (2008) 886-898.
[62] J.J. Arroyo-Crespo, et al., Anticancer activity driven by drug linker modification in a polyglutamic acid-based combination-drug conjugate. Adv. Funct. Mater 28(13) (2018).
[63] L. Hu, P. Zhang, X. Wang, X. Cheng, J. Qin, R. Tang, pH-sensitive carboxymethyl chitosan hydrogels via acid-labile ortho ester linkage for potential biomedical applications, Carbohydr Polym 178 (2017) 166-179.
[64] J. Tian, V.J. Stella, Degradation of paclitaxel and related compounds in aqueous solutions III: Degradation under acidic pH conditions and overall kinetics, J Pharm Sci 99 (2010) 1288-98.

[65] P.T. Wong, S.K. Choi, Mechanisms of drug release in nanotherapeutic delivery systems, Chem Rev 115 (2015) 3388-432.
[66] E. Desmet, A. Ramadhas, J. Lambert, M. Van Gele, In vitro psoriasis models with focus on reconstructed skin models as promising tools in psoriasis research, Exp Biol Med (Maywood) 242(11) (2017) 1158-1169.
[67] C.K. Sen, G.M. Gordillo, S. Roy, R. Kirsner, L. Lambert, T.K. Hunt, F. Gottrup, G.C. Gurtner, M.T. Longaker, Human skin wounds: a major and snowballing threat to public health and the economy, Wound Repair Regen 17(6) (2009) 763-71.
[68] F. Gottrup, A specialized wound-healing center concept: importance of a multidisciplinary department structure and surgical treatment facilities in the treatment of chronic wounds, Am J Surg 187(5, Supplement 1) (2004) S38-S43.
[69] V.A. Ziboh, C.C. Miller, Y. Cho, Metabolism of polyunsaturated fatty acids by skin epidermal enzymes: generation of antiinflammatory and antiproliferative metabolites, Am J Clin Nutr 71(1 Suppl) (2000) 361S-6S.
[70] C.N. Serhan, N. Chiang, T.E. Van Dyke, Resolving inflammation: dual anti-inflammatory and pro-resolution lipid mediators, Nat Rev Immunol 8(5) (2008) 349-61.
[71] R. De Caterina, M.I. Cybulsky, S.K. Clinton, M.A. Gimbrone, P. Libby, The omega-3 fatty acid docosahexaenoate reduces cytokine-induced expression of proatherogenic and proinflammatory proteins in human endothelial cells, Arterioscler Thromb 14(11) (1994) 1829-36.
[72] R. De Caterina, J.K. Liao, P. Libby, Fatty acid modulation of endothelial activation, Am J Clin Nutr 71(1 Suppl) (2000) 213S-23S.
[73] E. Arab-Tehrany, M. Jacquot, C. Gaiani, M. Imran, S. Desobry, M. Linder, Beneficial effects and oxidative stability of omega-3 long-chain polyunsaturated fatty acids, Trends Food Sci Tech 25(1) (2012) 24-33.

FINAL CONCLUSIONS

FINAL CONCLUSIONS

During the development of this Thesis, we demonstrated the applicability of polymer therapeutics as platform technology to topically administer bioactive agents or drugs for the treatment, among others, of skin disorders such as psoriasis or wound healing.

Herein, we highlight the main conclusions resulting from this work:

1. We have developed *ex vivo* human skin models using human skin explants from donors as a useful tool to validate polymer-based treatments. We established a healthy skin model as well as an inflammatory skin model by treating the explants with a combination of LPS and EGF.

   The established *ex vivo* models have been validated as relevant preclinical models of disease for skin disorders. We evaluated tissue viability both in the healthy and in the inflammatory model by means of MTT assay as well as by immunohistochemistry, and several inflammatory markers were also used to analyze the inflammatory process. Finally, we detected the modulation of the release of pro-inflammatory cytokines to the culture media, demonstrating the inflammatory effect produced by the combined action of LPS and EGF.

2. We have characterized a preclinically relevant acute psoriatic mice model for testing and validating the polypeptide-based therapies developed. By topical application of imiquimod (IMQ) cream, we triggered the intrinsic characteristics of the psoriasis disease. We evaluated for ten days the progression and maintenance of the disease, by assessing the morphology of the skin using PASI score and also H&E staining, focusing on specific parameters of the disease, such as the epidermal thickening. We also studied the increase in spleen weight after the application of IMQ, correlated with the synthesis of cytokines. Finally, we identified specific pro-inflammatory cytokines related to the human disease both in tissue and in serum.

3. To improve and optimize the penetration of nanocarriers through the skin, we have developed and fully characterized a hyaluronic-poly-L-glutamate cross-

polymer (HA-CP) vehicle (composed by hyaluronic acid (HA) and poly-L-glutamic acid (PGA) cross-linked through lysine moieties). We validated and demonstrated its properties as skin penetration enhancer by means of its use with a family of amphiphilic block copolymers of different nature and consequently different solution conformation, thereby modulating the final skin permeation enhancement. Changes in the nanocarrier solution conformation were driven by the presence of Phe as aminoacid in the polymer chain, as well as the polymer size among other features.

4. We have developed a family of polymer-drug conjugates, based on the biodegradable carrier poly-L-glutamic acid (PGA), incorporating a corticosteroid (fluocinolone acetonide) by means an ester bond for the topical treatment of psoriasis. An exhaustive characterization using several techniques were employed to fully characterize our conjugates in relevant solutions, establishing a relation between the structure and their biological activity.

5. *In vitro* evaluation of the developed conjugates in relevant skin cell lines revealed the absence of toxicity up to the concentrations tested. Cellular internalization and anti-inflammatory activity studies demonstrated the ability of the conjugates to penetrate into the skin cells and maintain the anti-inflammatory activity of the drug once conjugated to the PGA.

6. *Ex vivo* evaluation of the conjugate alone or applied in the HA-CP vehicle as penetration enhancer demonstrated its presence in the viable epidermis. Moreover, using two *ex vivo* models, our developed inflammatory *ex vivo* human skin model and a reconstructed inflammatory skin equivalents model (in collaboration with Freie Universität Berlin, Prof S. Hedtrich), we demonstrated the enhanced activity of the conjugate to reduce the release of IL-6 compared to the free drug.

7. *In vivo* evaluation in our established psoriatic mice model demonstrated the anti-inflammatory/anti-psoriatic efficacy and safety of our conjugate compared to the free drug demonstrating the importance of the use of adequate linking chemistry

in order to control drug release kinetics in the adequate skin layers. Of note, the conjugate applied in the HA-CP vehicle revealed enhanced activity and effectiveness, demonstrating also the importance of the selection of an appropriate vehicle to improve the penetration through the skin. HA-CP showed high hydration properties which synergizes with the anti-inflammatory effects of the corticosteroid conjugate, resulting in a significantly improved therapeutic approach for psoriasis.

8. Finally, we have developed a new family of polymer-drug conjugates, using PGA as a carrier, incorporating different loadings of an omega 3 fatty acid (diDHA) by means of an ester bond for the topical treatment of wound healing. We thoroughly studied the physico-chemical characteristics of the conjugate optimizing diDHA loading, and the *in vitro* biological evaluation revealed its suitability for wound healing applications, enhancing the closure of the wound.

9. The family of PGA-diDHA conjugates were validated *in vivo* in a wound healing scenario using an ischemia-reperfusion (I/R) model in collaboration with Hospital La Fe (Dr P. Sepúlveda) clearly showing the advantages of polymer conjugation. Infusion of the conjugates and free diDHA in an *in vivo* I/R rat model showed that infarct size was significantly reduced when PGA-diDHA6.4 was administrated before reperfusion in comparison with free diDHA at the same dose. Collectively, our data showed that PGA-diDHA6.4 could be effective in mitigating I/R-induced injury thereby providing a new therapeutic agent for future clinical studies.

APPENDIX

THESIS PROJECT, OBJECTIVES,

MAIN METHODOLOGY,

RESULTS AND CONCLUSIONS IN SPANISH

1. Introducción y antecedentes de la Tesis

La administración local de agentes bioactivos representa la principal vía de administración para lograr una actividad terapéutica local debido a su idoneidad y asequibilidad en comparación con otras vías de administración, como la intravenosa e intramuscular, lo que mejora el cumplimiento del tratamiento por parte del paciente y la aceptación por parte del clínico [1]. Los principales lugares del cuerpo que pueden beneficiarse de la administración local son la piel, la vagina, los ojos o la nariz, pero también otros órganos, como el corazón, a los que se puede llegar mediante dispositivos que actúan como reservorio y son capaces de mejorar el transporte del fármaco a través del endotelio. El principal reto de la vía de administración tópica es sortear eficientemente las barreras biológicas para lograr una concentración óptima del agente terapéutico en el lugar de acción deseado, durante el tiempo necesario para llevar a cabo la actividad farmacológica [2].

La piel es el órgano más extenso del cuerpo humano, por lo que representa la principal barrera biológica del cuerpo frente a amenazas externas [3]. La piel está compuesta por distintas capas, divididas principalmente entre la epidermis y la dermis. Esta complejidad fisiológica ejerce una protección a nuestro organismo, sin embargo, también evita la penetración de agentes terapéuticos cuando se administran de forma tópica, y por tanto su efectividad se encuentra limitada. Además, muchos de los medicamentos tópicos actualmente utilizados o en ensayos clínicos carecen de las características físico-químicas adecuadas para su administración a través de la piel. Por este motivo, actualmente se están desarrollado varias estrategias para mejorar las propiedades físico-químicas de los agentes terapéuticos de acuerdo con las características del sitio de acción deseado, mejorando la administración tópica así como la estabilidad de los fármacos. Algunos métodos incluyen la utilización de profármacos [4] o el desarrollo de nanomedicinas mediante la conjugación de agentes terapéuticos a diferentes portadores con características específicas [5]. Dichas nanomedicinas protegen al agente terapéutico frente a la degradación prematura y también interactúan con varios componentes de la piel, incrementando su penetración a través de las diferentes capas de la piel, y aumentando el tiempo de retención en el sitio de acción deseado [6, 7].

Los portadores de tamaño nanométrico son especialmente útiles para la administración pasiva de agentes terapéuticos, induciendo el tránsito a través de la piel sin necesidad de aporte de energía o de receptores específicos. Algunos de los nanotransportadores más utilizados son las nanopartículas, los liposomas, las micropartículas, los nanocristales, los polímeros, los niosomas, los dendrímeros, entre otros [8, 9].

En esta Tesis se describe un enfoque específico de la nanomedicina mediante la utilización de Polímeros Terapéuticos [10], cuyo principal objetivo en este trabajo es aumentar la penetrabilidad de los agentes bioactivos a través de la piel, mejorar sus propiedades físico-químicas y liberar el fármaco de una manera controlada en la capa de la piel específica. Los Polímeros Terapéuticos engloban una amplia variedad de sistemas macromoleculares, presentando la mayoría una estructura común basada en un enlace químico (covalente) entre el agente(s) bioactivo y el transportador polimérico que es soluble en medio acuoso. Las principales ventajas de la conjugación de fármacos a los transportadores poliméricos se pueden resumir en: (i) mayor solubilidad en medios acuosos, (ii) control sobre el tamaño final del conjugado (tamaño nanométrico), (iii) protección del agente terapéutico contra la degradación por enzimas proteolíticas o absorción celular inespecífica, (iv) prevención o reducción de la agregación, la inmunogenicidad y la antigenicidad, (v) farmacocinética modificada tanto a nivel celular como incluso subcelular y (vi) liberación controlada y sostenida del fármaco en el lugar de acción específico gracias a los enlaces polímero-fármaco biosensibles en presencia de condiciones específicas [11]. Además, el desarrollo de nuevos Polímeros Terapéuticos basados en la utilización de polímeros biodegradables y biocompatibles, como los aminoácidos, supone un avance frente a las limitaciones que presentan otros polímeros que no son biodegradables [12]. En esta Tesis, nos centramos en la utilización de poliglutamatos (PGA) para llevar a cabo la conjugación de fármacos, basándonos en los buenos resultados obtenidos en ensayos clínicos del conjugado PGA-paclitaxel (Opaxio^{TM}) para el tratamiento de varios tipos de cáncer [13].

Cabe destacar que la correcta selección del vehículo para la administración de estos polímeros es un parámetro crítico para favorecer la eficacia y la aceptabilidad de las formulaciones tópicas, ya que la permeabilidad a través de las diferentes capas de la piel está modulada y relacionada con las propiedades del vehículo utilizado [14], por lo que las propiedades físico-químicas del vehículo condicionan su efecto sobre la piel. Por ello,

en este trabajo se propone la utilización de un nuevo vehículo basado en el ácido hialurónico [15, 16], para favorecer la penetración de estos polímeros a través de la piel.

En esta Tesis nos hemos centrado en la administración tópica de terapias avanzadas validando una nueva plataforma de administración de fármacos a nivel tópico basada en la utilización de Polímeros Terapéuticos, principalmente para patologías de la piel (como la psoriasis o la cicatrización de heridas), pero también hemos explorado ligeramente un enfoque de administración local para disminuir el daño de la lesión por isquemia/reperfusión (I/R) en el corazón.

2. Objetivos de la investigación

La presente tesis doctoral se centra en el desarrollo de plataformas poliméricas para la administración de fármacos de manera tópica como nuevos enfoques de tratamiento, por ejemplo, para trastornos de la piel, como la psoriasis y la cicatrización de heridas. El desarrollo de nuevos conjugados poliméricos debe basarse en enfoques sintéticos bien establecidos así como en el diseño racional de los conjugados, seguido de una caracterización físico-química exhaustiva y una evaluación biológica completa en modelos preclínicos relevantes, con el objetivo de avanzar hacia un posible escenario clínico.

Este objetivo general puede resumirse en los siguientes objetivos específicos:

1. Desarrollo y caracterización exhaustiva de modelos de piel humana *ex vivo* sanos e inflamatorios, así como un modelo preclínico de psoriasis en ratones, ambos como plataformas para evaluar y validar terapias avanzadas basadas en polipéptidos. (Capítulo II)

2. Síntesis, caracterización físico-química completa y evaluación biológica de nuevos materiales a base de ácido hialurónico reticulado y polipéptidos (solos o en combinación) como portadores capaces de mejorar la penetración de fármacos a través de la piel. (Capítulo III)

3. Diseño, síntesis y caracterización físico-química exhaustiva de conjugados de ácido poli-L-glutámico y corticosteroides para el tratamiento tópico de la psoriasis. Optimización de la química de conjugación y evaluación biológica para lograr una

prueba de concepto para mejorar la actividad antiinflamatoria y antipsoriásica después de la conjugación. (Capítulo IV)

4. Diseño, síntesis, caracterización físico-química exhaustiva y evaluación biológica en modelos preclínicos relevantes de una familia de conjugados de ácido poli-L-glutámico para los trastornos de cicatrización de heridas (incluida la cicatrización de heridas en la piel y en el tejido cardíaco). (Capítulo V)

3. Metodología

3.1. Materiales e instrumentación

3.1.1. Materiales

Todos los reactivos y disolventes utilizados durante el desarrollo de la presente Tesis fueron de grado analítico o superior, sin purificación adicional (a no ser que se indique lo contrario en el correspondiente apartado). Generalmente, las reacciones llevadas a cabo en disolventes orgánicos se realizaron bajo atmósfera inerte de nitrógeno o argón. El agua utilizada era desionizada, presentando una conductancia menor que 0.06 μS (agua milliQ).

Los métodos más empleados para llevar a cabo la purificación de los conjugados poliméricos fueron principalmente la cromatografía por exclusión de tamaño, utilizando resina Sephadex® LH-20 medium (disolventes orgánicos) o Sephadex® G-25 medium (fase acuosa). Además, se utilizó la diálisis (con membranas de 3, 30 kDa) y la ultrafiltración (Vivaspin®).

Los animales de experimentación utilizados en la Tesis, se adquirieron en Envigo Laboratories Inc. (España). Se utilizaron ratones machos de 6 semanas de la cepas BALB/c OlaHsd.

3.1.2. Instrumentación

Espectroscopía de Resonancia Magnética Nuclear (RMN): Los espectros de RMN se llevaron a cabo en un sistema Bruker Advance AC 300 (Billerica MA, USA) utilizando al menos 5 mg de compuesto, temperatura ambiente y disolventes deuterados. Los datos obtenidos se analizaron mediante el software Topspin (Bruker GmbH, Karlsruhe, Germany).

Espectroscopía Ultravioleta-Visible (UV-Vis): Los espectros fueron adquiridos en un espectrofotómetro Jasco V-630 (JASCO Corporation, Spain) a 25˚C con celdas de cuarzo de 1 cm y ancho de banda de 0.5 nm.

Espectroscopia por dicroísmo circular: Se llevó a cabo en un espectrómetro J-815 CD Spectrometer equipado con un soporte de celda termostatizado (PTC-423), un refrigerante (JASCO Corporation, Spain) y flujo controlado de nitrógeno (~2.7 L.min-1) (Afriso Euro-Index, Germany). Las muestras se midieron en agua MilliQ, PB 7.4 y a diferentes pHs (7.4 y 5.5) para polímeros en la forma sal sódica. Las medidas se realizaron en cubetas de cuarzo, de d= 0.1 cm y por triplicado.

Dispersión de Luz Dinámica (DLS): Las medidas tanto de tamaño de partícula como de potencial Z se realizaron a 25˚C en un dispositivo Malvern Zetasizer Nano ZS equipado con un láser (532 nm), utilizando un ángulo de dispersión fijo de 90˚ (Malvern Instruments Ltd., UK). La celda utilizada fue DTS 1070. Para las medidas de tamaño, el tiempo de equilibrado fue de 0 min con atenuación automática. El índice de refracción del disolvente (agua) fue 1.330 y, por lo tanto, la viscosidad fue 0.8872. Para el análisis de los diferentes polímeros se utilizó el índice de refracción del látex de poliestireno (1.590). Cada muestra se midió tres veces con 10 submedidas.

Cromatografía de permeabilidad en gel en medios acuosos: Las mediciones en medios acuosos que contienen 150 mM de $NaNO_3$, se realizaron utilizando 5 mM de tampón fosfato (PB) a pH 5 y 0.005 % (p/p) de azida sódica como aditivo en un sistema AF2000 de Postnova Analytics (Landsberg, Germany). El sistema fue configurado para funcionar con una bomba isocrática (PN1130), un muestreador automático (PN5300), un índice de refracción (RI, PN3150), 21 ángulos múltiples de dispersión de luz (MALS, PN3621) y detectores ultravioleta-visible (UV-Vis) (PN3211). La columna utilizada fue TSKgel G6000PWXL, empleando un caudal de trabajo de 0.8 mL/min a 30°C. El índice de refracción y la dispersión de luz multiángulo se utilizaron para la detección y la determinación del peso molecular.

Microscopía Electrónica de Transmisión (TEM): Las imágenes se adquirieron en un microscopio de transmisión electrónica EM 410 Philips. Para su preparación, las muestras se adsorbieron en rejillas de cobre recubiertas por una película de carbón de 200 mallas. Seguidamente, se realizó una tinción de contraste negativo con una disolución de ácido fosfotúngstico al 0.1%.

Victor^2 Wallac^{TM} para medidas de absorbancia o fluorescencia: Para determinar absorbancias o fluorescencias se utilizó un equipo Victor^2 Wallac^{TM} 1420 (Perkin Elmer, Spain) utilizando placas de 96 pocillos y las correspondientes longitudes de onda (emisión/excitación) propias de cada compuesto.

Cromatografía líquida de alta eficacia (HPLC): La determinación analítica de la cantidad de fármaco libre y la cinética de liberación de los fármacos se realizó en un sistema HPLC Waters (Waters Corporation, S.A, Spain) provisto de bombas binarias 2x515, automuestreador 717 Plus, FLD 2475 y PDA 2996. Las medidas se realizaron utilizando una columna analítica RP C-18 Licrospher (125x4.0mm) (Scharlab S.L., Spain). Los cromatogramas fueron tratados con el software Empower 2.0 (Waters Corporation, S.A, Spain).

Microscopía Confocal: Las imágenes fueron adquiridas con un microscopio (invertido) láser confocal Leica, modeloTCS SP8 AOBS (Leica Microsystems Heidelberg and MBH, Germany). Todas las imágenes se adquirieron bajo las mismas condiciones y se analizaron mediante el software de Leica LAS AF Lite (Leica Microsystems Heidelberg and MBH, Germany).

3.2. Métodos más relevantes

3.2.1. Protocolos de síntesis

Síntesis de un polímero entrecruzado de ácido hialurónico (HA) y ácido poli-glutámico (PGA): Paralelamente se preparan cuatro soluciones: HA (100 mg, 0.249 mmol, 1 eq.) (solución A) y PGA (2.6 mg, 0.017 mmol, 0.07 eq.) (solución B) se disuelven por separado en agua destilada. (C) DMTMM·Cl utilizado como agente de acoplamiento (44 mg, 0.159 mmol, 0.6 eq. a ácidos carboxílicos totales) se disuelve en agua destilada. La sal de clorhidrato de L-lisina (1.5 mg, 0.008 mmol, 0.03 eq. a ácidos carboxílicos totales) se disuelve en agua destilada. A continuación, la solución B se agrega a la A, seguidamente se agrega C y se mezcla, ajustando el pH a 7 con unos pocos microlitros de 1 M NaOH. La solución se agita durante 15 minutos. A continuación, se añade D y se ajusta el pH a 8.5 con unos pocos microlitros de 1 M NaOH. La mezcla se deja reaccionar durante toda noche a temperatura ambiente. Tras ello, el producto es purificado por diálisis usando Vivaspin®, utilizando una membrana MWCO de 30 kDa. En primer lugar, el producto se lava con 5 mM tampón fosfato (PB) utilizando un pH de

7.5, y seguidamente, se lava con agua destilada. La solución final es liofilizada, obteniendo un polvo blanco.

Síntesis general de los copolímeros en bloque a partir de polietilenglicol (PEG): La síntesis de los copolímeros en bloque compuestos por PEG-poliaminoácido se efectúa ajustando la relación [monómero]/[iniciador] para obtener el grado de polimerización deseado. Brevemente, el monómero NCA (3.923 mmol, 10 eq.) se pesa en un tubo de Schlenk, equipado con una barra de agitación y secado a 80ºC en un horno durante al menos 24 h antes de comenzar la reacción. El tubo es purgado con ciclos de argón/vacío, y el monómero se disuelve en 4 mL de DMF seco. A continuación, el macroiniciador MeO-PEG-NH_2 se pesa en un vial, se purga con argón y se disuelve en 1 mL de DMF seco. Tras ello, la solución iniciadora se agrega a la solución de monómero, manteniéndose la atmósfera de argón a 4ºC bajo agitación vigorosa durante 3 - 4 días. Finalmente, la mezcla de reacción se vierte sobre más de 50 mL de Et_2O, y el precipitado obtenido se filtra y lava con Et_2O adicional. Tras ello, se realiza una purificación adicional mediante suspensión en THF y precipitación sobre el exceso de Et_2O, se filtra y se seca bajo la corriente de N_2.

Marcaje con Cyanine 5.5 (Cy5.5) para estudios de internalización en piel: El marcaje con Cy5.5 se realizó mediante la conjugación a los materiales basados en el HA mediante enlace tipo amida. Brevemente y a modo de ejemplo, HA-CP (100 mg, 0.249 mmol, 1 eq.) se disuelve en agua destilada. Paralelamente, el agente de acoplamiento DMTMM·Cl (3.4 mg, 0.012 mmol, 0.05 eq) se disuelve en agua y la solución de DMTMM·Cl se añade a la solución HA-CP, ajustando el pH a 7 con unos pocos microlitros de 1 M NaOH. La activación del acoplamiento del ácido carboxílico a través de DMTMM·Cl se lleva a cabo durante 30 minutos. A continuación, se añade la solución de Cy5.5 (1.8 mg, 0.003 mmol, 0.01 eq.) previamente preparada en una mezcla de H_2O:DMSO (1:1), y se ajusta el pH a 8.5 con unos pocos microlitros de 1 M NaOH. La solución azul resultante de la reacción de conjugación se deja actuar durante 72 horas a temperatura ambiente. Tras ello, el producto se purifica por diálisis usando Vivaspin® (MWCO 30 kDa). El producto se debe lavar con 5 mM PB a un pH de 7.5, y seguidamente con agua destilada. Finalmente, la solución resultante se liofiliza, obteniendo un polvo azul.

El contenido de Cy5.5 se determinó por espectroscopia UV-Vis, con filtro de excitación de 680 nm de longitud de onda y filtro de emisión de 595 nm a través de una curva de calibrado previa.

Protocolo para la conjugación de Acetónido de Fluocinolona (FLUO) al PGA: La conjugación se llevó a cabo para alcanzar alrededor de un 8% molar de FLUO en relación con los residuos de glutamato, a través de enlaces tipo éster. Como ejemplo para describir la síntesis, utilizamos un lote de 200 mg de PGA.

Brevemente, en un matraz provisto con un agitador magnético y una entrada y salida de nitrógeno, se agrega PGA en forma ácida (200 mg, 1.55 mmol) y se disuelve en DMF anhidro (5 mL) bajo atmósfera de nitrógeno. Seguidamente, se agrega FLUO (140.27 mg, 0.3 mmol, 0.2 eq. a unidades de ácido glutámico) disuelto en 1 mL DMF y se permite que la mezcla se agite durante diez minutos. Tras ello, la mezcla de reacción se enfría en baño de hielo, y se agrega 1 mL de DMF con DMAP (1.9 mg, 0.0155 mmol, 0.01 eq. a unidades de ácido glutámico) y 4 mL de DMF con EDAC (89.22 mg, 0.465 mmol, 0.3 eq. a unidades de ácido glutámico). La mezcla se deja reaccionar durante 72 horas. La cromatografía de capa fina (MeOH) confirma el consumo de FLUO. La solución final se purifica mediante cromatografía de exclusión de tamaño utilizando Sephadex® LH-20 y después de evaporar el DMF (en condiciones de vacío) el residuo se disuelve con 0.5 M $NaHCO_3$ para pasarlo a forma sal y volver a purificarlo con Sephadex® G-25. Finalmente, la suspensión acuosa resultante se liofiliza obteniendo un polvo blanco.

Marcaje con Oregon Green (OG) 488 Cadaverina para estudios de internalización celular y en piel: El marcaje con OG se realizó mediante la conjugación al conjugado polímero-fármaco o al polímero mediante enlace tipo amida. Brevemente, siguiendo el protocolo descrito para la síntesis del conjugado PGA-FLUO, después de agregar el PGA y el fármaco disueltos en DMF, se añaden 2.745 mg de DMTMM·BF_4 ($8.366x10^{-3}$ mmol, 0.02 eq.) a la solución y se deja transcurrir durante diez minutos a temperatura ambiente. A continuación, se añaden 0.01 eq. del fluoróforo OG y se ajusta el pH a 8 mediante la adición de DIEA. La mezcla se deja reaccionar durante 48 horas a temperatura ambiente y protegida de la luz. Tras ello, el disolvente es eliminado a vacío, y el producto se disuelve con 0.5 M $NaHCO_3$ para pasarlo a forma sal. Finalmente, se procede a su purificación mediante los métodos estándar de diálisis, Sephadex® G-25 o

precipitación ácido-base. Finalmente, la suspensión acuosa resultante se liofiliza obteniendo un polvo naranja.

El contenido de OG se determinó por espectroscopia UV-Vis, con filtro de excitación de 490 nm de longitud de onda y filtro de emisión de 535 nm a través de una curva de calibrado previa.

3.3. Ensayos *In vitro*

Degradaciones con Catepsina B: La biodegradabilidad de varios conjugados polímero-fármaco en presencia de la enzima lisosomal catepsina B fue evaluada *in vitro*. Brevemente, se prepararon disoluciones de 2 mg/mL de polímero en tampón acetato (para 3 mg de polímero, 700 μL de tampón acetato 20 mM, pH 6, 100 μL de EDTA 2 mM, 100 μL de DTT 5 mM). A continuación, se añadieron 6.25 unidades de catepsina B disueltas en 100 μL de tampón acetato pH 6, 20 mM. Las mezclas se mantuvieron a 37°C bajo agitación, y se tomaron alícuotas a diferentes tiempos (0, 0.5, 1, 3, 6, 10, 24, 30, 48 y 72 horas). La concentración de fármaco liberada en cada tiempo de estudio se analizó mediante HPLC.

Cultivos celulares: Las células HaCaT (CLS Cell Lines Servic, Germany) se cultivaron en medio DMEM Glutamax alto en glucosa (Fisher, Spain) mientras que los fibroblastos humanos (Hospital La Fe, Spain) y la línea celular Raw264.7 CLS Cell Lines Service, Germany) se cultivaron en medio DMEM (Sigma-Aldrich Chemical Co., Spain). Los medios de cultivo fueron complementados con un 2% de penicilina/estreptomicina y 50 mL de suero fetal bovino (FBS). Las células se mantuvieron a 37°C en atmósfera con un 5% de CO_2. En las 3 líneas celulares, el medio se renovó cada 2 - 3 días y se pasaron al menos una vez por semana cuando se alcanzó el 80% de confluencia.

Ensayos de viabilidad celular (MTS): Las células se sembraron en placas estériles de 96 pocillos a una concentración de 4000 células/cm^2 para HaCaT, 2000 células/cm^2 para los fibroblastos y 6000 células/cm^2 para Raw264.7. Después de la siembra, las placas se incubaron durante 24 horas y transcurrido ese tiempo se añadieron los tratamientos (previamente filtrados con un filtro de 0.22 μm). Transcurridas 72 horas de incubación, se añadió 20 μL de la mezcla MTS/PMS (20:1) a cada pocillo, y la placa se incubó durante 3 horas más (2 horas en el caso de Raw264.7) en oscuridad. Transcurrido este tiempo, la densidad óptica de cada pocillo se midió

espectrofotométricamente a 490 nm utilizando el equipo Victor^2 Wallac^{TM} (Perkin Elmer, Spain). Los valores de absorbancia se representaron como porcentaje de viabilidad celular tomando como 100% de viabilidad celular células control no tratadas.

Internalización de los conjugados marcados con OG mediante citometría de flujo: Las células HaCaT fueron sembradas en placas de 6 pocillos a una densidad de células de 118751 células/cm^2, y se incubaron durante 24 horas. El estudio se realizó transcurridas las 24 horas tanto a 4°C como a 37°C. Para el experimento a 4°C, las células se pre-incubaron a esa temperatura durante 30 minutos antes de empezar el experimento. Para ambas temperaturas, 30 minutos antes de añadir el compuesto a estudiar, se añadió 0.4 µL de una solución de 5 µM de inhibidor de catepsina B CA-074 (alcanzando una concentración final de 2 µM). Seguidamente, se añadieron 15 µL de una solución del conjugado marcado con OG a diferentes tiempos (0 a 27 horas), tanto a las células incubadas a 37°C como a 4°C. Tras ello, las placas se colocaron en hielo, las células fueron lavadas dos veces con PBS-BSA 0.1% y se añadieron 400 µL de tripsina para levantar las células. Finalmente, las células se resuspendieron en 600 µL de medio celular y se depositaron en tubos de citometría de flujo. El pellet se analizó con el citómetro de flujo Becton Dickinson FACS Calibur cytometer (California, USA) equipado con un láser de argón (488 nm) y filtro de emisión de 550 nm. Los datos se expresaron en porcentaje de células positivas. Se utilizaron células incubadas sin polímero para eliminar la fluorescencia de fondo.

Internalización celular por microscopía confocal: Las células fueron incubadas en las mismas condiciones que para citometría de flujo, pero la siembra se realizó sobre un cristal para recoger posteriormente las muestras y analizarlas mediante microscopía confocal. Al igual que en la citometría de flujo, primero se añadió el inhibidor de catepsina B (misma cantidad que para citometría) 30 minutos antes de la adición del conjugado marcado con OG. Seguidamente, se añadieron 15 µL de una solución del conjugado marcado con OG a diferentes tiempos (0 a 72 horas) y las células se incubaron a 37°C. 30 minutos antes de efectuar el lavado de las células con PBS-BSA 0.1%, se añadió el marcador nuclear (Hoetch, 1 µL de una disolución 5 mM) y lisosomal (Lysotracker Red, 0.75 µL de una disolución 100 µM). Finalmente, las células se lavaron con PBS-BSA al 0.1%, y el cristal fue acoplado a una cámara para microscopía con medio nuevo, conteniendo 2 µM de CA-074. Las imágenes fueron capturadas con un

microscopio DM IRE2 invertido, excitando con los láseres de argón (OG 496 nm), HeNe (Lysotracker Red 594 nm) y diodo azul (Hoetch 405 nm).

Evaluación de la actividad antiinflamatoria en Raw264.7: Se sembraron 50 µL de células en placas de 96 pocillos a una concentración de 6000 células/cm^2. Después de 24 horas, se evaluó la combinación de 25 µL de lipopolisacárido (LPS) de *E. coli* (5 ng/mL) para inducir la síntesis de citoquinas proinflamatorias, junto con 25 µL de cada tratamiento: FLUO libre (0.49 ng/mL), PGA-FLUO (a los mismos equivalentes de FLUO libre) y PGA. Todos los tratamientos fueron filtrados antes de añadirlos al pocillo (tamaño de poro 0.22 µm). Las células fueron incubadas con muestras o controles durante 72 horas. Tras ello, las placas de 96 pocillos fueron centrifugadas durante 5 minutos, a 22°C y 400 rcf, y 90 µL del sobrenadante fueron recogidos y congelados hasta su uso. Para la cuantificación de citoquinas proinflamatorias se utilizó un ensayo LUMINEX® (kit Affymetrix m Th1/2/9/9/17/22/Treg 17plex, eBioscience, Spain). Este estudio se analizó mediante el equipo LUMINEX 200 (LUMINEX corporation, USA), y los resultados se expresaron como porcentaje de inhibición de cada citoquina.

3.4. Ensayos *Ex vivo*

3.4.1. Estudios de penetración a través de piel humana mediante celdas de difusión de Franz

Las muestras de piel se obtuvieron de mujeres sanas que se sometieron a cirugía plástica (reducciones de pecho) después del consentimiento informado por escrito (piel cedida por Hospital La Fe, Valencia, Spain). Inmediatamente después de la escisión, se eliminó el tejido graso subcutáneo con un bisturí. La piel se cortó en trozos de 4 cm^2, se envolvió en papel de aluminio y se almacenó a -20ºC hasta su uso. El estudio de penetración a través de la piel humana se desarrolló utilizando las celdas de difusión de Franz (Logan Instruments Corp., EE.UU.).

La piel fue fijada entre el compartimento donador y el receptor, de modo que el estrato córneo se colocó hacia arriba. La cámara receptora se llenó con 8 mL de PBS 0.01 M, pH 7.4 y se mezcló con una barra agitadora magnética, mientras que la temperatura se mantuvo a 37ºC. Se colocó la piel entre las celdas y se aplicó en el compartimento donador 100 µL del tratamiento de estudio marcado con el fluoróforo correspondiente, a una concentración de 10 mg/mL, para poder observar su penetración a través de la piel

mediante microscopia confocal. Además, se tomaron alícuotas del compartimento receptor a tiempo 0, 8 y 24 horas (dependiendo del estudio realizado). Los 2 mL de la muestra tomada se rellenaron inmediatamente con solución fresca. Después de 8 o 24 horas de ensayo, las muestras de piel se lavaron dos veces con PBS-BSA 0.1% y se mantuvieron en paraformaldehído (PFA) al 4% durante 24 horas a temperatura ambiente. A continuación, las muestras se lavaron con un 30% de sacarosa en solución de PBS, y se mantuvieron en ella 24 horas a 4ºC. Finalmente, las muestras de piel se lavaron dos veces con PBS y se conservaron en una solución de criopreservación (40% PB 0.1 M, 30% etilenglicol y 30% glicerol) a 4ºC hasta su utilización. A continuación, las muestras de piel se incluyeron en el medio de inclusión de temperatura de corte óptima (OCT) y se realizaron cortes de 5 µm con el criostato (versión CM1850 UV, Leica, Alemania), para analizar las muestras finalmente mediante microscopía confocal. Los núcleos celulares fueron marcados con DAPI para diferenciar las distintas capas de la piel. Las imágenes se capturaron con un microscopio DM IRE2 invertido equipado con un objetivo de inmersión en aceite λ-blue 40x y se manipularon con un sistema TCS SP2, equipado con un divisor de haz óptico acústico (AOBS). La excitación se realizó con un láser de argón (OG, 496 nm), diodo azul (DAPI, 405 nm) y diodo rojo (Cy5.5 o Dil, 675 nm). Las imágenes se procesaron con el software LCS (versión 2.5.1347a, Leica, Alemania). También se analizó el tejido control, el cual siguió el mismo tiempo de estudio utilizando como tratamiento agua MilliQ para establecer la autofluorescencia. Además, utilizando el programa Image J se realizaron medidas de la intensidad de fluorescencia para cada fluoróforo (cuantificando 5 veces por muestra), y el resultado se expresó en píxeles frente al grosor de la piel (µm). La intensidad del control fue restada en cada caso.

3.4.2. Viabilidad del tejido y evaluación de la actividad antiinflamatoria de los conjugados en un modelo de inflamación en piel humana *ex vivo*

Las muestras de piel se obtuvieron de mujeres sanas que se sometieron a cirugía plástica (reducciones de pecho) después del consentimiento informado por escrito (piel cedida por Hospital La Fe, Valencia, Spain). Inmediatamente después de la escisión, se eliminó el tejido graso subcutáneo con un bisturí. La piel fue cortada aproximadamente en 1 cm^2 y se colocó en unas rejillas metálicas situadas en placas de 6 pocillos, de modo que el la dermis estaba en contacto con el medio de cultivo DMEM, complementado con 50 mL de suero fetal bovino, 5.5 mL de penicilina/estreptomicina y 50 µL anfotericina

B, quedando la epidermis expuesta al aire. El modelo de piel se incubó a 37ºC y 5% de CO_2. El modelo inflamatorio fue inducido mediante la adición de una combinación de 2.5 ng/mL de factor de crecimiento epidérmico (EGF) y 15 µg/mL de LPS de *E. coli* al medio de crecimiento durante 24 horas (ver **Capítulo II** para más detalles).

Después de 24 horas en cultivo, se aplicaron los tratamientos. El control negativo y el control no tratado fueron evaluados para asegurar el desarrollo del modelo. 3 µL de una solución a 10 mg/mL de los tratamientos bajo estudio fueron aplicados tópicamente durante 24, 48 o 72 horas (según experimento). Después de este tiempo, las muestras de piel se lavaron dos veces con PBS y se introdujeron en 4 mL de solución de MTT (2 mg/mL) a 37ºC. Después de 4 horas de incubación, las muestras de piel fueron lavadas dos veces con PBS e introducidas en 4 mL de DMSO, para extraer el formazán de la piel. Después de 15 horas de extracción, la absorbancia fue leída a 490 nm usando el lector de placas Victor^{2}Wallac™.

Finalmente, para cuantificar los niveles de citoquinas proinflamatorias secretadas por la piel, se recogieron los medios de cultivo en condiciones estandarizadas después de cada tiempo de tratamiento, y se conservaron a -80ºC hasta su uso. Las concentraciones de IL-6 se midieron mediante el ensayo ELISA (Invitrogen, Spain) y se determinaron de acuerdo con las soluciones estándar.

3.5. Ensayos *In vivo*

3.5.1. Consideraciones éticas

Los experimentos con animales se realizaron de acuerdo con las directrices del Consejo de la Comunidad Europea (86/609/CCE) y con el Real Decreto español 1201/2005. Los procedimientos experimentales realizados durante esta Tesis fueron aprobados por el comité institucional sobre el cuidado y uso de animales, así como realizados por personal acreditado y capacitado. Los ratones utilizados se mantuvieron durante todo el proceso en una instalación libre de patógenos específicos (SPF), a una temperatura y humedad específica, y bajo un ciclo de luz-oscuridad de 12 horas. Además, como alimento se proporcionó pienso estandarizado libre de alfalfa y agua *ad-libitum*. Durante los estudios, se evaluó el aspecto y comportamiento general, la conducta de acicalamiento y el peso corporal desde el comienzo del experimento para garantizar el bienestar animal.

3.5.2. Establecimiento de un modelo murino de psoriasis mediante la aplicación de la imiquimod en forma de crema

Ratones machos BALB/c (BALB/cOlaHsd) de 6 semanas de edad fueron utilizados para todos los procedimientos experimentales. Un día antes de la primera aplicación de imiquimod (IMQ) en forma de crema, se afeitó aproximadamente 2x3 cm de la parte posterior de los ratones. Los síntomas similares a los de la psoriasis fueron inducidos por la aplicación diaria durante 7 días consecutivos de 62.5 mg de crema de IMQ disponible comercialmente (5%) (Imunocare; Industrial Farmacéutica Cantabria, S.A., Spain) tanto en la espalda como en la oreja derecha, lo que se traduce en una dosis diaria de 3.125 mg del compuesto activo. Después de los 7 días de aplicación, la progresión de la enfermedad se estudió durante 10 días más, para evaluar los días adecuados para añadir los tratamientos posteriores asegurando el mantenimiento de la enfermedad. Después de este periodo, los animales fueron sacrificados utilizando una atmósfera de CO_2 y los órganos de interés fueron aislados y evaluados.

3.5.3. Evaluación de la actividad antipsoriática de los conjugados poliméricos

Mediante estudios previos se establecieron 7 días de aplicación de la crema de IMQ y 5 días de tratamiento con los polímeros sintetizados. Por lo tanto, siete días después de la inducción de la enfermedad, los ratones fueron divididos en grupos representativos. Se utilizaron ratones sanos y sin tratar como control negativo y positivo, respectivamente. Se realizaron estudios previos para optimizar la concentración óptima equivalente de FLUO, seleccionando 0.15% equivalentes de FLUO para realizar el experimento con todos los tratamientos. Los conjugados se disolvieron en nuestro nuevo vehículo de ácido hialurónico entrecruzado con PGA (HA-CP) al 1% (ver **Capítulo III** para más detalles), y en una crema base (Cold cream®, Farmacia BOIX, Spain). La FLUO libre se disolvió con 0.5 mL de Hydrolite® (Guinama S.L., Spain) y se incorporó a la crema base. El vehículo HA-CP y la crema base se aplicaron también como control, siguiendo el mismo procedimiento. Todos los tratamientos fueron inmediatamente aplicados tópicamente en la espalda y en la oreja derecha del ratón durante 5 días consecutivos desde la última aplicación de la crema de IMQ. La seguridad de los tratamientos se evaluó mediante el seguimiento del peso corporal cada dos días desde el principio del experimento en comparación con los animales sanos. El grosor epidérmico de las orejas fue medido antes de cada tratamiento cada 2 días desde el inicio del experimento. Además, durante todo el estudio se utilizó la escala PASI para evaluar

visualmente parámetros presentes en la enfermedad, como eritema, descamación de la piel y grosor epidérmico (relacionado con el endurecimiento de la piel). Después de los 5 días de tratamiento, los ratones fueron sacrificados utilizando una atmósfera de CO_2 y se extrajeron los órganos principales, la piel, las orejas y la sangre para su análisis posterior. El peso del bazo se midió al final del experimento usando para ello una balanza de precisión. En estudios posteriores se evaluó el grosor epidérmico de la piel de la espalda y de la oreja mediante histología hematoxilina-eosina, así como los niveles de citoquinas proinflamatorias relacionadas con la enfermedad (IL-23 y INF-γ) tanto en tejido como en suero.

4. Resultados

4.1. Desarrollo de modelos relevantes para la evaluación de nanomedicinas: modelo de inflamación en piel humana *ex vivo y* un modelo murino de psoriasis (Capítulo II).

La psoriasis es una enfermedad cutánea inflamatoria crónica, autoinmune, genéticamente heterogénea y específica de los seres humanos [17]. Durante la última década, nuestro conocimiento sobre el desarrollo y la patogénesis de la enfermedad ha aumentado, lo que ha promovido al desarrollo de modelos *ex vivo* e *in vivo* precisos que favorezcan la comprensión de los mecanismos genéticos e inmunológicos que contribuyen al desarrollo de la enfermedad. Por lo tanto, cualquier modelo desarrollado debe reflejar las características críticas de la enfermedad humana y responder de manera similar a los tratamientos previamente desarrollados [18].

A lo largo del presente trabajo de Tesis, se presenta una caracterización detallada de dos modelos *ex vivo* (piel sana e inflamada) y un modelo *in vivo* de ratones psoriásicos. Estos modelos han sido empleados para evaluar la seguridad de los conjugados sintetizados, así como su actividad antiinflamatoria; el modelo inflamatorio *ex vivo* nos ha servido como plataforma para hacer un primer cribado de la actividad antiinflamatoria de los conjugados polímero-fármaco, para posteriormente evaluar en el modelo *in vivo* de psoriasis los que ofrezcan un mejor potencial terapéutico.

El modelo *ex vivo* de inflamación en piel humana desarrolla características histológicas similares a la enfermedad humana, como por ejemplo el engrosamiento de la capa epidérmica de la piel, manteniendo la estructura y viabilidad de las células de la piel. Además, la inducción de la inflamación en la piel ha promovido la liberación de

citoquinas proinflamatorias al medio de cultivo, permitiendo la evaluación de la capacidad antiinflamatoria de los conjugados.

Por otra parte, el desarrollo de un modelo agudo de psoriasis en ratón ha reproducido fielmente las características más descriptivas de la patología humana. Nuestras investigaciones han permitido evaluar la progresión y el mantenimiento de la enfermedad con el paso del tiempo. Este modelo se caracteriza por presentar características intrínsecas de la enfermedad humana tanto en la espalda como en la oreja del ratón, como enrojecimiento y descamación de la piel, así como engrosamiento epidérmico. Asimismo, hemos identificado características distintivas de este tipo de modelo inducido por la aplicación de IMQ en forma de crema, como es el aumento de tamaño del bazo [19-21], el cual está íntimamente relacionado con la síntesis de citoquinas proinflamatorias, ya que se encuentran elevadas tanto en suero como en tejido.

Por lo tanto, estos modelos presentan características similares a la enfermedad humana, ofreciendo una plataforma útil para poder evaluar terapias antiinflamatorias y antipsoriáticas.

4.2. Desarrollo de un nuevo material a base de ácido hialurónico (HA) entrecruzado con ácido poli-L-glutámico (PGA) el cual potencia la penetración a través de la piel en comparación con HA lineal (Capítulo III). Manuscrito en preparación

Como se ha discutido anteriormente en varios capítulos de este trabajo de Tesis, las características físico-químicas tanto de las nanomedicinas así como del vehículo en el que se apliquen a nivel tópico van a condicionar la penetración a través de la piel. La utilización de vehículos basados principalmente en el ácido hialurónico (HA) [22], ha demostrado su idoneidad para aplicaciones dérmicas y cosméticas [16].

A lo largo de este capítulo de Tesis, hemos diseñado una nueva plataforma de administración tópica, basada en la utilización del HA como base biodegradable para nuestro vehículo. Este vehículo llamado ácido hialurónico-poli-L-glutamato (HA-CP) está compuesto por el entrecruzamiento de dos polímeros biodegradables, HA y PGA, a través de L-lisina.

Utilizando metodologías bien establecidas, pudimos llevar a cabo la síntesis del vehículo HA-CP, el cual fue caracterizado mediante una exhaustiva caracterización

físico-química utilizando una batería de técnicas, como RMN y cromatografía de exclusión por tamaño (SEC). Los resultados obtenidos mediante RMN revelaron que nuestro material entrecruzado presentaba mayor peso molecular y radio hidrodinámico que el HA lineal, sugiriendo que la reacción de entrecruzamiento se había desarrollado con éxito. Además, mediante los estudios realizados por SEC, cabe destacar que la población de aminas libres se ve disminuida con la progresión de la reacción, mientras que la viscosidad se ve aumentada, debido a la formación de enlaces tipo amida que promueven la reacción de entrecruzamiento del HA-CP. Además, se pudo observar una disminución progresiva del pH de la reacción como consecuencia de la liberación de protones en cada formación del enlace amida.

Además, estudiamos en profundidad las características del biomaterial HA-CP como vehículo para aplicaciones tópicas en la piel. Se realizó un estudio de degradación por SEC en presencia de la enzima hialuronidasa [23], comparando el biomaterial HA-CP con HA lineal, demostrando que nuestro nuevo vehículo presentaba una degradación mucho más lenta, constante y sostenida a lo largo del tiempo, debido principalmente a las diferentes conformaciones estructurales de ambos materiales. Además, estudios de penetración a través de la piel revelaron que nuestro biomaterial HA-CP es capaz de alcanzar en mayor medida la epidermis que el HA lineal, el cual se encuentra principalmente en el estrato córneo, como ya demostraron otros autores [24]. Por último, ensayos de hidratación en voluntarios humanos demostraron que a tiempos largos de estudio nuestro HA-CP fue capaz de prolongar y mejorar la hidratación de la piel en comparación con HA.

Como hemos podido corroborar en este trabajo, el entrecruzamiento del HA con el PGA modifica las características físico-químicas del HA y favorece la penetración del biomaterial a través de la piel. Por ello, nuestro último esfuerzo se centró en estudiar la capacidad de nuestro vehículo como potenciador de la penetración de diferentes transportadores, como micelas polipeptídicas. Para la síntesis de estas micelas, se sintetizaron diferentes copolímeros utilizando polietilenglicol (PEG) como parte hidrofílica y como parte hidrofóbica se utilizó poli-fenilalanina (PPhe) y poli-bencil-L-glutamato (PBG) con diferentes grado de polimerización (10, 20, 40). La caracterización físico-química de estas micelas reveló que las que poseían mayor grado de polimerización (40) precipitaban en solución, probablemente debido a un desequilibrio de la relación hidrofílica y lipofílica, por lo que fueron descartadas del estudio. Los copolímeros PEG-

PBG mostraron unos valores de concentración micelar crítica más altos que los derivados de PEG-PPhe, indicando que los copolímeros de PEG-PPhe tienen un comportamiento más compacto en solución acuosa. Además, estos resultados fueron corroborados mediante cromatografía por exclusión de tamaño en medio orgánico (GPC), en los cuales los copolímeros basados en PPhe presentaron un fuerte comportamiento de agregación en comparación con PBG. Por último, las 4 micelas presentaron un tamaño entre 12 y 30 nm, lo cual coindice con las imágenes de microscopio electrónico de transmisión (TEM).

Así pues, estudiamos la penetración de las micelas marcadas con el fluoróforo Dil embebidas en el vehículo HA-CP a través de piel humana. Este estudio nos permitió demostrar la capacidad de nuestro vehículo para mejorar la penetración de las micelas a través de la piel, y por tanto, resaltar su utilización como vehículo para posibles aplicaciones tópicas de nanomedicinas.

4.3. Diseño racional de conjugados basados en poliglutamatos, incorporando un corticosteroide para el tratamiento de la psoriasis (Capítulo IV, manuscrito en revisión (Journal of Controlled Release)**).**

A lo largo de este capítulo de Tesis, hemos diseñado un nuevo conjugado polímero-fármaco incorporando el corticosteroide acetónido de fluocinolona (FLUO). El objetivo de esta conjugación es mejorar la penetración del fármaco a través de la piel y que su liberación se lleve a cabo de manera controlada y sostenida en la epidermis.

Para desarrollar este conjugado, se ha empleado una química optimizada, dotando al conjugado de un enlace sensible al pH (éster) para obtener una liberación controlada del fármaco. El conjugado PGA-FLUO presentaba un tamaño hidrodinámico constante con valores alrededor de 100 nm en todos los medios acuosos evaluados mediante dispersión dinámica de luz (DLS). Además, descubrimos que el conjugado era capaz de autoensamblarse en nanoestructuras mayores debido al balance hidrofílico-hidrofóbico, presentando una morfología esférica mediante TEM. Adicionalmente, se comprobó que el pH de la solución acuosa utilizada (pH 7.4 o 5.5) induce un cambio significativo en la cinética de liberación del fármaco y su estructura secundaria, influyendo por tanto en la disposición interna del fármaco en el esqueleto polipeptídico, tal y como pudimos observar tras los análisis llevados a cabo por cromatografía líquida de alta eficacia (HPLC) y dicroísmo circular (CD). La distinta estructura secundaria del conjugado parece modificar accesibilidad al fármaco, por lo que se ve favorecida su liberación a pH 7.4, del

mismo modo que se favorece el acceso de la enzima proteolítica catepsina B. Además, la liberación del fármaco una vez el conjugado se aplica en el vehículo HA-CP es más sostenida y constante en el tiempo, característica clave a la hora de controlar la actividad biológica en la epidermis.

La evaluación biológica del conjugado PGA-FLUO *in vitro* en líneas celulares de la piel demostró su internalización en los queratinocitos y colocalización en los lisosomas. Además, se comprobó la capacidad antiinflamatoria del conjugado en macrófagos estimulados con LPS, ya que el conjugado presentaba una mayor disminución de los niveles de citoquinas proinflamatorias en comparación con el fármaco libre. Estudios de penetración a través de la piel nos permitieron demostrar la presencia del conjugado en la epidermis, aumentando su cantidad si el conjugado se aplicaba con el vehículo HA-CP. Además, en dos modelos *ex vivo* de inflamación (definidos en el **Capítulo II**), se demostró nuevamente la mejoría de la capacidad antiinflamatoria del conjugado comparado con el fármaco libre, mediante la disminución de la liberación de IL-6. Por último, debemos destacar que la presencia del vehículo HA-CP en la aplicación del conjugado resultó en una mayor disminución de los niveles de IL-6.

Finalmente, el conjugado fue validado *in vivo* en un modelo murino de psoriasis (definido en el **Capítulo II**). En este modelo, se comparó la actividad del fármaco libre frente al conjugado, ambos aplicados en crema. Los resultados demostraron una mayor capacidad antipsoriática del conjugado, reduciendo parámetros significativos de la enfermedad como el engrosamiento epidérmico, el tamaño del bazo (un ~60% de reducción de peso del bazo con respecto al control positivo) y los niveles de citoquinas proinflamatorias características de la enfermedad (INF-γ y IL-23) en suero y tejido. Es de destacar que el grupo tratado con el conjugado aplicado en el vehículo HA-CP demostró una mayor capacidad de reducción de todos los parámetros estudiados en comparación con el conjugado aplicado en crema, alcanzando niveles similares a los controles sanos.

Mediante este estudio se demostró nuevamente una mejora de la actividad del conjugado frente al fármaco libre. Además, la administración del conjugado en nuestro vehículo HA-CP presentó en todos los casos un mayor efecto terapéutico, probándose la importancia de la correcta administración de los conjugados a nivel tópico mediante la elección de vehículos que promuevan su penetración a través de la piel.

4.4. Diseño racional de conjugados basados en poliglutamatos, incorporando un ácido graso omega 3 para mejorar la cicatrización de heridas y disminuir el daño producido por isquemia/reperfusión (I/R) en el corazón (Capítulo IV). Manuscrito en preparación

Tras la mejora terapéutica obtenida mediante la conjugación de fármacos al PGA para aplicaciones tópicas, durante este capítulo de Tesis se desarrolló una nueva familia de conjugados poliméricos con una estructura similar, incorporando distintas cargas de un ácido graso omega 3, llamado ácido docosahexaenoico (DHA), el cual ha demostrado eficacia terapéutica para en la cicatrización de heridas [25-27]. Para este trabajo, utilizamos DHA con dos cadenas poliinsaturadas, al que llamamos diDHA, para favorecer la conjugación al PGA. La conjugación se efectuó mediante un enlace tipo éster sensible al pH, con el objetivo de mejorar la estabilidad y actividad del diDHA.

La síntesis de los conjugados fue previamente optimizada facilitando la conjugación de distintas cargas de diDHA al polímero (2.2, 6.4 y 9.1 mol%). Hemos demostrado que la conjugación al PGA mejoró la solubilidad del diDHA en medios acuosos, así como su estabilidad y protección durante el tiempo, independientemente de la carga de diDHA en los conjugados. Mediante estudios de RMN pudimos evidenciar que después de 28 días de estudio, el diDHA sufrió una degradación de un 50%, mientras que los conjugados PGA-diDHA sólo mostraron un 10% de degradación, y además, estos estudios fueron corroborados mediante ensayos de peroxidación de lípidos. Adicionalmente, hemos demostrado que la carga de diDHA en los conjugados condiciona las propiedades físico-químicas del mismo, ya que a mayor carga de diDHA el conjugado presenta tamaños más pequeños y valores de concentración de agregación crítica menores, tras los análisis llevados a cabo mediante DLS y fluorímetro.

La familia de conjugados obtenida fue evaluada *in vitro*, en dos líneas celulares de la piel, demostrando una citotoxicidad del 100% el fármaco libre a las mayores concentraciones testadas, en comparación con los conjugados que mantuvieron el 100% de viabilidad celular a todas las concentraciones testadas. Además, en un estudio de cierre de herida en fibroblastos, el conjugado con carga intermedia de diDHA (PGA-diDHA6.4) favoreció el cierre de heridas respecto al diDHA libre. Por último, estudiamos la capacidad de penetración de los conjugados con mayor y menor carga de diDHA

marcados con OG (PGA-diDHA2.2-OG y PGA-diDHA9.1-OG) a través de la piel, demostrando que menores cargas de diDHA favorecen su penetración.

Basándonos en estos resultados, realizamos el estudio de liberación de fármaco con los conjugados con menor carga de diDHA, en el que comprobamos que la liberación de diDHA en el conjugado con carga intermedia (PGA-diDHA6.4) era casi el doble en comparación con el conjugado con carga baja (PGA-diDHA2.2) (5% y 3% de diDHA liberado, respectivamente). Mediante estos estudios también comprobamos que a pH 7.4 la liberación era mayor que a pH 5.5, y al igual que ocurría con otros conjugados desarrollados durante esta Tesis (**Capítulo IV**), observando cambios conformacionales a cada pH mediante CD.

Tanto los resultados experimentales en el modelo de cierre de herida como el estudio de la penetración a través de la piel, indicaron que los dos conjugados más efectivos eran los que presentaban una menor carga de diDHA (PGA-diDHA2.2 y PGA-DHA6.4) debido a sus características físico-químicas. Estos resultados sientan las bases para realizar estudios posteriores *in vivo* de rata diabética, en el cual se validarán estos dos conjugados y se evaluará su capacidad para favorecer la proliferación celular y disminuir la inflamación en la zona de la herida.

Finalmente, también demostramos la capacidad de los conjugados PGA-diDHA para mejorar el proceso de curación tras el daño al corazón producido por I/R asociado a infarto agudo de miocardio (IAM). La evaluación *in vitro* utilizando un ensayo de lactato deshidrogenasa reveló que el conjugado PGA-diDHA6.4 redujo el daño a las células cardíacas en comparación con el diDHA libre. Además, la infusión de los conjugados y diDHA libre en un modelo *in vivo* de I/R en ratas mostró que el tamaño del infarto se redujo significativamente cuando se administró PGA-diDHA6.4 antes de la reperfusión, en comparación con el diDHA libre en la misma dosis (12 % vs 28% de área infartada con o sin tratamiento, respectivamente). En conclusión, nuestros datos mostraron que la conjugación del diDHA podría ser un tratamiento efectivo para mitigar la lesión inducida por I/R.

5. Conclusiones

Durante el desarrollo de esta Tesis hemos demostrado la aplicabilidad de los polímeros terapéuticos como una nueva plataforma de administración tópica de diferentes agentes bioactivos o fármacos para el tratamiento, entre otras, de enfermedades de la piel,

como la psoriasis o la cicatrización de heridas. A continuación, destacamos las principales conclusiones de este trabajo:

1. Se han desarrollado modelos *ex vivo* de piel humana utilizando explantes de piel a partir de donantes, como una herramienta útil para validar los tratamientos basados en polímeros. Hemos establecido un modelo de piel sana así como un modelo inflamatorio tratando los explantes con una combinación de LPS y EGF.

   Los modelos *ex vivo* establecidos han sido validados como modelos preclínicos de enfermedad relevantes para los trastornos de la piel. La viabilidad de la piel fue evaluada en ambos modelos mediante ensayo MTT e inmunohistoquímica, y varios marcadores inflamatorios también se utilizaron para analizar el proceso inflamatorio. Finalmente, se detectó la modulación de la liberación de citoquinas proinflamatorias en el medio de cultivo, demostrando el efecto inflamatorio producido por la acción combinada de LPS y EGF.

2. Se ha caracterizado un modelo agudo de ratón psoriásico preclínicamente relevante, en el cual poder testar y validar las terapias basadas en polipéptidos que han sido desarrolladas. Mediante la aplicación tópica de una crema compuesta por imiquimod (IMQ), desarrollamos las características intrínsecas de la enfermedad de la psoriasis. Se evaluó durante 10 días la progresión y el mantenimiento de la enfermedad, mediante la valoración de la morfología de la piel utilizando la puntuación PASI y también la tinción H&E, centrándonos en parámetros específicos de la enfermedad, como el engrosamiento epidérmico. También se estudió el aumento del peso del bazo tras la aplicación de IMQ, el cual está relacionado con la síntesis de citoquinas. Finalmente, identificamos varias citoquinas proinflamatorias específicas relacionadas con la enfermedad humana, tanto en tejido como en suero.

3. Para mejorar y optimizar la penetración de los nanoportadores a través de la piel, hemos desarrollado y caracterizado completamente un nuevo vehículo basado en un polímero entrecruzado de ácido hialurónico-poli-L-glutamato (HA-CP) (compuesto por ácido hialurónico (HA) y ácido poli-L-glutámico (PGA) entrecruzados a través de fragmentos de lisina). Además, validamos y demostramos sus propiedades como potenciador de la penetración mediante su uso con una familia de copolímeros en bloque anfifílicos de diferente naturaleza

y consecuentemente presentando una conformación en solución diferente, modulando así la mejora de la permeación cutánea. Los cambios en la conformación de los portadores fueron impulsados por la presencia de Phe como aminoácido en la cadena de polímeros, así como por el tamaño del polímero, entre otras características.

4. Se ha desarrollado una nueva familia de conjugados polímero-fármaco, basados en el ácido poli-L-glutámico (PGA) como portador biodegradable, el cual incorpora un corticosteroide (acetónido de fluocinolona) mediante una unión tipo éster para el tratamiento tópico de la psoriasis. Se empleó una exhaustiva caracterización utilizando varias técnicas para caracterizar plenamente nuestros conjugados poliméricos en soluciones relevantes, estableciendo una relación entre la estructura y la actividad biológica.

5. La evaluación *in vitro* de los conjugados desarrollados en líneas celulares relevantes de la piel reveló la ausencia de toxicidad hasta las concentraciones probadas. Los estudios de internalización celular y actividad antiinflamatoria demostraron la capacidad de los conjugados para penetrar en las células de la piel y mantener la actividad antiinflamatoria del fármaco una vez se encuentra conjugado al PGA.

6. La evaluación *ex vivo* de los conjugados solos o aplicados en el vehículo HA-CP (como potenciador de la penetración) demostró su presencia en la epidermis viable. Además, utilizando dos modelos *ex vivo*, nuestro modelo de inflamatorio *ex vivo* de piel humana y un modelo reconstituido de inflamación a partir equivalentes cutáneos (en colaboración con la Freie Universität Berlin, Prof. S. Hedtrich), demostramos que el conjugado presentaba mayor capacidad para reducir la liberación de IL-6 en el medio de cultivo, en comparación con el fármaco libre.

7. La evaluación *in vivo* en nuestro modelo de ratón psoriásico demostró la eficacia antiinflamatoria/antipsoriásica y la seguridad de nuestro conjugado en comparación con el fármaco libre, verificando la importancia del uso de una química de enlace adecuada para controlar la cinética de liberación de los fármacos en las capas cutáneas adecuadas. Cabe destacar que el conjugado aplicado en nuestro novedoso vehículo HA-CP reveló una mayor actividad y

eficacia, demostrando la importancia de un vehículo adecuado para mejorar la penetración a través de la piel. HA-CP mostró altas propiedades de hidratación que se sinergizan con los efectos antiinflamatorios del conjugado, resultando en un enfoque terapéutico significativamente mejorado para la psoriasis.

8. Finalmente, se ha desarrollado una nueva familia de conjugados poliméricos, utilizando PGA como portador, incorporando diferentes cargas de un ácido graso omega 3 (diDHA) por medio de un enlace éster para el tratamiento tópico de la cicatrización de heridas. Las características físico-químicas del conjugado fueron estudiadas a fondo, y la evaluación biológica *in vitro* reveló su idoneidad para aplicaciones de cicatrización de heridas, mejorando el cierre de la herida.

9. La familia de conjugados PGA-diDHA fue validada en un escenario de curación de heridas *in vivo* utilizando un modelo de isquemia-reperfusión (I/R) en colaboración con el Hospital La Fe (Dr. P. Sepúlveda) mostrando claramente las ventajas de la conjugación a polímeros. La infusión de los conjugados y el diDHA libre en un modelo *in vivo* de I/R en rata mostró que el tamaño del infarto se redujo significativamente cuando se administró el conjugado PGA-diDHA6.4 antes de la reperfusión en comparación con el diDHA libre a la misma dosis. En conclusión, nuestros datos demostraron que el conjugado PGA-diDHA6.4 podría ser efectivo para mitigar la lesión inducida por I/R, proporcionando así un nuevo agente terapéutico para futuros estudios clínicos.

6. Referencias

[1] H.-Y. Chen, J.-Y. Fang, Therapeutic patents for topical and transdermal drug delivery systems, Expert Opin Ther Pat 10(7) (2000) 1035-1043.
[2] D. Singh Malik, N. Mital, G. Kaur, Topical drug delivery systems: a patent review, Expert Opin Ther Pat 26(2) (2016) 213-28.
[3] P.A.J. Kolarsick, M.A. Kolarsick, C. Goodwin, Anatomy and Physiology of the Skin, Journal of the Dermatology Nurses' Association 3(4) (2011) 203-213.
[4] J.Y. Fang, Y.L. Leu, Prodrug strategy for enhancing drug delivery via skin, Curr Drug Discov Technol 3(3) (2006) 211-24.
[5] R. Saraceno, A. Chiricozzi, M. Gabellini, S. Chimenti, Emerging applications of nanomedicine in dermatology, Skin Res Technol 19(1) (2013) e13-9.
[6] F. Alexis, E. Pridgen, L.K. Molnar, O.C. Farokhzad, Factors affecting the clearance and biodistribution of polymeric nanoparticles, Mol Pharm 5(4) (2008) 505-15.
[7] A. Kumari, S.K. Yadav, S.C. Yadav, Biodegradable polymeric nanoparticles based drug delivery systems, Colloids Surf B Biointerfaces 75(1) (2009) 1-18.

[8] B.C. Palmer, L.A. DeLouise, Nanoparticle-Enabled Transdermal Drug Delivery Systems for Enhanced Dose Control and Tissue Targeting, Molecules 21(12) (2016).
[9] B.D. Kurmi, P. Tekchandani, R. Paliwal, S.R. Paliwal, Transdermal Drug Delivery: Opportunities and Challenges for Controlled Delivery of Therapeutic Agents Using Nanocarriers, Curr Drug Metab 18(5) (2017) 481-495.
[10] R. Duncan, The dawning era of polymer therapeutics, Nat Rev Drug Discov 2 (2003) 347-60.
[11] R. Duncan, Polymer therapeutics as nanomedicines: new perspectives, Curr Opin Biotech 22(4) (2011) 492-501.
[12] R. Duncan, R. Gaspar, Nanomedicine(s) under the microscope, Mol Pharm 8(6) (2011) 2101-41.
[13] S.D. Chipman, F.B. Oldham, G. Pezzoni, J.W. Singer, Biological and clinical characterization of paclitaxel poliglumex (PPX, CT-2103), a macromolecular polymer-drug conjugate, Int J Nanomedicine 1(4) (2006) 375-83.
[14] G.E. Flaten, Z. Palac, A. Engesland, J. Filipović-Grčić, Ž. Vanić, N. Škalko-Basnet, In vitro skin models as a tool in optimization of drug formulation, Eur J Pharm Sci 75 (2015) 10-24.
[15] S. Berkó, M. Maroda, M. Bodnár, G. Erős, P. Hartmann, K. Szentner, P. Szabó-Révész, L. Kemény, J. Borbély, E. Csányi, Advantages of cross-linked versus linear hyaluronic acid for semisolid skin delivery systems, Eur Polym J 49(9) (2013) 2511-2517.
[16] S. Khunmanee, Y. Jeong, H. Park, Crosslinking method of hyaluronic-based hydrogel for biomedical applications, Journal of Tissue Engineering 8 (2017) 16.
[17] M.A. Lowes, A.M. Bowcock, J.G. Krueger, Pathogenesis and therapy of psoriasis, Nature 445 (2007) 866.
[18] J.E. Gudjonsson, A. Johnston, M. Dyson, H. Valdimarsson, J.T. Elder, Mouse models of psoriasis, J Invest Dermatol 127(6) (2007) 1292-308.
[19] L. van der Fits, S. Mourits, J.S. Voerman, M. Kant, L. Boon, J.D. Laman, F. Cornelissen, A.M. Mus, E. Florencia, E.P. Prens, E. Lubberts, Imiquimod-induced psoriasis-like skin inflammation in mice is mediated via the IL-23/IL-17 axis, J Immunol 182 (2009) 5836-45.
[20] H. Vinter, K. Kragballe, T. Steiniche, M. Gaestel, L. Iversen, C. Johansen, Tumour necrosis factor-alpha plays a significant role in the Aldara-induced skin inflammation in mice, Br J Dermatol 174(5) (2016) 1011-21.
[21] A. Ueyama, M. Yamamoto, K. Tsujii, Y. Furue, C. Imura, M. Shichijo, K. Yasui, Mechanism of pathogenesis of imiquimod-induced skin inflammation in the mouse: a role for interferon-alpha in dendritic cell activation by imiquimod, J Dermatol 41(2) (2014) 135-43.
[22] L. Kenne, S. Gohil, E.M. Nilsson, A. Karlsson, D. Ericsson, A. Helander Kenne, L.I. Nord, Modification and cross-linking parameters in hyaluronic acid hydrogels—Definitions and analytical methods, Carbohyd Polym 91(1) (2013) 410-418.
[23] F. Tranchepain, B. Deschrevel, M.N. Courel, N. Levasseur, D. Le Cerf, C. Loutelier-Bourhis, J.C. Vincent, A complete set of hyaluronan fragments obtained from hydrolysis catalyzed by hyaluronidase: Application to studies of hyaluronan mass distribution by simple HPLC devices, Anal Biochem 348(2) (2006) 232-242.
[24] M. Essendoubi, C. Gobinet, R. Reynaud, J.F. Angiboust, M. Manfait, O. Piot, Human skin penetration of hyaluronic acid of different molecular weights as probed by Raman spectroscopy, Skin Res Technol 22(1) (2016) 55-62.
[25] E.L. Arantes, N. Dragano, A. Ramalho, D. Vitorino, G.F. de-Souza, M.H. Lima, L.A. Velloso, E.P. Araújo, Topical Docosahexaenoic Acid (DHA) Accelerates Skin Wound Healing in Rats and Activates GPR120, Biol Res Nurs 18(4) (2016) 411-9.

[26] J.C. McDaniel, M. Belury, K. Ahijevych, W. Blakely, Omega-3 fatty acids effect on wound healing, Wound Repair Regen 16(3) (2008) 337-45.
[27] C.R. Cardoso, M.A. Souza, E.A. Ferro, S. Favoreto, J.D. Pena, Influence of topical administration of n-3 and n-6 essential and n-9 nonessential fatty acids on the healing of cutaneous wounds, Wound Repair Regen 12(2) (2004) 235-43.